UNIVERSIDADE FEDERAL DO RIO GRANDE DO SUL
INSTITUTO DE QUÍMICA
PROGRAMA DE PÓS-GRADUAÇÃO EM QUÍMICA

ISOXAZOLINAS. UMA CLASSE DE MATERIAIS AVANÇADOS REVISITADA

Aline Tavares

Tese

Porto Alegre, Novembro/2010.

UNIVERSIDADE FEDERAL DO RIO GRANDE DO SUL
INSTITUTO DE QUÍMICA
PROGRAMA DE PÓS-GRADUAÇÃO EM QUÍMICA

ALINE TAVARES

Tese apresentada como requisito parcial para a
obtenção do grau de Doutor em Química

Prof. Dr. Aloir Antonio Merlo
Orientador

Porto Alegre, Novembro/2010.

A presente tese foi realizada inteiramente pela autora, exceto as colaborações as quais serão devidamente citadas nos agradecimentos, no período entre Novembro de 2006 e Novembro de 2010, no Instituto de Química da Universidade Federal do Rio Grande do Sul sob Orientação do Professor Doutor Aloir Antonio Merlo. A tese foi julgada adequada para a obtenção do título de Doutor em Química pela seguinte banca examinadora:

Comissão Examinadora:

Prof. Dr. Ivan Helmuth Bechtold

Universidade Federal de Santa Catarina - UFSC

Prof. Dr. Günter Ebeling

Universidade Federal do Rio Grande do Sul - UFRGS

Prof. Dr. Nilo Zanatta

Universidade Federal de Santa Maria - UFSM

Prof[a]. Dr[a]. Iêda Maria Begnini

Fundação Universidade Regional de Blumenau - FURB

Prof. Dr. Aloir Antonio Merlo

Orientador

Aline Tavares

"Não me pergunte quem sou
e não me diga para permanecer o mesmo"

Michel Foucault

AGRADECIMENTOS

Ao Felipe, meu amor, companheiro, psicólogo e parceiro, pela amizade, paciência e compreensão nesta longa vida acadêmica.

Aos meus pais e irmã, os quais amo muito, pelo carinho e incentivo. É graças a vocês que hoje sou quem sou.

Ao Prof. Aloir só posso oferecer a minha sincera gratidão pela maravilhosa orientação, amizade e ensinamentos durante os quatro anos de convivência.

Ao Prof. Paulo Schneider, pela amizade e disponibilidade em ajudar nas discussões a respeito dos espectros de RMN.

À Profª. Leandra Campo pela contribuição na realização das análises de ultravioleta.

Ao Prof. Paulo Brenner e ao químico Júlio pela realização das medidas de DSC.

Ao Prof. Celso Moro, pelo empréstimo das cubetas de quartzo.

Aos Profs. Livotto, Paulo Gonçalves e Hubert pelos cálculos computacionais.

Aos funcionários do Instituto de Química Régis, sempre disponível a ajudar, Joyce, pela colaboração nos experimentos de RMN e também Edson, Carlos e Raul.

Aos companheiros e amigos de laboratório Dani, Eric, Guilherme, Helena, Joel, Ju, Laura, Mari, Marcelo M., Rafa, Raoní, Rodrigo, Sérgio, Si, Tiago, pelas horas compartilhadas no trabalho e pelas tantas conversas, cafés, churrascos, risadas, cantorias... como amigo! À Bárbara, a aluna "maluquinha" de iniciação científica que me ajudou na realização deste trabalho e agora amiga para sempre! Fico feliz de ter colaborado na formação profissional dessa guria que traz Kit-Kat do Chuí: quem sabe um dia trabalharemos juntas novamente! Em especial à Lili, pelas conversas e conselhos... e pelos seus maravilhosos quitutes que alimentaram o meu doutorado, claro!

À Sílvia, ex-colega de faculdade e hoje grande amiga e incentivadora, por tudo que compartilhamos juntas na nossa jornada.

À Mariane, que deu sorte para o Inter na conquista do bi da libertadores. Ao Pedroso, amigão, pelos cafezinhos e conversas nas idas fugidas ao R.U. e a todos os amigos que fiz dentro dessa Universidade.

Ao Instituto de Química da UFRGS pela disponibilidade dos equipamentos para realização das análises no infravermelho, UV-vis, RMN, análise elementar e DSC.

Aos órgãos financiadores CNPq e CAPES pelas bolsas concedidas e PADCT pelo suporte financeiro à pesquisa.

SUMÁRIO

SUMÁRIO DAS FIGURAS, ESQUEMAS E TABELAS

LISTA DE ABREVIATURAS

APT	Teste do próton ligado (*Attached Proton Test)*
Ar	Arila
CL	Cristal líquido
Col.	Colaboradores
Cr	Fase cristalina
DCC	1,3-Diciclohexilcarbodiimida
DMAP	4-(*N*,*N*-dimetilamino)piridina
DSC	Calorimetria exploratória diferencial (*Differential Scanning Calorimetry)*
GC-MS	Cromatografia gasosa acoplada à espectrometria de massas (*Gas Chromatography-Mass Spectrometry*)
HMQC	Correlação heteronuclear ^{1}H-^{13}C com detecção de hidrogênio (*Heteronuclear Multiple Quantum Coherence*)
HOMO	Orbital molecular ocupado de mais alta energia (*Highest Occupied Molecular Orbital*)
I	Estado líquido isotrópico
IV	Infravermelho (*Infrared)*
LC	Líquido-cristalino
LCDs	Mostradores de cristal líquido (*Liquid Crystal Displays*)
LUMO	Orbital molecular não ocupado de mais baixa energia (*Lowest Unoccupied Molecular Orbital*)
MMI	Material molecular inteligente
MOLP	Microscopia óptica de luz polarizada
m. p.	Melting point
N	Mesofase nemática
n	Número de carbonos
OLEDs	Diodos orgânicos emissores de luz (*Organic light emitting diodes*)
p. f.	Ponto de fusão
ppm	Partes por milhão
Ref.	Referência
RMN	Ressonância Magnética Nuclear
SmA	Mesofase esmética A
SmC	Mesofase esmética C
TGA	Análise termogravimétrica (*Thermogravimetric Analysis)*
TMS	Trimetilsilano
UV-vis	Ultravioleta visível
ΔH	Variação de entalpia
λ	Comprimento de onda

RESUMO

Este trabalho descreve a síntese e caracterização de séries inéditas de materiais líquido-cristalinos contendo o *N*-heterociclo isoxazolina. Este anel foi obtido a partir da reação de cicloadição [3+2] 1,3-dipolar de óxidos de nitrila a diferentes dipolarófilos. As propriedades térmicas foram analisadas por MOLP, DSC e TGA, e as propriedades ópticas através de espectros de absorção.

O presente trabalho apresenta três publicações, um artigo submetido e dois em fase final de redação, todos relacionados à Tese. Na primeira publicação (*Eur. J. Org. Chem*. **2009**, 889-897) foi obtida uma coleção de isoxazolinas que serviram como intermediários na síntese dos compostos líquido-cristalinos finais. Da coleção foram selecionados os intermediários 3-4-(alquiloxi)fenil]-4,5-dihidroisoxazoil-5-metanol e ácido 3-[4-(alquiloxi)fenil]-4,5-dihidroisoxazoil-5-carboxílico para a transformação nos respectivos cristais líquidos. Além do cicloaduto esperado, em um dos casos obteve-se o cicloaduto 2:1 na reação entre o óxido de nitrila e o ácido vinilacético. Os compostos finais apresentaram mesofases nemática e esmética C. Na segunda publicação (*J. Braz. Chem. Soc.* **2009**, *20*, 1742-1752) foram obtidas três novas séries homólogas contendo o heterociclo isoxazolina através de uma síntese envolvendo as reações de esterificação, proteção de grupos funcionais e acoplamento de Sonogashira. Neste trabalho foi realizado um estudo sistemático em relação às propriedades líquido-cristalinas através da variação do número de átomos de carbonos metilênicos e da inversão do grupo polar carbonílico como grupo conector dos anéis. Os compostos finais exibiram mesofases nemática e esmética C. Na terceira publicação (*Liq. Cryst.* **2010**, *37*, 159-169) foram obtidas duas séries de cristais líquidos contendo o anel isoxazolina ligado a diferentes grupos arilacetilênicos. As séries mostraram mesofase nemática monotrópica para os derivados de fenilacetileno. Quando a unidade aromática foi substituída por naftilacetileno os compostos apresentaram mesofase esmética A enantiotrópica.

No quarto trabalho submetido à Revista *Mater. Chem. Phys.* uma série de *O*-benzoiloximas foi sintetizada a partir da reação de esterificação entre oximas e derivados do ácido benzóico. Os compostos apresentaram mesofases N e SmA enantiotrópicas e fluorescência, com decomposição da amostra após o primeiro ciclo de aquecimento. Também foi sintetizado um homólogo da série contendo o anel isoxazolínico via reação entre uma oxima e o ácido 3-[4-octiloxi)fenil]-4,5-dihidroisoxazoil-5-carboxílico, com mesofase esmética B. No quinto trabalho, em fase final de redação, foi investigado detalhadamente o

comportamento térmico da série homóloga de cicloadutos 2:1. A elucidação estrutural foi feita via técnicas de ressonância magnética nuclear (^{1}H, ^{13}C, COSY, HMBC e HMQC), DSC, microscopia e estudo fotofísico. Cálculos teóricos também foram feitos para a compreensão mecanística da formação do aduto 2:1 em detrimento do aduto 1:1. Os compostos mostraram mesofases esméticas com decomposição da amostra após o primeiro ciclo de aquecimento. Nos ciclos subseqüentes observou-se que apesar da decomposição, as amostras apresentaram mesofase esmectogênica com textura *Schlieren*, sugerindo mesofase SmC. No sexto trabalho, em fase final de redação, foram sintetizadas duas séries de CLs contendo o anel isoxazolínico 3,5-dissubstituído variando-se o número de carbonos metilênicos entre o anel e um grupo éster. Assim, foram analisadas as propriedades mesomórficas destes materiais em relação às temperaturas de transição e estrutura química. Os compostos apresentaram mesofases N e SmA.

ABSTRACT

The synthesis and characterization of novel series of liquid crystalline materials containing *N*-heterocyclic isoxazoline are described. These molecules were obtained from the reaction of 1,3-dipolar cycloaddition of nitrile oxides to different compounds containing double bonds. Thermal properties were analyzed by MOLP, DSC and TGA, and optical properties by absorption spectra.

This work presents three publications, one submitted article and two in final stages of writing, all related to the thesis. In the first publication (*Eur. J. Org. Chem.* **2009**, 889-897) was obtained a collection of isoxazoline as intermediates in the synthesis of liquid crystalline compounds. The intermediates 3-[4-(alkyloxy)phenyl]-4,5-dihydroisoxazol-5-yl methanol and 3-[4-(alkyloxy)phenyl]-4,5-dihydroisoxazole-5-carboxylic acid were selected for the transformation in the respectives LCs. Besides the expected cycloadducts, in one case we obtained the 2:1 cycloadduct in the reaction between nitrile oxide and vinylacetic acid. The final compounds showed nematic and smectic C mesophases. In the second publication (*J. Braz. Chem. Soc* **2009**, *20*, 1742-1752) were obtained three new homologous series containing the isoxazoline heterocycle through the reactions esterification, protection of functional groups and Sonogashira coupling. This work represents a systematic study with respect to the LCs properties by varying the number of methylene carbon atoms and the inversion of the polar carbonyl group as connector rings. The final compounds exhibited nematic and smectic C mesophases. In the third publication (*Liq.Cryst.* **2010**, *37*, 159-169) were obtained two series of liquid crystals containing the isoxazoline ring connected to different groups arylacetylenenes. The series showed monotropic nematic mesophase for derivatives of phenylacetylene. When a unit has been replaced by naphtilacetylene the compounds showed smectic A enantiotropic mesophase.

In the fourth paper submitted to *Mater. Chem. Phys.* a series of *O*-benzoyloximes was synthesized from the esterification reaction between oximes and derivatives of benzoic acid. The compounds present N and SmA enantiotropic mesophases and fluorescence, with decomposition of the sample after the first heating cycle. Was also synthesized a homologous series containing the isoxazoline ring by reaction between an oxime and the 3-[4-(octyloxy)phenyl]-4,5-dihydroisoxazole-5-carboxylic acid, with smectic B behavior. In the fifth study, in the final stages of writing, was investigated in detail the thermal behavior of homologous series of 2:1 cycloadducts. The structure was determined by nuclear magnetic

resonance (^{1}H, ^{13}C, COSY, HMBC and HMQC), DSC, microscopy and photophysical study. Theoretical calculations were also obtained to understand the mechanism of the formation of 2:1 adduct instead of the 1:1 adduct. The compounds showed smectic mesophases with decomposition of the sample after the first heating cycle. In the sixth work in the final stages of writing, were synthesized two series of LCs containing 3,5-disubstituted isoxazoline ring varying the number of methylene carbon atoms between the ring and an ester group. Thus, we analyzed the mesomorphic properties of these materials in relation to transition temperatures and chemical structure. The compounds exhibited N and SmA mesophases.

CAPÍTULO 1

As isoxazolinas fazem parte de uma interessante classe de compostos heteropentaciclos. A síntese de novas moléculas contendo este heterociclo constitui uma importante área de investigação devido ao seu potencial aplicativo em diversas áreas do conhecimento científico.

Por exemplo, o anel 2-isoxazolina está presente em produtos biológicos[1] tais como bactericidas e fungicidas, farmacológicos[2], com destaque para os antiinflamatórios e antidepressivos, agroquímicos[3] e também na área de materiais[4]. Como exemplo, a isoxazolina **1** apresentou alta atividade antibacteriana contra *S. aureus* e *S. paratyhi A*[5] e a isoxazolina **2** mostrou-se como um bom agente anti-HIV-1[2a] (Figura 1).

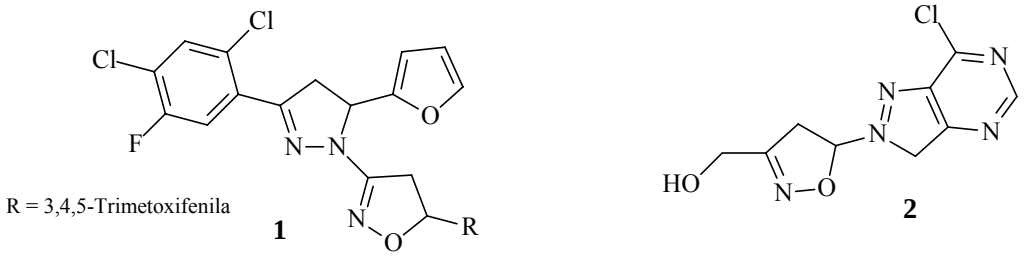

Figura 1. Estrutura química de isoxazolinas com atividade biológica.

Em síntese orgânica este heterociclo tem se mostrado um intermediário versátil uma vez que a ruptura do anel leva a compostos importantes tais como β-aminoácidos[6], cetonas α,β-insaturadas[8b], β-aminoálcoois[7], β-dióis[8b], etc (Figura 2). Além destas aplicações, moléculas orgânicas contendo esse anel também são utilizadas na produção de materiais sensíveis a efeitos externos, os quais podem ser utilizados na preparação de mostradores de

[1] (a) Cannon, J. G.; Mohan, P.; Bojarski, J.; Long, J. P.; Bhatnagar, R. K.; Leonard, P. A.; Flynn, J. R.; Chatterjee, T. K. *Med. Chem. Res*. **1988**, *8*, 313; (b) Gaonkar, S. L.; Rai, K. M. L.; Prabhuswamy, B. *Med. Chem. Res.* **2007**, *15*, 407.

[2] (a) Xiang, Y.; Chen, J.; Schinazi, R. F.; Zhao, K. *Bioorg. Med. Chem. Lett.* **1996**, *6*, 1051; (b) Zhang, L.; Anzalone, L.; Ma, P.; Kauffman, G. S.; Storace, L.; Ward, R. *Tetrahedron Lett*. **1996**, *37*, 4455; (c) Dallanoce, C.; Meroni, G.; De Amici, M.; Hoffmann, C.; Klotz, K-N.; De Micheli, C. *Bioorg. Med. Chem.* **2006**, *14*, 4393; (d) Wade, P. A.; Pillay, M. K.; Singh, S. M. *Tetrahedron Lett.* **1982**, *23*, 4563.

[3] Milinkevich, K. A.; Yoo, C. L.; Sparks, T. C.; Lorsbach, B. A.; Kurth, M. J. *Bioorg. Med. Chem. Lett.* **2009**, *19*, 5796.

[4] Torroba, T. *J. Prakt. Chem.* **1999**, *341*, 99.

[5] Shah, T.; Desai, V. *J. Serb. Chem. Soc.* **2007**, *72*, 443.

[6] Fuller, A. A.; Chen, B.; Minter, A. R.; Mapp, A. K. *J. Am. Chem. Soc.* **2005**, *127*, 5376.

[7] Aschwanden, P.; Kvarno, L.; Geisser, R. W.; Kleinbeck, F.; Carreira, E. *Org. Lett.* **2005**, *7*, 5741.

[8] (a) Jäger, V.; Colinas, P. A. "*Nitrile Oxides"* em *The Chemistry of Heterocyclic Compounds*. Vol. 59; Padwa, A. e Pearson, W. H., Eds.; Wiley: New York, 2002; (b) Kozikowski, A. P. *Acc. Chem. Res.* **1984**, *17,* 410; Aschwanden, P.; Kvaerno, L.; Geisser, R. W.; Kleinbeck, F.; Carreira, E. M. *Org. Lett.* **2005**, *7*, 5741.

cristais líquidos. Isto ainda é pouco difundido nessa área, mas apresenta grande potencial na preparação de interessantes materiais orgânicos[9].

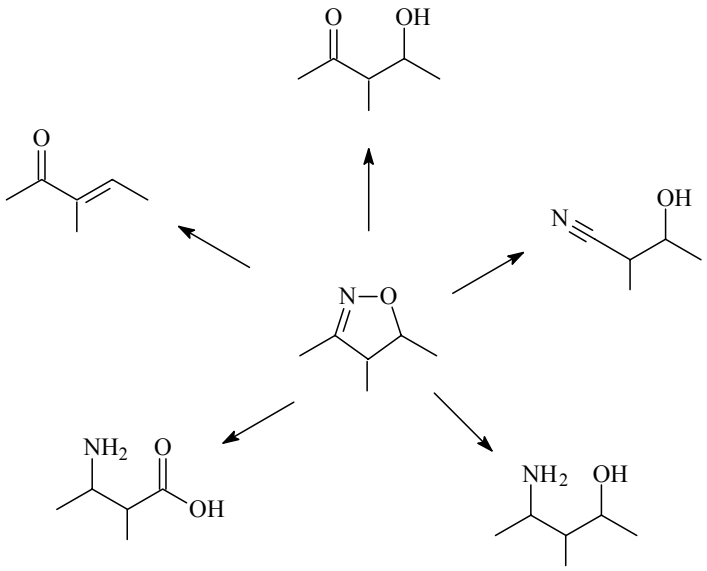

Figura 2. A potencialidade do anel isoxazolina na obtenção de derivados importantes para a síntese orgânica sintética.

A síntese e aplicação de cristais líquidos funcionais, também conhecidos como *materiais moleculares inteligentes* (MMI)[10], é de grande importância para o desenvolvimento de diversas áreas de pesquisa[11]. Cristais líquidos são materiais orgânicos com importantes aplicações científicas e tecnológicas devido à sua anisotropia geométrica, a qual gera propriedades ópticas, elétricas e magnéticas devido ao alinhamento molecular alcançado com estímulo elétrico ou magnético e por causa da sua propriedade intrínseca de auto-organização.

Na área tecnológica a sua aplicação mais difundida é em mostradores de cristal líquido (*LCDs*). Na física, os cristais líquidos encontram aplicações como semicondutores[12]. Na química, uma possível aplicação é a sua utilização como precursores moleculares em síntese orgânica. Nas áreas farmacêutica e medicinal têm-se estudado o uso dos CLs como veículos transportadores de fármacos que regulam a liberação de substâncias neles incorporadas, como

---

[9] (a) Tavares, A.; Schneider, P. H.; Merlo, A. A. *Eur. J. Org. Chem.* **2009**, 889; (b) Tavares, A.; Livotto, P. R.; Gonçalves, P. F. B.; Merlo, A. A. *J. Braz. Chem. Soc.* **2009**, *20*, 1742; (c) Tavares, A.; Ritter, O. M. S.; Vasconcelos, U. B.; Arruda, B. C.; Schrader, A.; Schneider, P. H.; Merlo, A. A. *Liq. Cryst.* **2010**, *37*, 159; (d) Passo, J. A.; Vilela, G. D.; Schneider, P. H.; Ritter, O. M. S.; Merlo, A. A. *Liq. Cryst.* **2008**, *35*, 833; (e) Ritter, O. M. S.; Giacomelli, F. C.; Passo, J. A.; Silveira, N. P.; Merlo, A. A. *Polym. Bull.* **2006**, *56*, 549; (f) Umesha, K. B.; Rai, K. M. L.; Nagappa, N.; Mahadeva, J. *Indian J. Chem., Sect. B: Org. Chem. Incl. Med. Chem.* **2004**, *43*, 2635.

[10] (a) Kato, T. *Science* **2002**, *295*, 2414; (b) Lehn, J-M. *Science* **2002**, *295*, 2400.

[11] Goodby, J. W.; Bruce, D. W.; Hird, M.; Imrie, C.; Neal, M. *J. Mater. Chem*. **2001**, *11*, 2631.

[12] Shimura, H.; Yoshio, M.; Hamasaki, A.; Mukai, T.; Ohno, H.; Kato, K. *Adv. Mater*. **2009**, *21*, 1591.

algumas drogas anticâncer[13]. Deve-se observar que os próprios DNA e RNA são polímeros capazes de gerar mesofase.

Também, os cristais líquidos vêm sendo investigados devido ao seu potencial de aplicação nas indústrias de cosméticos, alimentícia e medicinal.

De acordo com o interesse, certas propriedades podem ser geradas a partir da funcionalização de um cristal líquido, como a incorporação de anéis heterocíclicos, por exemplo. Devido ao desvio da linearidade, o uso destes anéis contribui para os estudos referentes à compreensão sobre a influência dos fatores estéricos, eletrônicos e estruturais, que se relacionam com a estrutura molecular, e que irão influenciar nas propriedades mesomórficas. O primeiro autor que mostrou que heterociclos incorporados na estrutura molecular de um composto permitiam a formação de mesofases foi Vorländer no início do século XX[14].

Em trabalhos prévios de nosso grupo de pesquisa[9d,e] foi mostrado que polímeros contendo o anel isoxazolínico apresentam comportamento líquido-cristalino com mesofase nemática (Figura 3).

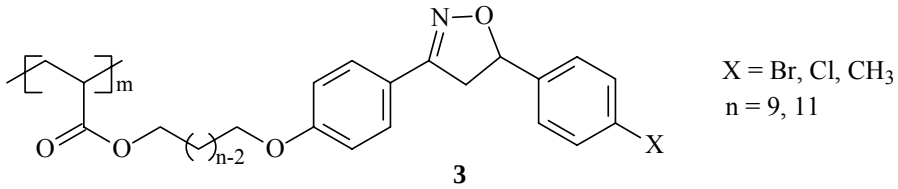

3

Figura 3. Exemplo de cristal líquido polimérico.

Kovganko *et al.*[15] investigaram a síntese e as propriedades líquido-cristalinas de duas séries de moléculas contendo o anel isoxazol, obtido a partir da oxidação do anel isoxazolina (Figura 4). Os compostos sintetizados apresentaram fases SmA, SmC e N.

4 **5**

R = cadeias alquílicas

Figura 4. Exemplos de cristais líquidos contendo o anel isoxazol.

[13] Formariz, T. P.; Urban, M. C. C.; Silva, A. A. J.; Gremiao, M. P. D.; Oliveira, A. G. *Rev. Bras. Cienc. Farm.* **2005**, *41*, 301.
[14] (a) Vorländer, D. *Z. Phys. Chem.* **1923**, *105*, 211; (b) Bruce, D.; Heyns, K.; Vill, V. *Liq. Cryst.* **1997**, *23*, 813.
[15] Kovganko, V. N.; Kovganko, N. N. *Russ. J. Org. Chem.* **2006**, *42*, 243.

Além dos anéis isoxazol e isoxazolina, existem inúmeros exemplos de CLs contendo heterociclos[16]. Por exemplo, Cristiano e col.[17] publicaram um estudo sobre moléculas com formato curvo contendo o anel 1,3,4-oxadiazol e grupos tolano. Os compostos apresentaram mesofases líquido-cristalinas típicas de compostos calamíticos (Figura 5).

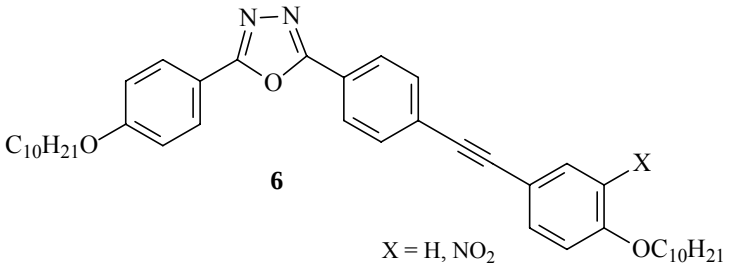

6

Figura 5. Exemplo de cristal líquido com estrutura molecular curva.

Normalmente os CLs são compostos formados por moléculas alongadas que contêm vários anéis aromáticos. Quando tais materiais têm uma geometria molecular adequada que permita uma alta conjugação π ao longo desses anéis eles poderão apresentar fluorescência, que é uma propriedade muito interessante para aplicação em dispositivos eletroluminescentes tais como OLEDs[18] e sondas fluorescentes[19].

Vieira e col.[20] publicaram em 2008 a síntese de uma série de derivados de 2,1,3-benzotiadiazóis com diferentes grupos arilacetilenos terminais (Figura 6). Em relação ao comportamento mesomórfico, os compostos apresentaram preferencialmente mesofases SmC e N. O estudo fotofísico mostrou que os compostos também apresentam fluorescência.

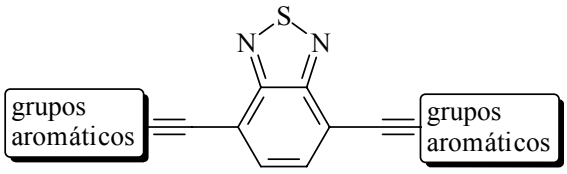

7

Figura 6. Exemplos de cristais líquidos contendo o anel benzotiadiazol.

---

[16] (a) Qu, S.; Chen, X.; Shao, X.; Li, F.; Zhang, H.; Wang, H.; Zhang, P.; Yu, Z.; Wu, K.; Wang, Y.; Li, M. *J. Mater. Chem*. **2008**, *18*, 3954; (b) Wang, C-S.; Wang, I-W.; Cheng, K-L.; Lai, C. K. *Tetrahedron* **2006**, *62*, 9383; (c) Han, J.; Chang, X-Y.; Zhu, L-R.; Wang, Y-M.; Meng, J-B.; Lai, S-W.; Chui, S. S-Y. *Liq. Cryst.* **2008**, *35*, 1379; (d) Han, J.; Zhang, F-Y.; Chen, Z.; Wang, J-Y.; Zhu, L-R.; Pang, M-L.; Meng, J-B. *Liq. Cryst.* **2008**, *35*, 1359; (e) Kozmík, V.; Polásek, P.; Seidler, A.; Kohout, M.; Svoboda, J.; Novotná, V.; Glogarová, M.; Pociecha, D. *J. Mater. Chem.* **2010**, *20*, 7430.

[17] Cristiano, R.; Santos, D. M. P. O.; Gallardo, H. *Liq. Cryst.* **2005**, *32*, 7.

[18] (a) Lydon, D. P.; Porrès, L.; Beeby, A.; Marder, T. B.; Low, P. J. *New J. Chem*. **2005**, *29*, 972; (b) Giménez, R.; Piñol, M.; Serrano, J. L. *Chem. Mater.* **2004**, *16*, 1377.

[19] (a) Maeda, H.; Maeda, T.; Mizuno, K.; Fujimoto, K.; Shimizu, H.; Inouye, M. *Chem. Eur. J*. **2006**, *12*, 824; (b) Wicklein, A.; Muth, M-A.; Thelakkat, M. *J. Mater. Chem.* **2010**, *20*, 8646.

[20] Vieira, A. A.; Cristiano, R.; Bortoluzzi, A. J.; Gallardo, H. *J. Mol. Struct.* **2008**, *875*, 364.

Também, um material orgânico que possuir um sistema π eletrônico conjugado com grande deslocalização da nuvem eletrônica pode ser um promissor semicondutor, pois o comportamento dos seus orbitais moleculares será parecido com o comportamento das bandas eletrônicas de um semicondutor inorgânico[21].

CLs contendo grupos funcionais do tipo uréia, amida, peptídeos, ácidos, entre outros, são capazes de formar géis, ou seja, podem ser aplicados como gelatinizantes orgânicos. A incorporação de pelo menos um destes grupos permitirá que o composto forme, de maneira espontânea, uma rede supramolecular termorreversível de fibras auto-organizáveis via interações intermoleculares não covalentes (por exemplo, ligações de hidrogênio e interações π-π).

A presença de agregados de fibras (diâmetro normalmente na ordem de centenas de nanômetros) pode admitir interessantes propriedades aos géis líquido-cristalinos[22]. Estes mantêm a propriedade estímulo-resposta dos CLs, ou seja, respondem a estímulos externos, e por isso têm apresentado uma promissora abordagem para o desenvolvimento de materiais moleculares funcionais[23], além de atrair atenção pelas suas excelentes propriedades eletro-ópticas[24] e eletrônicas[25]. Também, apresentam potencial para uso como sensores e no campo dos *displays* apresentam resposta mais rápida e mais brilho do que os *displays* de CL puro[26], entre outros[27].

A Figura 7 descreve as potencialidades do anel isoxazolínico como precursor molecular em diversas áreas do conhecimento científico. Assim, nesta Tese explorou-se o vértice do pentágono que contempla os cristais líquidos isoxazolínicos.

---

[21] (a) Newma, C. R.; Frisbie, C. D.; Filho, D. A. S.; Brédas, J. L.; Ewbank, P. C.; Mann, K. R. *Chem. Mater.* **2004**, *16*, 4436; (b) Sun, Y.; Duan, L.; Wei, P.; Qiao, J.; Dong, G.; Wang, L.; Qiu, Y. *Org. Lett.* **2009**, *11*, 2069; (c) Chow, C-F.; Roy, V. A. L.; Ye, Z.; Lam, M. H. W.; Lee, C. S. Lau, K. C. *J. Mater. Chem.* **2010**, *20*, 6245; (d) Vlachos, P.; Mansoor, B.; Aldred, M. P.; O'Neill, M.; Kelly, S. M. *Chem. Commun.* **2005**, 2921.
[22] Kato, T.; Hirai, Y.; Nakaso, S.; Moriyama, M. *Chem. Soc. Rev.* **2007**, *36*, 1857.
[23] Shinkai, S.; Murata, K. J. *Mater. Chem.* **1998**, *8*, 485.
[24] (a) Kato, T. *Science* **2002**, *295*, 2414; (b) He, J.; Yan, B.; Yu, B.; Bao, R.; Wang, X.; Wang, Y. *J. Colloid Interf. Sci*. **2007**, *316,* 825.
[25] (a) Mizoshita, N.; Monobe, H.; Inoue, M.; Ukon, M; Watanabe, T.; Shimizu, Y.; Hanabusa K.; Kato, K. *Chem. Commun.* **2002**, 428; (b) Wang, C.; Zhang, D.; Xiang, J.; Zhu, D. *Langmuir* **2007**, *23*, 9195; (c) Tong, X.; Zhao, Y.; An, B-K.; Park, S. Y. *Adv. Funct. Mater*. **2006**, *16*, 1799.
[26] Mizoshita, N.; Suzuki, Y.; Kishimoto, K.; Hanabusa K.; Kato, T. *J. Mater. Chem.* **2002**, *12*, 2197.
[27] (a) Kato, T.; Kondo, G.; Hanabusa, K. *Chem. Lett*. **1998**, *3*, 193; (b) Kato, T.; Mizoshita, N.; Moriyama, M.; Kitamura, T. *Top. Curr. Chem.* **2005**, *256*, 219; (c) Kim, T. H.; Choi, M. S.; Sohn, B. H.; Park, S.-Y.; Lyoo, W. S.; Lee, T. S. *Chem. Commun.* **2008**, 2364.

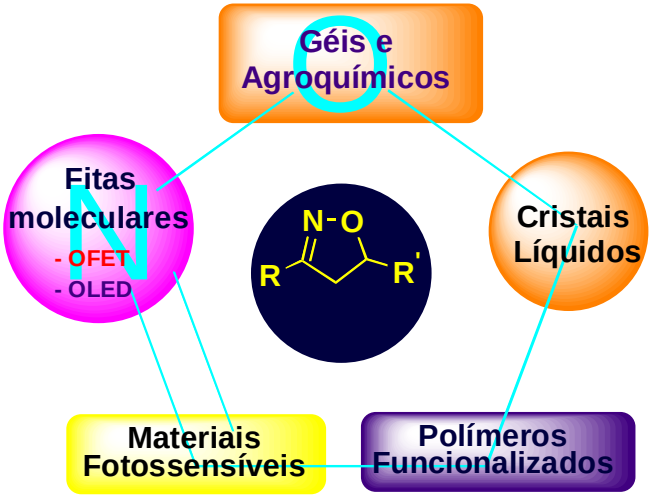

Figura 7. Potencial aplicativo do anel isoxazolínico como precursor de materiais com as mais diversas aplicações.

CAPÍTULO 2

2.1 ANEL ISOXAZOLINA. UMA CLASSE DE MATERIAIS AVANÇADOS REVISITADA.

Os compostos heterocíclicos compreendem uma enorme fração dos compostos descritos na literatura. Das 55 milhões de substâncias químicas registradas na base de dados do *Chemical Abstracts* (Outubro, 2010) aproximadamente metade são heterociclos.

Os compostos orgânicos que possuem anéis pentagonais contendo dois ou mais heteroátomos como nitrogênio, oxigênio, selênio ou enxofre na sua estrutura molecular (Figura 8), apresentam uma função importante na síntese de novos materiais. Isto é conseqüência das alterações que o heteroátomo causa nas propriedades estruturais e eletrônicas da molécula devido à presença de pares de elétrons e da diferença de eletronegatividade entre o heteroátomo e o carbono na estrutura cíclica, levando a novas propriedades físico-químicas e reatividade, as quais podem ser exploradas na preparação de compostos orgânicos com propriedades específicas.

Nesse sentido, o anel isoxazolínico é um representante importante do grupo dos ciclos 1,2-azóis. Este anel caracteriza-se por possuir dois heteroátomos: um átomo de oxigênio na posição 1 e um átomo de nitrogênio na posição 2 do anel, com uma insaturação sp^2 entre a ligação N-C (Figura 8).

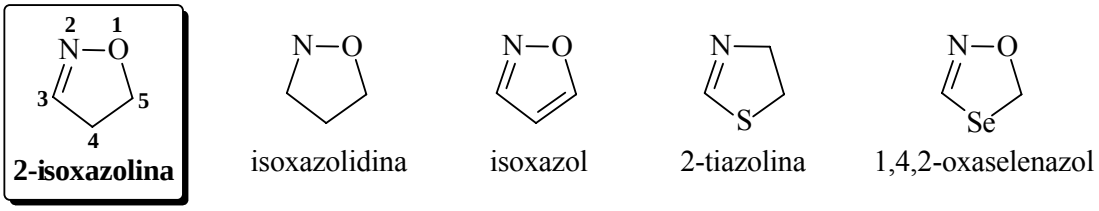

Figura 8. Exemplos de heterociclos pentagonais. Em destaque o anel 2-isoxazolina.

Existem diversas metodologias para a obtenção de compostos cíclicos. Por exemplo, as adições aldólicas exibem grande potencial sintético nas reações que ocorrem de forma intramolecular, isto é, quando estão presentes na mesma molécula uma carbonila e um enolato, resultando na formação de um sistema cíclico[28]. Esse tipo de reação é particularmente interessante na formação de anéis de cinco ou seis membros. Dentre as reações de cicloadição, o exemplo mais conhecido é a reação de Diels-Alder, que fornece anéis de seis

[28] Saito, S.; Yamamoto, H. *Chem. Eur. J.* **1999**, *5*, 1959.

membros. Para a obtenção de anéis de cinco membros, a reação de cicloadição 1,3-dipolar é a metodologia mais utilizada.

Alguns métodos para a síntese de 2-isoxazolinas são: ciclização nitrosativa de 3-cloro-1-nitropropano[29], a partir de nitrato de sódio e *n*-propilnitrito; reação entre 3-isoxazolin-5-ona com olefinas[30]; também as reações fotoquímicas de ciclopropanos 1,2-dissustituídos com $NOBF_4$[31]; reações envolvendo dipolarófilos contendo selênio[32], entre outros. Entretanto, o método mais utilizado para a síntese de 2-isoxazolinas é a reação de cicloadição 1,3-dipolar, com inúmeros exemplos na literatura.

2.1.1 Reação de cicloadição 1,3-dipolar: obtenção de 2-isoxazolinas.

Nas reações de cicloadição a união de 2 sistemas π leva à formação de 2 novas ligações σ. As reações de cicloadição 1,3-dipolar são um tipo de reação pericíclica, as quais são caracterizadas por um processo de reorganização contínua e concertada de elétrons. Isto significa que, quando concertadas, um único estado de transição cíclico está envolvido, sem a formação de intermediários no processo, como pode ser visto no Esquema 1[33].

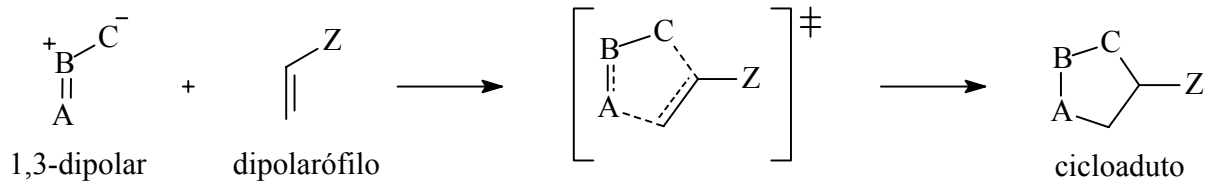

Esquema 1. Exemplo geral de uma reação de cicloadição, mostrando o estado de transição cíclico.

A principal rota para a obtenção do anel isoxazolínico é a partir da reação de cicloadição 1,3-dipolar entre um óxido de nitrila e um alceno[8a, 34]. Essas reações são análogas às reações de Diels-Alder uma vez que são concertadas e eletronicamente definidas como um sistema de 6 elétrons. Nestas adições uma espécie irá participar com 4 elétrons distribuídos sobre 3 átomos (chamado de componente 1,3-dipolar) e a outra com 2 elétrons distribuídos

[29] (a) Wade, P. A.; Price, D. T. *Tetrahedron Lett.* **1989**, *30*, 1185; (b) Wade, P. A.; D'Ambrosio, S. G.; Price, D. T. *J. Org. Chem.* **1995**, *60*, 6302.
[30] Higashida, S.; Nakashima, H.; Tohda, Y.; Tani, K.; Nishiwaki, N.; Ariga, M. *Heterocycles* **1992**, *34*, 1511.
[31] Mizuno, K.; Ichinose, N.; Tamai, T.; Otsuji, Y. *J. Org. Chem.* **1992**, *57*, 4669.
[32] Segi, M.; Tanno, K.; Kojima, M.; Honda, M.; Nakajima, T. *Tetrahedron Lett.* **2007**, *48*, 2303.
[33] Houk, K. N.; Sims, J.; Watts, C. R.; Luskus, L. J. *J. Amer. Chem. Soc.* **1973**, *95*, 7301.
[34] (a) Carey, F. A.; Sundberg, R. J. *Advanced Organic Chemistry, Part B: Reactions and Synthesis.* Plenum Press, 2008; (b) Rodrigues, R. C. *Synthetic Commun.* **2001**, *31*, 3075; (c) Huisgen R. *1,3-Dipolar Cycloadditon Chemistry.* Padwa, A., Ed.; Vol. 1. Wiley: New York, 1984.

sobre 2 átomos (chamado de dipolarófilo), levando ao anel isoxazolínico. Deste modo, estas cicloadições são definidas como reações [3+2], onde os números representam o número de átomos envolvidos na formação do anel.

As espécies 1,3-dipolar têm um sistema eletrônico π com 2 orbitais preenchidos e um vazio e são análogas aos ânions alílico ou propargílico. Estes compostos apresentam estruturas de ressonância como exemplificado na Figura 9, onde se pode ver a distribuição de cargas nas posições 1 e 3.

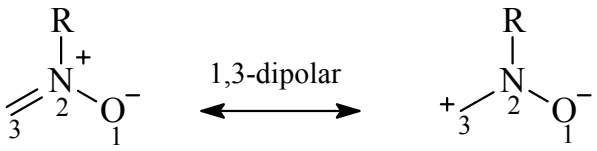

Figura 9. Estrutura de ressonância e distribuição de cargas em uma nitrona (exemplo de composto 1,3-dipolar).

Os compostos 1,3-dipolar do tipo alila são curvos e caracterizam-se pela presença de quatro elétrons π em três orbitais *p* paralelos e perpendiculares ao plano do 1,3-dipolar. Já os ânions do tipo propargila são lineares e com um orbital π ortogonal extra[35] (Figura 10).

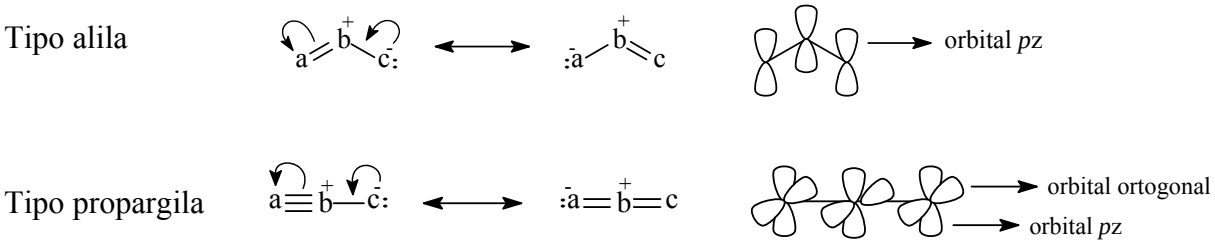

Figura 10. Geometria e orbitais dos compostos 1,3-dipolar do tipo alila e propargila.

Dentre os diversos compostos 1,3-dipolar que podem ser utilizados nas reações de cicloadição, destacam-se os exemplos mostrados na Figura 11. Estes compostos variam bastante em estabilidade, sendo que alguns podem ser isolados e armazenados, enquanto outros são instáveis e devem ser gerados *in situ*, como no caso dos óxidos de nitrila.

[35] Fleming, I. *Frontier Orbitals and Organic Chemical Reation.* John Wiley, N. Y. 1976.

1,3-Dipolos do tipo alila

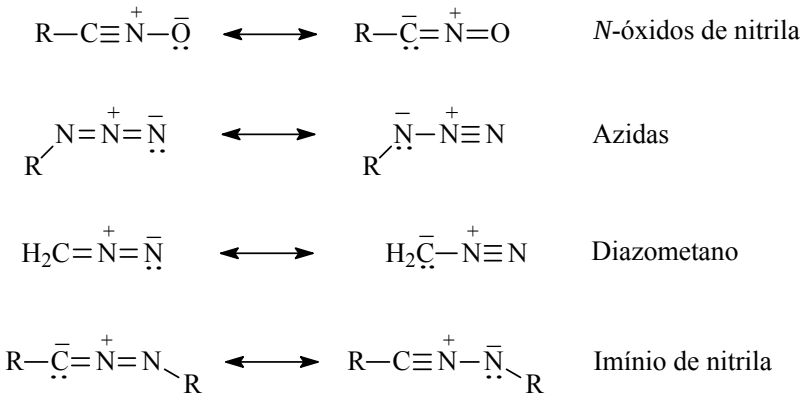

1,3-Dipolos do tipo propargila

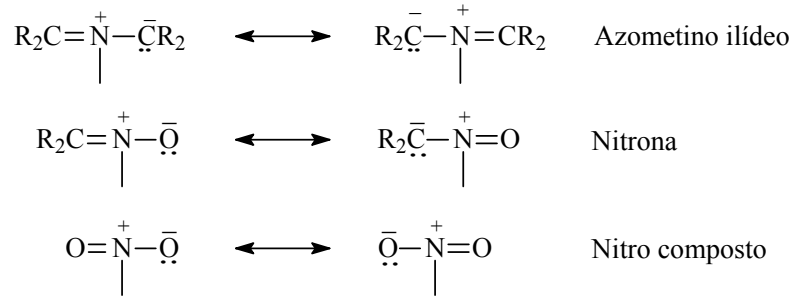

Figura 11. Exemplos de compostos 1,3-dipolar.

Dentre as espécies 1,3-dipolar mostradas na Figura 11, o óxido de nitrila é o composto utilizado para a formação do anel isoxazolínico. Existem dois métodos para a sua formação: a partir da desidrogenação oxidativa de oximas e da desidratação de nitro compostos (Esquema 2). Freqüentemente, ele é gerado *in situ* no meio reacional a partir de uma aldoxima ou cetoxima em meio oxidante. Para isso, dois agentes de oxidação podem ser utilizados: hipoclorito de sódio 5% (NaOCl) e *N*-clorosuccinimida (NCS)[36].

[36] Fener, H. *Nitrile oxides, nitrones, and nitronates in organic synthesis: novel strategies in synthesis.* 2ª Ed. Wiley-Interscience: New Jersey. 2008.

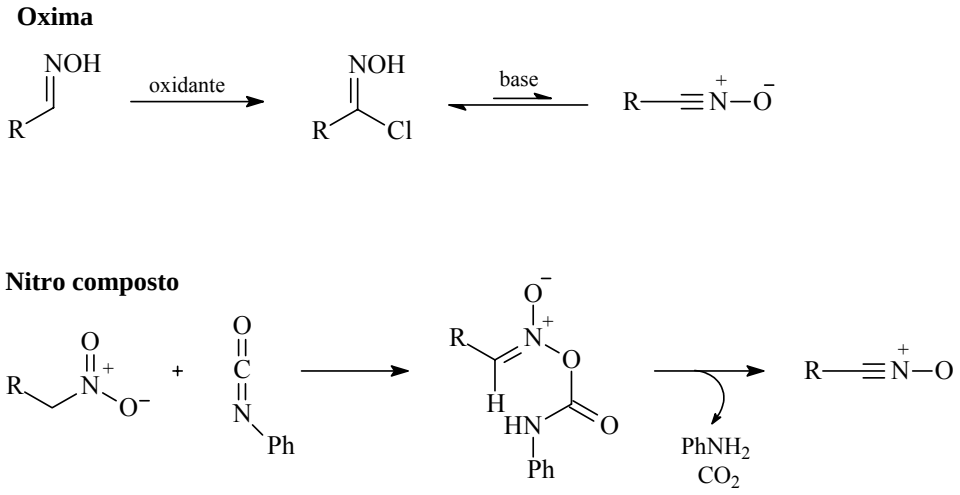

Esquema 2. Dois métodos para formação do óxido de nitrila: um a partir de oxima e outro de nitro composto.

As oximas, responsáveis pela geração dos óxidos de nitrila, são obtidas a partir de aldeídos ou cetonas através da reação com cloridrato de hidroxilamina[37]. Observa-se, nestas reações, a formação dos isômeros *E* e *Z* (Esquema 3), com a predominância para formação do isômero *E*.

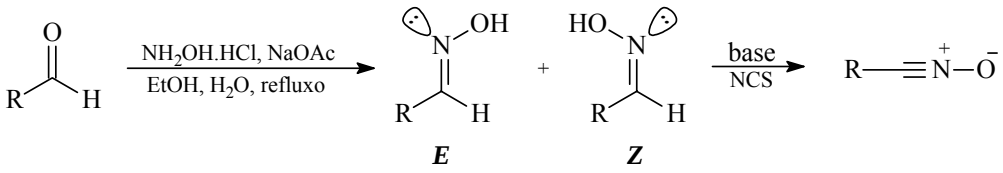

Esquema 3. Formação das oximas *E* e *Z*, precursoras do óxido de nitrila.

As atribuições dos deslocamentos químicos de RMN de ^{1}H e ^{13}C para os isômeros *E* e *Z* de algumas oximas são encontradas na literatura[38] e alguns dados podem ser vistos na Tabela 1, Entradas 1 e 2.

A análise dos deslocamentos dos átomos de hidrogênio e carbono imínicos, além dos carbonos C_1 e C_4, são de maior relevância. A partir dos dados apresentados na Tabela 1 pode-se observar que a configuração da oxima tem uma forte influência sobre os deslocamentos químicos dos átomos de carbono e hidrogênio imínicos. Assim, os sinais dos hidrogênios imínicos dos isômeros *Z* aparecem em campo mais alto do que os isômeros *E*, o que é coerente com oximas análogas derivadas do anisaldeído[38]. Este resultado sugere que a

[37] Lee, G. A. *Synthesis* **1982**, 508.
[38] (a) Gordon, M. S.; Sojka, S. A.; Krause, J. G. *J. Org. Chem.* **1984**, *49*, 2326; (b) Owston, N. A.; Parker, A. J.; Williams, J. M. *Org. Lett.* **2007**, *9*, 3599; (c) Danoff, A.; Franzen-Sieveking, M.; Lichter, R. L.; Fanso-Free, S.

densidade eletrônica no carbono imínico do isômero *E* é menor (mais desblindado) em relação ao isômero *Z*[39,40].

Durante a realização deste trabalho foi possível a atribuição e a determinação da proporção dos isômeros *E* e *Z* na preparação das oximas utilizadas nesta tese, conforme Capítulo 5.1, página 53[9a] (Figura 12). Os deslocamentos químicos das oximas **9** (*E*/*Z*) e **10** (*E*) estão apresentados na Tabela 1, Entradas 3, 4 e 5, e estão de acordo com a literatura.

Tabela 1. Deslocamentos químicos de RMN de ^{13}C e ^{1}H das oximas **8**, **9** e **10**.

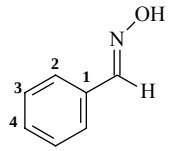

8-*E*

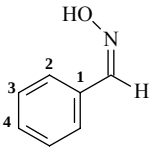

8-*Z*

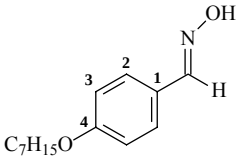

9-*E*

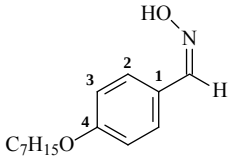

9-*Z*

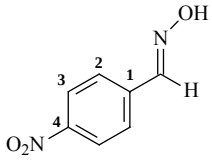

10-*E*

		C_1	C_2	C_3	C_4	C=N	CH_2O	H-C=N	Ref.
1	**8**-isômero *E*	131,8	127,0	128,4	130,2	150,3	-	8,1	38
2	**8**-isômero *Z*	130,7	128,0	129,2	130,3	145,5	-	7,2	38
3	**9**-isômero *E*	125,3	128,5	114,8	160,6	149,5	67,8	8,1	nesta tese
4	**9**-isômero *Z*	124,0	132,9	114,4	160,2	146,0	67,7	7,3	nesta tese
5	**10**-isômero *E**	139,0	127,1	123,6	147,7	146,8	-	8,2	nesta tese

*O isômero *Z* não foi detectado nos espectros RMN de ^{1}H e ^{13}C neste trabalho. Sharghi em uma publicação de 2001, mostrou que o sinal do hidrogênio imínico do isômero *E* aparece em campo mais alto do que o isômero *Z*[41].

Os deslocamentos químicos de ^{13}C seguem a mesma tendência. Por exemplo, o átomo de carbono imínico do isômero **9**-*Z* aparece em 146,0 ppm (Entrada 4, Tabela 1), enquanto que para o **9**-*E* aparece em 149,5 ppm (Entrada 3, Tabela 1). Para a oxima **8** o deslocamento químico do carbono imínico do isômero *E* também aparece deslocado para campo baixo (Entradas 1 e 2, Tabela 1). Os valores listados na Tabela 1 mostraram que o deslocamento químico de ^{13}C do carbono imínico são menos sensíveis ao efeito dos substituintes em comparação com os átomos de carbono do anel aromático.

N. Y. *Org. Mag. Ress*. **1979**, *12*, 83; (d) Halkier, B. A.; Olsens, C. E.; Moller, B. L. *J. Biol. Chem.* **1989**, *264*, 19487.

[39] G. C. Levy, G. C.; Lichter, R. L.; Nelson, G. L.; *Carbon-13 Nuclear Magnetic Resonance Spectroscopy*, Wiley-Interscience, New York, 1980, p 55-57.

[40] (a) Karabatsos, G. J.; Taller, R. A.; Vane, F. M. *J. Am. Chem. Soc.* **1963**, *85*, 2326; (b) Heinisch, G.; Holzer, W. *Tetrahedron Lett.* **1990**, *31*, 3109; (c) De Rosa, M.; Brown, K.; McCoy, M.; Ong, K.; Sanford, K. *J. Chem. Soc. Perkin Trans. 1* **1993**, 1787; (d) Gunn, B. C.; Stevens, M. F. G. *J. Chem. Soc. Perkin Trans. 1* **1973**, 1682.

[41] Sharghi, H.; Sarvari, M. H. *Synlett* **2001**, 99.

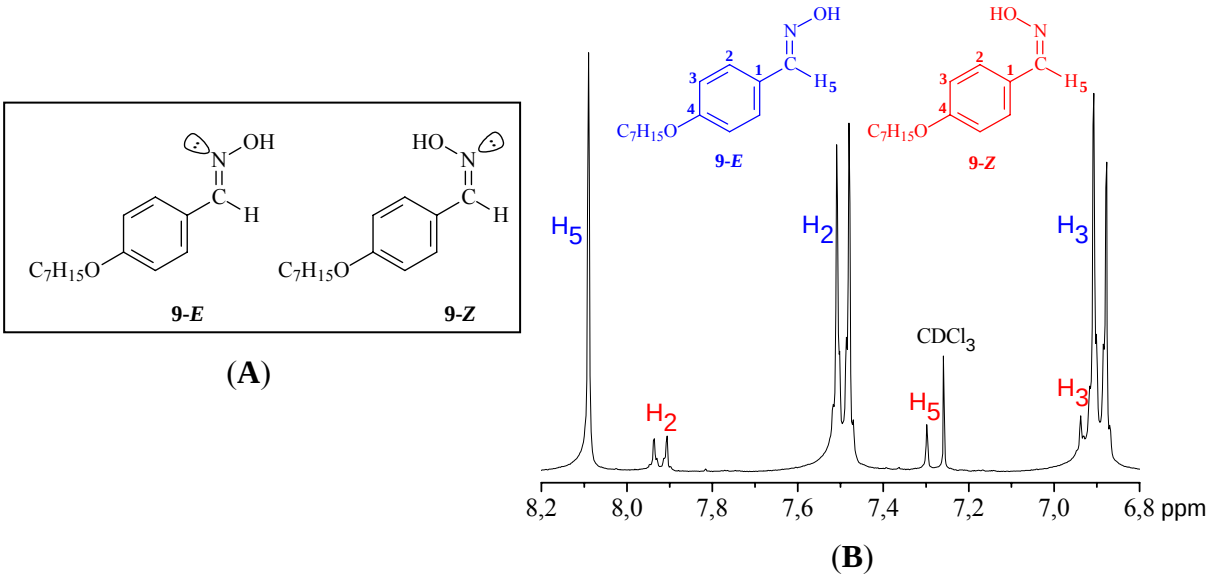

Figura 12. Em (A) oximas *E* e *Z* e em (B) espectro parcial de RMN de ^{1}H (300 MHz, $CDCl_3$) do composto **9**.

É interessante também analisar o efeito do substituinte na posição *para* do anel aromático sobre os deslocamentos dos átomos de carbono C_1 e C_4. Quando o substituinte é retirador de elétrons, o carbono C_4 torna-se mais blindado e seu deslocamento químico é para campo alto (Figura 13A). Este comportamento pode ser claramente observado comparando as oximas **9** e **10** (Entradas 3, 4 e 5, Tabela 1). Provavelmente este efeito é devido à maior capacidade do grupo nitro de estabilizar a carga negativa no átomo de carbono C_4 em relação ao grupo alcóxi (Figura 13B). No caso do carbono C_1, ele está mais deficiente eletronicamente quando o substituinte é o grupo nitro, deslocando o seu sinal para campo mais baixo.

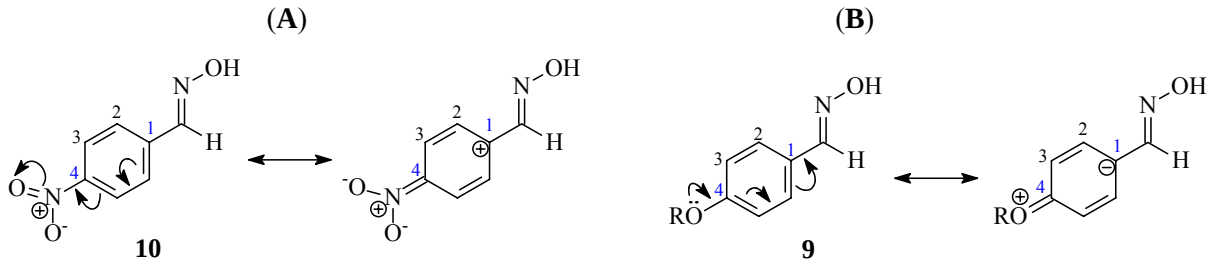

Figura 13. Influência do efeito eletrônico sobre os carbonos C_1 e C_4. Em (A) grupo retirador e em (B) grupo doador.

Nas reações de cicloadição 1,3-dipolar uma grande variedade de dipolarófilos (alcenos e alcinos) pode ser utilizada. Dependendo da escolha do par de reagentes diferentes anéis

podem ser formados (Tabela 2). Para a produção do anel isoxazolínico, por exemplo, a espécie 1,3-dipolar deve ser um óxido de nitrila e o dipolarófilo um alceno, o qual pode ser funcionalizado ou não.

Tabela 2. Exemplos de compostos heterocíclicos formados a partir da reação de cicloadição 1,3-dipolar.

1,3-dipolar	Dipolarófilo	Heterociclo
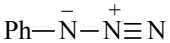	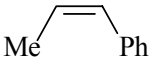	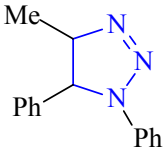 Anel triazol
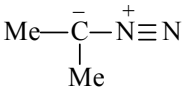	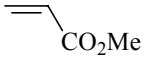	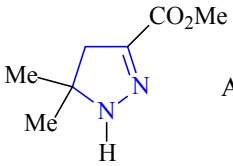 Anel pirazol
$PhSO_2CBr{=}NOH$, base		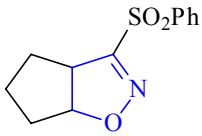 Anel isoxazolina
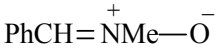	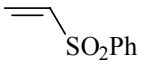	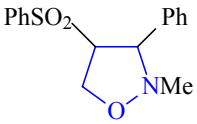 Anel isoxazolidina
	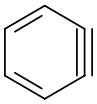	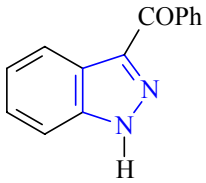 Anel pirazol
PhCCl=NOH, Et_3N	PhC=S	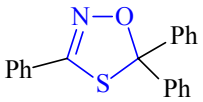 Anel oxatiazolidina

Uma característica importante da reação de Diels-Alder é a formação de anéis com alto controle da estereoquímica, uma conseqüência do mecanismo concertado destas adições. Isto é perdido, em parte, nas cicloadições 1,3-dipolar devido à natureza polar dos reagentes. Assim, elas podem passar tanto por um mecanismo concertado quanto radicalar[42].

Em geral, observa-se um mecanismo concertado para as cicloadições 1,3-dipolar. Nestes casos, o estado de transição é governado pelos orbitais moleculares de fronteira dos substratos. Isto é explicado pela Teoria dos Orbitais Moleculares de Fronteira, que considera

[42] Huisgen, R. *J. Org. Chem.* **1976**, *41*, 403.

as interações entre orbitais moleculares do composto 1,3-dipolar e do dipolarófilo, explicando a regio e estereoquímica do cicloaduto formado.

Assim, as cicloadições podem ser divididas em 3 tipos: ***i.*** cicloadição controlada pelos orbitais HOMO do 1,3-dipolar e LUMO do dipolarófilo; ***ii.*** cicloadição controlada pelos orbitais LUMO do 1,3-dipolar e HOMO do dipolarófilo; *iii*. cicloadição controlada pelos orbitais HOMO ou LUMO de ambos. O tipo de interação dominante dependerá da diferença de energia entre os pares de orbitais moleculares. As interações entre o HOMO e o LUMO que tiverem as menores diferenças de energia serão predominantes. Quando a energia dos orbitais é muito próxima, a reação pode ser controlada simultaneamente por ambos o HOMO e LUMO do 1,3-dipolar e dipolarófilo. Isto pode ser manipulado eletronicamente através da adição de grupos retiradores ou doadores de elétrons. Também, os reagentes serão preferencialmente orientados, ou seja, a interação mais forte vai acontecer, entre os carbonos que têm os maiores coeficientes dos dois orbitais alinhados.

A maioria dos casos descritos na literatura constata que as cicloadições 1,3-dipolar acontecem com uma regioquímica bem definida no fechamento do anel, ou seja, com alta regiosseletividade. Em especial, as cicloadições com óxidos de nitrila mostram-se bastante regiosseletivas. A questão da regiosseletividade deve ser considerada quando o alceno for substituído. Com esta condição, a cicloadição pode fornecer a mistura dos regioisômeros 3,5- e 3,4-dissubstituídos (posição relativa entre os grupos R e R' e o átomo de oxigênio do anel), conforme mostra o Esquema 4.

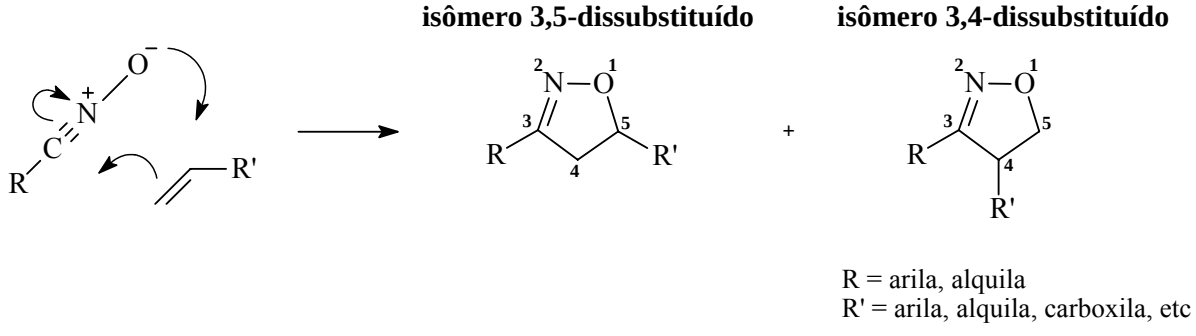

Esquema 4. Modelo geral de uma reação de cicloadição 1,3-dipolar com óxido de nitrila, mostrando os dois regioisômeros que podem ser formados.

Como já foi visto, a formação dos isômeros 3,5- e 3,4-dissubstituídos dependerá dos coeficientes atômicos e das energias relativas dos orbitais HOMO e LUMO[43]. Na Figura 14A

[43] Carruthers, W. *Cycloadditon Reactions in Organic Synthesis*. Pergamon Press, 1990.

está representada uma interação predominante acontecendo entre o HOMO do dipolarófilo e o LUMO do óxido de nitrila. O tipo dos orbitais moleculares envolvidos pode ser definido através de cálculos teóricos. Assim, o isômero 3,5 se forma quando acontecer a Combinação 1 (Figura 14B), e o isômero 3,4 se forma quando acontecer a Combinação 2 (Figura 14B). Além do fator eletrônico que favorece a formação do isômero 3,5, deve-se levar em conta que o arranjo *anti* dos substituintes ligados aos componentes reativos favorece a aproximação no estado de transição[44].

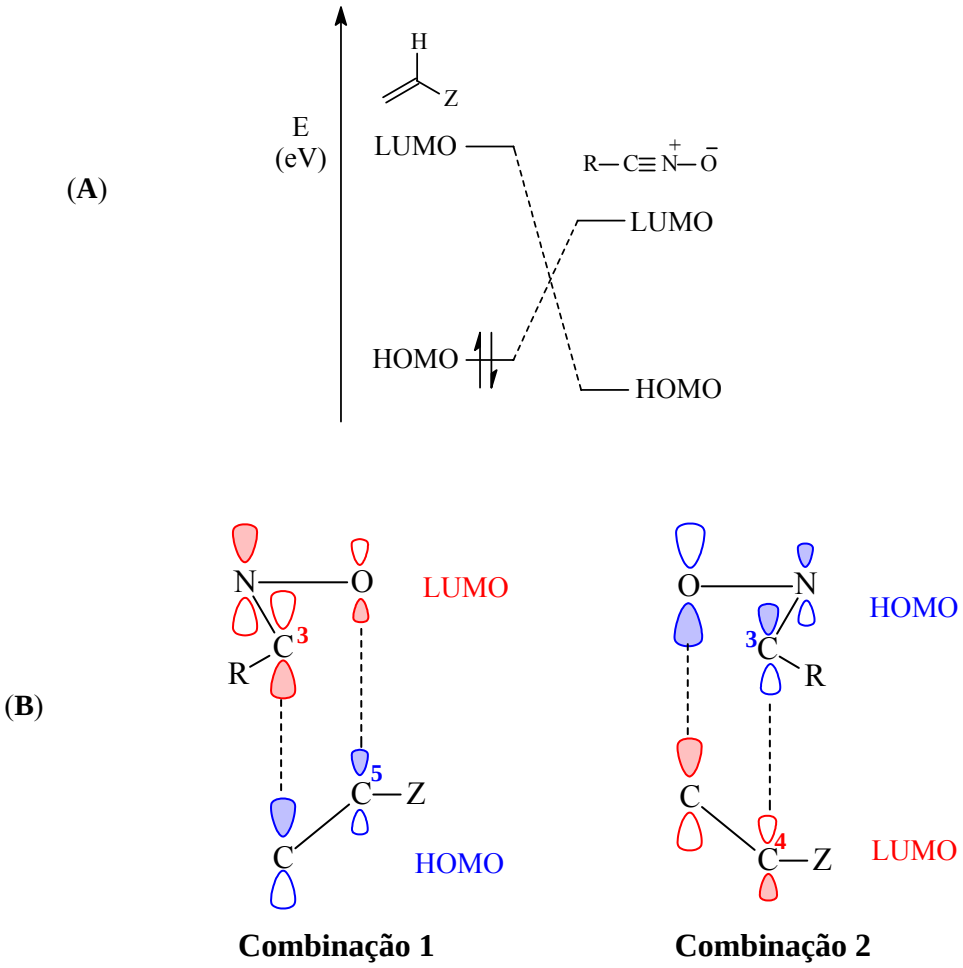

Figura 14. Em (A): cicloadição 1,3-dipolar controlada pelo HOMO do dipolarófilo e LUMO do 1,3-dipolar. Em (B): interação orbitalar levando à formação dos isômeros 3,5 ou 3,4-dissubstituído.

A identificação do anel heterociclo e dos seus isômeros pode ser facilmente detectada por espectroscopia de RMN. Essa identificação é feita pela análise dos deslocamentos químicos, isto é, através da posição relativa dos sinais nos espectros de RMN de ^{1}H e ^{13}C. Freqüentemente, os hidrogênios metilênicos diastereotópicos apresentam um padrão de

[44] Domingo, L. R.; Chamorro, E.; Pérez, P. *Eur. J. Org. Chem.* **2009**, 3036.

multiplicidade na forma de duplo dubleto. Os derivados 3,5-dissubstituídos apresentam dois conjuntos de sinais dos hidrogênios diastereotópicos localizados em aproximadamente 3,3 ppm e 3,8 ppm, enquanto que o isômero-3,4 apresenta os dois sinais em aproximadamente 4,5 ppm e 5,1 ppm[45], como mostrado na Figura 15.

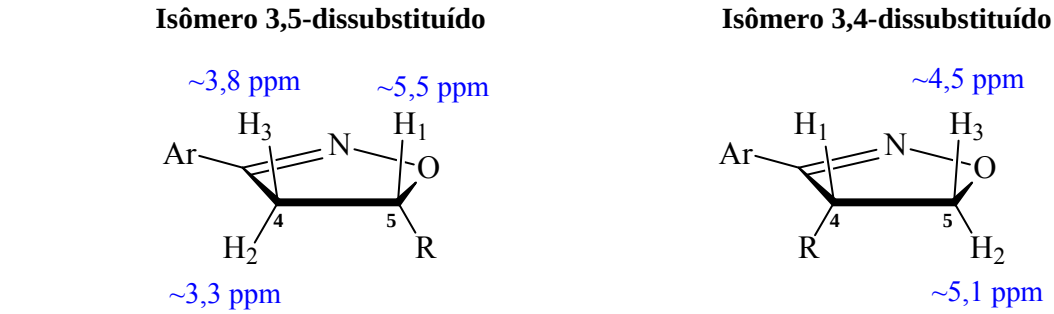

Figura 15. Deslocamentos químicos dos hidrogênios diastereotópicos dos isômeros 3,4 e 3,5 do anel isoxazolínico.

Também, pode-se confirmar a formação do anel a partir da análise das constantes de acoplamento do espectro de RMN de ^{1}H. Em um sistema cíclico de cinco membros observa-se a tendência de acoplamentos: $J_{gem} > J_{cis} > J_{trans}$, como pode ser visto na Figura 16. A diferenciação entre os hidrogênios é conseqüência da interação orbitalar entre os hidrogênios ligados a carbonos vizinhos, que é mínima quando os orbitais estão perpendiculares e máxima quando o ângulo entre os orbitais é 0º ou 180º. Esta interação é descrita pela correlação de Karplus[46]. Como o anel isoxazolina tem configuração de envelope faz com que o H_1 tenha um ângulo diedro de aproximadamente 109º com o H_2 (J_{trans}) e de 0º com o H_3 (J_{cis}), causando a diferença nas constantes de acoplamento.

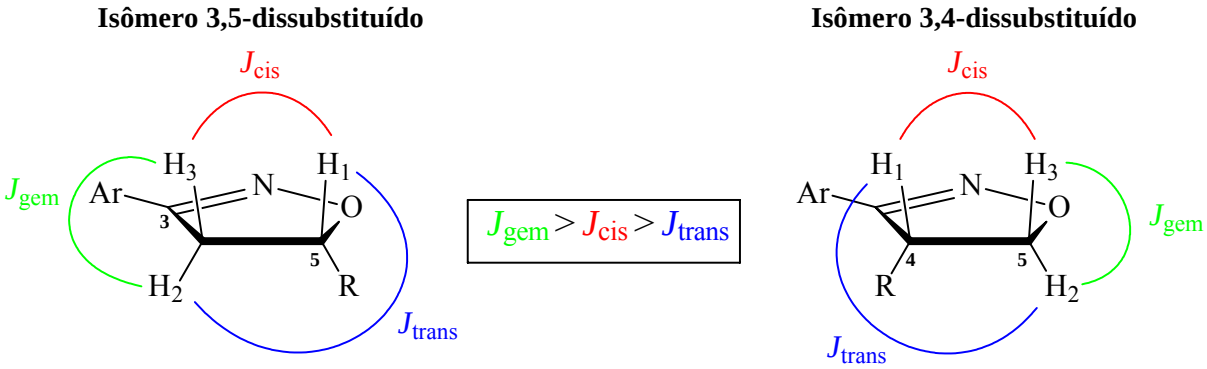

Figura 16. Constantes de acoplamento em um sistema cíclico pentagonal.

[45] Kateley, L. J.; Martin, W. B.; Wiser, D. C.; Brummond, C. A. *J. Chem. Educ.* **2002**, *79*, 225.
[46] Fieser, L. M. and Fieser, M. *Natural Products Related to Phenanthrene,* Reinhold, New York, 1949, p. 184.

2.1.2 Reação de Acoplamento Cruzado de Sonogashira: Ferramenta Importante na Síntese de Cristais Líquidos.

Uma das reações mais utilizada na química orgânica sintética para a formação de ligações C-C é o acoplamento de Sonogashira[47,48]. Este acoplamento consiste na reação entre um grupo R-X (onde R são grupos arila, vinila, benzila ou alila) e um alcino terminal na presença de catalisador de paládio e iodeto de cobre (I) com amina como solvente, como mostra o Esquema 5.

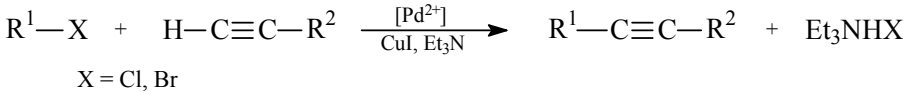

Esquema 5. Acoplamento de Sonogashira catalisado por paládio.

As condições reacionais dependem fortemente da reatividade do haleto, do alcino e da base. Para haletos orgânicos a ordem de reatividade observada é: iodeto de vinila, brometo de vinila > iodeto de arila > cloreto de vinila > brometo de arila. A ordem de reatividade de algumas bases é: *n*-$BuNH_2$ > Et_3N > *i*-Pr_2NH > Et_2NH, piperidina, pirrolidina > *i*-Pr_2NH.

Essa reação tem aplicação comercial na síntese de produtos farmacêuticos como a terbinafina[49]. Também, é amplamente explorada na síntese de intermediários para a síntese de produtos naturais[50], materiais avançados como cristais líquidos[51], para formação de polímeros e oligomeros[52], na área de nanocompostos[53], compostos luminescentes[54], entre outros (Esquema 6).

---

[47] Sonogashira, K.; Tohda, Y.; Hagihara, N. *Tetrahedron Lett.* **1975**, *50*, 4467.
[48] Farias, R. F. *Química de Coordenação,* Editora Átomo, São Paulo, 2009.
[49] Oh, C. H.; Jung, S. H. *Tetrahedron Lett.* **2000**, *41*, 8513.
[50] Balavoine, F.; Madec, D.; Mioskowski, C. *Tetrahedron Lett.* **1999**, *40*, 8351.
[51] (a) Chinchilla, R.; Nájera, C. *Chem. Rev.* **2007**, *107*, 874; (b) An, Z.; Yu, J.; Domercq, B.; Jones, S. C.; Barlow, S.; Kippelen, B.; Marder, S. R. *J. Mater. Chem.* **2009**, *19*, 6688; (c) Vasconcelos, U. B.; Dalmolin, E.; Merlo, A. A. *Org. Lett.* **2005**, *7*, 1027; (d) Bouchta, A.; Nguyen, H. T.; Achard, M. F.; Hardouin, F.; Destrade, C.; Twieg, R. J.; Maaroufi, A.; Isaert, N. *Liq. Cryst.* **1992**, *12*, 575;
[52] (a) Trumbo, D. L.; Marvel, C. S. *J. Pol. Sci. Part A: Pol. Chem.* **1986**, *24*, 2311; (b) Ting, C-H.; Chen, J-T.; Hsu, C-S. *Macromol.* **2002**, *35*, 1180.
[53] (a) Chanteau, S. H.; Tour, J. M. *J. Org. Chem.* **2003**, *68*, 8750; (b) Rapenne, G.; Jimenez-Bueno, G. *Tetrahedron* **2007**, *63*, 7018.
[54] Maeda, H.; Maeda, T.; Mizuno, K.; Fujimoto, K.; Shimizu, H.; Inouye, M. *Chem. Eur. J.* **2006**, *12*, 824.

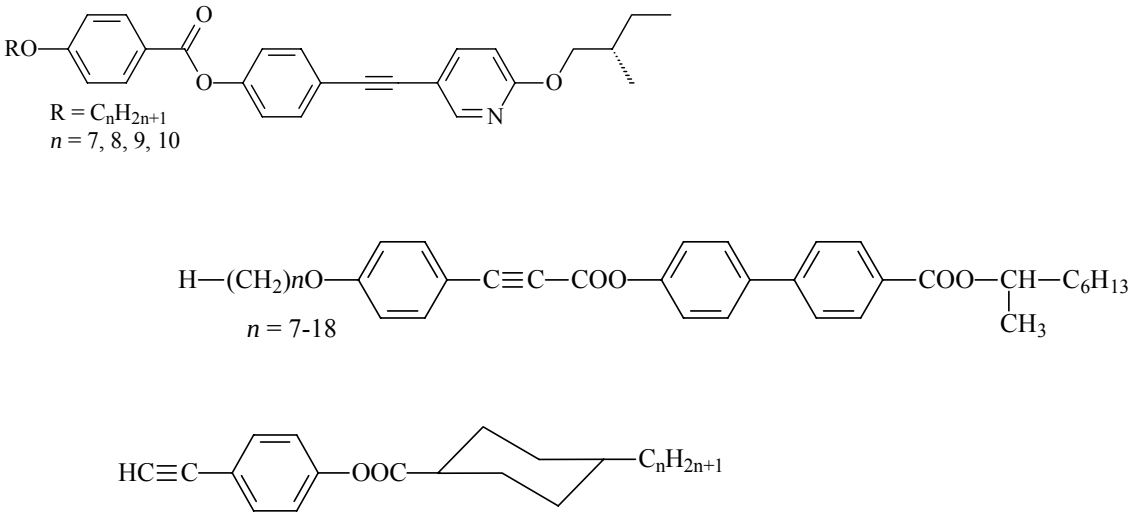

Esquema 6. Moléculas obtidas a partir do acoplamento de Sonogashira em pelo menos uma etapa reacional.

A fim de melhorar os rendimentos da reação e/ou tentar diminuir a produção do diino como subproduto de acoplamento, diversas alterações já foram realizadas no procedimento original do protocolo de Sonogashira. Por exemplo, reações livres de cobre[55] ou de Pd[56], com diferentes complexos de Pd[57], em meio aquoso[58], com líquidos iônicos[59], trocando a amina por outra base[60], entre outras modificações.

Apesar de esta reação ser bastante utilizada, seu mecanismo ainda não é totalmente esclarecido. Na Figura 17 está apresentado um ciclo catalítico com o complexo $[PdL_2Cl_2]$ (onde L é o ligante) aceito para este tipo de acoplamento, proposto por Sonogahira em 2002[61]. O mecanismo é dividido em um sistema com três ciclos, um principal (*Ciclo 1*) e dois adjacentes (*Ciclos 2 e 3*).

No primeiro ciclo o Pd^{2+} converte-se a Pd^0, a qual é a espécie ativa que vai iniciar o ciclo. Neste caso a trietilamina extrai o hidrogênio do alcino terminal, assistida pelo sal de cobre, formando o cuprato de alquinila através da adição de iodeto de cobre. Esse intermediário cuprato é mais reativo que o alcino inicial. Nesta etapa é formado o produto de

[55] (a) Soheili, A.; Albaneze-Walker, J.; Murry, J. A.; Dormer, P. G.; Hughes, D. L. *Org. Lett.* **2003**, *5*, 4191; (b) Gallagher, W. P.; Maleczka, R. E. *J. Org. Chem.* **2003**, *68*, 6775.
[56] Thathagar, M. B.; Beckers, J.; Rothenberg, G. *Green Chem.* **2004**, *6*, 215.
[57] Liao, Y.; Fathi, R.; Reitman, M.; Zhang, Y.; Yang, Z. *Tetrahedron Lett.* **2001**, *42*, 1815.
[58] (a) Liang, B.; Dai, M.; Chen, J.; Yang, Z. *J. Org. Chem.* **2005**, *70*, 391; (b) Chow, H.; Wan, C.; Low, K.; Yeung, Y. *J. Org. Chem.* **2001**, *66*, 1910.
[59] Park, S. B.; Alper, H. *Chem. Commun.* **2004**, 1306.
[60] Chou, M.; Mandal, A. B.; Leung, M. *J. Org. Chem.* **2002**, *67*, 1501.
[61] Sonogashira, K. *J. Organomet. Chem.* **2002**, *653*, 46.

homoacoplamento (diino), como principal produto lateral, a partir de uma eliminação redutiva formando a espécie ativa de Pd^0.

No ciclo principal o Pd^0 sofre adição oxidativa do haleto de arila, voltando ao estado de Pd^{2+}. No ciclo adjacente 3 o intermediário Pd^{2+} sofre uma transmetalação entre o cuprato e o haleto. Por último ocorre uma segunda eliminação redutiva regenerando o catalisador Pd^0 e formando o produto de acoplamento arilacetilênico desejado.

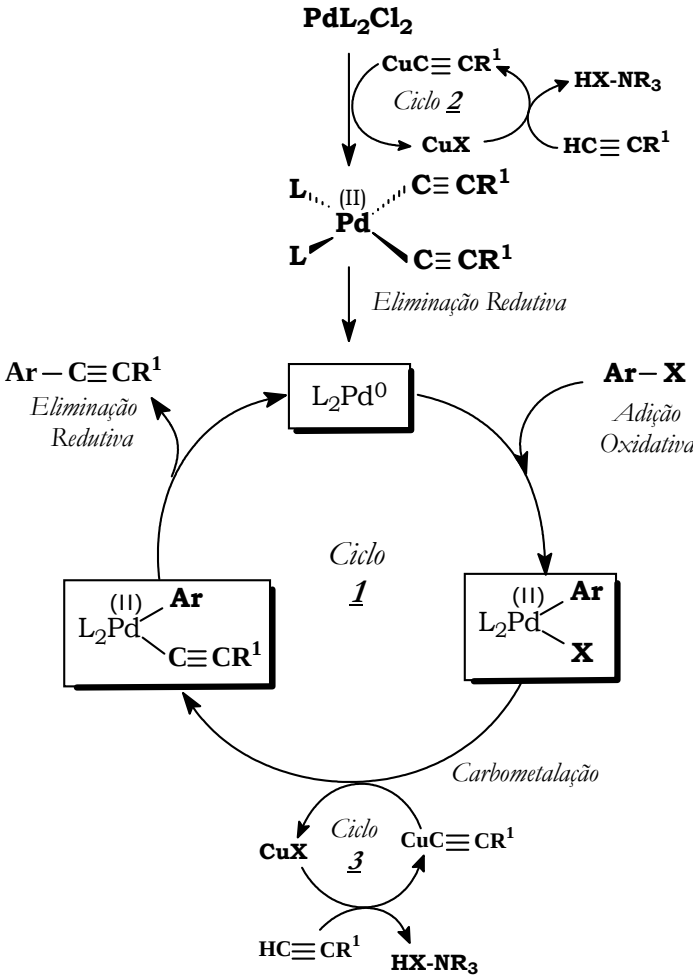

Figura 17. Ciclo catalítico da reação de Sonogashira.

2.2 CRISTAIS LÍQUIDOS. MATERIAIS MOLECULARES INTELIGENTES.

A ciência dos CL iniciou com os trabalhos de Friedrich Richard Kornelius Reinitzer (1858-1927), no ano de 1888. Botânico austríaco, Reinitzer investigava as propriedades físico-químicas de vários derivados do colesterol quando observou que o benzoato de colesterila apresentava dois pontos de fusão[62]. A partir desta observação, em trabalho conjunto com o físico alemão Otto Lehmann[63] (1855-1922), propuseram em 1900 o termo *flüssige kristalle* (cristal líquido) para descrever o novo fenômeno que haviam descoberto.

Assim, o termo cristal líquido é associado a certos materiais orgânicos e à fase termodinâmica de existência do fenômeno. A maioria das substâncias apresenta três estados: sólido, líquido e gasoso, onde a diferença entre estes estados está relacionada aos diferentes graus de ordem das moléculas no material. A fase líquido-cristalina, também chamada de mesofase (mesomorfo, do Grego *mesos morphe*: entre dois estados), é a fase que apresenta um grau de ordem molecular intermediário entre o estado líquido e o sólido (Figura 18).[64]

Em um sólido cristalino as moléculas (ou átomos) estão organizadas espacialmente ocupando posição e orientação definidas, com ordem orientacional e posicional de curto e longo alcance. Neste sentido, os sólidos são sistemas anisotrópicos que apresentam o fenômeno da birrefringência. A birrefringência é um fenômeno que aparece quando um material apresenta dois índices de refração distintos, sendo um paralelo e outro perpendicular ao seu eixo óptico, onde este é o eixo de simetria da organização molecular. No estado líquido as moléculas não possuem ordem posicional e orientacional e podem se mover de forma aleatória (por isso o estado líquido é chamado de isotrópico: suas propriedades são as mesmas em qualquer direção investigada). Assim, um cristal líquido é um fluido anisotrópico que apresenta ordem molecular intermediária entre as ordens posicional e orientacional dos sólidos cristalinos e a desordem dos líquidos isotrópicos[65]. Deste modo, os CLs apresentam birrefringência dos sólidos combinada com a fluidez e mobilidade dos líquidos.

---

[62] Reinitzer, F. *Monatsh. Chem*. **1888**, *9*, 941. Versão em inglês: Reinitzer, F. *Liq. Cryst.* **1989**, *5*, 7.
[63] Lehmann, O. *Z. Phys. Chem.* **1889**, *4*, 462.
[64] (a) Gennes, P. G.; Prost, J. *The Physics of Liquid Crystals,* Clarendon Press, Oxford University Press, 1993; (b) Stevenson, C. L.; Bennett, D. B.; Leghuga-Ballesteros, D. *J. Pharm. Sciences* **2005**, *94*, 1861; (c) Brown, G. H. *J. Chem. Educ.* **1983**, *60*, 900; (d) Bechtold, I. H. *Rev. Bras. Ensino Fis*. **2005**, *27*, 333.
[65] (a) Dunmur, D. A. *Liquid Crystals: Fundamentals.* Word Scientific Publishing, 2002; (b) Chandrasekhar, S. *Liquid Crystals*. 2ª ed., Cambridge University Press, New York, 1994.

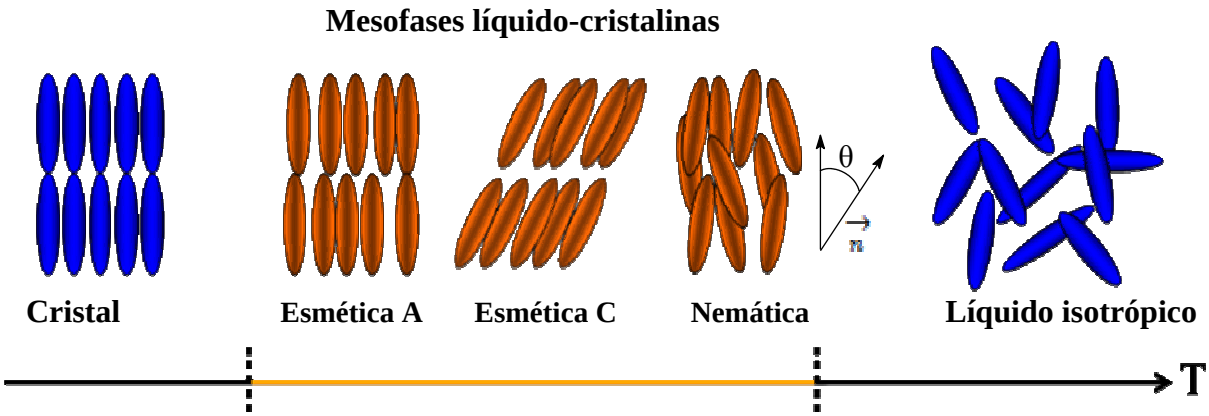

Figura 18. Ilustração esquemática do arranjo molecular no estado cristal, mesofase líquido-cristalina e estado líquido isotrópico em função da temperatura. $\vec{n}$ representa o diretor da fase.

Os requerimentos necessários para um composto calamítico não-linear apresentar propriedades mesomórficas são[66]: as moléculas devem ter uma forma geométrica bastante alongada e linear; devem apresentar grupos retiradores e doadores de elétrons, gerando dipolos permanentes; e apresentar grupos centrais rígidos e altamente polarizáveis, para permitir uma boa compactação das camadas de moléculas. Além disso, um pré-requisito fundamental para a formação de fases líquido-cristalinas é a necessidade de elevada anisotropia (as propriedades variam de acordo com a direção em que são medidas), como na sua forma geométrica. Outras anisotropias observadas nos CLs são a elétrica e magnética. A anisotropia óptica, por exemplo, permite modular a luz para mostrar ou não alguma informação. Esse efeito é a base de todas as aplicações tecnológicas dos CLs.

Também existem CLs com formas estruturais não-convencionais, bem diferentes dos bastões clássicos (calamíticos), como as formas de S, V, Y, *boomerang* e banana[67] (Figura 19).

Quando heterociclos são incorporados na estrutura molecular causam desvios na linearidade destes compostos[68]. Para os anéis isoxazolínicos e isoxazólicos, por exemplo, estudos através de cálculos computacionais mostram que os ângulos das ligações exocíclicas são 156,10º e 156,70º, respectivamente, conforme Figura 20.

---

[66] Collins, P. J.; Hird, M. *Introduction of Liquid Crystals*. Chemistry and Physics. CRC Press, 1997.
[67] (a) Tschierske, C. *Nature* **2002**, *419*, 681; (b) Lee, S. K.; Li, X.; Kang. S.; Tokita, M.; Watanabe, J. *J. Mat. Chem.* **2009**, *19*, 4517; (c) Ros, M. B.; Serrano, J. L.; de la Fuente, M. R.; Folcia, C. L. *J. Mater. Chem.* **2005**, *15*, 5093; (d) Saez, I. M.; Goodby, J. W.; *J. Mater. Chem.* **2005**, *15*, 26; (e) Dunemann, U.; Schroder, M. W.; Pelzl, G.; Diele, S.; Weissflog, W. *Liq. Cryst.* **2005**, *32*, 151; (f) Yoshizawa, A.; Kasai, H.; Ogasawara, F.; Nagashima, Y.; Kawaguchi, T. *Liq. Cryst.* **2007**, *34*, 547; (g) Dingemans, T. J.; Samulski, E. T. *Liq. Cryst.* **2000**, *27*, 131; (h) Vorländer, D.; Apel, A. *Ber.* **1932**, *65*, 1101.
[68] (a) Zafiropoulos, N. A.; Choi, E-J.; Dingemans, T.; Lin, W.; Samulski, E. *Chem. Mater.* **2008**, *20*, 3821; (b) Seed, A. *Chem. Soc. Rev*. **2007**, *36*, 2046.

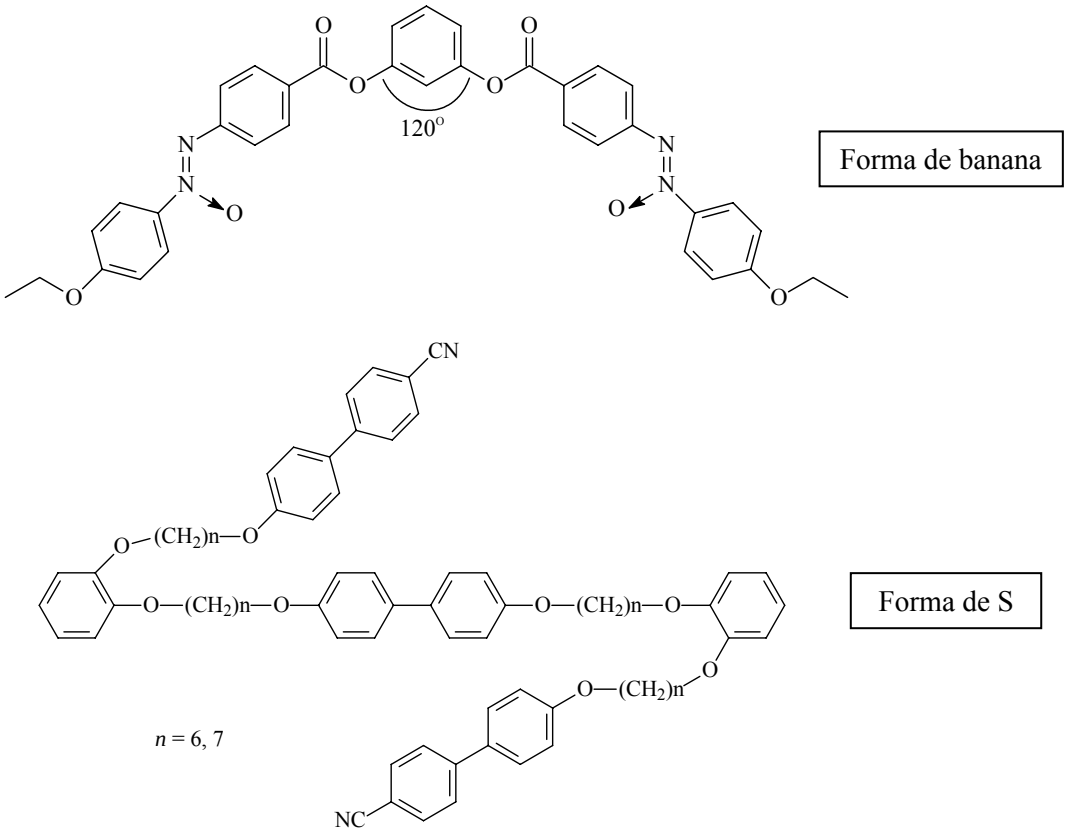

Figura 19. Exemplos de moléculas LC com arquitetura não-convencional.

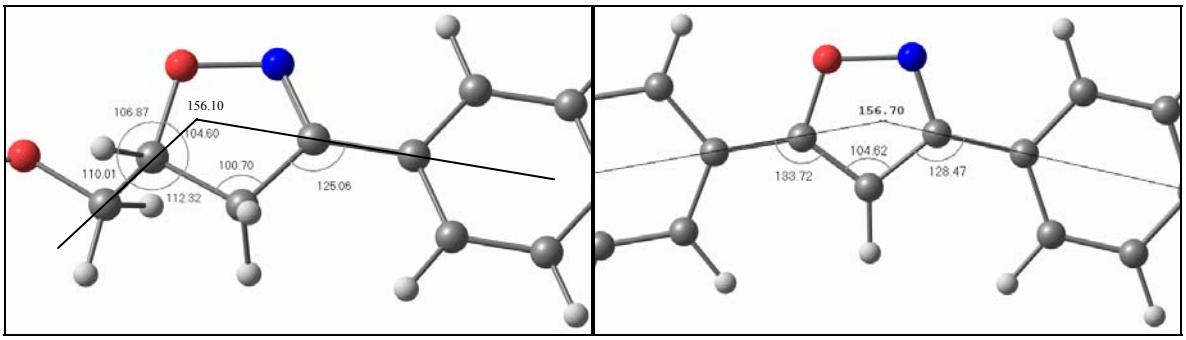

(**A**) (**B**)

Figura 20. Ângulos das ligações exocíclicas dos anéis: (A) isoxazolina e (B) isoxazol, determinados por cálculos computacionais.

Alguns exemplos de materiais líquido-cristalinos com arquitetura não convencional que se ouve falar comumente são a lecitina[69], o DNA[70], a celulose e o grafite[71].

[69] Santos, O. D. H.; Miotto, J. V.; Morais, J. M.; Rocha- Filho, P. A. *J. Disper. Sci. Technol.* **2005**, *26*, 243.
[70] Kassapidou, K.; van der Maarela, J. R. C. *Eur. Phys. J. B* **1998**, *3*, 471.
[71] Konovalova, L. Ya.; Negodyaeva, G. S.; Kalashnik, A. T.; Rudinskaya, G. V.; Mil'kova, L. P.; Pozhalkin, N. S.; Iovleva, M. M. *Fibre Chem.* **1994**, *26*, 170.

2.2.1 Classificação dos Cristais Líquidos

A transição de uma fase cristal para uma fase líquido-cristalina pode ser induzida tanto pelas interações que ocorrem entre as moléculas assim como por processos térmicos e/ou concentração de solventes. Assim, os materiais que apresentam mesofases são classificados como **termotrópicos** ou **liotrópicos**, dependendo do parâmetro indutor da fase, ou seja, o que induz o ordenamento local das moléculas.

- **Cristais líquidos termotrópicos:** como o próprio nome sugere, o parâmetro indutor da fase é a temperatura. São constituídos por substâncias orgânicas onde a unidade responsável pelo mesomorfismo é a própria molécula ou mistura de moléculas, que devem apresentar alta anisotropia de forma (anisometria). Para esse tipo de CL as mesofases podem ser classificadas como *enantiotrópicas* ou *monotrópicas*. Quando o material é submetido a ciclos de aquecimento e resfriamento e a mesofase (ou mesofases) ocorre reversivelmente nos dois sentidos, são chamadas de enantiotrópicas. Isso quer dizer que quando o cristal líquido é aquecido as moléculas mudarão de ordenamento permitindo o aparecimento da mesofase. Quando a temperatura alcançar a temperatura de isotropização (líquido isotrópico) perde-se qualquer tipo de ordem molecular, porém, ao resfriar a amostra, observa-se novamente a mesofase, indicando que o ordenamento molecular foi reconstruído, indicando uma fase termodinamicamente estável. Porém, quando o material é submetido ao mesmo ciclo de temperatura e a mesofase é observada somente no resfriamento, é dita monotrópica e é característica de uma fase termodinamicamente instável.

A importância dos CLs termotrópicos está relacionada às suas aplicações tecnológicas na fabricação de dispositivos eletro-ópticos e sensores de temperatura e pressão.

- **Cristais líquidos liotrópicos:** neste caso a fase líquido-cristalina é dependente da relação soluto-solvente e/ou da temperatura. Nesse caso não se fala em substâncias puras, mas sim em misturas de moléculas anfifílicas e solventes. Moléculas polares anfifílicas são caracterizadas por possuírem, na mesma molécula, dois grupos com propriedades de solubilidade diferentes, ou seja, possuem uma cabeça polar hidrofílica (normalmente iônica, altamente solúvel na água) e uma cauda apolar hidrofóbica (normalmente cadeias alifáticas, altamente solúveis em hidrocarbonetos). Em uma solução aquosa os compostos irão se auto-organizar em superestruturas na forma de micelas (agregados moleculares), apresentando a condição necessária para o aparecimento de mesofase. Por exemplo, obtém-se um CL liotrópico pela mistura de um surfactante (sabão), água e álcool. Em solventes orgânicos, o

mesmo tipo de cristal líquido forma micelas reversas. Assim, as micelas constituem a unidade estrutural responsável pelo aparecimento das mesofases.

Hoje em dia, os CL liotrópicos representam uma importante área de pesquisa na biologia e medicina devido à grande semelhança de seus agregados com a membrana celular e estruturas no interior da célula[72], permitindo o estudo sobre o funcionamento das membranas biológicas. Estudos citados por Stevenson e col. em 2005[73] estimam que cerca de 5% das moléculas orgânicas possuem mesomorfismo termotrópico e incontáveis moléculas apresentam mesomorfimo liotrópico.

2.2.2 Tipos de Cristais Líquidos Termotrópicos.

Tanto os CL termotrópicos quanto os liotrópicos apresentam seus tipos particulares de mesofases. Os cristais líquidos termotrópicos mais conhecidos e difundidos são aqueles formados por moléculas alongadas em forma de bastão (Figura 21), chamados de calamíticos. Quando têm a forma de disco são chamados de discóticos.

No trabalho desta Tese serão estudas as propriedades dos CL termotrópicos calamíticos e, por isso, nas seções seguintes será dada uma abordagem maior para as propriedades destes CLs.

• **Cristais Líquidos Calamíticos.** A principal característica dos CLs calamíticos é que são formados por moléculas de forma linear alongada com formato de bastão (do inglês *rod-like*), onde o comprimento (*l*) é bem maior que o diâmetro (*d*), ou seja, apresenta anisometria geométrica em uma direção, como representado na Figura 21, onde:

A e **B** são núcleos rígidos
Y é um grupo ponte;
R e **R'** são grupos flexíveis e
X e **Z** são grupos laterais.

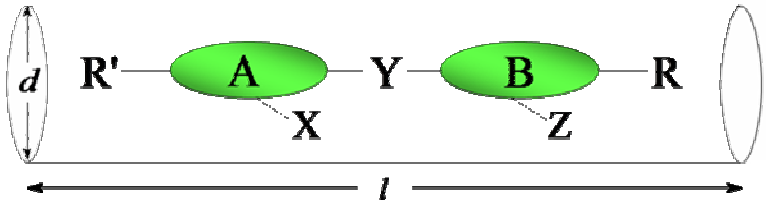

Figura 21. Modelo esquemático da estrutura molecular alongada de um CL calamítico do tipo bastão.

Basicamente, as moléculas são formadas por uma parte central rígida (grupos **A** e **B)**. Isso é importante para manter a anisometria molecular em forma de bastão (alongada) e

[72] (a) Brown, G. H.; Wolken, J. J.; *Liquid Crystals and Biological Structures*. Academic Press, N. York, 1979; (b) Burducea, G. *Rom. Rep. Phys.* **2004**, 66.
[73] Stevenson, C. L.; Bennett, D. B.; Leghuga-Ballesteros, D. *J. Pharm. Sci*. **2005**, *94*, 1861.

permitir interações que favoreçam o alinhamento das moléculas. Porém, também é necessária certa flexibilidade para manter o ponto de fusão baixo. Normalmente são grupos polarizáveis e responsáveis pela anisotropia. Os mais utilizados são anéis aromáticos (piridina, benzeno) e heterociclos, que podem estar condensados ou ligados por um grupo conector **Y**. Em geral, estes são grupos funcionais com ligações múltiplas que restringem rotações livres para manter a rigidez, linearidade e a polarização anisotrópica da molécula. Os grupos funcionais como carbonos *sp* e sp^2, iminas ou ésteres são os mais representativos.

Os grupos **R** e **R'** são unidades terminais longas posicionados no eixo molecular, conferindo flexibilidade e garantindo a anisometria do sistema. Podem ser cadeias alquílicas (lineares, ramificadas, quirais ou aquirais) ligadas diretamente ao núcleo rígido ou através de grupos éter ou éster, carbonos sp^2 ou heteroátomos como enxofre e nitrogênio, que podem aumentar a ressonância do sistema, favorecendo a estabilidade da mesofase. Também, é possível a combinação **R** = cadeia flexível e **R'**= grupo polar como CN e Br, entre outros. Os grupos **X** e **Z** são grupos laterais ligados ao anel aromático, que podem estar presentes ou não na molécula. Normalmente os mais utilizados são os grupos altamente polarizáveis e pequenos, como átomos de flúor ou grupos NO_2, CN, OH e C≡C, desde que não alterem a anisotropia do CL.

- **Cristais Líquidos Discóticos.** Em relação aos CL discóticos, a principal característica é que são formados por moléculas em forma de disco, apresentando anisometria em duas direções (Figura 22). Devido a essa geometria, os CLs discóticos têm a propriedade de se auto-montarem formando mesofases colunares organizadas. Como resultado dessas estruturas organizadas, os CLs discóticos podem transportar cargas e têm sido utilizados como semicondutores[74].

[74] (a) Sergeyev, S.; Pisula, W.; Geerts, Y. H. *Chem. Soc. Rev.* **2007**, *36*, 1902; (b) Pisula, W.; Tomovic, Z.; Wegner, M.; Graf, R.; Pouderoijen, M. J.; Meijer, E. W.; Schenning, A. P. H. J. *J. Mat. Chem.* **2008**, *18*, 2968; (c) An, Z.; Yu, J.; Domercq, B.; Jones, S. C.; Barlow, S.; Kippelen, B.; Marder, S. R. *J. Mat. Chem.* **2009**, 19, 6688; (d) Adam, D.; Schuhmacher, P.; Simmerer, J.; Haussling, L.; Siemensmeyer, K.; Etzbach, K. H.; Ringsdorf, H.; Haarer, D. *Nature* **1994**, *371*, 141; (e) Gupta, S. K.; Raghunathan, V. A.; Kumar, S. *New J. Chem.* **2009**, *33*, 112.

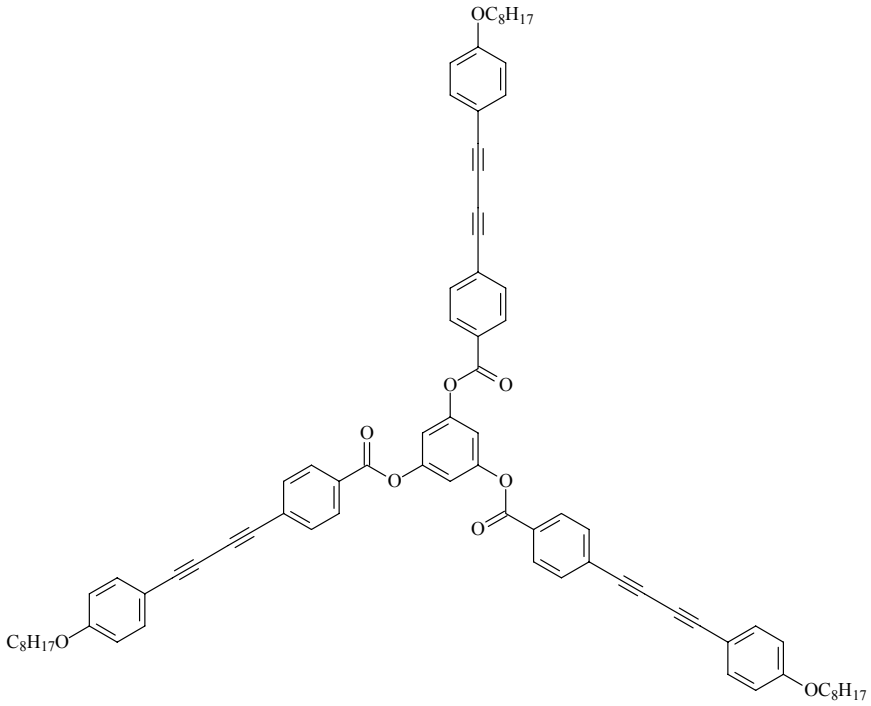

Figura 22. Estrutura de um CL discótico[75].

2.3 TIPOS DE MESOFASES TERMOTRÓPICAS CALAMÍTICAS

Nos CLs pode haver diferentes graus de ordem, variando desde valores próximos ao líquido (desordem) até a ordem em uma dimensão dos sólidos, dando origem a diferentes mesofases. Cada mesofase pode apresentar uma ou mais texturas diferentes, que vai depender do arranjo das suas moléculas. Assim, dentro do grupo dos CLs termotrópicos calamíticos, as mesofases líquido-cristalinas foram classificadas por Friedel, em 1922, em três grandes grupos de acordo com as propriedades ópticas e grau de ordenamento molecular: fase nemática, fase esmética e fase colestérica[76].

Dessa forma, as mesofases são caracterizadas pelos graus de liberdade que as moléculas de CL apresentam, através das simetrias de translação e rotação. Nesse sentido, as transições de fase ocorrem pela quebra na ordem posicional e/ou orientacional das moléculas, aumentando ou diminuindo seus graus de liberdade. Cabe ressaltar que as mesofases aparecem apenas em materiais cujas moléculas apresentam anisotropia de forma (alongadas ou achatadas, por exemplo).

[75] Chang, J. Y.; Yeon, J. R.; Shin, Y. S.; Han, M. J.; Hong, S-K. *Chem. Mater.* **2000**, *12*, 1076.
[76] Friedel, G. *Ann. de Physique* **1922**, *18*, 273.

Apesar das diferenças quanto à natureza e ao processo de obtenção, a mesma classificação pode ser aplicada para os CLs liotrópicos, os quais foram descobertos após essa classificação (1950), considerando as propriedades de simetria que caracterizam as mesofases.

2.3.1 A mesofase nemática e suas texturas.

A fase nemática (N) é a mesofase com menor nível de ordem molecular (Figura 23), e é a mais encontrada dentre as mesofases. É a fase que mais se aproxima do estado líquido isotrópico em relação ao ordenamento molecular (possui ordem orientacional de longo alcance) e às temperaturas de transição mesofase-isotrópico, exibindo a fluidez típica de líquidos. A ordem orientacional apenas é possível se as moléculas forem alongadas e anisométricas (sem simetria esférica), com fracas interações laterais. Devido à ausência de ordem posicional de curto alcance das moléculas nessa fase, estas podem mover-se livremente ao redor do seu eixo molecular maior tendendo a ficar paralelas entre si e a uma determinada direção preferencial no espaço, definida por um vetor chamado diretor da fase $\vec{n}$. Devido à alta fluidez das moléculas nessa fase, os cristais líquidos N que apresentam transições líquido-cristalinas à temperatura ambiente são os mais utilizados na fabricação de *LCDs* desde o final da década de 60.

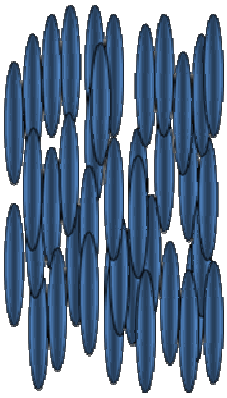

Figura 23. Representação esquemática das moléculas na mesofase nemática.

A caracterização da mesofase é feita visualmente através de um microscópio óptico de luz polarizada. Observando uma amostra entre polarizadores cruzados, texturas com cores de intensidades diferentes serão observadas como resultado da interação da luz polarizada com a amostra de CL em função da propriedade de birrefringência.

Cada mesofase pode apresentar diversas texturas e a observação microscópica destas texturas pode revelar informações importantes a respeito da ordem das mesofases. Isto é

possível porque é o alinhamento das moléculas que determina o tipo de textura que será observada.

Os defeitos ou descontinuidades (descritos por avançada teoria matemática)[77], identificam os diferentes tipos de mesofases e aparecem na textura na forma de pontos de imperfeição, como as texturas *Schlieren*. Na Figura 24 podem-se observar pontos semelhantes a cruzes (defeitos), onde regiões claras e escuras se encontram. Normalmente essas cruzes têm duas, quatro ou até seis regiões claras.

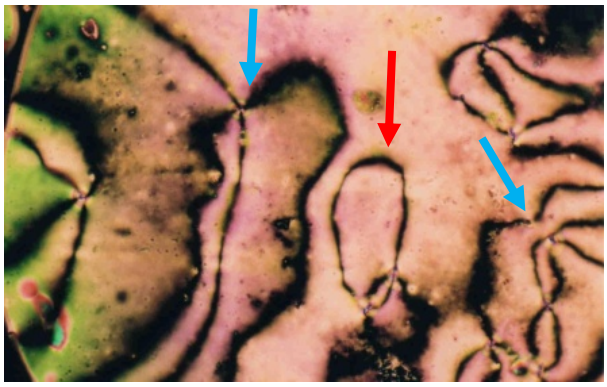

Figura 24. Textura *Schlieren* de um CL nemático. Os defeitos (descontinuidades) estão indicados pelas setas azuis. Quando os ramos se encontram formam um laço (*loop*), indicado pela seta vermelha.

Existem três tipos principais de texturas[78]: **planar degenerada** e **planar homogênea**, nas quais as moléculas estão orientadas paralelas ao plano dos vidros (Figura 25A); e **homeotrópica**, onde as moléculas estão perpendiculares ao plano dos vidros (Figura 25B). Como as observações são realizadas com a amostra confinada entre duas lâminas de vidro, o alinhamento é quase sempre perturbado devido a essas superfícies. Os maiores fatores que podem causar distúrbio nas orientações são: a estrutura da própria molécula, impurezas e imperfeições no vidro. A espessura da amostra também pode causar alguma influência. Por exemplo, uma textura homeotrópica perfeita deve aparecer totalmente escura quando observada no microscópio óptico de luz polarizada.

[77] Kelly, G.; Mottram, N.; Ramage, A. *The effect of elastic anisotropy on nematic disclination lines*, British Liquid Crystal Society, 2002.
[78] Dierking, I. *Textures of Liquid Crystals.* Weinheim: Wiley-VCH, 2003.

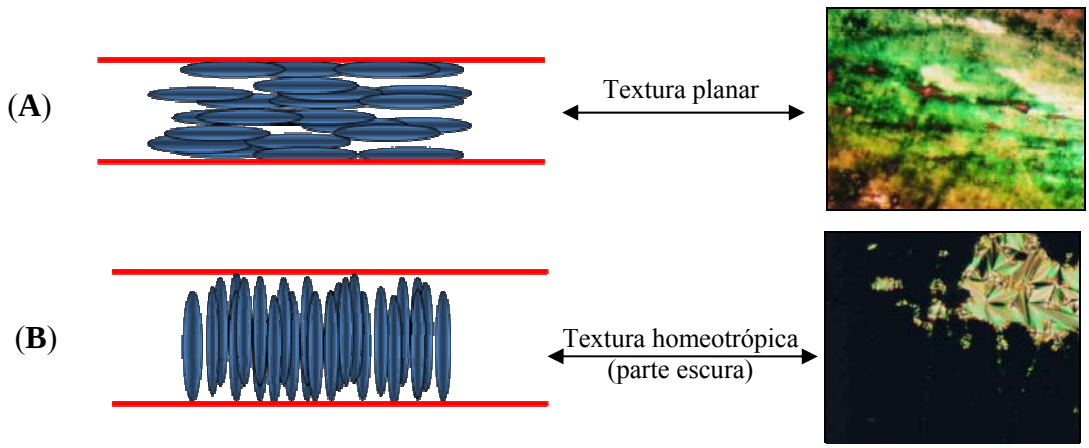

Figura 25. Representação das moléculas (bastões azuis) orientadas: (A) paralelamente ao vidro e a textura planar observada na fotomicrografia obtida por MOLP; (B) perpendicularmente ao vidro e a textura homeotrópica (parte escura) observada na fotomicrografia obtida por MOLP.

A mesma textura pode acontecer em diferentes mesofases, porém, algumas são exclusivas de uma determinada fase, o que contribui para a sua classificação. Por exemplo, a textura *marble* ocorre somente na mesofase N.

As moléculas LC calamíticas que mostram fase nemática com transições em temperatura ambiente são utilizadas para *displays* de televisão e computadores.

2.3.2 A mesofase esmética e suas texturas.

As mesofases esméticas (Sm), além da ordem orientacional de longo alcance bem definida, também possuem ordem posicional de curto alcance ao longo de uma dimensão, o que dá origem à formação de camadas periódicas de moléculas, as quais podem deslizar livremente umas sobre as outras. Essa fase é mais viscosa que a mesofase N porque tem ordem em uma dimensão (posicional) e assim se aproxima mais do estado sólido (em relação ao ordenamento molecular).

As fases mais observadas são a esmética A (SmA) e a esmética C (SmC). Na SmA as moléculas estão orientadas com seu eixo de simetria perpendicular ao plano das camadas e com uma ordem posicional entre as moléculas dentro da mesma camada (Figura 26A). A mesofase SmB é mais ordenada que a SmA. As moléculas estão arranjadas em camadas com seus eixos perpendiculares ao plano da camada e, também, apresentam alguma ordem posicional dentro da camada, formando estruturas hexagonais (Figura 26B). Na SmC a diferença é que o eixo molecular maior está organizado, em média, paralelo à direção definida pelo vetor $\vec{n}$, ou seja, está inclinado de um ângulo θ em relação à normal às camadas (Figura 26C).

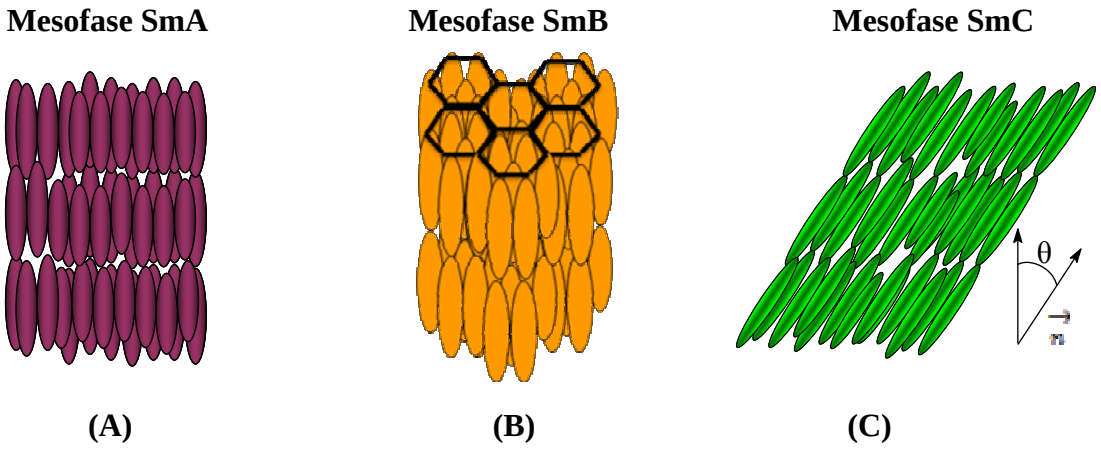

Figura 26. Representação esquemática das moléculas nas mesofases: (A) SmA, (B) SmB e (C) SmC.

Hoje em dia são conhecidos muitos tipos diferentes de estruturas esméticas (SmA, SmB, SmC... SmK, de acordo com a ordem cronológica da sua descoberta), as quais são diferenciadas pelo grau de ordem orientacional e posicional molecular dentro da estratificação e pelo ângulo de inclinação θ[79].

Algumas texturas podem ajudar na classificação das diversas mesofases esméticas. Por exemplo, a textura focal cônica em forma de leque (*fan*) ocorre principalmente nas SmA e SmB. Na SmC, esta textura aparece sempre na forma de leque quebrado (*broken fan*).

Nos CLs termotrópicos as transições de fases são dependentes da temperatura. Assim, várias mesofases podem ocorrer em um mesmo composto. Por exemplo, uma molécula pode apresentar transição do estado cristalino para fase N e após para líquido isotrópico, diretamente. Outro pode apresentar uma transição do estado cristalino para SmC, depois para SmA, seguida de N para finalmente alcançar o líquido isotrópico. Quando várias mesofases podem ser distinguidas, diz-se que o composto apresenta o fenômeno do polimorfismo.

2.3.3 Mesofase colestérica

A mesofase colestérica (Ch) é muito parecida com a fase N, exceto por suas moléculas apresentarem atividade óptica, ou seja, é uma mesofase nemática quiral, sendo comumente encontrada em compostos que contêm pelo menos um centro estereogênico[79]. Neste caso, além das moléculas tenderem a ficar arranjadas paralelamente (mesma ordem orientacional da fase N), elas se torcem ligeiramente a partir de uma camada até a próxima, resultando numa

[79] Singh, S. *Liquid Crystals. Fundamentals.* Word Scientific Publishing, 2002.

periodicidade espacial na forma de hélice (Figura 27). Essa propriedade dá origem a propriedades ópticas bastante peculiares a esta fase.

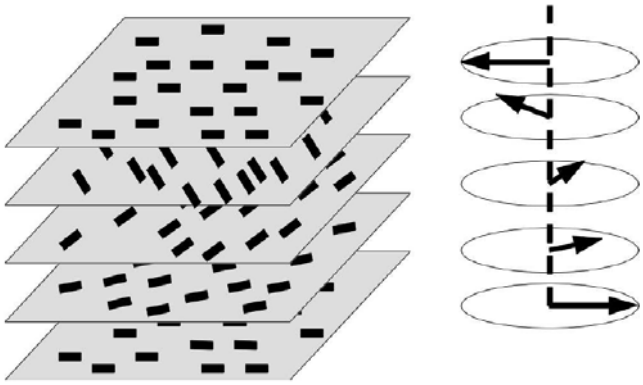

Figura 27. Representação esquemática das moléculas na mesofase colestérica. (Figura retirada da referência 64d).

2.3.4 Caracterização das mesofases

A caracterização das diversas mesofases é feita visualmente e comparada com bancos de dados de texturas já existentes na literatura[78-80]. A técnica mais utilizada no estudo das texturas de mesofases é a microscopia óptica de luz polarizada (MOLP). Quando os polarizadores estão em posição cruzada os planos da luz estão perpendiculares entre si e nenhuma luz é transmitida, ou seja, se não há um material que desvie o plano dessa luz polarizada, como um líquido isotrópico, a luz passa pelo primeiro polarizador mas não pode atravessar o segundo, gerando uma textura escura. Porém, quando um material birrefringente é colocado entre os polarizadores, a luz sofrerá uma defasagem óptica de modo que haverá transmitância da luz pelo segundo polarizador, levando à formação das mais diversas texturas e cores dos CLs.

O microscópio óptico de luz polarizada (Figura 28) é acoplado a um controlador de temperatura (*hotstage*). Quando o material no estado cristalino é sujeito a aquecimento, a energia fornecida quebra a rede cristalina levando à fase líquido-cristalina (mesofase). Assim, é possível observar, através de vários ciclos de aquecimento e resfriamento, o comportamento mesomórfico e as temperaturas de transição de fases. Para essa análise a amostra é solubilizada em um solvente volátil e filtrada sob papel Millipore® para a retirada de impurezas sólidas (vindas da própria síntese e manipulação do material) e confinada entre duas lâminas de vidro.

[80] Demus, D.; Richter, L. *Textures of Liquid Crystals.* Weinheim: VCH, 1978.

Figura 28. Foto do microscópio óptico, sistema de aquecimento e câmera fotográfica acoplada utilizados na caracterização das texturas deste trabalho.

Outra análise térmica, utilizada para complementar a MOLP, é a calorimetria exploratória diferencial (DSC), que fornece informações sobre a estabilidade térmica da molécula, temperaturas de transição de fases e valores de entalpia e entropia para cada transição envolvida. A medida da variação de entalpia (ΔH) é importante porque pode fornecer informações a respeito da estrutura organizacional da molécula na mesofase. Para uma correta atribuição dos picos, essa análise deve ser associada a outras técnicas, como a microscopia óptica. Para essa análise a amostra também é filtrada sob papel Millipore®.

A técnica de difração de Raios-X da fase LC é uma técnica bastante apropriada para obter informações sobre a estrutura da mesofase do material. Quando os raios incidem sobre um cristal, ocorre a penetração do raio na rede cristalina, os raios-X interagirão com os elétrons do material e serão difratados. Para se analisar a difração, basta colocar um dispositivo capaz de captar os raios difratados e traçar o espalhamento, ou seja, o desenho da forma da rede cristalina ou estrutura que refletiu e difratou os raios-X.

Outras técnicas podem ser utilizadas como microscopia de transmissão eletrônica (TEM), teste da miscibilidade e TGA.

3. OBJETIVOS

Este trabalho tem como objetivos gerais o desenho, síntese e caracterização de uma coleção de moléculas isoxazolínicas assim como a sua derivatização para a preparação de novos materiais orgânicos.

3.1 OBJETIVOS ESPECÍFICOS

> Estudo da reação de cicloadição 1,3-dipolar e síntese regiosseletiva de precursores isoxazolínicos como potenciais candidatos para gerar mesomorfismo;

> Síntese, caracterização e análise do comportamento mesomórfico de novas séries homólogas de cristais líquidos derivados dos precursores que contêm o heterociclo isoxazolina 3,5-dissubstituído;

> Síntese, caracterização e análise do comportamento mesomórfico e óptico de cristais líquidos derivados de *O*-benzoiloximas.

CAPÍTULO 4

4.1 MÉTODOS DE ANÁLISE

As análises espectroscópicas de ressonância magnética nuclear de hidrogênio e carbono foram obtidas em um espectrômetro Varian 300MHz. As amostras foram dissolvidas nos solventes DMSO ou clorofórmio deuterados. Os deslocamentos químicos são dados em ppm e foram referenciados ao TMS.

As análises de espectrometria de massas foram realizadas em um cromatógrafo gasoso Varian Saturn 2100T equipado com coluna Sil Pona CB (100,0 m x 0,25 mm) e He como gás de arraste ou no equipamento Shimadzu QP5050 acoplado ao cromatógrafo gasoso Shimadzu GC-17A com coluna DB-17. As condições operacionais foram ajustadas conforme a necessidade da análise. As análises de espectrometria de massas de alta resolução foram realizadas em um equipamento Micromass Q-Tof Micro. Trabalhou-se em condições de *tunning* otimizadas para ionização por *eletrospray* íon positivo.

Os espectros no IV foram realizados com 16 varreduras em equipamento Perkin-Elmer Spectrum One FTIR utilizando cristais de NaCl. Os espectros de ATR foram obtidos no equipamento Varian 640. Os espectros são dados em número de onda (cm^{-1}).

As microanálises (C, H, N) foram determinadas no equipamento Perkin-Elmer 2400.

Os espectros no UV-vis foram realizados em um espectrofotômetro Perkin-Elmer modelo Lambda-16. As medidas de fluorescência foram feitas em um espectrofluorímetro Hitachi modelo F-4500.

Os pontos de fusão e as fotos das texturas foram obtidos em um microscópio óptico de luz polarizada da marca Mettler Toledo equipado com um *hotstage* FP82. Uma câmera fotográfica Olympus BX43 acoplada ao microscópio registrou as fotomicrografias das texturas das mesofases. As velocidades de aquecimento e resfriamento foram de 10 ºC.min^{-1}.

As análises de DSC foram medidas em um calorímetro DSC-2910 da TA Instruments, utilizando como referência interna o índio.

Os cálculos computacionais foram realizados nos grupos de pesquisa de Química Teórica da UFRGS e Centro Universitário La Salle - Canoas.

Os experimentos de difração de Raios-X foram realizados no Instituto de Física da Universidade Federal de Santa Catarina. Foi utilizado um difratômetro modelo X`Pert-PRO com radiação Cu Kα1 (λ = 1,5405 Å). Os *scans* foram realizados em modo contínuo de 2^o a 30^o (2θ) e a radiação difratada foi coletada com o detector X'Celerator.

4.2 SINOPSE DOS ARTIGOS PUBLICADOS.

Neste capítulo serão apresentados os principais pontos dos artigos publicados, bem como dos artigos que estão em fase final de redação e o trabalho submetido. Para uma melhor compreensão desta sinopse e dos artigos, a numeração das Figuras e Tabelas seguiram a ordem da Tese, no entanto, a numeração dos compostos aqui apresentados seguirá a numeração do artigo correspondente.

4.2.1 Primeiro artigo: **"3,5-Disubstituted Isoxazolines as Potential Molecular Kits for Liquid-Crystalline Materials".** *Eur. J. Org. Chem.* **2009**, 889-897.

O primeiro trabalho realizado consistiu na síntese do anel isoxazolina e posteriores substituições nas posições 3 e 5 desse anel com diferentes grupos polares (Figura 29). Também, pretendeu-se mostrar a versatilidade do anel isoxazolínico como uma metodologia rápida e versátil para a preparação do anel isoxazol a partir de uma única etapa reacional.

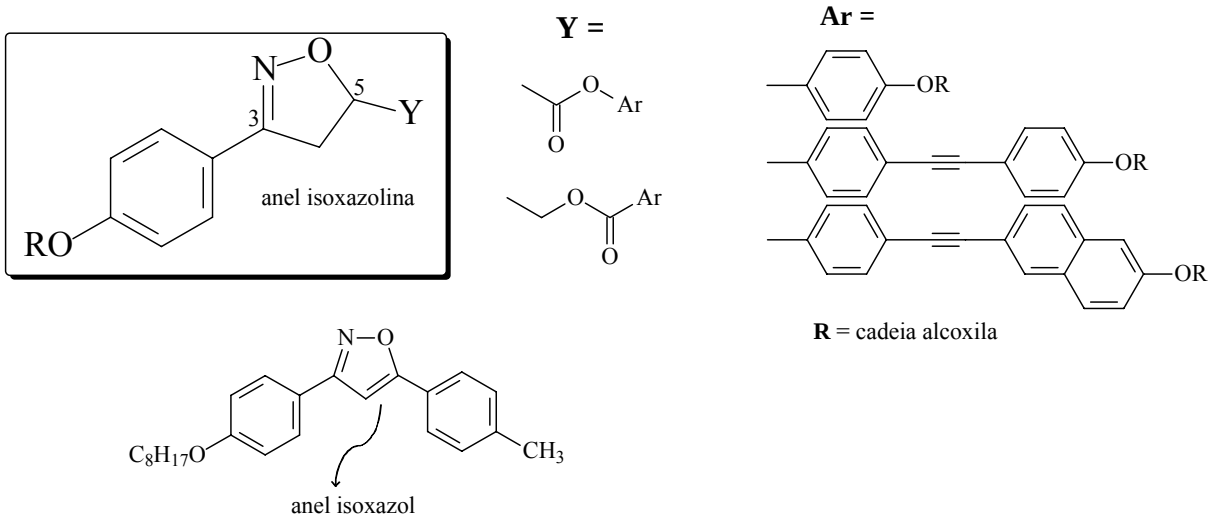

Figura 29. Estruturas representativas dos compostos isoxazolínicos sintetizados.

A preparação do anel isoxazolínico é realizada através da reação de cicloadição entre um óxido de nitrila e um alceno. Os óxidos de nitrila, por sua vez, são obtidos a partir de oximas. Assim, preparou-se a série de oximas **3a-d** através da reação entre o 4-hidroxibenzaldeído e cloridrato de hidroxilamina e também oximas substituídas com os grupos polares Br (**4e**), CN (**4f**) e NO_2 (**4g**). Todas as sínteses apresentaram rendimentos de bons a excelentes.

A série **3a-d** formou uma mistura de isômeros *E* e *Z*, com predominância do isômero *E*. Já as outras oximas geraram somente o isômero *E*. A determinação estrutural dos isômeros foi obtida a partir da análise dos deslocamentos químicos de RMN de ^{1}H e ^{13}C.

Preparadas e caracterizadas as oximas, pode-se sintetizar as isoxazolinas. Isto ocorreu através da reação de cicloadição 1,3-dipolar entre óxidos de nitrila, que é gerado *in situ* no meio reacional, e um dipolarófilo. Essa reação acontece através da adição gota-a-gota de uma solução de oxima em clorofórmio à uma solução contendo o NCS, piridina e o dipolarófilo, a zero grau.

Assim, foi obtida uma coleção de isoxazolinas (**6-12**, Tabela 3) a partir de diferentes oximas e dipolarófilos com rendimentos entre 25 e 89%, com exceção das reações entre a oxima ciano com ácido acrílico (Entrada 6) e acrilamida (Entrada 18), onde não houve formação de produto e a reação entre a oxima **3a** e o ácido vinilacético, onde se obteve somente o cicloaduto 2:1 e não o esperado 1:1 (Entrada 21). Esta reação será discutida posteriormente.

Tabela 3. Cicloadição 1,3-dipolar entre as oximas **3a-d** e **4e-g** e os dipolarófilos **5a-g**.[a]

Experimento	Oxima	Dipolarófilo (Y)	Produto	R. (%)[b]
1	**3a**	CO_2H (**5a**)	**6a**	80
2	**3b**		**6b**	66
3	**3c**		**6c**	83
4	**3d**		**6d**	89
5	**4e**		**6e**	47
6	**4f**		**6f**[c]	-
7	**4g**		**6g**	25
8	**3a**	CH_2OH (**5b**)	**7a**	36
9	**3b**		**7b**	36
10	**3c**		**7c**	38
11	**3d**		**7d**	41
12	**3a**	$CO_2{}^{n}Bu$ (**5c**)	**8a**	31
13	**3b**		**8b**	65
14	**3c**		**8c**	38
15	**3d**		**8d**	62
16	**3a**	$CONH_2$ (**5d**)	**9a**	50
17	**3b**		**9b**	78
18	**4f**		**9c**[c]	-
19	**4g**		**9d**	45
20	**3c**	CN (**5e**)	**10**	43
21	**3a**	CH_2CO_2H (**5f**)	**11a**[d]	-
22	**3b**	*p*-MeC_6H_4 (**5g**)	**12**	60

[a]Condições reacionais: dipolarófilo (2,3 mmol), NCS (2,3 mmol), oxima (2,0 mmol), piridina (3,0 mmol), solvente (8 mL); [b]Rendimento isolado; [c]Não houve reação; [d]Formação do cicloaduto 2:1.

A caracterização do anel isoxazolínico foi realizada por espectroscopia de RMN de ^{1}H e ^{13}C. A identificação é feita pela análise dos deslocamentos químicos e das constantes de acoplamento.

Da coleção de isoxazolinas produzidas foram selecionados os intermediários 3-[4-(alquiloxi)fenil]-4,5-dihidroisoxazoil-5-metanol (**7a-d**) e os ácidos 3-[4-(alquiloxi)fenil]-4,5-dihidroisoxazoil-5-carboxílicos (**6a-d**) para a transformação nos respectivos cristais líquidos.

O desenho dos compostos-alvo será baseado na estrutura não simétrica contendo o anel isoxazolina. Assim, diferentes unidades aromáticas (ver Figura 29) foram utilizadas para redimensionar a anisotropia molecular (tornar a molécula mais parecida com a forma de um bastão) e aumentar a conjugação e planaridade.

Para isso, diversos intermediários foram preparados para atingir-se o objetivo final. O primeiro composto líquido-cristalino (**19**) foi obtido via reação de esterificação entre a isoxazolina **6a** (Tabela 3) e um fenol intermediário usando-se DCC e DMAP em THF com 70% de rendimento.

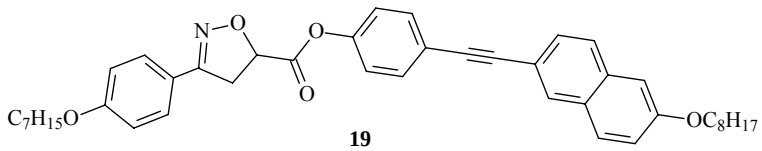

19

Para a síntese dos segundo e terceiro compostos líquido-cristalinos **21** e **23** foram realizadas reações de esterificação entre a isoxazolina **7a** (Tabela 3) e derivados do ácido benzóico.

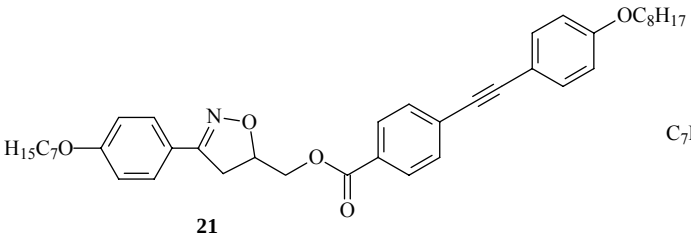

21

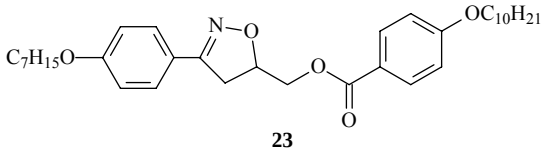

23

Todos os compostos finais apresentaram comportamento líquido-cristalino. Os composto **19** exibiu mesofase N enantiotrópica e o **21** exibiu mesofase N monotrópica. Já o composto **23** mostrou mesofase SmC monotrópica.

Ainda para mostrar a capacidade do anel isoxazolina em gerar materiais líquido-cristalinos, foi realizada uma reação de oxidação da isoxazolina **12b** com MnO_2 com ótimo rendimento.

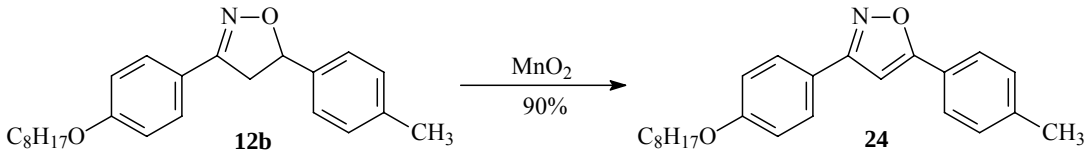

O isoxazol **24** mostrou comportamento líquido-cristalino com mesofase nemática numa ampla faixa de temperatura.

Deste modo, pode-se mostrar que compostos que contêm o anel isoxazolina são intermediários interessantes na síntese de materiais com propriedades líquido-cristalinas.

4.2.2 Segundo artigo: **"3-Arylisoxazolyl-5-Carboxylic Acid and 5-(Hydroxymethyl)-3-Aryl-2-Isoxazoline as Molecular Platforms for Liquid-Crystalline Materials".** *J. Braz. Chem. Soc.* **2009**, *20*, 1742-1752.

Neste trabalho foi realizado um estudo sistemático da relação *estrutura x propriedade* dos compostos finais obtidos de dois precursores isoxazolínicos da Tabela 3. A relação foi avaliada através da variação do número de átomos de carbonos metilênicos do grupo Y e da inversão do grupo polar carbonílico como grupo conector dos anéis, como destacado na Figura 29.

Após a preparação de todos os compostos intermediários necessários, foram obtidas três novas séries homólogas inéditas e mais um composto, em um total de 15 compostos (Figura 30), contendo o heterociclo isoxazolina através de uma síntese envolvendo as reações de esterificação, proteção de grupos funcionais e acoplamento de Sonogashira.

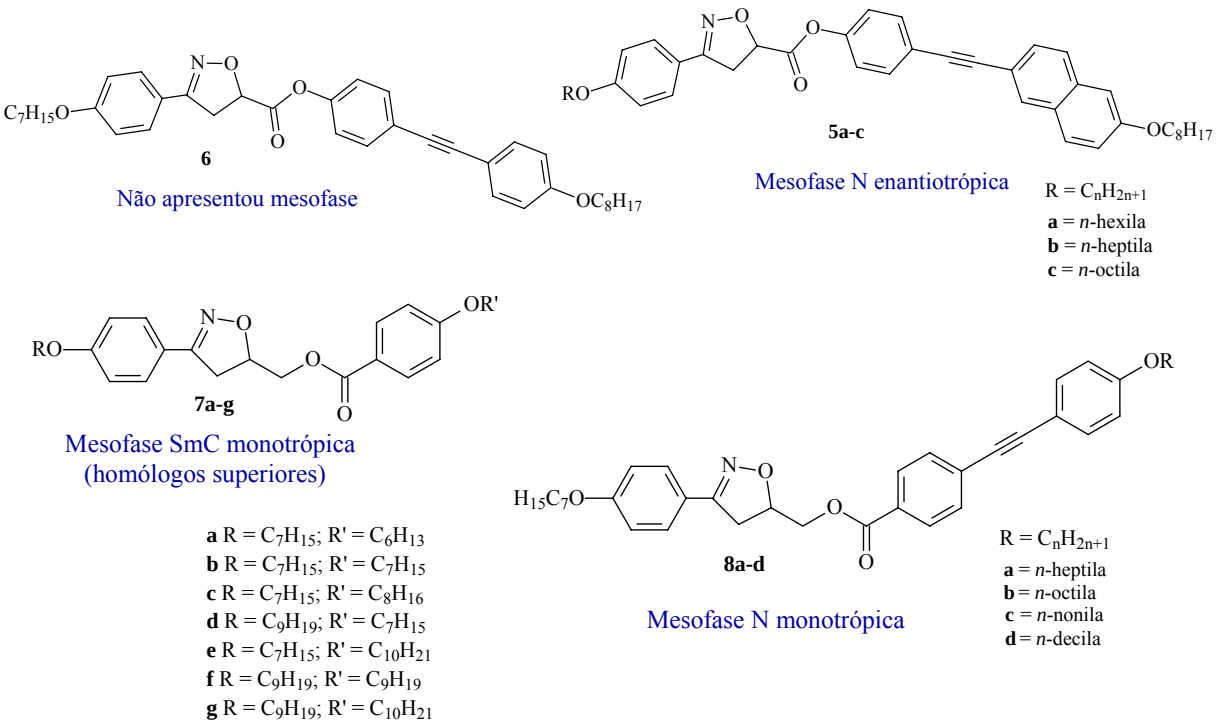

Figura 30. Estruturas dos compostos isoxazolínicos sintetizados.

Com exceção do composto **6**, todos os outros materiais exibiram comportamento líquido-cristalino. O aparecimento de mesofase N na série **5a-c** e o não aparecimento de mesofase no composto **6** pode estar relacionado ao maior alongamento molecular alcançado com a presença do grupo naftila na série **5a-c**, o que leva à maior rigidez e planaridade molecular.

Comparando as séries **5** e **8** observa-se a mesma mesofase nemática, porém ela é observada somente no resfriamento para a série **8**. Isto pode estar relacionado à presença do grupo fenila na série **8** e naftila na série **5**, onde este estabiliza melhor a mesofase. Também pode estar havendo influência do carbono metilênico inserido na série **8**.

Comparando as séries **7** e **8**, ambas têm o carbono metilênico inserido na sua estrutura, porém a série **7** apresentou mesofase SmC monotrópica, e somente nos compostos homólogos com as maiores cadeias alquílicas laterais. A série **8**, por apresentar maior anisotropia de forma, exibiu uma mesofase mais estável.

Um estudo teórico mostrou que a inserção do carbono metilênico muda drasticamente a disposição dos planos nos compostos das séries **7** e **8**. Comparando com a série **5**, esta série possui os compostos mais planares. Assim, os planos distintos gerados pelo carbono sp^2 estão desfavorecendo a interação molecular gerando mesofases monotrópicas.

4.2.3 Terceiro artigo: **"Synthesis of Liquid-crystalline 3,5-Diarylisoxazolines".** *Liq. Cryst.* **2010**, *37*, 159-169.

Na terceira publicação as isoxazolinas utilizadas como moléculas precursoras foram planejadas a fim de permitir a inserção de unidades tolano de um lado ou do outro do anel isoxazolínico, como mostrado na Figura 31, variando os grupos **X** e **Z**.

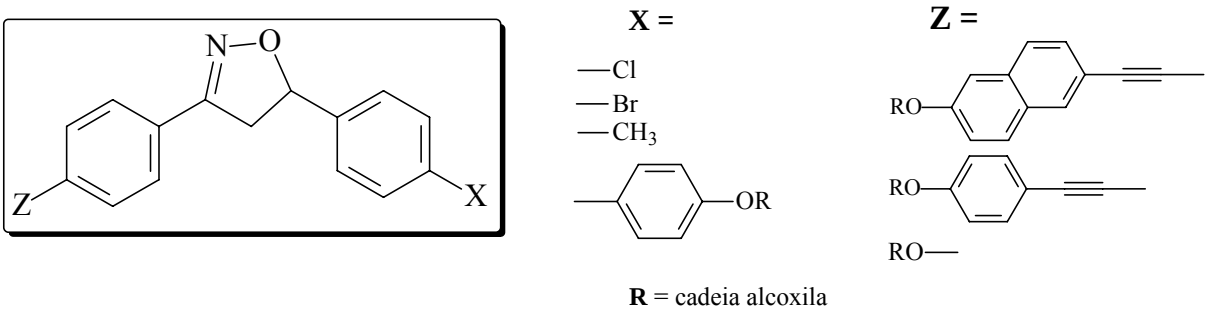

Figura 31. Estruturas representativas dos compostos isoxazolínicos sintetizados.

Após a preparação de todos os compostos intermediários necessários, foram obtidas duas séries inéditas e mais três compostos líquido-cristalinos contendo o anel isoxazolina ligado a diferentes grupos arilacetilênicos, como pode ser visto na Figura 32.

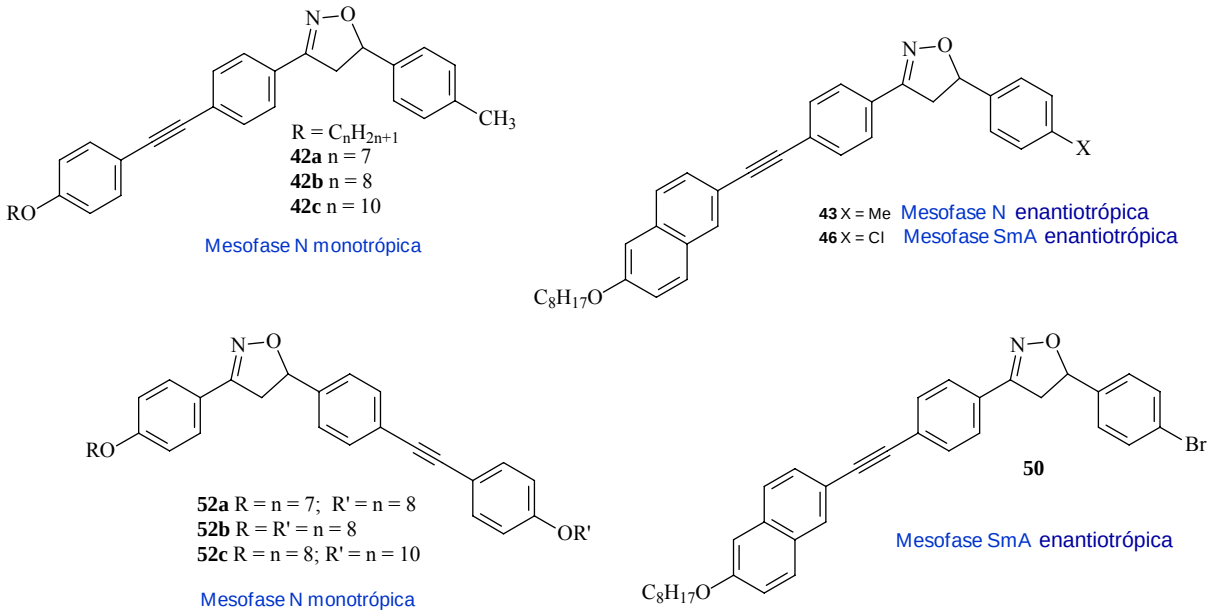

Figura 32. Estruturas dos compostos isoxazolínicos líquido-cristalinos sintetizados.

Todos os compostos exibiram comportamento líquido-cristalino. Os compostos das séries **42** e **52**, derivados de fenilacetileno, apresentaram mesofase N monotrópica. Quando a unidade aromática foi substituída por naftilacetileno nos compostos **43**, **46** e **50**, observou-se

mesofases enantiotrópicas, provavelmente devido a maior anisotropia molecular e planaridade causados pelo novo grupo.

4.3 SINOPSE DOS ARTIGOS EM FASE FINAL DE REDAÇÃO E SUBMETIDO.

4.3.1 Artigo submetido à Revista *Materials Chemistry and Physics* **"Thermal Elimination of *O*-Benzoyloximes. Consequences on the Chemical Stability and Mesomorphic Behavior".**

No desenvolvimento do trabalho relativo ao artigo descrito no item 4.2.3 foram preparados diversos intermediários. Entre estes, foi observado que alguns apresentavam fluorescência e comportamento mesomórfico.

Devido a isso, neste trabalho a oxima **4** foi utilizada como intermediário na síntese de uma série inédita de *O*-benzoiloximas a partir da reação de esterificação entre uma série de oximas e derivados do ácido benzóico. Também, foi sintetizado um composto homólogo contendo o anel isoxazolínico via reação entre a oxima **4** e o ácido 3-[4-octiloxi)fenil]-4,5-dihidroisoxazoil-5-carboxílico (Tabela 3), como mostrado na Figura 33.

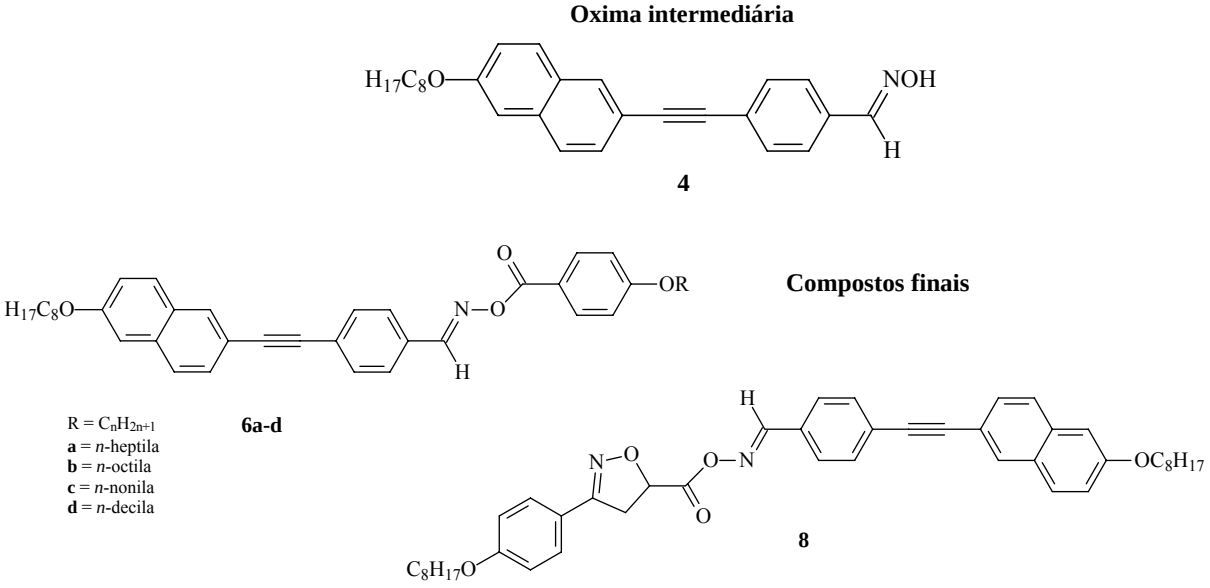

Figura 33. Estruturas dos compostos líquido-cristalinos sintetizados.

As propriedades líquido-cristalinas foram investigas através de DSC e MOLP. Observou-se, por DSC, um comportamento diferente nos 1º e 3º ciclos de aquecimento tanto para o composto **6c** quanto para o **8**, indicando possível degradação das amostras com a

temperatura (Figura 34). A análise dos outros compostos da série mostrou o mesmo comportamento.

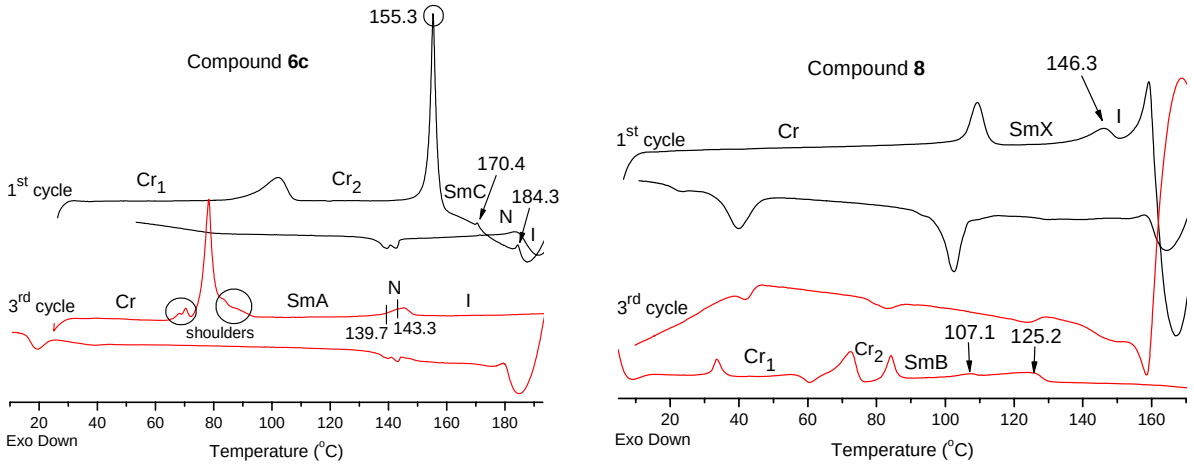

Figura 34. Termogramas de DSC dos compostos **6c** and **8** nos 1º e 3º ciclos de aquecimento e resfriamento a 10 ^{o}C min^{-1}.

Então se submeteu o composto **6b** a ciclos de aquecimento/resfriamento por DSC onde a temperatura máxima utilizada foi de aproximandamente 10 ºC abaixo do ponto de clareamento. Mesmo assim observou-se decomposição contínua da amostra.

A análise de MOLP mostrou que os compostos da série **6** apresentavam mesofases N e SmA após o 1º ciclo de aquecimento/resfriamento. O homólogo **8**, contendo o anel isoxazolínico, exibiu mesofase SmB após o mesmo tratamento térmico.

A fim de entender melhor os resultados obtidos por DSC, foi realizada um análise de Raio-X, onde se observou uma diminuição do espaçamento entre as camadas após o 1º aquecimento, indicando uma mudança da estrutura molecular para o composto **6a**.

Cálculos teóricos foram realizados e mostraram a possibilidade de rotação da ligação N-O, levando à conformação *cis*. Assim, foi proposta uma eliminação induzida por calor, formando nitrila e derivados de ácido benzóico. Análises de ATR de uma amostra submetida a tratamento térmico mostraram o aparecimento da banda de estiramento da ligação C≡N, confirmando uma possível formação de nitrila.

4.3.2 Artigo em fase final de redação: **"The 2:1 Cycloadduct from [3+2] 1,3-dipolar Cycloaddition Reaction. Synthesis and Liquid Crystal Behavior".**

No quinto trabalho, em fase final de redação, foi investigado o comportamento da cicloadição entre oximas e o ácido vinilacético, além de um estudo detalhado do comportamento térmico da série homóloga de cicloadutos 2:1 (**11a-d**), a qual foi obtida inesperadamente na ocasião da produção da Tabela 3.

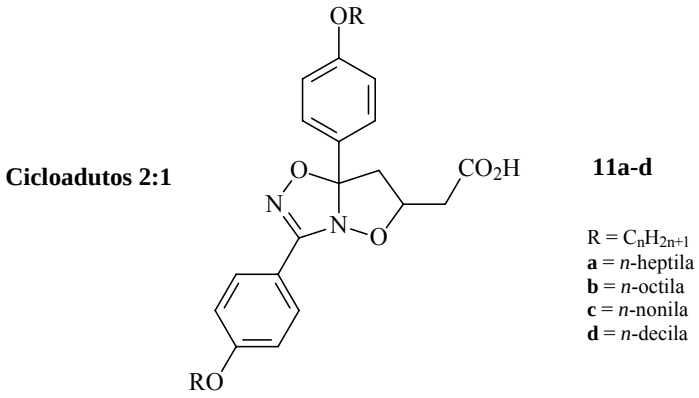

Em relação ao mecanismo desta cicloadição, sugerimos uma adição subseqüente de óxido de nitrila em um cicloaduto intermediário, onde a ligação C=N deste cicloaduto estaria atuando como dipolarófilo para a segunda cicloadição, como mostrado no Esquema 7.

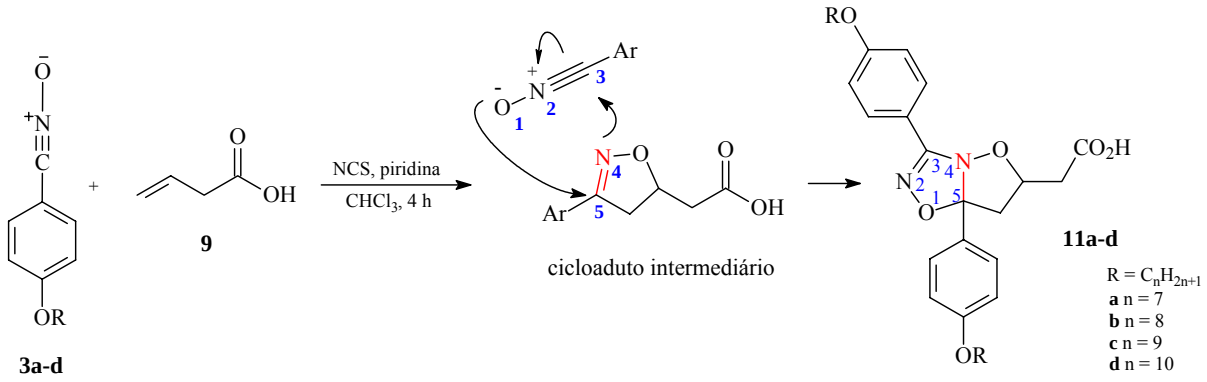

Esquema 7. Síntese da série homóloga **11a-d** de cicloadutos 2:1.

A fim de entender esse mecanismo, foi realizado um estudo teórico para a compreensão da formação do aduto 2:1 em detrimento do aduto 1:1. Este estudo mostrou que a menor diferença de energia entre os orbitais das três espécies existentes no meio reacional é entre o óxido de nitrila e o cicloaduto intermediário, levando assim ao aduto 2:1 (Figura 35).

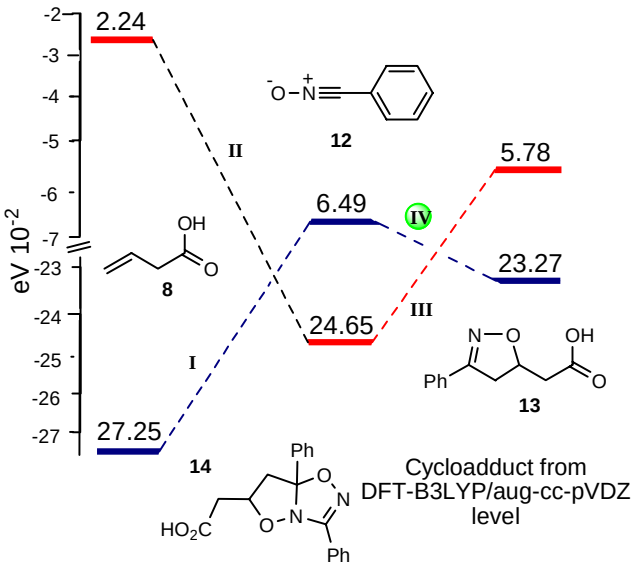

Figura 35. Energias dos orbitais moleculares HOMO e LUMO (eV x10^{-2}) calculadas para o ácido vinilacético (**8**), óxido de benzonitrila (**12**) e isoxazolina (**13**).

A elucidação estrutural dos compostos foi feita via técnicas de ressonância magnética nuclear (^{1}H, ^{13}C, COSY, HMBC e HMQC), DSC, microscopia e estudo fotofísico, além de IR e espectrometria de massas de baixa e alta resolução. Os compostos mostraram mesofases esméticas com decomposição da amostra após o primeiro ciclo de aquecimento. Nos ciclos subseqüentes observou-se que apesar da decomposição, as amostras apresentaram mesofase esmectogênica com textura *Schlieren*, sugerindo mesofase SmC.

4.3.3 Artigo em fase final de redação: **"Síntese e Propriedades Mesomórficas dos Ésteres Aromáticos 3,5-Dissubstituídos Benzoatos de 4,5-dihidroisoxazoíla".**

Neste sexto trabalho, em fase final de redação, foram sintetizadas duas séries homólogas inéditas de CLs contendo o anel isoxazolínico 3,5-dissubstituído e avaliada a relação *estrutura x propriedade* gerada pela variação de espaçadores internos, ou seja, dos carbonos metilênicos entre o anel e um grupo éster, como mostra a Figura 36.

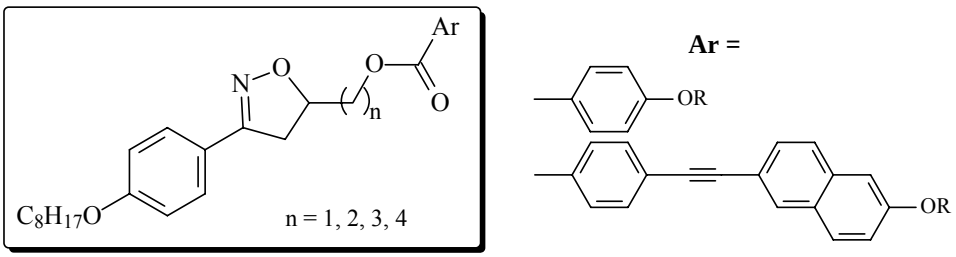

Figura 36. Estruturas representativas dos compostos isoxazolínicos sintetizados.

Após a preparação de todos os compostos intermediários necessários, foram obtidas as séries de compostos homólogos inéditos **5a-d** e **9a-d** com diferente número de carbonos metilênicos na cadeia alquílica interna (Figura 37).

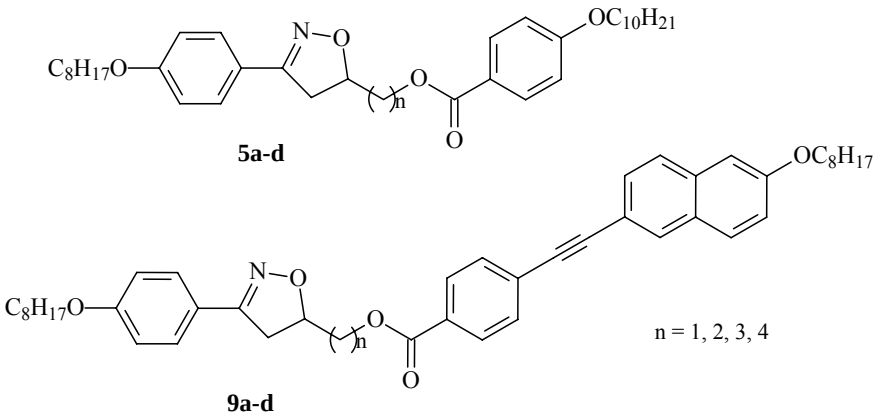

Figura 37. Estruturas dos compostos isoxazolínicos líquido-cristalinos sintetizados.

A mesofase para os compostos da série **5** foi identificada como SmC a partir da observação da textura de leque quebrado por microscopia óptica. A identificação da mesofase N dos compostos da série **9** foi realizada a partir da observação visual das texturas *Schlieren* e planar e pelos baixos valores de entalpia da transição I→mesofase. Os compostos desta série têm estrutura molecular em forma de bastão mais pronunciada que a dos compostos da série **5** e, conseqüentemente, apresentaram mesofase mais estável (enantiotrópica).

A Figura 38A mostra a variação nas temperaturas de transição com o aumento do número de átomos de carbonos na cadeia carbônica interna. Ambas as transições cristal-isotrópico e isotrópico-SmC (para os compostos **5a** e **5b**) diminuem à medida que a cadeia aumenta. Também, é observado um efeito par-ímpar nestas transições e nos valores de entalpia. O comportamento da entropia indica a natureza da transição envolvida. Na Figura 38B pode-se observar uma tendência crescente no valor das entropias de fusão com o aumento do número de átomos de carbonos metilênicos, além do efeito par-ímpar. Os maiores valores de entropia são observados para os compostos com número ímpar de átomos de carbonos (**5a** e **5c**), o que está indicando um melhor empacotamento molecular destas moléculas na transição do que aquelas com número par de átomos de carbono, o que pode ser conseqüência de uma maior linearidade destas moléculas.

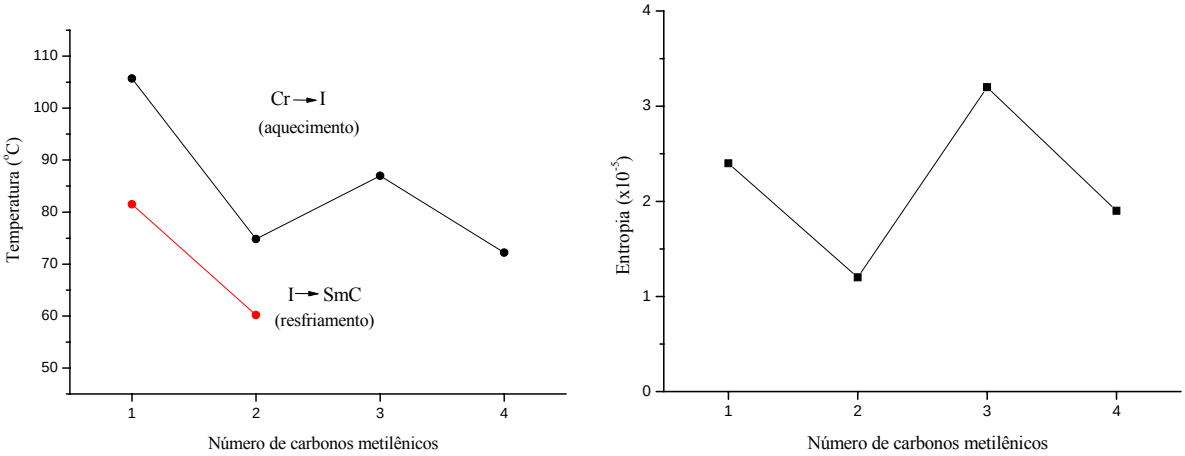

Figura 38. Gráficos do número de átomos de carbonos metilênicos (*n*) na cadeia alquílica interna para os compostos da série **5a-d** em função (A) das temperaturas de transição de fase e (B) da entropia da transição Cr→I.

A Figura 39A mostra a variação das temperaturas de transição com o aumento do número de átomos de carbonos na cadeia carbônica interna para a série **9**. Ambas as transições isotrópico→N e cristal→N diminuem à medida que a cadeia aumenta, assim como pode ser observado um efeito par-ímpar nestas transições. Os valores de entalpia também mostraram este efeito e são consistentes com a mesofase N menos ordenada. Os valores de entropia apresentaram o mesmo comportamento que os compostos da série **5**, porém neste caso os valores são menores uma vez que se trata de transições Cr→mesofase, as quais são fases mais ordenadas que a fase isotrópica (Figura 39B).

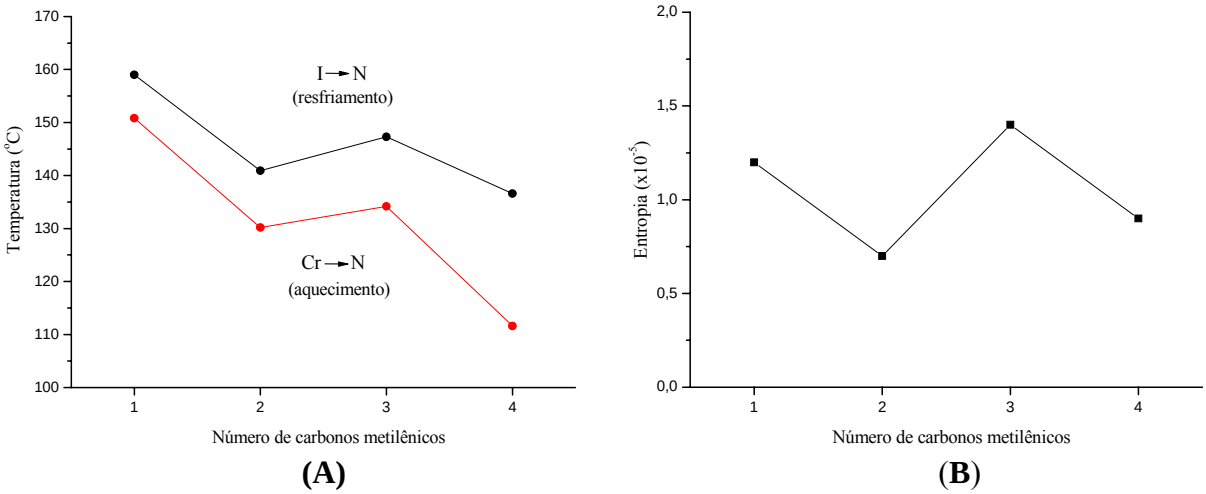

Figura 39. Gráficos do número de átomos de carbonos metilênicos (*n*) na cadeia alquílica interna para os compostos da série **9a-d** em função (A) das temperaturas de transição de fase e (B) da entropia da transição Cr→N (aquecimento).

Também foram realizados estudos teóricos para avaliar a influência do número de carbonos na cadeia alquílica interna. A análise da conformação mais estável para a série **5** mostrou que os compostos **5a** e **5c** têm os seus eixos moleculares mais colineares e coplanares que os compostos **5b** e **5d**, o que vai permitir um melhor empacotamento molecular na transição líquido-cristalina, o que está de acordo com os maiores valores de entalpia encontrados para aqueles compostos.

CAPÍTULO 5

CAPÍTULO 5.1 - *Eur. J. Org. Chem.* **2009**, 889-897 - **DOI: 10.1002/ejoc.200801026**

3,5-Disubstituted Isoxazolines as Potential Molecular Kits for Liquid-crystalline Materials.

Aline Tavares,[a] Paulo H. Schneider,[a] and Aloir A. Merlo*[a]

Keywords: 3,5-Disubstituted Isoxazoline / [3+2] 1,3-Dipolar cycloaddition / Sonogashira Coupling / Liquid Crystals

A collection of 3,5-disubstituted isoxazolines were synthesized using [3+2] 1,3-dipolar cycloaddition. Some isoxazolines were selected and transformed into liquid crystals. The new LC compounds exhibited nematic and smectic C mesophases.

[a] Organic Department, Chemistry Institute, UFRGS, Bento Gonçalves avenue, 9500, Campus do Vale, Porto Alegre, RS, Brazil, 91501970
Fax: +55 51 3308 7304
E-mail: aloir@iq.ufrgs.br
Supporting information for this article is available on the WWW under http://www.eurjoc.org/ or from the author.

Introduction

The 1,3-dipolar [3+2] cycloaddition of nitrile oxides to olefins offers a convenient one-step route for construction of a variety of five-membered heterocycles known as isoxazolines.[1] Pharmacologically, this class of heterocycles has been reported to possess interesting biological activities as well as analgesic, anti-inflammatory and hypoglycemic properties.[2-5] Isoxazolines are also synthetically versatile intermediates that readily undergo further transformations, such as alkylation,[6] dehydrogenation to isoxazoles,[7]and reductive cleavage to expose functionalities such a β-hydroxy ketones, α,β-unsaturated ketones,[8] β-amino acids or γ-amino alcohols.[9]

Nitrogen- and oxygen-containing heterocycles also play an important role in the synthesis of novel liquid-crystalline (LC) materials. One important heterocycle moiety used in LC materials is the isoxazole ring and its variants. While the [3+2]-cycloaddition approach has been used to synthesize the isoxazole directly from activated alkynes and nitrile oxides, the literature reports only moderate yields and low regioselectivities.[10-12] To increase both the yield and regioselectivity of the cycloaddition step, we envisage that the isoxazoline intermediate emerge as an excellent alternative to prepare the isoxazole ring with fair to good yields and high regioselectivity. The oxidation reaction of the corresponding 3,5-isoxazoline prepared by cycloaddition is an easy and efficient approach to synthesize the isoxazole ring. Moreover, by attaching suitable aryl groups at C-3 and C-5 positions of the isoxazoline ring, interesting LC properties can emerge. In this sense, the isoxazoline moiety can be considered a useful molecular kit of interesting organic materials[13].

In this article we describe the 1,3-dipolar cycloaddition of nitrile oxides to dipolarophiles to produce 3,5-disubstituted isoxazoline rings which are potential candidates for liquid-crystalline materials. For this purpose we selected three 3,5-disubstituted isoxazoline compounds synthesized in this work to demonstrate that these heterocycles can serve as molecular kits in the synthesis of new compounds with mesogenic properties. Four LC compounds were prepared by a simple and easy modification of the original isoxazoline ring (Figure 1) by adding two "molecular wings," bearing one or more aromatic rings at the 3- and 5-positions of the isoxazoline system.

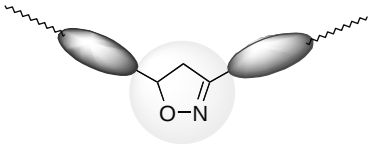

Figure 1. General structure of the isoxazolinic LC.

Results and Discussion

Synthesis of the Isoxazolines 6-12.

Two main methodologies were used to prepare the isoxazoline LC materials. First, to form the isoxazoline, a [3+2] cycloaddition reaction between a nitrile oxide (generated by *in situ* oxidation of the corresponding aldoxime) and an alkene was performed. The Sonogashira reaction was then used as the second methodology to install the triple bond into the molecular wings of the final compounds. The preparation of the aldoximes **3a-d** is outlined in Scheme 1. They were prepared from aldehyde **1** in two steps following classical procedures. In the first step, *p*-hidroxybenzaldehyde (**1**) was alkylated by treatment with alkylbromides in 70-90% yields. In the second step, the oximes were synthesized by reaction of **2a-d** with a solution of hydroxylamine hydrochloride in good yields (73-93%).

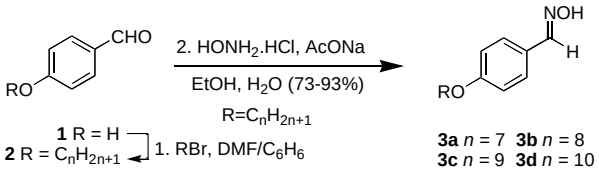

Scheme 1. Synthesis of aldoximes **3a-d.**

Oximes containing a polar group (X) at the *para* position of the aromatic ring **4e** (X=Br), **4f** (X=CN) and **4g** (X=NO_2) were also prepared in good yields by exposure of 4-substituted benzaldehyde to a solution of hydroxylamine hydrochloride.

The oximes prepared in this work were obtained as a mixture of the *(E)*- and (*Z*)-isomers. The structural assignments of these intermediates were made based on their ^{1}H and ^{13}C chemical shifts. The signal of the iminyl hydrogen of the *Z*-isomer always appears at a higher field than the *E*-isomer in accordance with the reported oxime analogs derived from anisaldehyde.[15a,b] The ^{13}C resonance line for the iminyl carbon atom follows the same tendency. For instance, the chemical shifts of the iminyl carbon for the *E*-isomer are always shifted to downfield, whereas that of the the *Z*-isomer is shifted upfield. The chemical shift is an indication of the charge distribution on the iminyl carbon atom. In this situation, the charge distribution values observed for the *E*-isomers were smaller compared to the those of the *Z*-isomers.[14-19]

The 1,3-dipolar [3+2] cycloaddition reactions were examined using seven different oxime benzaldehydes **3a-d/4e-g** with seven dipolarophiles **5a-g** (Scheme 2, Table 1). The yields of the isoxazolines **6-12** is described in Table 1. All the cycloadducts were characterized by ^{1}H and ^{13}C NMR spectroscopic techniques and melting points. The regiochemistry was established from ^{1}H and ^{13}C NMR. In all cases, the reaction of oxime benzaldehydes with **5a-g** (via the nitrile oxide intermediate) was completely regioselective giving only 3,5-disubstituted isoxazolines while no traces of the 3,4-regioisomer was detected.[20]

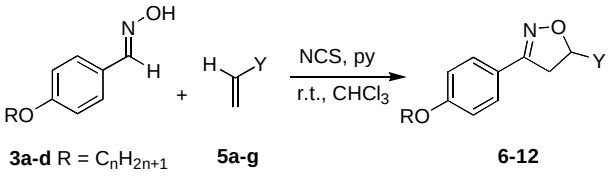

Scheme 2. Preparation of isoxazolines **6-12**.

In nearly all cases, the yields were in the range of 40 to 90%. A low yield was obtained with the allylic alcohol dipolarophile **(5b)**, which gave the 3,5-disubstituted isoxazoline **7a-d**, and is known to be considerably less reactive than the other dipolarophiles used in this work. When the aldoxime **4f**, having the cyano group, reacted with dipolarophile **5a** or **5d**, no cycloadducts **6f** or **9f** were observed (entries 6 and 18).

Table 1. 1,3-Dipolar [3+2] Cycloaddition of oximes **3a-d** and **4e-g** with dipolarophiles **5a-g**.[a]

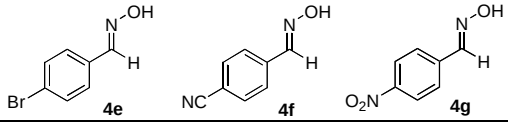

Entry	Aldoxime	Dipolarophile		Aduct	Yield (%)[b]
1	**3a**			**6a**	80
2	**3b**			**6b**	66
3	**3c**			**6c**	83
4	**3d**	**5a**	Y = CO_2H	**6d**	89
5	**4e**			**6e**	47
6	**4f**			**6f**[c]	-
7	**4g**			**6g**	25
8	**3a**			**7a**	36
9	**3b**	**5b**	Y = CH_2OH	**7b**	36
10	**3c**			**7c**	38
11	**3d**			**7d**	41
12	**3a**			**8a**	31
13	**3b**	**5c**	Y = $CO_2{}^n$Bu	**8b**	65
14	**3c**			**8c**	38
15	**3d**			**8d**	62
16	**3a**			**9a**	50
17	**3b**	**5d**	Y = $CONH_2$	**9b**	78
18	**4f**			**9f**[c]	-
19	**4g**			**9g**	45
20	**3c**	**5e**	Y = CN	**10c**	43
21	**3a**	**5f**	Y = CH_2CO_2H	**11a**[d]	-
22	**3b**	**5g**	Y = *p*-MeC_6H_4	**12b**	60

[a] Reaction conditions: dipolarophile (2.3 mmol), NCS (2.3 mmol), oxime (2 mmol), pyridine (3 mmol), solvent (8 mL). [b] Isolated yields. [c] No reaction. [d] 2:1 Cycloadduct, see discussion in the text.

The ^{13}C and ^{1}H spectra of the isoxazolines exhibited well-defined resonances lines for the C_3 and C_5 carbon atoms and for the corresponding hydrogen atoms. The ^{1}H NMR spectrum of cycloadduct **7a**, for instance, showed four sets of doubled dublet of resonance lines centered at 3.24 ppm, 3.36 ppm, 3.68 and 3.86 ppm that belong to the ABX and AMX pattern related to the chemically and magnetically nonequivalent protons. The resonance lines of the selected carbon atoms of the isoxazoline ring confirm the correct regiochemistry during the [3+2] cycloaddition event. Thus, from the ^{13}C NMR spectrum of **7a** we can observe only two signals centered at 36.5 and 80.9 ppm which are consistent with 3,5 regioisomer[20,21] (see Supporting Information).

The cycloaddition reaction between the oxime **3a** and the dipolarophile **5f** described in Table 1 gave the product **11a** (Figure 2), exclusively in 30% yield and not the expected 3,5-isoxazoline. The structure of the new condensed product **11a**, which was characterized as 2:1 cycloadduct, was confirmed by NMR, mass spectroscopy, elemental analysis and thermal analysis. These results can be rationalized considering the low dipolarophilic reactivity of the vinylacetic acid (**5f**) in comparison with the 3,5-isoxazoline formed *in situ*. Once the 3,5-isoxazoline is formed by the reaction of aryl nitrile oxide and **5f**, the polarization of the C=N bond by the oxygen atom enhances the dipolarophilic character of this C=N bond, and drives the addition of a second equivalent of aryl nitrile oxide to the initially formed isoxazoline.[22]

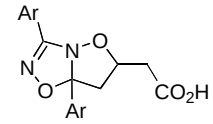

Ar = *p*-$C_nH_{2n+1}OC_6H_4$

11a *n* = 7

Figure 2. The 2:1 cycloadduct **11a**.

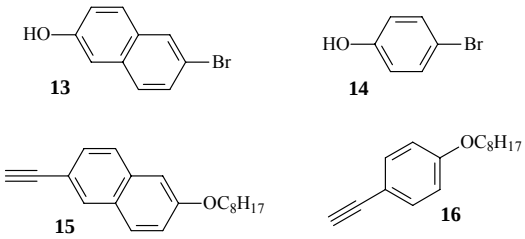

Figure 3. Terminal acetylenes **15** and **16**.

Synthesis of Selected Liquid-Crystalline Materials.

Having accomplished the preparation of the 3,5-disubstituted isoxazolines (Table 1) we could now explore this heterocyclic class as a molecular kit in order to obtaining a new class of the calamitic liquid crystals. In this way, the potential LC materials are reached through an *elongating molecular strategy* from these key intermediates. This elongation builds off the rigid isoxazoline core to form a more polarizable and mesogenic one. Our idea was to explore the synthetic potential of this class of compounds bearing a functional group by attaching a proper aromatic moiety. The isoxazolines **6a** and **7a** were chosen due to their possession of carboxyl and hydroxyl functional groups, which could be used to reach the desired LC materials. In addition, a simple oxidation step on the isoxazoline ring *such as* **12b** affords the liquid crystal compound in a straightforward fashion.

By a Sonogashira reaction an arylacetilenic group was installed on one side of the isoxazoline ring. The Figure 3 shows two acetylene derivatives which are necessary to elongate the isoxazolines **6a** and **7a**. The compounds **15** and **16** were synthesized in three steps following a methodology described previously.[23] Thus, the alkylation of 6-bromo-2-naphtol (**13**) or *p*-bromophenol (**14**) with *n*-alkylbromide gave the corresponding alkylaryl ethers in 85-95% yields. Installation of the acetylene unit was accomplished by Sonogashira alkynylation[24] of the alkylaryl ethers derived from **13** or **14** with 2-methyl-3-butyn-2-ol (mebynol). The terminal acetylenes **15** and **16** were smoothly reached by releasing acetone using KOH and isopropanol.[25]

The second Sonogashira reaction allowed further elongation of the acetylene derivatives **15** and **16** by connecting another aromatic ring. Thus, the reaction of the protected bromophenols[26] **17b** and **15** under palladium-copper cross-coupling,[24,27] gave the desired phenol **18** after hydrolysis of the acetyl group in good yields (Scheme 3).

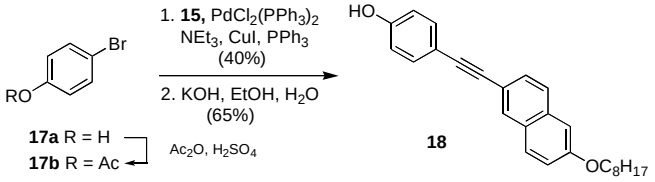

Scheme 3. Synthesis of **18**.

The chemical linkage between **18** and **6a** to obtain the final liquid crystal compound **19** was mediated by DCC/DMAP protocol[28] in 70% of yield (Figure 4). The thermal analysis (DSC) and polarized optical microscopy studies (POM) showed that **19** is a thermotropic liquid crystal. When the compound **19** was cooled from the isotropic phase, it clearly presented typical schlieren textures with singularities points and two- and four-brush defect characteristic of the nematic phase. The optical, thermal and thermodynamic data for these compounds are summarized in Table 2.

The DSC traces (Figure 5) of **19** exhibit I → N → K on cooling. However, this compound showed enantiotropic behavior when analyzed by POM. On slow heating the sample **19** enters into the nematic phase at 144.5 °C and melts to an isotropic liquid at 148.0 °C. The range of temperature for the mesophase is small for **19** (ΔT 3.5 °C). The transition enthalpy for the isotropic to nematic transition of the **19** is rather low 0.015 kcal.mol^{-1}. This value is consistent with a less ordered nematic mesophase.

Table 2. Transition temperatures and enthalpies (Δ*H*) for compounds **19**, **21**, **23** and **24**.[a]

Entry	Phase transition temperature [°C] Heating	Cooling	Δ*H* [kcal mol^{-1}] Melt[d]	Iso phase K[e]
19	K 144.5[b] N 148.0 I	I 144.9 N 136.9 K	6.74	I 0.015 N 6.59 K
21	K 138.4 I	I 134.3[c] N 120.2 K	13.91	I 0.67 N 13.53 K
23	K 102.5 I	I 75.7[c] SmC[f] 71.2 K	13.40	I 2.81 SmC 11.79 K
24	K 105.9 N 132.2 I	I 131.1 N 82.2 K	5.82	I 0.076 N 5.87 K

[a] Scan rate: 10 °C min^{-1} for all samples. K denotes crystal phase, SmC = smectic C phase and N = nematic phase. [b] Data obtained from POM study. [c] Monotropic behaviour. [d] Enthalpies (second heating/cooling stage) were determined from the crystal phase to the LC phase. [e] Cooling. [f] On slow cooling the samples crystallized. On fast cooling the sample displayed an unstable mesophase SmC during the crystallization process.

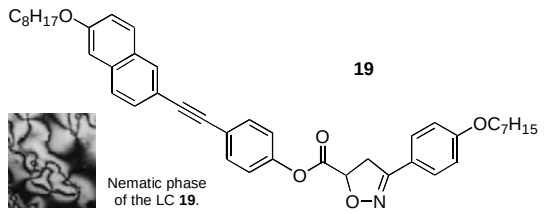

Figure 4. Chemical structure of **19**.

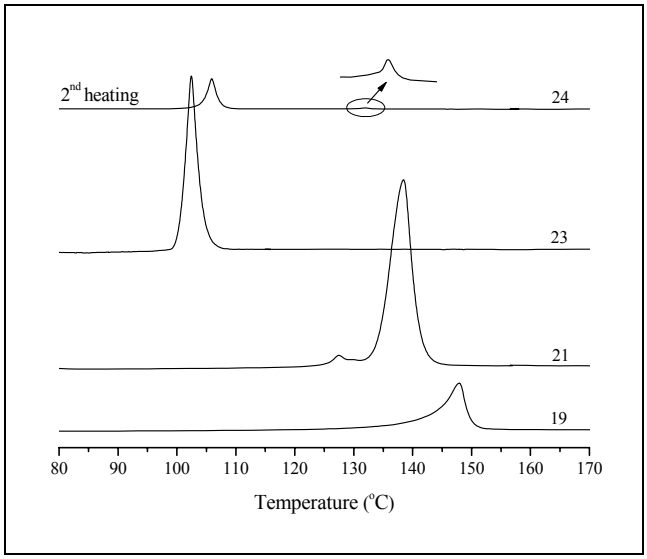

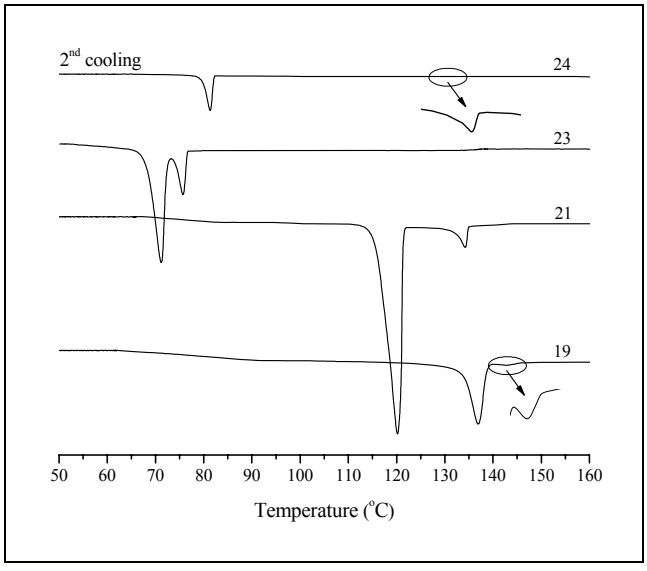

Figure 5. DSC curves of the LC compounds **19**, **21, 23** and **24** on second heating and cooling run.

The isoxazoline **7a** was selected to prepare the liquid crystal compounds **21** and **23**. Figure 6 contains the general chemical structure of the final liquid crystals compounds as well as the optical texture micrographs of the mesophase. For these purposes, the ester linkage was introduced by esterification reaction of the bromoacid **20** with **7a** by DCC/DMAP protocol. Application of the same cross-coupling reaction conditions of the alkyne **16** and the ester derivative from acid **20** afforded the liquid-crystalline compound **21** in 40 % of yield (2 steps). The data collected in Table 2 for this compound show that the mesophase appears only during the cooling cycle. No mesophase was observed on heating when the sample was analysed under POM observation. The compound **21** displayed planar thread-like texture which is characteristic of liquid-crystalline nematic phase. It should be noted that the enthalpy value for this nematic-isotropic transition of **21** is larger than the conventional nematic ↔ isotropic transition enthalpies (< 0.50 kcal.mol^{-1}) of calamitic liquid crystals. This may be indicating that relatively strong intermolecular interactions exist in the nematic phase and could be attributed to an inversion of the carboxylate group in **21** compared with in **19**.

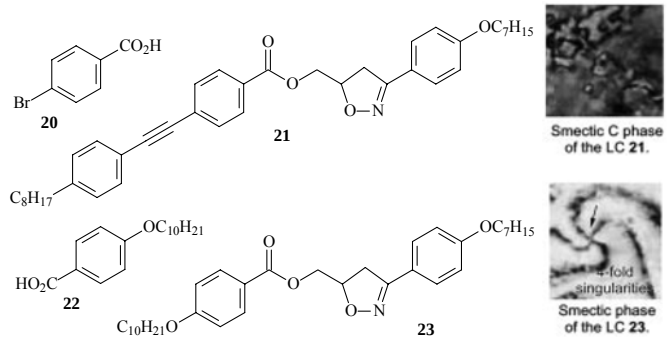

Figure 6. Chemical intermediates **20**, **22** and final liquid crystals isoxazolines **21** and **23**.

Liquid crystal **23** was prepared from **7a** by a short and fast method. The esterification reaction (DCC-DMAP) between **7a** and the popular acid **22** widely used in LC synthesis[29] gave the LC product. The phase behaviour of compound **23** is similar to compound **21**. On heating, the sample **23** melts to isotropic state at 102.5 °C. However on cooling, the sample enters into the smectic C phase at 75.7 °C and finally crystallizes at 71.2 °C (Table 2, Figure 5). The schlieren texture observed for this sample shows a disclination point where four black brushes (disclination lines) meet and it was assigned as smectic C phase. In smectic C phase, only 4-fold singularities are observed; nematics may in addition show singularities with two brushes, as showed by compound **19**. For comparison the mesophase range of the LC **21** is larger than the LC **23** due to the phenylacetylene substructure present in **21**. The transition enthalpy for the isotropic to smectic transition of the **23** is higher than **21**. The enthalpy value suggests a more ordered phase going from isotropic to smectic phase compared to compound **21**.

The final demonstration the potential of isoxazolines in LC materials is outlined in Scheme 4. The isoxazoline **12b** was oxidized to the isoxazole **24** when exposed to manganese (IV) dioxide.[30] The compound **24** was easily purified through a simple filtration to remove the inorganic materials and recrystallized in ethanol. The optical, thermal and thermodynamic data (Table 2) and the DSC traces (Figure 5) for compound **24** clearly reveals that it exhibits a large enantiotropic nematic mesophase. When the sample is cooled from its isotropic phase, the nematic phase appears exhibiting planar thread-like texture which is characteristic of liquid-crystalline nematic phase.[31] On heating, sample **24** enters into the nematic phase at 105.9 °C and finally melts to an isotropic liquid at 132.2 °C. The range of temperature for the mesophase is 26.3 °C. The two peaks observed at 105.9 °C and 132.2 °C were associated with **K** → **N** and **N** → **I** transitions, respectively. As expected for Isotropic ↔ Nematic transition

enthalpies the value of 0.076 kcal.mol^{-1} is in accordance with a less ordered nematic mesophase.

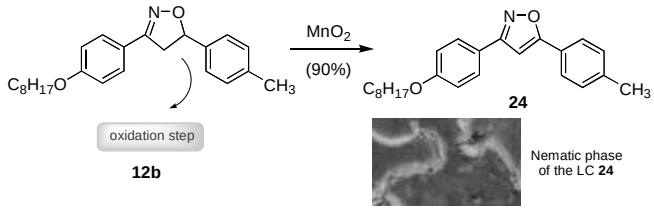

Scheme 4. Preparation of isoxazole LC **24**.

Conclusions

We have synthesized and characterized a number of isoxazolines comprising aryl and polar groups at 3- and 5-positions, using the 1,3-dipolar [3+2] cycloaddition reactions of nitrile oxides and alkenes. The straightforward access to 2-isoxazolines is an excellent manner to obtain a molecular kits to prepare versatile intermediates that can be transformed into LC materials. In this work, the isoxazolines **6a** and **7a** were chosen and chemically modified through a linkage of arylacetilenic moiety at the polar group. Also, we selected the isoxazoline **12b** and performed the oxazoline-oxazole transformation through an oxidation reaction. In this sense were synthesized four new LC materials **19**, **21**, **23** and **24**. In all chemical operations, the compounds exhibited mesomorphic behavior; the nematic phase was observed for the compounds **19**, **21** and **24** and smectic C phase was detected for the compound **23**. For the less reactive dipolarophile vinylacetic acid (**5f**), the 2:1 cycloadduct was obtained exclusively and not the expected 1:1 cycloadduct. New liquid crystals derived from the isoxazolines listed in Table 1 are in progress and will be reported in due course.

Experimental Section

Instruments and Techniques. 4-Hydroxybenzaldehyde, 1-bromoalkanes, hydroxylamine hydrochloride, acrylic acid, *N*-chlorosuccinimide (NCS), KOH, sodium acetate, ethanol, chloroform, butyl acrylate, acrylonitrile, 4-bromobenzaldehyde, acetonitrile and toluene were used without further purification from Aldrich. Pyridine and allylic alcohol were distilled under reduced pressure. All other commercial solvents and reagents were used without further purification. The melting points and mesophase transition temperatures and textures of the samples were measured on a Mettler Toledo FP82HT Hot Stage FP90 Central Processor and DSC 2910 TA Instruments. Nuclear magnetic resonance spectra were obtained on a Varian 300 MHz instrument. Chemical shift are given in parts per million (δ) and are referenced from tetramethylsilane (TMS). Infrared spectra were recorded on a Perkin-Elmer Spectrum One FTIR Spectrometer Instruments using NaCl plates in case of solids and as thin film supported between NaCl plates in case of liquids and are reporter as wavenumber (cm^{-1}). Low-resolution mass spectra were obtained on a Shimadzu CG-MS-QP5050 Mass Spectrometer interfaced with a Shimadzu GC-17A. Gas Chromatograph equipped with a DB-17 MS capillary column. ESI-MS data were collected on a Waters® Micromass® Q-Tof micro™ mass spectrometer with Z-spray electrospray source. Samples were infused from a 100 μL gas-tight syringe at 5 μL min^{-1}, via a syringe pump. Instrument settings were unexceptional: capillary voltage 4500 V, cone voltage 50 V, source temperature 100 ºC, desolvation gas temperature 100 ºC. Nitrogen was used as the desolvation gas. CHN analyses were performed on a Perkin-Elmer 2400 CHN Elemental Analyzer. All reactions involving Sonogashira's coupling were performed in one-neck round-bottom flask equipped with septum stoppers and charged with triethylamine (Et_3N), aromatic iodide and alkyne under argon atmosphere for 30 min. Copper(I) iodide (CuI), triphenylphosphane (PPh_3) and *bis*-(triphenylphosphane)palladium (II) chloride [$PdCl_2(PPh_3)_2$] were then added.

Alkylation reactions. The 4-(*n*-alkyloxy)benzaldehydes (**2a-d**) were prepared from benzaldehyde (**1**) were obtained according to reference 23b and 32. **Synthesis of aldoximes.** The 4-(*n*-alkyloxy)benzaldehyde oximes (**3a-d** and **4e-g**) were synthesized from the corresponding 4-(*n*-alkyloxy)benzaldehydes according to references 13a, 33, 34, 35 and 36. See Supporting Information for experimental procedure and spectral characterization.

Cycloaddition reactions. A solution of the corresponding oxime (2 mmol) was added dropwise to an ice-cooled solution of $CHCl_3$ (8 mL), dipolarophile (2.3 mmol), pyridine (3 mmol) and *N*-chlorosuccinimide (NCS) (2.3 mmol) under argon for 40 min. The reaction was then stirred at room temperature for 4 h. The solution was washed with water and dried over Na_2SO_4. The filtrate was evaporated under a reduced pressure and the residue was purified by recristalization from toluene.

3-[4-(Heptyloxy)phenyl]-4,5-dihydroisoxazole-5-carboxylic acid (6a). Yield: 240 mg, 80%; white solid; mp 149 ºC. ^{1}H NMR ($CDCl_3$): δ = 0.89 (m, 3H, CH_3), 1.38 (m, 8H, $(CH_2)_4$), 1.79 (m, 2H, C$\underline{H}_2$CH$_2$O), 3.62 (d, *J* = 9.0 Hz, 2H, C$\underline{H}_2$CH), 3.98 (t, *J* = 6.6 Hz, 2H, CH_2O), 5.12 (t, *J* = 9.0 Hz, 1H, CH$_2$C$\underline{H}$), 6.90 (d, *J* = 8.7 Hz, 2H, Ar), 7.60 (d, *J* = 8.7 Hz, 2H, Ar), 8.10 (b, 1H, OH); ^{13}C NMR ($CDCl_3$/DMSO-d_6): δ = 13.7, 22.2, 25.5, 28.6, 28.7, 31.3, 38.8, 67.7, 77.4, 114.3, 120.5, 128.0, 155.3, 160.5, 172.0; IR 3182, 2925, 2854, 1720, 1610, 1517, 1461, 1377, 1252, 1183, 1043, 1010, 897, 829, 721, 666. Elemental analysis (%) for $C_{17}H_{23}NO_4$ (305.37): calcd. C 66.86, H 7.59, N 4.59; found C 66.96, H 7.62, N 4.71. **3-[4-(Octyloxy)phenyl]-4,5-dihydroisoxazole-5-carboxylic acid (6b).** Yield: 105 mg, 66%; white solid; mp 143 ºC. ^{1}H NMR ($CDCl_3$): δ = 0.89 (m, 3H, CH_3), 1.39 (m, 10H, $(CH_2)_5$), 1.79 (m, 2H, C$\underline{H}_2$CH$_2$O), 3.63 (d, *J* = 9.0 Hz, 2H, C$\underline{H}_2$CH), 3.98 (t, *J* = 6.6 Hz, 2H, CH_2O), 5.13 (t, *J* = 9.0 Hz, 1H, CH$_2$C$\underline{H}$), 5.80 (b, 1H, OH), 6.90 (d, *J* = 8.7 Hz, 2H, Ar), 7.60 (d, *J* = 8.7 Hz, 2H, Ar); ^{13}C NMR ($CDCl_3$/DMSO-d_6): δ = 13.7, 22.2, 25.6, 28.7, 28.8, 29.0, 31.4, 38.9, 67.7, 77.4, 114.3, 120.5, 128.1, 155.3, 160.5, 172.1; IR 3184, 2925, 2854, 1720, 1610, 1519, 1461, 1377, 1253, 1183, 1045, 1010, 895, 828, 721, 665. Elemental analysis (%) for $C_{18}H_{25}NO_4$ (319.40): calcd. C 67.69, H 7.89, N 4.39; found C 67.58, H 7.92, N 4.51.

3-[4-(Nonyloxy)phenyl]-4,5-dihydroisoxazole-5-carboxylic acid (6c). Yield: 138 mg, 83%; white solid; mp 141 ºC. ^{1}H NMR ($CDCl_3$): δ = 0.88 (m, 3H, CH_3), 1.38 (m, 12H, $(CH_2)_6$), 1.78 (m, 2H, C$\underline{H}_2$CH$_2$O), 3.62 (d, *J* = 9.0 Hz, 2H, C$\underline{H}_2$CH), 3.98 (t, *J* = 6.6 Hz, 2H, CH_2O), 5.11 (t, *J* = 9.0 Hz, 1H, CH$_2$C$\underline{H}$), 6.70 (b, 1H, OH), 6.90 (d, *J* = 8.7 Hz, 2H, Ar), 7.59 (d, *J* = 8.7 Hz, 2H, Ar); ^{13}C NMR ($CDCl_3$/DMSO-d_6): δ = 13.8, 22.3, 25.6, 28.8, 28.9, 29.0, 29.1, 31.5, 38.9, 67.8, 77.4, 114.3, 120.6, 128.1, 155.3, 160.5, 172.2; IR 3183, 2925, 2854, 1721, 1608, 1518, 1461, 1377, 1253, 1182, 1045, 1010, 898, 828, 721, 667. Elemental analysis (%) for $C_{19}H_{27}NO_4$ (333.43): calcd. C 68.44, H 8.16, N 4.20; found C 68.32, H 8.09, N 4.32.

3-[4-(Decyloxy)phenyl]-4,5-dihydroisoxazole-5-carboxylic acid (6d). Yield: 309 mg, 89%; white solid; mp 138 ºC. ^{1}H NMR ($CDCl_3$): δ = 0.88 (m, 3H, CH_3), 1.38 (m, 14H, $(CH_2)_7$), 1.79 (m, 2H, C$\underline{H}_2$CH$_2$O), 3.62 (d, *J* = 9.0 Hz, 2H, C$\underline{H}_2$CH), 3.98 (t, *J* = 6.6 Hz, 2H, CH_2O), 5.12 (t, *J* = 9.0 Hz, 1H, CH$_2$C$\underline{H}$), 6.90 (d, *J* = 8.7 Hz, 2H, Ar), 7.59 (d, *J* = 8.7 Hz, 2H, Ar); ^{13}C NMR ($CDCl_3$/DMSO-d_6): δ = 13.8, 22.3, 25.6, 28.8, 28.9, 29.0, 29.2, 30.6, 31.5, 38.9, 67.7, 77.4, 114.3, 120.5, 128.1, 155.3, 160.5, 172.1; IR 3183, 2925, 2854, 1720, 1610, 1517, 1461, 1377, 1251, 1183, 1042, 1010, 898, 830, 721, 665. Elemental analysis (%) for $C_{20}H_{29}NO_4$ (347.45): calcd. C 69.14, H 8.41, N 4.03; found C 69.23, H 8.33, N 4.12.

3-(4-Bromophenyl)-4,5-dihydroisoxazole-5-carboxylic acid (6e). Yield: 127 mg, 47%; brown solid; mp 173-175 ºC. ^{1}H NMR ($CDCl_3$): δ = 3.62 (d,

J = 9.3 Hz, 2H, C$\underline{H}_2$CH), 5.16 (t, *J* = 9.3 Hz, 1H, CH$_2$C$\underline{H}$), 7.55 (s, 4H, Ar); ^{13}C NMR (CDCl$_3$/DMSO-d$_6$): δ = 38.5, 77.8, 124.4, 127.4, 128.1, 131.7, 155.0, 171.8; IR 3200-3100, 2924, 2854, 1726, 1592, 1462, 1377, 1225, 899, 824. Elemental analysis (%) for $C_{10}H_8BrNO_3$ (270.08): calcd. C 44.47, H 2.29, N 5.19; found C 44.56, H 2.41, N 5.25.

3-(4-Nitrophenyl)-4,5-dihydroisoxazole-5-carboxylic acid (6g). Yield: 118 mg, 25%; white solid; mp 130 ºC. ^{1}H NMR (CDCl$_3$/DMSO-d$_6$): δ = 3.69 (d, *J* = 9.3 Hz, 2H, C$\underline{H}_2$CH), 5.25 (m, 1H, CH$_2$C$\underline{H}$), 7.45 (b, 1H, OH), 7.87 (d, *J* = 8.4 Hz, 2H, Ar), 8.27 (d, *J* = 8.4 Hz, 2H, Ar). Elemental analysis (%) for $C_{10}H_8N_2O_5$ (236.18): calcd. C 50.85, H 3.41, N 11.86; found C 50.78, H 3.49, N 12.01.

{3-[4-(Heptyloxy)phenyl]-4,5-dihydroisoxazol-5-yl} methanol (7a). Yield: 419 mg, 36%; white solid; mp 96 ºC. ^{1}H NMR (CDCl$_3$): δ = 0.89 (m, 3H, CH$_3$), 1.41 (m, 8H, (CH$_2$)$_4$), 1.79 (m, 2H, C$\underline{H}_2$CH$_2$O), 2.10 (broad, 1H, OH), 3.24 (dd, *J* = 16.5, 7.8 Hz, 1H, N=CC$\underline{H}$HCH), 3.36 (dd, *J* = 16.5, 10.5 Hz, 1H, N=CCH$\underline{H}$CH), 3.67 (dd, *J* = 12.0, 4.8 Hz, 1H, CHC$\underline{H}$HOH), 3.85 (dd, *J* = 12.0, 3.3 Hz, 1H, CHCH$\underline{H}$OH), 3.97 (t, *J* = 6.6 Hz, 2H, CH$_2$O), 4,83 (m, 1H), 6.89 (d, *J* = 9.0 Hz, 2H, Ar), 7.58 (d, *J* = 8,7 Hz, 2H, Ar); ^{13}C NMR (CDCl$_3$): δ = 13.9, 22.5, 25.8, 28.9, 29.0, 31.6, 36.5, 63.4, 68.0, 80.9, 114.5, 121.5, 128.1, 156.5, 160.5; IR 3294, 3187, 2923, 2854, 1610, 1517, 1463, 1377, 1253, 1181, 1049, 875, 820, 721, 665. Elemental analysis (%) for $C_{17}H_{25}NO_3$ (291.39): calcd. C 70.07, H 8.65, N 4.81; found C 70.12, H 8.71, N 4.89.

{3-[4-(Octyloxy)phenyl]-4,5-dihydroisoxazol-5-yl} methanol (7b). Yield: 219 mg, 36%; white solid; mp 94 ºC. ^{1}H NMR (CDCl$_3$): δ = 0.89 (m, 3H, CH$_3$), 1.41 (m, 10H, (CH$_2$)$_5$), 1.78 (m, 2H, C$\underline{H}_2$CH$_2$O), 2.99 (broad, 1H, OH), 3.24 (dd, *J* = 16.8, 8.1 Hz, 1H, N=CC$\underline{H}$HCH), 3.34 (dd, *J* = 16.8, 10.5 Hz, 1H, N=CCH$\underline{H}$CH), 3.67 (dd, *J* = 12.0, 4.8 Hz, 1H, CHC$\underline{H}$HOH), 3.83 (dd, *J* = 12.0, 3.3 Hz, 1H, CHCH$\underline{H}$OH), 3.96 (t, *J* = 6.6 Hz, 2H, CH$_2$O), 4,81 (m, 1H), 6.87 (d, *J* = 9.0 Hz, 2H, Ar), 7.56 (d, *J* = 8.7 Hz, 2H, Ar); ^{13}C NMR (CDCl$_3$): δ = 13.9, 22.5, 25.8, 29.0, 29.1, 29.2, 31.7, 36.5, 63.4, 68.0, 80.9, 114.5, 121.4, 128.1, 156.5, 160.5; IR 3294, 3189, 2923, 2854, 1608, 1517, 1463, 1377, 1254, 1181, 1049, 876, 820, 721, 668. Elemental analysis (%) for $C_{18}H_{27}NO_3$ (305.42): calcd. C 70.79, H 8.91, N 4.59; found C 70.65, H 8.86, N 4.80.

{3-[4-(Nonyloxy)phenyl]-4,5-dihydroisoxazol-5-yl} methanol (7c). Yield: 122mg, 38%; white solid; mp 98 ºC. ^{1}H NMR (CDCl$_3$): δ = 0.89 (m, 3H, CH$_3$), 1.43 (m, 12H, (CH$_2$)$_6$), 1.79 (m, 2H, C$\underline{H}_2$CH$_2$O), 2.10 (broad, 1H, OH), 3.24 (dd, *J* = 16.8, 8.1 Hz, 1H, N=CC$\underline{H}$HCH), 3.36 (dd, *J* = 16.8, 10.5 Hz, 1H, N=CCH$\underline{H}$CH), 3.67 (dd, *J* = 12.0, 4.8 Hz, 1H, CHC$\underline{H}$HOH), 3.86 (dd, *J* = 12.0, 3.3 Hz, 1H, CHCH$\underline{H}$OH), 3.97 (t, *J* = 6.6 Hz, 2H, CH$_2$O), 4,84 (m, 1H), 6.89 (d, *J* = 9.0 Hz, 2H, Ar), 7.58 (d, , *J* = 8,7 Hz 2H, Ar); ^{13}C NMR (CDCl$_3$): δ = 13.9, 22.5, 25.8, 29.0, 29.1, 29.2, 29.3, 31.7, 36.5, 63.3, 68.0, 80.9, 114.4, 121.5, 128.0, 156.4, 160.5; IR 3294, 3189, 2923, 2854, 1611, 1515, 1463, 1377, 1254, 1182, 1048, 876, 820, 721, 666. Elemental analysis (%) for $C_{19}H_{29}NO_3$ (319.44): calcd. C 71.44, H 9.15, N 4.38; found C 71.65, H 9.25, N 4.50.

{3-[4-(Decyloxy)phenyl]-4,5-dihydroisoxazol-5-yl} methanol (7d). Yield: 273 mg, 41%; white solid; mp 95 ºC. ^{1}H NMR (CDCl$_3$): δ = 0.89 (m, 3H, CH$_3$), 1.43 (m, 14H, (CH$_2$)$_7$), 1.79 (m, 2H, C$\underline{H}_2$CH$_2$O), 2.05 (broad, 1H, OH), 3.24 (dd, *J* = 16.5, 7.8 Hz, 1H, N=CC$\underline{H}$HCH), 3.37 (dd, *J* = 16.5, 10.5 Hz, 1H, N=CCH$\underline{H}$CH), 3.67 (dd, *J* = 12.0, 4.8 Hz, 1H, CHC$\underline{H}$HOH), 3.86 (dd, *J* = 12.0, 3.3 Hz, 1H, CHCH$\underline{H}$OH), 3.98 (t, *J* = 6.6 Hz, 2H, CH$_2$O), 4,84 (m, 1H), 6.90 (d, *J* = 9.0 Hz, 2H, Ar), 7.58 (d, *J* = 8.7 Hz, 2H, Ar); ^{13}C NMR (CDCl$_3$): δ = 14.0, 22.6, 25.9, 29.1, 29.2, 29.3, 29.4, 29.5, 31.8, 36.5, 63.5, 68.0, 80.9, 114.5, 121.5, 128.1, 156.6, 160.6; IR 3294, 3187, 2923, 2854, 1610, 1515, 1463, 1377, 1256, 1182, 1047, 877, 820, 721, 667. Elemental analysis (%) for $C_{20}H_{31}NO_3$ (333.47): calcd. C 72.04, H 9.37, N 4.20; found C 71.98, H 9.24, N 4.45.

Butyl 3-(4-heptyloxyphenyl)-4,5-dihydroisoxazole-5-carboxylate (8a). Yield: 112 mg, 31%; yellow solid; mp 34 ºC. ^{1}H NMR (CDCl$_3$): δ = 0.91 (m, 6H, (CH$_3$)$_2$), 1.38 (m, 10H, (CH$_2$)$_5$), 1.67 (m, 2H, C$\underline{H}_2$CH$_2$OCO), 1.79 (m, 2H, C$\underline{H}_2$CH$_2$O), 3.60 (d, *J* = 10.2 Hz, 1H, C$\underline{H}$HCH), 3.61 (d, *J* = 8.4 Hz, 1H, CH$\underline{H}$CH), 3.98 (t, *J* = 6.6 Hz, 2H, CH$_2$O), 4.20 (t, *J* = 6.6 Hz, 2H, CH$_2$OCO), 5.13 (dd, *J* = 8.4, 10.2 Hz, 1H, CHHC$\underline{H}$), 6.90 (d, *J* = 9.0 Hz, 2H, Ar), 7.60 (d, *J* = 9.0 Hz, 2H, Ar); ^{13}C NMR (CDCl$_3$): δ = 13.5, 13.9, 18.9, 22.4, 25.8, 28.9, 29.0, 30.3, 31.6, 39.0, 65.6, 68.0, 77.7, 114.5, 120.7, 128.3, 155.5, 160.8, 170.3; IR 2923, 2854, 1737, 1610, 1519, 1456, 1377, 1264, 1210, 1017, 879, 828, 722, 664. Elemental analysis (%) for $C_{21}H_{31}NO_4$ (361.48): calcd. C 69.78, H 8.64, N 3.87; found: C 69.58, H 8.59, N 3.98.

Butyl 3-(4-octyloxyphenyl)-4,5-dihydroisoxazole-5-carboxylate (8b). Yield: 244 mg, 65%; yellow solid; mp 35 ºC. ^{1}H NMR (CDCl$_3$): δ = 0.91 (m, 6H, (CH$_3$)$_2$), 1.38 (m, 12H, (CH$_2$)$_6$), 1.67 (m, 2H, C$\underline{H}_2$CH$_2$OCO), 1.79 (m, 2H, C$\underline{H}_2$CH$_2$O), 3.60 (d, *J* = 9.9 Hz, 1H, C$\underline{H}$HCH), 3.61 (d, *J* = 8.1 Hz, 1H, CH$\underline{H}$CH), 3.98 (t, *J* = 6.6 Hz, 2H, CH$_2$O), 4.20 (t, *J* = 6.6 Hz, 2H, CH$_2$OCO), 5.13 (dd, *J* = 8.1, 9.9 Hz, 1H, CHHC$\underline{H}$), 6.90 (d, *J* = 9.0 Hz, 2H, Ar), 7.60 (d, *J* = 9.0 Hz, 2H, Ar); ^{13}C NMR (CDCl$_3$): δ = 13.5, 14.0, 18.9, 22.5, 25.9, 29.0, 29.1, 29.2, 30.3, 31.7, 39.0, 65.6, 68.0, 77.7, 114.5, 120.6, 128.3, 155.5, 160.8, 170.4; IR 2923, 2854, 1738, 1612, 1519, 1458, 1377, 1264, 1210, 1019, 881, 827, 722, 666. Elemental analysis (%) for $C_{22}H_{33}NO_4$ (375.51): calcd. C 70.37, H 8.86, N 3.73; found C 70.18, H 8.69, N 3.90.

Butyl 3-(4-nonyloxyphenyl)-4,5-dihydroisoxazole-5-carboxylate (8c). Yield: 151 mg, 38%; yellow solid; mp 40 ºC. ^{1}H NMR (CDCl$_3$): δ = 0.91 (m, 6H, (CH$_3$)$_2$), 1.38 (m, 14H, (CH$_2$)$_7$), 1.67 (m, 2H, C$\underline{H}_2$CH$_2$OCO), 1.79 (m, 2H, C$\underline{H}_2$CH$_2$O), 3.60 (d, *J* = 9.9 Hz, 1H, C$\underline{H}$HCH), 3.61 (d, *J* = 8.4 Hz, 1H, CH$\underline{H}$CH), 3.98 (t, *J* = 6.6 Hz, 2H, CH$_2$O), 4.20 (t, *J* = 6.6 Hz, 2H, CH$_2$OCO), 5.13 (dd, *J* = 8.4, 9.9 Hz, 1H, CHHC$\underline{H}$), 6.91 (d, *J* = 9.0 Hz, 2H, Ar), 7.60 (d, *J* = 9.0 Hz, 2H, Ar); ^{13}C NMR (CDCl$_3$): δ = 13.5, 14.0, 18.9, 22.5, 25.8, 29.0, 29.1, 29.2, 29.4, 30.3, 31.7, 39.0, 65.6, 68.0, 77.7, 114.5, 120.7, 128.3, 155.5, 160.8, 170.4; IR 2923, 2854, 1737, 1610, 1517, 1456, 1377, 1264, 1210, 1017, 880, 828, 722, 667. Elemental analysis (%) for $C_{23}H_{35}NO_4$ (389.54): calcd. C 70.92, H 9.06, N 3.60; found C 70.98, H 9.12, N 3.69.

Butyl 3-(4-decyloxyphenyl)-4,5-dihydroisoxazole-5-carboxylate (8d). Yield: 250 mg, 62%; yellow solid; mp 44 ºC. ^{1}H NMR (CDCl$_3$): δ = 0.91 (m, 6H, (CH$_3$)$_2$), 1.38 (m, 16H, (CH$_2$)$_8$), 1.67 (m, 2H, C$\underline{H}_2$CH$_2$OCO), 1.79 (m, 2H, C$\underline{H}_2$CH$_2$O), 3.60 (d, *J* = 10.2 Hz, 1H, C$\underline{H}$HCH), 3.61 (d, *J* = 8.4 Hz, 1H, CH$\underline{H}$CH), 3.98 (t, *J* = 6.6 Hz, 2H, CH$_2$O), 4.20 (t, *J* = 6.6 Hz, 2H, CH$_2$OCO), 5.13 (dd, *J* = 8.4, 10.2 Hz, 1H, CHHC$\underline{H}$), 6.90 (d, *J* = 9.0 Hz, 2H, Ar), 7.60 (d, *J* = 9.0 Hz, 2H, Ar); ^{13}C NMR (CDCl$_3$): δ = 13.5, 14.0, 18.9, 22.5, 25.9, 29.0, 29.1, 29.2, 29.4, 29.5, 30.3, 31.7, 39.0, 65.6, 68.0, 77.7, 114.5, 120.7, 128.3, 155.5, 160.8, 170.3; IR 2923, 2854, 1737, 1611, 1519, 1457, 1377, 1264, 1210, 1018, 879, 829, 722, 667. Elemental analysis (%) for $C_{24}H_{37}NO_4$ (403.56): calcd. C 71.43, H 9.24, N 3.47; found C 71.52, H 9.34, N 3.59.

3-[4-(Heptyloxy)phenyl]-4,5-dihydroisoxazole-5-carboxamide (9a). Yield: 152 mg, 50%; white solid; mp 185 ºC. ^{1}H NMR (CDCl$_3$/DMSO-d$_6$): δ = 0.88 (m, 3H, CH$_3$), 1.39 (m, 8H, (CH$_2$)$_4$), 1.79 (m, 2H, C$\underline{H}_2$CH$_2$O), 3.68 (m, 2H, C$\underline{H}_2$CH), 3.99 (t, *J* = 6.6 Hz, 2H, CH$_2$O), 5.11 (dd, *J* = 6.6, 9.9 Hz, 1H, CH$_2$C$\underline{H}$), 5.57 (s, 1H, N$\underline{H}$H), 6.79 (s, 1H, NH$\underline{H}$), 6.92 (d, *J* = 9.0 Hz, 2H, Ar), 7.59 (d, *J* = 9.0 Hz, 2H, Ar); ^{13}C NMR (CDCl$_3$/DMSO-d$_6$): δ = 12.2, 20.4, 23.8, 26.8, 26.9, 29.6, 65.9, 76.7, 112.8, 119.1, 126.5, 153.9, 158.6, 170.7; IR 3394, 3186, 2925, 2854, 1655, 1610, 1460, 1377, 1255, 1114, 1048, 906, 875, 822, 722, 667. Elemental analysis (%) for $C_{17}H_{24}N_2O_3$ (304.39): calcd. C 67.08, H 7.95, N 9.20; found C 67.06, H 7.89, N 9.30.

3-[4-(Octyloxy)phenyl]-4,5-dihydroisoxazole-5-carboxamide (9b). Yield: 496 mg, 78%; white solid; mp 185 ºC. ^{1}H NMR (CDCl$_3$/DMSO-d$_6$): δ = 0.88 (m, 3H, CH$_3$), 1.37 (m, 10H, (CH$_2$)$_5$), 1.80 (m, 2H, C$\underline{H}_2$CH$_2$O), 3.64 (m, 2H, C$\underline{H}_2$CH), 3.99 (t, *J* = 6.6 Hz, 2H, CH$_2$O), 5.11 (dd, *J* = 6.6, 10.5 Hz, 1H, CH$_2$C$\underline{H}$), 5.58 (s, 1H, N$\underline{H}$H), 6.79 (s, 1H, NH$\underline{H}$), 6.92 (d, *J* = 8.1 Hz, 2H, Ar), 7.59 (d, *J* = 8.1 Hz, 2H, Ar); ^{13}C NMR (CDCl$_3$/DMSO-d$_6$):

δ = 12.1, 20.3, 23.7, 26.8, 26.9, 27.0, 29.5, 65.8, 76.7, 112.7, 119.0, 126.4, 153.4, 158.5, 170.5; IR 3394, 3187, 2924, 2854, 1655, 1610, 1460, 1377, 1256, 1114, 1049, 906, 875, 823, 722, 667. Elemental analysis (%) for $C_{18}H_{26}N_2O_3$ (318.42): calcd. C 67.90, H 8.23, N 8.80; found C 67.92, H 8.16, N 8.85.

3-(4-(Nitrophenyl)-4,5-dihydroisoxazole-5-carboxamide (9g). Yield: 106 mg, 45%; white solid; mp 220 ºC (thermal degradation after isotropic temperature). ^{1}H NMR ($CDCl_3$/DMSO-d_6): δ = 3.67 (m, 2H, C$\underline{H}_2$CH), 5.15 (dd, *J* = 11.4, 6.6 Hz, 1H, CH$_2$C$\underline{H}$), 6.41 (s, 1H, N$\underline{H}$H), 6.84 (s, 1H, NH$\underline{H}$), 7.78 (d, *J* = 9.0 Hz, 2H, Ar), 8.21 (d, *J* = 9.0 Hz, 2H, Ar); ^{13}C NMR ($CDCl_3$/DMSO-d_6): δ = 36.9, 78.4, 122.4, 126.4, 133.5, 146.9, 153.8, 170.7; IR 3310, 3192, 1670, 1578, 1346, 875, 851, 752, 722. Elemental analysis (%) for $C_{10}H_9N_3O_4$ (235.20): calcd. C 51.07, H 3.86, N 17.87; found C 51.12, H 3.89, N 17.94.

3-[4-(Nonyloxy)phenyl]-4,5-dihydroisoxazole-5-carbonitrile (10c). Yield: 136 mg, 43%; white solid; mp 65ºC. ^{1}H NMR ($CDCl_3$): δ = 0.92 (m, 3H, CH$_3$), 1.35 (m, 12H, (CH$_2$)$_6$), 1.80 (m, 2H, C$\underline{H}_2$CH$_2$O), 3.68 (dd, *J* = 16.5, 6.6 Hz, 1H, C$\underline{H}$HCH), 3.75 (dd, *J* = 16.5, 10.2 Hz, 1H, CH$\underline{H}$CH), 3.99 (t, *J* = 6.6 Hz, 2H, CH$_2$O), 5.34 (dd, *J* = 6.6, 10.2 Hz, 1H, CHHC$\underline{H}$), 6.93 (d, *J* = 8.7 Hz, 2H, Ar), 7.59 (d, *J* = 8.7 Hz, 2H, Ar); ^{13}C NMR ($CDCl_3$): δ = 14.0, 22.5, 25.8, 29.0, 29.1, 29.2, 29.4, 31.7, 41.3, 66.2, 68.1, 114.8, 117.2, 119.4, 128.6, 155.8, 161.4; IR 2924, 2853, 1607, 1516, 1461, 1377, 1362, 1257, 1175, 1014, 935, 876, 860, 839, 812, 723, 666. Elemental analysis (%) for $C_{19}H_{26}N_2O_2$ (314.43): calcd. C 72.58, H 8.33, N 8.91; found C 72.51, H 8.58, N 8.94.

3,7a-*bis*(4-Heptyloxyphenyl)-7,7a-dihydro-6*H*-isoxazolo[2,3-*d*][1,2,4]-oxadiazol-6-yl)acetic acid (11a). Yield: 83 mg, 30%; white solid; mp 110-113 ºC. HRMS (ESI): m/z calcd for $[M]^+$ 552.3199, found $[M+1]^+$ 553.3298; $[M+Na]^+$ calcd 575.3097, found 575.3068. EIMS: m/z 233, 135 (100 %), 134, 107, 106, 90, 78. ^{1}H NMR ($CDCl_3$): δ = 0.89 (m, 6H, (CH$_3$)$_2$), 1.38 (m, 16H, (CH$_2$)$_8$), 1.79 (m, 4H, (C$\underline{H}_2$CH$_2$O)$_2$), 2.87 (dd, *J* = 15.6, 7.5 Hz, 1H, NCC$\underline{H}$HCH), 3.05 (dd, *J* = 15.6, 6.0 Hz, 1H, NCCH$\underline{H}$CH), 3.28 (dd, *J* = 16.8, 6.9 Hz, 1H, CHC$\underline{H}$HCO$_2$H), 3.59 (dd, *J* = 16.8, 10.5 Hz, 1H, CHCH$\underline{H}$CO$_2$H), 3.98 (m, 4H, (CH$_2$O)$_2$), 5.17 (m, 1H), 6.89 (d, *J* = 8.4 Hz, 2H, Ar), 6.93 (d, *J* = 8.4 Hz, 2H, Ar), 7.60 (d, *J* = 8,7 Hz, 2H, Ar), 7.85 (d, *J* = 8.7 Hz, 2H, Ar); ^{13}C NMR ($CDCl_3$/DMSO-d_6): δ = 14.0, 22.5, 25.8, 25.9, 28.9, 29.0, 29.1, 31.7, 37.5, 40.4, 68.1, 68.2, 76.3, 114.4, 114.6, 121.3, 122.4, 128.3, 129.5, 156.4, 160.8, 162.7, 166.3, 168.8; IR 3228, 2924, 2854, 1787, 1684, 1608, 1517, 1464, 1377, 1254, 1176, 1098, 1015, 876, 834, 812, 722, 666; Elemental analysis (%) for $C_{32}H_{44}N_2O_6$ (552.71): calcd. C 69.54, H 8.02, N 5.07; found C 68.93, H 8.03, N 4.79.

5-(4-Methylphenyl)-3-(4-octyloxyphenyl)-4,5-dihydroisoxazole (12b). Yield: 220 mg, 60%; white solid; mp 110-113 ºC. ^{1}H NMR ($CDCl_3$): δ = 0.89 (m, 3H, CH$_3$), 1.38 (m, 10H, (CH$_2$)$_5$), 1.80 (m, 2H, C$\underline{H}_2$CH$_2$O), 2.31 (s, 3H, CH$_3$), 3.30 (dd, *J* = 16.6, 7.8 Hz, 1H, C$\underline{H}$HCH), 3.71 (dd, *J* = 16.4, 10.7 Hz, 1H, CH$\underline{H}$CH), 4.0 (t, *J* = 6.4 Hz, 2H, CH$_2$O), 5.60 (dd, *J* = 10.8, 8.0 Hz, 1H, CHHC$\underline{H}$), 6.93 (d, *J* = 8.8 Hz, 2H, Ar), 7.28 (d, *J* = 8.4 Hz, 2H, Ar), 7.32 (d, *J* = 8.6 Hz, 2H, Ar), 7.68 (d, *J* = 8.8 Hz, 2H, Ar); ^{13}C NMR ($CDCl_3$): δ = 14.1, 21.1, 22.6, 25.9, 29.1, 29.2, 29.3, 31.8, 43.3, 68.0, 82.2, 114.5, 121.6, 125.8, 128.1, 129.3, 137.8, 137.9, 155.7, 160.6; IR 2922, 2853, 1904, 1701, 1605, 1515, 1460, 1376, 1255, 1174, 1112, 1044, 1021, 904, 837, 812, 714, 657. Elemental analysis (%) for $C_{24}H_{31}NO_2$ (365.52): calcd. C 78.87, H 8.55, N 3.83; found: C 78.89, H 8.53, N 3.79.

2-Ethynyl-6-(octyloxy)naphtalene (15). Compounds **15** and **16** were synthesized according to reference 23-25. Yield: 1,55 g 69%; white solid; mp 36 ºC. ^{1}H NMR ($CDCl_3$): δ = 0.89 (m, 3H, CH$_3$), 1.40 (m, 10H, (CH$_2$)$_5$), 1.83 (m, 2H, C$\underline{H}_2$CH$_2$O), 3.10 (s, 1H, HCC), 4.04 (t, *J* = 6.6 Hz, 2H, CH$_2$O), 7.07 (d, *J* = 2.4 Hz, 1H, Ar), 7.15 (dd, *J* = 9.0, 2.4 Hz, 1H, Ar), 7.47 (dd, *J* = 8.4, 1.5 Hz, 1H, Ar), 7.65 (m, 2H, Ar), 7.93 (s, 1H, Ar); ^{13}C NMR ($CDCl_3$): δ = 14.1, 22.6, 26.1, 29.1, 29.2, 29.3, 31.8, 68.1, 76.6, 84.2, 106.4, 116.7, 119.7, 126.7, 128.1, 129.0, 129.2, 132.1, 134.4, 157.9; IR 3314, 2904, 2109, 1630, 1602, 1500, 1466, 1377, 1266, 1225, 1173, 1030, 891, 849, 812, 722, 646.

1-Ethynyl-4-(octyloxy)benzene (16).[23-25] Yield: 1,10 g 60%; colorless liquid. ^{1}H NMR ($CDCl_3$): δ = 0.90 (m, 3H, CH$_3$), 1.38 (m, 10H, (CH$_2$)$_5$), 1.77 (m, 2H, C$\underline{H}_2$CH$_2$O), 2.99 (s, 1H, HCC), 3.94 (t, *J* = 6.6 Hz, 2H, CH$_2$O), 6.82 (d, *J* = 8.4 Hz, 2H, Ar), 7.41 (d, *J* = 8.4 Hz, 2H, Ar); ^{13}C NMR ($CDCl_3$): δ = 14.1, 22.6, 26.0, 29.1, 29.2, 29.3, 31.8, 68.1, 75.6, 83.7, 113.9, 114.4, 133.5, 159.5; IR 3318, 2927, 2856, 2108, 1607, 1507, 1469, 1289, 1248, 1170, 1026, 832, 724, 641.

4-Bromophenyl acetate (17b). This compound was prepared according to previous report.[26] Yield: 3,78 g 88%; pale yellow liquid. ^{1}H NMR ($CDCl_3$): δ = 2.29 (s, 3H, CH$_3$), 6.98 (d, *J* = 8.7 Hz, 2H, Ar), 7.48 (d, *J* = 8.7 Hz, 2H, Ar); ^{13}C NMR ($CDCl_3$): δ = 20.9, 118.7, 123.3, 132.3, 149.6, 168.9; IR 1761, 1485, 1369, 1197, 1068, 1013, 908, 843, 794, 710, 674.

4-[(6-Octyloxy-2-naphthyl)ethynyl]phenol (18). This compound was prepared according to reference 27. Yield: 204 mg, 55%; brown solid; mp 126-128 ºC. ^{1}H NMR ($CDCl_3$/DMSO-d_6): δ = 0.89 (m, 3H, CH$_3$), 1.38 (m, 10H, (CH$_2$)$_5$), 1.82 (m, 2H, C$\underline{H}_2$CH$_2$O), 4.06 (t, *J* = 6.3 Hz, 2H, CH$_2$O), 6.84 (d, *J* = 8.1 Hz, 2H, Ar), 7.12 (m, 2H, Ar), 7.40 (d, *J* = 8.1 Hz, 2H, Ar), 7.50 (d, *J* = 8.4 Hz, 1H, Ar), 7.64 (d, *J* = 8.4 Hz, 1H, Ar), 7.68 (d, *J* = 9.0 Hz, 1H, Ar), 7.91 (s, 1H, Ar); ^{13}C NMR ($CDCl_3$/DMSO-d_6): δ = 13.9, 22.5, 25.9, 29.0, 29.1, 29.2, 31.6, 67.9, 87.9, 89.3, 106.4, 113.9, 115.6, 118.3, 119.4, 126.5, 128.2, 128.7, 128.9, 130.5, 132.9, 133.7, 157.3, 157.5; IR 2925, 2855, 1727, 1466, 1377, 1251, 1182, 898, 876, 829, 721, 666.

4-[(6-Octyloxy-2-naphthyl)ethynyl]phenyl 3-(4-heptyloxyphenyl)-4,5-dihydroisoxazole-5-carboxylate (19). Compounds **19**, **21** and **23** were prepared according to protocol reaction DCC/DMAP/DCM following the experimental procedure described in reference 28. Yield: 115 mg, 70%; white solid; mp 144.5 ºC. ^{1}H NMR ($CDCl_3$): δ = 0.88 (m, 6H, (CH$_3$)$_2$), 1.38 (m, 18H, (CH$_2$)$_9$), 1.82 (m, 4H, (C$\underline{H}_2$CH$_2$O)$_2$), 3.75 (m, 2H, C$\underline{H}_2$CH), 3.98 (t, *J* = 6.6 Hz, 2H, CH$_2$O), 4.07 (t, *J* = 6.6 Hz, 2H, CH$_2$O), 5.37 (dd, *J* = 7.2, 11.1 Hz, 1H, CH$_2$C$\underline{H}$), 6.92 (d, *J* = 8.7 Hz, 2H, Ar), 7.14 (m, 4H, Ar), 7.50 - 7.72 (m, 7H, Ar), 7.96 (s, 1H, Ar); ^{13}C NMR ($CDCl_3$): δ = 14.0, 14.1, 22.5, 22.6, 25.9, 26.1, 28.9, 29.0, 29.1, 29.2, 29.3, 31.7, 31.8, 39.2, 68.0, 68.1, 77.7, 87.9, 90.4, 106.5, 114.7, 117.6, 119.7, 120.5, 121.3, 121.6, 126.8, 128.3, 128.5, 128.8, 129.2, 131.3, 132.7, 134.2, 149.9, 155.6, 157.9, 161.0, 168.5; IR 2924, 2854, 1763, 1596, 1464, 1378, 1224, 1045, 897, 859, 818, 722, 666. Elemental analysis (%) for $C_{43}H_{49}NO_5$ (659.85): calcd. C 78.27, H 7.48, N 2.12; found C 78.48, H 7.58, N 2.07.

[3-(4-Heptyloxyphenyl)4,5-dihydroisoxazol-5-yl]methyl 4-[(octyloxy phenyl)ethynyl]benzoate (21). Yield: 63,0 mg, 40%; orange solid; mp 138.4 ºC. ^{1}H NMR ($CDCl_3$): δ = 0.89 (m, 6H, (CH$_3$)$_2$), 1.38 (m, 18H, (CH$_2$)$_9$), 1.79 (m, 4H, (C$\underline{H}_2$CH$_2$O)$_2$), 3.24 (dd, *J* = 16.5, 6.6 Hz, 1H, N=CC$\underline{H}$HCH), 3.52 (dd, *J* = 16.5, 10.5 Hz, 1H, N=CCH$\underline{H}$CH), 3.98 (m, 4H, (CH$_2$O)$_2$), 4.43 (dd, *J* = 12.0, 5.4 Hz, 1H, CHC$\underline{H}$HOCO), 4.50 (dd, *J* = 12.0, 4.2 Hz, 1H, CHCH$\underline{H}$OCO), 5.08 (m, 1H), 6.87 (d, *J* = 9.0 Hz, 2H, Ar), 6.92 (d, *J* = 8.7 Hz, 2H, Ar), 7.45 (d, *J* = 9.0 Hz, 2H, Ar), 7.51 (d, *J* = 8.4 Hz, 2H, Ar), 7.62 (d, *J* = 9.0 Hz, 2H, Ar), 7.97 (d, *J* = 8.4 Hz, 2H, Ar); ^{13}C NMR ($CDCl_3$): δ = 14.0, 22.5, 22.6, 25.8, 25.9, 28.9, 29.0, 29.1, 29.3, 31.6, 31.7, 37.5, 65.7, 68.0, 77.8, 87.3, 92.9, 114.3, 114.5, 114.6, 121.3, 128.1, 128.3, 128.6, 129.6, 131.2, 133.1, 155.8, 159.6, 160.7, 165.7; IR 2924, 2855, 1723, 1600, 1517, 1465, 1377, 1286, 1251, 1177, 1108, 1045, 890, 834, 765, 721, 695, 666. Elemental analysis (%) for $C_{40}H_{49}NO_5$ (623.82): calcd. C 77.01, H 7.92, N 2.25; found C 76.96, H 8.07, N 2.14.

[3-(4-Heptyloxyphenyl)4,5-dihydroisoxazol-5-yl]methyl 4-decyloxyben-zoate (23). Yield: 83,0 mg, 60%; white solid; mp 102.5 ºC. ^{1}H NMR ($CDCl_3$): δ = 0.89 (m, 6H, (CH$_3$)$_2$), 1.38 (m, 22H, (CH$_2$)$_{11}$), 1.79 (m, 4H, (C$\underline{H}_2$CH$_2$O)$_2$), 3.22 (dd, *J* = 16.5, 6.9 Hz, 1H, N=CC$\underline{H}$HCH), 3.49 (dd, *J* = 16.5, 10.8 Hz, 1H, N=CCH$\underline{H}$CH), 3.98 (t, *J* = 6.6 Hz, 4H, (CH$_2$O)$_2$), 4.44 (m, 2H, CHC$\underline{H}_2$OCO), 5.06 (m, 1H), 6.85 (d, *J* = 8.7 Hz, 2H, Ar), 6.91 (d, *J* = 8.4 Hz, 2H, Ar), 7.61 (d, *J* = 8.7 Hz, 2H, Ar), 7.95 (d, *J* = 9.0 Hz, 2H, Ar); ^{13}C NMR ($CDCl_3$): δ = 14.0, 14.1, 22.5, 22.6, 25.9, 28.9, 29.0, 29.1,

29.2, 29.3, 29.5, 31.7, 31.8, 37.6, 65.2, 68.0, 68.1, 78.0, 114.0, 114.6, 121.5, 121.6, 128.2, 131.7, 155.8, 160.7, 163.1, 166.0; IR 2924, 2854, 1715, 1606, 1510, 1466, 1377, 1249, 1169, 1127, 1014, 882, 834, 768, 722, 699, 666, 649. Elemental analysis (%) for $C_{34}H_{49}NO_5$ (551.76): calcd. C 74.01, H 8.95, N 2.54; found C 74.15, H 9.13, N 2.54.

3-(4-Octyloxyphenyl)-5-(4-methylphenyl)isoxazole (24). This compound was prepared according to previous report.[30] Yield: 131 mg, 90%; white solid; mp 105.9 ºC. ^{1}H NMR ($CDCl_3$): δ = 0.89 (m, 3H, CH_3), 1.38 (m, 10H, $(CH_2)_5$), 1.80 (m, 2H, $C\underline{H}_2CH_2O$), 2.41 (s, 3H, CH_3), 4.00 (t, *J* = 6.6 Hz, 2H, CH_2O), 6.72 (s, 1H), 6.97 (d, *J* = 8.7 Hz, 2H, Ar), 7.28 (d, *J* = 8.1 Hz, 2H, Ar), 7.72 (d, *J* = 8.1 Hz, 2H, Ar), 7.78 (d, *J* = 8.7 Hz, 2H, Ar); ^{13}C NMR ($CDCl_3$): δ = 14.1, 21.5, 22.6, 26.0, 29.1, 29.2, 29.3, 31.8, 68.1, 96.7, 114.8, 121.5, 124.9, 125.7, 128.1, 129.6, 140.4, 160.6, 162.6, 170.3; IR 2924, 2854, 1618, 1464, 1377, 1270, 1180, 951, 875, 837, 807, 722, 666. Elemental analysis (%) for $C_{24}H_{29}NO_2$ (363.50): calcd. C 79.30, H 8.04, N 3.85; found C 79.24, H 8.09, N 3.80.

Supporting Information (see also the footnote on the first page of this article): Spectral and analytical data on isolated products, including ^{1}H, ^{13}C NMR, IR, DSC and polarizing optical micrographs of the texture of the LCs, are supplied.

Acknowledgments

This work was supported by the Conselho Nacional de Desenvolvimento Científico e Tecnológico (project MCT/CNPq nº 555785/2006-8) and the Coordenação de Aperfeiçoamento de Pessoal de Nível Superior (CAPES) for a fellowship.

[1] a) S. Kobayashi, K. A. Jorgensen, *Cycloaddition Reactions in Organic Synthesis*, Wiley-VCH, Weinheim, **2002**. b) K. V. Gothelf, K. A. Jorgensen, *Chem. Rev.* **1998**, *98*, 863-909. c) A. Padwa, W. H. Pearson, *The Chemistry of Heterocyclic Compounds: Synthetic Applications of 1,3-Dipolar Cycloaddition Chemistry Toward Heterocycles and Natural Products*, John Wiley & Sons, New York, **2002**, vol. 59. d) K. B. G. Torssell, *Nitrile Oxides, Nitrones and Nitronates in Organic Synthesis*, VCH, New York, **1988**. e) R. Huisgen, *J. Org. Chem*. **1976**, *41*, 403-419. f) K. N. Houk, J. Sims, R. E. Duke, R. W. Strozier, J. K. George, *J. Am. Chem. Soc.* **1973**, *95*, 7287-7301 g) A. Ros, E. Alvarez, H. Dietrich, R. Fernández, J. M. Lassaletta, *Synlett* **2005**, 2899-2904. h) H. Yamamoto, S. Hayashi, M. Kubo, M. Harada, M. Hasegawa, M. Noguchi, M. Sumimoto, K. Hori, *Eur. J. Org. Chem*. **2007**, 2859-2864.

[2] a) P. A. Kozikowski, *Acc. Chem. Res*. **1984**, *17*, 410-416. b) J. A. Bull, E. P. Balskus, R. A. J. Horan, M. Langner, S. V. Ley, *Angew. Chem. Int. Ed*. **2006**, *45*, 6714-6718.

[3] a) P. Conti, C. Dallanoce, M. De Amici, C. De Micheli, K.-N. Klotz, *Bioorg. Med. Chem*. **1998**, 6, 401-408. b) L.-H. Zhang, J. C. Chung, T. D. Costello, I. Valvis, P. Ma, S. Kauffman, R. Ward, R. *J. Org. Chem*. **1997**, *62*, 2466-2470. c) N. Zanatta, J. M. F. M. Schneider, P. H. Schneider, A. D. Wouters, H. G. Bonacorso, M. A. P. Martins, L. A. Wessjohann, *J. Org. Chem*. **2006**, *71*, 6996-6998.

[4] a) D.-H. Ko, M. F. Maponya, M. A. Khalil, E. T. Oriaku, Z. You, H. Lee, *J. Med. Chem. Res*. **1998**, *8*, 313-323. b. J. Wityak, T. M. Sielecki, D. J. Pinto, G. Emmett, J. Y. Sze, J. Liu, A. E. Tobin, S. Wang, B. Jiang, P. Ma, S. A. Mousa, R. R. Wexler, R. E. Olson, *J. Med. Chem.* **1997**, *40*, 50-60.

[5] a) P. J. Zimmermann, J. Y. Lee, I. Hlobilova, R. Endermann, D. Habich, V. Jager, *Eur. J. Org. Chem*. **2005**, 3450-3460. b) S. A. Mousa, J. Wityak, *Cardiovascular Drug Reviews* **1998**, *16*, 48-61.

[6] V. Jäger, W. Schwab, *Tetrahedron Lett*. **1978**, *34*, 3129-3132.

[7] K. P. Park, C.-Y. Shiue, L. B. Clapp, *J. Org. Chem.* **1970**, *35*, 2065-2067.

[8] a) P. Aschwanden, L. Kvaerno, R. W. Geisser, F. Kleinbeck, E. M. Carreira, *Org. Lett*. **2005**, *7*, 5741-5742. b) J. W. Bode, E. M. Carreira, *Org. Lett*. **2001**, *3*, 1587-1590.

[9] a) A. A. Fuller, B. Chen, A. R. Minter, A. K. Mapp, *J. Am. Chem. Soc*. **2005**, *127*, 5376-5383. b) J. A. Kenar, *J. Am. Oil Chem. Soc.* **2002**, *79*, 351-356.

[10] a) V. Kumar, R. Aggarwal, S. P. Singh, *J. Fluorine Chem*. **2006**, *127*, 880-888 b) M. Tanaka, T. Haino, K. Ideta, K. Kubo, A. Mori, Y. Fukazawa, *Tetrahedron* **2007**, *63*, 652-665. c) C. K. Y. Lee, A. J. Herlt, G. W. Simpson, A. C. Willis, C. J. Easton, *J. Org. Chem.* **2006**, *71*, 3221-3231. d) F. Machetti, L. Cecchi, E. Trogu, F. De Sarlo, *Eur. J. Org. Chem*. **2007**, 4352-4359. e) H. A. Gallardo, R. Cristiano, F. Ely, *Liq. Cryst*. **2005**, *32*, 15-25. f) H. A. Gallardo, R. Cristiano, A. A. Vieira, R. A. W. Neves Filho, R. M. Srivastava, *Synthesis*, **2008**, 605-609. g) H. A. Gallardo, R. Cristiano, F. Ely, *Liq. Cryst*. **2006**, *33*, 381-390.

[11] C. K. Y. Lee, A. B. Holmes, B. Al-Duri, G. A. Leeke, R. C. D. Santos, J. P. K. Seville, *Chem. Commun.* **2004**, *22*, 2622-2623.

[12] To regioselective copper(I)-catalyzed cycloaddition reaction, see T. V. Hansen, P. Wu, V. V. Fokin, *J. Org. Chem.* **2005**, *70*, 7761-7764.

[13] a) J. A. Passo, G. D. Vilela, P. H. Schneider, O. M. S. Ritter, A. A. Merlo, *Liq. Cryst*. **2008**, *35*, 833-840. b) V. N. Kovganko, N. N. Kovganko, *Russian J. Org. Chem*. **2006**, *42*, 696-700. c) O. M. S. Ritter, F. C. Giacomelli, J. A. Passo, N. P. Silveira, A. A. Merlo, *Polymer Bull.* **2006**, *56*, 549-561. d) U. M. Kauhanka, M. M. Kauhanka, *Liq. Cryst.* **2006**, *33*, 121-127. e) K. B. Umesha, K. M. L. Raí, N. Mahadeva, *Indian J. Chem. Sec B – Org. Chem. Including Med. Chem*. **2004**, *43*, 2635-2640. f) V. Bezborodov, N. Kauhanka, V. Lapanik, *Mol. Cryst. Liq. Cryst*. **2004**, *411*, 1145-1152. g) V. N, Kovganko, N. N. Kovganko, *Russian J. Org. Chem*. **2005**, *41*, 1165-1169. h) M. Tanaka, T. Haino, K. Ideta, K. Kubo, A. Mori, Y. Fukuzawa, *Tetrahedron*, **2007**, *63*, 652-665.

[14] J. B. Stothers, *Carbon-13 NMR Spectroscopy.* Academic Press, New York, **1972**.

[15] a) M. S. Gordon, S. A. Sojka, J. G. Krause, *J. Org. Chem*. **1984**, *49*, 97-100. b) N. A. Owston, A. J. Parker, J. M. J. Williams, *Org. Lett*. **2007**, *9*, 3599-3601. c) A. Danoff, M. Franzen-Sieveking, R. L. Lichter, S. N. Y. Fanso-Free, *Org. Mag. Ress.* **1979**, *12*, 83-86. d) B. A. Halkier, C. E. Olsens, B. L. Moller, *J. Biol. Chem*. **1989**, *264*, 19487-19494. e) G. C. Levy, R. L. Lichter, G. L. Nelson, *Carbon-13 Nuclear Magnetic Resonance Spectroscopy,* Wiley-Interscience, New York, **1980**. f) J. Esteban, A. M. Costa, F. Urpí, J. Vilarrasa, *Tetrahedron Lett*. **2004**, *45*, 5563-5567.

[16] G. J. Karabatsos, R. A. Taller, F. M. Vane, *J. Am. Chem. Soc*. **1963**, *85*, 2326-2327.

[17] G. Heinisch, W. Holzer, *Tetrahedron Lett.* **1990**, *31*, 3109-3112.

[18] M. De Rosa, K. Brown, M. McCoy, K. Ong, K. Sanford, *J. Chem. Soc. Perkin Trans. 1*, **1993**, 1787-1790.

[19] B. C. Gunn, M. F. G. Stevens, *J. Chem. Soc. Perkin Trans. 1*, **1973**, 1682-1688.

[20] L. J. Kateley, W. B. Martin, D. C. Wiser, C. A. Brummond, *J. Chem. Edu.* **2002**, *79*, 225-227.

[21] a) F. A. C. Andrade, *J. Braz. Chem. Soc*. **1998**, *9*, 85-86. b) A. A. Merlo, O. M. S. Ritter, F. V. Pereira, C. H. Vieira, N. P. Silveira, *J. Braz. Chem. Soc*. **2001**, *12*, 184-191.

[22] a) J.-P. Gilbert, R. Jacquier, C. Pétrus, *Bull. Soc. Chem. France* **1979**, II-281-288. b) J.-F. Wang, D.-Q. Wei, C.-F. Wang, Y. Ye, Y.-X. Li, Y. Luo, W.-W. Wang, L.-Z. Liu, Y.-F. Zhao, *J. of Theoretical and Computational Chem*. **2007**, *6*, 861-867. c) We have synthesized four compounds **11a-d**. All compounds displayed the same spectral data. A complete thermal study of the LC properties of this class the compounds are under analysis and will be reported soon.

[23] a) U. B. Vasconcelos, E. Dalmolin, A. A. Merlo, *Org. Lett*. **2005**, *7*, 1027-1030. b) U. B. Vasconcelos, A. A. Merlo, *Synthesis* **2006**, *7*, 1141-1147. c) U. B. Vasconcelos, G. D. Vilela, A. Schrader, A. C. A. Borges, A. A. Merlo, *Tetrahedron*. **2008**, *64*, 4619-4626.

[24] a) K. Sonogashira, Y. Tohda, N. Hagihara, *Tetrahedron Lett*. **1975**, *16*, 4467-4470. b) R. Chinchilla, C. Nájera, *Chem. Rev*. **2007**, *107*, 874-922. c) R. Cristiano, D. M. P. O. Santos, G. Conte, H. Gallardo, *Liq. Cryst.* **2006**, *33*, 997-1003. d) D. M. Price, S. M. Dirk, F. Maya, J. M. Tour, *Tetrahedron* **2003**, *59*, 2497-2518.

[25] A. P. Melissaris, M. H. Litt, *Macromolecules* **1994**, *27*, 883-887.

[26] B. Neises, W. Steglich, *Angew. Chem., Int. Ed. Engl.* **1978**, *17*, 569-583.

[27] S. Takahashi, Y. Kuroyama, K. Sonogashira, N. Hagihara, *Synthesis* **1980**, 627-630.

[28] B. Neises, W. Steglich, *Angew. Chem., Int. Ed. Engl.* **1978**, *17*, 522-524.

[29] N. Gimeno, M. B. Ros, M. R. De la Fuente, J. L. Serrano, *Chem. Mater.* **2008,** *20*, 1262-1271.

[30] a) R. J. K. Taylor, M. Reid, J. Foot, S. A. Raw, *Acc. Chem. Res.* **2005**, *38*, 851-869. b) R. M. Srivastava, A. A. Lima, O. S. Viana, M. J. C. Silva, M. T. J. A. Catanho, J. O. F. Morais, *Bioorganic & Medicinal Chemistry* **2003**, *11*, 1821-1827.

[31] a) G. W. Gray, J. W. Goodby, *Smectic Liquid Crystals: Textures and Structures*, Leonard Hill, Glasgow and London, **1984**. b) L. Li, C. D. Jones, J. Magolan, R. P. Lemieux, *J. Mat. Chem.* **2007**, *17*, 2313-2318.

[32] C. Weygand, R. Gabler, *J. Prakt Chem.* **1940**, *155*, 332-341.

[33] K.-C. Liu, B. R. Shelton, R. K. Howe, *J. Org. Chem.* **1980**, *45*, 3916-3918.

[34] R. F. Collins, *J. Pharm. Pharmacol*. **1962**, *14*, 48-58.

[35] A. V. Narsaiah, *Advanced Synthesis & Catalysis* **2004**, *11*, 1271-1274.

[36] L. Field, P. B. Hughmark, S. H. Shumaker, W. S. Marshall, *J. Am. Chem. Soc*. **1961**, *83*, 1983-1987.

SUPPORTING INFORMATION - CAPÍTULO 5.1

3,5-Disubstituted Isoxazolines as Potential Molecular Kits for Liquid-crystalline Materials

*Aline Tavares, Paulo H. Schneider and Aloir A. Merlo**

Instituto de Química, UFRGS, Av. Bento Gonçalves, 9500 - 91501-970, Porto Alegre-RS, Brasil

Experimental Section.

Alkylation reactions.[1] To 80 mL CH_3CN and 4-hydroxybenzaldehyde (42 mmol) was added potassium hydroxide (46 mmol). The solution was stirred at room temperature for 1h and then the bromoalkanes (46 mmol) corresponding were added. The reaction mixture was refluxed for 4 h and the precipitate was filtered off. The filtrate was evaporated in vacuum and purified by distillation under a reduced pressure. All the aldehydes were obtained as pale yellow viscous liquids.

4-(Heptyloxy)benzaldehyde (2a). Yield: 9,10 g, 90%; bp 139 ^oC (0.5 mmHg) (lit.[2] bp 162-164 ^oC). ^1H NMR ($CDCl_3$): δ = 0.90 (m, 3H, CH_3), 1.42 (m, 8H, $(CH_2)_4$), 1.84 (m, 2H, $C\underline{H}_2CH_2O$), 4.04 (t, *J* = 6.6 Hz, 2H, CH_2O), 6.99 (d, *J* = 8.7 Hz, 2H, Ar), 7.82 (d, *J* = 8.7 Hz, 2H, Ar), 9.87 (s, 1H, CHO); ^{13}C NMR ($CDCl_3$): δ = 13.9, 22.4, 25.8, 28.8, 28.9, 31.6, 68.3, 114.6, 129.5, 131.9, 164.2, 190.9; IR 2930, 2858, 2802, 2736, 1693, 1602, 1510, 1259, 1018, 833, 724, 665.

4-(Octyloxy)benzaldehyde (2b). Yield: 7,10 g, 72%; bp 158 ^oC (0.5 mmHg) (lit.[2] bp 162-163 ^oC). ^1H NMR ($CDCl_3$): δ = 0.89 (m, 3H, CH_3), 1.42 (m, 10H, $(CH_2)_5$), 1.82 (m, 2H, $C\underline{H}_2CH_2O$), 4.04 (t, *J* = 6.6 Hz, 2H, CH_2O), 6.99 (d, *J* = 8.7 Hz, 2H, Ar), 7.83 (, *J* = 8.7 Hz d, 2H, Ar), 9.87 (s, 1H, CHO); ^{13}C NMR ($CDCl_3$): δ = 14.0, 22.6, 25.8, 28.9, 29.1, 29.2, 31.7, 68.3, 114.6, 129.4, 131.8, 164.2, 191.0; IR 2931, 2858, 2802, 2735, 1694, 1602, 1509, 1259, 1017, 834, 726, 665.

4-(Nonyloxy)benzaldehyde (2c). Yield: 8,4 g 80%; bp 175 ^oC (0.5 mmHg) (lit.[2] bp 181-183 ^oC). ^1H NMR ($CDCl_3$): δ = 0.89 (m, 3H, CH_3), 1.42 (m, 12H, $(CH_2)_6$), 1.81 (m, 2H, $C\underline{H}_2CH_2O$), 4.03 (t, *J* = 6.6 Hz, 2H, CH_2O), 6.99 (d, *J* = 8.7 Hz, 2H, Ar), 7.82 (d, *J* = 8.7 Hz, 2H, Ar), 9.86 (s, 1H, CHO); ^{13}C NMR ($CDCl_3$): δ = 13.9, 22.3, 25.6, 28.7, 28.9, 29.0, 29.1, 31.5, 68.0, 114.4, 129.3, 131.6, 163.9, 190.5; IR 2930, 2859, 2802, 2734, 1694, 1602, 1508, 1259, 1016, 833, 724, 665.

4-(Decyloxy)benzaldehyde (2d). Yield: 7,70 g, 70%; bp 184-186 ^oC (0.5 mmHg). ^1H NMR ($CDCl_3$): δ = 0.89 (m, 3H, CH_3), 1.42 (m, 14H, $(CH_2)_7$), 1.81 (m, 2H, $C\underline{H}_2CH_2O$), 4.04 (t, *J* = 6.6 Hz, 2H, CH_2O), 6.98 (d, *J* = 8.7 Hz, 2H, Ar), 7.83 (d, *J* = 8.7 Hz, 2H, Ar), 9.87 (s, 1H, CHO); ^{13}C NMR ($CDCl_3$): δ = 14.0, 22.6, 25.9, 28.9, 29.2, 29.3, 29.4, 29.5, 31.8, 68.3, 114.6, 129.7, 131.9, 164.2, 190.7; IR 2930, 2858, 2802, 2734, 1694, 1602, 1510, 1259, 1015, 835, 724, 665.

Synthesis of aldoximes.[3] To a corresponding alkylated product (23 mmol) and hydroxylamine hydrochloride (68 mmol) was added 40 mL of ethanol. The reaction mixture was stirred for

[1] U. B. Vasconcelos, A. A. Merlo, *Synthesis* **2006**, *7*, 1141-1147.
[2] C. Weygand, R. Gabler, *J. Prakt Chem.* **1940**, *155*, 332-341.
[3] K.-C. Liu, B. R. Shelton, R. K. Howe, *J. Org. Chem.* **1980**, *45*, 3916-3918.

10 minutes and then sodium acetate (90 mmol) in water (20 mL) was added. The mixture was heated at reflux during 1 hour. The reaction mixture was cooled and the white crystals were filtered off, washed with 50 mL of EtOH/H_2O mixture (15:35 mL) and dried under a reduced pressure.

(*E*)-4-(Heptyloxy)benzaldehyde oxime (3a). Yield: 2,20g, 93%; white solid; mp 54 °C. ^{1}H NMR ($CDCl_3$): δ = 0.89 (m, 3H, CH_3), 1.38 (m, 8H, $(CH_2)_4$), 1.79 (m, 2H, C$\underline{H}_2$CH_2O), 3.97 (t, *J* = 6.6 Hz, 2H, CH_2O), 6.89 (m, 2H (*E*-isomer), 2H (*Z*-isomer), Ar), 7.31 (s, 1H, C$\underline{H}$NOH (*Z*-isomer)), 7.50 (d, *J* = 8.7 Hz, 2H, Ar), 7.92 (d, *J* = 8.7 Hz, 2H, Ar (*Z*-isomer)), 8.09 (s, 1H, C$\underline{H}$NOH), 9.15 (b, 1H, OH); ^{13}C NMR ($CDCl_3$): δ = 13.9, 22.4, 25.7, 28.8, 28.9, 31.5, 67.7 (*Z*-isomer), 67.8, 114.4 (*Z*-isomer), 114.8, 124.0 (*Z*-isomer), 125.3, 128.5, 132.9 (*Z*-isomer), 146.0 (*Z*-isomer), 149.5, 160.2 (*Z*-isomer), 160.6; IR 3246, 2922, 2854, 1607, 1463, 1377, 1253, 951, 876, 836, 721, 666.

(*E*)-4-(Octyloxy)benzaldehyde oxime (3b). Yield: 1,80 g, 75%; white solid; mp 67 °C (lit.[4] mp 81-83 °C). ^{1}H NMR ($CDCl_3$): δ = 0.88 (m, 3H, CH_3), 1.35 (m, 10H, $(CH_2)_5$), 1.78 (m, 2H, C$\underline{H}_2$CH_2O), 3.97 (t, *J* = 6.6 Hz, 2H, CH_2O), 6.89 (m, 2H (*E*-isomer), 2H (*Z*-isomer), Ar), 7.31 (s, 1H, C$\underline{H}$NOH (*Z*-isomer)), 7.50 (d, *J* = 8.7 Hz, 2H, Ar), 7.93 (d, *J* = 8.7 Hz, 2H, Ar (*Z*-isomer)), 8.09 (s, 1H, C$\underline{H}$NOH), 8.75 (b, 1H, OH); ^{13}C NMR ($CDCl_3$): δ = 14.0, 22.6, 25.9, 29.1, 29.2, 29.3, 31.8, 67.7 (*Z*-isomer), 67.8, 114.4 (*Z*-isomer), 114.7, 123.9 (*Z*-isomer), 125.3, 128.1, 132.5 (*Z*-isomer), 145.9 (*Z*-isomer), 149.9, 160.3 (*Z*-isomer), 160.6; IR 3246, 2923, 2854, 1607, 1464, 1374, 1253, 953, 876, 835, 722, 666.

(*E*)-4-(Nonyloxy)benzaldehyde oxime (3c). Yield: 2,20g, 86%; white solid; mp 80 °C. ^{1}H NMR ($CDCl_3$): δ = 0.88 (m, 3H, CH_3), 1.35 (m, 12H, $(CH_2)_6$), 1.78 (m, 2H, C$\underline{H}_2$CH_2O), 3.97 (t, *J* = 6.6 Hz, 2H, CH_2O), 6.89 (m, 2H (*E*-isomer), 2H (*Z*-isomer), Ar), 7.31 (s, 1H, C$\underline{H}$NOH (*Z*-isomer)), 7.50 (d, *J* = 8.7 Hz, 2H, Ar), 7.93 (d, *J* = 8.7 Hz, 2H, Ar (*Z*-isomer)), 8.09 (s, 1H, C$\underline{H}$NOH), 8.54 (b, 1H, OH); ^{13}C NMR ($CDCl_3$): δ = 14.1, 22.6, 25.9, 29.1, 29.2, 29.3, 29.4, 31.8, 68.0 (*Z*-isomer), 68.1, 114.5 (*Z*-isomer), 114.8, 123.9 (*Z*-isomer), 125.5, 128.5, 132.9 (*Z*-isomer), 146.0 (*Z*-isomer), 150.0, 160.3 (*Z*-isomer), 160.6; IR 3246, 2922, 2853, 1607, 1463, 1377, 1253, 951, 876, 834, 722, 666.

(*E*)-4-(Decyloxy)benzaldehyde oxime (3d). Yield: 2,1g, 73%; white solid; mp 55 °C. ^{1}H NMR ($CDCl_3$): δ = 0.88 (m, 3H, CH_3), 1.35 (m, 14H, $(CH_2)_7$), 1.79 (m, 2H, C$\underline{H}_2$CH_2O), 3.97 (t, *J* = 6.6 Hz, 2H, CH_2O), 6.89 (m, 2H (*E*-isomer), 2H (*Z*-isomer), Ar), 7.30 (s, 1H, C$\underline{H}$NOH (*Z*-isomer)), 7.49 (d, *J* = 8.7 Hz, 2H, Ar), 7.92 (d, *J* = 8.7 Hz, 2H, Ar (*Z*-isomer)), 8.09 (s, 1H, C$\underline{H}$NOH); ^{13}C NMR ($CDCl_3$/DMSO-d_6): δ = 13.9, 22.4, 25.9, 29.1, 29.2, 29.3, 29.4, 29.5, 31.5, 67.6 (*Z*-isomer), 67.7, 114.4 (*Z*-isomer), 114.7, 124.0 (*Z*-isomer), 125.5, 128.3, 132.7 (*Z*-isomer), 146.0 (*Z*-isomer), 149.9, 160.1 (*Z*-isomer), 160.5; IR 3246, 2921, 2854, 1607, 1463, 1377, 1255, 953, 874, 835, 722, 666.

[4] R. F. Collins, *J. Pharm. Pharmacol*. **1962**, *14*, 48-58.

4-Bromobenzaldehyde oxime (4e). Yield: 2,80 g, 47%; white solid; mp 112 °C (lit.[5] mp 110-112 °C). ^{1}H NMR ($CDCl_3$): δ = 7.47 (m, 4H, Ar), 8.07 (s, 1H, CHNOH), 10.50 (s, 1H, OH); ^{13}C NMR ($CDCl_3$): δ = 124.6, 128.7, 131.0, 132.3, 149.7; IR 3295, 1588, 1489, 1317, 1210, 1068, 971, 873, 819.

4-Cyanobenzaldehyde oxime (4f). Yield: 2,60 g, 60%; yellow solid; mp 174 °C (thermal degradation after isotropic temperature - lit.[6] mp 174-176 °C). ^{1}H NMR ($CDCl_3$/DMSO-d_6): δ = 7.58 (d, *J* = 8.4 Hz, 2H, Ar), 7.67 (d, *J* = 8.4 Hz, 2H, Ar); 8.11 (s, 1H, CHNOH), 9.66 (b, 1H, OH).

4-Nitrobenzaldehyde oxime (4g). Yield: 3,25g, 98%; mp 128 °C (lit.[7] mp 132-133 °C). ^{1}H NMR ($CDCl_3$): δ = 7.76 (d, *J* = 9.0 Hz, 2H, Ar), 8.11 (s, 1H, OH), 8.21 (s, 1H, CHNOH), 8.25 (d, *J* = 9.0 Hz, 2H, Ar); ^{13}C NMR ($CDCl_3$/DMSO-d_6) δ 123.6, 127.1, 139.0, 146.8, 147.7; IR 3305, 1606, 1538, 1350, 968, 845, 749.

Table of Contents

[5] A. V. Narsaiah, *Advanced Synthesis & Catalysis* **2004**, *11*, 1271-1274.
[6] L.-H. Zhang, J. C. Chung, T. D. Costello, I. Valvis, P. Ma, S. Kauffman, R. Ward, R. *J. Org. Chem*. **1997**, *62,* 2466-2470.
[7] L. Field, P. B. Hughmark, S. H. Shumaker, W. S. Marshall, *J. Am. Chem. Soc.* **1961**, *83*, 1983-1987.

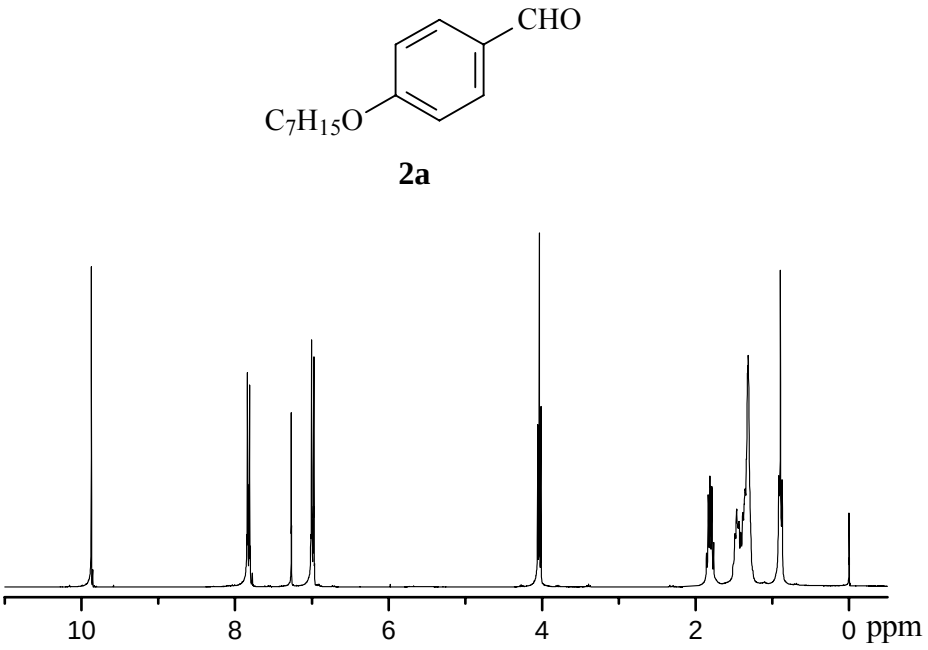

Figure S1. ^{1}H NMR spectrum of compound **2a** ($CDCl_3$, 300 MHz).

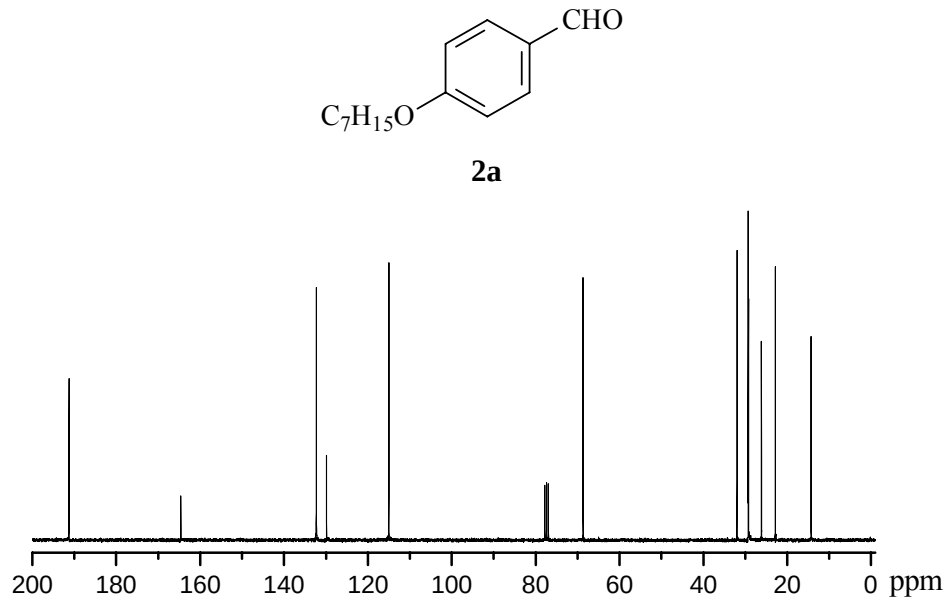

Figure S2. ^{13}C NMR spectrum of compound **2a** ($CDCl_3$, 75 MHz).

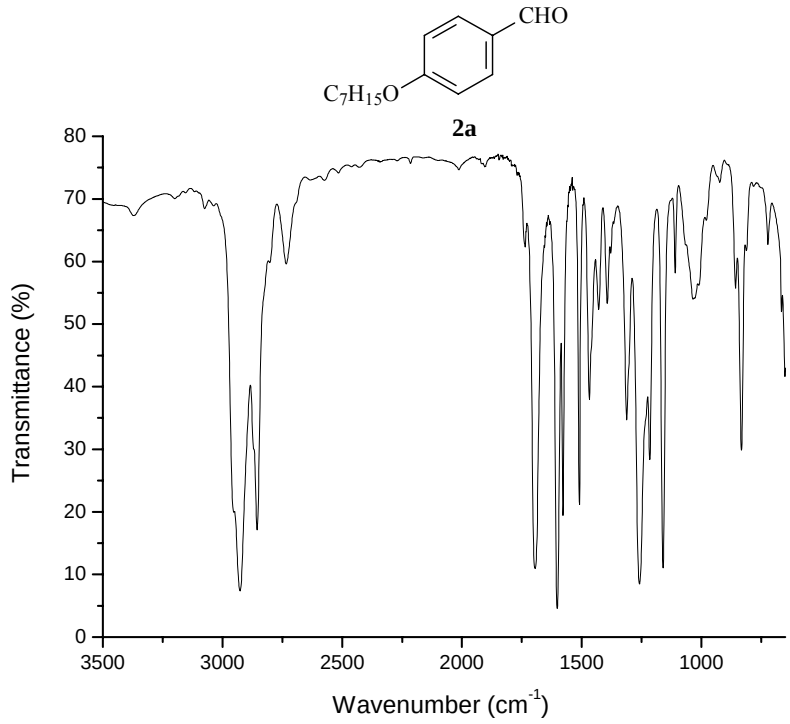

Figure S3. FT-IR spectrum of compound **2a** (neat liquid, thin film).

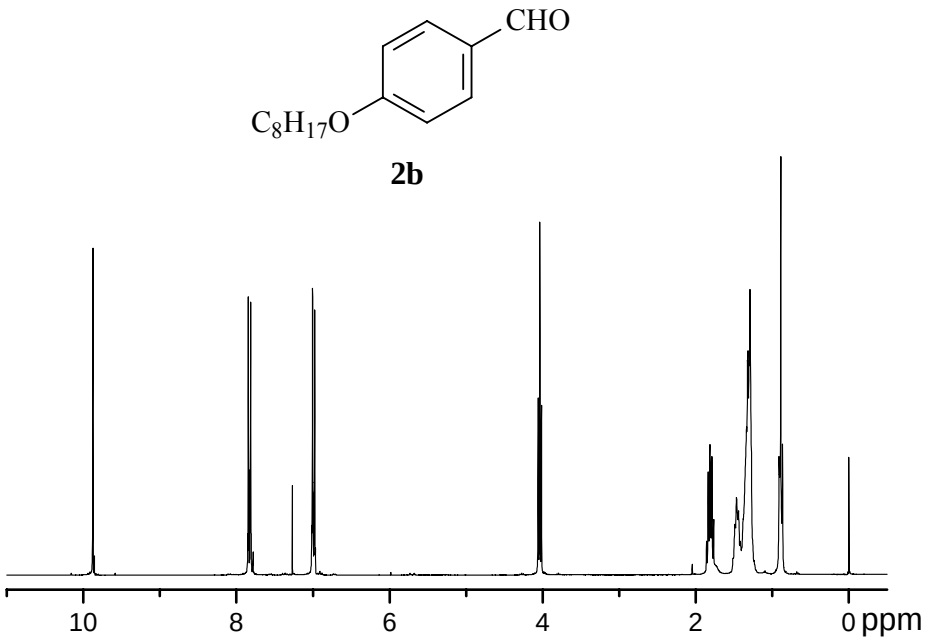

Figure S4. ^1H NMR spectrum of compound **2b** ($CDCl_3$, 300 MHz).

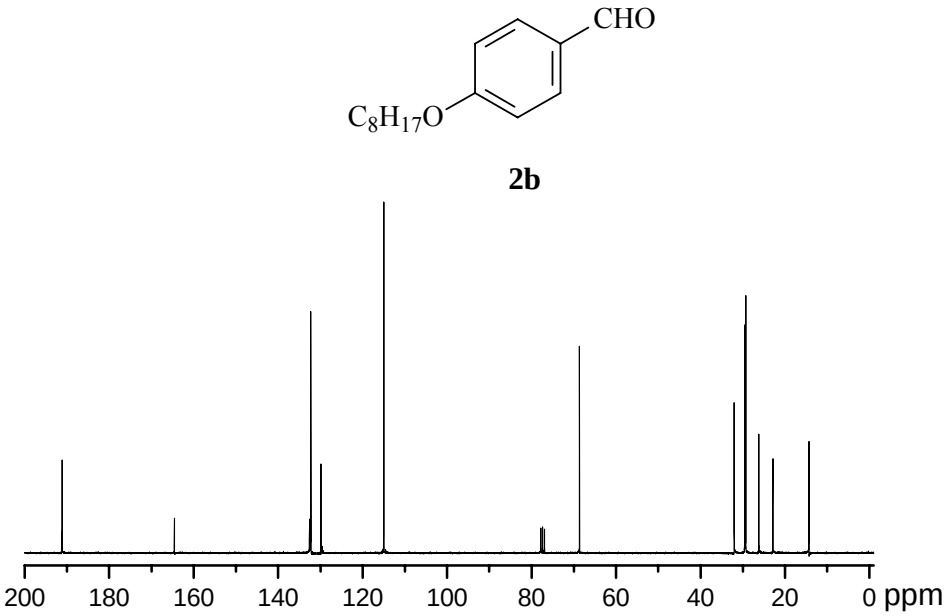

Figure S5. ^{13}C NMR spectrum of compound **2b** ($CDCl_3$, 75 MHz).

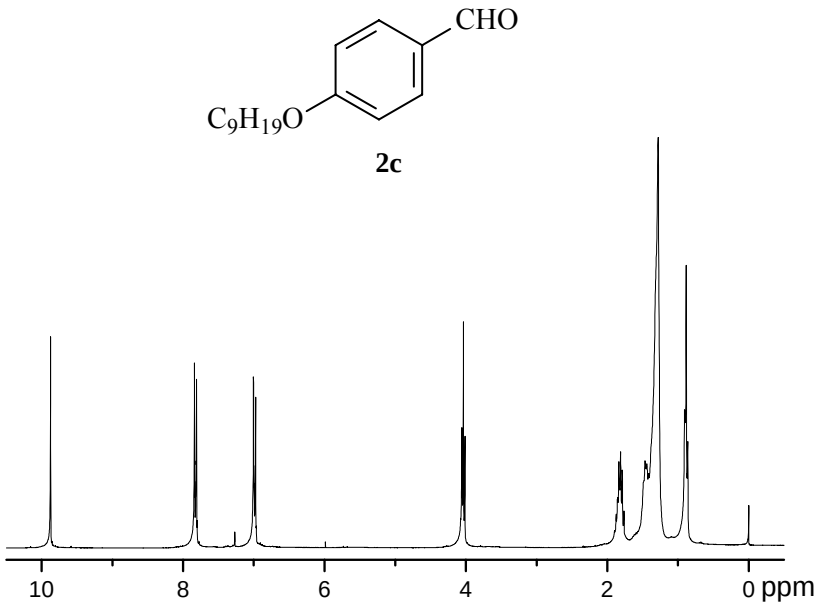

Figure S6. ^{1}H NMR spectrum of compound **2c** ($CDCl_3$, 300 MHz).

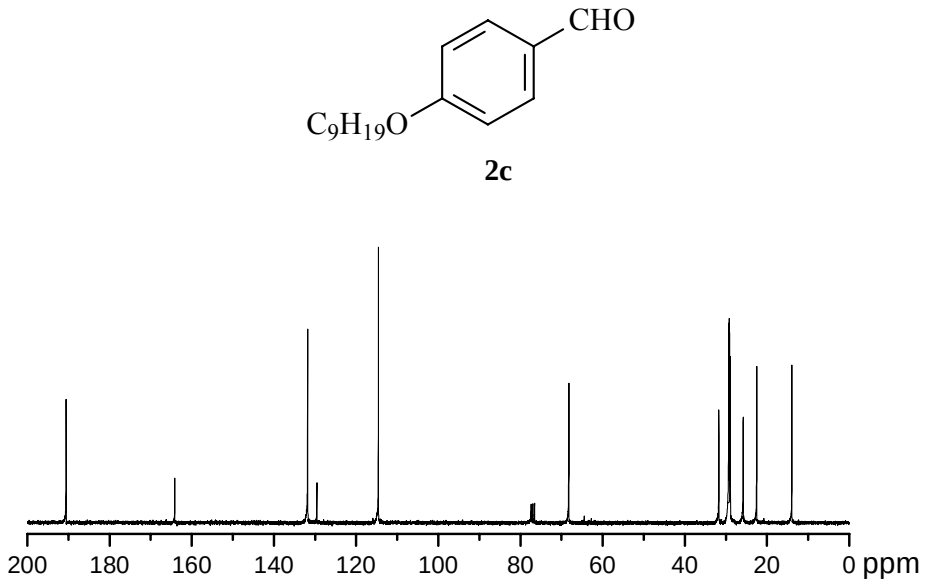

Figure S7. ^{13}C NMR spectrum of compound **2c** ($CDCl_3$, 75 MHz).

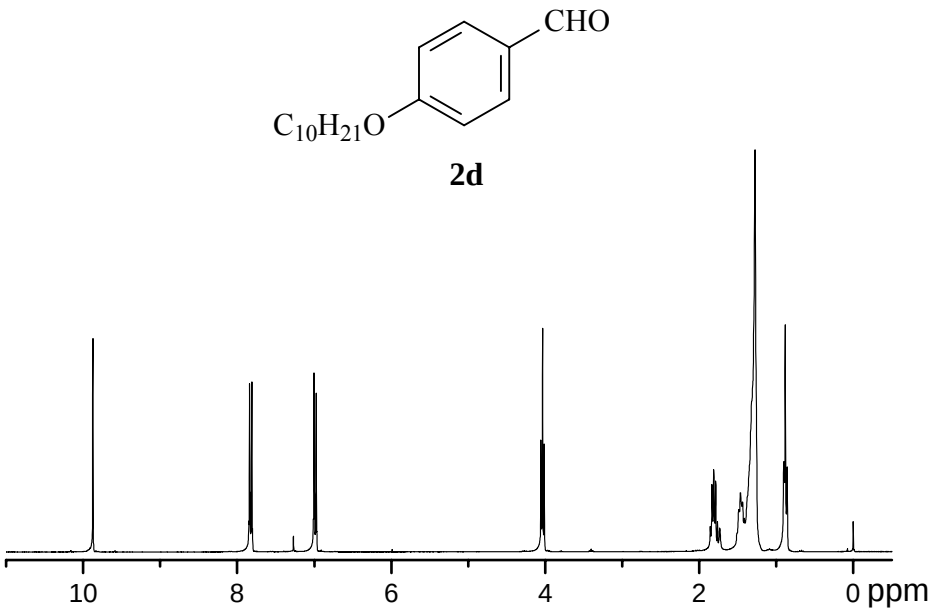

Figure S8. ^{1}H NMR spectrum of compound **2d** ($CDCl_3$, 300 MHz).

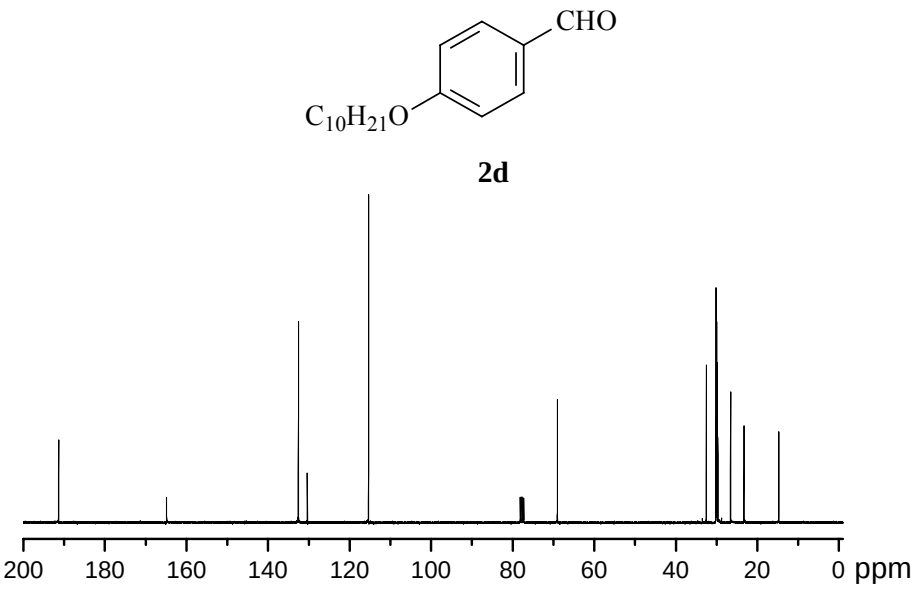

Figure S9. ^{13}C NMR spectrum of compound **2d** ($CDCl_3$, 75 MHz).

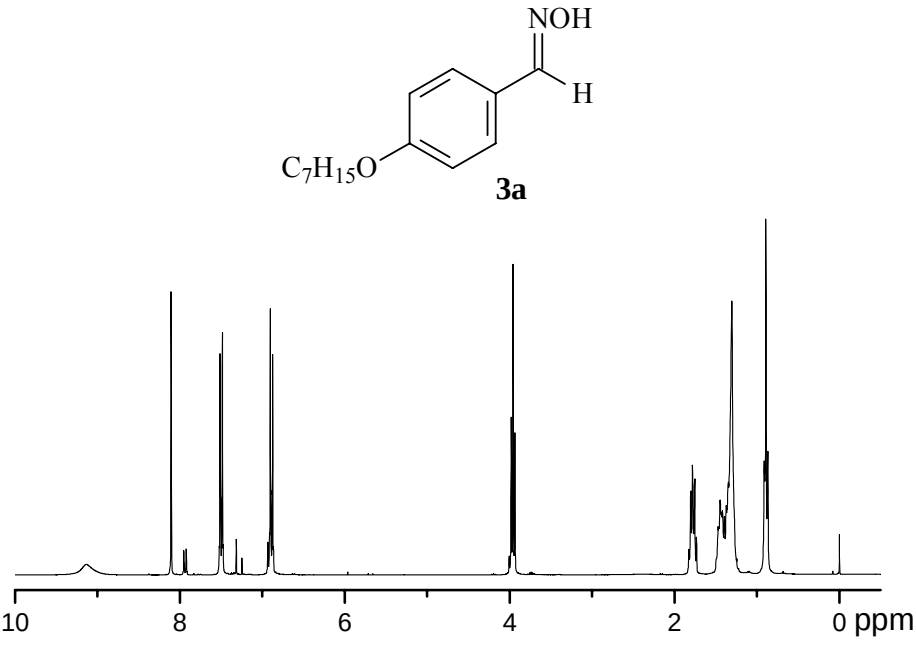

Figure S10. ^{1}H NMR spectrum of compound **3a** ($CDCl_3$, 300 MHz).

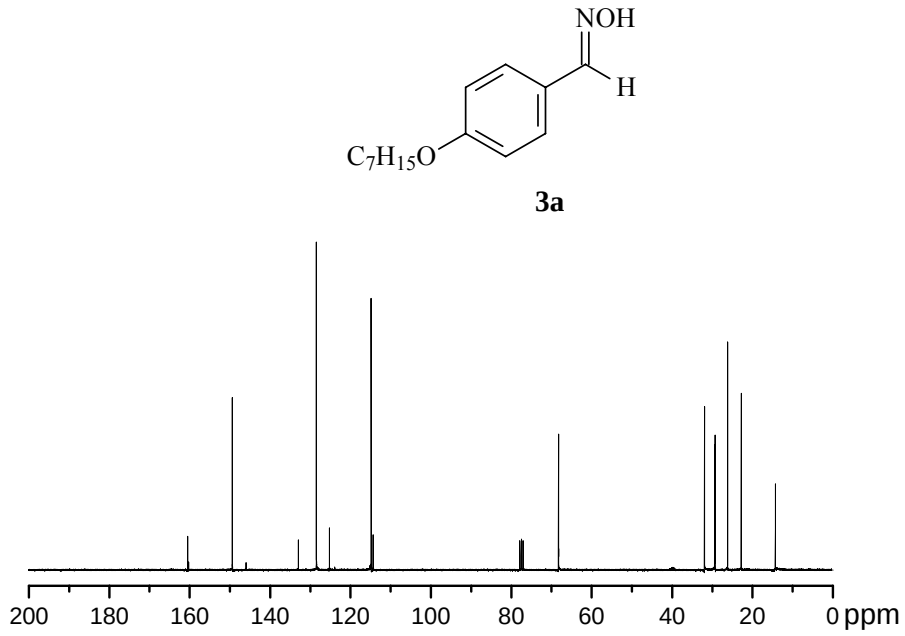

Figure S11. ^{13}C NMR spectrum of compound **3a** ($CDCl_3$, 75 MHz).

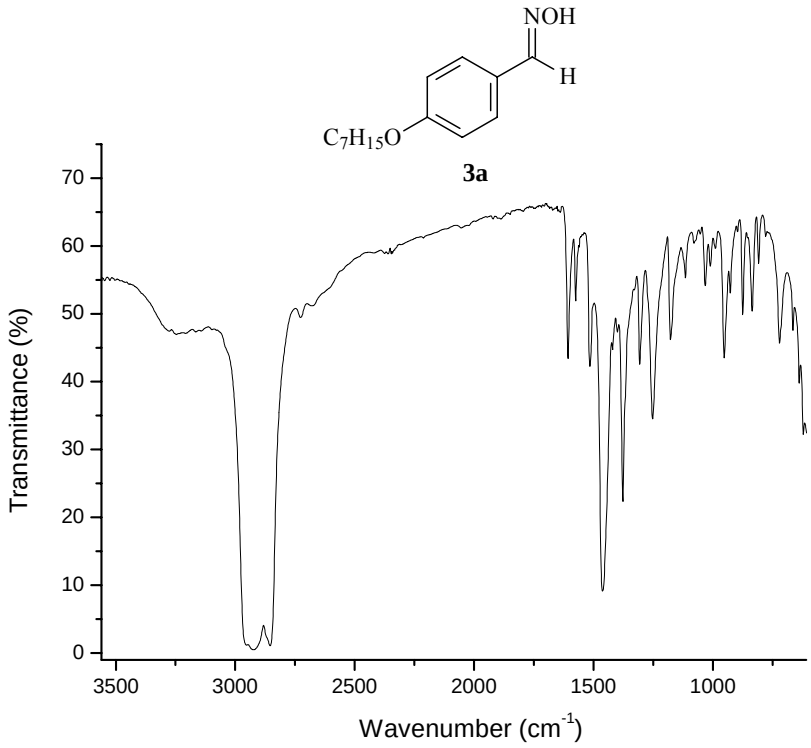

Figure S12. FT-IR spectrum of compound **3a** (nujol).

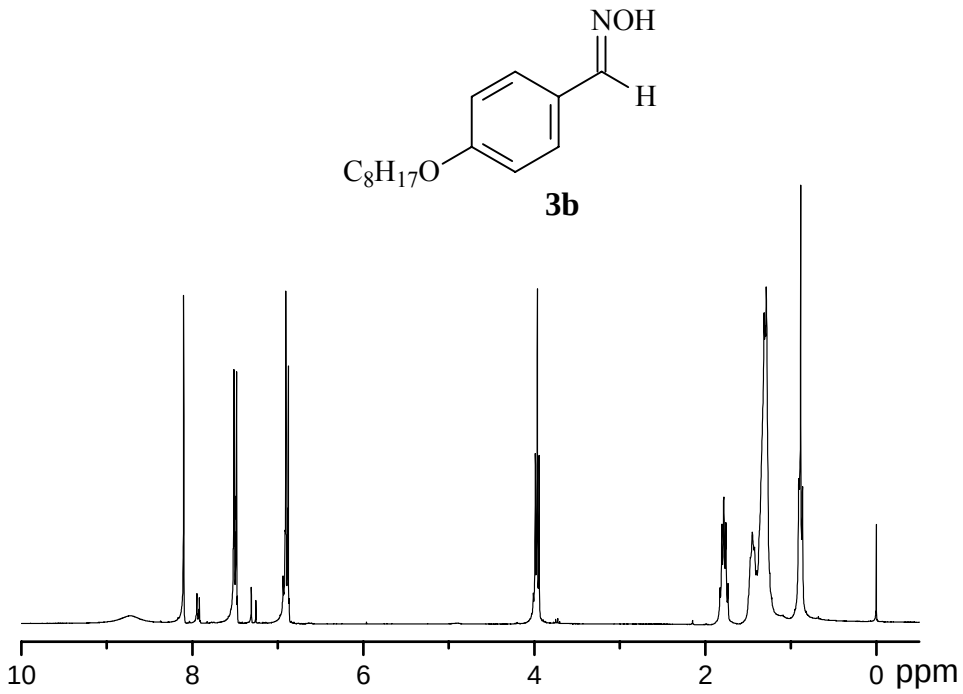

Figure S13. ^{1}H NMR spectrum of compound **3b** ($CDCl_3$, 300 MHz).

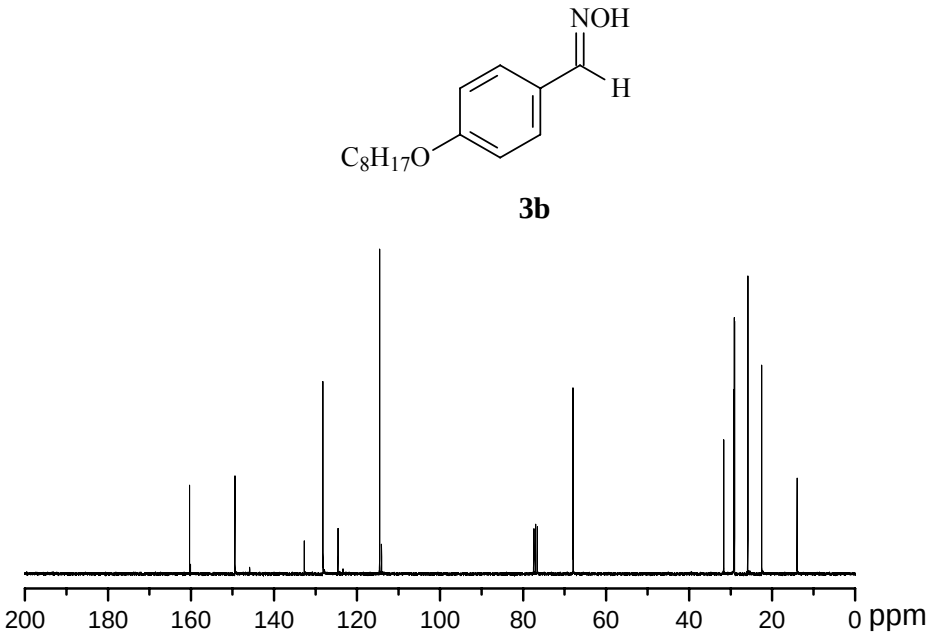

Figure S14. ^{13}C NMR spectrum of compound **3b** ($CDCl_3$, 75 MHz).

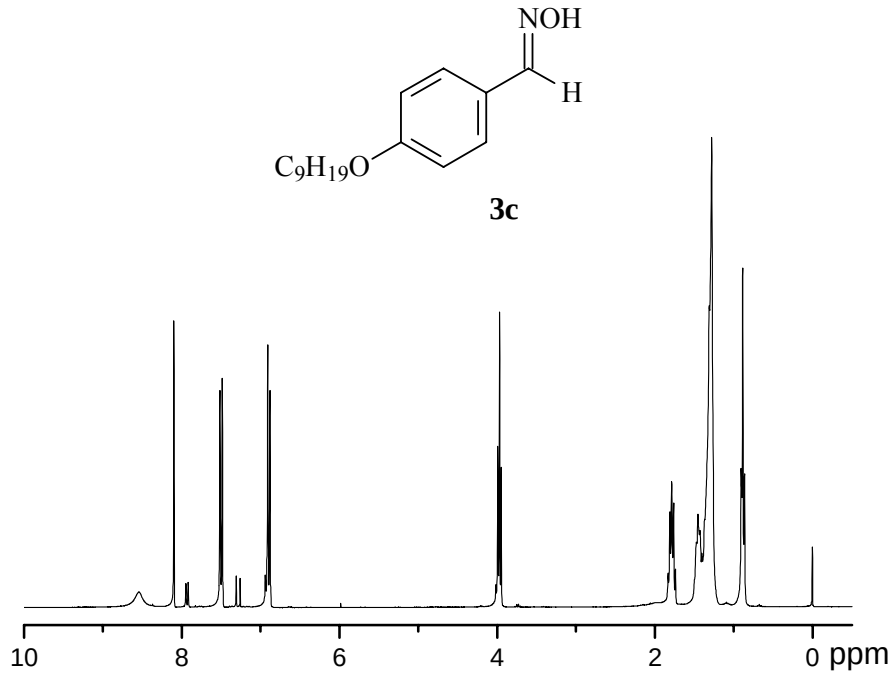

Figure S15. ^{1}H NMR spectrum of compound **3c** ($CDCl_3$, 300 MHz).

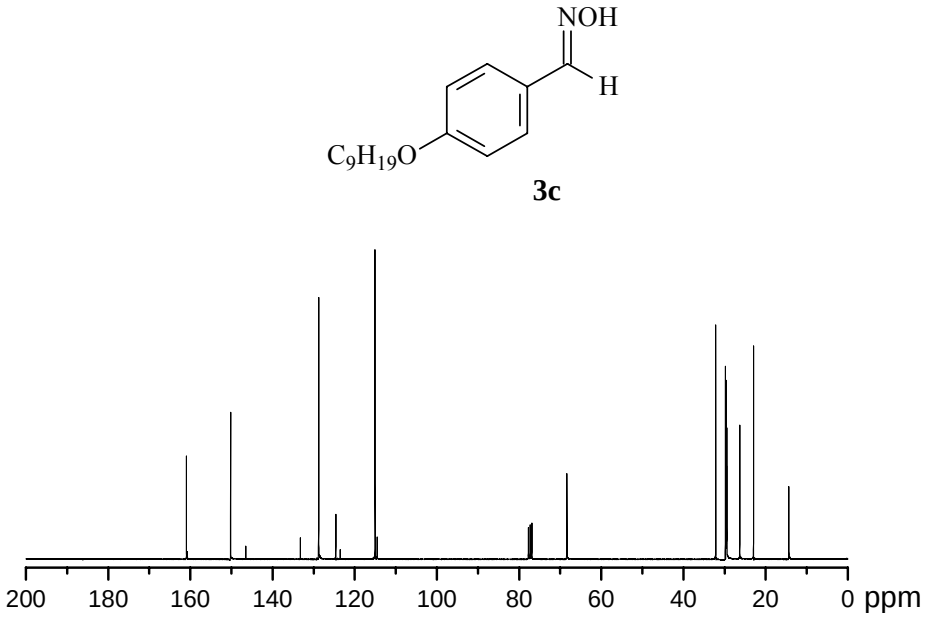

Figure S16. ^{13}C NMR spectrum of compound **3c** ($CDCl_3$, 75 MHz).

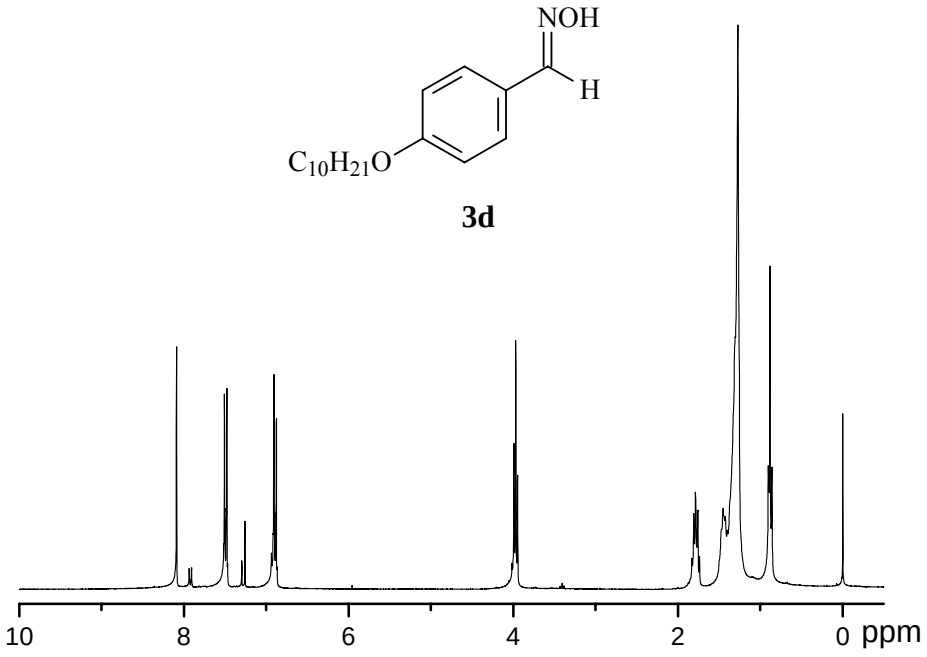

Figure S17. ^{1}H NMR spectrum of compound **3d** ($CDCl_3$, 300 MHz).

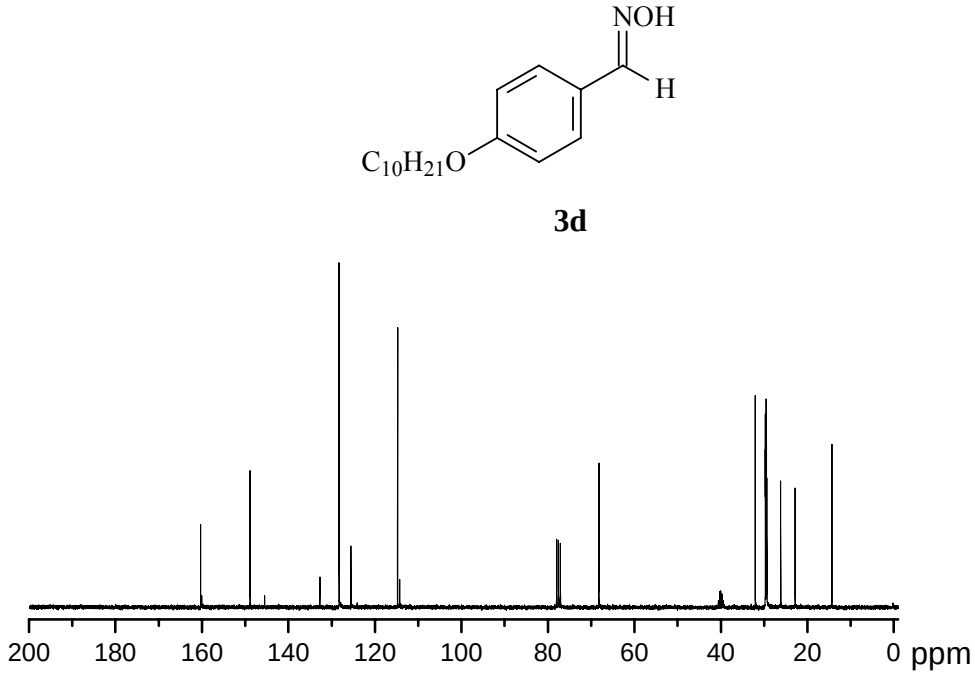

Figure S18. ^{13}C NMR spectrum of compound **3d** ($CDCl_3$/DMSO-d_6, 75 MHz).

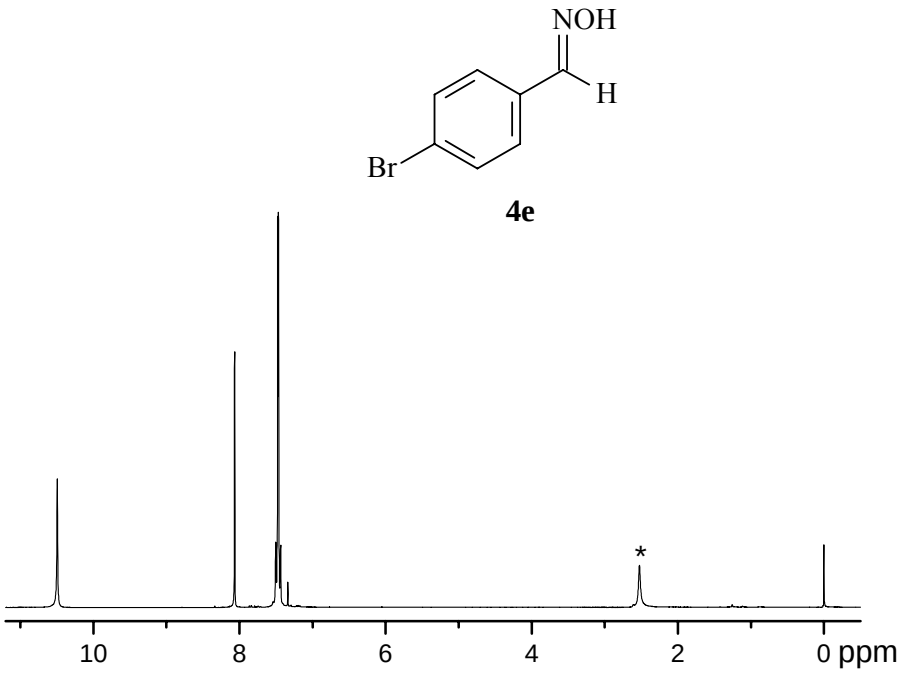

Figure S19. ^{1}H NMR spectrum of compound **4e** ($CDCl_3$, 300 MHz). *Solvent impurity.

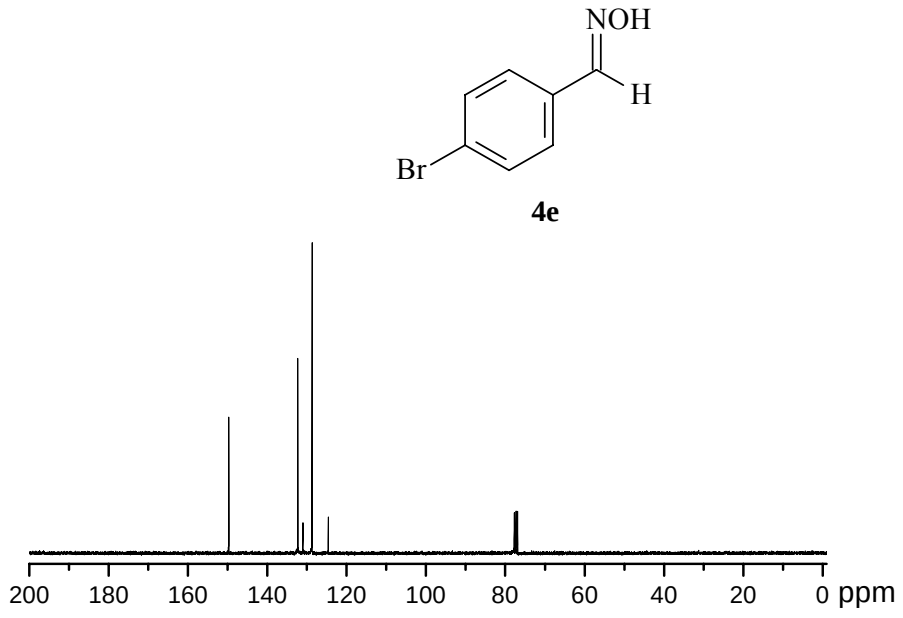

Figure S20. ^{13}C NMR spectrum of compound **4e** ($CDCl_3$, 75 MHz).

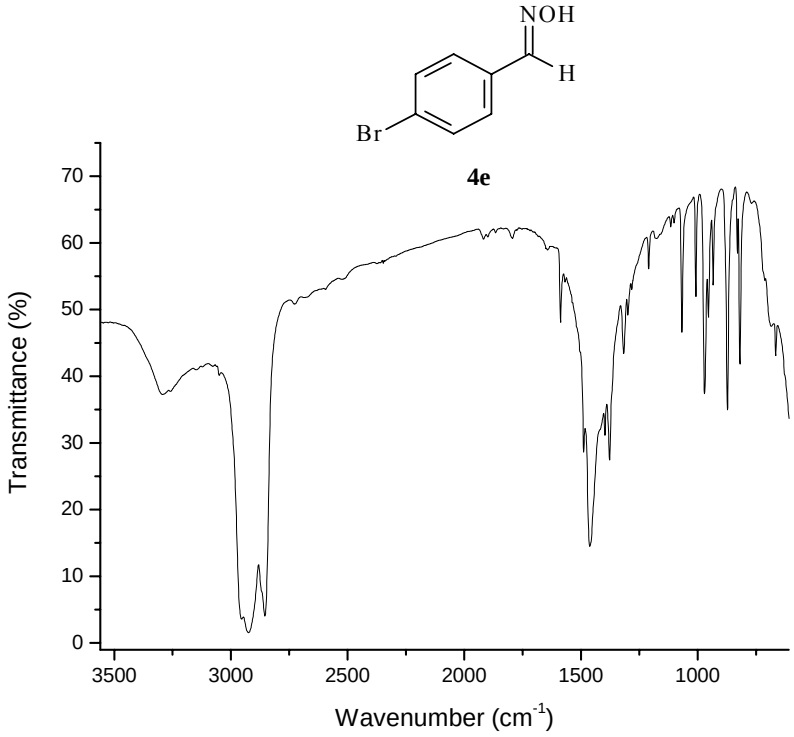

Figure S21. FT-IR spectrum of compound **4e** (nujol).

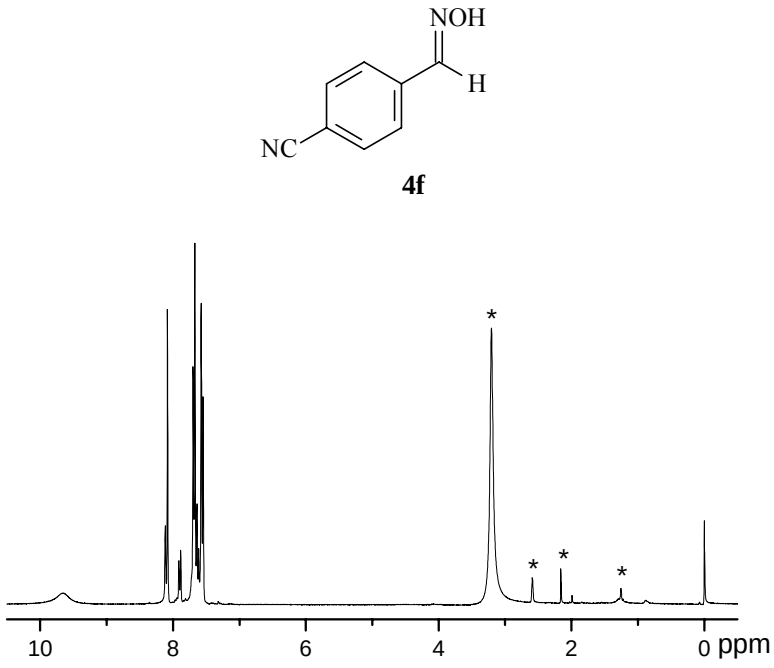

Figure S22. ^{1}H NMR spectrum of compound **4f** ($CDCl_3$/DMSO-d_6, 300 MHz). *Solvent impurity.

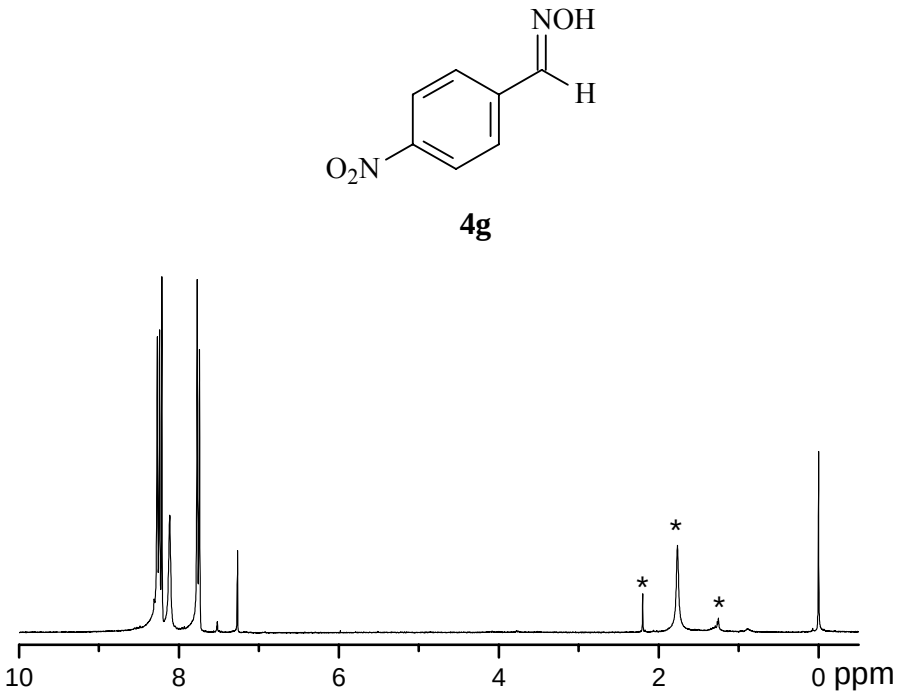

Figure S23. ^{1}H NMR spectrum of compound **4g** ($CDCl_3$, 300 MHz). *Solvent impurity.

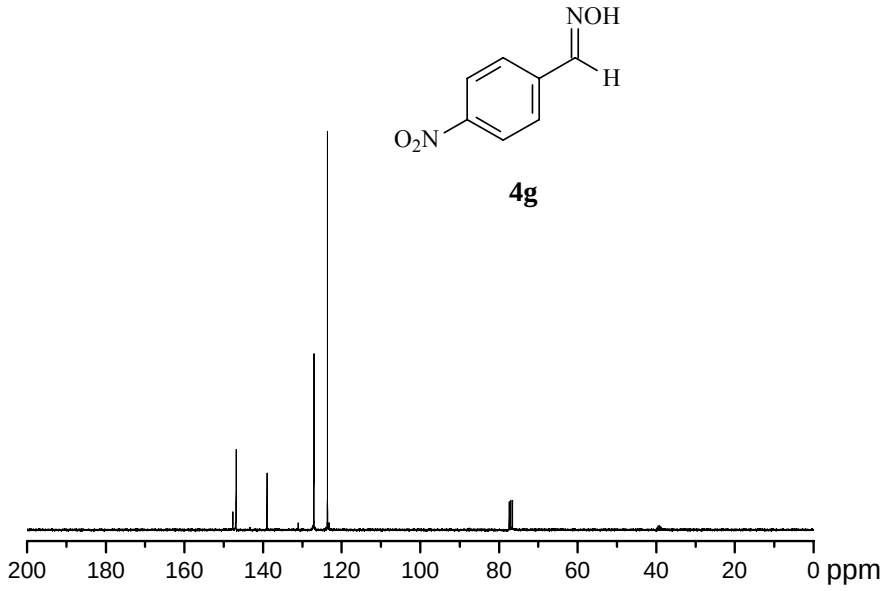

Figure S24. ^{13}C NMR spectrum of compound **4g** ($CDCl_3$/DMSO-d_6, 75 MHz).

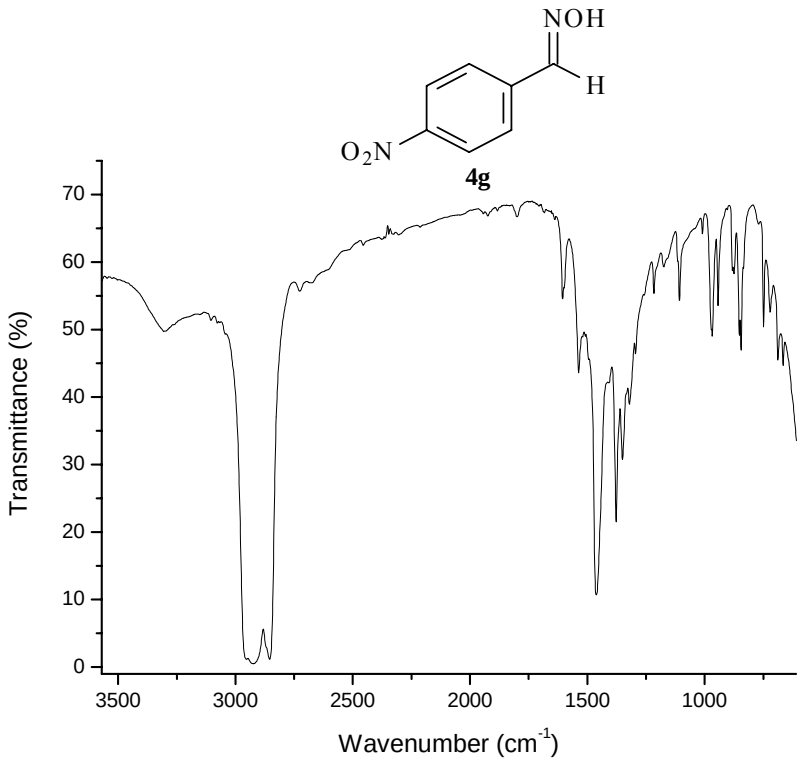

Figure S25. FT-IR spectrum of compound **4g** (nujol).

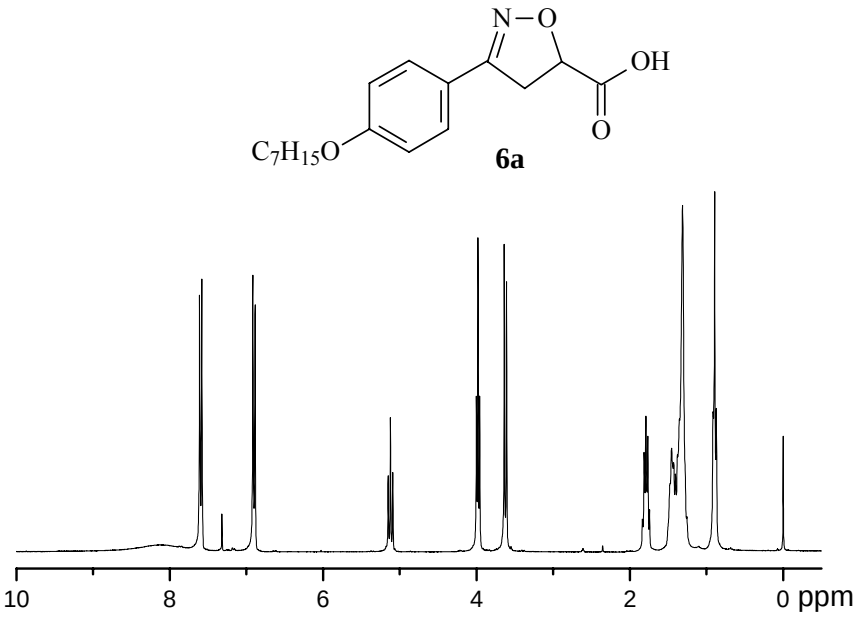

Figure S26. ^{1}H NMR spectrum of compound **6a** ($CDCl_3$, 300 MHz).

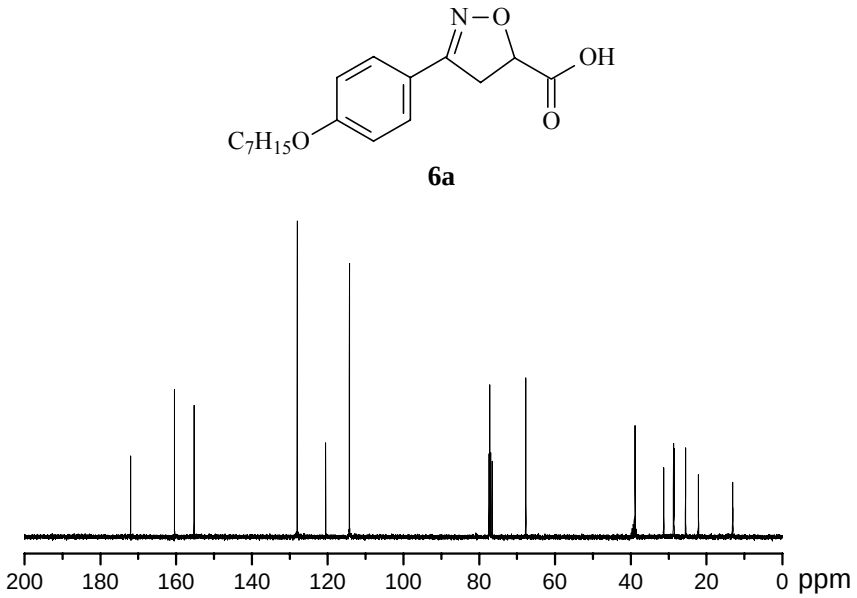

Figure S27. ^{13}C NMR spectrum of compound **6a** ($CDCl_3$/DMSO-d_6, 75 MHz).

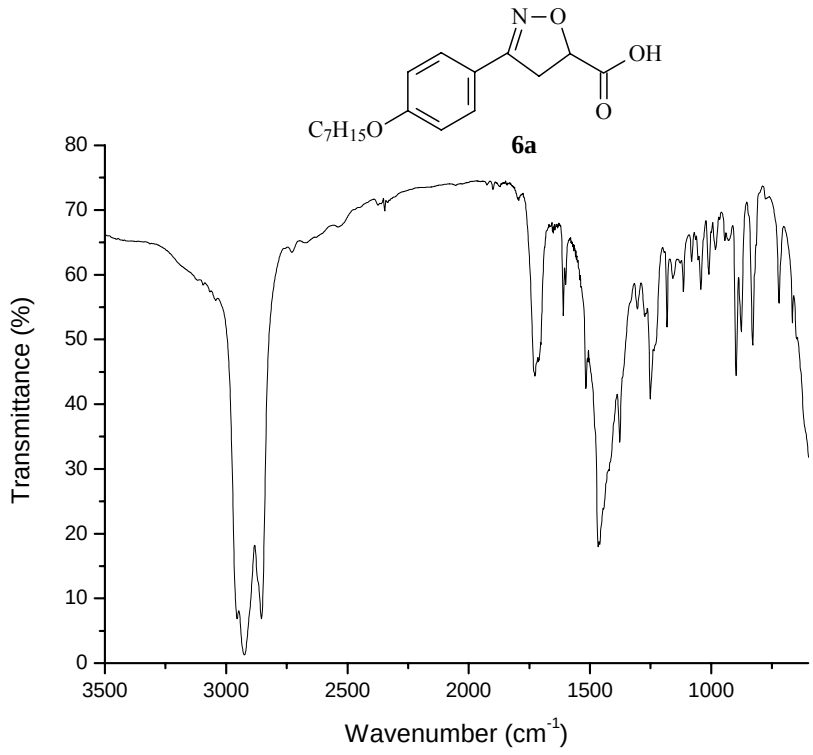

Figure S28. FT-IR spectrum of compound **6a** (nujol).

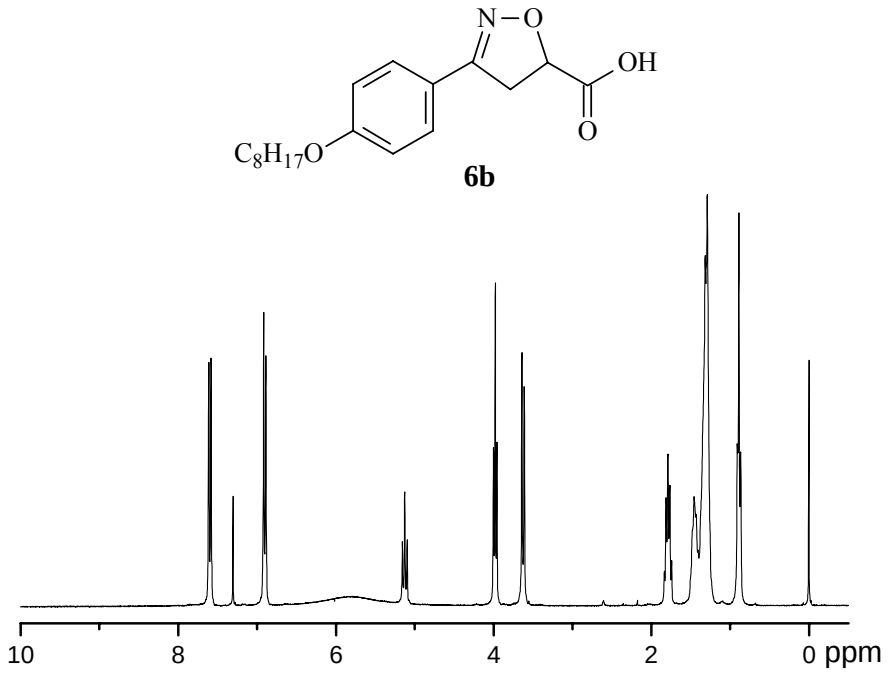

Figure S29. ^{1}H NMR spectrum of compound **6b** ($CDCl_3$, 300 MHz).

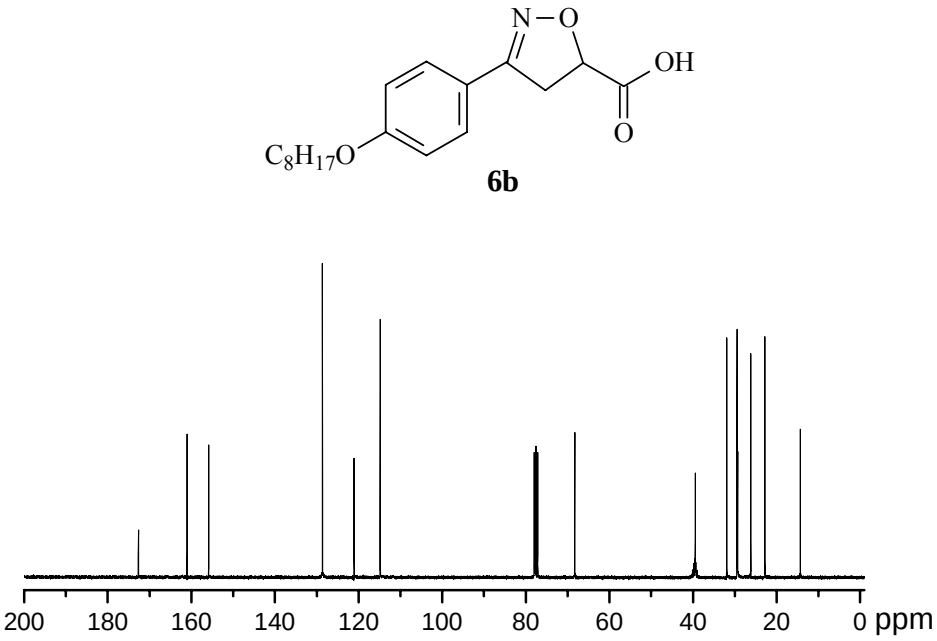

Figure S30. ^{13}C NMR spectrum of compound **6b** ($CDCl_3$/DMSO-d_6, 75 MHz).

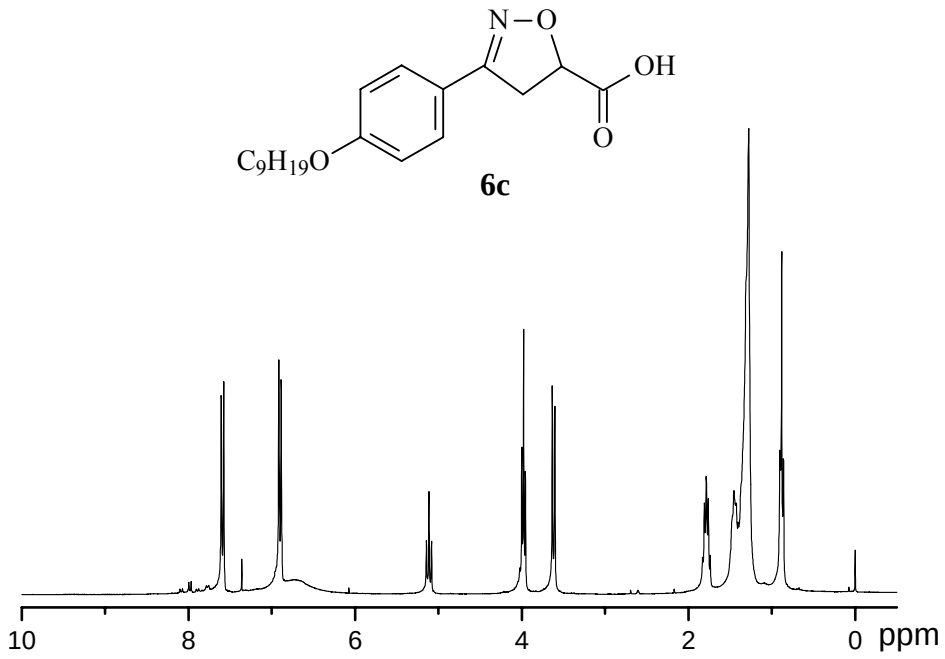

Figure S31. ^{1}H NMR spectrum of compound **6c** ($CDCl_3$, 300 MHz).

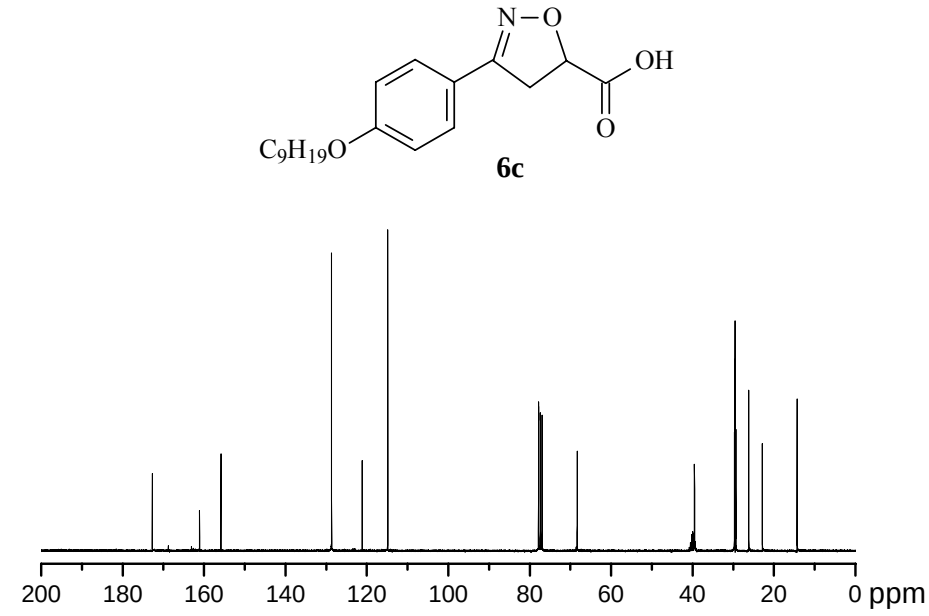

Figure S32. ^{13}C NMR spectrum of compound **6c** ($CDCl_3$/DMSO-d_6, 75 MHz).

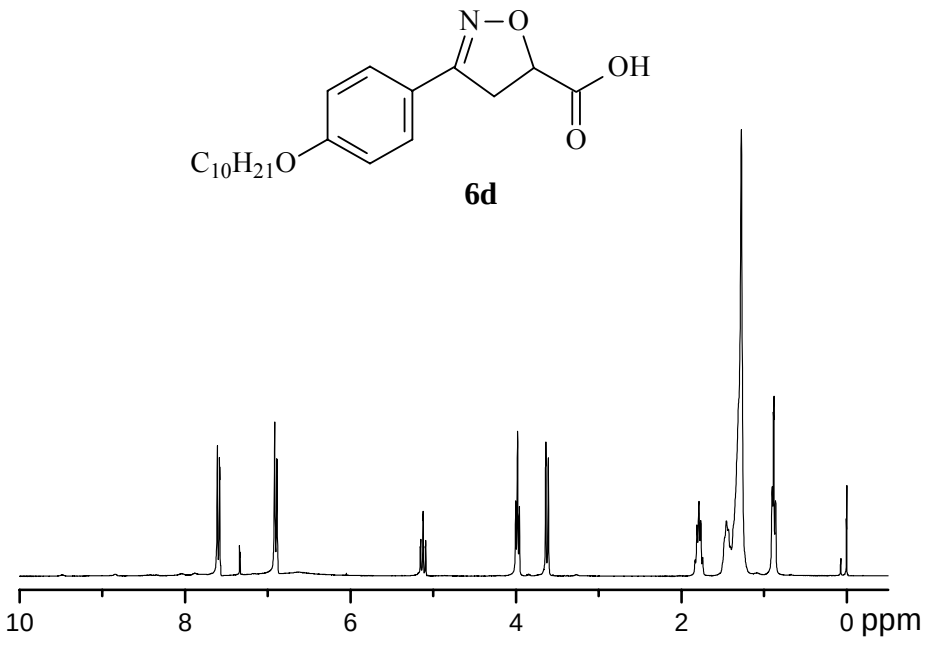

Figure S33. ^{1}H NMR spectrum of compound **6d** ($CDCl_3$, 300 MHz).

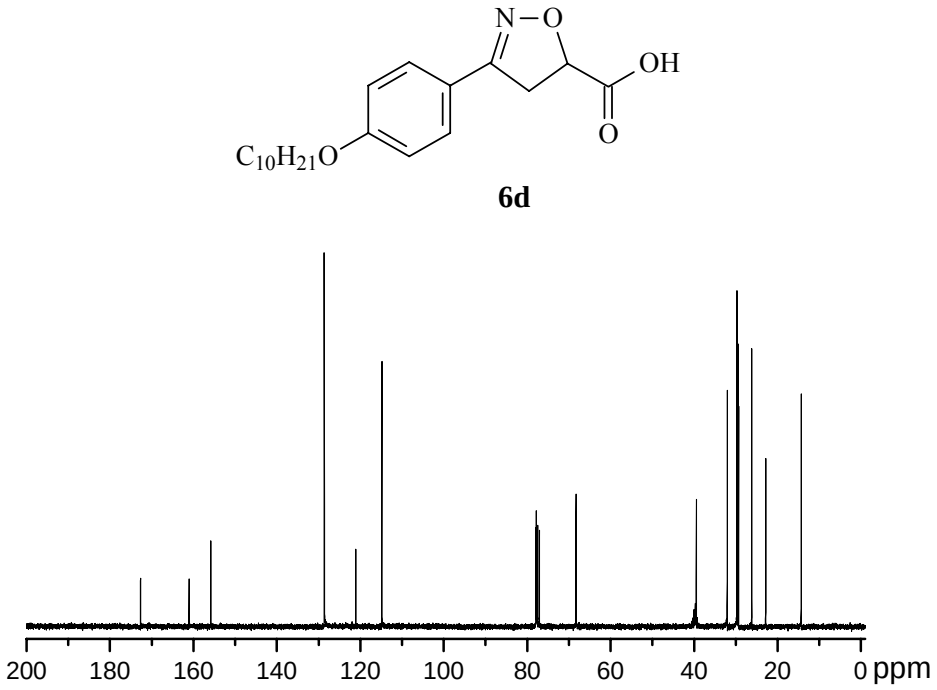

Figure S34. ^{13}C NMR spectrum of compound **6d** ($CDCl_3$/DMSO-d_6, 75 MHz).

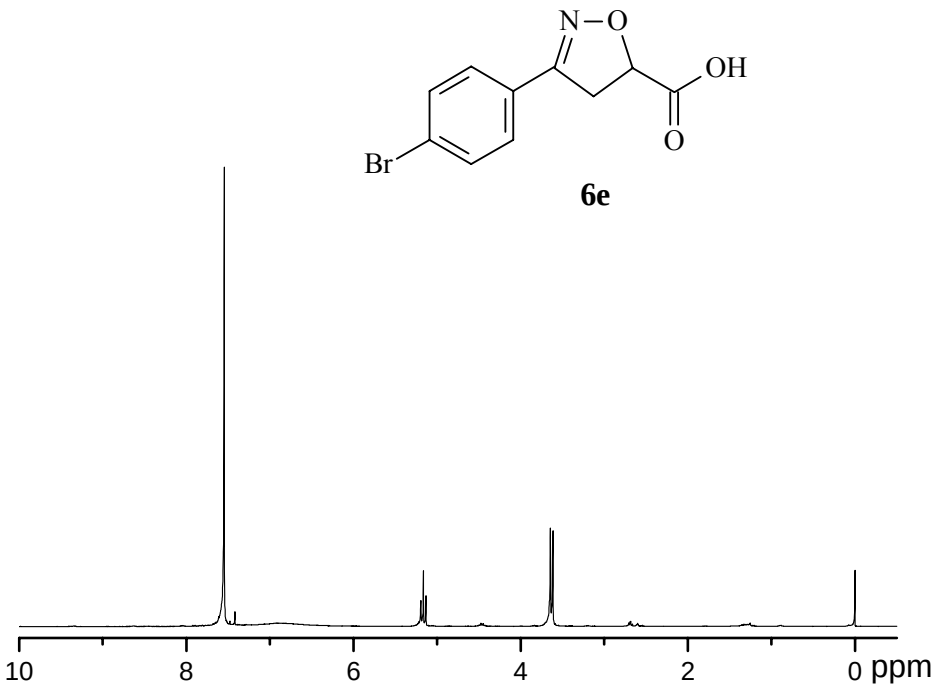

Figure S35. ^{1}H NMR spectrum of compound **6e** ($CDCl_3$, 300 MHz).

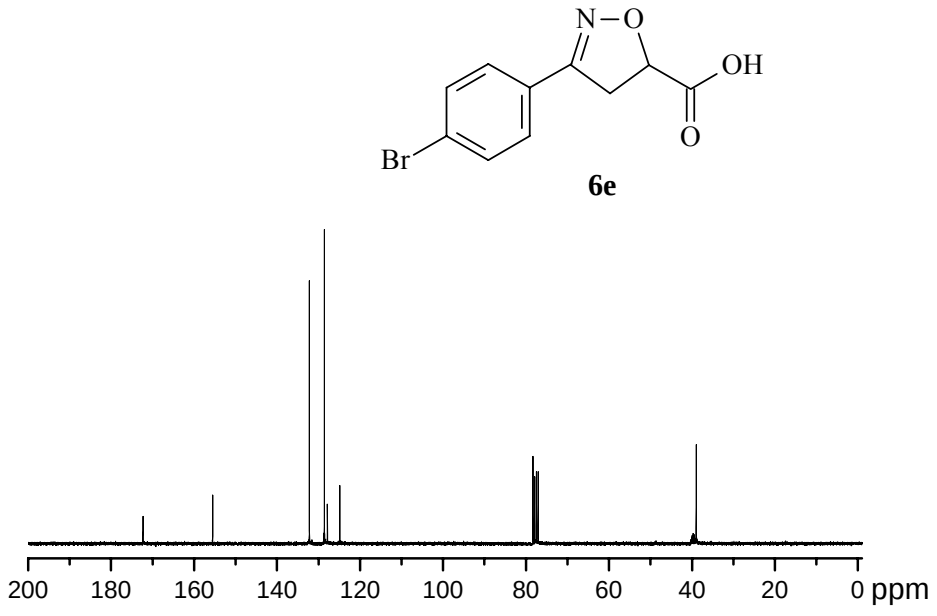

Figure S36. ^{13}C NMR spectrum of compound **6e** ($CDCl_3$/DMSO-d_6, 75 MHz).

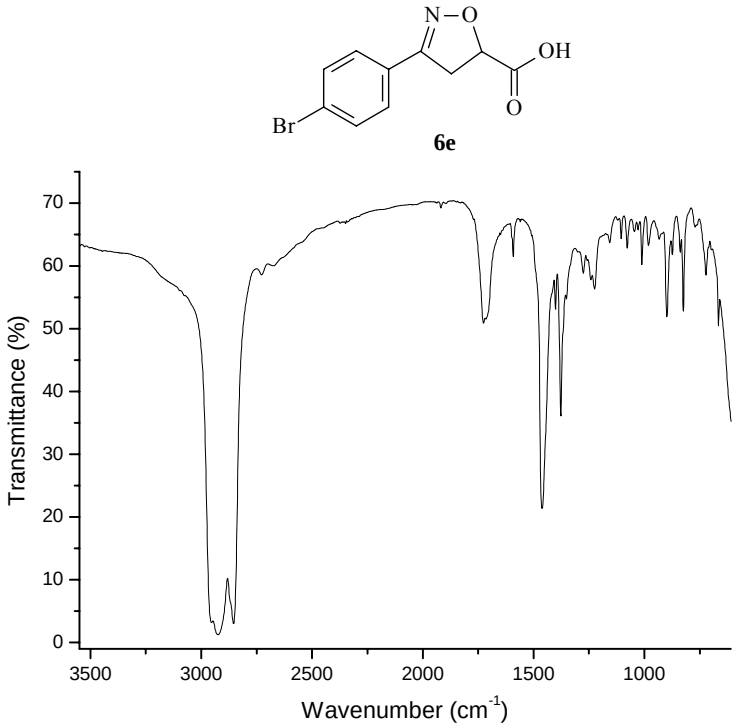

Figure S37. FT-IR spectrum of compound **6e** (nujol).

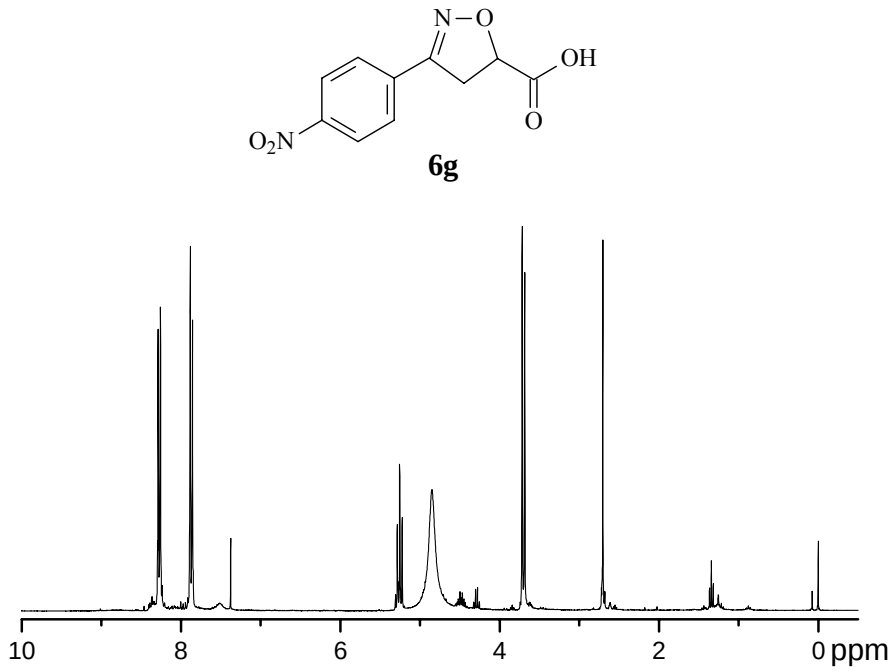

Figure S38. ^{1}H NMR spectrum of compound **6g** ($CDCl_3$/DMSO-d_6, 300 MHz).

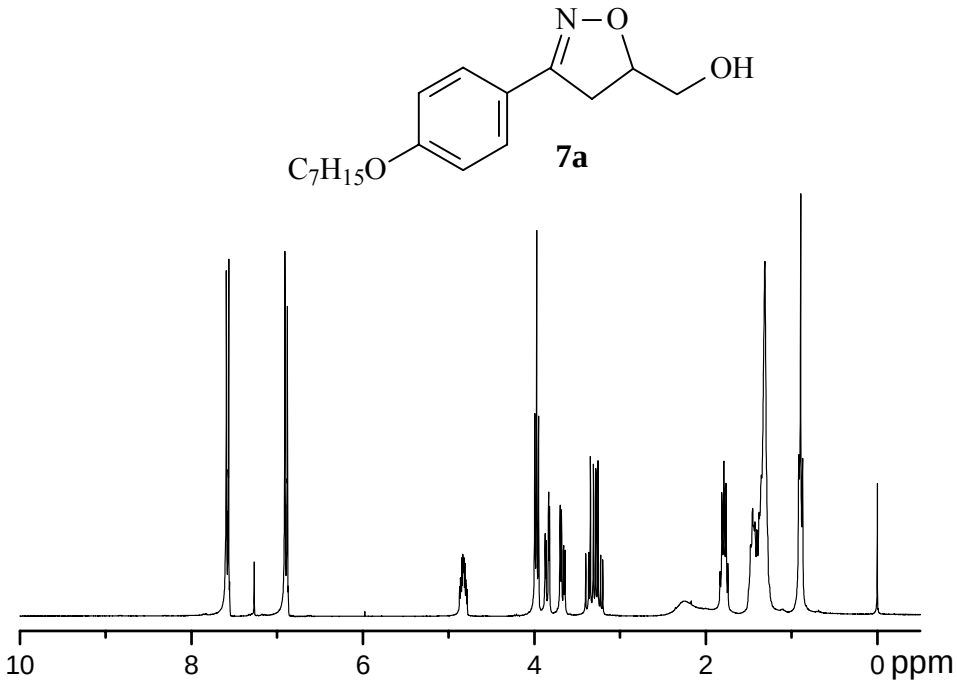

Figure S39. ^{1}H NMR spectrum of compound **7a** ($CDCl_3$, 300 MHz).

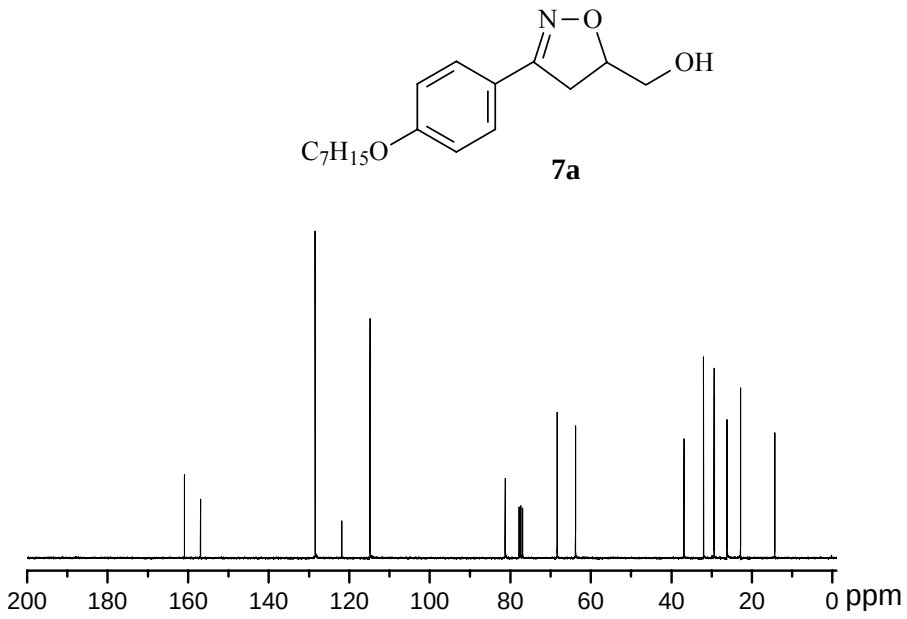

Figure S40. ^{13}C NMR spectrum of compound **7a** ($CDCl_3$, 75 MHz).

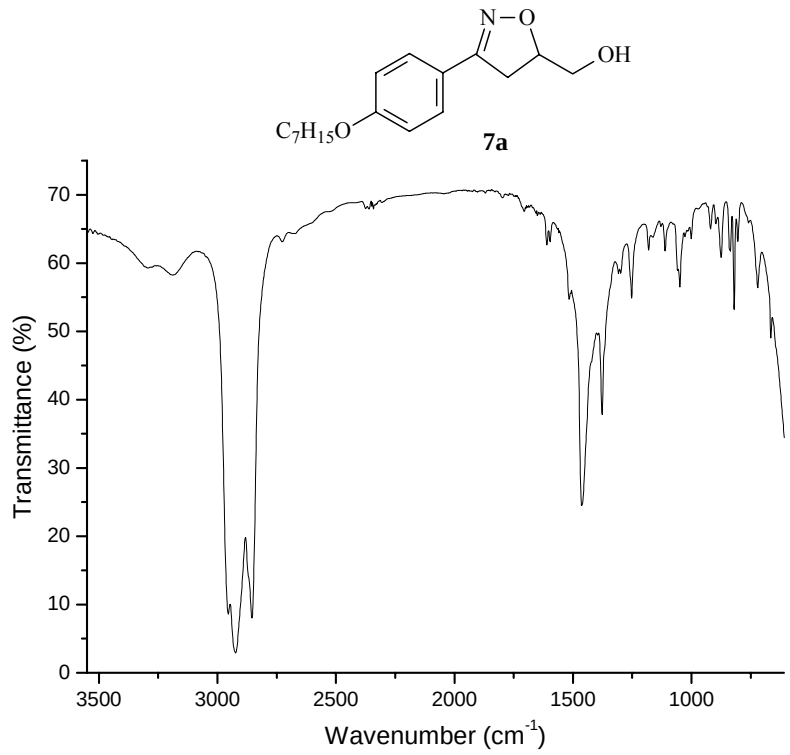

Figure S41. FT-IR spectrum of compound **7a** (nujol).

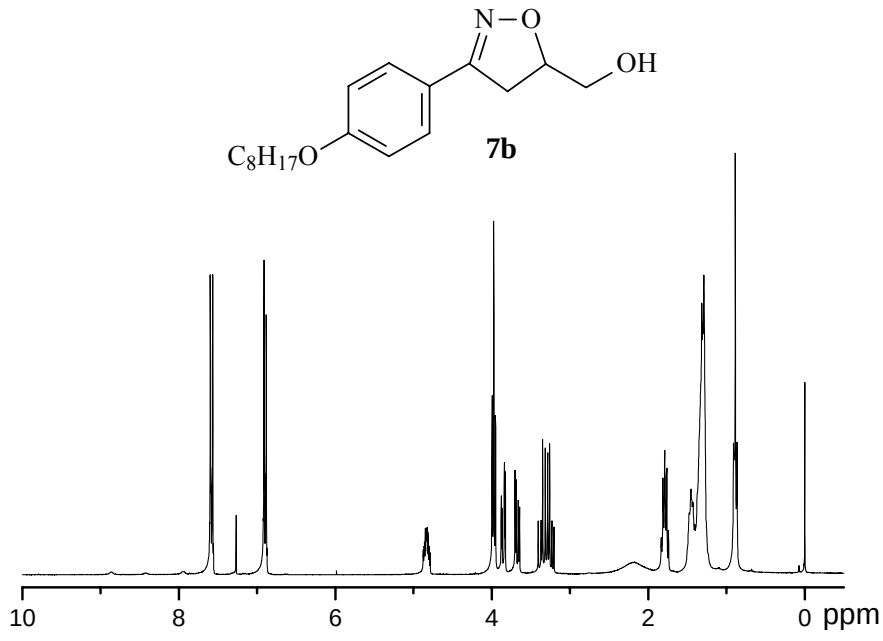

Figure S42. ^{1}H NMR spectrum of compound **7b** ($CDCl_3$, 300 MHz).

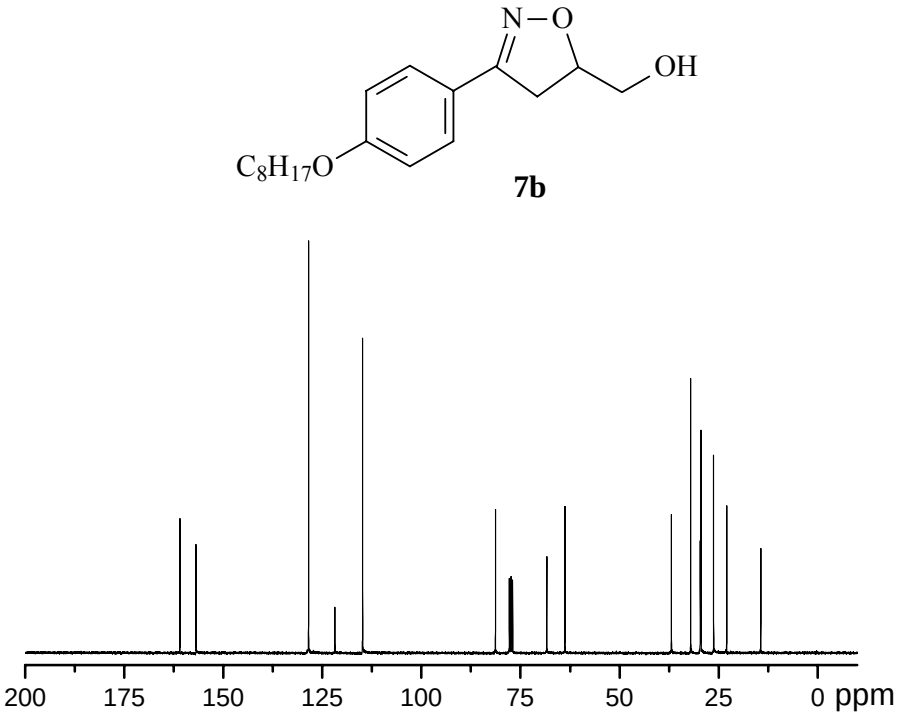

Figure S43. ^{13}C NMR spectrum of compound **7b** ($CDCl_3$, 75 MHz).

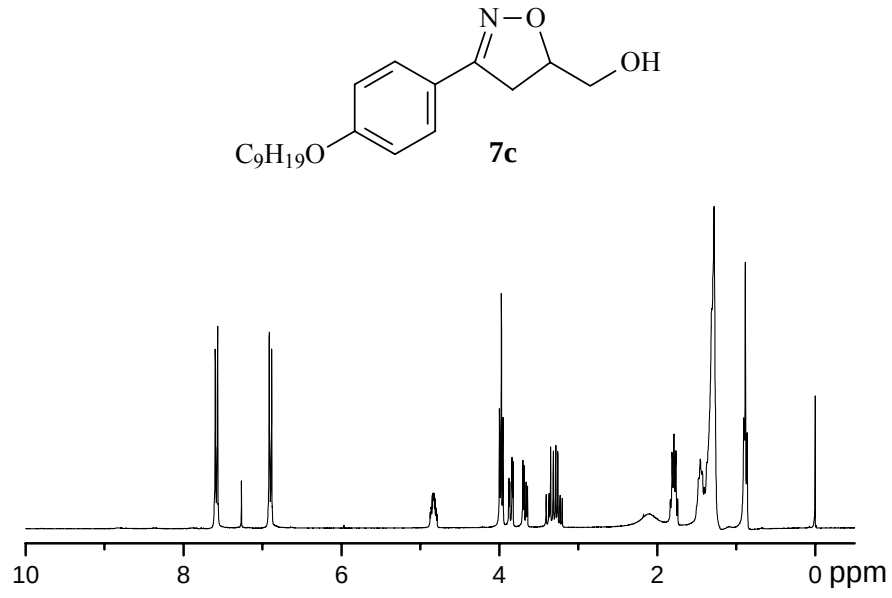

Figure S44. ^{1}H NMR spectrum of compound **7c** ($CDCl_3$, 300 MHz).

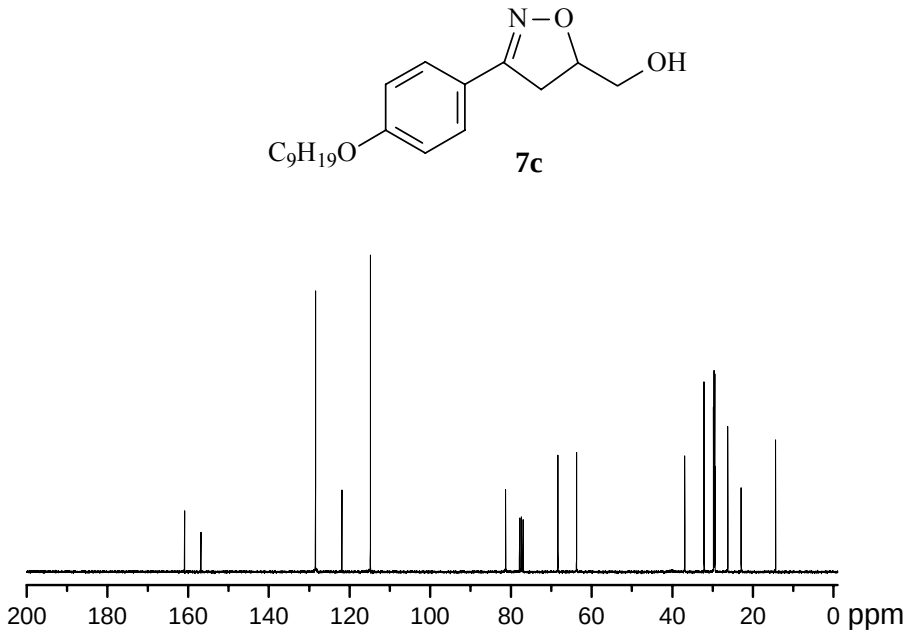

Figure S45. ^{13}C NMR spectrum of compound **7c** ($CDCl_3$, 75 MHz).

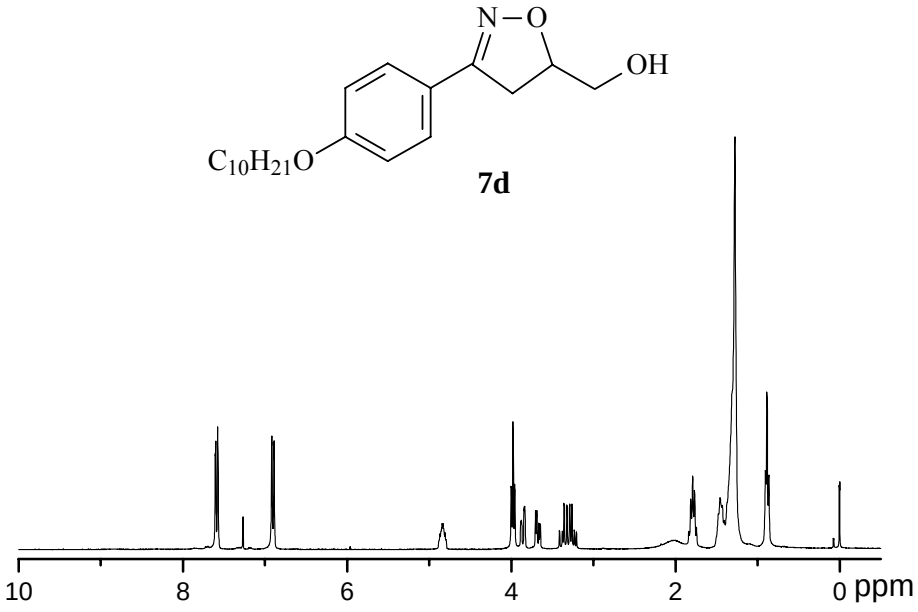

Figure S46. ^{1}H NMR spectrum of compound **7d** ($CDCl_3$, 300 MHz).

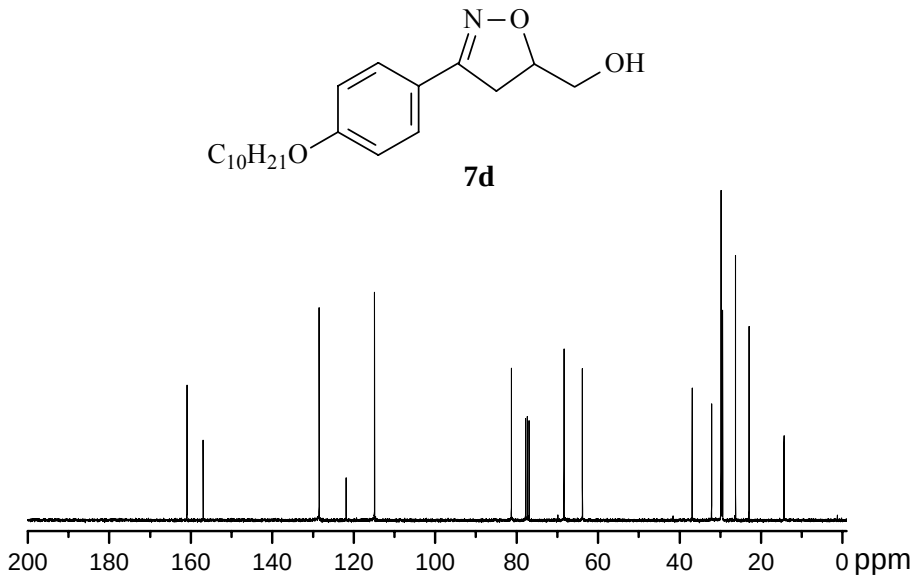

Figure S47. ^{13}C NMR spectrum of compound **7d** ($CDCl_3$, 75 MHz).

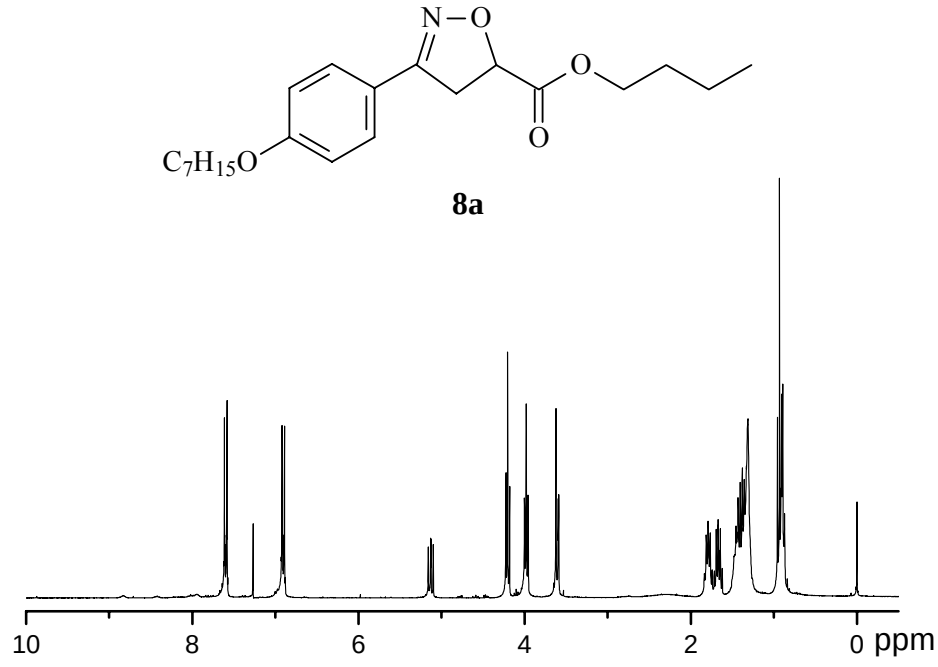

Figure S48. ^{1}H NMR spectrum of compound **8a** ($CDCl_3$, 300 MHz).

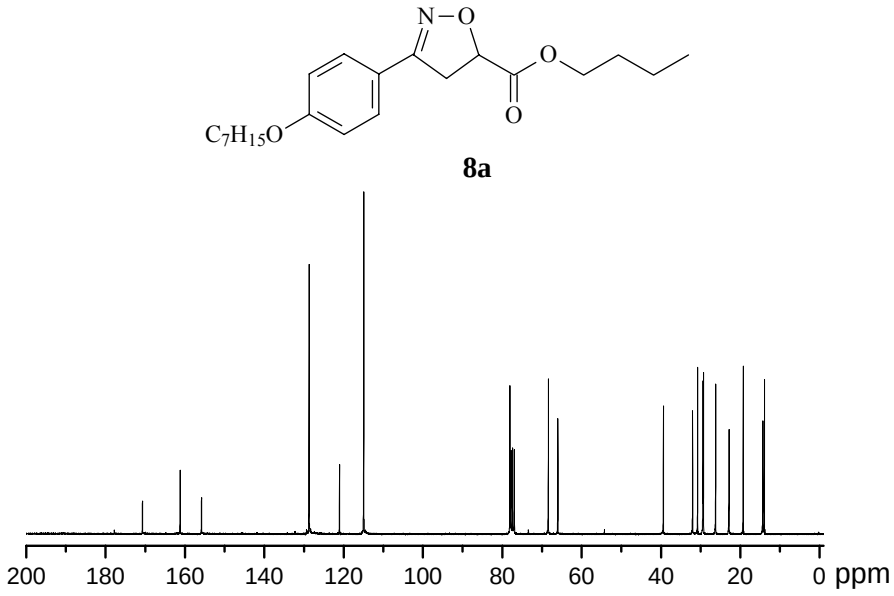

Figure S49. ^{13}C NMR spectrum of compound **8a** ($CDCl_3$, 75 MHz).

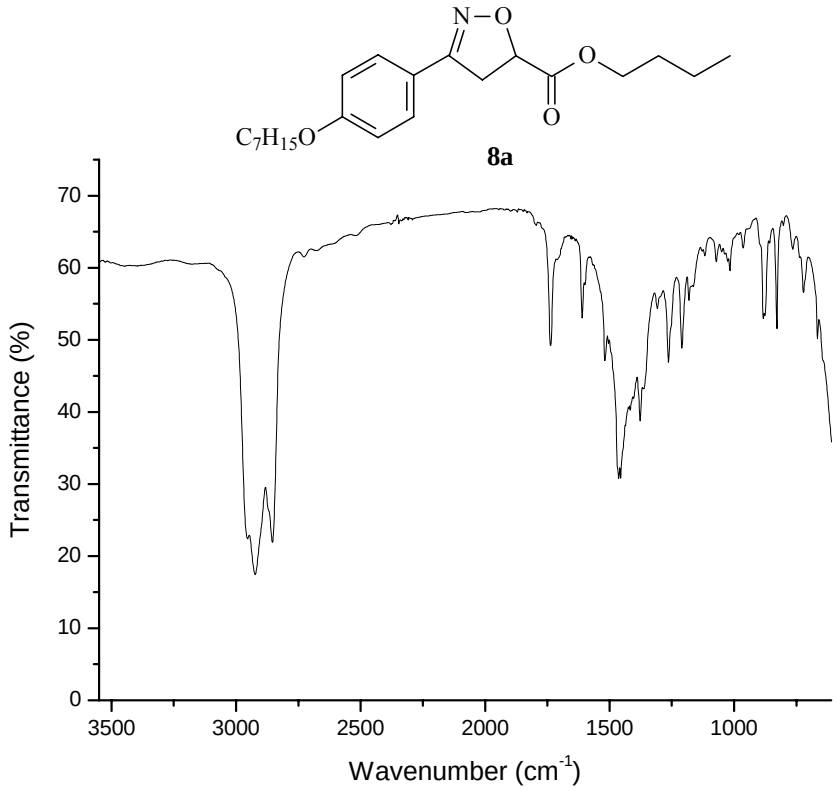

Figure S50. FT-IR spectrum of compound **8a** (nujol).

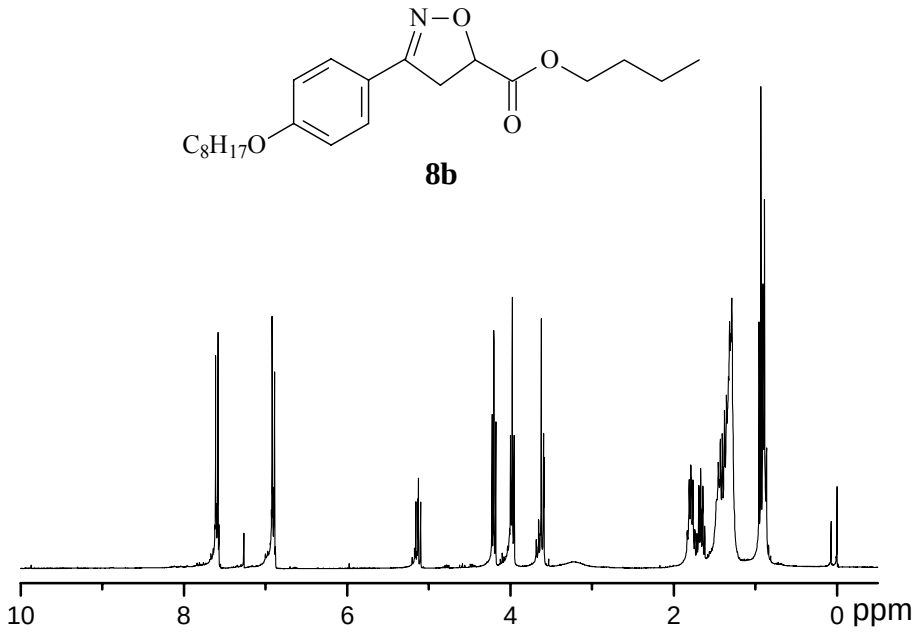

Figure S51. ^{1}H NMR spectrum of compound **8b** ($CDCl_3$, 300 MHz).

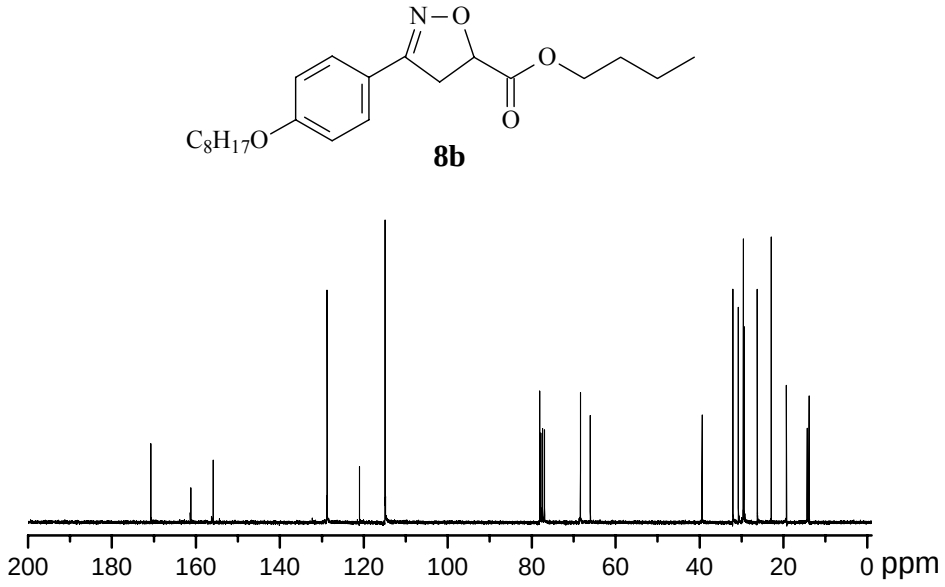

Figure S52. ^{13}C NMR spectrum of compound **8b** ($CDCl_3$, 75 MHz).

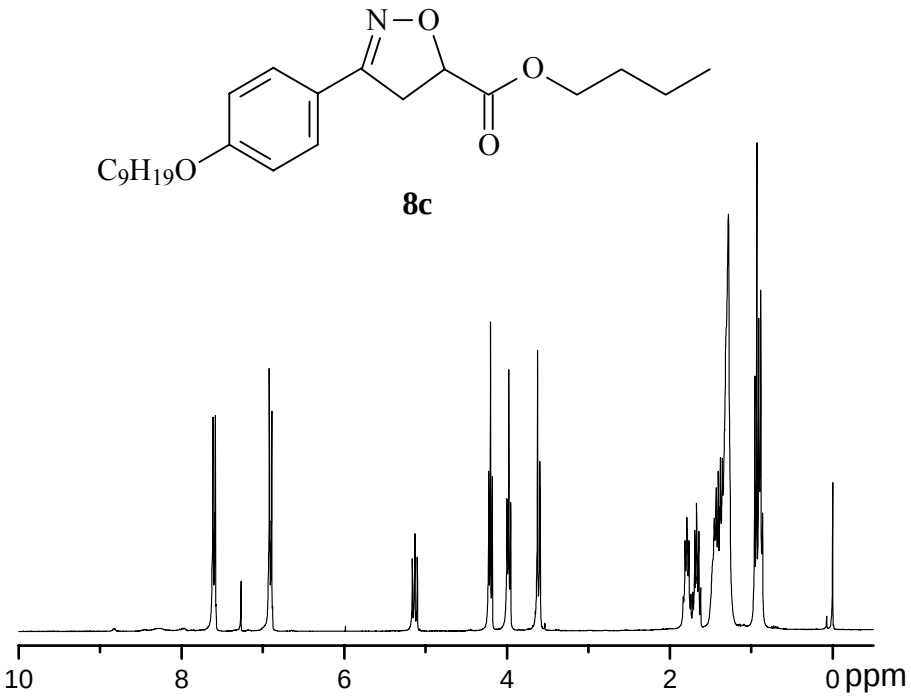

Figure S53. ^{1}H NMR spectrum of compound **8c** ($CDCl_3$, 300 MHz).

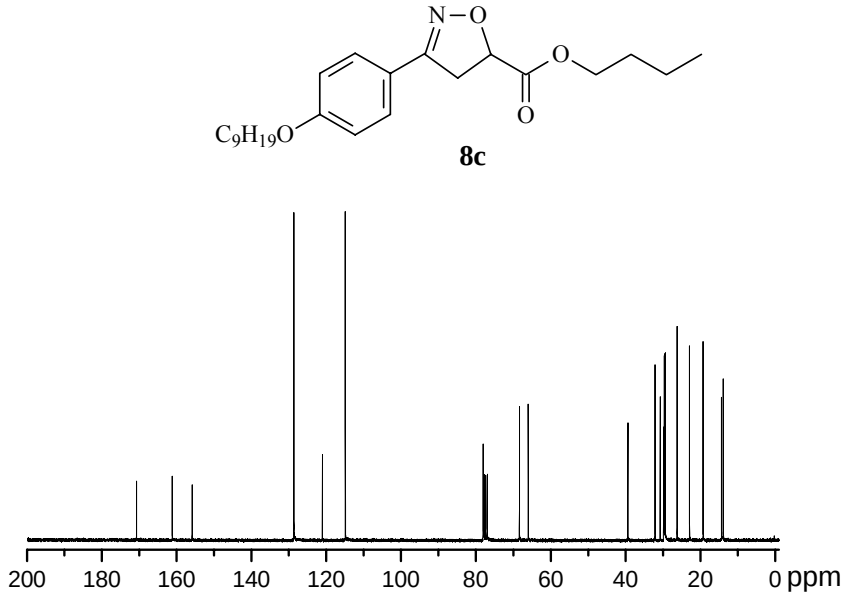

Figure S54. ^{13}C NMR spectrum of compound **8c** ($CDCl_3$, 75 MHz).

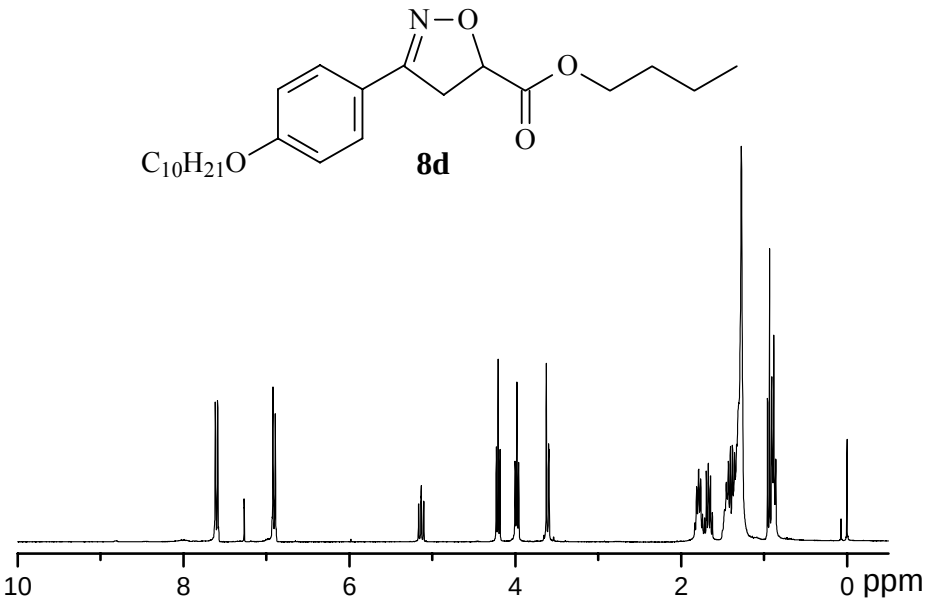

Figure S55. ^{1}H NMR spectrum of compound **8d** ($CDCl_3$, 300 MHz).

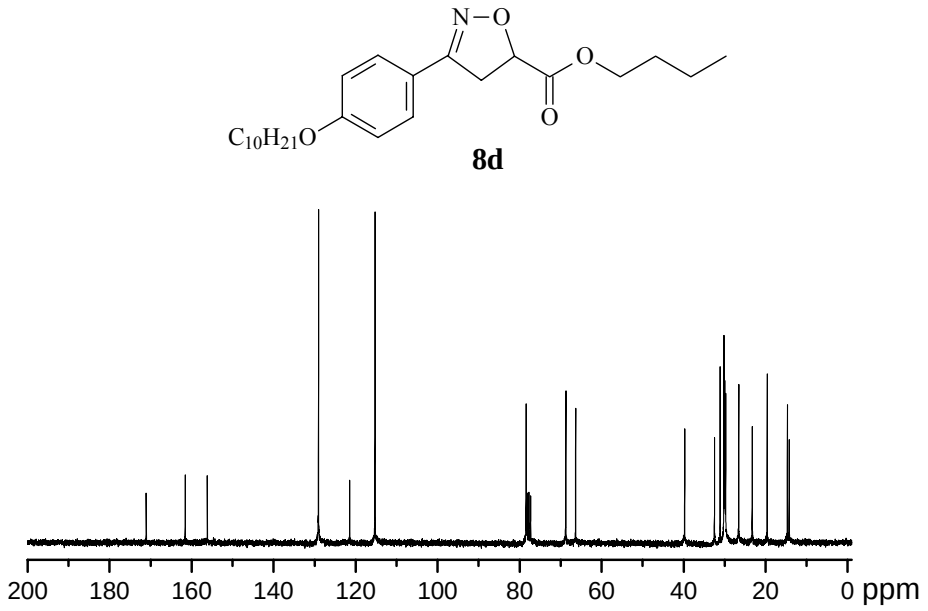

Figure S56. ^{13}C NMR spectrum of compound **8d** ($CDCl_3$, 75 MHz).

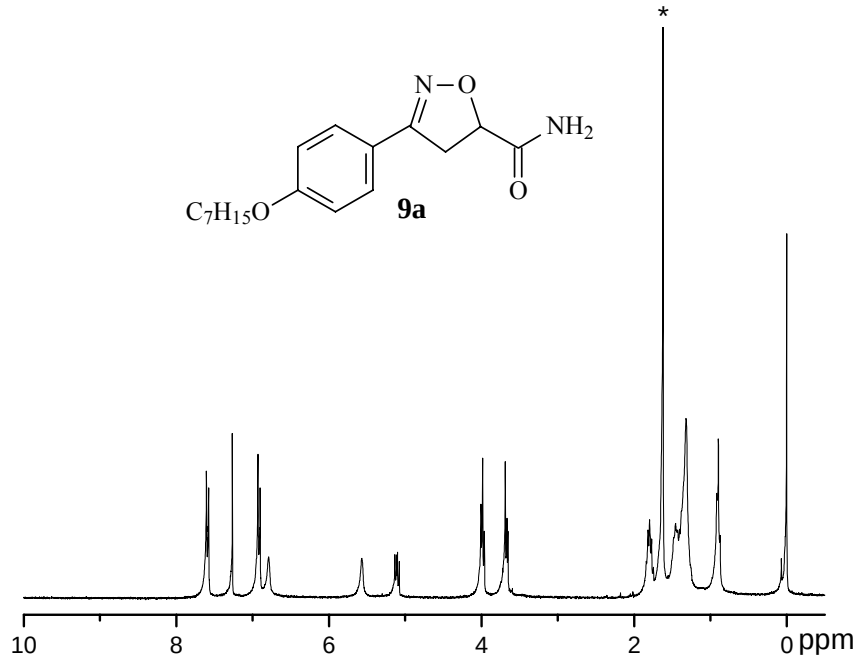

Figure S57. ^{1}H NMR spectrum of compound **9a** ($CDCl_3$/DMSO-d_6, 300 MHz). *Solvent impurity.

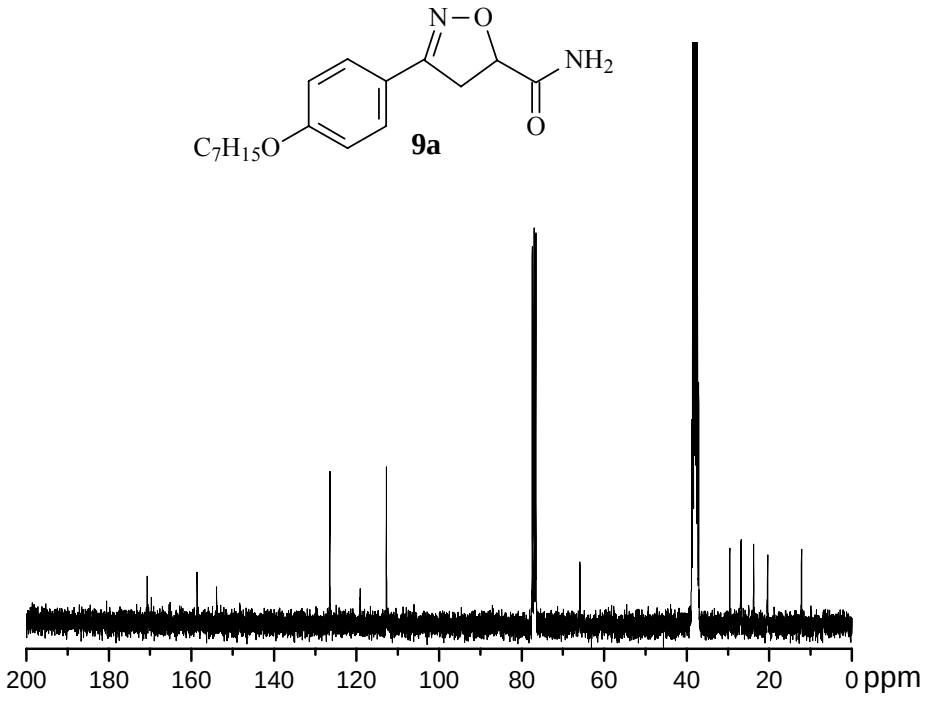

Figure S58. ^{13}C NMR spectrum of compound **9a** ($CDCl_3$/DMSO-d_6, 75 MHz).

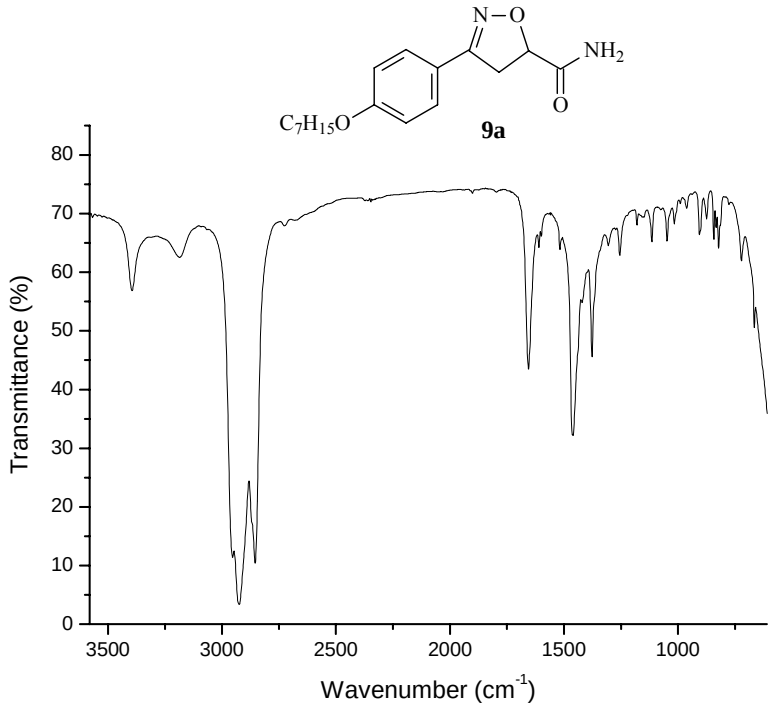

Figure S59. FT-IR spectrum of compound **9a** (nujol).

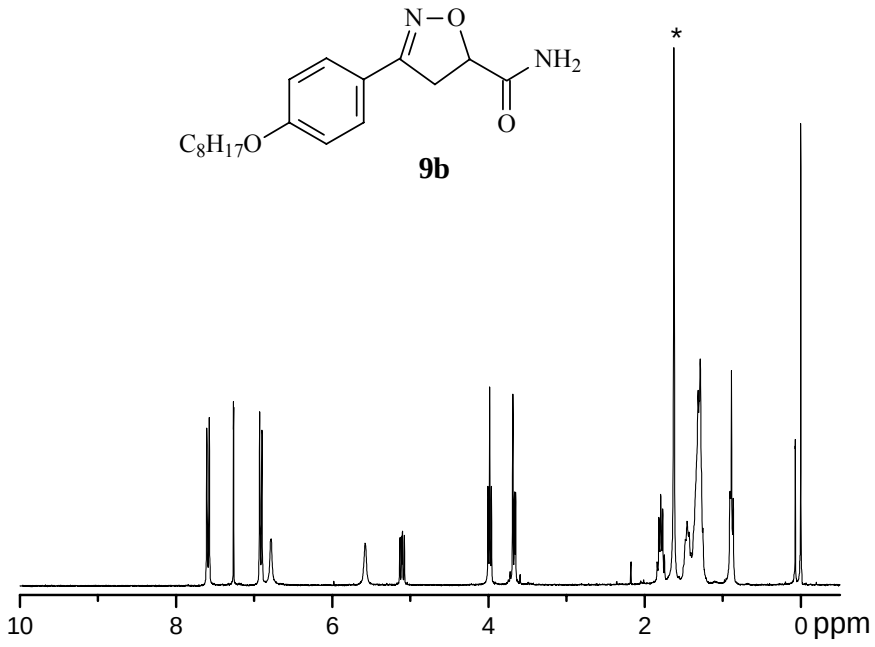

Figure S60. ^{1}H NMR spectrum of compound **9b** ($CDCl_3$/DMSO-d_6, 300 MHz). *Solvent impurity.

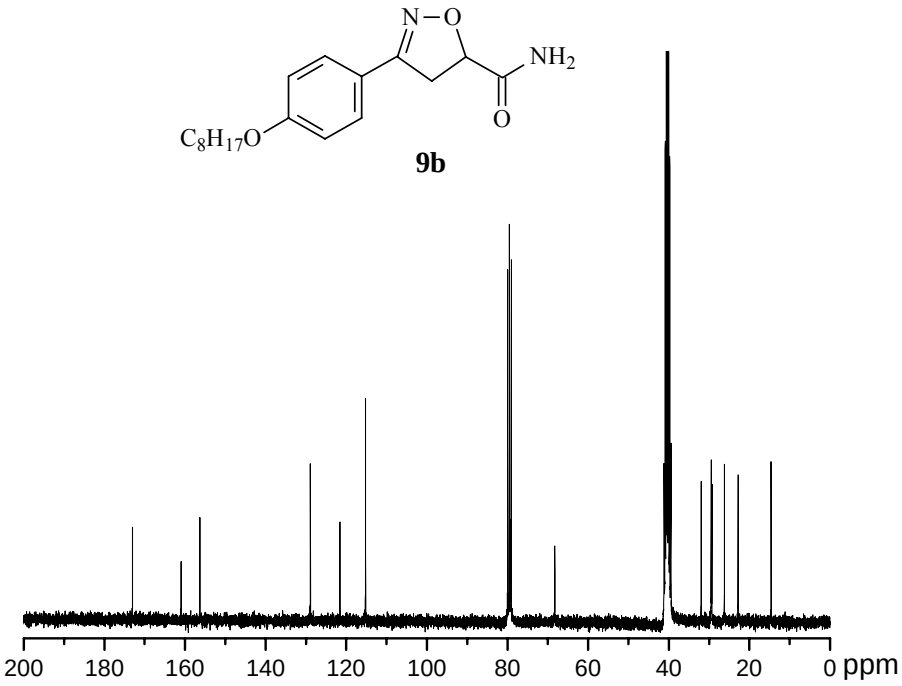

Figure S61. ^{13}C NMR spectrum of compound **9b** ($CDCl_3$/DMSO-d_6, 75 MHz).

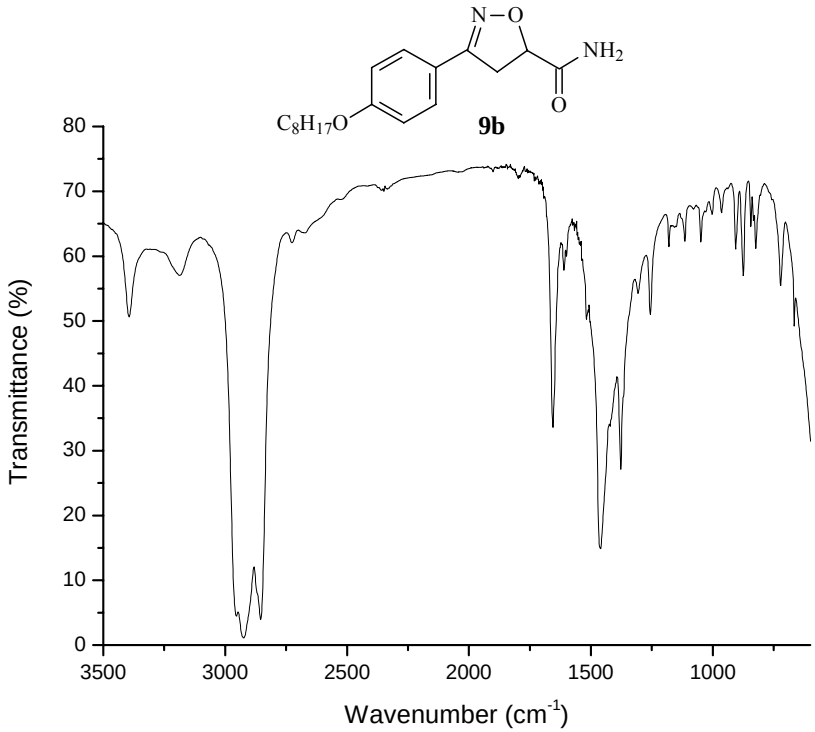

Figure S62. FT-IR spectrum of compound **9b** (nujol).

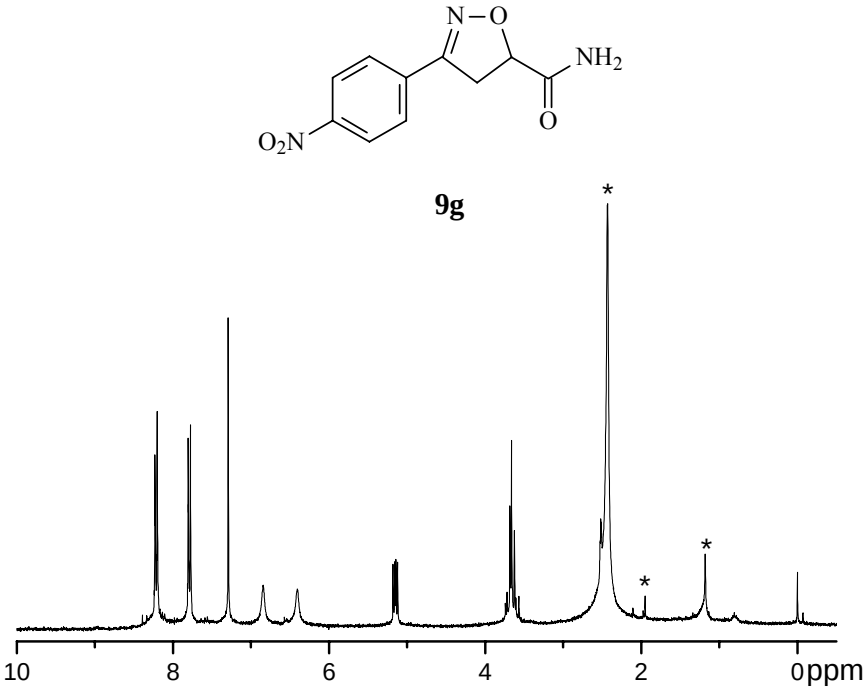

Figure 63. ^{1}H NMR spectrum of compound **9g** ($CDCl_3$/DMSO-d_6, 300 MHz). *Solvent impurity.

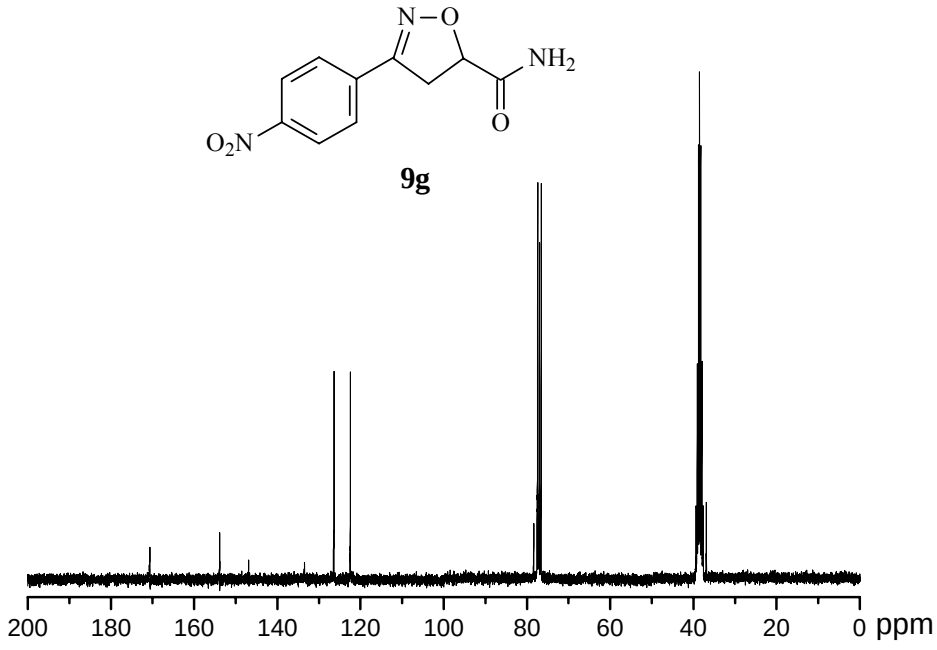

Figure S64. ^{13}C NMR spectrum of compound **9g** ($CDCl_3$/DMSO-d_6, 75 MHz).

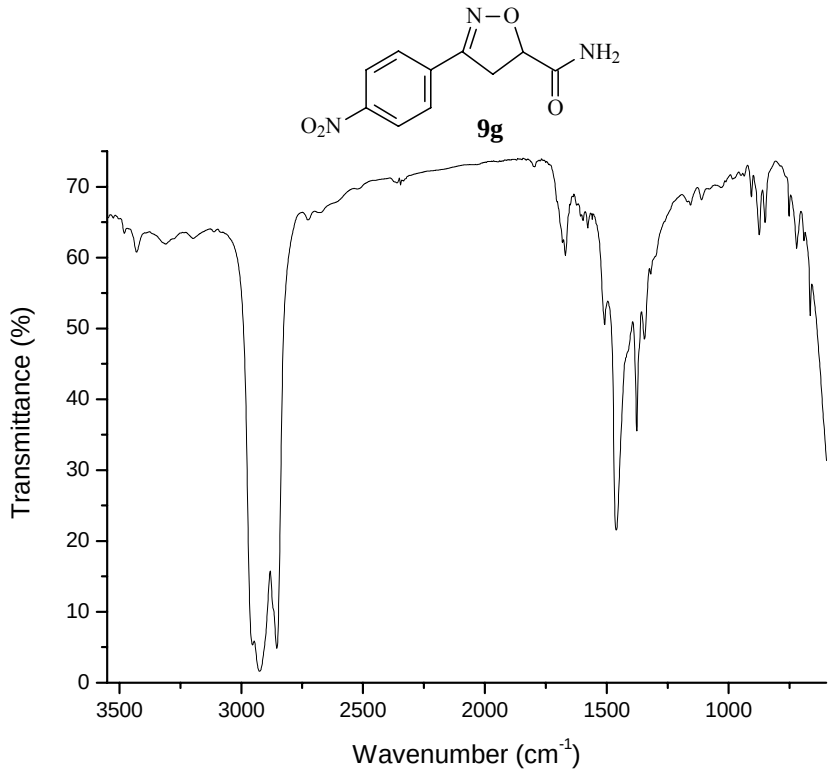

Figure S65. FT-IR spectrum of compound **9g** (nujol).

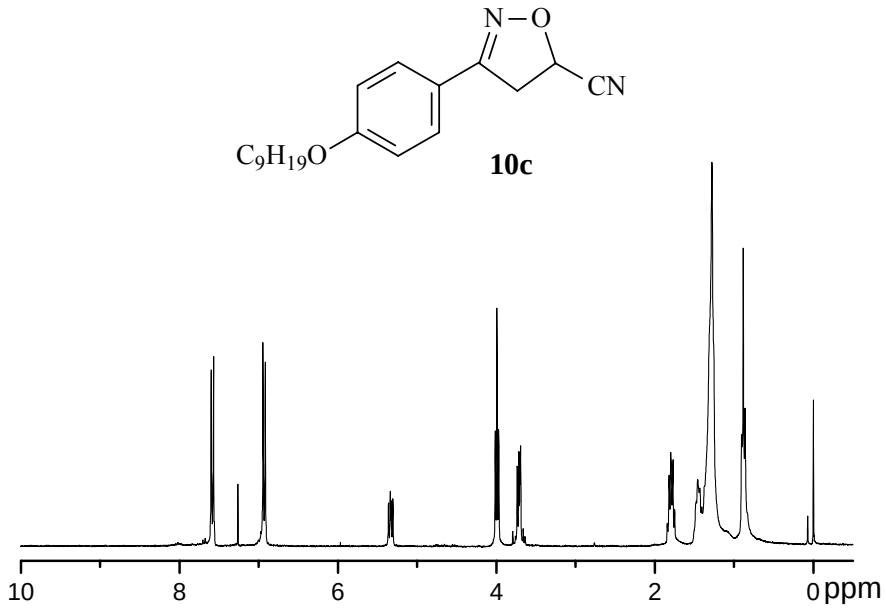

Figure S66. ^{1}H NMR spectrum of compound **10c** ($CDCl_3$, 300 MHz)**.**

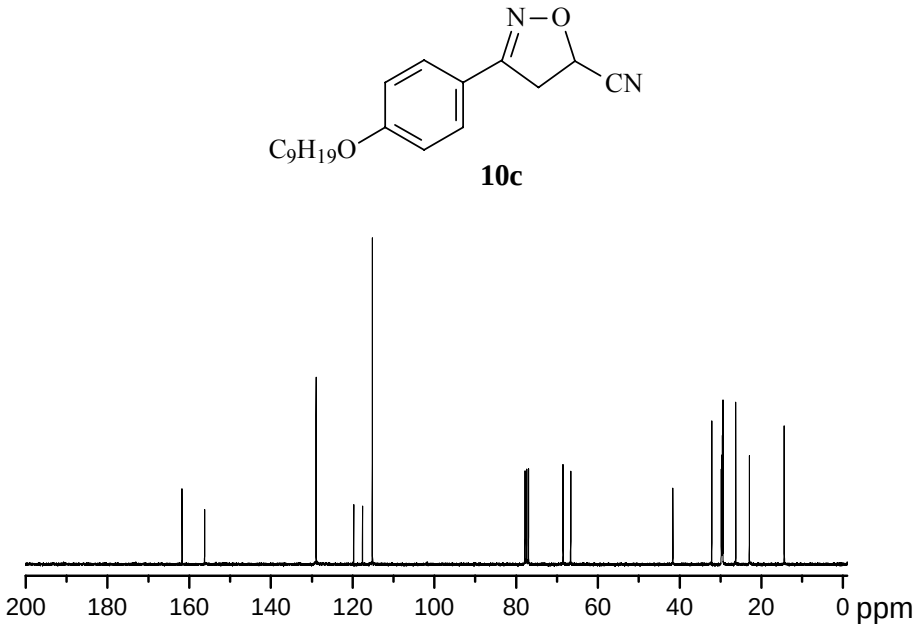

Figure S67. ^{13}C NMR spectrum of compound **10c** ($CDCl_3$, 75 MHz).

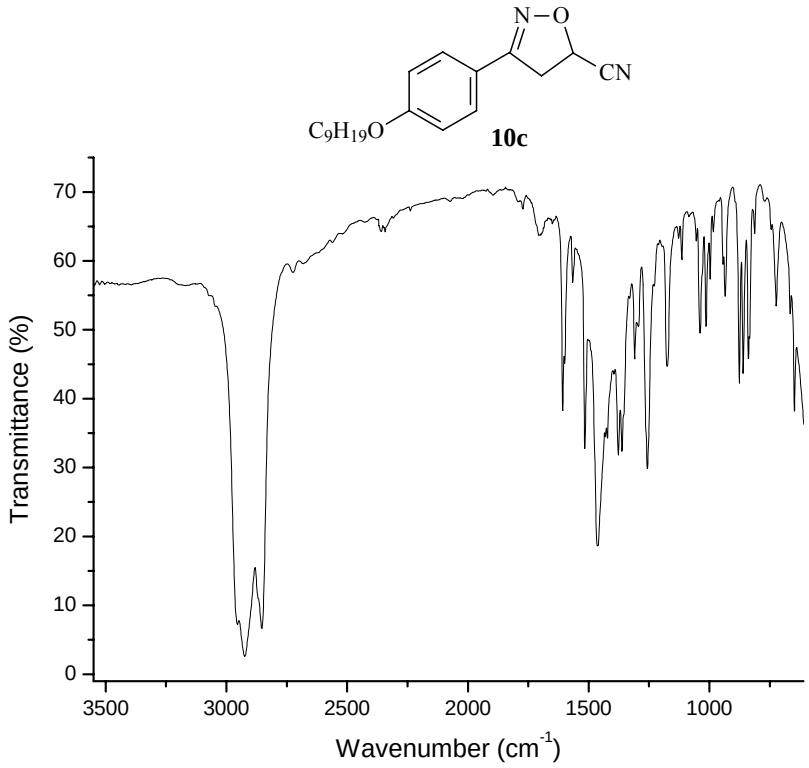

Figure S68. FT-IR spectrum of compound **10c** (nujol).

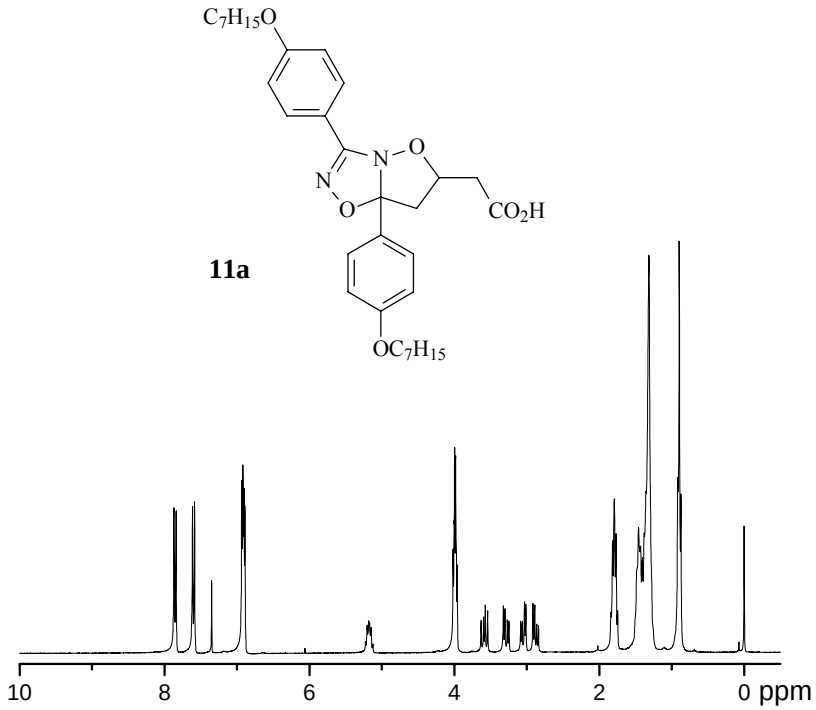

Figure S69. ^{1}H NMR spectrum of compound **11a** ($CDCl_3$, 300 MHz)**.**

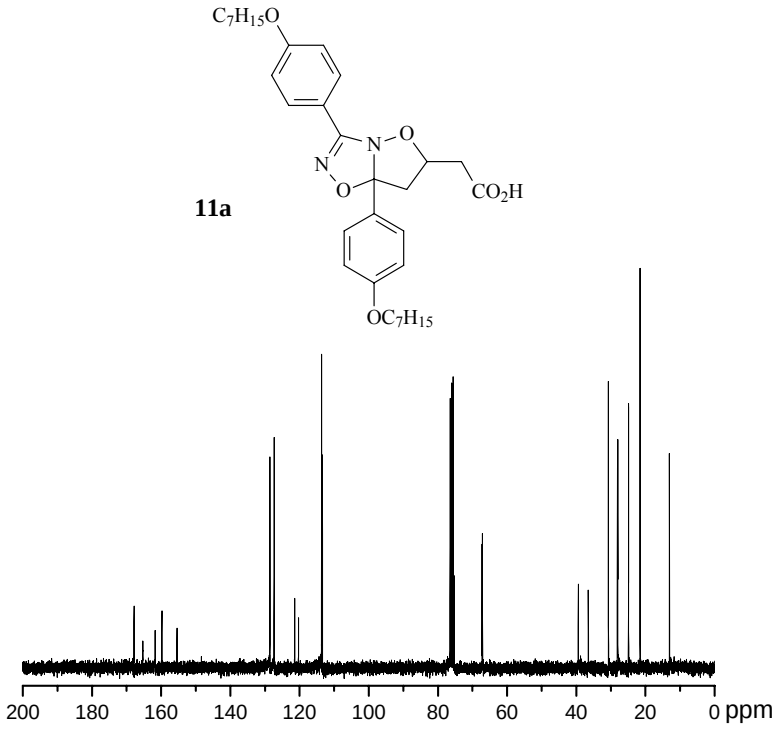

Figure S70. ^{13}C NMR spectrum of compound **11a** ($CDCl_3$/DMSO-d_6, 75 MHz).

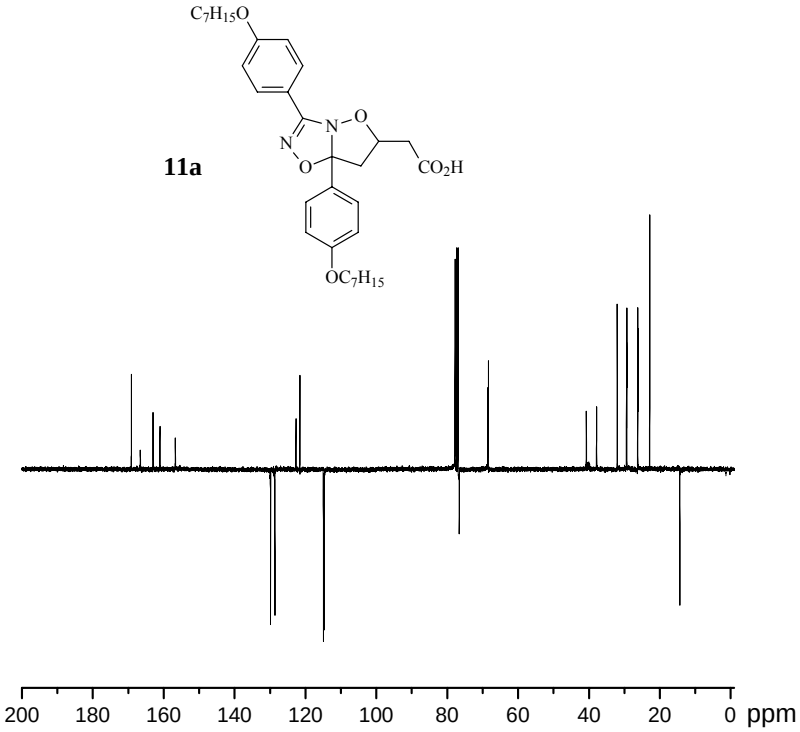

Figure S71. APT spectrum of compound **11a** ($CDCl_3$/DMSO-d_6, 75 MHz).

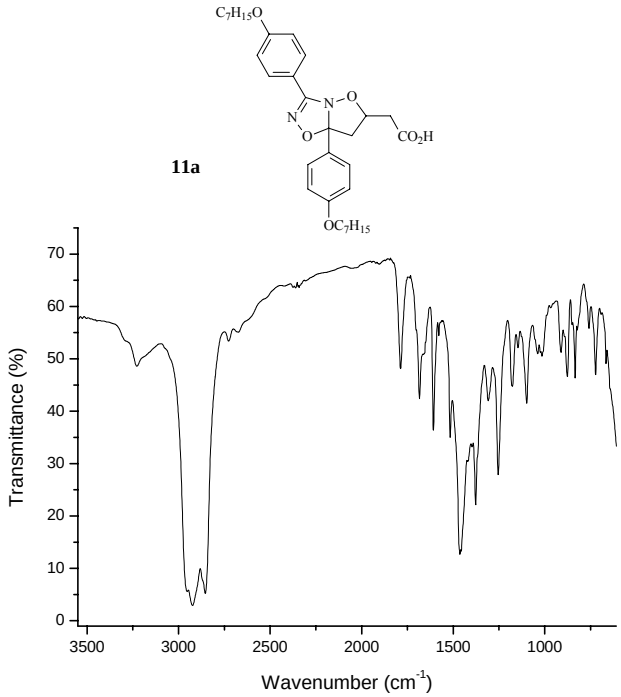

Figure S72. FT-IR spectrum of compound **11a** (nujol).

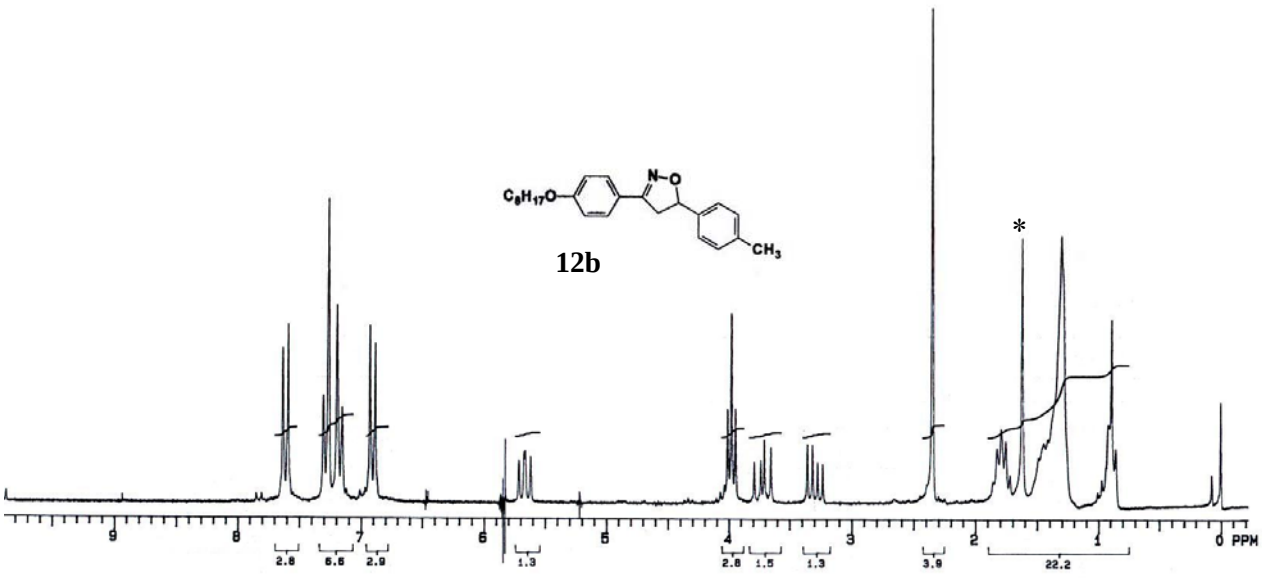

Figure S73. ^{1}H NMR spectrum of compound **12b** ($CDCl_3$, 200 MHz)**.** *Solvent impurity.

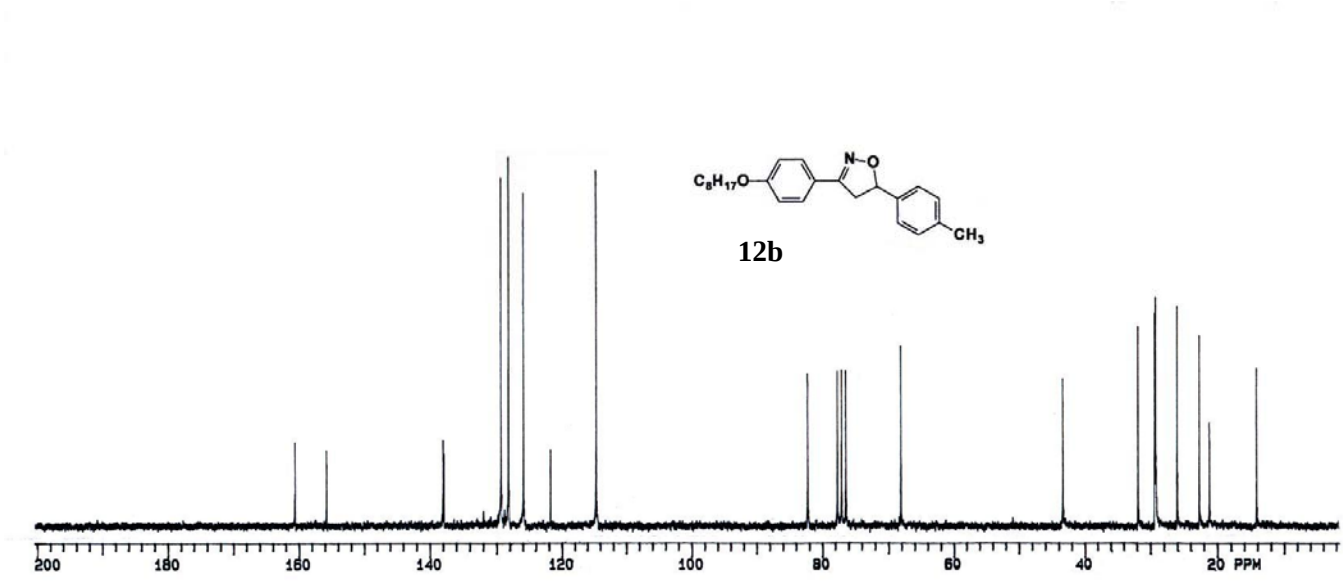

Figure S74. ^{13}C NMR spectrum of compound **12b** ($CDCl_3$, 50 MHz).

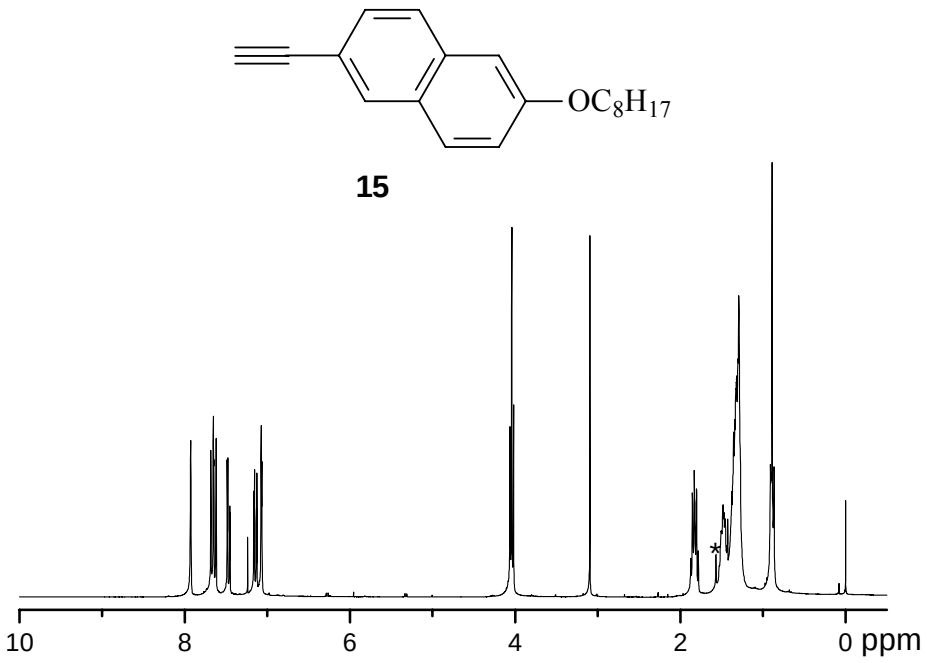

Figure S75. ^{1}H NMR spectrum of compound **15** ($CDCl_3$, 300 MHz). *Solvent impurity.

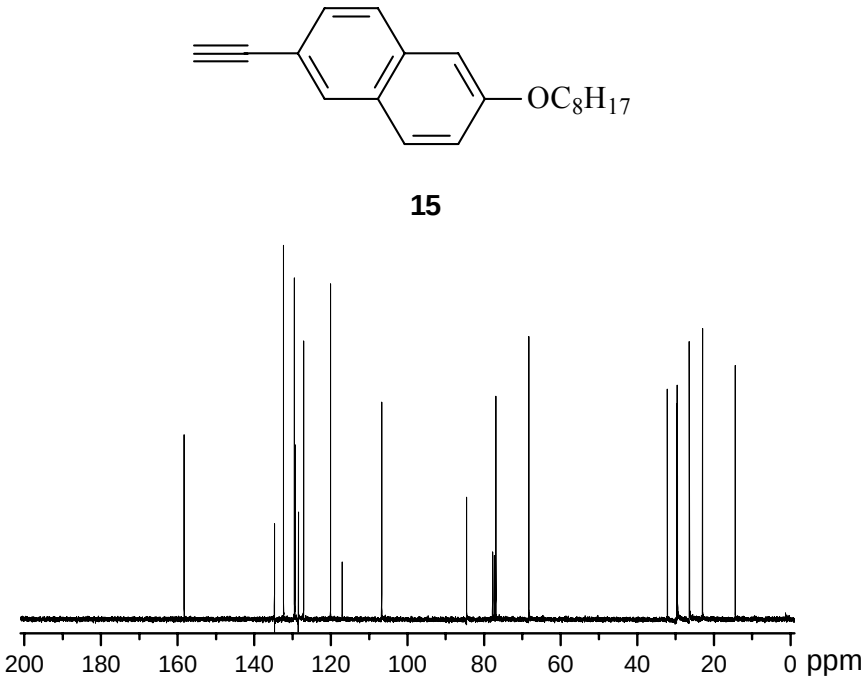

Figure S76. ^{13}C NMR spectrum of compound **15** ($CDCl_3$, 75 MHz).

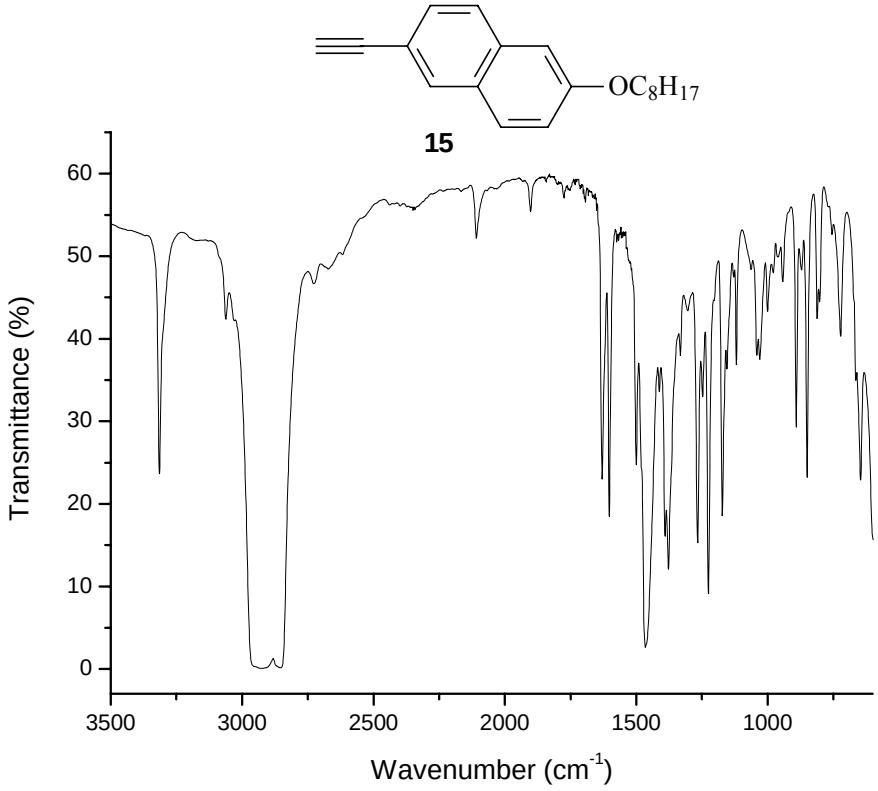

Figure S77. FT-IR spectrum of compound **15** (nujol).

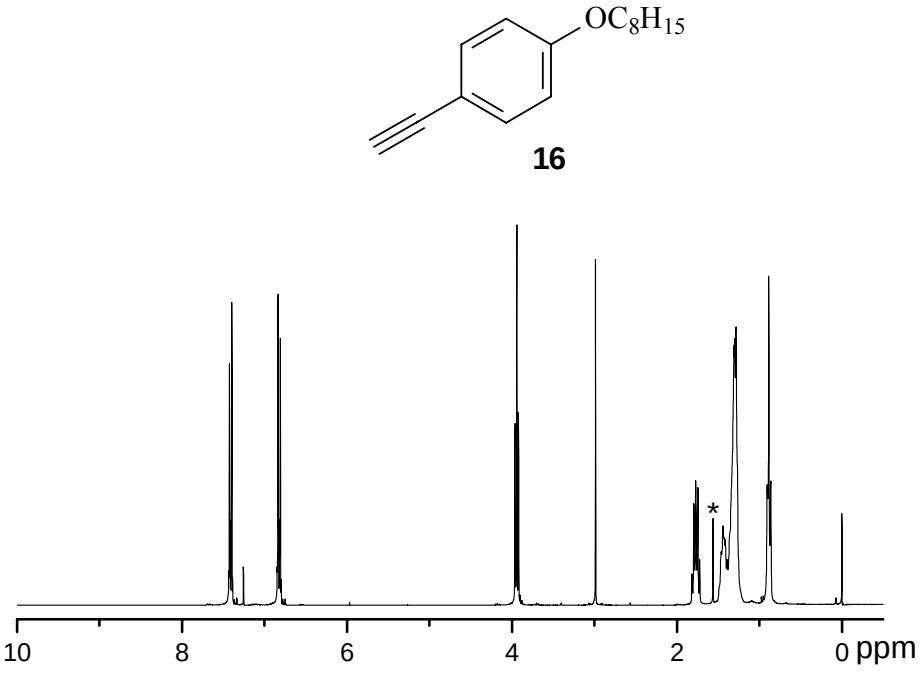

Figure S78. ^{1}H NMR spectrum of compound **16** ($CDCl_3$, 300 MHz). *Solvent impurity.

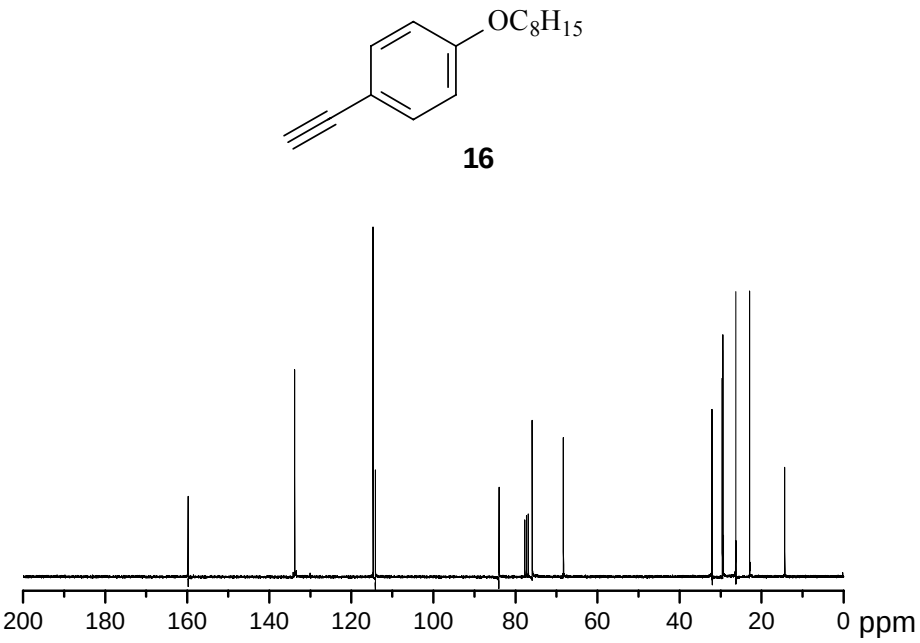

Figure S79. ^{13}C NMR spectrum of compound **16** ($CDCl_3$, 75 MHz).

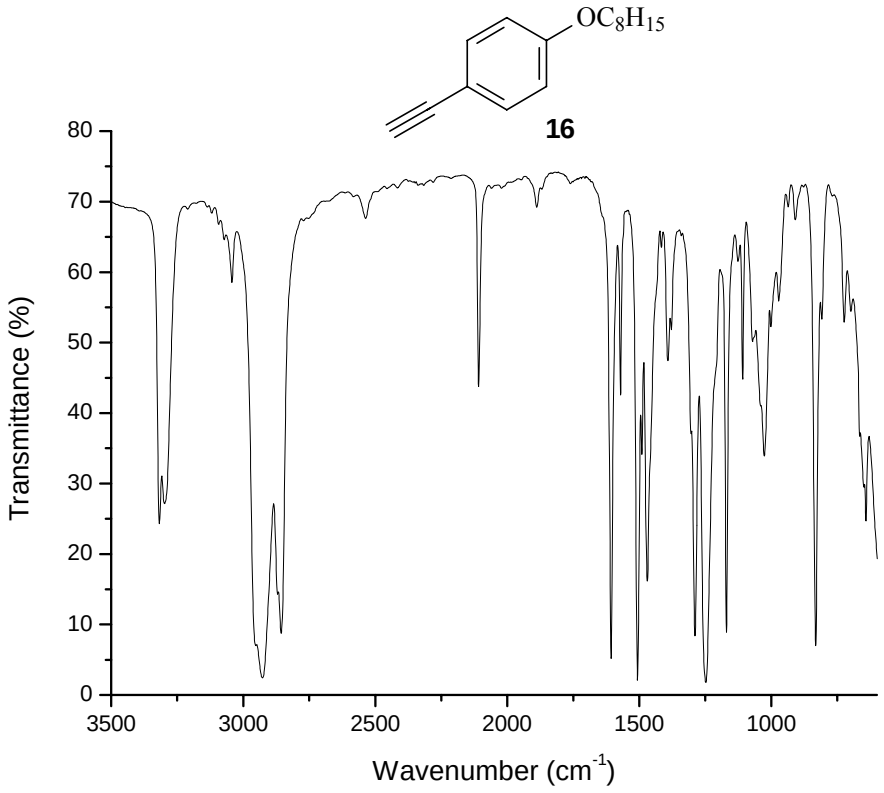

Figure S80. FT-IR spectrum of compound **16** (neat liquid, thin film).

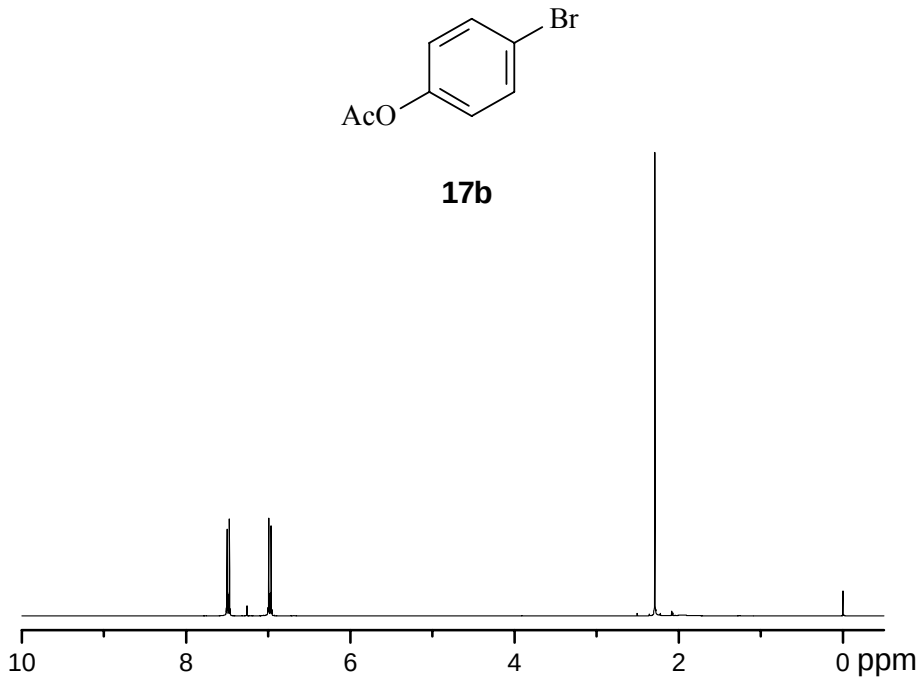

Figure S81. ^{1}H NMR spectrum of compound **17b** ($CDCl_3$, 300 MHz).

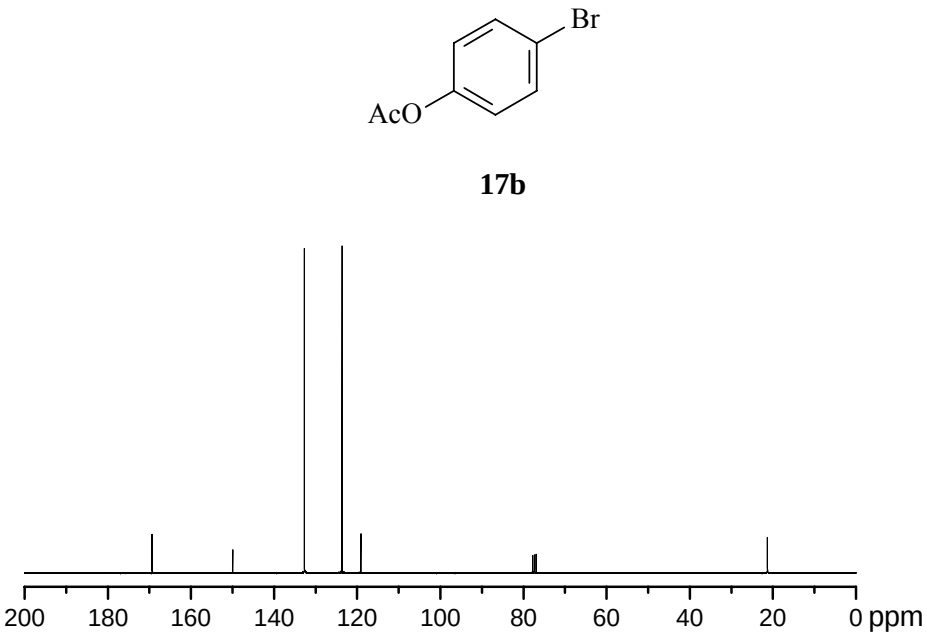

Figure S82. ^{13}C NMR spectrum of compound **17b** ($CDCl_3$, 75 MHz).

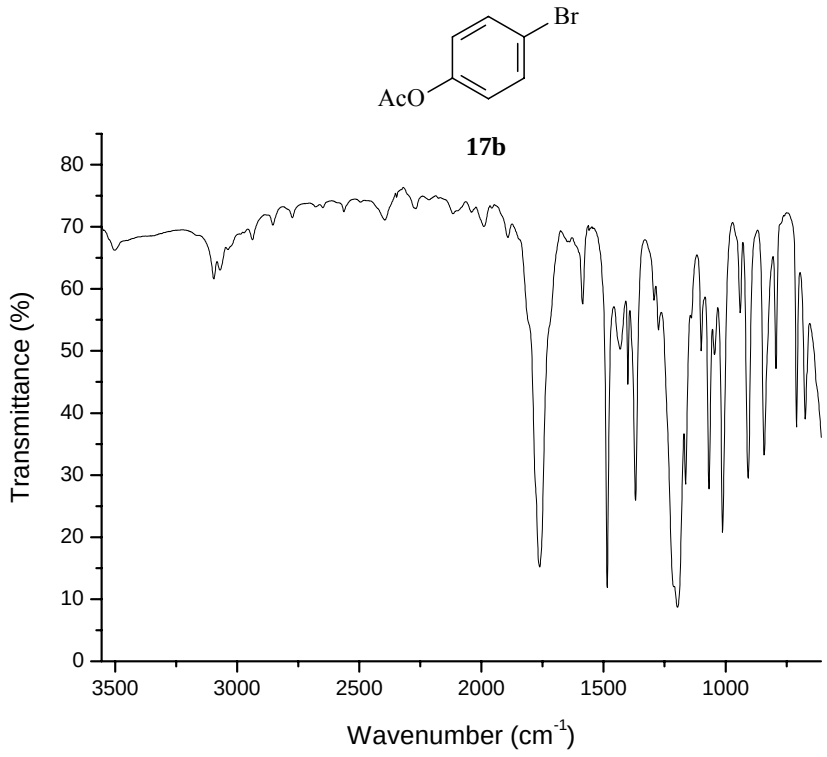

Figure S83. FT-IR spectrum of compound **17b** (neat liquid, thin film).

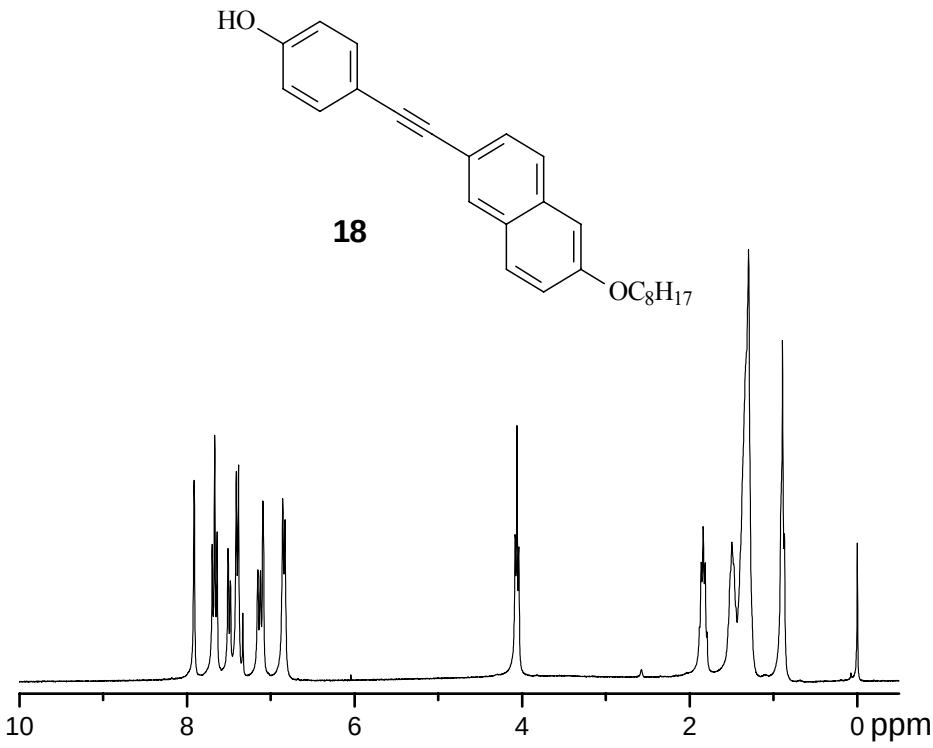

Figure S84. ^{1}H NMR spectrum of compound **18** ($CDCl_3$/DMSO-d_6, 300 MHz).

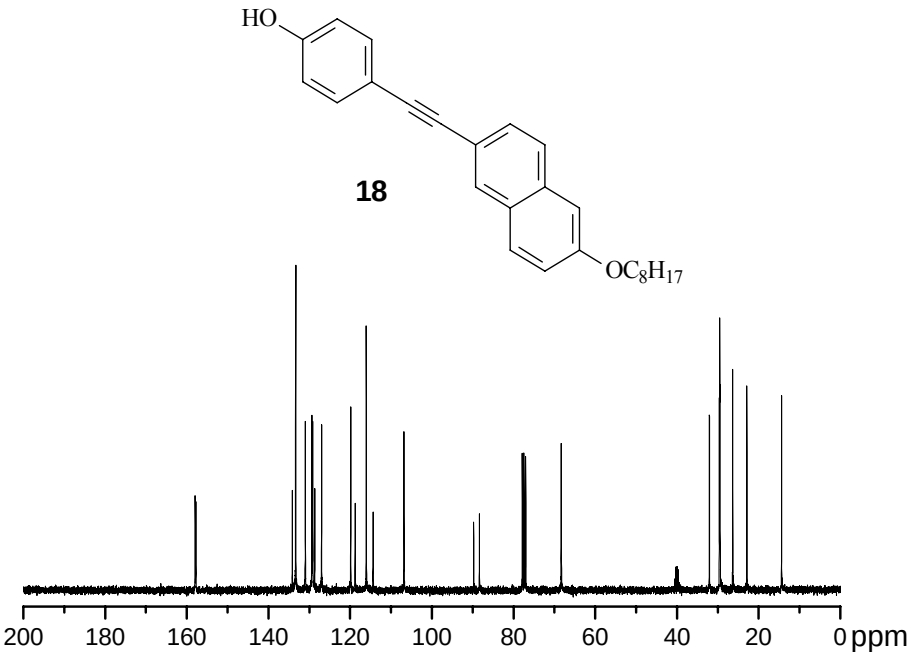

Figure S85. ^{13}C NMR spectrum of compound **18** ($CDCl_3$/DMSO-d_6, 75 MHz).

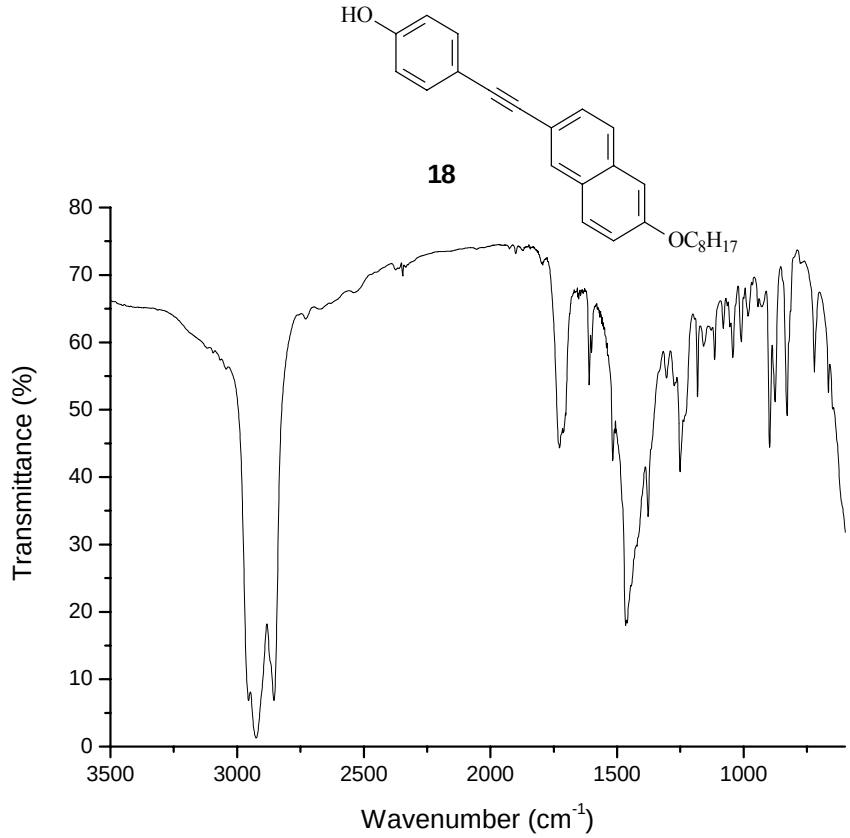

Figure S86. FT-IR spectrum of compound **18** (nujol).

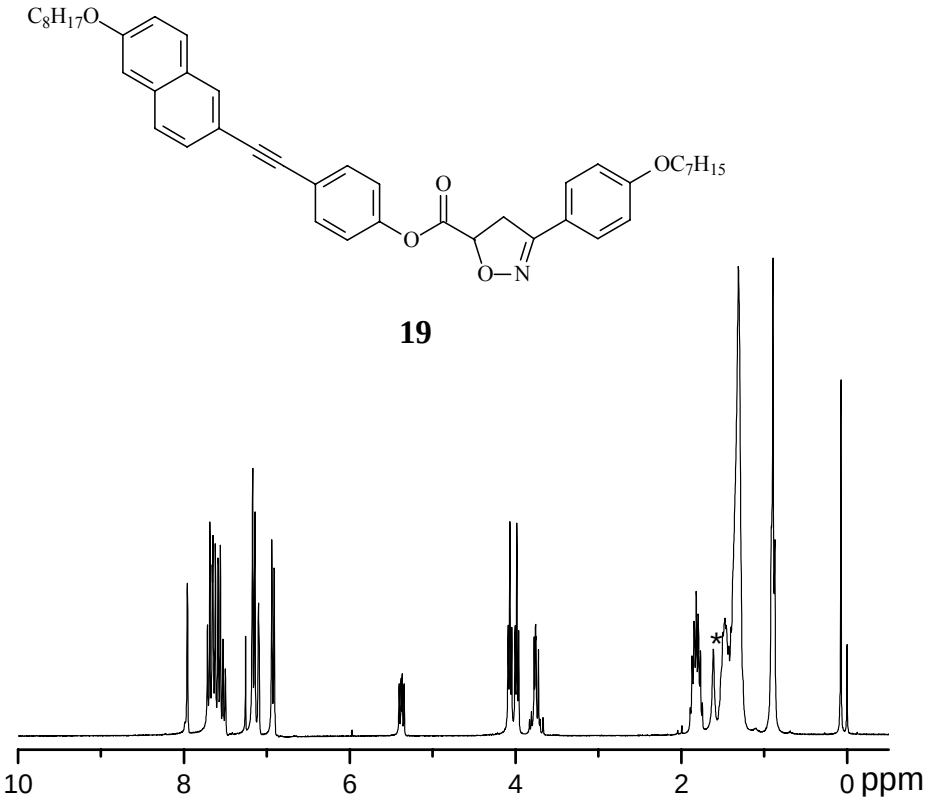

Figure S87. ^{1}H NMR spectrum of compound **19** ($CDCl_3$, 300 MHz). *Solvent impurity.

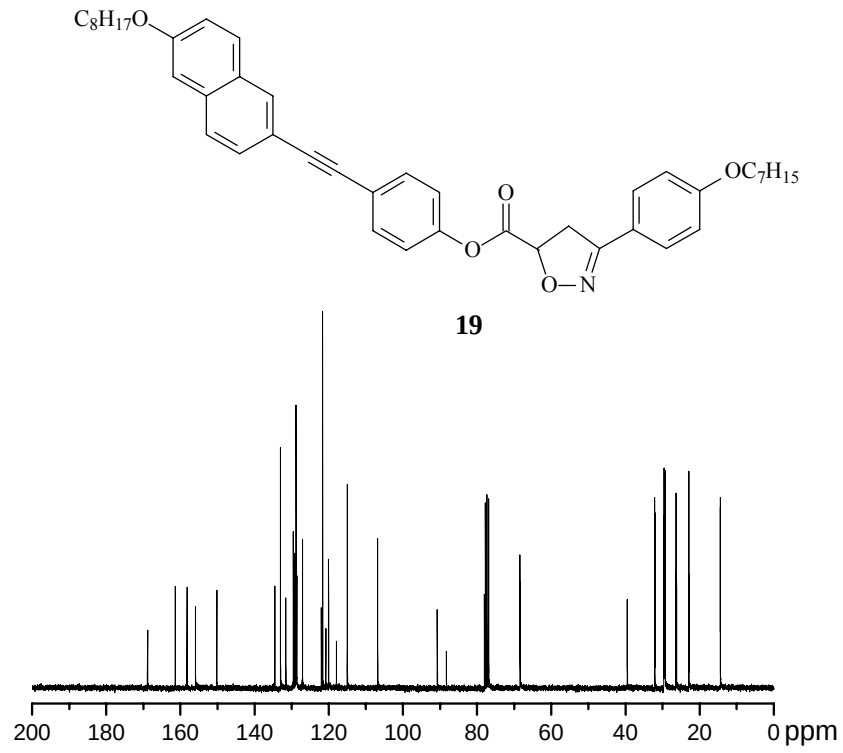

Figure S88. ^{13}C NMR spectrum of compound **19** ($CDCl_3$, 75 MHz).

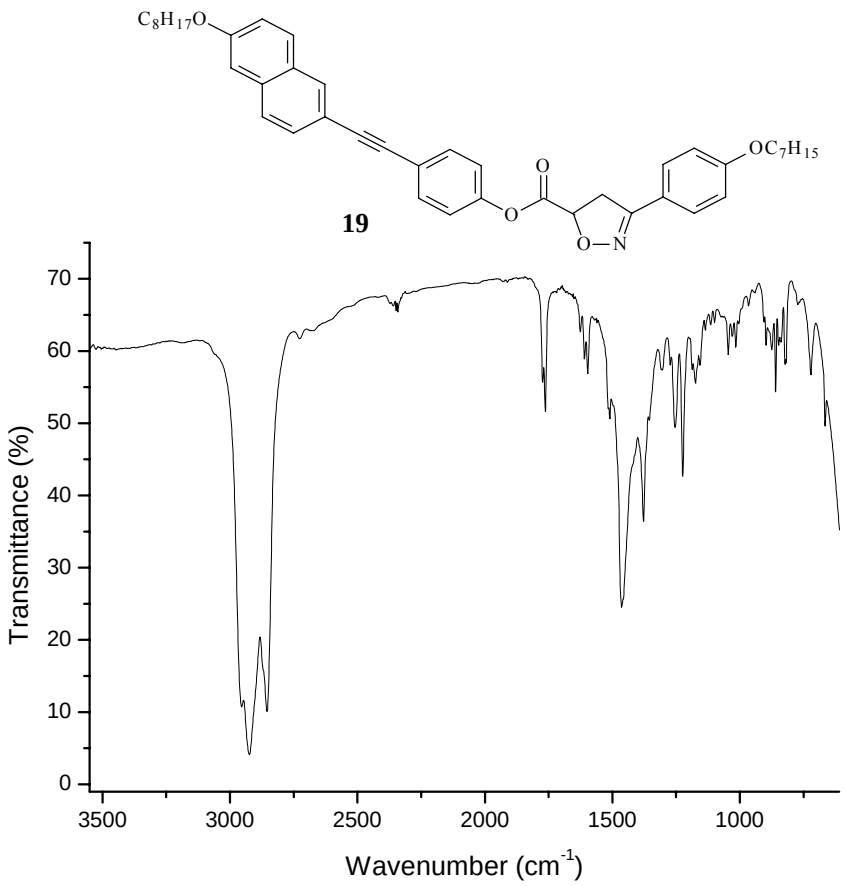

Figure S89. FT-IR spectrum of compound **19** (nujol).

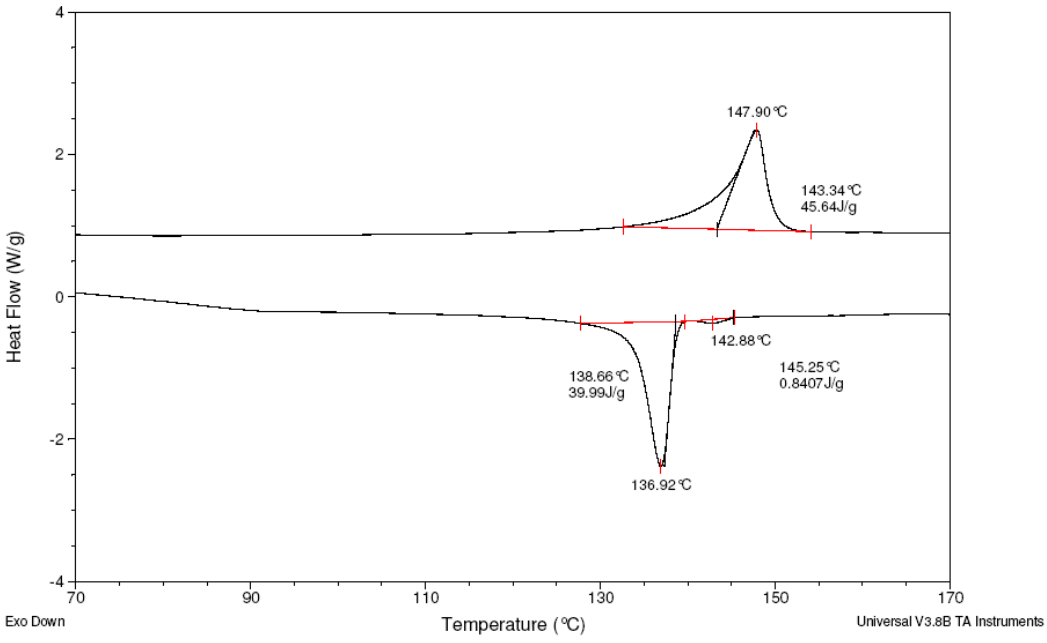

Figure S90. DSC thermogram of compound **19** on 2nd cycle at 10 °C min^{-1}.

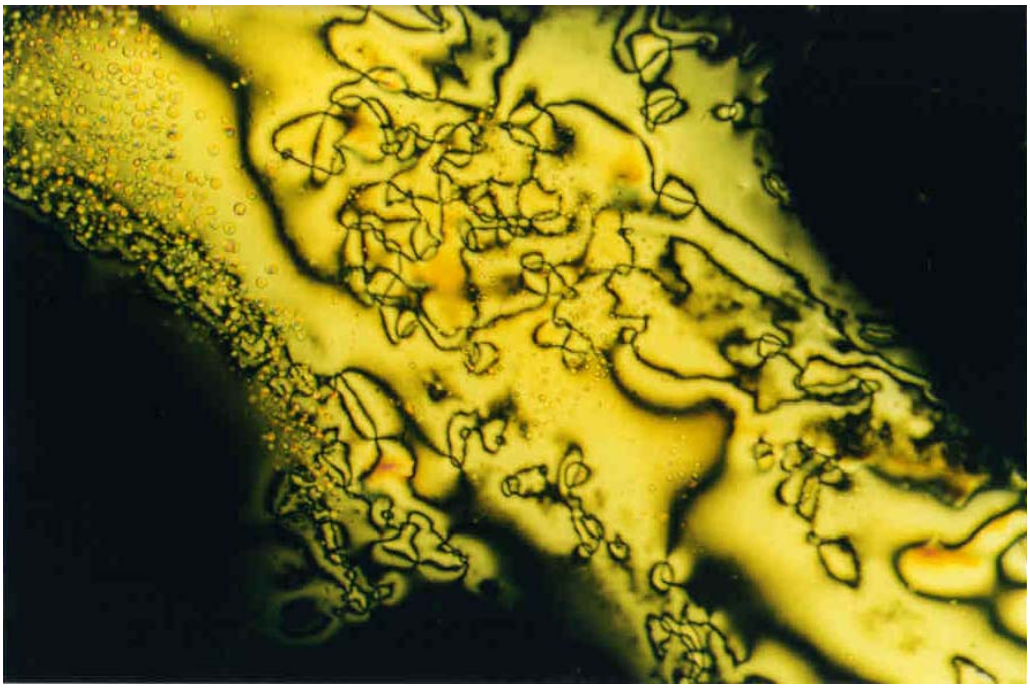

Figure S91. Texture schlieren of the nematic phase for **19** on cooling at 141.7 ^{o}C (10x).

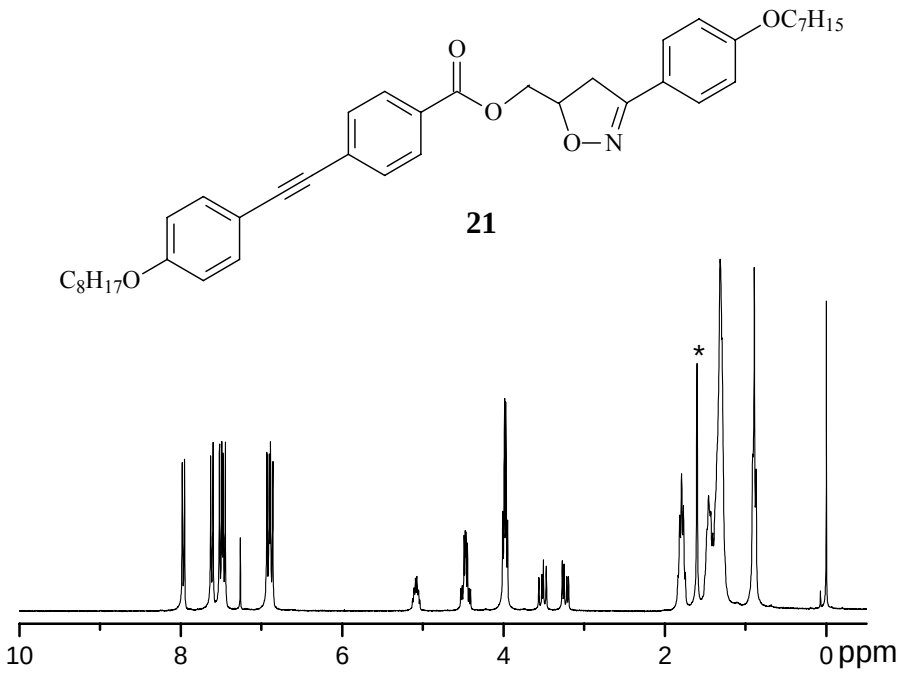

Figure S92. ^{1}H NMR spectrum of compound **21** ($CDCl_3$, 300 MHz). *Solvent impurity.

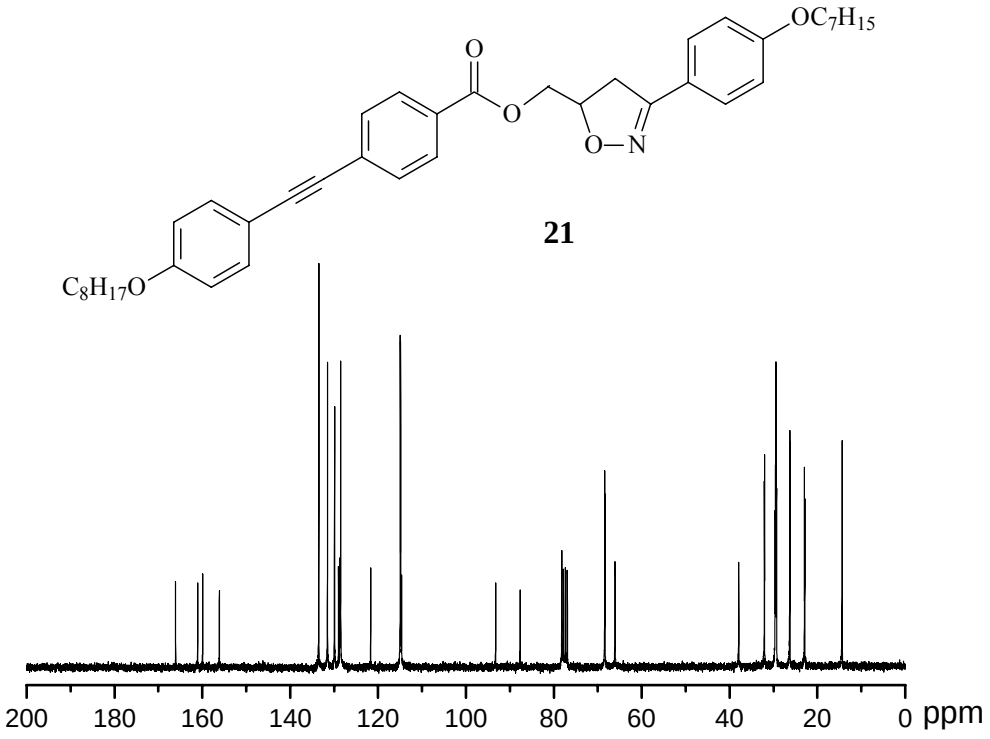

Figure S93. ^{13}C NMR spectrum of compound **21** ($CDCl_3$, 75 MHz).

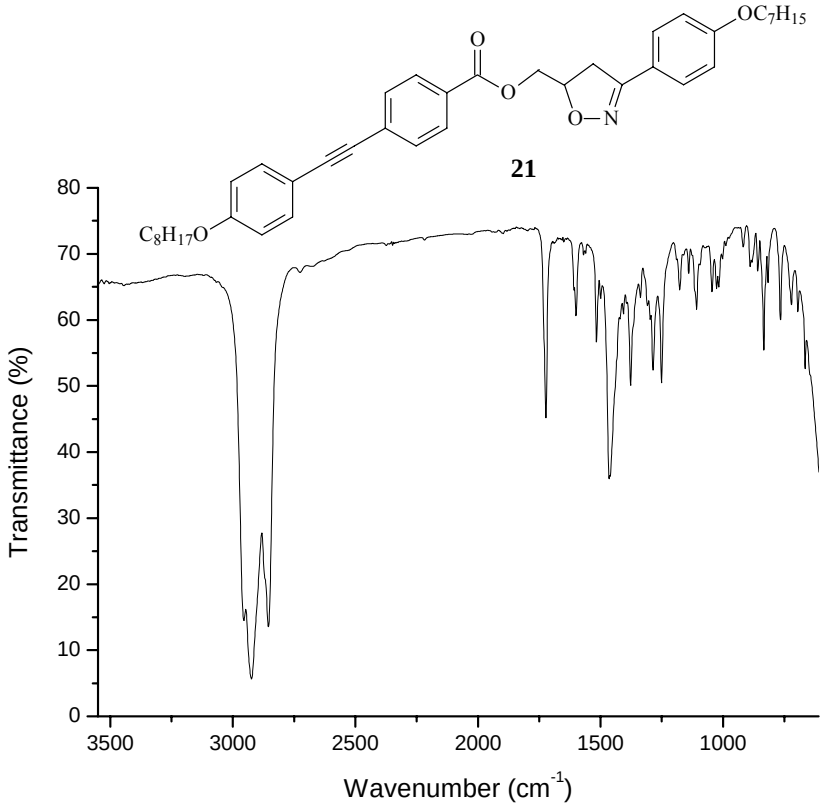

Figure S94. FT-IR spectrum of compound **21** (nujol).

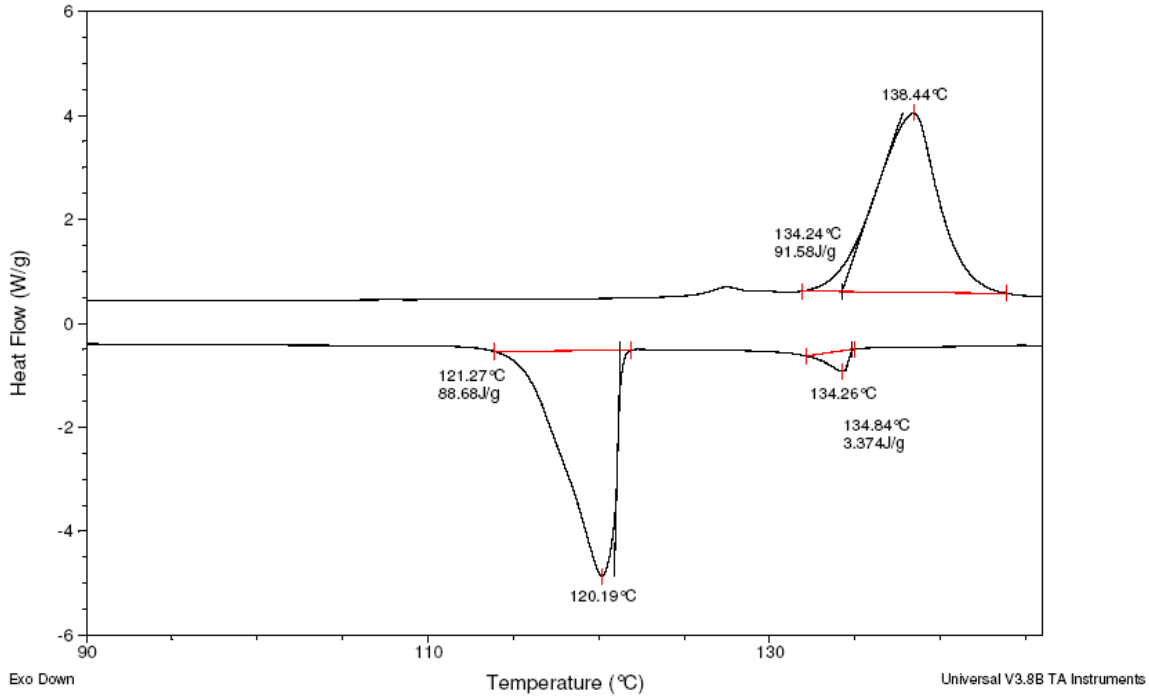

Figure S95. DSC thermogram of compound **21** on 2nd cycle at 10 °C min^{-1}.

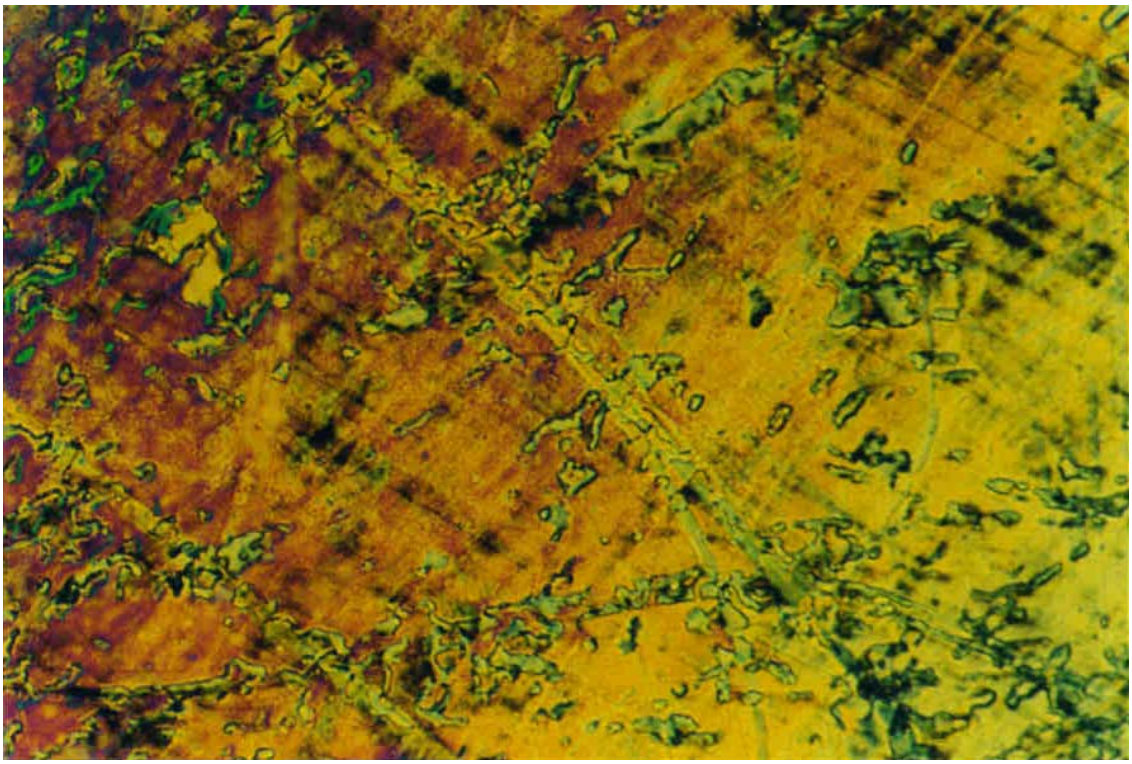

Figure S96. Texture planar of the nematic phase for **21** on cooling at 131.6 °C (10x).

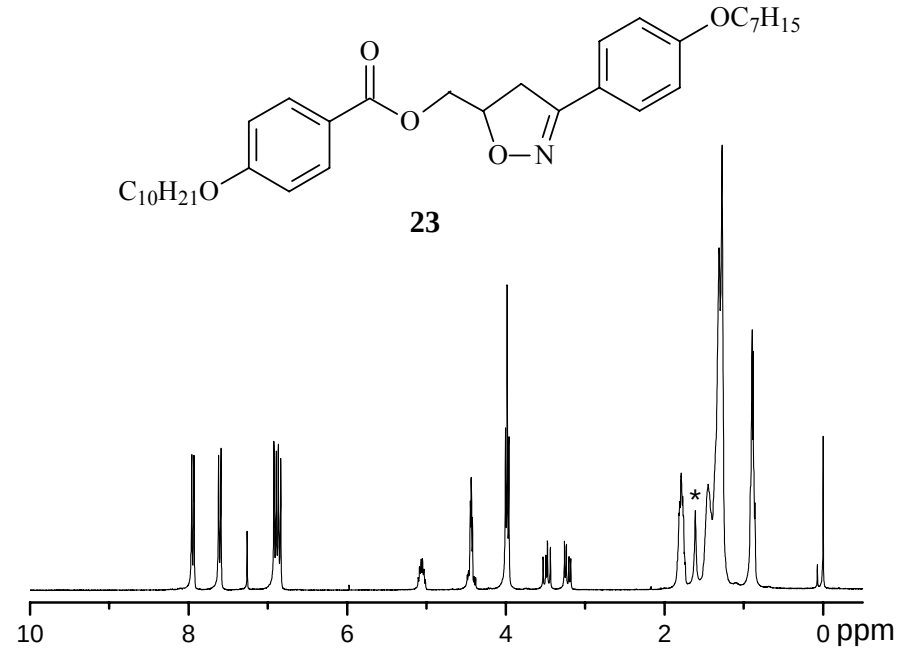

Figure S97. ^{1}H NMR spectrum of compound **23** ($CDCl_3$, 300 MHz). *Solvent impurity.

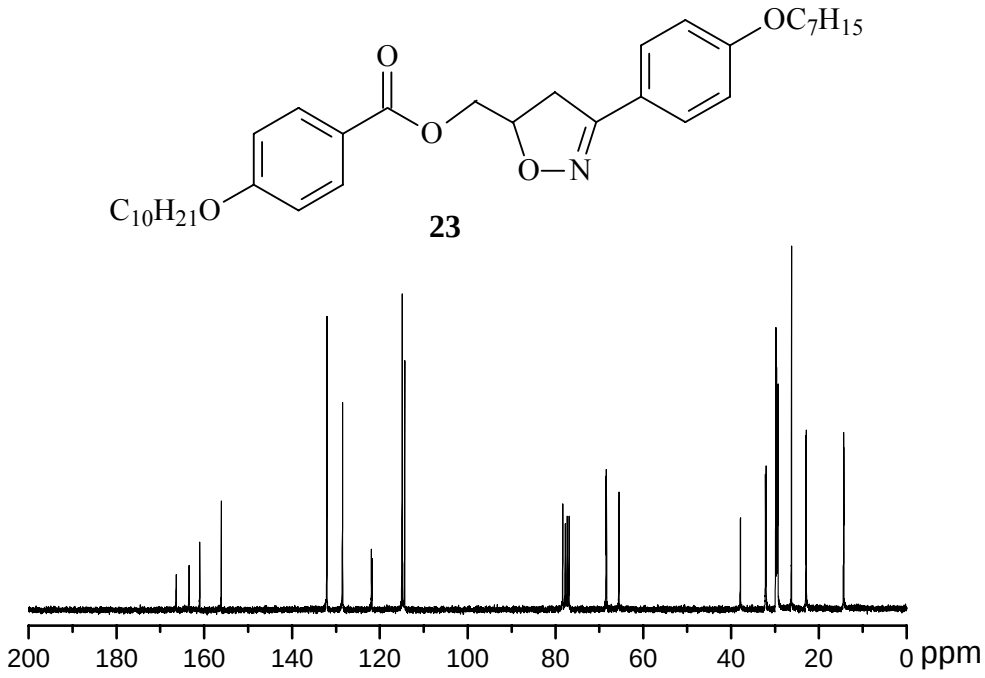

Figure S98. ^{13}C NMR spectrum of compound **23** ($CDCl_3$, 75 MHz).

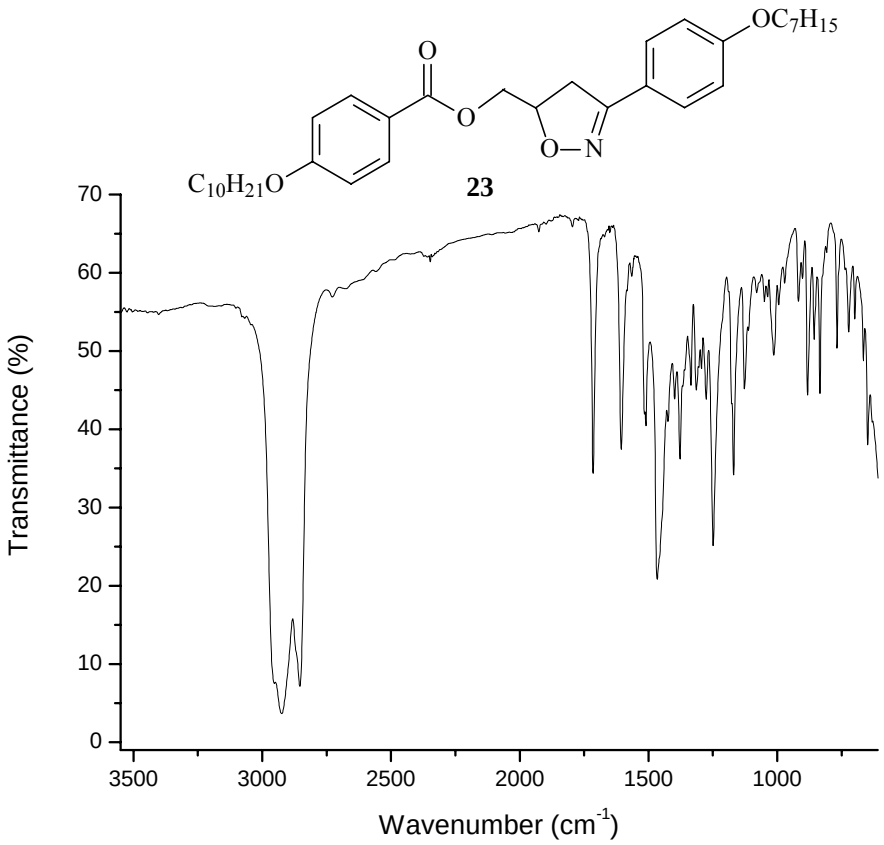

Figure S99. FT-IR spectrum of compound **23** (nujol).

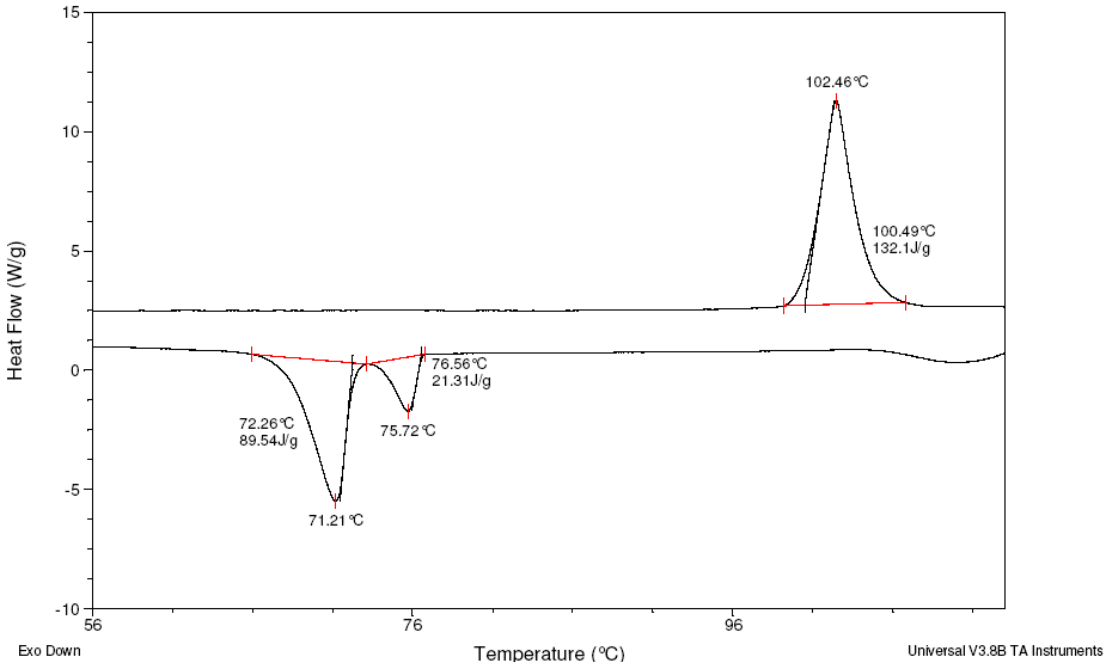

Figure S100. DSC thermogram of compound **23** on 2nd cycle at 10 °C min-1.

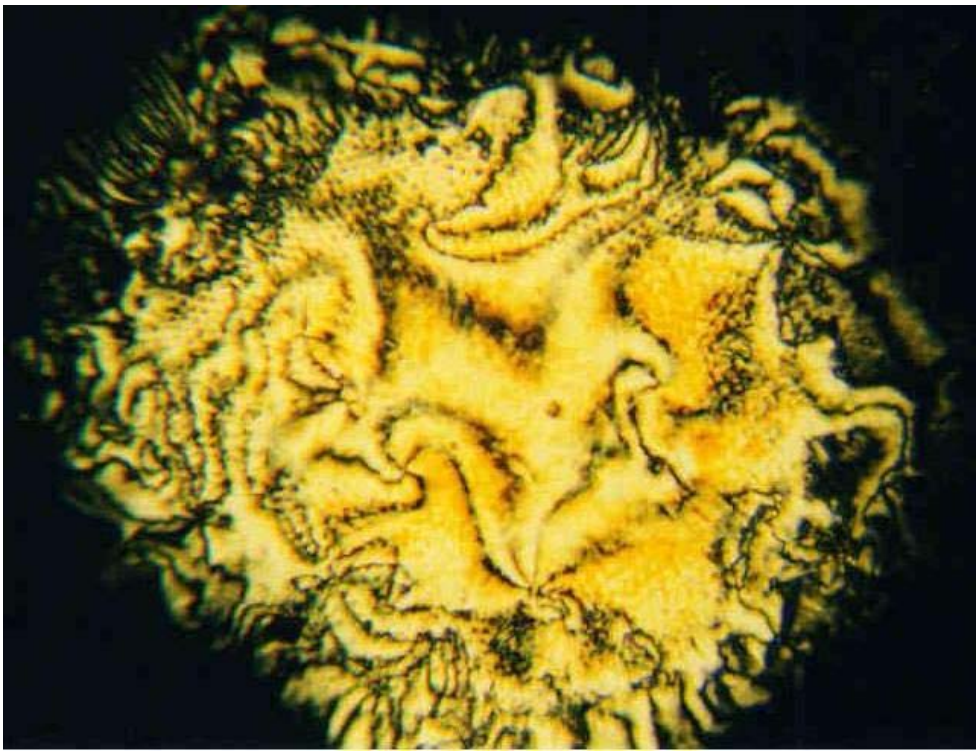

Figure S101. Texture schlieren of the smetic C phase of **23** at 74.0 ^{o}C (10x).

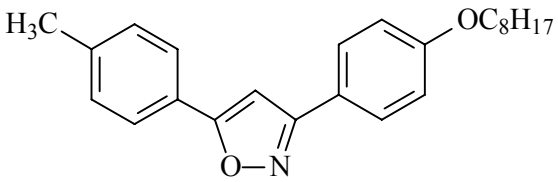

24

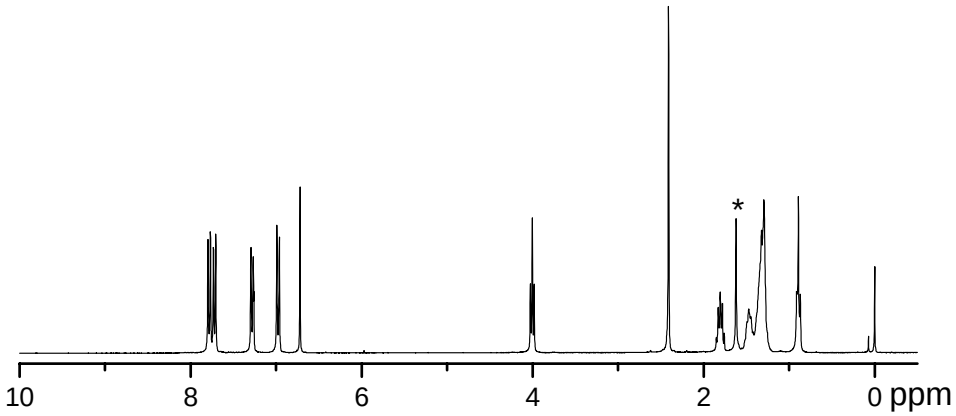

Figure S102. ^{1}H NMR spectrum of compound **24** ($CDCl_3$, 300 MHz). *Solvent impurity.

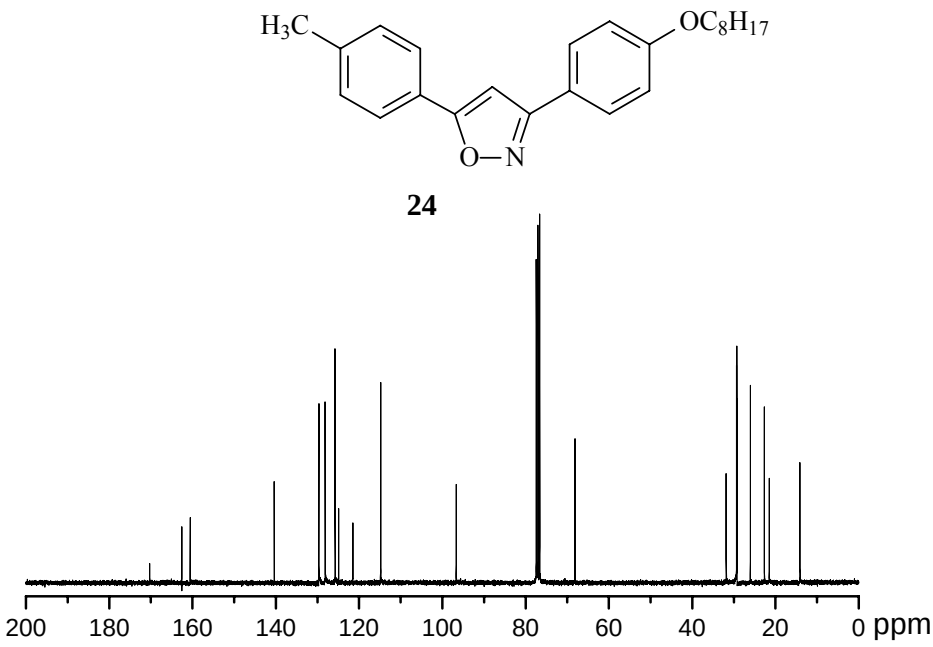

Figure S103. ^{13}C NMR spectrum of compound **24** ($CDCl_3$, 75 MHz).

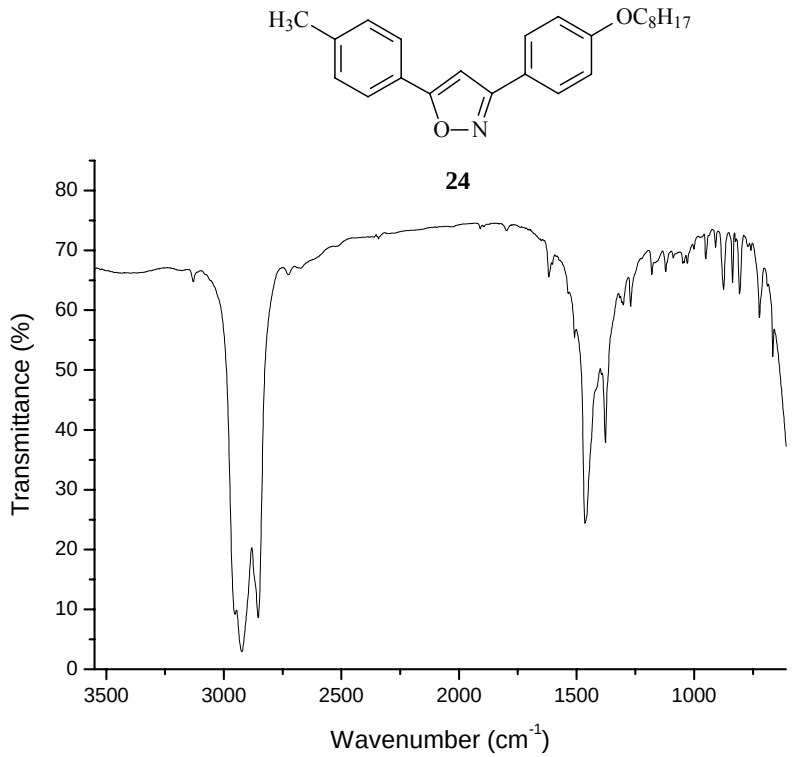

Figure S104. FT-IR spectrum of compound **24** (nujol).

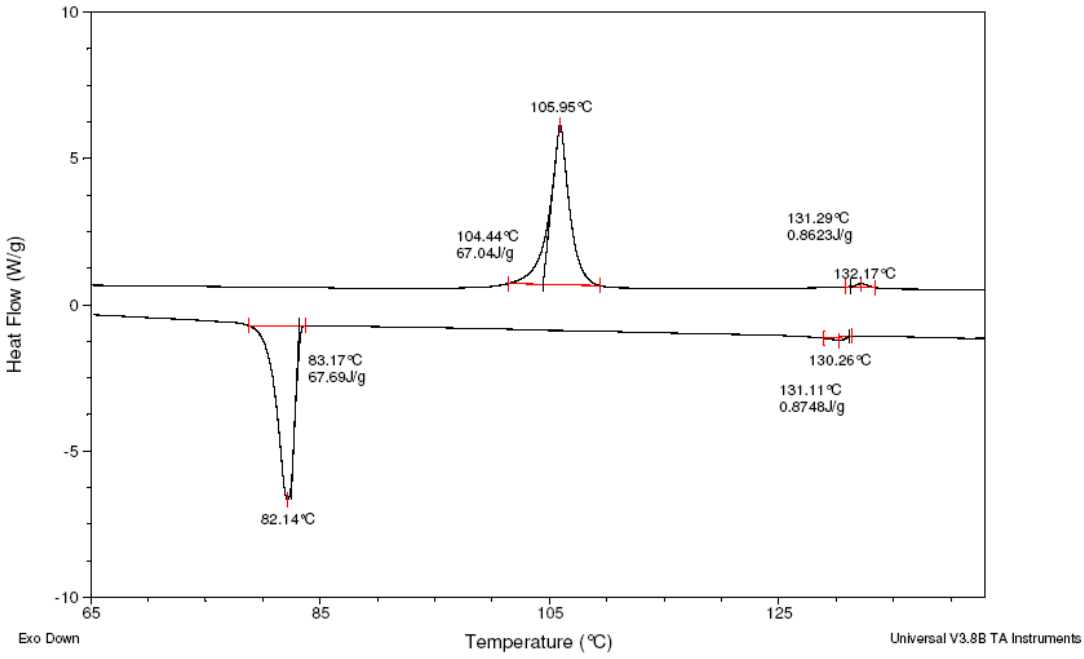

Figure S105. DSC thermogram of compound **24** on 2nd cycle at 10 ^{o}C min^{-1}.

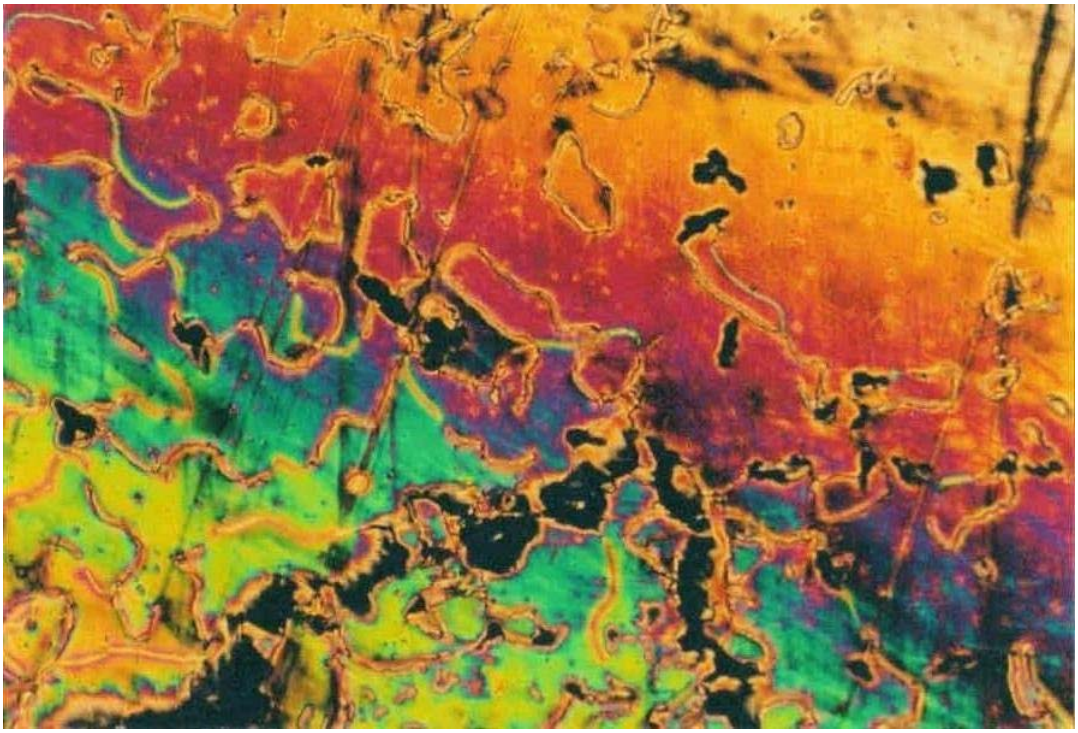

Figure S106. Texture planar of the nematic phase of **24** on cooling at 121.6 ^{o}C (10x).

CAPÍTULO 5.2 - *J. Braz. Chem. Soc.* **2009**, *20*, 1742-1752 –

DOI: 10.1590/S0103-50532009000900025

3-Arylisoxazolyl-5-Carboxylic Acid and 5-(Hydroxymethyl)-3-Aryl-2-Isoxazoline as Molecular Platforms for Liquid-Crystalline Materials.

Aline Tavares,[a] Paolo R. Livotto,[a] Paulo F. B. Gonçalves[b] and Aloir A. Merlo*[a]

[a]Instituto de Química. Universidade Federal do Rio Grande do Sul, 91501-970. Porto Alegre-RS, Brazil
[b]Centro Universitário La Salle, 92010-000. Canoas-RS, Brazil

A síntese de uma plataforma molecular para materiais líquido-cristalinos derivados do ácido 3-arilisoxazolil-5-carboxílico (**1**) e do 5-(hidroximetil)-3-aril-2-isoxazolina (**2**) é descrita. Os intermediários **1** e **2** são obtidos através da reação de cicloadição [3+2] 1,3-dipolar entre arilóxidos de nitrilas e os dipolarófilos ácido acrílico e álcool alílico, respectivamente. Os compostos cristais líquidos são sintetizados através de uma estratégia de alongamento molecular do núcleo primitivo isoxazolínico pela conexão de subunidades arilacetilênicas, as quais foram obtidas da reação de Sonogashira. Sob essas condições, séries de cristais líquidos **5a-c, 6, 7a-g** e **8a-d** têm sido sintetizadas com rendimentos de médios para bons. Os compostos finais apresentam propriedades líquido-cristalinas nematogênica e esmectogênica. Um cálculo *ab initio* no nível B3LYP/6-31G(d,p) é também apresentado e alguns parâmetros estruturais obtidos são analisados.

The synthesis of the molecular platform for liquid-crystalline materials based on 3-arylisoxazolyl-5-carboxylic acid (**1**) and 5-(hydroxymethyl)-3-aryl-2-isoxazoline (**2**) is described. The key intermediates **1** and **2** are obtained by [3+2] 1,3-dipolar cycloaddition reaction between an arylnitrile oxide and an acrylic acid and allylic alcohol as the dipolarophile. The liquid crystals (LC) compounds are synthesized through an *molecular elongation strategy* from the initial isoxazolinic core by connecting the arylacetylene moiety obtained from the Sonogashira reaction. Under these conditions, the series of liquid crystals **5a-c, 6, 7a-g** and **8a-d** have been successfully synthesized in fair to good yields. The final compounds display nematic and smectic liquid-crystalline properties. The structural properties of the series of the liquid crystals has been studied using *ab initio* methods at level B3LYP/6-31G(d,p). The equilibrium geometries in the gas phase are presented and analyzed.

Keywords: 3,5-Disubstituted isoxazolines, [3+2] 1,3-dipolar cycloaddition, liquid crystals, molecular platform.

Introduction

The [3+2] 1,3-dipolar cycloaddition reaction of a nitrile oxide to an alkene or alkyne has proven to be extremely useful in the preparation of a variety of compounds in organic chemistry. Among the various classes of compounds which are prepared from these cycloadducts are enones,[1] 1,3-amino alcohols,[2] β,γ-dihydroxy ketones[3] and β-hydroxy ketones.[4] In the area of materials, the construction of the isoxazoline and

isoxazole rings by this methodology constitute an easy way to prepare a molecular platform for the synthesis of smart molecules, such as polymers and non-polymer liquid-crystallines materials.[5]

Our previous results showed that the introduction of an isoxazoline ring flanked by aromatic rings or polar groups opened a route to prepare useful intermediates in the field of liquid crystals.[6] Herein we describe the preparation of four homologous series of 3,5-disubstituted isoxazoline rings. A complete study of the thermal behavior of these compounds is also presented with the goal to understanding the correlation between the molecular structure and liquid crystal parameters.

Based upon the considerations discussed above, we now report a convenient and practical route to the synthesis of isoxazoline ring platform for liquid crystal (LC) materials. The compounds from series **5** and **6** are derived from 3-arylisoxazolyl-5-carboxylic acid (**1**) while the members of the homologous series **7** and **8** are derived from 5-(hydroxymethyl)-3-aryl-2-isoxazoline (**2**).

Results and Discussion

Synthesis

To synthesize the isoxazoline LC, the molecular platforms **1** and **2** bearing carboxyl or hydroxyl groups suitable for further derivation were prepared (Chart I). The acid **1a-d** and alcohol **2a-d** were obtained using [3+2] 1,3-dipolar cycloadditions according to reference 6.

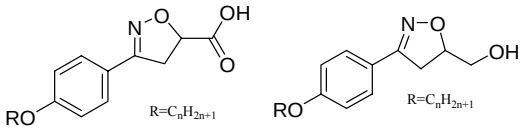

1a n = *n*-heptyl; **1b** n = *n*-octyl; **1c** n = *n*-nonyl; **1d** n = *n*-decyl.

2a n = *n*-heptyl; **2b** n = *n*-octyl; **2c** n = *n*-nonyl; **2d** n = *n*-decyl.

Chart I. The isoxazoline platforms **1** and **2**.

To achieve our goal of the isoxazoline LC material it was necessary to synthesize the phenols **3** and **4** as the chemical counterparts of the acid **1**. The synthesis of the key intermediates **3** is reported elsewhere.[6] Compound **4** was prepared following the experimental procedure to **3**.

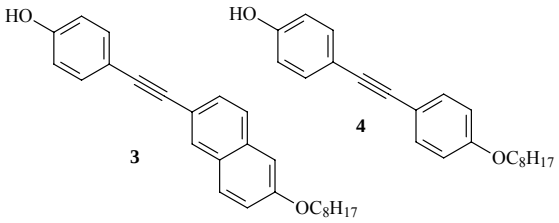

The chemical connection between the intermediates **3** and **4** and acid **1** was made through an esterification reaction using the DCC-DMAP protocol. Thus, the compounds **5a-c** and **6** were synthesized as representative members of these homologous series.

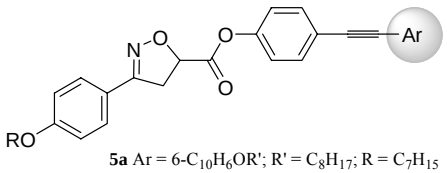

5a Ar = 6-$C_{10}H_6OR'$; R' = C_8H_{17}; R = C_7H_{15}
5b Ar = 6-$C_{10}H_6OR'$; R' = C_8H_{17}; R = C_8H_{17}
5c Ar = 6-$C_{10}H_6OR'$; R' = C_8H_{17}; R = $C_{10}H_{21}$
6 Ar = 4-C_6H_4OR'; R' = C_8H_{17}; R = C_7H_{15}

The third and fourth homologous series **7a-g** and **8a-d** are derived from 5-(hydroxymethyl)-3-aryl-2-isoxazoline (**2**). The compounds **7a-g** were quickly prepared by an esterification reaction (DCC/DMAP) between the corresponding *p*-*n*-alkoxybenzoic acid[7] and the alcohol **2**. In order to synthesize the elongated (anisotropic) liquid-crystalline isoxazolines **8a-d**, we again applied the DCC/DMAP protocol to introduce the ester linkage by reaction of *p*-bromobenzoic acid with the alcohol **2a**. To accomplish the synthesis of the homologous series **8a-d** the triple bond was inserted through the Sonogashira cross-coupling reaction between the 1-alkoxy-4-ethynylbenzene[8] and the ester derived from *p*-bromobenzoic acid.

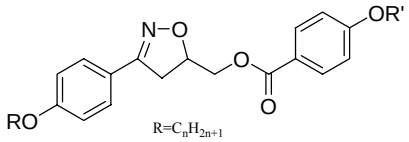

7a R = C_7H_{15}; R' = C_6H_{13}
7b R = C_7H_{15}; R' = C_7H_{15}
7c R = C_7H_{15}; R' = C_8H_{17}
7d R = C_9H_{19}; R' = C_7H_{15}
7e R = C_7H_{15}; R' = $C_{10}H_{21}$
7f R = C_9H_{19}; R' = C_9H_{19}
7g R = C_9H_{19}; R' = $C_{10}H_{21}$

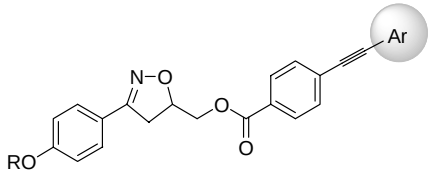

Ar = 4-C_6H_4OR'

8a R = C_7H_{15}; R' = C_7H_{15}
8b R = C_7H_{15}; R' = C_8H_{17}
8c R = C_7H_{15}; R' = C_9H_{19}
8d R = C_7H_{15}; R' = $C_{10}H_{21}$

Liquid-crystalline behavior

Thermal analysis of all isoxazolines **5a-c, 6, 7a-g** and **8a-d** was performed by differential scanning calorimetry (DSC). The texture of the mesophase[9] was identified by microscopy studies on cooling from the isotropic liquid state of the samples (Figure 1). The transition temperatures and enthalpy values were collected from a second heating scan and is compiled in Table 1. Polarizing optical photomicrographs of the representative LCs are shown in Figure 1. The 3-phenylisoxazolyl-5-carboxylate esters **5a-c** exhibited enantiotropic liquid-crystalline properties (Figure 1a and 1b). The ester **6** did not exhibit mesomorphic behavior under optical polarized

light microscopy (Figure 1c). The LC 5-(hydroxymethyl)-3-aryl-2-isoxazolyl benzoates **7c-g** and **8a-d** displayed monotropic liquid-crystalline phase while the smectic C and nematic mesophases were observed in these series (Table 1), respectively.

The mesophase characterization was made by polarized optical microscopy studies (POM, Figure 1) and the enthalpy values were obtained from DSC traces (Figure 2). The schlieren textures of series **5a-c** and **7d-g** show singularity lines with two and four dark brushes, which correspond to the extinction orientation of the liquid crystals. The singularity points are defects in the structure where two or four brushes meet. In the smectic C phase, only singularities with four brushes are observed

Table 1. Transition temperatures (°C) for homologous series **5a-c**, **6**, **7a-g** and **8a-d** and enthalpies values (ΔH, kcal.mol^{-1}).

Entry	R/R´	Phase transition temperatures (°C)		ΔT^d	Enthalpies values	
	C_nH_{2n+1}	Heating	Cooling		Melt[c]	Iso - phase – K[d]
		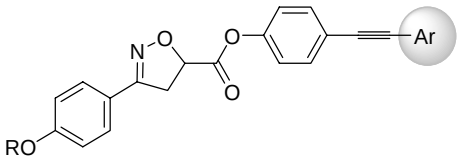		**5** Ar = 6-$C_{10}H_6OR'$; R = R' = C_nH_{2n+1} **6** Ar = 4-C_6H_4OR'; R = R' = C_nH_{2n+1}		
5a	7/8	K 144.5[a] N 148.0[a] I	I 142.9 N 136.9 K	3.5	6.74	I 0.015 N 6.59 K
5b	8/8	K 134.4[a] N 150.5[a] I	I 144.0 N 127.3 K	16.1	6.05	I 0.031 N 6.00 K
5c	10/8	K 142.6[a] N 151.0[a] I	I 149.5[a] N 130.7 K	8.4	5.93	I [f] N 6.01 K
6	7/8	K 129.5 I	I 116.1 K	-	12.31	I 12.74 K
		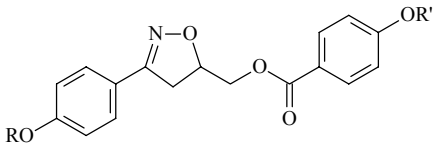		R = R' = C_nH_{2n+1}		
7a	7/6	K 100.8 I	I 73.7 K	-	13.07	I 12.87 K
7b	7/7	K 97.8 I	I 73.7 K	-	15.10	I 15.29 K
7c	7/8	K 96.7 I	I 78.6[b,e] K	-	12.64	I 12.64 K
7d	9/7	K 93.8 I	I 76.9[b] SmC 64.8 K	12.1	18.69	I 4.19 SmC 10.88 K
7e	7/10	K 102.5 I	I 75.7[b] SmC 71.2 K	4.5	13.40	I 2.81 SmC 11.79 K
7f	9/9	K 91.9 I	I 82.5[b] SmC 58.1 K	24.4	12.79	I 3.01 SmC 6.15 K
7g	9/10	K 100.4 I	I 83.3[b] SmC 68.2 K	15.1	16.67	I 3.66 SmC 11.82 K
		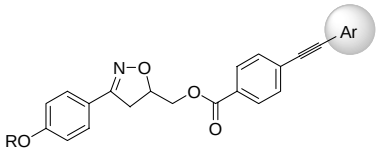		Ar = 4-C_6H_4OR'; R = R' = C_nH_{2n+1}		
8a	7/7	K 134.7 I	I 125.8[a,b] N 118.0 K	7.8	6.26	I [f] N 8.36 K
8b	7/8	K 138.4 I	I 134.3[b] N 120.2 K	14.1	13.91	I 0.67 N 13.53 K
8c	7/9	K 133.5 I	I 120.0[b] N 116.7 K	3.3	15.01	I 0.087 N 15.66 K
8d	7/10	K 137.8 I	I 132.5[b] N 121.4 K	11.1	11.94	I 0.72 N 11.01 K

Scan rate: 10 °C min^{-1} for all samples; K = Crystal phase; SmC = Smectic C phase and N = Nematic phase. a. Transition temperatures were obtained from POM analyze. b. Monotropic behavior. c. Enthalpies values (second heating/cooling stage) were determined from crystal phase to LC phase or isotropic phase for compound **6**. d. Heating for **5a-c** and cooling for **7a-g** and **8a-d**. e. Upon slow cooling the samples crystallizes. Upon fast cooling the sample displayed a very short range of the SmC phase during the crystallization process. f. Enthalpy value not determined.

(Figure 1e and 1f). Nematic phase may also showed singularities with two brushes (Figure 1a and 1b). The homologous series **8a-d** exhibited a thread-like texture when the sample was sandwiched between two glass plates that had not been rubbed or treated (Figure 1d). This texture is usually observed in thin samples placed

between two crossed polarizers. The dark lines, the so-called threads, are line singularities, which either connect two point defects or form closed loops. The planar thread-like texture is characteristic of liquid-crystalline nematic phase.

Compounds **5a-c** displayed enantiotropic nematic phase whereas compound **6** is a non-mesomorphic compound. The non-liquid crystal **6** melts at 129.5 ^{o}C

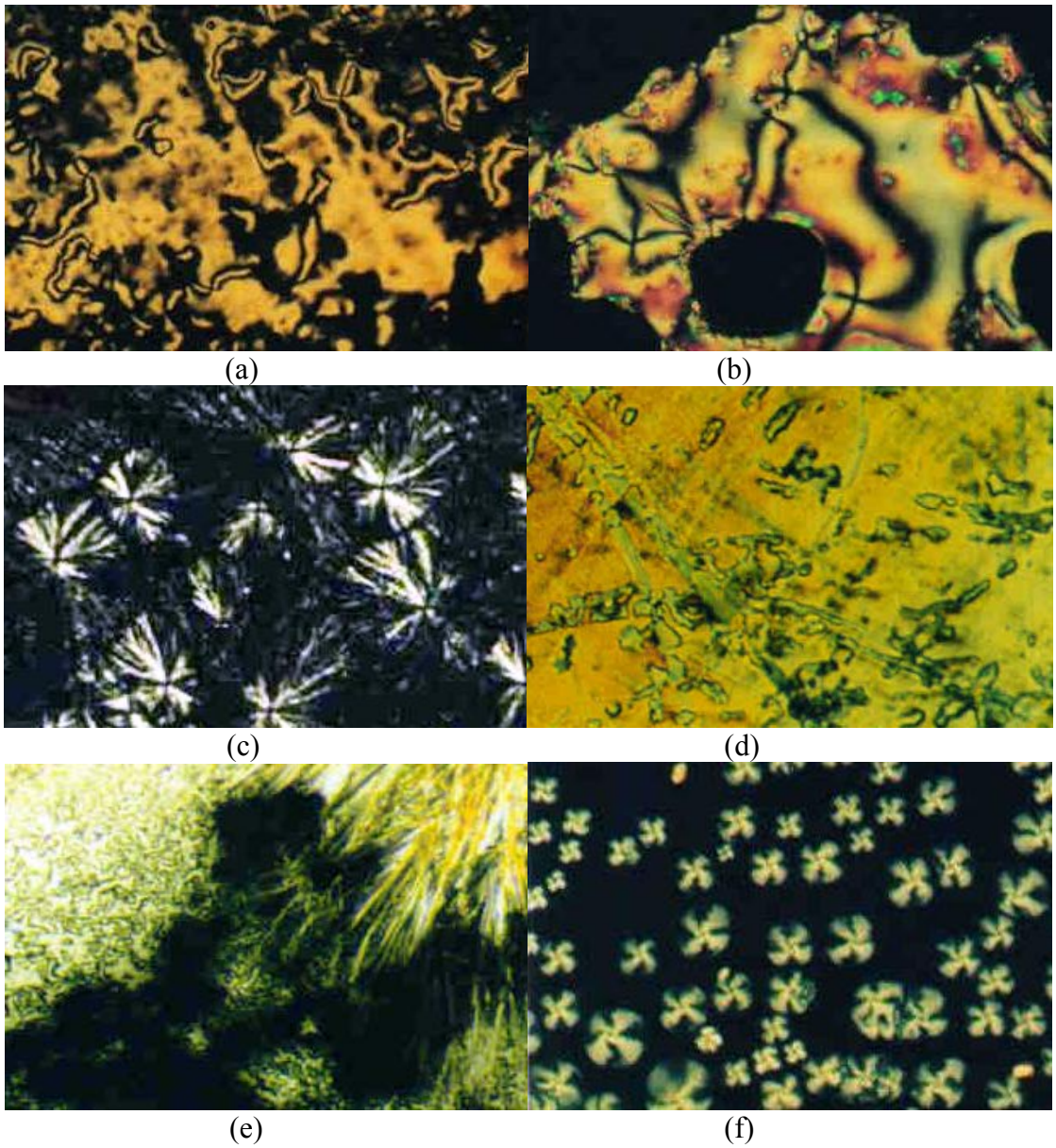

Figure 1. Polarizing optical photomicrographs (10x). (a) The planar thread-like texture on cooling of **5a** (141.7°C); (b) schlieren texture of **5b** on heating (145.8 °C); (c) crystal phase ("pom-pom" texture) of **6** on cooling (107.8 °C); (d) nematic planar texture of **8d** on cooling (129.7 °C); (e) the coexisting of smectic C and crystal phase of **7d** on cooling (67.2 °C); (f) the schlieren texture of the smectic C phase (color-four-fold rosette and black-isotropic liquid) of **7g** on cooling (83.0 °C).

from its crystalline state to an isotropic liquid and it crystallizes at 116.1 ^{o}C without any trace of a LC mesophase (Figure 1c and 2). The lack of LC behavior for this compound is probably related to the geometrical anisotropy when the napthyl group is changed to phenyl group.

Compounds belong to **5a-c** series showed enantiotropic behavior when analyzed by POM. However, the DSC traces of the **5a** did not exhibit K $\rightarrow$ N on heating and whereas **5c** did not exhibit I $\rightarrow$ N on cooling (Figure 2). For example, on heating, the sample **5a** enters into the nematic phase at 144.5 ^{o}C and melts to an isotropic liquid at 148.0 ^{o}C. The range of temperature for the mesophase is small for **5a** (ΔT = 3.5 ^{o}C) and large for **5b** (ΔT = 16.1 ^{o}C) and **5c** (ΔT = 8.4 ^{o}C). On cooling, the mesophase range follows the same tendency. They

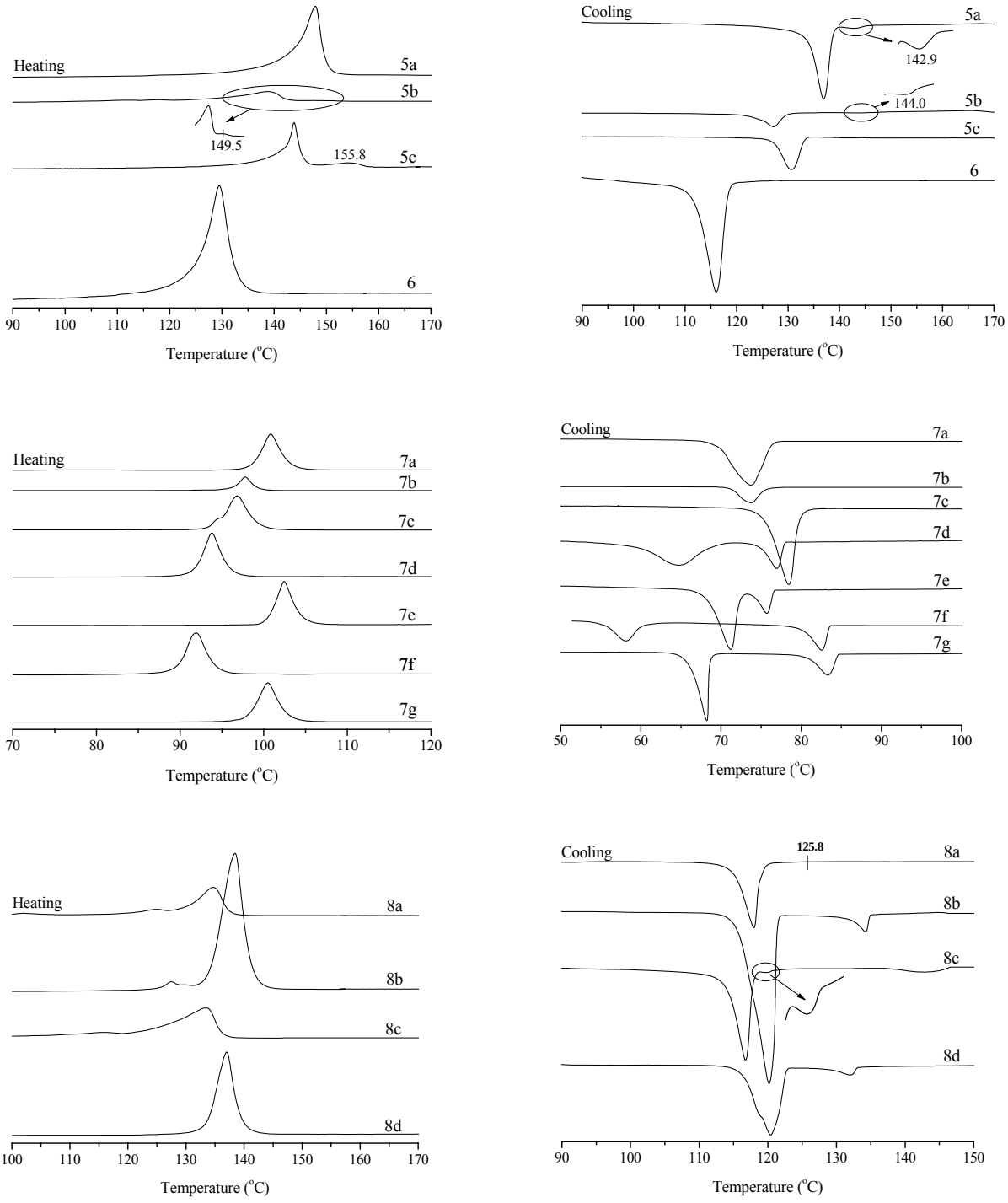

Figure 2. DSC thermograms of compounds **5a-c, 6, 7a-g** and **8a-d** on 2nd cycle at 10 °C min^{-1}.

are larger for compounds **5b** (ΔT = 16.7 °C) and **5c** (ΔT = 18.8 °C) than for **5a** (ΔT = 6.0 °C), while the transition enthalpies (Table 1) for the isotropic to nematic transition of the **5a-c** are rather low. These values are consistent with a less ordered nematic mesophase.

The third homologous series **7a-g** displayed a monotropic smectic C mesophase only for the superior members **7c-g**. For the first and second member (**7a** and **7b**) of this series no mesophase was observed. While the next member **7c** exhibited a monotropic smectic C phase.The smectic C phase appeared only under fast cooling and the mesophase range was too short to be determined under these conditions. On cooling, **7c** crystallizes at 78.6 °C. The broken-fan focal conic texture of the SmC phase appears during the crystallization process. The broken-fan can be visualized simultaneously with the crystals and

they disappear very fast. This situation makes it impossible to get some information about the range of this mesophase. Upon slow cooling, no traces of the mesophase were detected and observed. For the superior members **7d-g** the range of the monotropic SmC phase was determined. The DSC traces are shown in Figure 2 and the thermal data for this series is shown in Table 1. The melting points of these compounds display a regular tendency if we compare them in *pairs*. The compounds containing odd carbon atoms in their alkyl chains melt at higher temperatures than the next member having an even carbon in the alkyl chains. For instance, the melting points of **7a**, **7c**, **7e** and **7g** are higher than **7b**, **7d** and **7f**. Figure 3a shows the dependence of the melting points on the number of carbon atoms in the alkyl tail for the **7a-g** homologues. Also, from Figure 3a it is possible to see that the melting point decreases with the increase of *n* in the alkyl chain on going from **7a** to **7d**. The melting point for **7e** doesn't follow the tendency, and it is higher than **7d**. However it is possible to establish the same correlation between the melting point and the length of the terminal *n*-alkyl chain to the last three members of this series. For instance **7e** with an odd number of carbon atoms in its alkyl chain has a higher melting point than **7f**. The melting points of compounds **7e-g** display an odd-even effect as seen with the four first compounds. The deviation observed jumping from **7a-d** to **7e-g** may be associated with the increase in the molecular weight of the latter compounds. The tendency observed in both groups of the LC series **7a-d** and **7e-g** related to the lowering of the melting point is probably a manifestation of the lipophilic effect as the length of the alkyl chains increase. The transition enthalpies of the isotropic to smectic transitions of **7d-g** are higher than for both **5a-c** and **8a-d**. The enthalpy value suggests a more ordered phase going from isotropic to smectic phase compared to compounds **5a-c** or **8a-d**.

In general, as the length of the alkyl chains increases the mesophase range becomes wider, especially with respect to smectic phase; the opposite is observed for the nematic phase (see discussion for **8a-d** below). The reduction of the length of the alkyl chain may be responsible for the absence of the mesophase. A delicate balance between many structural parameters favors the appearance of the mesophase for the intermediate compounds **7c-g**. The inversion of the ester group and the insertion of a methylene unit between the isoxazolyl and carboxyl groups are other two factors that should have considered when we compare the compounds **7a-g** with **5a-c** and **6**.

In contrast to the compounds **5a-c,** the homologous series **8a-d** displayed monotropic nematic mesophases with planar thread-like textures. The thermal, optical and thermodynamic data of these compounds are compiled in Table 1. All compounds displayed similar thermal behavior. The DSC traces are shown in Figure 2. For **8a** and **8c** (ΔT = 7.8 ^{o}C; ΔT = 3.3 ^{o}C) the mesophase range was smaller than for **8b** and **8d** (ΔT = 14.1 ^{o}C; ΔT = 11.1 ^{o}C). The melting points of this series have the same tendency observed to the series **7a-g**. The LCs **8a** and **8c** melt at lower temperature than **8b** and **8d**. The LCs with odd carbon atoms in the alkyl group, considering R plus R', melt *c.a.* 4 ^{o}C above the LCs containing even carbon atoms on their terminal tails. The transition temperatures I $\rightarrow$ N obtained on cooling exhibited the same behavior. For example, on cooling, **8b** and **8d** enter into the nematic phase at higher temperature than **8a** and **8c**.

The usual even-odd alternations of temperature range of the crystal-isotropic phase and of the isotropic-nematic phase transition are observed. For the odd number of the carbon atoms the mesophase range is higher than for the even number of the carbon atoms in the alkyl tail. Figure 3b shows the dependence of the transition temperatures on the number of carbon atoms in the alkyl tail for the **8a-d** series. The tendency observed upon heating of the melting points is similar to the transition temperatures I $\rightarrow$ N observed on cooling process. The compounds that have an odd number of carbon atoms exhibit higher values than for those with an even number of carbon atoms. This can be seen in Figure 3b – the superior line is related to the melting point and inferior line is associated with the temperature when the compounds **8a-d** enter into nematic phase. It should be noted that, when compared with **8b** and **8d,** the enthalpy values for these isotropic-nematic transitions of **8c** also showed the odd-even effect. The enthalpy value of the **8a** was too small to be detected by DSC. The phase transition for this member was observed with a polarizing microscope. However the values for the compounds with odd carbon atoms in the alkyl tail, **8b** and **8d**, are larger than the conventional nematic $\leftrightarrow$ isotropic transition enthalpies (<0.50 kcal mol^{-1}) for calamitic liquid crystals. In addition, these enthalpy values for compounds **8a-d** are higher than series **5a-c**. This may be indicating that relatively strong intermolecular interactions might exist in its nematic phase and could be attributed to the inversion of the carboxylate group between **5a-c** and **8a-d**.

A theoretical study was performed in order to understand the phase behavior and correlate it to the structural features of these compounds. We selected the LC compounds **5b**, **7b** and **8c** as a representative of this study and their energy and its corresponding geometry of all model systems were obtained by full optimization without any constraint. The calculation was performed with the GAUSSIAN 98[10] program using the B3LYP hybrid functional,[10] employing a 6-31G(d,p) basis set.

The molecular shape of a compound has a critical effect on its liquid-crystalline behavior. Two facts are important and need to discussed relating to the mesomorphic behavior of the calamitic liquid crystals (rod-like mesogen). First, the linear-shape of the calamitic LC changes to a bent-shape with the introduction of five-membered heterocycles into the center of the mesogenic core.[11] The bent-shape is a consequence of the relative position of the substituent bonded at the heterocyclic

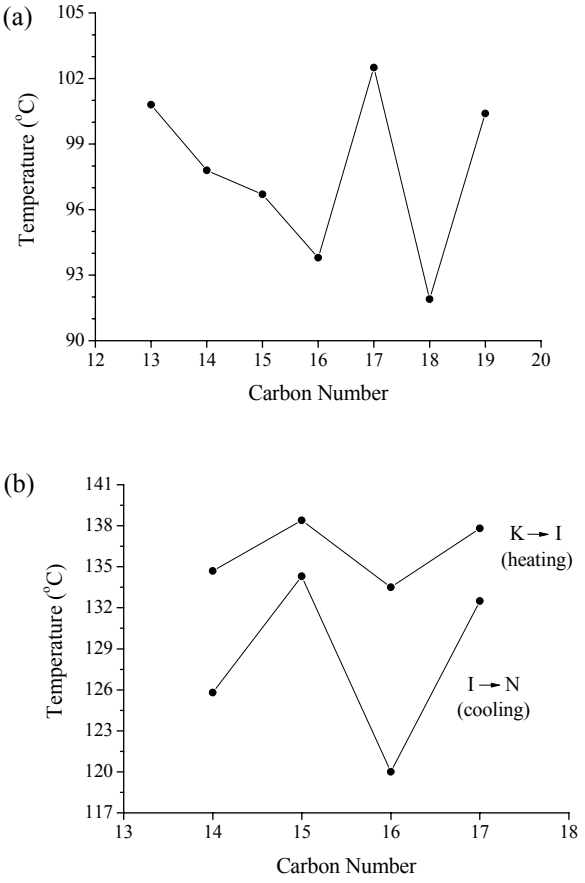

Figure 3. (a) Plot of melting point against the number of carbon atoms of the homologues **7a-g**. (b) Plot of transition temperatures against the number of carbon atoms (*n*) in the alkoxy chain of the compounds **8a-d**. Melting points (above); I-N transition temperature (below, on cooling).

group. So, the deviation of linearity is an important structural parameter that should be taken into account. Second, the 3,5-disubstitued isoxazoline ring has two non-coplanar aromatic groups bonded at 3- and 5-position of the isoxazoline ring. The non-linearity of the isoxazolina ring along with the non-coplanarity of the two aryl groups located at C_3 and C_5 on the heterocyclic ring are determine whether a stable liquid-crystalline phase forms. To minimize this unfavorable disposition of the groups in the 3- and 5-carbon atom of the isoxazoline ring, the final central core must be as long as possible and possess high polarizability. In this way, the potential LC materials are reached through an *elongating molecular strategy* from the isoxazoline intermediates. This elongation builds off the rigid isoxazoline core to form a more polarizable and mesogenic one.

The mesomorphic behavior found in this work is due to the presence of the long aromatic moiety laterally bonded to the isoxazoline ring. However, in some cases the molecular dimensions (length-to-breadth ratio) of the aromatic moiety are not sufficient to overcome the non-coplanarity of the aryl group connected on the isoxazoline ring. In this situation no mesophase or unstable mesophase (*i.e*, monotropic behavior) appears. By changing the hybridization of the C_4 and C_5 carbon atoms of the isoxazolinic system the liquid-crystalline state forms vigorously. Our previous work showed that oxidation of the isoxazoline to isoxazol ring yield LC materials with a large enantiotropic nematic mesophase.[6] The appearance of stable mesophase in isoxazol systems[12] is due to the substitution of a tetrahedral to planar carbon in the heterocyclic so that the two aryl and the isoxazoyl groups are coplanar and thus fully conjugated.

Table 2 shows the three lowest-energy conformations of the **5b**, **7b** and **8c** compounds. The other conformations of these compounds are not energetically favorable (by more than 1.00 kcal mol^{-1}) and these contributions can be neglected because they are local minima. The energy profile of the conformational population largely favors the conformation shown in Table 2. Therefore, we focused our analysis on the lowest-energy conformations so that the high energy conformations are not considered during this study. Modeling of these structures allows certain interesting conclusions to be drawn concerning their mesomorphic behavior. The distance between the oxygen of the carboxylate group and the hydrogen (O_{45}-H_{42}) for the **5b**, O_{44}-H_{39} for the **7b** and **8c** are 2.375, 2.465 and 2.45 Å, respectively. These values reveal a weak hydrogen bond in these conformers and they supported that this interaction is important to maintain the conformers in their lowest-energy state. As we can see in the Figure 4a, the hydrogen atom bonded to carbon 4 in the isoxazolinic ring shows a more positive charge than the others, interacting to the carboxylic oxygen as a weak hydrogen bond.

The dipole moment of these conformers may also play an additional role in the stabilization of the mesomorphic state. Compound **5b** has the lowest value whereas **8c** presents the highest value. A probable conclusion about this data is that compounds having the smallest molecular dipole values display enantiotropic behavior as we can see from the data for series **5a-c** (Table 1). On the other hand, compounds belonging to the series **7a-g** and **8a-d** having high values of the molecular dipole show monotropic LCs. A preliminary conclusion from the modeling data is that a large increase in the molecular dipole does not favor the formation of an enantiotropic mesophase (Table 1). However it is important to point out that monotropic behavior, or the absence of a mesogenic state, observed in the series **7a-g** and **8a-d** is mainly due to the deviations of the coplanarity between aromatic molecular segments connected by the polar isoxazoline ring.

The dihedral angle of the **5b**, **7b** and **8c** conformers was selected and they are listed in Table 2. The theoretical calculations reveal that rotation about C_1-C_{44} and C_1-C_{41} bond of the compounds **5b**, **7b** and **8c**, respectively, play an important role on their corresponding liquid crystalline behavior. The rotation about the C_1-C_{44} bond of **5b** yielded the more stable conformer which is separated by more than 1.00 kcal/mol

from the another unstable conformer of **5b** (not shown). The angle between two planes (right and left) of the molecule is about 135.9º. The dihedral angle O_2-C_1-C_{44}-O_{45} to the most stable conformation is 116.1º. This molecular arrangement favors mesophase formation probably due to the tendency of the polar mesogenic phase to self-assemble during the melting or passing from the isotropic to mesogenic state.

The insertion of methylene unit between the isoxazoline ring and carboxyl group changes the relative disposition of the two planes in the conformers of **7b** and **8c**. As we can see in Table 2 the conformers **7b** and **8c** present two distinct planes connected by the C_1-C_{44} bond. These planes are slightly collinear, twisted and non-coplanar. The estimated angles between these planes are 30.47° for **7b** and 28.45° for **8c** (Figure 4b,c). The dihedral angles O_2-C_1-C_{41}-O_{42} to the most stable conformation of the **7b** and **8c** are 163.5º and 163.3°, respectively. This arrangement favors the short-weak hydrogen bond interaction between O_{44}-H_{39} atoms in both rotamers. The conclusion that can be drawn from these data is that the methylene unit, as described above, produces two distinct planes which disfavor the molecular interaction in the liquid-crystalline state.

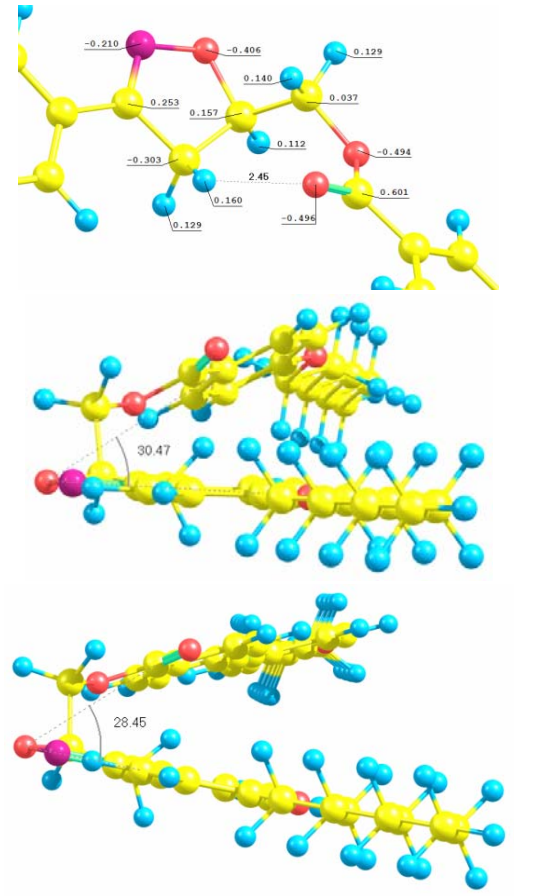

Figure 4. (a) Central core of the **8c** molecule showing the Mülliken charges and distance between oxygen of the carboxylate group and the hydrogen (2.45 Å, dotted line). (b) and (c) Diedral angle between molecular planes of the conformers - 30.47° for **7b** and 28.45° for **8c**.

The electrostatic interaction and dispersion interaction (van der Waals forces, π-stacking effects, etc) cannot compensate for the structural constraints that are imposed by the methylene group in the 5-(hydroxymethyl)-3-aryl-2-isoxazoline ring.

Experimental

Materials

Ethanol, diethyl ether, *p*-bromobenzoic acid, copper(I) iodide (CuI), triphenylphosphine (PPh_3), 4-(*N*,*N*-dimethylamino)pyridine (DMAP) and 1,3-dicyclohexylcarbodiimide (DCC) were used without further purification from Aldrich. The *p*-*n*-alkoxybenzoic acid and 1-alkoxy-4-ethynylbenzene were prepared according to references 7 and 8, respectively. *Bis*-(triphenylphosphine)palladium (II) chloride [$PdCl_2(PPh_3)_2$] was prepared following the procedure reported in reference 13. Triethylamine (Et_3N) was distilled over potassium hydroxide. Tetrahydrofuran (THF) was dried over sodium metal-benzophenone and distilled immediately before use. Anhydrous sodium sulphate (Na_2SO_4) was used to dry organic extracts.

Characterization

Nuclear magnetic resonance spectra were obtained on a Varian 300MHz instrument. Chemical shift are given in parts per million (δ) and are referenced from tetramethylsilane (TMS). GC-MS spectra are obtained using a Varian Saturn 2100T CG-MS equipped with a 100 meter CP Sil Pona CB (0.25 mm) column. The column temperature is started at 50 ^oC and is gradually ramped to 230 ^oC (15^oC min^{-1}) until the end of the run. Infrared spectra were recorded on a Perkin-Elmer Spectrum One FTIR Spectrometer Instruments using NaCl plates in case of solids (nujol dispersions) and as thin film supported between NaCl plates in case of liquids and are reporter as wavenumber (cm^{-1}). Elemental analyses were performed on a Perkin-Elmer model 2400 instrument. All new compounds **5a-c**, **6**, **7a-g** and **8a-d** gave satisfactory spectral, MS data and elemental analysis. The DSC analyses were obtained on a DSC 2910 TA Instruments.

Thermal characterization

Melting points, thermal transitions and mesomorphic textures were taken using an Olympus BX41 microscope equipped with a Mettler Toledo FP82 Hot Stage FP90 Central Processor. The rate of heating or cooling was 10 ºC min^{-1}.

Theoretical calculations

The energy and its corresponding geometry of all model systems were obtained by full optimization

without any constraint. The calculation was performed with the GAUSSIAN 98[10] program using the B3LYP hybrid funcional, employing a 6-31G(d,p) basis set.

Table 2. Lowest-energy conformations for the **5b, 7b** and **8c** compounds. The alkyl groups have been omitted for clarity.

Entry		Dipole	Dihedral angle
5b	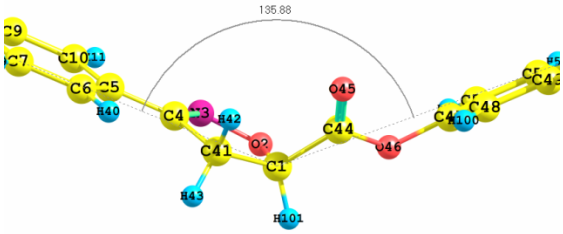	**1.93 D**	O_2-C_1-C_{44}-O_{45} 116.1°
7b	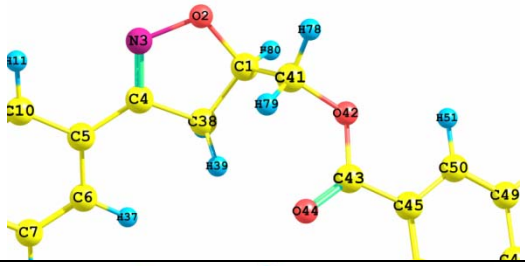	**3.79 D**	O_2-C_1-C_{41}-O_{42} 163.5°
8c	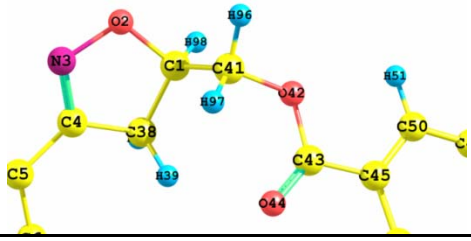	**4.82 D**	O_2-C_1-C_{41}-O_{42} 163.3°

Synthesis

The 3-arylisoxazolyl-5-carboxylic acid (**1a-d**) and 5-(hydroxymethyl)-3-aryl-2-isoxazoline (**2a-d**) were prepared according to our previus report.[6]

*4-[(6-Octyloxy-2-naphthyl)ethynyl]phenol (**3**).*

This compound was prepared according to previous report.[6,8] 4-[(4-Octyloxyphenyl)ethynyl]phenol (**4**) was obtained by procedures similar to that used to prepare compound **3** (Yield: 300 mg, 34%, three steps); white solid; m.p. 69.1 °C; IR ν_{max}/cm^{-1} 2925, 2855, 1727, 1466, 1377, 1251, 1182, 898, 876, 829, 721, 666. ^{1}H NMR (300 MHz, $CDCl_3$) δ 0.88 (m, 3H, CH_3), 1.39 (m, 10H, $(CH_2)_5$), 1.78 (m, 2H, $C\underline{H}_2CH_2O$), 3.97 (t, 2H, CH_2O, *J* = 6.6 Hz), 6.80 (d, 2H, Ar, *J* = 8.4 Hz), 6.86 (d, 2H, Ar, *J* = 8.4 Hz), 7.40 (m, 4H, Ar); ^{13}C NMR (75 MHZ, $CDCl_3$) δ 14.1, 22.6, 26.0, 29.1, 29.2, 29.3, 31.8, 68.1, 87.7, 88.0, 114.5, 115.4, 115.5, 115.9, 132.8, 133.0, 155.5, 159.0.

*4-[(6-Alkyloxy-2-naphthyl)ethynyl]phenyl 3-(4-alkyloxyphenyl)-4,5-dihydroisoxazole-5-carboxylate (**5a-c**).*

These compounds were prepared according to the protocol reaction DCC/DMAP/DCM following the experimental procedure described in reference 6.

Representative data for **5a**

Yield 115 mg; 70%; white solid; m.p. 144.5 °C; Anal. Found: C, 78.48; H 7.58, N 2.07; calcd for $C_{43}H_{49}NO_5$: C, 78.27; H, 7.48; N, 2.12%; IR ν_{max}/cm^{-1} 2924, 2854, 1763, 1596, 1464, 1378, 1224, 1045, 897, 859, 818, 722, 666; ^{1}H NMR (300 MHz, $CDCl_3$) δ 0.88 (m, 6H, $(CH_3)_2$), 1.38 (m, 18H, $(CH_2)_9$), 1.82 (m, 4H, $(C\underline{H}_2CH_2O)_2$), 3.75 (m, 2H, $C\underline{H}_2CH$), 3.98 (t, *J* = 6.6 Hz, 2H, CH_2O), 4.07 (t, *J* = 6.6 Hz, 2H, CH_2O), 5.37 (dd, *J* = 7.2, 11.1 Hz, 1H, $CH_2C\underline{H}$), 6.92 (d, *J* = 8.7 Hz, 2H, Ar), 7.14 (m, 4H, Ar), 7.50 - 7.72 (m, 7H, Ar), 7.96 (s, 1H, Ar); ^{13}C NMR ($CDCl_3$) δ 14.0, 14.1, 22.5, 22.6, 25.9, 26.1, 28.9, 29.0, 29.1, 29.2, 29.3, 31.7, 31.8, 39.2, 68.0, 68.1, 77.7, 87.9, 90.4, 106.5, 114.7, 117.6, 119.7, 120.5, 121.3, 121.6, 126.8, 128.3, 128.5, 128.8, 129.2, 131.3, 132.7, 134.2, 149.9, 155.6, 157.9, 161.0, 168.5; EI-MS: *m/z* 530, 468, 426, 371, 355, 304, 290, 279, 258, 233, 218 (100), 190, 129, 128, 116 and 91.

*4-[(4-Octyloxyphenyl)ethynyl]phenyl 3-(4-heptyloxyphenyl)-4,5-dihydroisoxazole-5-carboxylate (**6**)*

This compound was obtained by procedures similar to those used to prepare compound **5a.** Yield: 110 mg, 50%; white solid; m.p. 129.5 °C; Anal. Found: C, 76.58; H 7.68, N 2.42; calcd for $C_{39}H_{47}NO_5$: C, 76.82; H, 7.77; N, 2.30%; IR ν_{max}/cm^{-1} 2924, 2855, 1765, 1595, 1467, 1378, 1224, 1043, 896, 859, 820, 722, 666; ^{1}H NMR (300

MHz, $CDCl_3$) δ 0.88 (m, 6H, $(CH_3)_2$), 1.40 (m, 18H, $(CH_2)_9$), 1.78 (m, 4H, $(C\underline{H}_2CH_2O)_2$), 3.75 (m, 2H, $C\underline{H}_2CH$), 3.98 (m, 4H, CH_2O), 5.37 (dd, 1H, $CH_2C\underline{H}$, *J* = 7.2, 10.5 Hz), 6.86 (d, 2H, Ar, *J* = 8.4 Hz), 6.93 (d, 2H, Ar, *J* = 8.4 Hz), 7.13 (d, 2H, Ar, *J* = 8.4 Hz), 7.44 (d, 2H, Ar, *J* = 8.4 Hz), 7.52 (d, 2H, Ar, *J* = 8.4 Hz), 7.64 (d, 2H, Ar, *J* = 8.4 Hz); ^{13}C NMR (75 MHz, $CDCl_3$) δ 14.0, 14.1, 22.6, 22.7, 25.9, 26.0, 29.0, 29.1, 29.2, 29.3, 29.4, 31.7, 31.8, 39.3, 68.1, 68.2, 77.8, 87.0, 90.0, 114.5, 114.8, 120.5, 121.3, 121.9, 128.6, 132.6, 133.0, 149.8, 155.7, 159.3, 161.1, 168.6; EI-MS: *m/z* 609 [M^+], 496, 494, 480, 418, 380, 349, 321, 306, 305, 288, 258, 233, 218 (100), 205, 191, 129, 115 and 91.

*General procedure for synthesis of homologue series **7a-g***

The corresponding alcohol **2a** or **2c** (5.8 x 10^{-4} mol) and the respective *p-n*-alkoxybenzoic acid (5.8 x 10^{-4} mol) were suspended in dry THF (5 mL) and stirring for 15 min under argon atmosphere. Then DCC (8.7 x 10^{-4} mol) and DMAP (7.6 x 10^{-5} mol) were added. The reaction mixture was stirred for 24 h at room temperature. The white precipitate was filtered off and washed with THF. The solvent was removed and the crude product was recrystallized from ethanol (double recrystallization).

*Representative data for [3-(4-heptyloxyphenyl)-4,5-dihydroisoxazol-5-yl]methyl 4-decyloxybenzoate **(7e)***

Yield: 83,0 mg, 60%; white solid; m.p. 102.5 ^oC; Anal Found: C, 74.15; H, 9.13; N, 2.54; calcd for $C_{34}H_{49}NO_5$: C, 74.01; H, 8.95; N, 2.54%; IR ν_{max}/cm^{-1} 2924, 2854, 1715, 1606, 1510, 1466, 1377, 1249, 1169, 1127, 1014, 882, 834, 768, 722, 699, 666, 649; ^{1}H NMR (300, MHz, $CDCl_3$) δ 0.89 (m, 6H, $(CH_3)_2$), 1.38 (m, 22H, $(CH_2)_{11}$), 1.79 (m, 4H, $(C\underline{H}_2CH_2O)_2$), 3.22 (dd, *J* = 16.5, 6.9 Hz, 1H, N=CC$\underline{H}$HCH), 3.49 (dd, *J* = 16.5, 10.8 Hz, 1H, N=CCH$\underline{H}$CH), 3.98 (t, *J* = 6.6 Hz, 4H, $(CH_2O)_2$), 4.44 (m, 2H, CHC$\underline{H}_2$OCO), 5.06 (m, 1H), 6.85 (d, *J* = 8.7 Hz, 2H, Ar), 6.91 (d, *J* = 8.4 Hz, 2H, Ar), 7.61 (d, *J* = 8.7 Hz, 2H, Ar), 7.95 (d, *J* = 9.0 Hz, 2H, Ar); ^{13}C NMR (75 MHz, $CDCl_3$) δ 14.0, 14.1, 22.5, 22.6, 25.9, 28.9, 29.0, 29.1, 29.2, 29.3, 29.5, 31.7, 31.8, 37.6, 65.2, 68.0, 68.1, 78.0, 114.0, 114.6, 121.5, 121.6, 128.2, 131.7, 155.8, 160.7, 163.1, 166.0; EI-MS: *m/z* 436, 360, 325, 291, 290, 277, 274, 260, 235 (100), 190, 156, 116 and 91.

*General procedure of the series **8a-d***

(i) Esterification reaction: alcohol **2a** (4.4 mmol) and *p*-bromobenzoic acid (4.4 mmol) were suspended in dry THF (30 mL) and stirred for 15 min under argon atmosphere. Then DCC (6.6 mmol) and DMAP (0.58 mmol) were added. The reaction mixture was stirred for 24 h at room temperature. The white precipitate was filtered off and washed with THF. The solvent from the filtrate was removed and the solid was recrystallized twice from ethanol to afford the corresponding esters as white crystals in 70%-90% of yield. All the compounds gave satisfactory analytical data. *(ii) Sonogashira's coupling:* A one-neck round-bottom flask equipped with septum stoppers was charged with the ester produced in step (*i*) (0.8 mmol), the corresponding 1-alkoxy-4-ethynylbenzene (1.2 mmol) and Et_3N (20 mL) under argon atmosphere. The suspension was stirred for 20 min and then CuI (1.2 x 10^{-5} mol), PPh_3 (4.0 x 10^{-5} mol) and $[PdCl_2(PPh_3)_2]$ (0.8 x 10^{-5} mol) were added. The mixture was heated under reflux for 48 h. The solution was cooled to room temperature and the solid was filtered through a Celite® pad and washed with diethyl ether (2x100 mL). The filtrate was then extracted with H_2O (4 x 20 mL) and the organic extracts were dried (Na_2SO_4) and the solvent evaporated. The solid was recrystallized in ethanol affording the respective products.

*Representative data for [3-(4-heptyloxyphenyl)-4,5-dihydroisoxazol-5-yl]methyl 4-[(octyl oxyphenyl)ethynyl]benzoate **(8b)***

Yield: 63 mg; 40%; orange solid; m.p. 138.4 ^oC; Anal. Found: C, 76.96; H, 8.07; N, 2.14; calcd for $C_{40}H_{49}NO_5$: C, 77.01; H, 7.92; N, 2.25%; IR ν_{max}/cm^{-1} 2924, 2855, 1723, 1600, 1517, 1465, 1377, 1286, 1251, 1177, 1108, 1045, 890, 834, 765, 721, 695, 666; ^{1}H NMR (300 MHz, $CDCl_3$) δ 0.89 (m, 6H, $(CH_3)_2$), 1.38 (m, 18H, $(CH_2)_9$), 1.79 (m, 4H, $(C\underline{H}_2CH_2O)_2$), 3.24 (dd, 1H, N=CC$\underline{H}$HCH, *J* = 16.5, 6.6 Hz), 3.52 (dd, 1H, N=CCH$\underline{H}$CH, *J* = 16.5, 10.5 Hz), 3.98 (m, 4H, $(CH_2O)_2$), 4.43 (dd, 1H, CHC$\underline{H}$HOCO, *J* = 12.0, 5.4 Hz), 4.50 (dd, 1H, CHCH$\underline{H}$OCO, *J* = 12.0, 4.2 Hz), 5.08 (m, 1H), 6.87 (d, 2H, Ar, *J* = 9.0 Hz), 6.92 (d, 2H, Ar, *J* = 8.7 Hz), 7.45 (d, 2H, Ar, *J* = 9.0 Hz), 7.51 (d, 2H, Ar, *J* = 8.4 Hz), 7.62 (d, 2H, Ar, *J* = 9.0 Hz), 7.97 (d, 2H, Ar, *J* = 8.4 Hz); ^{13}C NMR (75 MHz, $CDCl_3$) δ 14.0, 22.5, 22.6, 25.8, 25.9, 28.9, 29.0, 29.1, 29.3, 31.6, 31.7, 37.5, 65.7, 68.0, 77.8, 87.3, 92.9, 114.3, 114.5, 114.6, 121.3, 128.1, 128.3, 128.6, 129.6, 131.2, 133.1, 155.8, 159.6, 160.7, 165.7; EI-MS: *m/z* 624 ([M + H]$^+$), 623 [M^+], 430, 364, 349, 333, 306, 290, 274, 260, 234 (100), 230, 204, 190, 116 and 91.

Conclusions

In this work a molecular platform for liquid-crystalline materials based on 3-arylisoxazolyl-5-carboxylic acid and 5-(hydroxymethyl)-3-aryl-2-isoxazoline was described. In this context, a new series of liquid-crystalline **5a-c**, **6a**, **7a-g** and **8a-d** derived from isoxazolinic molecular platforms were synthesized and their mesomorphic behavior was investigated using POM and DSC techniques. The compounds belonging to series **5a-c** showed an enantiotropic nematic phase while **6** was not mesogenic. The monotropic smectic C phase of the third series was observed in **7c-g**. The first two **7a-b** did not exhibit a smectic LC phase. The last series **8a-d** displayed a monotropic nematic phase. A theoretical study was performed in order to understand the phase

behavior and structural features of these compounds. The reported calculations further support the role of the insertion of a methylene unit between the isoxazoline ring and the carboxylate group disfavoring the molecular interaction in the liquid-crystalline state.

Acknowledgments

This work was supported by Conselho Nacional de Desenvolvimento Científico e Tecnológico (project MCT/CNPq Nº 555785/2006-8 and MCT/CNPq Universal Nº 471194/2008-5), PROCAD-CAPES, INCT-CMN/CNPq and Coordenação de Aperfeiçoamento de Pessoal de Nível Superior (CAPES) for fellowship.

Supplementary Information

Copies of ^{1}H NMR, ^{13}C NMR spectrum and ESI-MS are available free of charge at http://jbcs.sbq.org.br, as PDF file.

References

1. Carmella, P.; Grünanger, P.; *1,3-Dipolar Cycloaddition Chemistry*; Padwa, A., Ed.; Wiley: New York, 1984; Vol. 1, pp 291–392. Torsell, K. B. G.; *Nitrile Oxides, Nitrones and Nitronates*; VCH: Weinheim, 1988.

2. Kozikowski, A. P.; *Acc. Chem. Res*. **1984**, *17*, 410–416. Jager, V.; Muller, I.; *Tetrahedron* **1985**, *41*, 3519–3528.

3. Curran, D. P.; Zhang, J.; *J. Chem. Soc. Perkin Trans. I* **1991**, 2613–2625.

4. Kenar, J. A.; *J. Am. Oil Chem. Soc*. **2002**, *79*, 351-356.

5. Kovganko, V. N.; Kovganko, N. N.; *Russian J. Org. Chem*. **2006**, *42*, 696-700. Ritter, O. M. S.; Giacomelli, F. C.; Passo, J. A.; Silveira, N. P.; Merlo, A. A.; *Polymer Bull.* **2006**, *56*, 549-561. Kauhanka, U. M.; Kauhanka, M. M.; *Liq. Cryst.* **2006**, *33*, 121-127. Bezborodov, V.; Kauhanka, N.; Lapanik, V.; *Mol. Cryst. Liq. Cryst*. **2004**, *411*, 1145-1152.

6. Tavares, A.; Schneider, P. H.; Merlo, A. A.; *Eur. J. Org. Chem.* **2009**, 889–897. Passo, J. A.; Vilela, G. D.; Schneider, P. H.; Ritter, O. M. S.; Merlo, A. A.; *Liq. Cryst*. **2008**, *35*, 833-840.

7. Gimeno, N.; Ros, M. B.; De la Fuente, M. R.; Serrano, J. L.; *Chem. Mater.* **2008,** *20,* 1262-1271. Naoum, M. M.; Saad, G. R.; Nessim, R. I.; Abdel Aziz, T. A.; Seliger, H.; *Liq. Cryst*. **1997**, *23*, 789-795.

8. Vasconcelos, U. B.; Dalmolin, E.; Merlo, A. A.; *Org. Lett*. **2005**, *7*, 1027-1030. Vasconcelos, U. B.; Merlo, A. A.; *Synthesis* **2006**, *7*, 1141-1147. Vasconcelos, U. B.; Vilela, G. D.; Schrader, A.; Borges, A. C. A.; Merlo, A. A.; *Tetrahedron* **2008**, *64*, 4619-4626. Sonogashira, K.; Tohda, Y.; Hagihara, N.; *Tetrahedron Lett*. **1975**, *16*, 4467-4470. Chinchilla, R.; Nájera, C.; *Chem. Rev*. **2007**, *107*, 874-922. Cristiano, R.; Santos, D. M. P. O.; Conte, G.; Gallardo, H.; *Liq. Cryst.* **2006**, *33*, 997-1003. Melissaris, A. P.; Litt, M. H.; *Macromolecules* **1994**, *27*, 883-887.

9. Gray, G. W.; Goodby, J. W. G.; *Smectic Liquid Crystals. Textures and Structures*; Leonard Hill: London, 1984.

10. Frisch, M. J.; Trucks, G. W.; Schlegel, H. B.; Scuseria, G. E.; Robb, M. A.; Cheeseman, J. R.; Zakrzewski, V. G.; Montgomery J. A.; Stratmann, Jr., R. E.; Burant, J. C.; Dapprich, S.; Millam, J. M.; Daniels, A. D.; Kudin, K. N.; Strain, M. C.; Farkas, O.; Tomasi, J.; Barone, V.; Cossi, M.; Cammi, R.; Mennucci, B.; Pomelli, C.; Adamo, C.; Clifford, S.; Ochterski, J.; Petersson, G. A.; Ayala, P. Y.; Cui, Q.; Morokuma, K.; Malick, D. K.; Rabuck, A. D.; Raghavachari, K.; Foresman, J. B.; Cioslowski, J.; Ortiz, J. V.; Stefanov, B. B.; Liu, G.; Liashenko, A.; Piskorz, P.; Komaromi, I.; Gomperts, R.; Martin, R. L.; Fox, D. J.; Keith, T.; Al-Laham, M. A.; Peng, C. Y.; Nanayakkara, A.; Gonzalez, C.; Challacombe, M.; Gill, P. M. W.; Johnson, B.; Chen, W.; Wong, M. W.; Andres, J. L.; Gonzalez, C.; Head-Gordon, M.; Replogle, E. S.; Pople, J. A.; *Gaussian 98, Revision A.5.* Gaussian, Inc., Pittsburgh, PA. **1998**. Becke, A. D.; *J. Chem. Phys.* **1993**, *98*, 5648-5652. Lee, C.; Yang, W.; Parr, R. G.; *Phys. Rev. B* **1988**, *37*, 785-789.

11. Dingemans, T. J.; Samulski, E. T.; *Liq. Cryst.* **2000**, *27*, 131-136. Cai, R.; Samulsky, E. T.; *Liq. Cryst.* **1991**, *9*, 617-634.

12. Vieira, A.; Bryk, F.; Conte, G.; Bortoluzzi, A.; Gallardo, H.; *Tetrahedron Lett.* **2009**, *50*, 905-908. Gallardo H.; Cristiano, R.; Ely, F.; Vieira, A.; *Liq. Cryst.* **2006**, *33*, 381-390.

13. King, A. O.; Negishi, E. *J. Org. Chem*. **1978**, *43*, 358-360.

SUPPORTING INFORMATION – CAPÍTULO 5.2

3-Arylisoxazolyl-5-Carboxylic Acid and 5-(Hydroxymethyl)-3-Aryl-2-Isoxazoline as Molecular Platforms for Liquid-Crystalline Materials

Aline Tavares[a], *Paolo R. Livotto*[a], *Paulo F. B. Gonçalves*[b] *and Aloir A. Merlo*[a]*

[a]Instituto de Química, Universidad Federal do Rio Grande do Sul, 91501-970. Porto Alegre, RS – Brasil.

[b]Centro Universitário La Salle. 92010-000. Canoas, RS – Brasil.

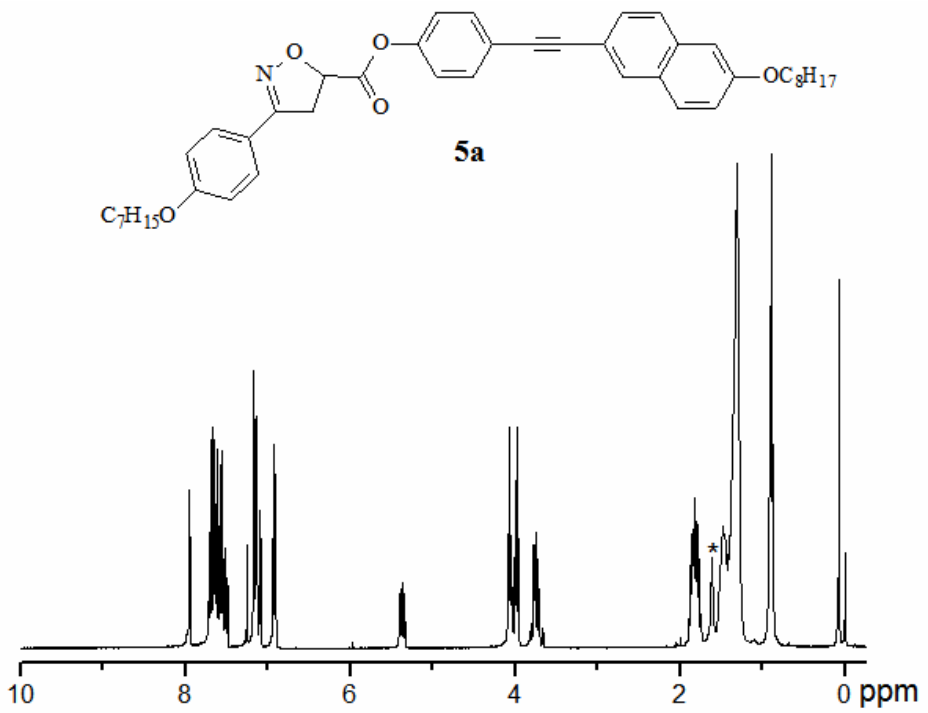

Figure S1. ^{1}H NMR spectrum of compound **5a** ($CDCl_3$, 300 MHz). *Solvent impurity.

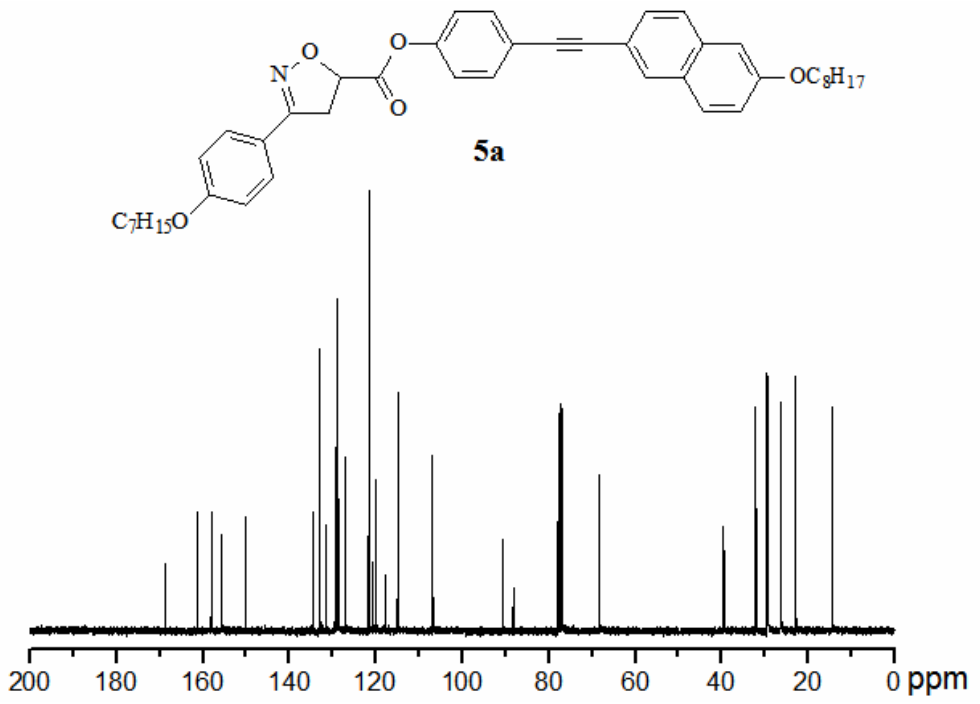

Figure S2. ^{13}C NMR spectrum of compound **5a** ($CDCl_3$, 75 MHz).

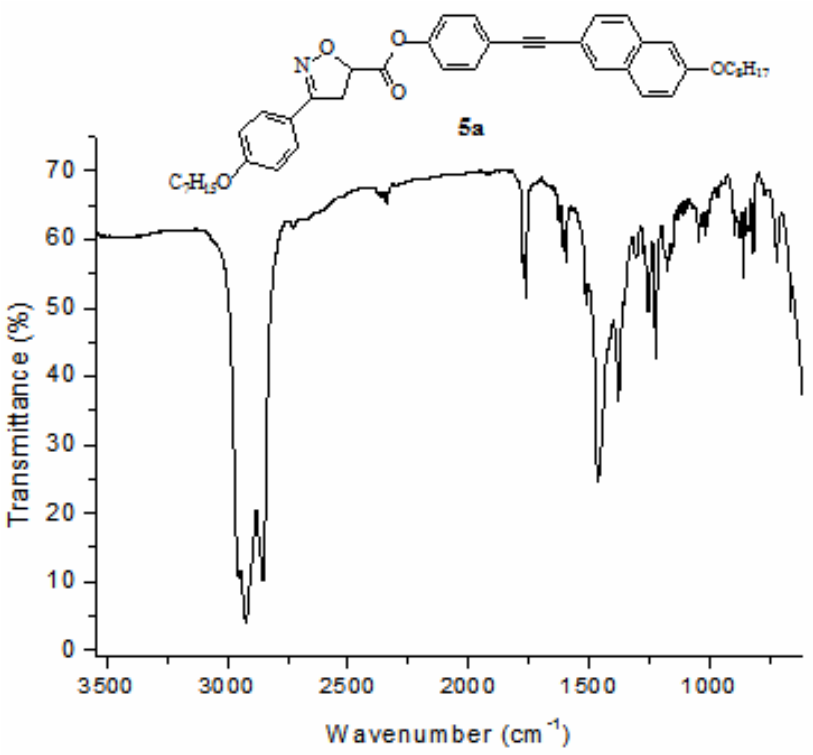

Figure S3. FT-IR spectrum of compound **5a** (nujol).

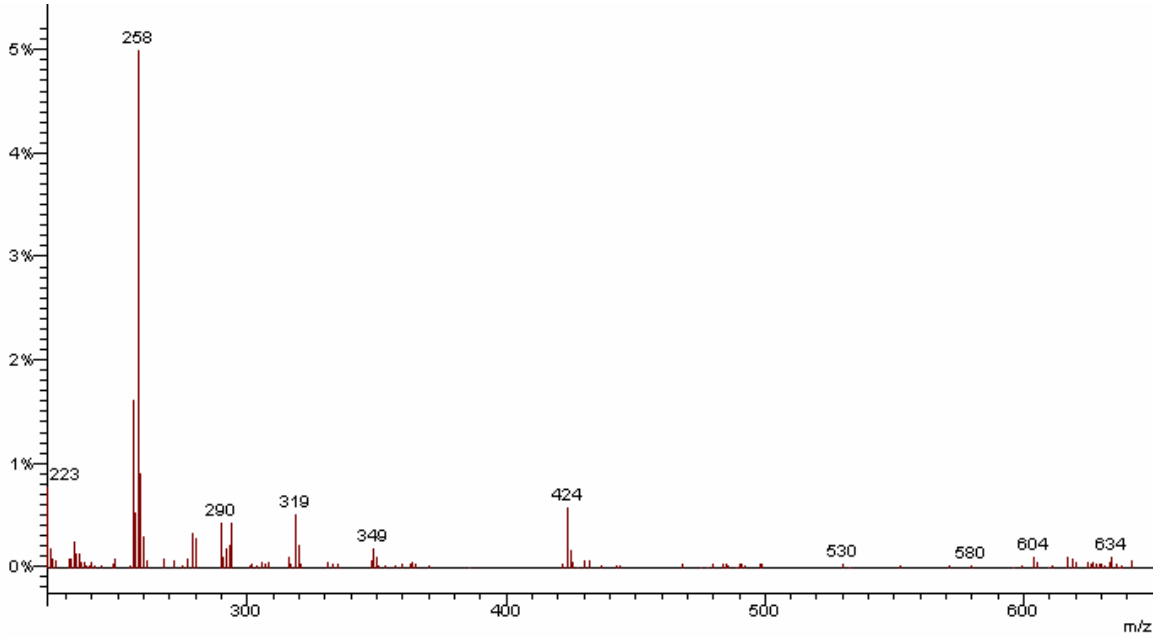

Figure S4. Mass spectra (EI-MS) of compound **5a**.

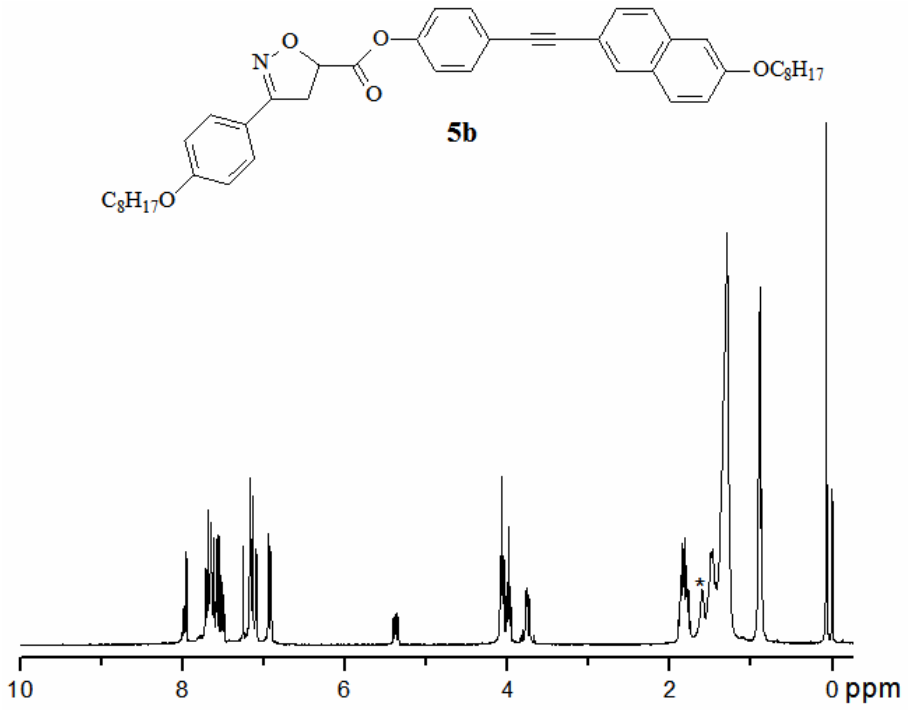

Figure S5. ^{1}H NMR spectrum of compound **5b** ($CDCl_3$, 300 MHz). *Solvent impurity.

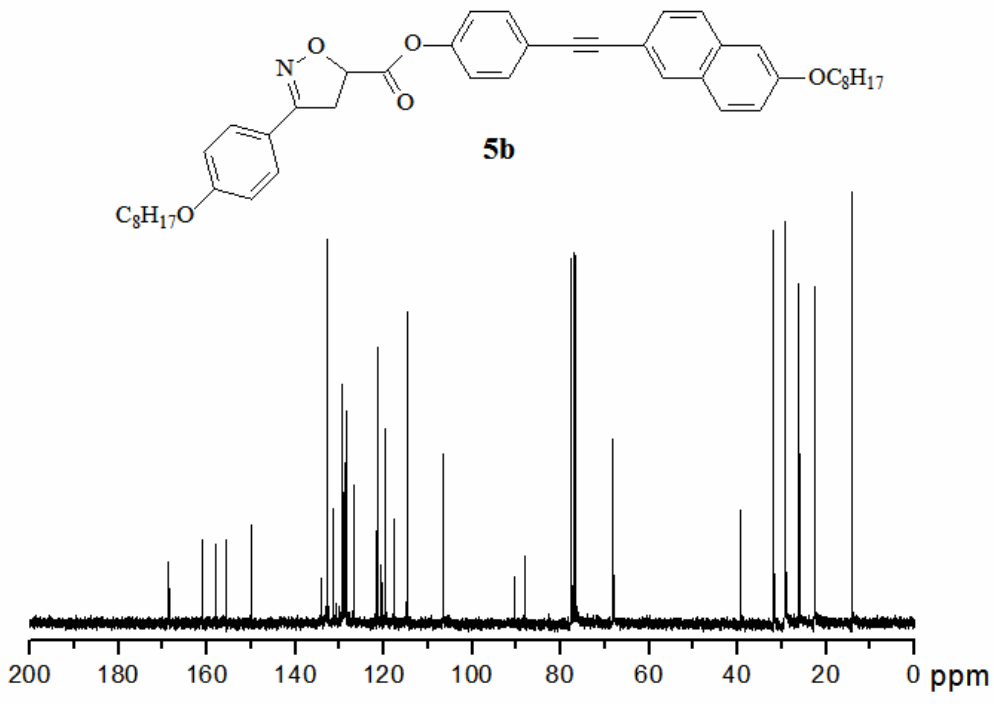

Figure S6. ^{13}C NMR spectrum of compound **5b** ($CDCl_3$, 75 MHz).

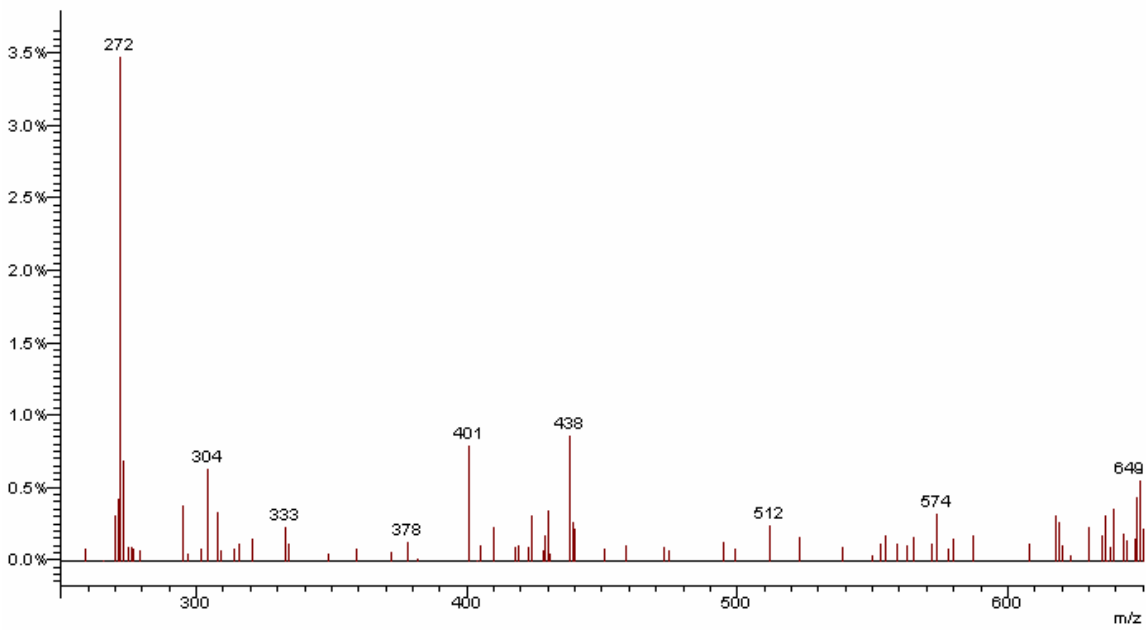

Figure S7. Mass spectra (EI-MS) of compound **5b**.

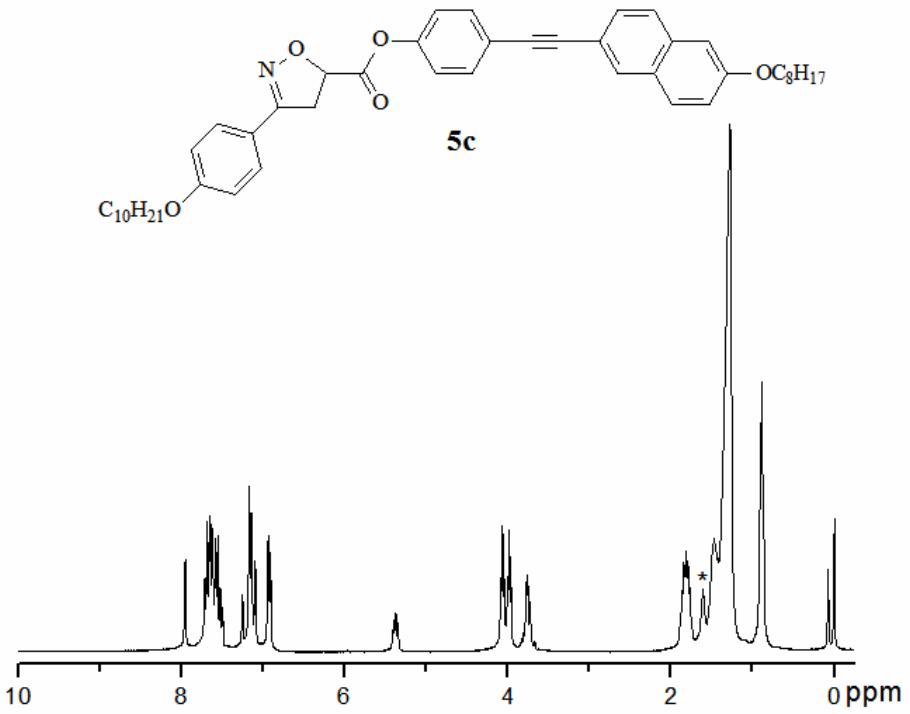

Figure S8. ^{1}H NMR spectrum of compound **5c** ($CDCl_3$, 300 MHz). *Solvent impurity.

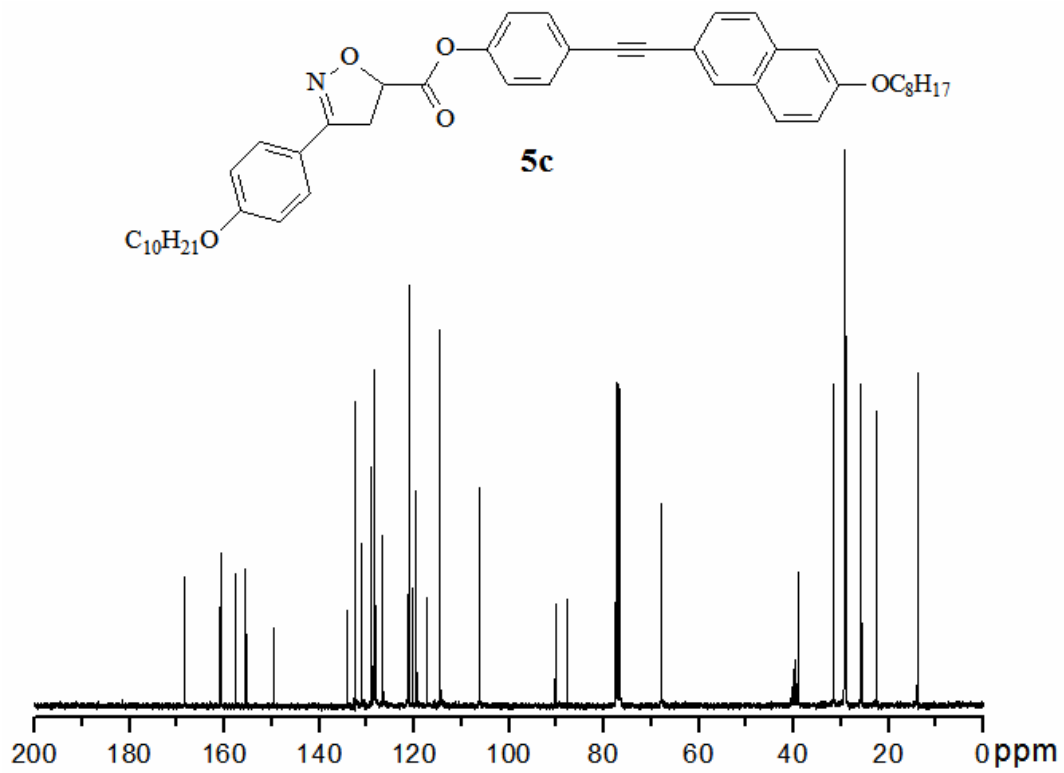

Figure S9. ^{13}C NMR spectrum of compound **5c** ($CDCl_3$/DMSO-d_6, 75 MHz).

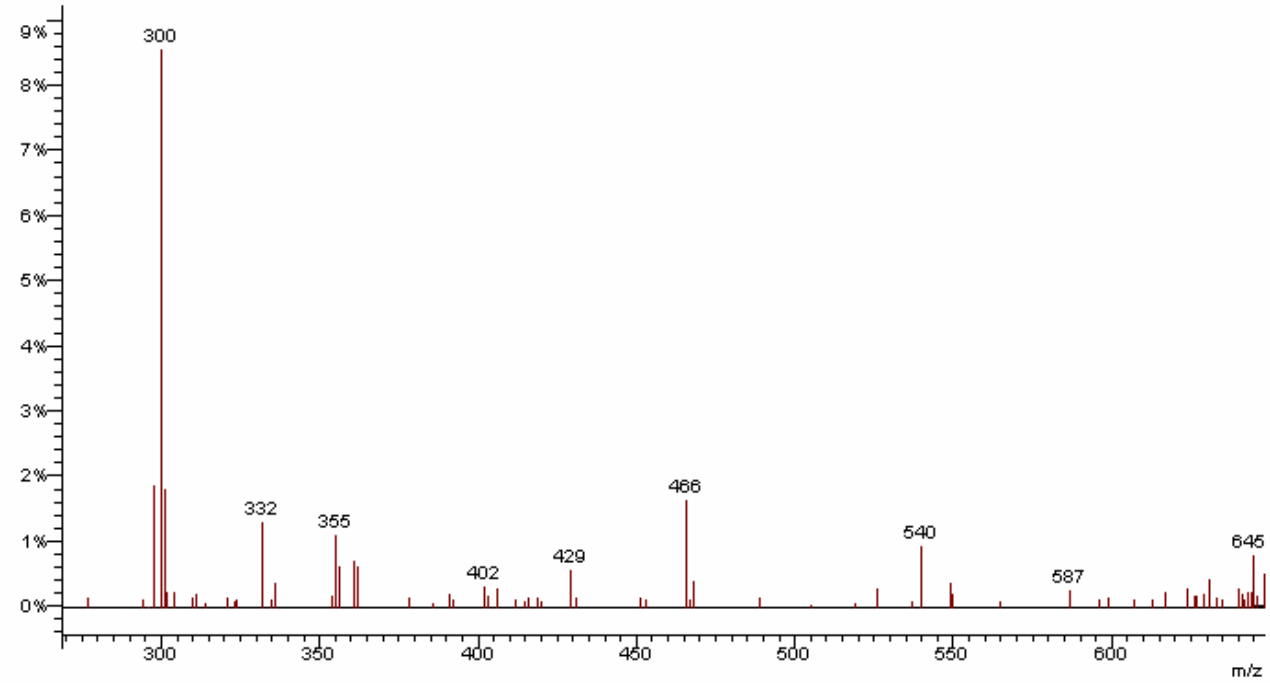

Figure S10. Mass spectra (EI-MS) of compound **5c**.

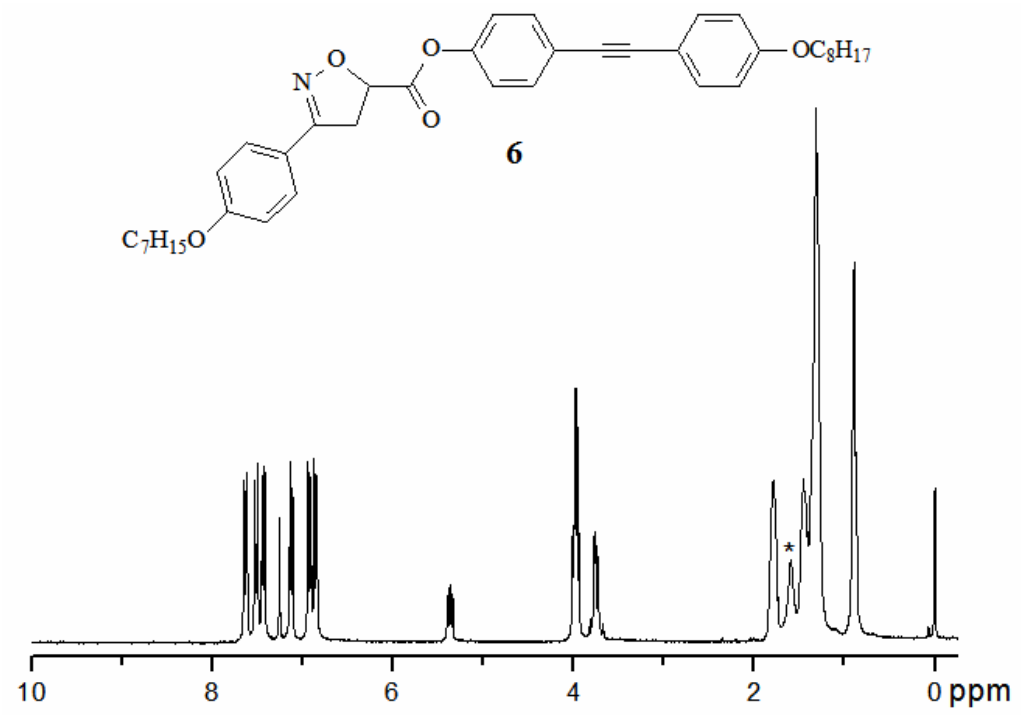

Figure S11. ^{1}H NMR spectrum of compound **6** ($CDCl_3$, 300 MHz). *Solvent impurity.

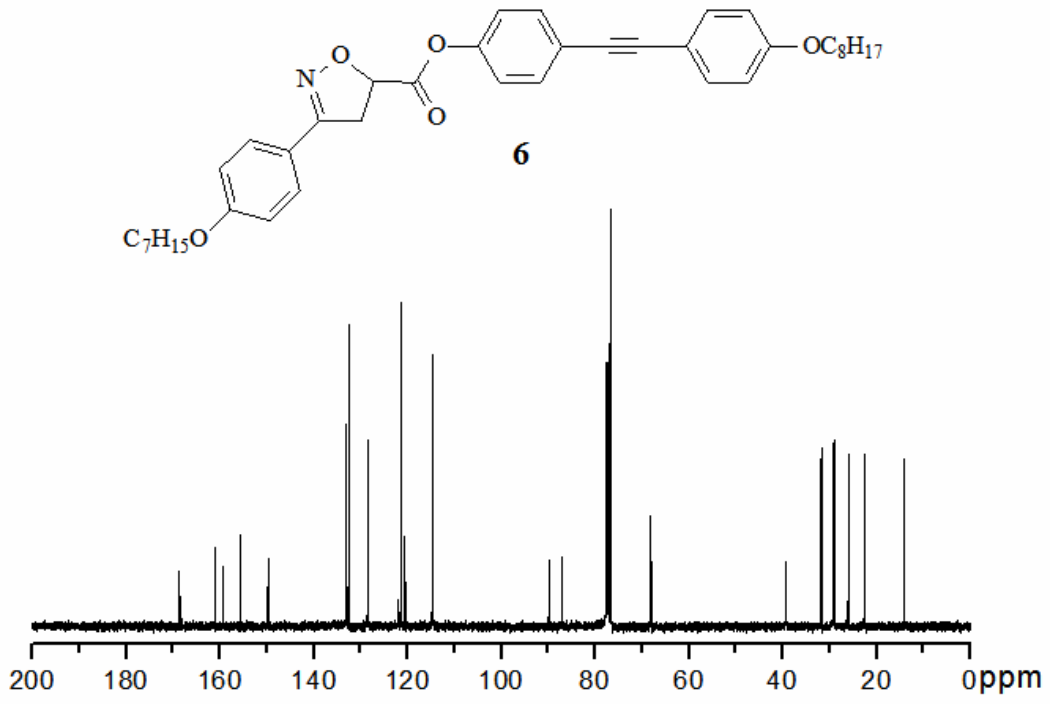

Figure S12. ^{13}C NMR spectrum of compound **6** ($CDCl_3$, 75 MHz).

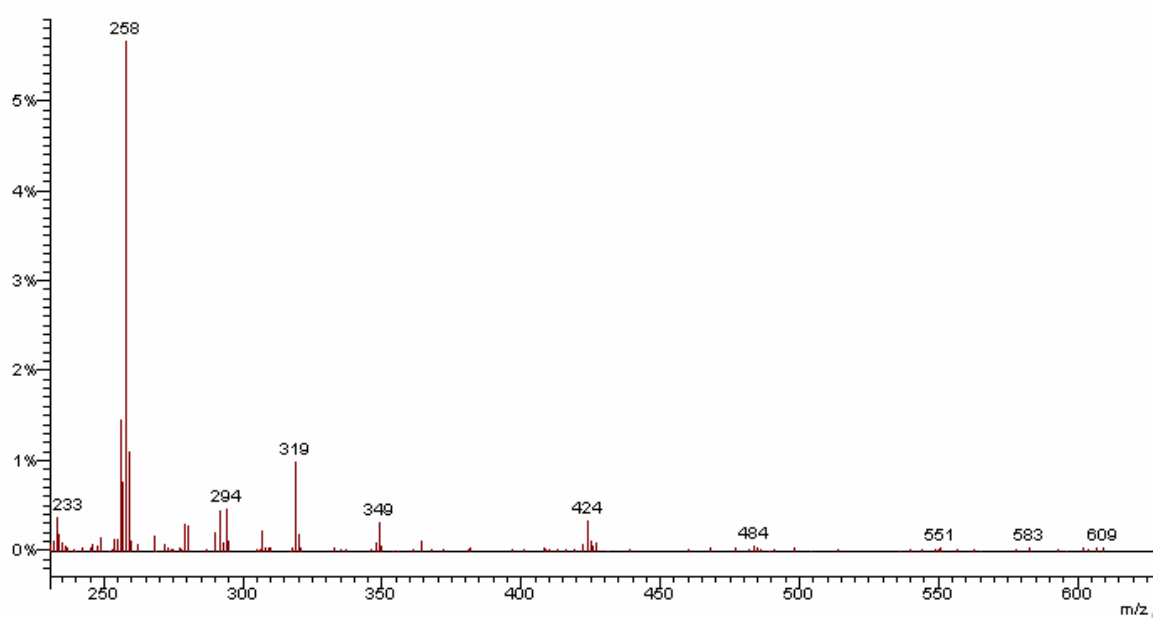

Figure S13. Mass spectra (EI-MS) of compound **6**.

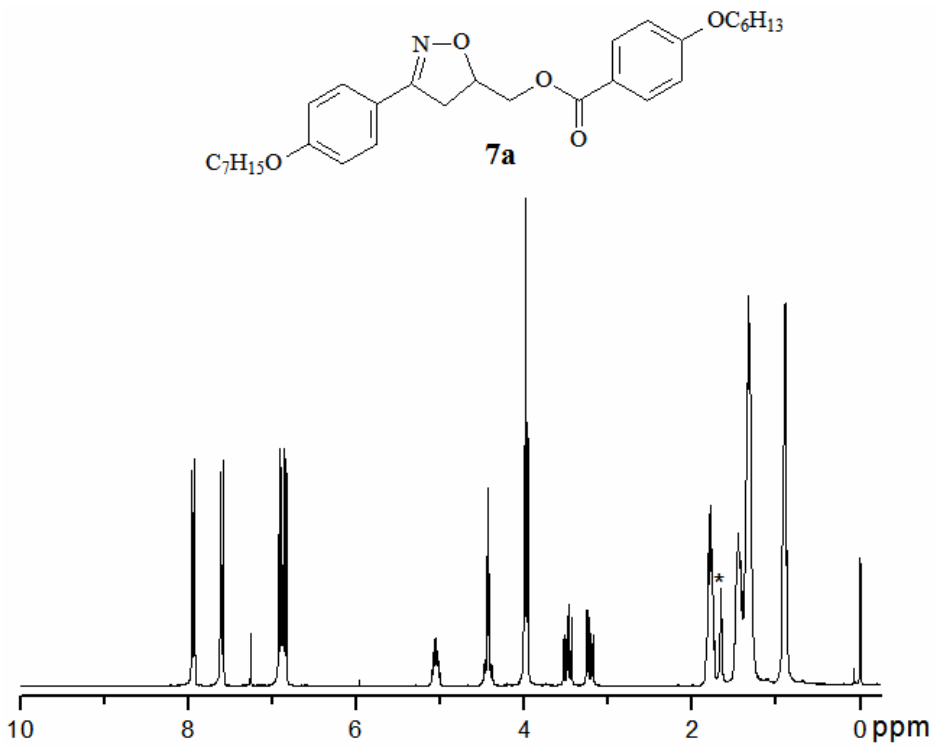

Figure S14. ^{1}H NMR spectrum of compound **7a** ($CDCl_3$, 300 MHz). *Solvent impurity

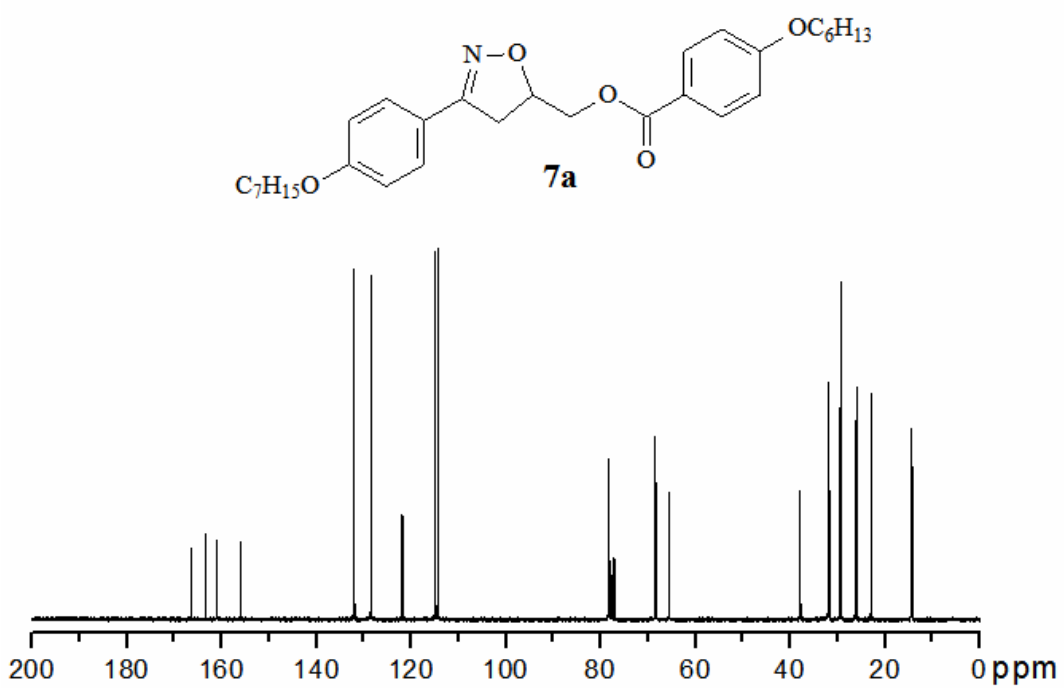

Figure S15. ^{13}C NMR spectrum of compound **7a** ($CDCl_3$, 75 MHz).

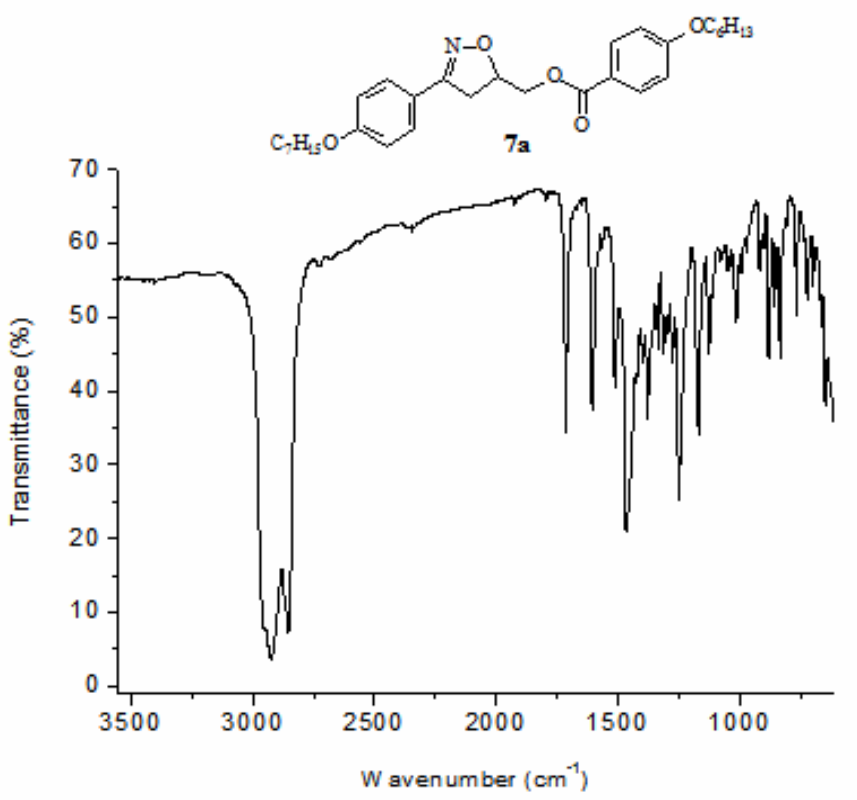

Figure S16. FT-IR spectrum of compound **7a** (nujol).

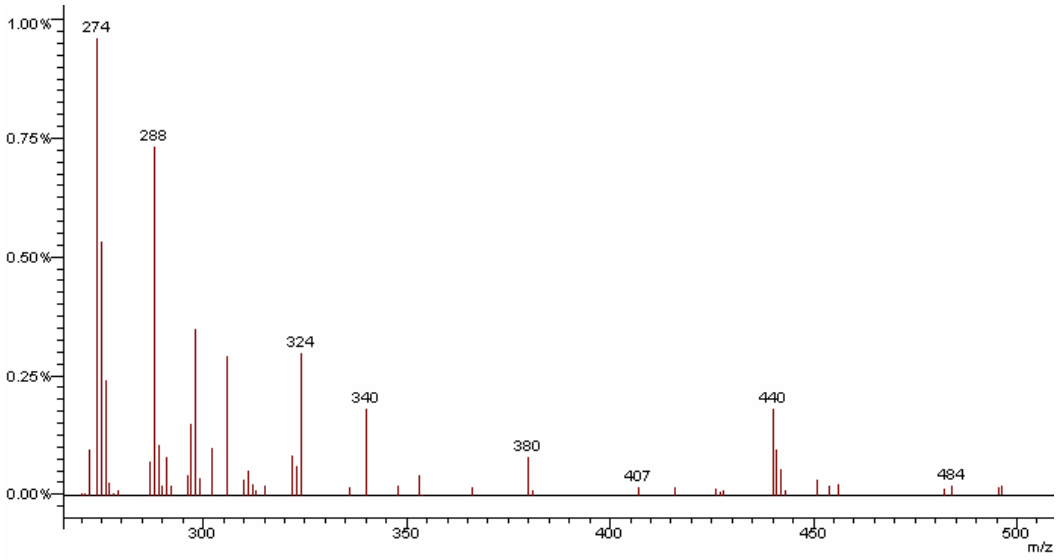

Figure S17. Mass spectra (EI-MS) of compound **7a**.

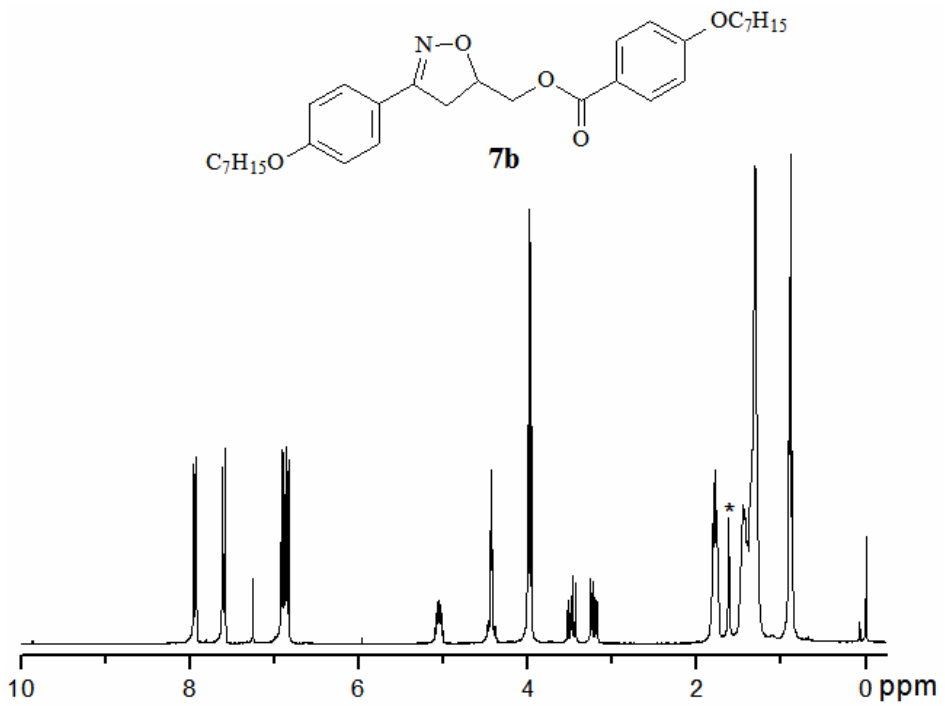

Figure S18. ^{1}H NMR spectrum of compound **7b** ($CDCl_3$, 300 MHz). *Solvent impurity.

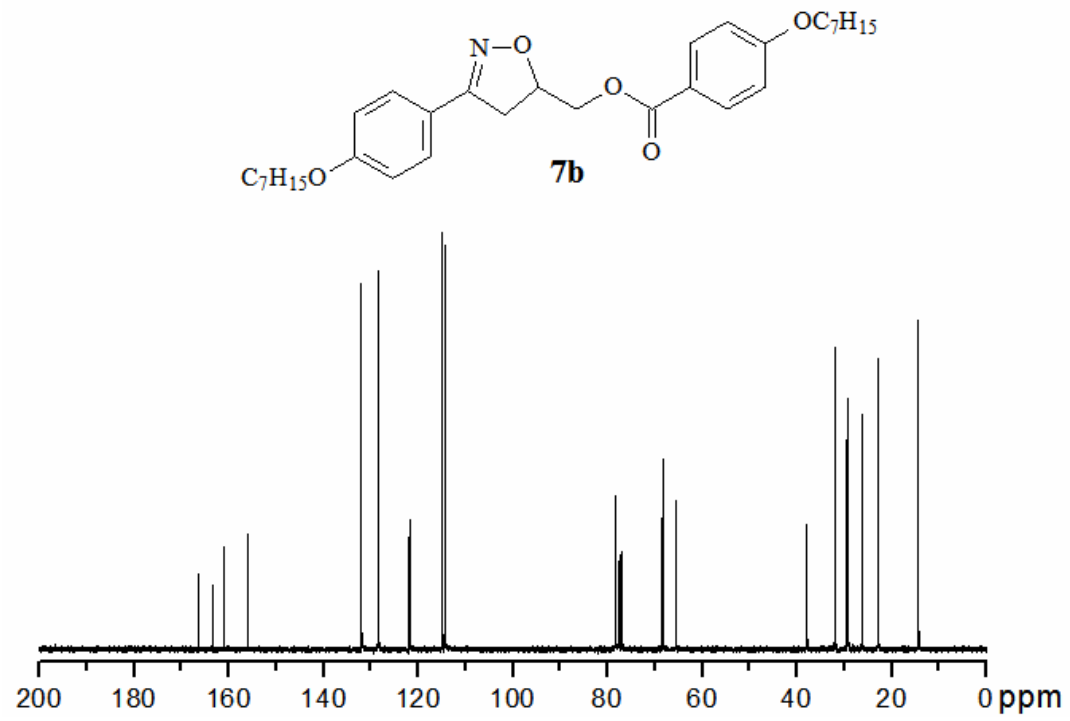

Figure S19. ^{13}C NMR spectrum of compound **7b** ($CDCl_3$, 75 MHz).

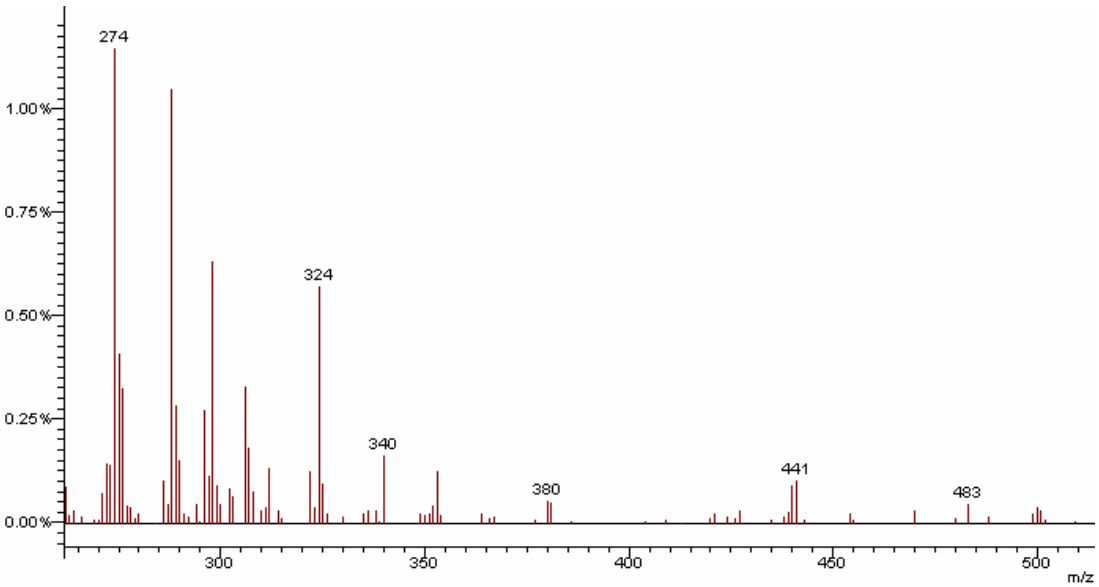

Figure S20. Mass spectra (EI-MS) of compound **7b**.

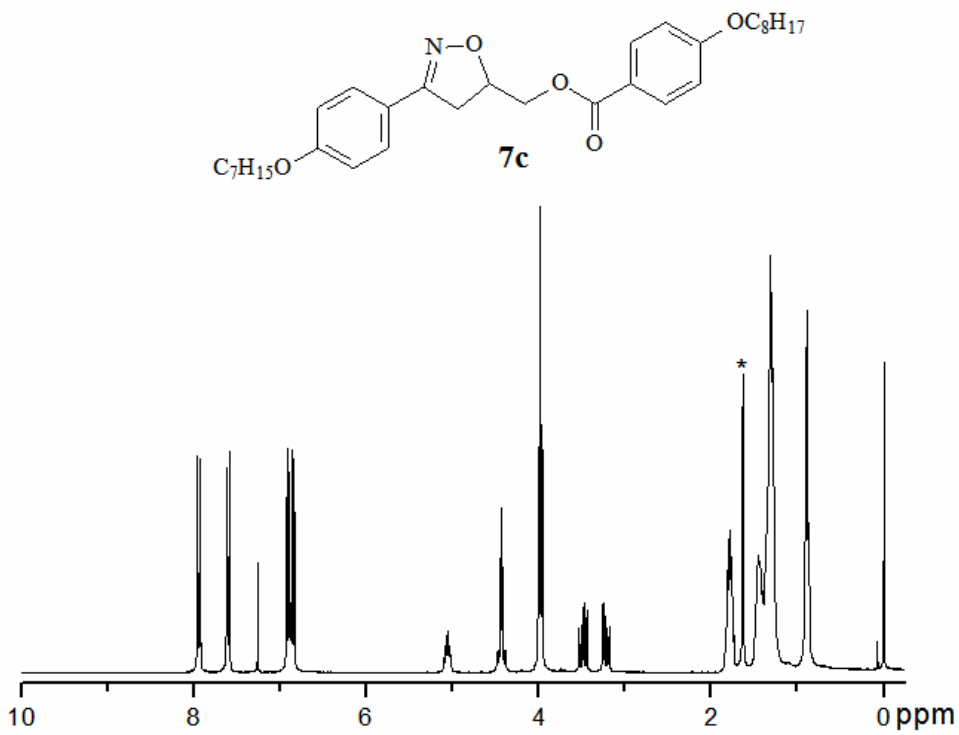

Figure S21. ^{1}H NMR spectrum of compound **7c** ($CDCl_3$, 300 MHz). *Solvent impurity.

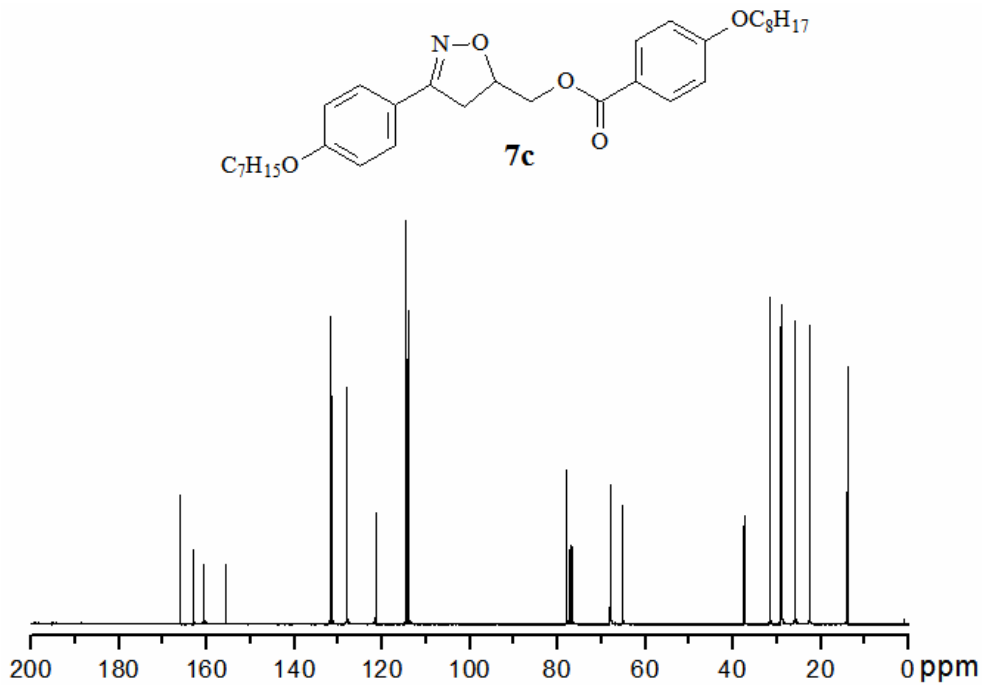

Figure S22. ^{13}C NMR spectrum of compound **7c** ($CDCl_3$, 75 MHz).

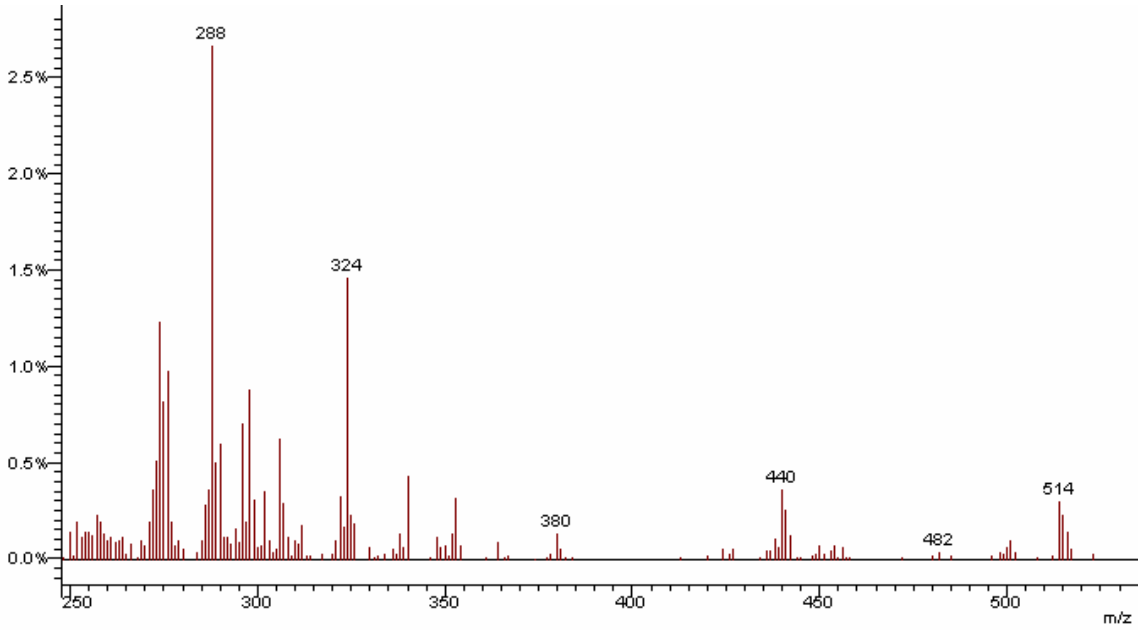

Figure S23. Mass spectra (EI-MS) of compound **7c.**

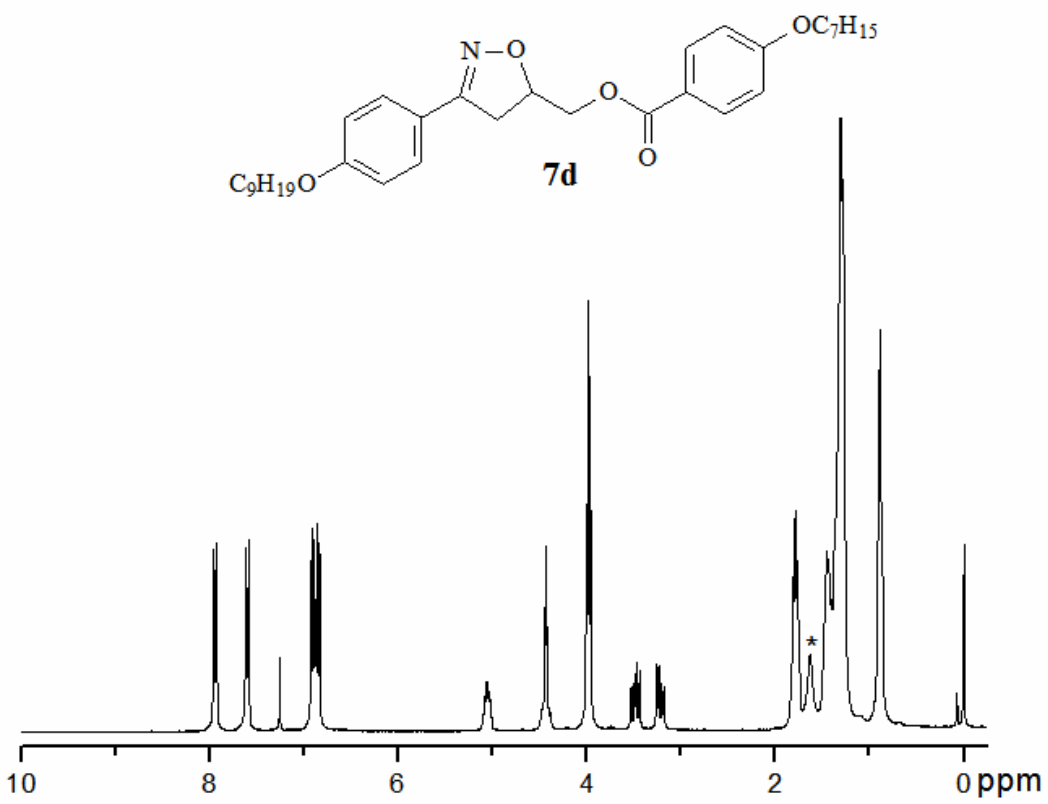

Figure S24. ^{1}H NMR spectrum of compound **7d** ($CDCl_3$, 300 MHz). *Solvent impurity.

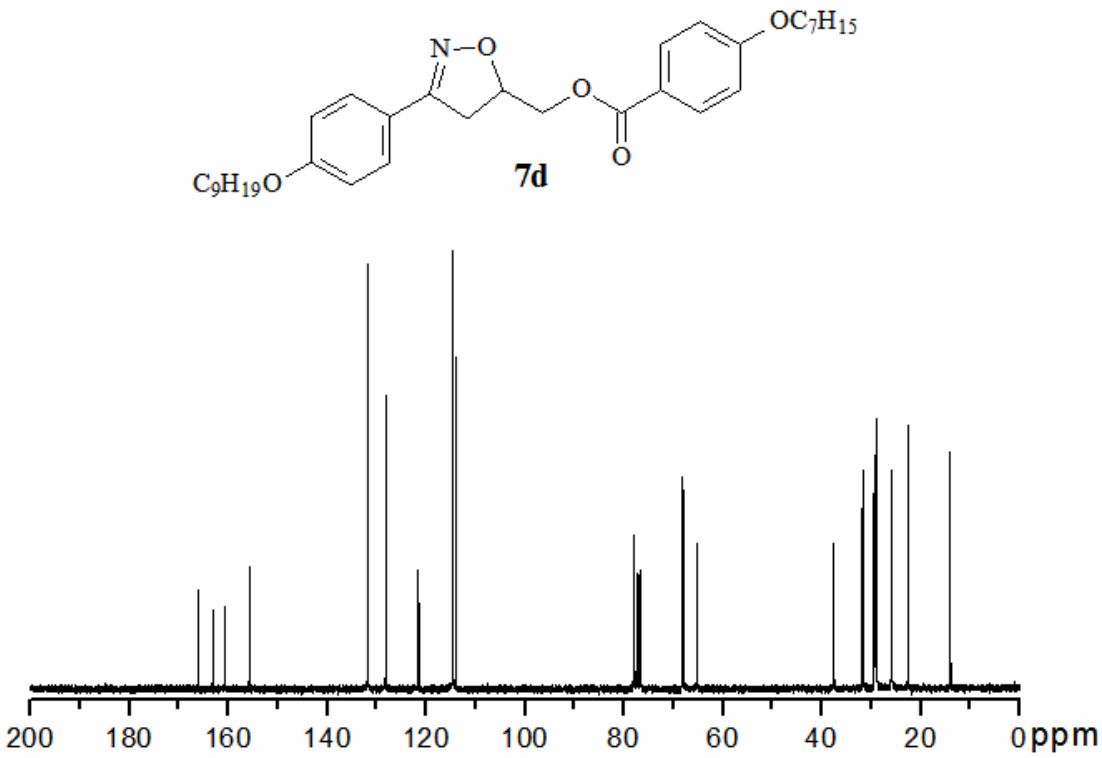

Figure S25. ^{13}C NMR spectrum of compound **7d** ($CDCl_3$, 75 MHz).

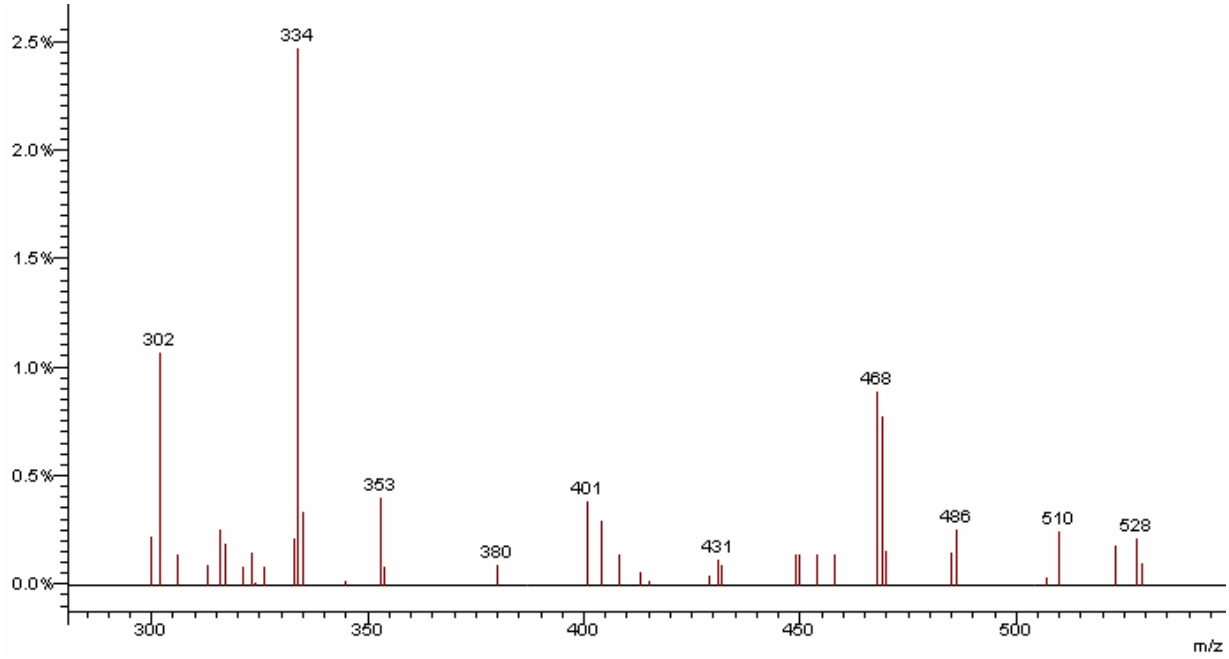

Figure S26. Mass spectra (EI-MS) of compound **7d**.

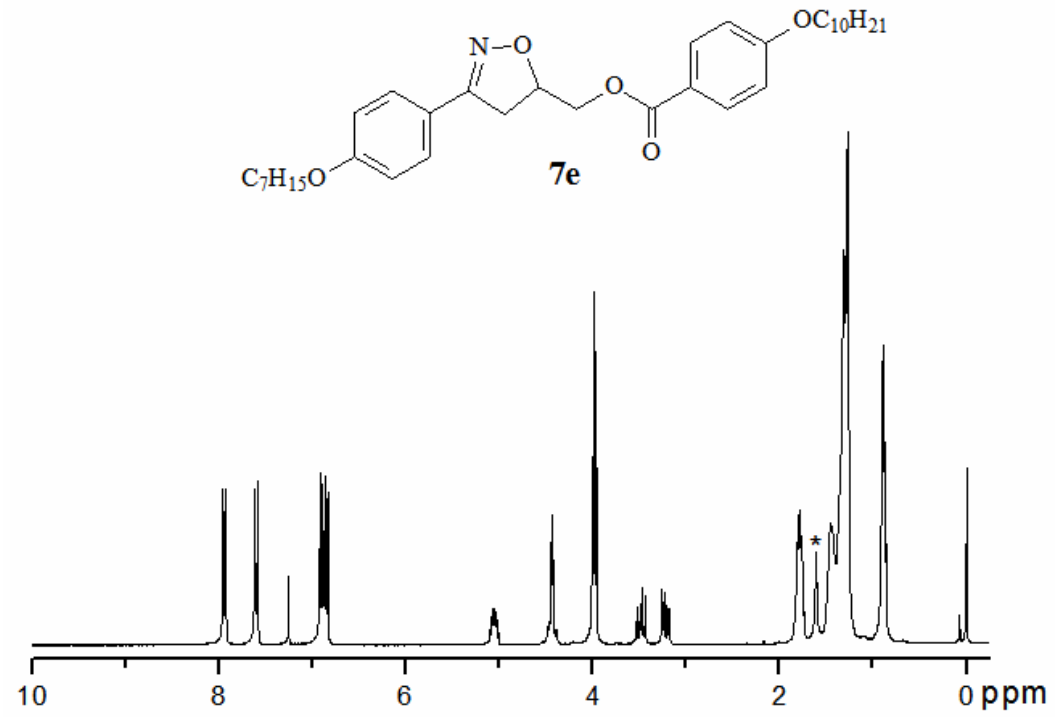

Figure S27. ^{1}H NMR spectrum of compound **7e** ($CDCl_3$, 300 MHz). *Solvent impurity.

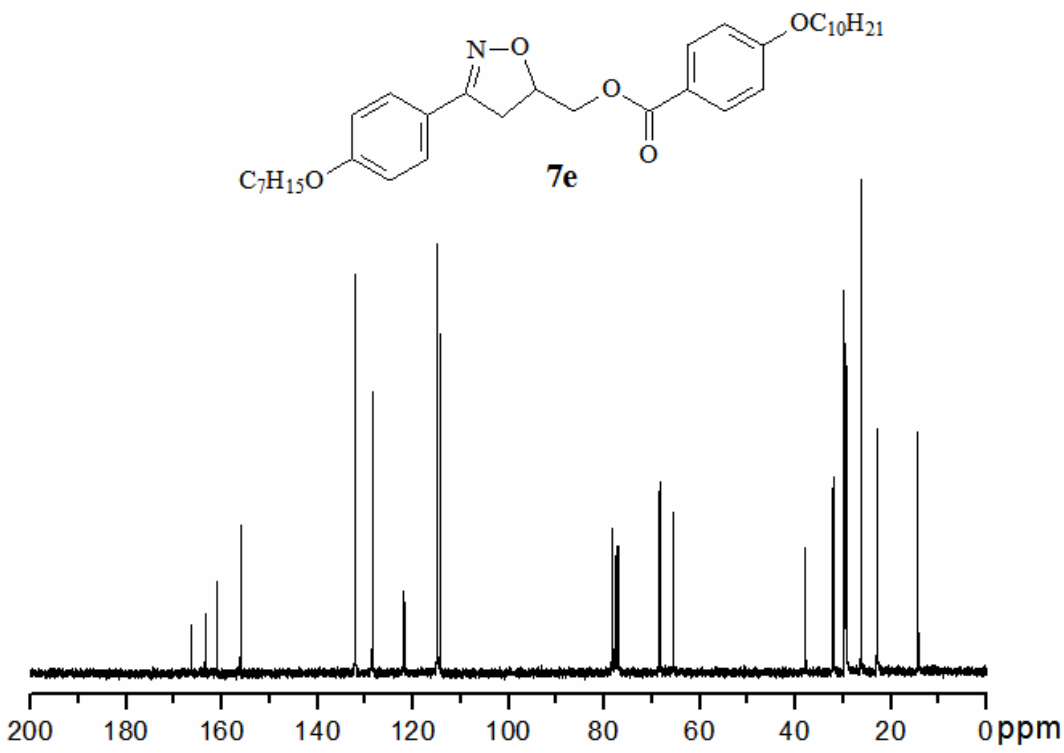

Figure S28. ^{13}C NMR spectrum of compound **7e** ($CDCl_3$, 75 MHz).

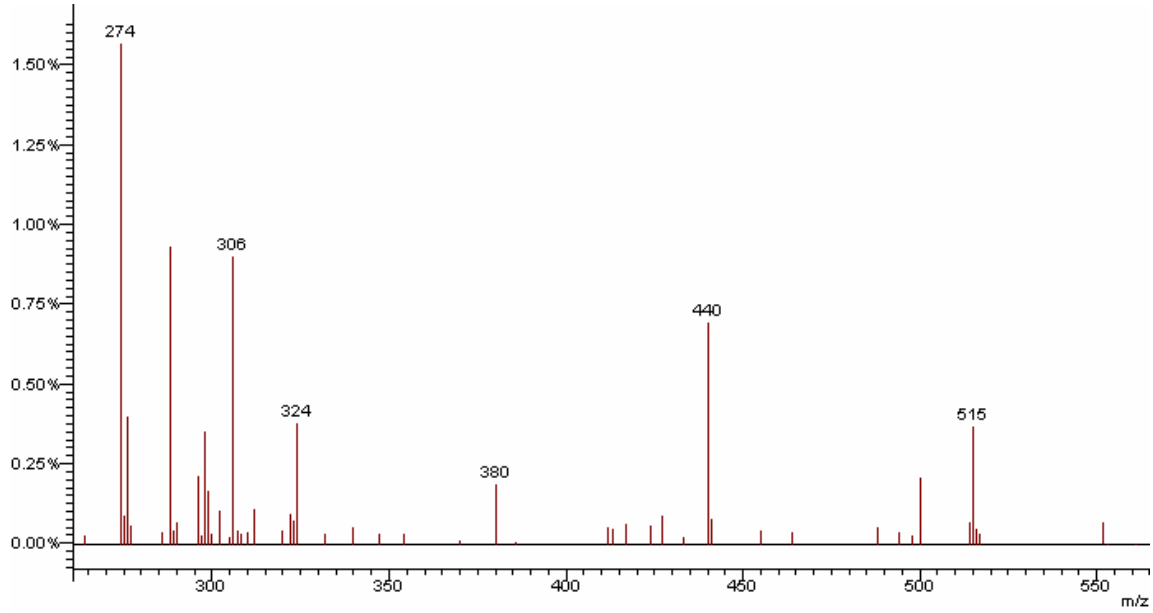

Figure S29. Mass spectra (EI-MS) of compound **7**e.

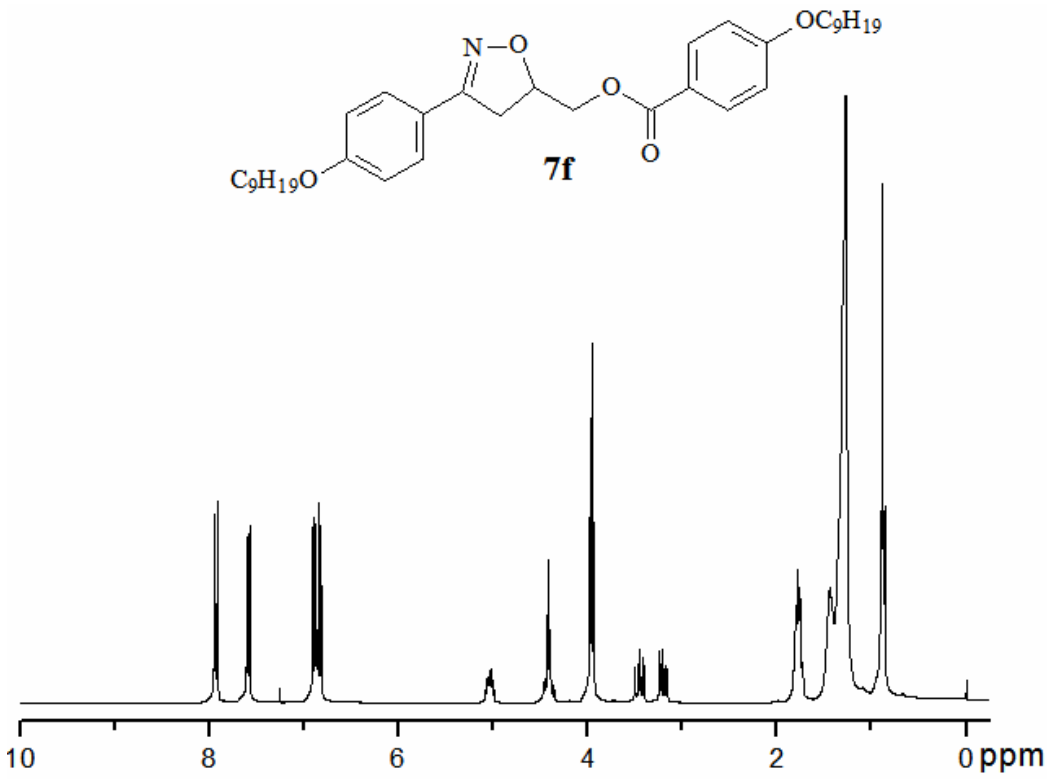

Figure S30. ^{1}H NMR spectrum of compound **7f** ($CDCl_3$, 300 MHz).

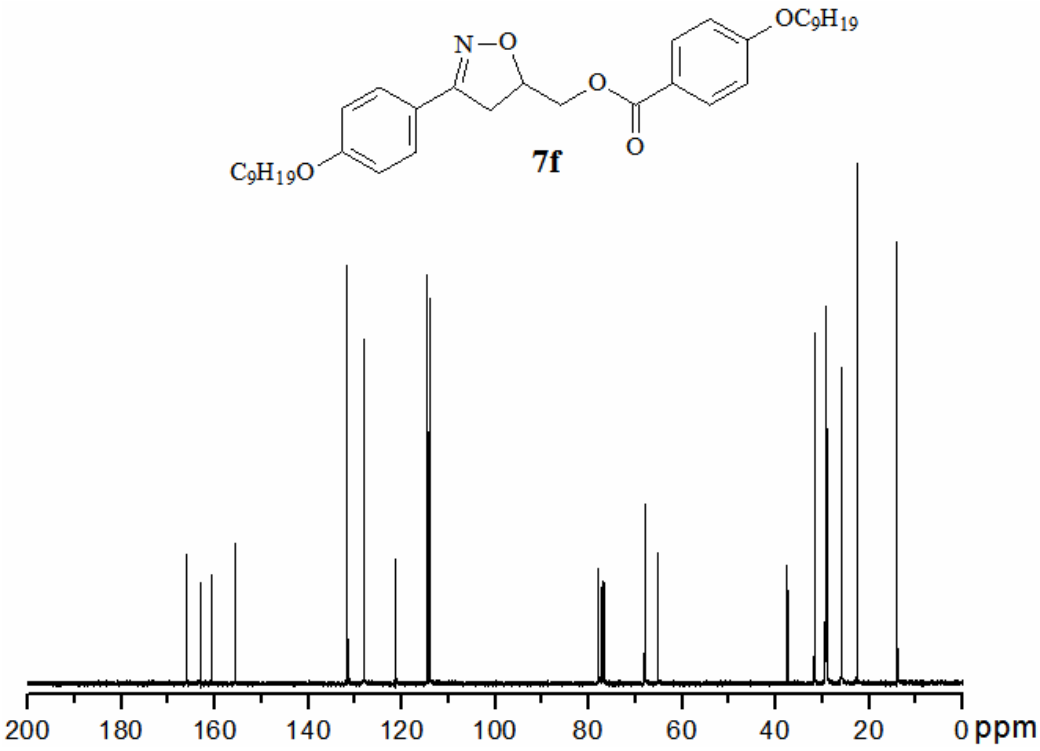

Figure S31. ^{13}C NMR spectrum of compound **7f** ($CDCl_3$, 75 MHz).

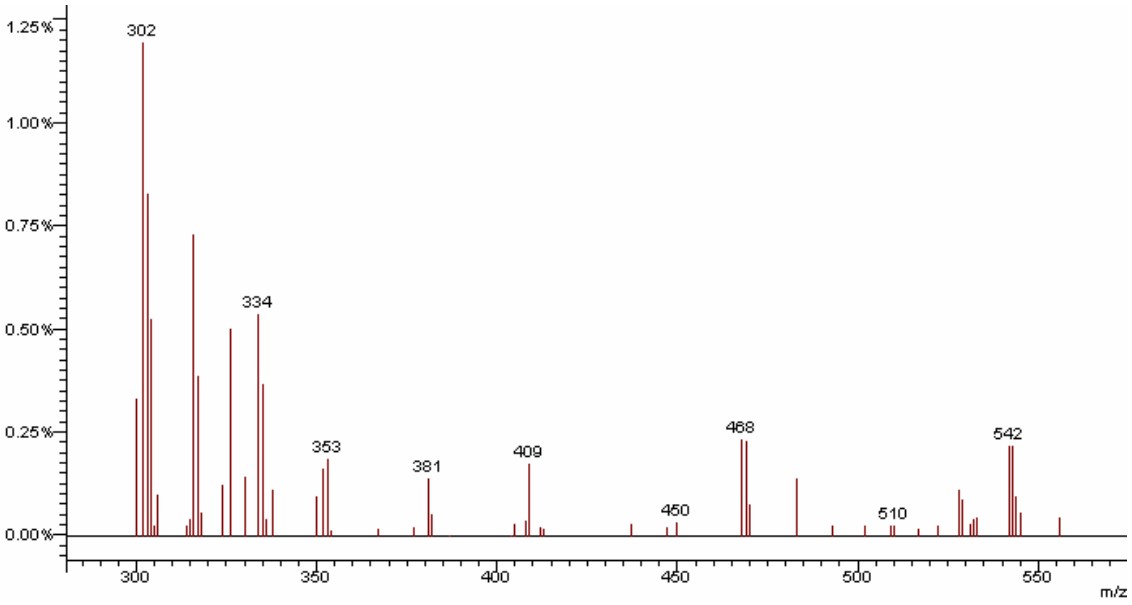

Figure S32. Mass spectra (EI-MS) of compound **7f**.

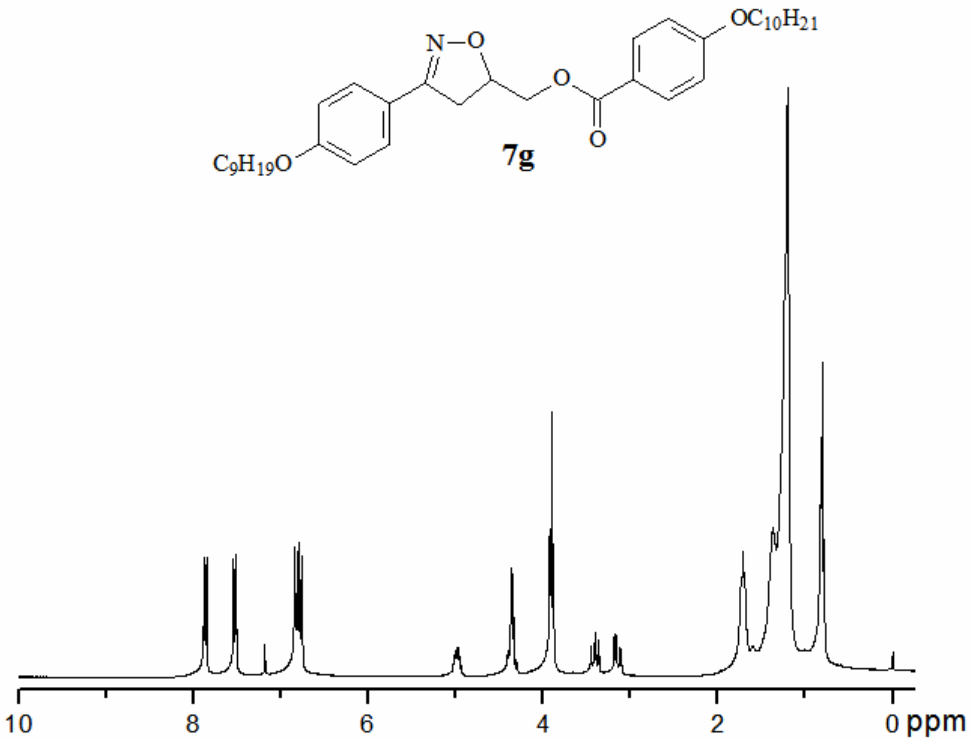

Figure S33. ^{1}H NMR spectrum of compound **7g** ($CDCl_3$, 300 MHz).

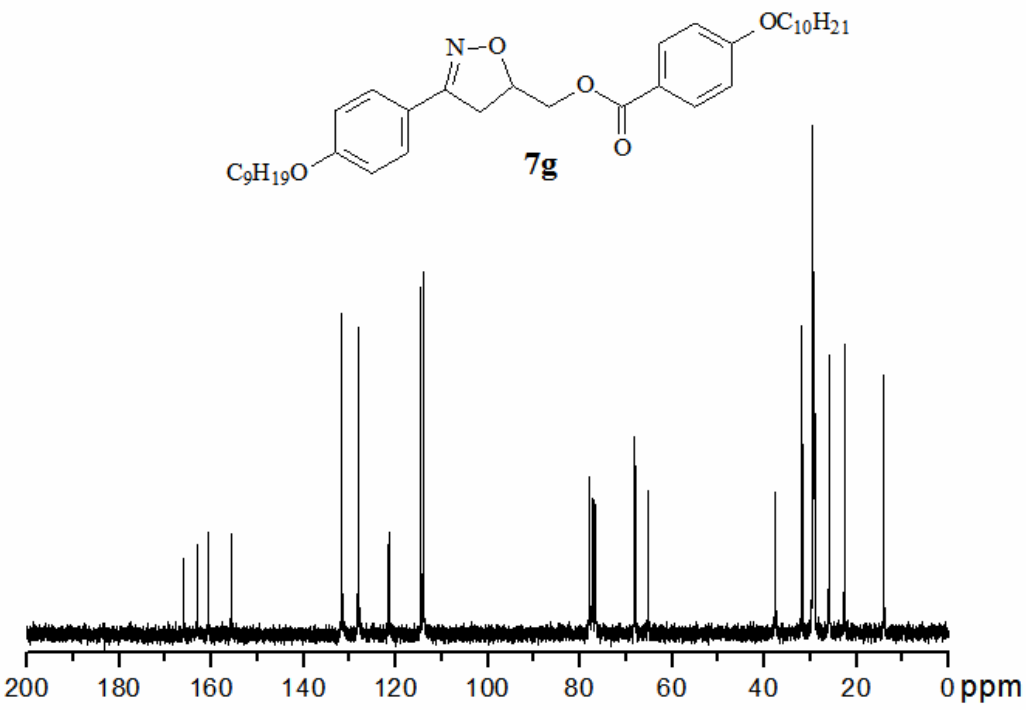

Figure S34. ^{13}C NMR spectrum of compound **7g** ($CDCl_3$, 75 MHz).

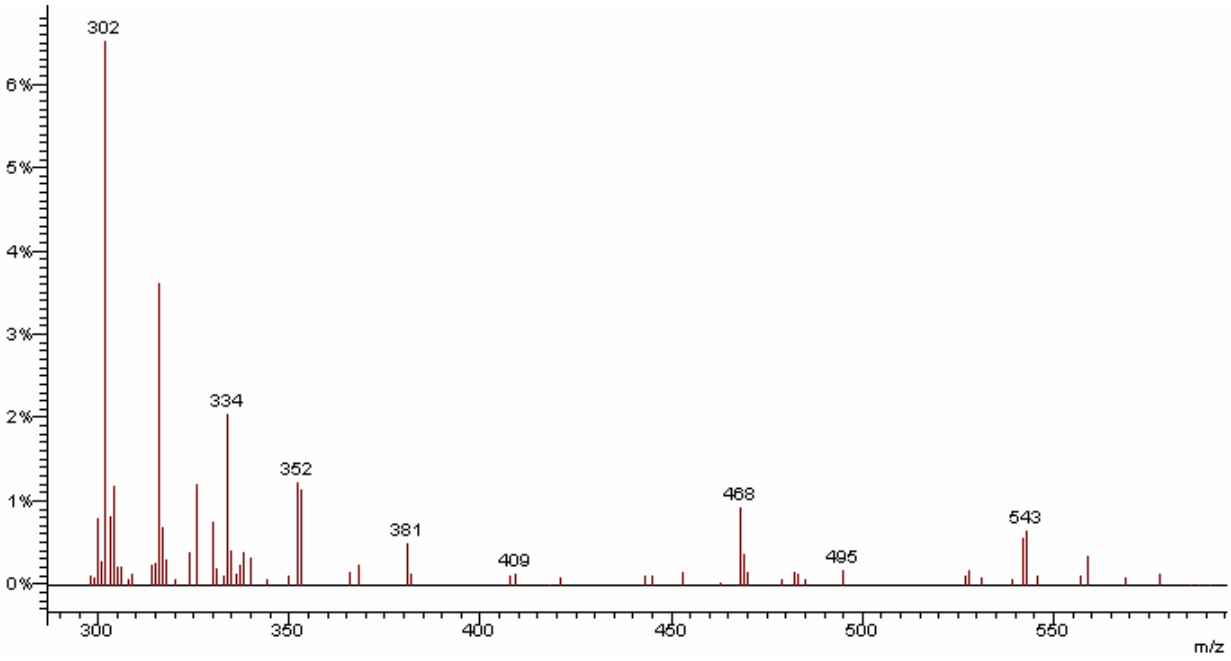

Figure S35. Mass spectra (EI-MS) of compound **7g**.

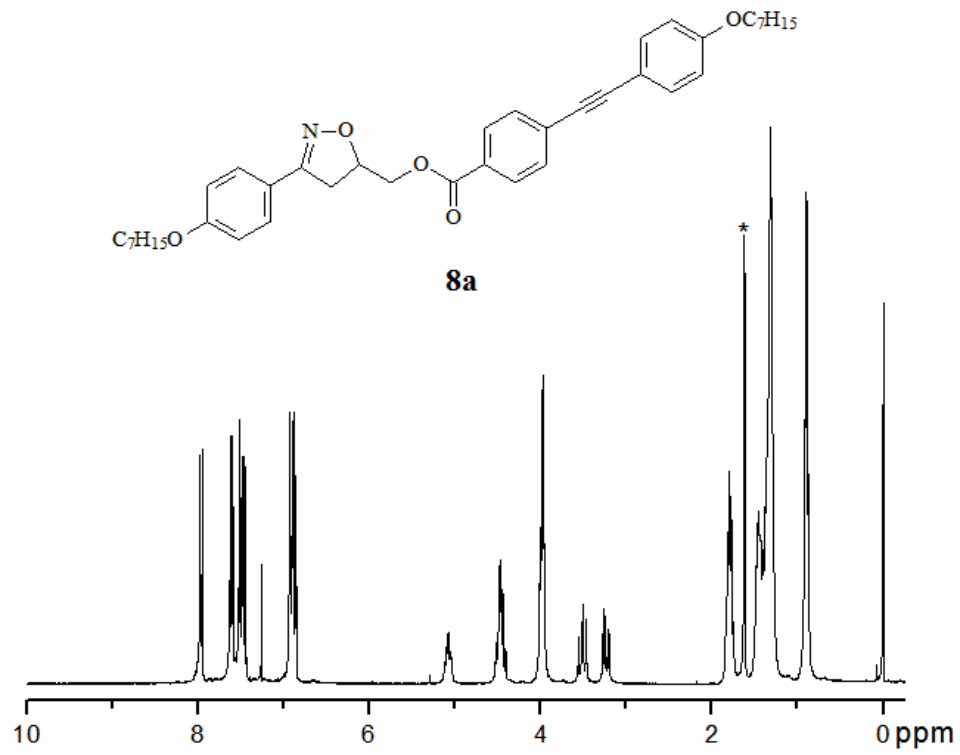

Figure S36. ^{1}H NMR spectrum of compound **8a** ($CDCl_3$, 300 MHz). *Solvent impurity.

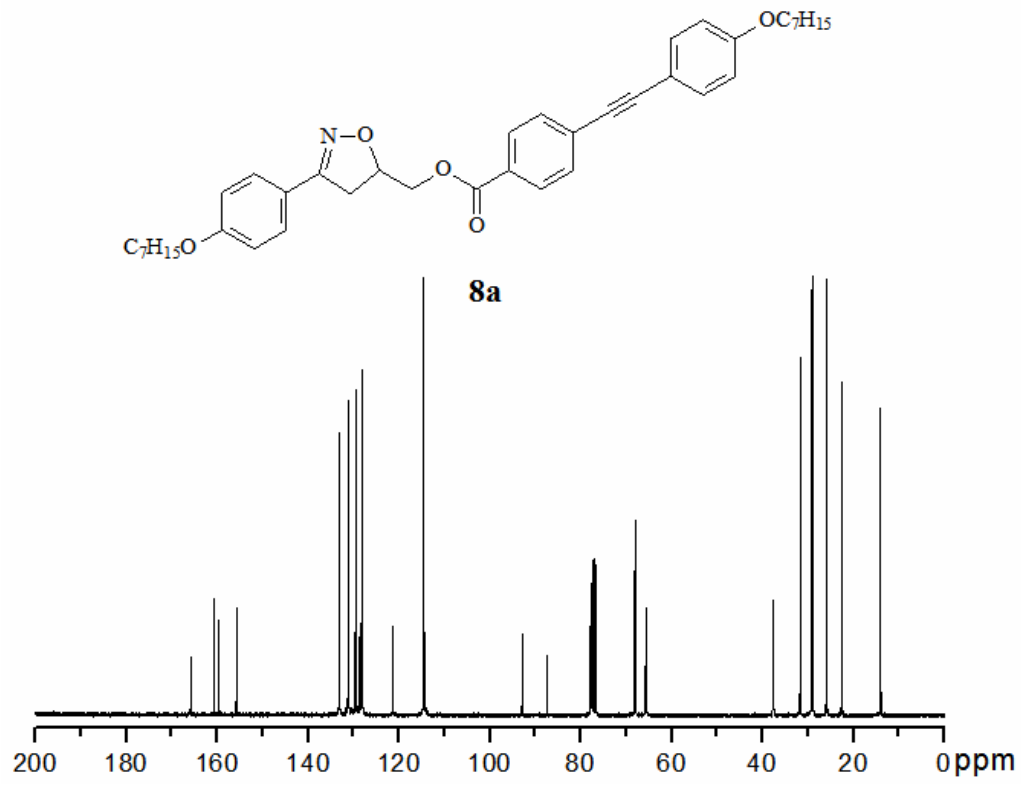

Figure S37. ^{13}C NMR spectrum of compound **8a** ($CDCl_3$, 75 MHz).

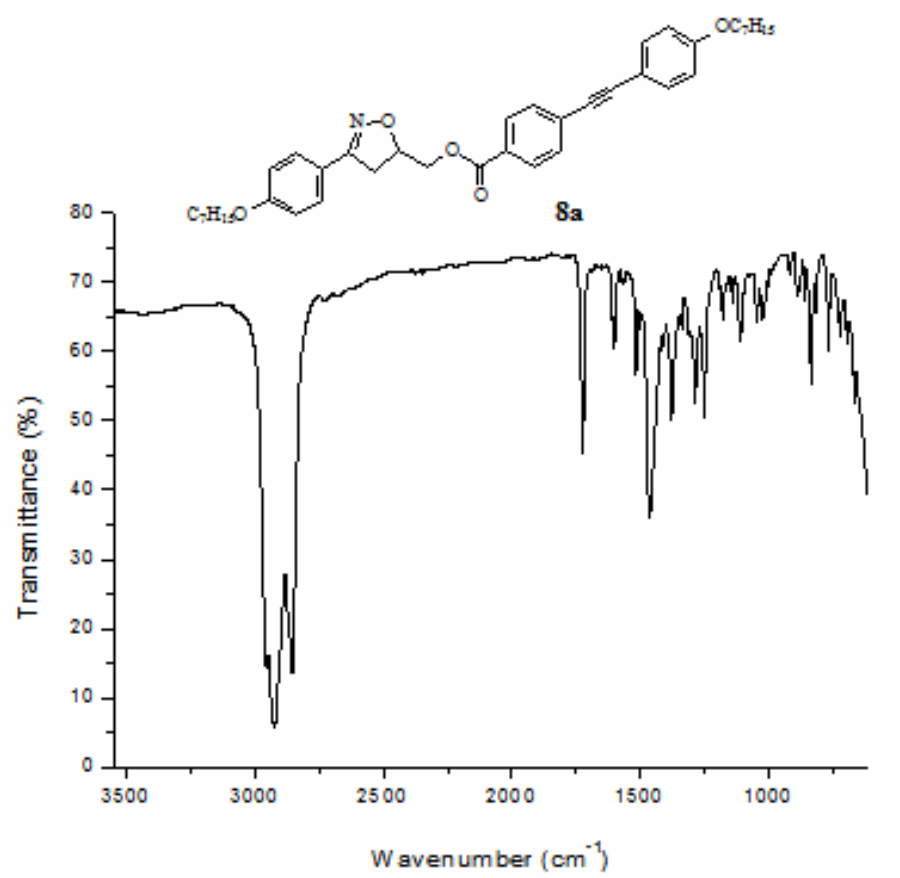

Figure S38. FT-IR spectrum of compound **8a** (nujol).

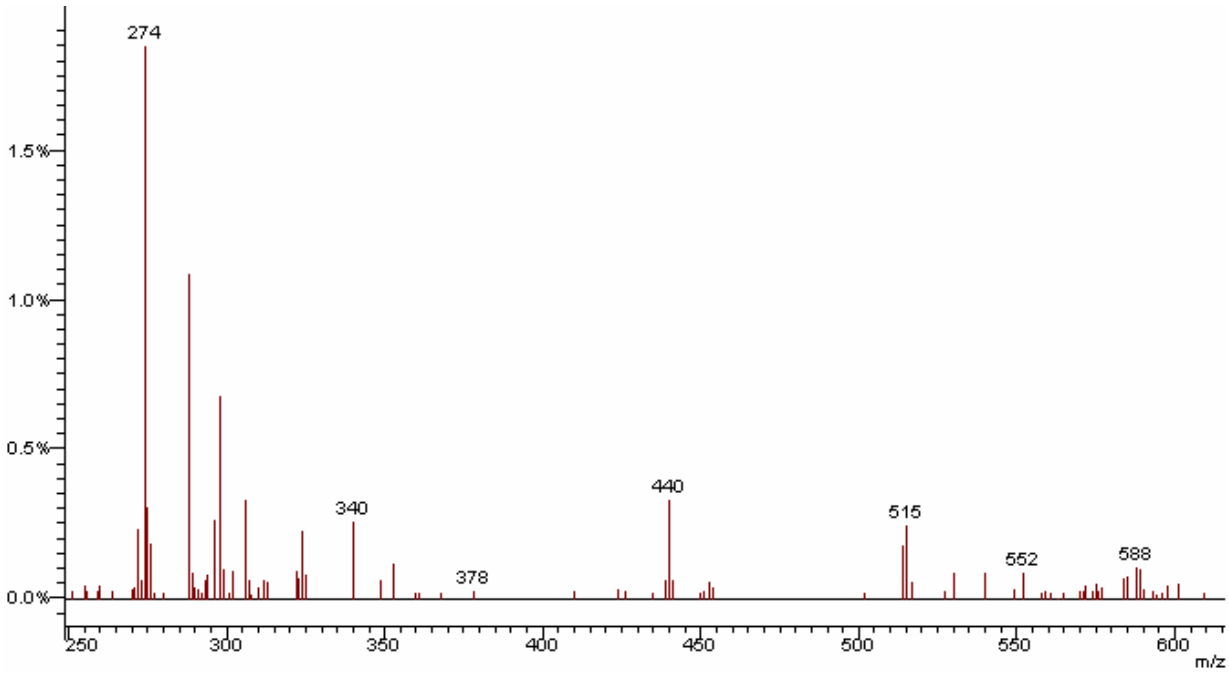

Figure S39. Mass spectra (EI-MS) of compound **8a**.

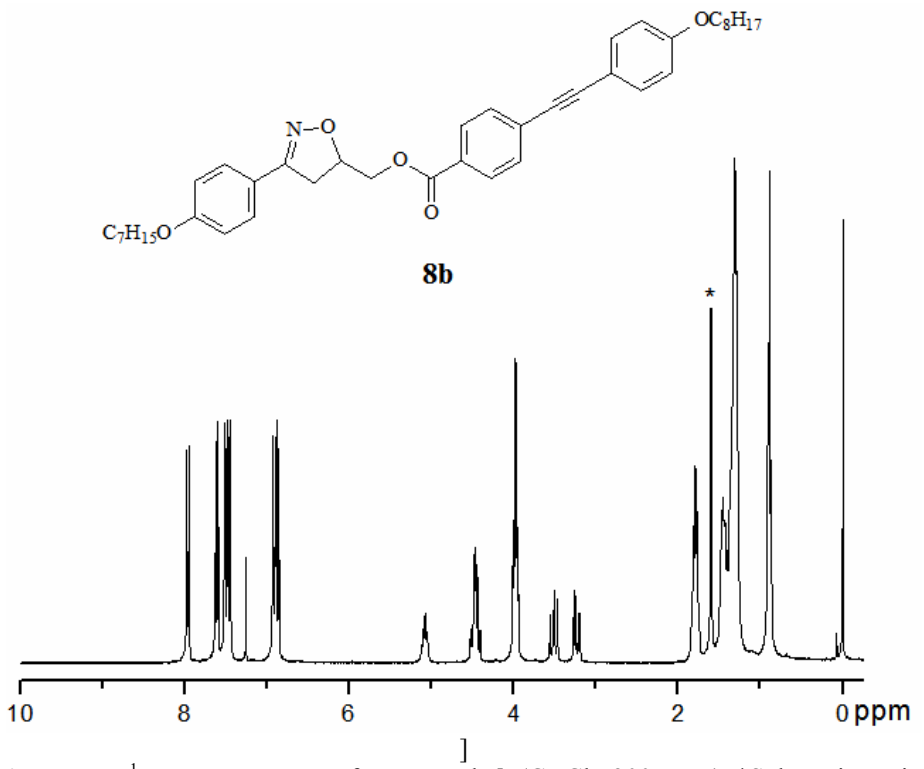

Figure S40. ^{1}H NMR spectrum of compound **8b** ($CDCl_3$, 300 MHz). *Solvent impurity.

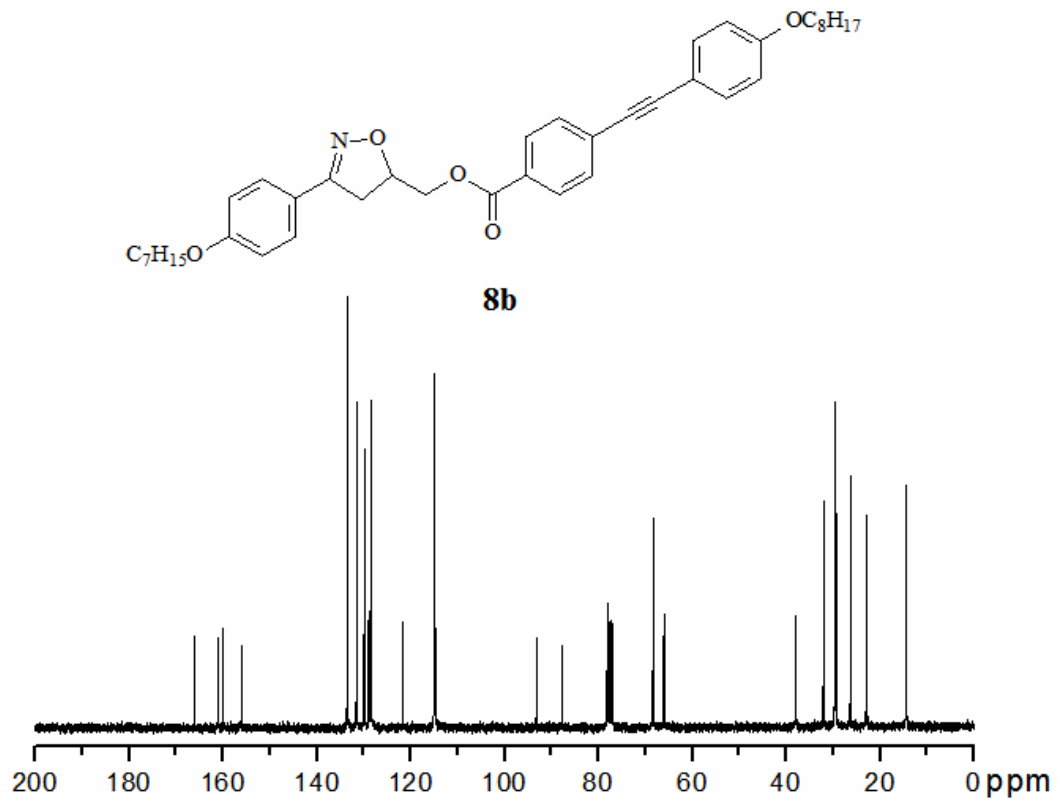

Figure S41. ^{13}C NMR spectrum of compound **8b** ($CDCl_3$, 75 MHz).

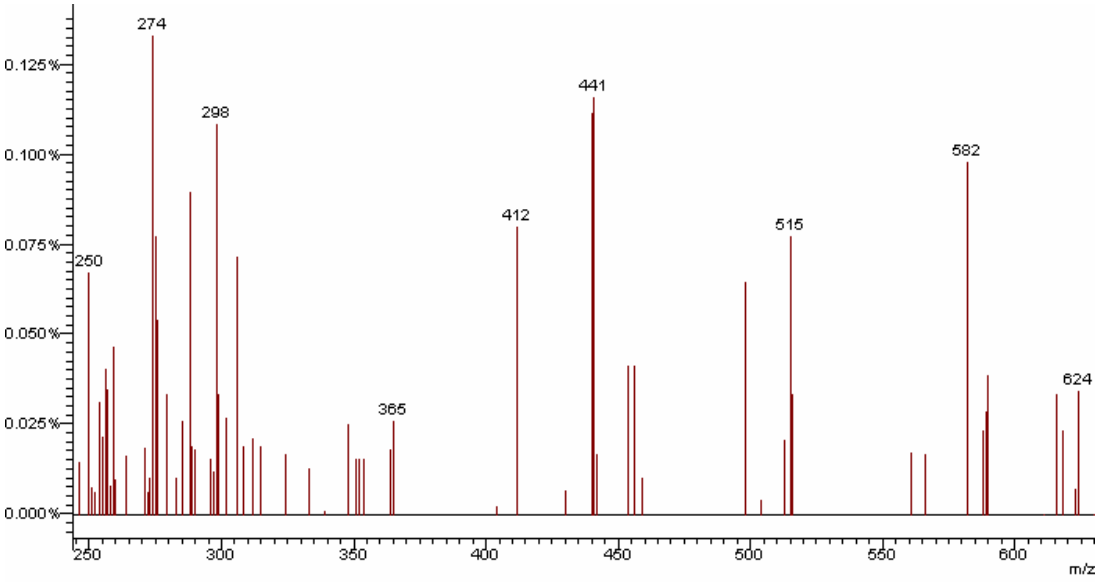

Figure S42. Mass spectra (EI-MS) of compound **8b**.

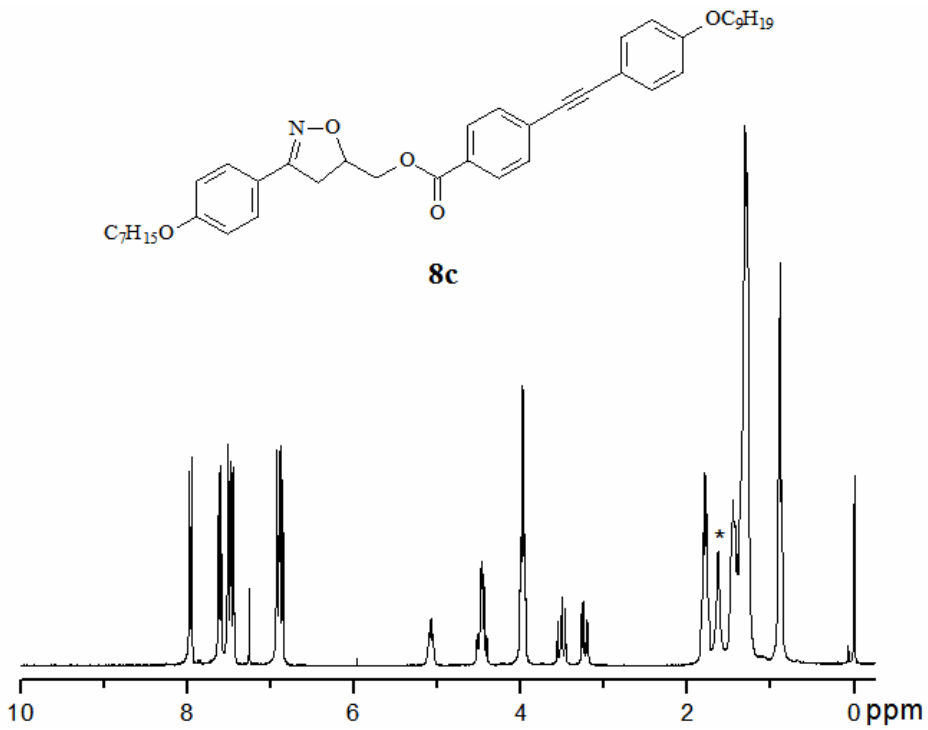

Figure S43. ^{1}H NMR spectrum of compound **8c** ($CDCl_3$, 300 MHz). *Solvent impurity.

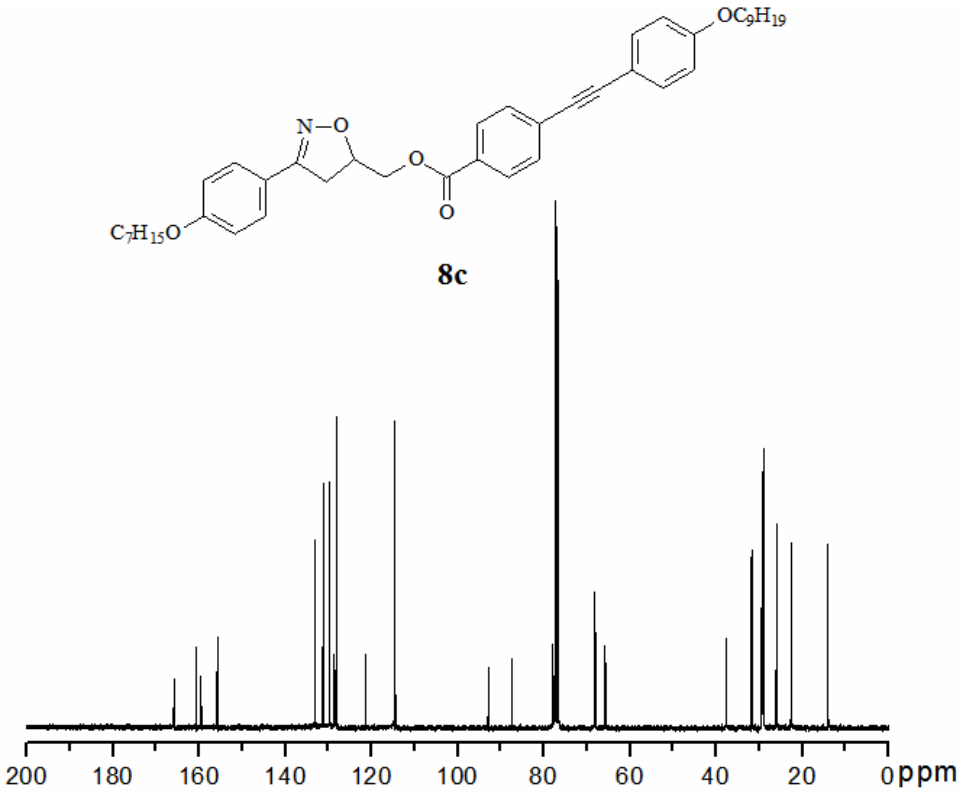

Figure S44. ^{13}C NMR spectrum of compound **8c** ($CDCl_3$, 75 MHz).

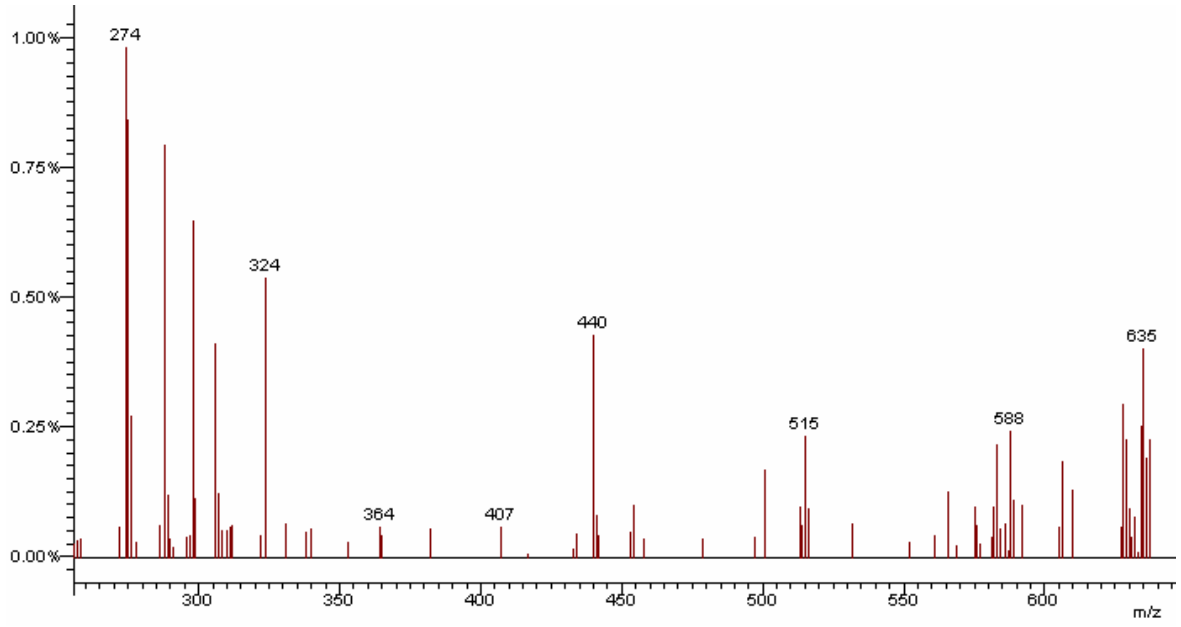

Figure S45. Mass spectra (EI-MS) of compound **8c**.

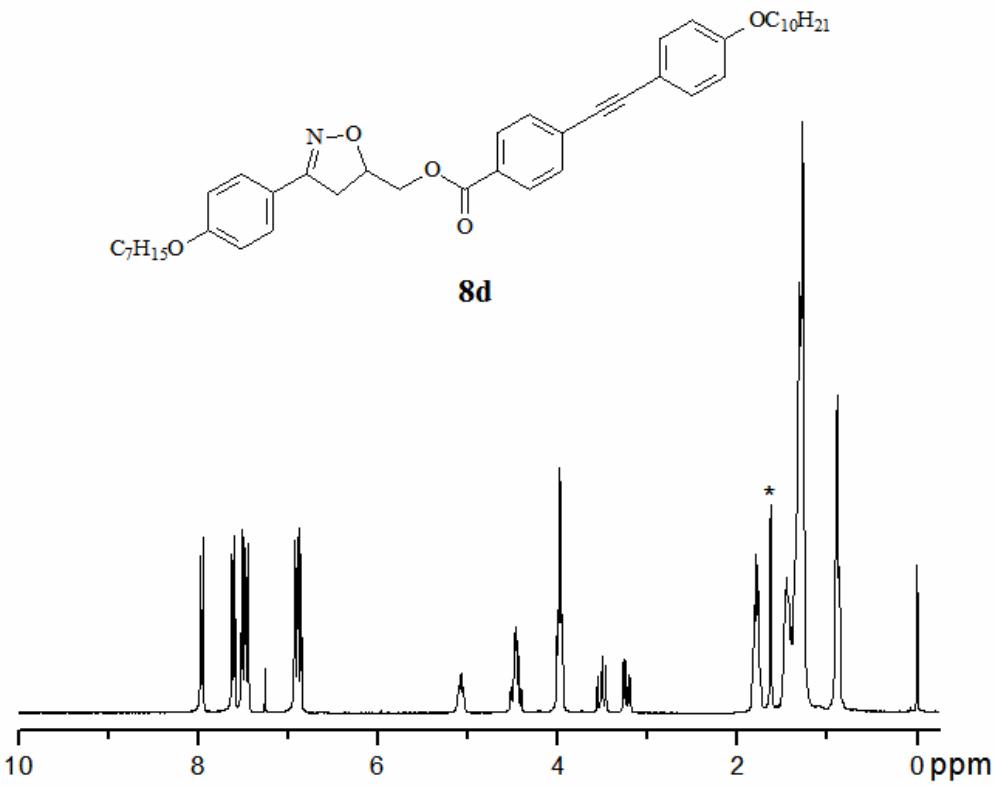

Figure S46. ^{1}H NMR spectrum of compound **8d** ($CDCl_3$, 300 MHz). *Solvent impurity

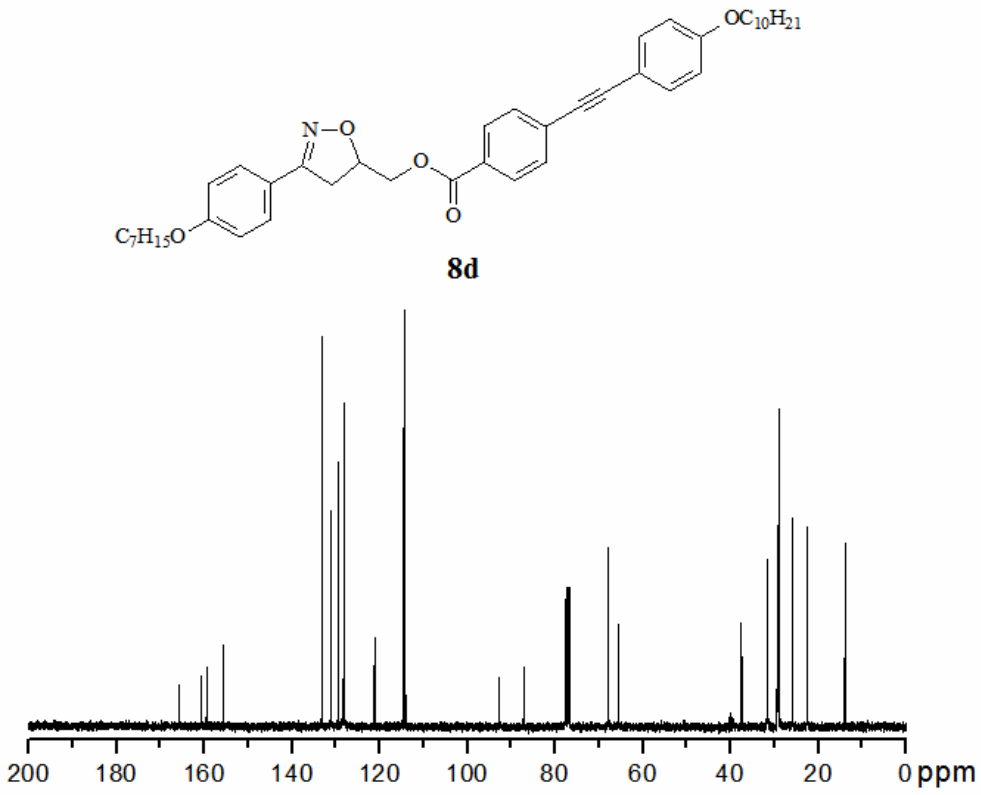

Figure S47. ^{13}C NMR spectrum of compound **8d** ($CDCl_3$/DMSO-d_6, 75 MHz).

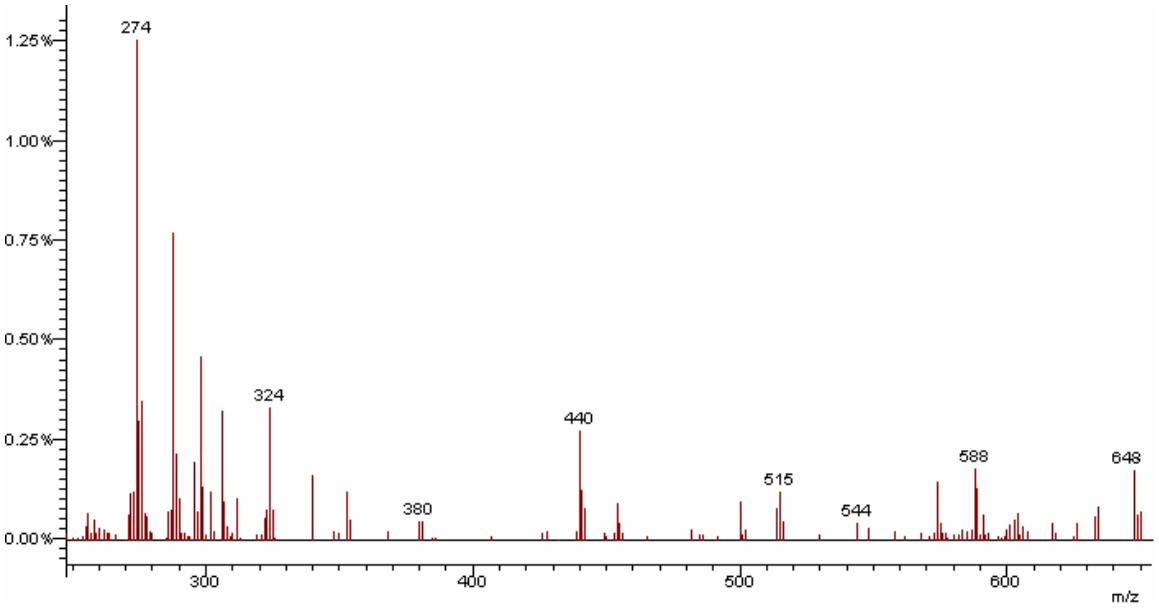

Figure S48. Mass spectra (EI-MS) of compound **8d.**

CAPÍTULO 5.3 - *Liq. Cryst.* **2010**, *37*, 159-169 **- DOI: 10.1080/02678290903432098**

Synthesis of liquid-crystalline 3,5-diarylisoxazolines

Aline Tavares,[a] Olga M. S. Ritter,[b] Ursula B. Vasconcelos,[c] Bárbara C. Arruda,[a] Abel Schrader,[a] Paulo H. Schneider[a] and Aloir A. Merlo[a*]

[a]Chemistry Institute, UFRGS, Porto Alegre, RS, Brazil; [b]Universidade Estadual do Oeste do Paraná, Centro de Engenharias e Ciências Exatas – Toledo, PR, Brazil; [c]Tanac S.A. Montenegro, RS.

(Received 21 August 2009; final form 21October 2009)

The synthesis and mesomorphic properties of new liquid-crystalline 3,5-disubstituted isoxazolines are presented and discussed. These isoxazoline derivatives have been synthesized by reacting oximes with the appropriate 4-substituted styrene dipolarophiles in the presence of *N*-chlorosuccinimide and pyridine. The isoxazolines **3a-d** and **7a-g** prepared by this methodology are used as scaffolds for further molecular derivation through a molecular elongation strategy. The selected scaffolds **3a-b** and **7f-g** were transformed into liquid crystals (LC) by the addition of an arylacetylene group at the C_3 or C_5 carbon atoms on the isoxazoline ring by a Sonogashira reaction. The relevant LC compounds **14a-c**, **15**, **16**, **17** and **18a-c** were synthesized in fair to good yields. The final compounds display both nematic and smectic A liquid-crystalline phases.

Keywords: isoxazoline liquid-crystalline; Sonogashira coupling; nitrile oxide [3+2] cycloaddition; mesomorphic behaviour.

Introduction

The 1,3-dipolar cycloaddition of a nitrile oxides to alkenes and alkynes has proved be an extremely useful strategy for the preparation of isoxazoline and isoxazole rings [1-7]. These compounds serve as useful building blocks in the synthesis of various compounds such as α,β-unsaturated ketones, 1,3-amino alcohols, β,γ-dihydroxy ketones and β-hydroxy ketones [6,7].

Previous studies of isoxazoline derivatives showed that these compounds exhibit a wide spectrum of pharmacological activities [8-10] and are key precursors for different natural products [11,12]. The isoxazoline was first used as structural molecular element of liquid crystals (LCs) by Daniel Vorlander nearly a century ago [13]. More recently, Bezborodov *et al.* [14] reported mesomorphic behavior of a series of isoxazolines. Other isoxazoline derivatives exhibiting mesomorphic properties were also developed by a Russian group [15,16]. We have recently reported that 3,5-disubstituted isoxazolines could easily be prepared using a [3+2] 1,3-dipolar cycloaddition reaction between nitrile oxides and alkenes [17-20]. As part of our continuing interest in the synthesis of new LCs containing the tolane structural unit in the 3- or 5-position of the isoxazoline ring we explored synthetic potential of the bromoisoxazoline in the preparation of new LC materials. The initial strategy utilized **3a-b** and **7f-g**, advanced intermediates in our research program involving the preparation of novel isoxazoline LCs, as key components for the synthesis of mesogenic 3,5-diarylisoxazolines. By using a Sonogashira reaction the third benzene ring was installed by connecting a triple bond to both sides of the isoxazoline ring. In this paper we describe the synthesis and the phase behavior of a series of novel 3,5-disubstituted isoxazoline compounds containing naphthyl and/or phenylacetylene groups attached to the heterocyclic ring. The isoxazolines **14a-c** and **18a-c** are composed of an arylphenylacetylene group linked at the 3- and 5-positions of the isoxazoline ring, respectively. Isoxazolines **15, 16** and **17** are composed of an arylnaphthylacetylene group linked at the 5-position of the isoxazoline ring. Figure 1 shows the general structure of the new 3,5-diarylisoxazolines synthesized in this work.

Results and Discussion

Synthesis

The synthesis of 3,5-diarylisoxazolines with non-symmetric phenyl groups was a ccomplished in a

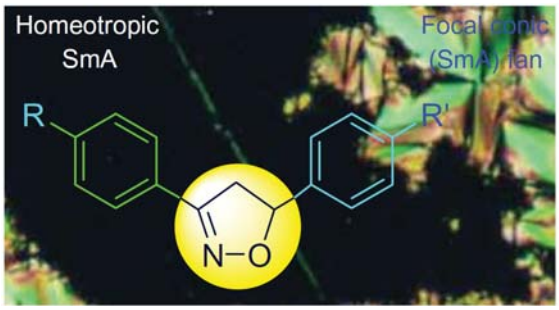

Figure 1. General chemical structure for 3,5-diaryl-isoxazolines.

straightforward manner by the 1,3-dipolar cycloaddition of nitrile oxides to alkenes. The synthesis of the first series of 3,5-isoxazolines **3a-d** and **4b** is outlined in Scheme 1. Compound **1** was used as a starting material in the synthesis of some of the final compounds described in this work. The flexible alkyl chain was introduced by an alkylation reaction of **1** following a procedure described by Hsiue and Chen [21]. The oxime derivatives were obtained through a condensation reaction using hydroxylamine salts under basic conditions. The synthesis of cycloadducts **3a-d** and **4b** were achieved by exposure of oximes to 4-substituted styrene **2** (X = Br and CH_3) through [3+2] 1,3-dipolar cycloaddition reaction shown in Scheme 1.

The second set of cycloadduct 3,5-disubstituted isoxazolines **7a-g** was prepared according to Scheme 2. In this set, we chose the aldehydes **5a-c** containing a more polar group at the *para* position of the benzene ring and three different dipolarophiles **2** (X = Me, Br, Cl).

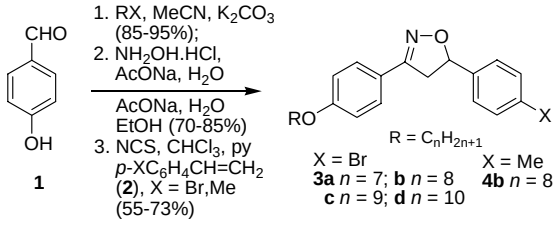

Scheme 1. Synthesis of the series of 3,5-diarylisoxazolines **3a-d** and **4b**.

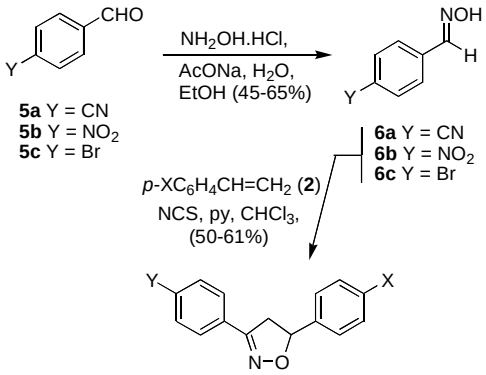

7a Y = NO_2, X = Cl; **7b** Y = NO_2, X = Br;
7c Y = NO_2, X = Me; **7d** Y = CN, X = Br;
7e Y = X = Br; **7f** Y = Br, X = Me;
7g Y = Br, X = Cl;

Scheme 2. Preparation of cycloadduct isoxazolines **7a-g**.

The final step in Schemes 1 and 2 is a one-pot reaction and was carried out in the following sequence (i) chlorination reaction of oximes with *N*-chlorosuccinimide (NCS) in chloroform solution to yield the arylhydroximinoyl chloride (**8**); (ii) addition of the dipolarophile; and (iii) dehydrohalogenation reaction by addition of pyridine as the basic agent for *in situ* generation of the nitrile oxide (**9**) (see [22] for a review, [23] for the isolation of hydroximinoyl chloride in NCS/dimethylformamide (DMF), [24] for hypochlorite oxidation, [25] for oxidation using hypervalent iodine reagents and [26] for oxidising system using bromide/organotin halide).

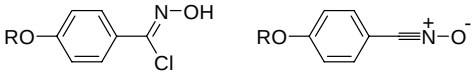

Chart 1 describes the chemical structures of the two acetylene derivatives which are necessary to elongate the isoxazolines **3a-b** and **7f-g** along both phenyl groups. The compounds **11a-d** and **13a-d** were synthesized in three steps by following the previously described method [27,28] from of *p*-bromophenol (**10**) or 6-bromo-2-naphthol (**12**) in three steps - alkylation reaction (85-95%), Sonogashira coupling [29-33] and deprotection reaction (71-81%) [34].

The synthesis of the final isoxazolines **14a-c** were reached by a second Sonogashira cross-coupling reaction between the precursor **7f** and three selected alkynes **11a**, **11b** and **11d** following the protocol of Wong *et al.* [33] according to Scheme 3. Compounds **14a-c** were obtained in moderate yields (65-70%). Following the procedure described above, isoxazolines **7f** and **7g** were selected and extended by connecting 6-octyloxy-2-ethynylnaphthalene (**13b**) in the Sonogashira step (Scheme 4).

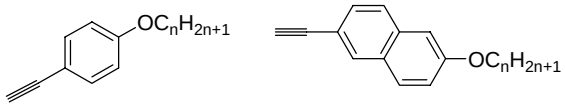

11a *n* = 7; **b** *n* = 8
c *n* = 9; **d** *n* = 10

13a *n* = 7; **b** *n* = 8
c *n* = 9; **d** *n* = 10

Chart 1. Terminal acetylenes **11a-d** and **13a-d**.

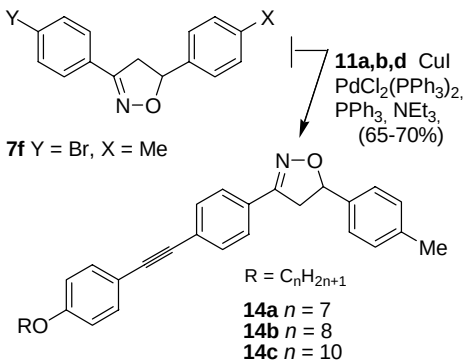

Scheme 3. Synthesis of selected isoxazolines **14a-c**.

As expected for **7g**, the regioselectivity observed in the alkynylation step is in accordance with previous reports as a result of the higher reactivity of the brominated position in relation to the chlorinated position [35-37]. The increase of the length-to-width ratio of the isoxazoline **15** and **16** and **17** favors the formation of stable liquid-crystalline phases [38].

The synthesis of isoxazoline **17** was accomplished as outlined in Scheme 5. The triple bond inserted between the isoxazoline scaffold and the naphthyl group was added by changing the chemical event sequence. Thus, we perform the second Sonogashira reaction directly after the [3+2] 1,3-dipolar cycloaddition. Firstly, the alkyne **13b** was coupled with aldehyde **5c** under Sonogashira condition and then reacting the product with hydroxylamine to yield the corresponding oxime. Finally, ring closure by 1,3-dipolar cycloaddition in the presence of pyridine and NCS yielded the cycloadduct **17**.

The construction of the triple bond at the right side of the isoxazoline allows us to prepare an elongated molecular framework with potential liquid crystal properties. Scheme 6 outlines the molecular construction of the target materials. The final isoxazolines **18a-c** containing two flexible chains at the 4-positions in both phenyl rings were prepared by a cross-coupling reaction of **3a-b** with **11b,d**. The conditions described by Wong *et al*. [33] (lower percentage of palladium(II) catalyst – 0.4 mol%) did not work very well when applied to the Pd-Cu

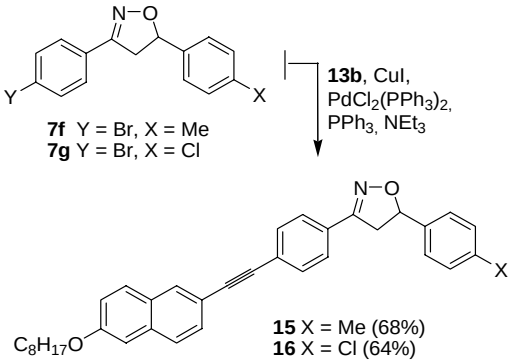

Scheme 4. Synthesis of the isoxazolines **15** and **16**.

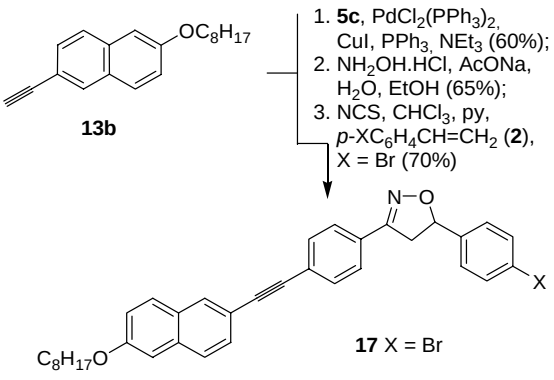

Scheme 5. Synthesis of the cycloadduct **17**.

cross-coupling reaction using isoxazolines **3a-b**. Under this condition, the starting material **3a-b** was recovered and no decomposition was detected. However, we have synthesized final targets **18a-c** in good yield following the procedure described by Price *et al.* [39-40]. In this case, the key to reaching the compounds is to use the '5,10,20 method'(5 mol% Pd:10 mol% Cu(I):20 mol% PPh_3) as described by the Tour report [34,40].

Thermal analysis of the 3,5-diarylisoxazolines

The thermal properties of new isoxazolines prepared in this work were analyzed by polarized-light optical microscopy (POM) and differential scanning calorimetry (DSC). The initial 3,5-disubstituted isoxazolines **3a-d, 4b** and **7a-g** are crystalline solids. As expected they are non-mesogenic compounds. The relevant compounds to be considered for LC analysis are **14a-c**, **15**, **16**, **17** and **18a-c**. The observed transition temperatures and enthalpies are tabulated in Table 1. The compounds **14b-c** and **18a-c** exhibit two peaks attributed to solid-to-solid phase transitions. For example, the DSC measurement of **14b** exhibited two endothermic peaks at 100 ^oC and 156 ^oC at a heating rate of 10 ^oC min^{-1}. Compound **14a** did not exhibit this $Cr \rightarrow Cr_1$ transition. It seems that the peak at 100 ^oC with small ΔH is due to the first crystal phase (Cr) to the second crystal phase (Cr_1) transition, and the other peak at 156 ^oC with a larger ΔH is attributed to the Cr_1 to isotropic phase transition. When the samples were placed between a clean untreated glass slide and a cover slip, and cooled at a rate of 10 ^oC min^{-1}, the POM studies revealed an absence of the mesophase for compounds **14a-c** and **18a-c**. However, the visualization of the texture is possible when the samples are heating 10 °C above clearing temperature followed by instantaneous cooling at room temperature. Thus, from the isotropic melt to any temperature below the isotropic temperature (*T*i), **14a-c** and **18a-c** developed schlieren and homeotropic textures, respectively. The texture, inside the region under observation, flashed very fast at the border and crystallizes quickly.

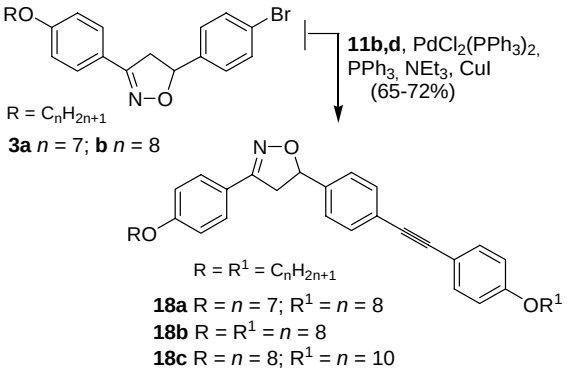

Scheme 6. Molecular construction of the isoxazolines **18a-c**.

Table 1. Transition temperatures (ºC) for the 3,5-diarylisoxazolines (2nd heating and cooling, 10 ºCmin^{-1}) and enthalpy (kcal.mol^{-1}).

Entry	Behaviour	Enthalpy (heating)
14a	Crystal $\underset{134}{\overset{155}{\rightleftharpoons}}$ N b Isotropic	Cr 6.9 N (-[b]) I
14b	Crystal $\underset{85}{\overset{100}{\rightleftharpoons}}$ Crystal 1 $\underset{136}{\overset{156}{\rightleftharpoons}}$ N b Isotropic	Cr 0.3 Cr_1 9.2 N (-[b]) I
14c	Crystal $\underset{82}{\overset{96}{\rightleftharpoons}}$ Crystal 1 $\underset{133}{\overset{154}{\rightleftharpoons}}$ N b Isotropic	Cr 0.4 Cr_1 8.8 N (-[b]) I
15	Crystal $\underset{137}{\overset{168}{\rightleftharpoons}}$ Nematic $\underset{191^a}{\overset{194}{\rightleftharpoons}}$ Isotropic	Cr 4.2 N 0.1 I
16	Crystal $\underset{150}{\overset{176}{\rightleftharpoons}}$ Smectic A $\underset{204}{\overset{212}{\rightleftharpoons}}$ Isotropic	Cr 6.8 SmA 0.9 I
17	Crystal $\underset{137}{\overset{170}{\rightleftharpoons}}$ Smectic A $\underset{183}{\overset{209}{\rightleftharpoons}}$ Isotropic	Cr 5.9 SmA 1.0 I
18a	Crystal $\underset{45}{\overset{57}{\rightleftharpoons}}$ Crystal 1 $\underset{113}{\overset{138}{\rightleftharpoons}}$ N b Isotropic	Cr 3.2 Cr_1 8.3 N (-[b]) I
18b	Crystal $\underset{42}{\overset{58}{\rightleftharpoons}}$ Crystal 1 $\underset{117}{\overset{140}{\rightleftharpoons}}$ N b Isotropic	Cr 4.0 Cr_1 11. N (-[b]) I
18c	Crystal $\underset{44}{\overset{57}{\rightleftharpoons}}$ Crystal 1 $\underset{110}{\overset{136}{\rightleftharpoons}}$ N b Isotropic	Cr 2.1 Cr_1 6.8 N (-[b]) I

[a] POM data. [b] The transition temperature and the enthalpy value were not measured because of the unstable monotropic nematic phase, see discussion in text. N = nematic phase.

As an example, nematic flashing micrograph (40x) displayed by compound **18b** on fast cooling (DSC trace inset) is shown in Figure 2. When the analysis was done without a cover slip the samples developed the droplet texture and crystallized a few seconds later.

The mesophase range in Table 1 was very short for all the compounds **14a-c** and **18a-c**. These values were not estimated due to their extremely short transition time (only enough to take a picture). This mesophase was assigned as a nematic phase [41,42]. Enantiotropic liquid-crystalline behavior was found for compounds **15**, **16** and **17**. The LC **15** showed a nematic phase while both **16** and **17** exhibited smectic A (SmA) phases. For instance, the DSC trace of **17** shows two endothermic peaks at 170 ^{o}C and 209 ^{o}C at a heating rate of 10 ^{o}Cmin^{-1}. The two peaks were associated with Cr $\rightarrow$ SmA and SmA $\rightarrow$ I transitions, respectively, during the microscopy studies. On slow cooling of the sample from the isotropic liquid it enters into the smectic phase with the formation of focal conic fans which is the typical of a smectic phase A. The thermal range of the mesophase, on heating, increases in the sequence **17** > **16** > **15** (ΔT = 39 ^{o}C for **17;** ΔT = 36 ^{o}C for **16**, ΔT = 26 ^{o}C for **15**). This behavior is a consequence of the efficiency of the terminal group in stabilising the LC phase. Thus, the order Br > Cl > CH_3 found in this work is in agreement with what is typically observed in low molecular mass LCs [17-20, 43, 44].

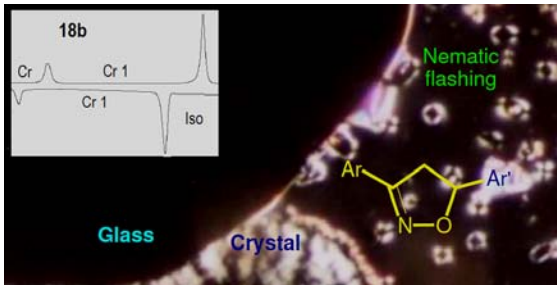

Figure 2. Nematic flashing micrograph (40x) displayed for compound **18b** on instantaneous cooling at room temperature (DSC trace inset).

The mesomorphic behavior of **14a-c**, **15**, **16**, **17** and **18a-c** can be understood in terms of the non-linearity of the isoxazoline ring coupled with the non-coplanarity of the two aryl groups located at C_3 and C_5 on the heterocyclic ring. To minimise this unfavorable disposition of the groups the final central core must be as long as possible and possess high polarisability. In this way, the potential LC materials are reached through a molecular elongation strategy from the isoxazoline intermediates. This elongation builds off the rigid isoxazoline core to form a more polarizable and mesogenic one.

Specifically, mesomorphic behavior found in this work is due to the presence of the extended aromatic group adjacent to the isoxazoline ring. However, in some cases the molecular dimensions (length-to-breadth ratio) of the aromatic group are not sufficient to overcome the non-coplanarity of the aryl group connected on the isoxazoline ring. In this situation no mesophase or an unstable mesophase, i.e. monotropic behavior, appears. By changing the phenyl group to a more polarizable naphthyl group at the C_3 carbon atom of the isoxazolinic system, a stable liquid-crystalline state becomes apparent. The appearance of a stable mesophase in **15**, **16** and **17** is due to the increased length-to-breadth ratio of the group bonded on the isoxazoline ring. The length-to-breadth ratio of the arylnaphthylacetylene is bigger than the arylphenylacetylene group in **14a-c** or **18a-c**.

Conclusions

We have synthesised a set of 3,5-disubstituted isoxazoline derivatives by [3+2] 1,3-dipolar cycloaddition. These intermediates can be used in the preparation of liquid-crystalline materials. We selected some appropriated isoxazolines containing halogen group at the *para* position of the aryl group to connect the triple bond through a Pd/Cu-catalyzed coupling reaction. Under these conditions, series of LCs have been successfully synthesised in fair to good yields. The final LC compounds **14a-c** and **18a-c**, containing the phenylacetylene group at the C_3 or C_5 atom on the isoxazoline ring, exhibited a monotropic nematic phase. By changing from a phenyl to a naphthylacetylene group at the C_3 atom on the isoxazolinic system the LC behaviour of the **15**, **16**, **17** changed to an enantiotropic phase. Compound **15** presented a nematic phase, whereas **16** and **17** exhibited SmA phases.

Experimental section

General

Nuclear magnetic resonance spectra were obtained on a Varian 200 and Varian Inova VNMRs 300 MHz instruments. Chemical shift values are given in parts per million (δ) and are referenced from tetramethylsilane (TMS). Infrared spectra were recorded on a Perkin-Elmer Spectrum One FTIR Spectrometer Instrument using NaCl plates in the case of solids and as thin film supported between KBr plates in case of liquids and are reporter as wavenumber (cm^{-1}). GC-MS low-resolution mass spectra were obtained using a Varian Saturn 2100T CG-MS equipped with a 100 meter CP Sil Pona CB (0.25 mm) column. The initial column temperature was 50 ^{o}C and was gradually ramped to 230 ^{o}C (15 ^{o}C min^{-1}). CHN analyses were performed on a Perkin-Elmer 2400 CHN Elemental Analyzer. DSC analyses were performed on a DSC 2910 TA. The melting points and textures of the samples were evaluated on a Mettler Toledo FP82HT Hot Stage with an FP90 central processor in conjunction with an Olympus BX43 polarizing microscope. 4-Hydroxybenzaldehyde, 1-bromoalkanes, hydroxylamine ydrochloride, 4-bromostyrene, 4-chlorostyrene, 4-

methylstyrene, chloroform, ethanol, *N*-chlorosuccinimide (NCS), potassium hydroxide, 4-bromobenzaldehyde, sodium acetate, acetonitrile and toluene were used without further purification from Aldrich Co. Pyridine was distilled under a reduce pressure. All other commercial solvents and reagents were used without further purification. All reactions involving Sonogashira couplings were performed in a one-neck round-bottom flask equipped with septum stoppers and charged with triethylamine (Et_3N), aromatic iodide and alkyne under an argon atmosphere for 30 min. Copper(I) iodide (CuI), triphenylphosphine (PPh_3) and *bis*-(triphenylphosphine)palladium(II) chloride [$PdCl_2(PPh_3)_2$] were then added.

Synthesis

4-*n*-Alkyloxybenzadehyde and the corresponding oximes were prepared from 4-hydroxybenzaldehyde (**1**) according to [17-20, 45, 46]. The general procedure for the preparation of 5-(4-bromophenyl)-3-[(4-*n*-alkyloxy)phenyl]-4,5-dihydroisoxazole **(3a-d)** is as follows.

General procedure. To a solution of the *p*-X-bromostyrene (**2**) (2 mmol), chloroform (4 mL), *N*-bromosuccinimide (2 mmol) and pyridine (3 mmol) at 0 ºC and under argon atmosphere was added dropwise the solution of oxime (1,7 mmol) in chloroform. The solution was heated to room temperature for 4 hours. The mixture was washed with HCl 1 M (3x20 mL), $NaHCO_3$ 10% (15 mL), water (15 mL) and brine (15 mL) and then dried with Na_2SO_4. After solvent evaporation the product was recrystallized from ethanol.

Data for *n*-heptyl **3a.** Yield 0.61g, 73%; white solid; mp 119-120 ºC. ^{1}H NMR ($CDCl_3$, 200 MHz): δ 0.9 (t, 3H, CH_3, J = 6.4 Hz), 1.3 (m, 8H, $(CH_2)_4$), 1.8 (quint, 2H, C$\underline{H}_2$CH_2O, J = 6.6 Hz), 3.2 (dd, 1H, C$\underline{H}$HCH, $^2J_{gem}$ = 16,6 Hz, $^3J_{trans}$ = 8.0 Hz), 3.7 (dd,1H, CH$\underline{H}$CH, $^2J_{gem}$ = 16.6 Hz, $^3J_{cis}$ = 10.8 Hz), 4.0 (t, 2H, CH_2O, J = 6.6 Hz), 5.6 (dd, 1H, CHHC$\underline{H}$, $^3J_{cis}$ = 10.8 Hz, $^3J_{trans}$ = 8 Hz), 6.9 (d, 2H, Ar, J = 8.8 Hz), 7.2 (d, 2H, Ar, J = 8.2 Hz), 7.5 (d, 2H, Ar, J = 8.4 Hz), 7.6 (d, 2H, Ar, J = 9.0 Hz). ^{13}C NMR ($CDCl_3$, 50 MHz): δ 14.0, 22.6, 25.9, 29.0, 29.1, 31.7, 43.4, 68.1, 81.4, 114.6, 121.4, 121.9, 127.5, 128.2, 131.7, 140.1, 155.6, 160.7. IR ν_{max}/cm^{-1}: 2923, 1610, 1598 (C=N), 1249, 1013, 813 (nujol).

Data for *n*-octyl **3b**. Yield 0.94g, 55%; white solid; mp 116-117 ºC. ^{1}H NMR ($CDCl_3$, 200 MHz): δ 0.9 (t, 3H, CH_3, J = 6.4 Hz), 1.3 (m, 10H, $(CH_2)_5$), 1.8 (quint, 2H, C$\underline{H}_2$CH_2O, J = 6.5 Hz), 3.2 (dd, 1H, C$\underline{H}$HCH, $^2J_{gem}$ = 16.6 Hz, $^3J_{trans}$ = 8.0 Hz), 3.7 (dd, 1H, CH$\underline{H}$CH, $^2J_{gem}$ = 16.4 Hz, $^3J_{cis}$ = 10.8 Hz), 4.0 (t, 2H, CH_2O, J = 6.6 Hz), 5.6 (dd, 1H, CHHC$\underline{H}$, $^3J_{cis}$ = 10.8 Hz, $^3J_{trans}$ = 8.0), 6.9 (d, 2H, Ar, J = 8.6 Hz), 7.2 (d, 2H, Ar, J = 8.4 Hz), 7.5 (d, 2H, Ar, J = 8.4 Hz); 7.6 (d, 2H, Ar, J = 8.6 Hz). ^{13}C NMR ($CDCl_3$, 50 MHz): δ 14.1, 22.6, 25.9, 29.1, 29.2, 29.3, 31.8, 43.4, 68.1, 81.4, 114.6, 121.4, 121.9, 127.5, 128.2, 131.8, 140.2, 155.6, 160.7. IR ν_{max}/cm^{-1}: 2922, 1615, 1590, 1250, 1024), 821, (nujol).

Data for *n*-nonyl **3c**. Yield 0.62g, 70%; white solid; mp 114-115 ºC. ^{1}H NMR ($CDCl_3$, 200 MHz): δ 0.8 (t, 3H, CH_3, J = 6.2 Hz), 1.2 (m, 12H, $(CH_2)_6$), 1.7 (m, 2H, C$\underline{H}_2$CH_2O), 3.2 (dd, 1H, C$\underline{H}$HCH, $^2J_{gem}$ = 16.6 Hz, $^3J_{trans}$ = 7.8 Hz), 3.6 (dd, 1H, CH$\underline{H}$CH, $^2J_{gem}$ = 16.4 Hz, $^3J_{cis}$ = 10.7 Hz), 4.0 (t, 2H, CH_2O, J = 6.6 Hz), 5.5 (dd, 1H, CHHC$\underline{H}$, $^3J_{cis}$ = 10.8 Hz, $^3J_{trans}$ = 8.0 Hz), 6.8 (d, 2H, Ar, J = 8.8 Hz), 7.2 (d, 2H, Ar, J = 8.6 Hz), 7.4 (d, 2H, Ar, J = 8.6 Hz), 7.5 (d, 2H, Ar, J = 8.8 Hz). ^{13}C NMR ($CDCl_3$, 50 MHz): δ 14.1, 22.6, 25.9, 29.1, 29.2, 29.4, 29.5, 31.8, 43.4, 68.1, 81.4, 114.6, 121.4, 121.9, 127.5, 128.2, 131.8, 140.2, 155.6, 160.7. IR ν_{max}/cm^{-1}: 2926, 1610, 1595, 1248, 1025, 825 (nujol).

Data for *n*-decyl **3d**. Yield 0.91g, 66%; white solid; mp 111-112 ºC. ^{1}H NMR ($CDCl_3$, 200 MHz): δ 0.8 (m, 3H, CH_3), 1.9 (m, 14H, $(CH_2)_7$), 1.7 (m, 2H, C$\underline{H}_2$CH_2O), 3.2 (m, 1H, C$\underline{H}$HCH), 3.8 (m, 1H, CH$\underline{H}$CH), 4.0 (t, 2H, CH_2O, J = 6.6 Hz), 5.5 (m, 1H, CHHC$\underline{H}$), 6.8 (d, 2H, Ar, J = 8.4 Hz), 7.2 (d, 2H, Ar, J = 8.0 Hz), 7.4 (d, 2H, Ar, J = 8.4 Hz), 7.5 (d, 2H, Ar, J = 8.2 Hz). ^{13}C NMR ($CDCl_3$, 50 MHz): δ 14.1, 22.6, 25.1, 29.1, 29.3, 29.4, 29.5, 31.8, 43.4, 68.1, 81.4, 114.6, 121.4, 121.9, 127.5, 128.2, 131.7, 140.1, 155.6, 160.7 (one signal of aliphatic C are missing due to overlap). IR ν_{max}/cm^{-1}: 2925, 1608, 1590, 1248, 1030, 829 (nujol).

Data for 3-(4-*n*-octyloxyphenyl)-5-*p*-tolyl-4,5-dihydroisoxazole (**4b**). Yield 0.44g, 60%; yellow pale solid; mp 94-95 ºC. ^{1}H NMR ($CDCl_3$, 200 MHz): δ 0.8 (m, 3H, CH_3), 1.3 (m, 10H, $(CH_2)_5$), 1.8 (quint, 2H, C$\underline{H}_2$CH_2O, J = 6.5 Hz), 2.3 (s, 3H, CH_3), 3.3 (dd, 1H, C$\underline{H}$HCH, $^2J_{gem}$ = 16.6 Hz, $^3J_{trans}$ = 7.8 Hz), 3.7 (dd, 1H, CH$\underline{H}$CH, $^2J_{gem}$ = 16.4 Hz, $^3J_{cis}$ = 10.7 Hz), 4.0 (t, 2H, CH_2O, J = 6.4 Hz), 5.6 (dd, 1H, CHHC$\underline{H}$, $^3J_{cis}$ = 10.8 Hz, $^3J_{trans}$ = 8.0 Hz), 6.9 (d, 2H, Ar, J = 8.8 Hz), 7.2 (d, 2H, Ar, J = 8.4 Hz), 7.3 (d, 2H, Ar, J = 8.6 Hz), 7.6 (d, 2H, Ar, J = 8.8 Hz). ^{13}C NMR ($CDCl_3$, 50 MHz): δ 14.1, 21.1, 22.6, 25.9, 29.1, 29.2, 29.3, 31.8, 43.3, 68.0, 82.2, 114.5, 121.6, 125.8, 128.1, 129.3, 137.8, 137.9, 155.7, 160.6. IR ν_{max}/cm^{-1}: 2922, 1607, 1598, 1249, 907, 829 (nujol).

Data for 4-cyanobenzaldehyde oxime (**6a**). Yield 0.730g, 50%; white solid; mp 174-175 ºC. (thermal degradation after isotropic temperature - lit. [47] mp 174-176 ºC).^{1}H NMR ($CDCl_3$, 200 MHz): δ 7.6 (d, 2H, Ar, J = 8.4 Hz), 7.7 (d, 2H, Ar, J = 8.6 Hz), 8.1 (s, 1H, HC=NOH), 11 (s, 1H, OH).

Data for 4-nitrobenzaldehyde oxime (**6b**). Yield 1.12g, 45%; yellow pale solid; mp 128-129 ºC (lit. [48] mp 132-

133 °C. ^{1}H NMR ($CDCl_3$, 200 Hz): δ 7.7 (d, 2H, Ar, *J* = 8.8 Hz), 8.2 (d, 2H, Ar, *J* = 8.8 Hz), 8.4 (s, 1H, HC=NOH), 9.0 (s, 1H, OH). ^{13}C NMR ($CDCl_3$, 50 MHz): δ 123.85, 127.29, 138.96, 146.8, 147.26. IR ν_{max}/cm^{-1}: 3289, 2930, 1640, 1599, 1534, 1456, 1347, 960, 841 (nujol).

Data for 4-bromobenzaldehyde oxime (**6c**). Yield 0.52g, 65%; white solid; mp 112-113 ºC (lit.[49] mp 110-112 °C). ^{1}H NMR ($CDCl_3$, 200 Hz): δ 7.5 (s, 4H, Ar), 8.0 (s, 1H, HC=NOH), 10.9 (s, 1H, OH). ^{13}C NMR ($CDCl_3$, 50 MHz): δ 123.2, 128.0, 131.6, 132.3, 148.0. IR ν_{max}/cm^{-1}: 3290, 1635, 1599, 1534, 1347, 1013, 841 (nujol).

Data for 5-(4-chlorophenyl)-3-(4-nitrophenyl)-4,5-dihydroisoxazole (**7a**). Yield 0.62g, 51%; mp 141-142 ºC. ^{1}H NMR ($CDCl_3$, 300 MHz): δ 3.3 (dd, 1H, C<u>H</u>HCH, $^2J_{gem}$ = 16.8 Hz, $^3J_{trans}$ = 8.4 Hz); 3.8 (dd, 1H, CH<u>H</u>CH, ^2J = 16.8 Hz, $^3J_{cis}$ = 11.4 Hz); 5.7 (dd, 1H, CHHC<u>H</u>, $^3J_{cis}$ = 11.2 Hz, $^3J_{trans}$ = 8.2 Hz); 7.3 (d, 2H, Ar, *J* = 8.7 Hz); 7.4 (d, 2H, Ar, *J* = 8.7 Hz); 7.8 (d, 2H, Ar, *J* = 8.7 Hz); 8.2 (d, 2H, Ar, *J* = 9.3 Hz). ^{13}C NMR ($CDCl_3$, 75 MHz): δ 42.5, 82.8, 124.0, 127.2, 127.4, 129.0, 134.4, 135.3, 138.6, 148.5, 154.6. IR ν_{max}/cm^{-1}: 2924, 1592, 1422, 1345, 1266, 1090, 1040, 869, 739 (nujol).

Data for 5-(4-bromophenyl)-3-(4-nitrophenyl)-4-5-dihydroisoxazole (**7b**). Yield 0.70g, 50%; mp 150-151 ºC. ^{1}H NMR ($CDCl_3$, 200 Hz): δ 3.2 (dd, 1H, C<u>H</u>HCH, $^2J_{gem}$ = 16.8 Hz, $^3J_{trans}$ = 8.4 Hz), 3.8 (dd, 1H, CH<u>H</u>CH, $^2J_{gem}$ = 16.8 Hz, $^3J_{cis}$ = 11.2 Hz), 5.7 (dd, 1H, CHHC<u>H</u>, $^3J_{cis}$ = 11.2 Hz, $^3J_{trans}$ = 8.6 Hz), 7.4 (d, 2H, Ar, *J* = 8.6 Hz), 7.6 (d, 2H, Ar, *J* = 9.2 Hz), 8.0 (d, 2H, Ar, *J* = 9.2 Hz), 8.2 (d, 2H, Ar, *J* = 8.2 Hz). ^{13}C NMR ($CDCl_3$, 50 MHz): 42.5, 82.8, 122.5, 124.0, 127.4, 127.5, 132.0, 135.2, 139.2, 148.5, 154.6. IR ν_{max}/cm^{-1}: 2922, 1592, 1422, 1345, 1266, 1072, 1011, 869, 739 (nujol).

Data for 3-(4-nitrophenyl)-5-*p*-tolyl-4,5-dihydroisoxazole (**7c**). Yield 0.69g, 61%; mp 122-123 ºC. ^{1}H NMR ($CDCl_3$, 300 MHz): δ 2.4 (s, 3H, $PhCH_3$), 3.3 (dd, 1H, C<u>H</u>HCH, $^2J_{gem}$ = 16.8 Hz, $^3J_{trans}$ = 8.4 Hz), 3.8 (dd, 1H, CH<u>H</u>CH, $^2J_{gem}$ = 16.6 Hz, $^3J_{cis}$ = 11.2 Hz), 5.8 (dd, 1H, CHHC<u>H</u>, $^3J_{cis}$ = 11.1 Hz, $^3J_{trans}$ = 8.7 Hz), 7.2 (d, 2H, Ar, *J* = 7.8 Hz), 7.3 (d, 2H, Ar, *J* = 8.1 Hz), 7.8 (d, 2H, Ar, *J* = 9.0 Hz), 8.3 (d, 2H, Ar, *J* = 8.7 Hz). ^{13}C NMR ($CDCl_3$, 75 MHz): δ 21.1, 42.3, 83.6, 124.0, 125.8, 127.4, 129.5, 135.6, 137.0, 138.4, 148.4, 154.6. IR ν_{max}/cm^{-1}: 1523, 1422, 1346, 1266, 896, 739 (neat).

Data for 4-[5-(4-bromophenyl)-4,5-dihydroisoxazol-3-yl]benzonitrile (**7d**). Yield 0.78g, 60%; mp 115-116 ºC. ^{1}H NMR ($CDCl_3$, 200 MHz): δ 3.4 (dd, 1H, C<u>H</u>HCH, $^2J_{gem}$ = 16.8 Hz, $^3J_{trans}$ = 8.4 Hz), 3.9 (dd, 1H, CH<u>H</u>CH, $^2J_{gem}$ = 16.8 H, $^3J_{cis}$ = 11.2 Hz), 5.8 (dd, 1H, CHHC<u>H</u>, $^3J_{cis}$ = 11.2 Hz, $^3J_{trans}$ = 8.6 Hz), 7.3 (d, 2H, Ar, *J* = 8.6 Hz), 7.5 (d, 2H, Ar, *J* = 9.2 Hz), 7.9 (d, 2H, Ar, *J* = 9.2 Hz), 8.3 (d, 2H, Ar, *J* = 8.2 Hz). IR ν_{max}/cm^{-1}: 1607, 1516, 1257, 1175, 1039, 1014, 876 (neat).

Data for 3,5-*bis*-(4-bromophenyl)-4,5-dihydroisoxazole (**7e**). Yield 0.86g, 55%; mp 132-133 ºC. **^{1}**H NMR ($CDCl_3$, 200 MHz): δ 3.1 (dd, 1H, C<u>H</u>HCH, $^2J_{gem}$ = 16.6 Hz, $^3J_{trans}$ = 8.3 Hz), 3.7 (dd, 1H, CH<u>H</u>CH, $^2J_{gem}$ = 16.8 Hz, $^3J_{cis}$ = 11 Hz), 5.6 (dd, 1H, CHHC<u>H</u>, $^3J_{cis}$ = 11.0 Hz, $^3J_{trans}$ = 8.3 Hz), 7.2 (d, 2H, Ar, *J* = 8.6 Hz), 7.4 (d, 2H, Ar, *J* = 8.6 Hz), 7.8 (d, 2H, Ar, *J* = 8.4 Hz), 8.3 (d, 2H, Ar, *J* = 8.6 Hz). ^{13}C NMR ($CDCl_3$, 50 MHz): 42.8, 82.0, 122.2, 124.5, 127.5, 128.0, 128.1, 131.9, 132.0, 139.6, 155.2. IR ν_{max}/cm^{-1}: 2923, 1460, 1376, 1070, 1005, 900, 874, 827, 721, 664 (nujol).

Data for 3-(4-bromophenyl)-5-*p*-tolyl-4,5-dihydroisoxazole (**7f**). Yield 0.67g, 53%; mp 142-143 °C. ^{1}H NMR ($CDCl_3$, 300 MHz): δ 2.3 (s, 3H, CH_3), 3.3 (dd, 1H, C<u>H</u>HCH, $^2J_{gem}$ = 16.5 Hz, $^3J_{trans}$ = 8.7 Hz), 3.7 (dd, 1H, CH<u>H</u>CH, $^2J_{gem}$ = 16.5 Hz, $^3J_{cis}$ = 10.8 Hz), 5.7 (dd, 1H, CHHC<u>H</u>, $^3J_{cis}$ = 10.8 Hz, $^3J_{trans}$ = 8.7 Hz), 7.2 (d, 2H, Ar, *J* = 8.1 Hz), 7.3 (d, 2H, Ar, *J* = 8.1 Hz), 7.5 (s, 4H, Ar). ^{13}C NMR ($CDCl_3$, 75 MHz): δ 21.1, 42.7, 82.9, 124.3, 125.8, 128.1, 128.5, 129.4, 131.9, 137.5, 138.2, 155.3. IR ν_{max}/cm^{-1}: 2922, 1459, 1397, 1376, 1071, 1006, 909, 830, 813 (nujol).

Data for 3-(4-bromophenyl)-5-(4-chlorophenyl)-4,5-dihydroisoxazole (**7g**). Yield 0.82g, 61%; mp 120-121 ºC. ^{1}H NMR ($CDCl_3$, 300 MHz): δ 3.4 (dd, 1H, <u>CH</u>HCH, $^2J_{gem}$ = 16.6 Hz, $^3J_{trans}$ = 8.2 Hz), 3.8 (dd, 1H, CH<u>H</u>CH, $^2J_{gem}$ = 16.5 Hz, $^3J_{cis}$ = 11.2 Hz); 5.7 (dd, 1H, CHHC<u>H</u>, $^3J_{cis}$ = 11.2 Hz, $^3J_{trans}$ = 8.2 Hz), 7.3 (d, 2H, Ar, *J* = 8.6 Hz), 7.4 (d, 2H, Ar, *J* = 8.6 Hz), 7.8 (d, 2H, Ar, *J* = 8.7 Hz), 8.2 (d, 2H, Ar, *J* = 9.0 Hz). ^{13}C NMR ($CDCl_3$, 75 MHz): δ 43.4, 82.4, 123.0, 127.4, 128.0, 130.0, 131.4, 132.3, 134.6, 143.6, 157.6.

1-Ethynyl-4-alkyloxybenzene. Compounds **11a-d** and **13a-d** were synthesised according to [27, 28].

Data for *n*-heptyl **11a**. Yield 1.64g, 76%; colorless oil. ^{1}H NMR ($CDCl_3$, 300 MHz): δ 0.9 (t, 3H, *J* = 6.4 Hz, CH_3), 1.3 (m, 8H, CH_2), 1.8 (quint, 2H, *J* = 6.9 Hz, CH_2), 3.0 (s, 1H, CH), 3.9 (t, 2H, *J* = 6.6 Hz, OCH_2), 6.8 (d, 2H, *J* = 8.8 Hz, Ar), 7.4 (d, 2H, *J* = 8.8 Hz, Ar). ^{13}C NMR ($CDCl_3$, 75 MHz): δ 159.5, 133.5, 114.4, 113.8, 83.7, 75.6, 68.0, 31.9, 29.3, 26.0, 25.9, 22.6, 14.0.

Data for *n*-octyl **11b**. Yield 1.77g, 77%; colorless oil. ^{1}H NMR ($CDCl_3$, 300 MHz): δ 0.9 (t, 3H, *J* = 6.4 Hz, CH_3), 1.3 (m, 10H, CH_2), 1.8 (quint, 2H, *J* = 6.8 Hz, CH_2), 3.0 (s, 1H, CH), 3.9 (t, 2H, *J* = 6.6 Hz, OCH_2), 6.8 (d, 2H, *J* = 8.8 Hz, Ar), 7.4 (d, 2H, *J* = 8.8 Hz, Ar). ^{13}C NMR ($CDCl_3$, 75 MHz): δ 159.5, 133.5, 114.4, 113.8, 83.7, 75.6, 68.0, 31.9, 29.5, 29.2, 26.0, 25.9, 22.6, 14.0.

Data for *n*-nonyl **11c**. Yield 1.73g, 71%; colorless oil. ^{1}H NMR ($CDCl_3$, 300 MHz): δ 0.9 (t, 3H, *J* = 6.4 Hz, CH_3), 1.3 (m, 12H, CH_2), 1.8 (quint, 2H, *J* = 6.8 Hz, CH_2), 3.0 (s, 1H, CH), 3.9 (t, 2H, *J* = 6.5 Hz, OCH_2), 6.8 (d, 2H, *J* = 8.8 Hz, Ar), 7.4 (d, 2H, *J* = 8.8 Hz, Ar). ^{13}C NMR ($CDCl_3$, 75 MHz): δ 159.5, 133.5, 114.4, 113.8, 83.7, 75.6, 68.0, 31.9, 29.5, 29.3, 29.1, 26.0, 25.9, 22.6, 14.0.

Data for *n*-decyl **11d**. Yield 2.10g, 80%; colorless oil. ^{1}H NMR ($CDCl_3$, 300 MHz): δ 0.9 (t, 3H, *J* = 6.4 Hz, CH_3), 1.3 (m, 14H, CH_2), 1.8 (quint, 2H, *J* = 6.9 Hz CH_2), 3.0 (s, 1H, CH), 3.9 (t, 2H, *J* = 6.6 Hz, OCH_2), 6.8 (d, 2H, *J* = 8.8 Hz, Ar), 7.4 (d, 2H, *J* = 8.8 Hz, Ar). ^{13}C NMR ($CDCl_3$, 75 MHz): δ 159.5, 133.5, 114.4, 113.8, 83.7, 75.6, 68.0, 31.9, 29.5, 29.3, 29.2, 29.1, 26.0, 25.9, 22.6, 14.0.

2-Alkyloxy-6-ethynylnaphthalene. Data for *n*-heptyl **13a**. Yield 2.02g, 76%; white solid. ^{1}H NMR ($CDCl_3$, 200 MHz): δ 0.9 (t, 3H, *J* = 8.4 Hz, CH_3), 1.3 (m, 8H, CH_2), 1.7-1.8 (m, 2H, CH_2), 3.1 (s, 1H, CH), 4.1 (t, 2H, *J* = 6.6 Hz, OCH_2), 7.1 (d, 1H, *J* = 2.2 Hz, Ar), 7.2 (dd, 1H, *J* = 6.4 Hz, 2.6 Hz, Ar), 7.4 (dd, 1H, *J* = 6.8 Hz, 2.0 Hz, Ar), 7.6 (d, 1H, *J* = 9.4 Hz, Ar), 7.7 (s, 1H, Ar); 7.8 (d, 1H, *J* = 1.4 Hz, Ar). ^{13}C NMR ($CDCl_3$, 50 MHz): δ 158.3, 134.8, 132.4, 129.6, 129.4, 128.5, 127.1, 120.2, 117.1, 106.8, 84.6, 78.0, 76.8, 68.5, 32.3, 29.8, 26.5, 23.1, 14.6. IR ν_{max}/cm^{-1}: 3315, 2924, 2853, 2108, 1601, 1463, 1390, 1225, 1172, 874, 646 (nujol).

Data for *n*-octyl **13b**. Yield 2.27g, 81%; white solid. ^{1}H NMR ($CDCl_3$, 200 MHz): δ 0.9 (t, 3H, *J* = 8.4 Hz, CH_3), 1.3 (m, 10H, CH_2), 1.7-1.8 (m, 2H, CH_2), 3.1 (s, 1H, CH), 4.1 (t, 2H, *J* = 6.6 Hz, OCH_2), 7.1 (d, 1H, *J* = 2.2 Hz, Ar), 7.2 (dd, 1H, *J* = 6.4 Hz, 2.6 Hz, Ar), 7.4 (dd, 1H, *J* = 6.8 Hz, 2.0 Hz, Ar), 7.6 (d, 1H, *J* = 9.4 Hz, Ar), 7.7 (s, 1H, Ar), 7.8 (d, 1H, *J* = 1.4 Hz, Ar). ^{13}C NMR ($CDCl_3$, 50 MHz): δ 158.3, 134.8, 132.4, 129.6, 129.4, 128.5, 127.1, 120.2, 117.1, 106.8, 84.6, 78.0, 76.8, 68.5, 32.3, 30.0, 29.7, 26.5, 23.1, 14.6. IR ν_{max}/cm^{-1}: 3315, 2924, 2853, 2108, 1601, 1463, 1390, 1225, 1172, 874, 646 (nujol).

Data for *n*-nonyl **13c**. Yield 2.12g, 72%; white solid. ^{1}H NMR ($CDCl_3$, 200 MHz): δ 0.9 (t, 3H, *J* = 8.4 Hz, CH_3), 1.3 (m, 12H, CH_2), 1.7-1.8 (m, 2H, CH_2), 3.1 (s, 1H, CH), 4.1 (t, 2H, *J* = 6.6 Hz, OCH_2), 7.1 (d, 1H, *J* = 2.2 Hz, Ar), 7.2 (dd, 1H, *J* = 6.4 Hz, 2.6 Hz, Ar), 7.4 (dd, 1H, *J* = 6.8 Hz, 2.0 Hz, Ar), 7.6 (d, 1H, *J* = 9.4 Hz, Ar), 7.7 (s, 1H, Ar), 7.8 (d, 1H, *J* = 1.4 Hz, Ar). ^{13}C NMR ($CDCl_3$, 50 MHz): δ 158.3, 134.8, 132.4, 129.6, 129.4, 128.5, 127.1, 120.2, 117.1, 106.8, 84.6, 78.0, 76.8, 68.5, 32.3, 30.0, 29.8, 29.6, 26.5, 23.1, 14.6. IR ν_{max}/cm^{-1}: 3315, 2924, 2853, 2108, 1601, 1463, 1390, 1225, 1172, 874, 646 (nujol).

Data for *n*-decyl **13d**. Yield 2.30g, 75%; white solid. ^{1}H NMR ($CDCl_3$, 200 MHz): δ 0.9 (t, 3H, *J* = 8.4 Hz, CH_3), 1.3 (m, 14H, CH_2), 1.7-1.8 (m, 2H, CH_2), 3.1 (s, 1H, CH), 4.1 (t, 2H, *J* = 6.6 Hz, OCH_2), 7.1 (d, 1H, *J* = 2.2 Hz, Ar), 7.2 (dd, 1H, *J* = 6.4 Hz, 2.6 Hz, Ar), 7.4 (dd, 1H, *J* = 6.8 Hz, 2.0 Hz, Ar), 7.6 (d, 1H, *J* = 9.4 Hz, Ar), 7.7 (s, 1H, Ar), 7.8 (d, 1H, *J* = 1.4 Hz, Ar). ^{13}C NMR ($CDCl_3$, 50 MHz): δ 158.3, 134.8, 132.4, 129.6, 129.4, 128.5, 127.1, 120.2, 117.1, 106.8, 84.6, 78.0, 76.8, 68.5, 32.3, 30.0, 29.8, 29.7, 29.6, 26.5, 23.1, 14.6. IR ν_{max}/cm^{-1}: 3315, 2924, 2853, 2108, 1601, 1463, 1390, 1225, 1172, 874, 646 (nujol).

Data for 3-{4-[(4'-heptyloxyphenyl)ethynyl]phenyl}-5-(*p*-tolyl)-4,5-dihydroisoxazole (**14a**). Yield 0.12g, 65%; white solid; mp 155 °C. ^{1}H NMR ($CDCl_3$, 200 MHz): δ 0.9-1.0 (m, 3H, CH_3), 1.4 (m, 8H, $(CH_2)_4$), 1.7-1.8 (m, 2H, $C\underline{H}_2CH_2O$), 2.3 (s, 3H, $PhCH_3$), 3.3 (dd, 1H, $C\underline{H}HCH$, $^2J_{gem}$ = 16.6 Hz, $^3J_{trans}$ = 8.4 Hz), 3.7 (dd, 1H, $CH\underline{H}CH$, $^2J_{gem}$ = 16.6 Hz, $^3J_{cis}$ = 11.0 Hz), 3.9 (t, 2H, CH_2O, *J* = 6.6 Hz), 5.7 (dd, 1H, $CHHC\underline{H}$, $^3J_{cis}$ = 10.8 Hz, $^3J_{trans}$ = 8.6 Hz), 6.8 (d, 2H, Ar, *J* = 8.8 Hz), 7.2 (d, 2H, Ar, *J* = 8.2 Hz), 7.3 (d, 2H, Ar, *J* = 8.2 Hz), 7.4 (d, 2H, Ar, *J* = 8.8 Hz), 7.5 (d, 2H, Ar, *J* = 8.2 Hz), 7.6 (d, 2H, Ar, *J* = 8.4 Hz). ^{13}C NMR ($CDCl_3$, 50 MHz): δ 14.1, 21.1, 22.6, 25.9, 29.0, 29.2, 31.7, 42.8, 68.0, 82.7, 87.6, 91.6, 114.5, 114.6, 125.3, 125.8, 126.5, 128.7, 129.4, 131.6, 133.6, 137.6, 138.0, 155.7, 159.4. EI-MS: *m/z* 452 [M+1], 225, 119 (100), 91. Anal. Calcd for $C_{31}H_{33}NO_2$: C, 82.45; H, 7.37; N, 3.10. Found: C, 82.55; H, 7.43; N, 3.30. IR ν_{max}/cm^{-1}: 2920, 2851, 1606, 1598, 1519, 1249, 907, 841, 813, 666 (neat).

Data for 3-{4-[(4'-octyloxyphenyl)ethynyl]phenyl}-5-(*p*-tolyl)-4,5-dihydroisoxazole (**14b**). Yield 0.12g, 67%; white solid; mp 156 °C. ^{1}H NMR ($CDCl_3$, 300 MHz): δ 0.9 (t, 3H, CH_3), 1.3 (m, 10H, $(CH_2)_5$), 1.8 (quint, 2H, $C\underline{H}_2CH_2O$, *J* = 6.8 Hz), 2.4 (s, 3H, $PhCH_3$), 3.3 (dd, 1H, $C\underline{H}HCH$, $^2J_{gem}$ = 16.5 Hz, $^3J_{trans}$ = 8.7 Hz), 3.7(dd, 1H, $CH\underline{H}CH$, $^2J_{gem}$ = 16.5 Hz, $^3J_{cis}$ = 11.1 Hz), 4.0 (t, 2H, CH_2O, *J* = 6.6 Hz), 5.7 (dd, 1H, $CHHC\underline{H}$, $^3J_{cis}$ = 10.8 Hz, $^3J_{trans}$ = 8.7 Hz), 6.9 (d, 2H, Ar, *J* = 8.7 Hz), 7.2 (d, 2H, Ar, *J* = 7.8 Hz), 7.3 (d, 2H, Ar, *J* = 7.8 Hz), 7.4 (d, 2H, Ar, *J* = 9.0 Hz), 7.5 (d, 2H, Ar, *J* = 8.7 Hz), 7.7 (d, 2H, Ar, *J* = 8.4 Hz). ^{13}C NMR ($CDCl_3$, 75 MHz): δ 14.1, 21.1, 22.6, 26.0, 29.0, 29.2, 29.3, 31.8, 42.8, 68.0, 82.8, 87.6, 91.6, 114.5, 114.6, 125.3, 125.9, 126.5, 128.7, 129.4, 131.6, 133.1, 137.6, 138.1, 155.7, 159.4. EI-MS: *m/z* 465 [M^+], 261, 225, 119 (100), 91. Anal. Calcd for $C_{32}H_{35}NO_2$: C, 82.54; H, 7.58; N, 3.01. Found: C, 82.68; H, 7.62; N, 3.23. IR ν_{max}/cm^{-1}: 2922, 2848, 1610, 1597, 1249, 907, 841, 813, 666 (neat).

Data for 3-{4-[(4'-decyloxyphenyl)ethynyl]phenyl}-5-(*p*-tolyl)-4,5-dihydroisoxazole (**14c**). Yield 0.14g, 70 %; white solid; mp 154 °C. ^{1}H NMR ($CDCl_3$, 200 MHz): δ 0.8-0.9 (m, 3H, CH_3), 1.8-2.0 (m, 16H, $(CH_2)_8$), 2.3 (s, 3H, $PhCH_3$), 3.3 (dd, 1H, $C\underline{H}HCH$, $^2J_{gem}$ = 16.6 Hz, $^3J_{trans}$ = 8.6 Hz), 3.7 (dd, 1H, $CH\underline{H}CH$, $^2J_{gem}$ = 16.6 Hz, $^3J_{cis}$ =

11.0 Hz), 3.9 (t, 2H, CH_2O, J = 6.4 Hz), 5.7 (dd, 1H, CHHC<u>H</u>, $^3J_{cis}$ = 11.0 Hz, $^3J_{trans}$ = 8.6 Hz), 6.9 (d, 2H, Ar, J = 8.8 Hz), 7.2 (d, 2H, Ar, J = 8.2 Hz), 7.3 (d, 2H, Ar, J = 8.0 Hz), 7.4 (d, 2H, Ar, J = 8.6 Hz), 7.5 (d, 2H, Ar, J = 8.2 Hz), 7.6 (d, 2H, Ar, J = 8.4 Hz). ^{13}C NMR ($CDCl_3$, 50 MHz): δ 14.1, 21.1, 22.6, 25.9, 29.1, 29.3, 29.4, 29.5, 30.1, 31.8, 42.8, 68.0, 82.7, 87.6, 91.6, 114.5, 114.6, 125.3, 125.8, 126.5, 128.7, 129.4, 131.0, 133.3, 137.6, 138.0, 155.7, 159.4 (one signal missing due to accidental equivalence). EI-MS: *m/z* 493 [M^+], 225, 119 (100), 91. Anal. Calcd for $C_{34}H_{39}NO_2$: C, 82.72; H, 7.96; N, 2.84. Found: C, 82.78; H, 7.97; N, 2.90. IR ν_{max}/cm^{-1}: 2925, 2848, 1604, 1599, 1249, 907, 841, 813, 666 (neat).

Data for 3-{4-[2-(6-octyloxy)naphthalene-2-yl]ethynylphenyl}-5-(*p*-tolyl)-4,5-dihydroisoxazole (**15**). Yield: 0.11g, 68%; brown solid; mp 168 ºC. ^{1}H NMR ($CDCl_3$, 300 Hz) δ 0.8 (t, 3H, CH_3, J = 7.2 Hz), 1.2-1.8 (m, 12H, $(CH_2)_6$), 2.4 (s, 3H, $PhCH_3$), 3.3 (dd, 1H, C<u>H</u>HCH, $^2J_{gem}$ = 16.2 Hz, $^3J_{trans}$ = 8.2 Hz), 3.7 (dd, 1H, CH<u>H</u>CH, $^2J_{gem}$ = 16.2 Hz, $^3J_{cis}$ = 11.0 Hz), 3.9 (t, 2H, CH_2O, J = 6.4 Hz), 5.7 (dd, 1H, CHHC<u>H</u>, $^3J_{cis}$ = 11.0 Hz, $^3J_{trans}$ = 8.2 Hz), 7.1-7.4 (m, 6H, Ar), 7.7-7.9 (m, 7H, Ar), 8.0 (s, 1H, Ar). ^{13}C NMR ($CDCl_3$, 75 MHz): δ 14.1, 21.2, 22.6, 26.0, 29.2, 29.3, 29.4, 31.8, 42.8, 68.0, 82.7, 88.6, 92.1, 106.4, 117.5, 119.7, 125.1, 125.8, 126.5, 126.8, 128.3, 128.7, 128.9, 129.3, 129.4, 131.4, 131.7, 134.3, 137.6, 138.0, 155.7, 157.9. EI-MS: *m/z* 516 [M + 1], 424, 402, 397, 386, 355, 129, 119 (100) and 91. Anal. Calcd for $C_{36}H_{37}NO_2$: C, 83.85; H, 7.23; N, 2.72. Found: C, 83.97; H, 7.42; N, 2.80. IR ν_{max}/cm^{-1}: 2920, 2851, 1607, 1599, 1517, 1286, 1250, 1107, 1025, 909, 841, 812, 720, 666 (neat).

Data for 5-(4-chlorophenyl)-3-{4-[2-(6-octyloxynaphthalen-2-yl)ethynyl]phenyl}-4,5-dihydroisoxazole (**16**). Yield 0.10g, 64%; pale yellow solid; mp 176 ºC. ^{1}H NMR ($CDCl_3$, 300 MHz): δ 0.8 (m, 3H, CH_3), 1.2-1.6 (m, 10H, $(CH_2)_5$), 1.8-1.9 (m, 2H, C<u>H</u>$_2$CH$_2$O), 3.3 (dd, 1H, C<u>H</u>HCH, $^2J_{gem}$ = 16.0 Hz, $^3J_{trans}$ = 8.0 Hz), 3.7 (dd, 1H, CH<u>H</u>CH, $^2J_{gem}$ = 16.0 Hz, $^3J_{cis}$ = 10.8 Hz), 3.9 (t, 2H, CH_2O, J = 6.4 Hz), 5.7 (dd, 1H, CHHC<u>H</u>, $^3J_{cis}$ = 10.8 Hz, $^3J_{trans}$ = 8.2 Hz), 7.1-7.4 (m, 6H, Ar,), 7.7-7.9 (m, 7H, Ar), 8.0 (s, 1H, Ar). ^{13}C NMR ($CDCl_3$, 75 MHz): δ 14.1, 22.7, 26.1, 29.1, 29.2, 29.3, 31.9, 43.0, 68.0, 82.0, 88.6, 92.3, 106.4, 117.5, 119.8, 125.4, 126.6, 126.8, 127.2, 128.3, 128.6, 128.8, 128.9, 129.3, 131.5, 131.8, 134.1, 134.3, 139.2, 155.6, 158.0. EI-MS: *m/z* 538 [M + 2], 536 [M^+], 424, 422, 406, 280, 255, 180, 139 (100), 113 and 111. Anal. Calcd for $C_{35}H_{34}ClNO_2$: C, 78.41; H, 6.39; N, 2.61. Found: C, 78.97; H, 7.37; N, 2.88. IR ν_{max}/cm^{-1}: 2923, 2854, 1625, 1605, 1495, 1469, 1411, 1392, 1259, 1212, 1171, 1095, 898, 858, 840, 824, 721, 666 (neat).

Data for 5-(4-bromophenyl)-3-{4-[2-(6-octyloxynaphthalen-2-yl)ethynyl]phenyl}-4,5-dihydroisoxazole (**17**). Yield 85.0 mg, 70%; pale yellow solid; mp 170 ºC. ^{1}H NMR ($CDCl_3$, 300 MHz): δ 0.9 (m, 3H, CH_3), 1.2-1.6 (m, 10H, $(CH_2)_5$), 1.9 (m, 2H C<u>H</u>$_2$CH$_2$O), 3.3 (dd, 1H, C<u>H</u>HCH, $^2J_{gem}$ = 16.3 Hz, $^3J_{trans}$ = 8.2 Hz), 3.7 (dd, 1H, CH<u>H</u>CH, $^2J_{gem}$ = 16.4 Hz, $^3J_{cis}$ = 11.0 Hz), 3.9 (t, 2H, CH_2O, J = 6.4 Hz), 5.7 (dd, 1H, CHHC<u>H</u>, $^3J_{cis}$ = 10.9 Hz, $^3J_{trans}$ = 8.2 Hz), 7.2-7.4 (m, 6H, Ar,), 7.7-7.9 (m, 7H, Ar), 8.0 (s, 1H, Ar). ^{13}C NMR ($CDCl_3$, 75 MHz): δ 14.0, 22.6, 26.9, 29.1, 29.3, 29.4, 31.8, 42.9, 68.1, 82.1, 88.5, 92.2, 106.5, 117.4, 119.8, 125.8, 126.6, 126.8, 127.7, 128.3, 128.6, 128.7, 129.2, 129.7, 131.4, 131.8, 131.9, 134.3, 139.8, 155.6, 158.0. EI-MS: *m/z* 582 [M + 2], 580 [M^+], 466, 450, 424, 355, 255, 185 (100), 182, 154, 129 and 113. Anal. Calcd for $C_{35}H_{34}BrNO_2$: C, 72.41; H, 5.90; N, 2.41. Found: C, 73.21; H, 6.03; N, 2.74. IR ν_{max}/cm^{-1}: 2923, 2854, 1623, 1605, 1469, 1259, 1211, 1171, 1075, 1013, 897, 855, 840, 821, 665 (neat).

Data for 3-(4-heptyloxyphenyl)-5-{4-[4-(octyloxyphenyl)ethynylphenyl]}-4,5-dihydroisoxazole (**18a**). Yield 77.0 mg, 70%; pale yellow solid; mp 138 ºC. ^{1}H NMR ($CDCl_3$, 300 MHz): δ 0.9-1.0 (m, 6H, $(CH_3)_2$), 1.4 (m, 18H, $(CH_2)_9$), 1.8 (m, 4H, $(C\underline{H}_2CH_2O)_2$), 3.3 (dd, 1H, C<u>H</u>HCH, $^2J_{gem}$ = 16.5 Hz, $^3J_{trans}$ = 8.1 Hz), 3.7 (dd, 1H, CH<u>H</u>CH, $^2J_{gem}$ = 16.6 Hz, $^3J_{cis}$ = 10.9 Hz), 3.9 (m, 4H, $(CH_2O)_2$), 5.7 (dd, 1H, CHHC<u>H</u>, $^3J_{cis}$ = 10.8 Hz, $^3J_{trans}$ = 8.1 Hz), 6.8 (d, 2H, Ar, J = 8.7 Hz), 6.9 (d, 2H, Ar, J = 9.0 Hz), 7.4 (d, 2H, Ar, J = 8.1 Hz), 7.5 (d, 2H, Ar, J = 8.7 Hz), 7.6 (d, 2H, Ar, J = 8.1 Hz), 7.7 (d, 2H, Ar, J = 9.0 Hz). ^{13}C APT NMR ($CDCl_3$, 75 MHz): δ 14.1 (2C), 22.5, 22.6, 25.9, 26.0, 28.9, 29.0-29.4 (5C), 31.7, 43.4, 68.0, 68.1, 81.8, 87.6, 89.8, 114.5, 114.6, 114.8, 121.5, 123.5, 125.8, 128.2, 131.7, 133.0, 140.7, 155.6, 159.2, 160.7. EI-MS: *m/z* 565 [M^+], 258, 218 (100). Anal. Calcd for $C_{38}H_{47}NO_3$: C, 80.67; H, 8.37; N, 2.48. Found: C, 80.88; H, 8.30; N, 2.75. IR ν_{max}/cm^{-1}: 2920, 2854, 1608, 1594, 1516, 1468, 1251, 1180, 1107, 898, 829, 719, 666 (neat).

Data for 3-(4-octyloxyphenyl)-5-{4-[4-(octyloxyphenyl)ethynylphenyl]}-4,5-dihydroisoxazole (**18b**). Yield 0.12g, 65%; pale yellow solid; mp 140 ºC. ^{1}H NMR ($CDCl_3$, 300 MHz): δ 0.9-1.0 (m, 6H, $(CH_3)_2$), 1.3 (m, 20H, $(CH_2)_{10}$), 1.7-1.8 (m, 4H, $(C\underline{H}_2CH_2O)_2$), 3.3 (dd, 1H, C<u>H</u>HCH, $^2J_{gem}$ = 16.5 Hz, $^3J_{trans}$ = 8.1 Hz), 3.7 (dd, 1H, CH<u>H</u>CH, $^2J_{gem}$ = 16.5 Hz, $^3J_{cis}$ = 10.8 Hz), 4.0 (m, 4H, $(CH_2O)_2$), 5.7 (dd, 1H, CHHC<u>H</u>, $^3J_{cis}$ = 10.8 Hz, $^3J_{trans}$ = 8.1 Hz), 6.8 (d, 2H, Ar, J = 8.7 Hz), 6.9 (d, 2H, Ar, J = 8.7 Hz), 7.4 (d, 2H, Ar, J = 8.1 Hz), 7.5 (d, 2H, Ar, J = 9.0 Hz), 7.6 (d, 2H, Ar, J = 8.1 Hz), 7.7 (d, 2H, Ar, J = 8.7 Hz). ^{13}C APT NMR ($CDCl_3$, 75 MHz): δ 14.1 (2C), 22.3, 22.6, 25.9, 26.0, 28.9, 29.0-29.4 (6C), 31.8, 43.4, 68.0, 68.2, 81.9, 87.6, 89.9, 114.5, 114.6, 114.8, 121.6, 123.5, 125.8, 128.2, 131.7, 133.0, 140.7, 155.7, 159.3, 160.7. EI-MS: *m/z* 579 [M^+], 272, 232 (100). Anal. Calcd for $C_{39}H_{49}NO_3$: C, 80.79; H, 8.52; N, 2.42. Found: C, 80.91; H, 8.59; N, 2.50. IR ν_{max}/cm^{-1}: 2925, 2850,

1605, 1592, 1514, 1250, 1181, 1107, 898, 829, 720, 666 (neat).

Data for 3-(4-octyloxyphenyl)-5-{4-[4-(decyloxyphenyl)ethynylphenyl]}-4,5-dihydroisoxazole (**18c**). Yield 87.0mg, 72%; pale yellow solid; mp 136 ºC. ^{1}H NMR ($CDCl_3$, 300 MHz): δ 0.8-0.9 (m, 6H, $(CH_3)_2$), 1.3 (m, 24H, $(CH_2)_{12}$), 1.8 (m, 4H, $(CH_2CH_2O)_2$), 3.3 (dd, 1H, CHHCH, $^2J_{gem}$ = 16.5 Hz, $^3J_{trans}$ = 8.1 Hz), 3.7 (dd, 1H, CHHCH, $^2J_{gem}$ = 16.5 Hz, $^3J_{cis}$ = 11.1 Hz), 3.97 (m, 4H, $(CH_2O)_2$), 5.7 (dd, 1H, CHHCH, $^3J_{cis}$ = 10.8 Hz, $^3J_{trans}$ = 8.1 Hz), 6.8 (d, 2H, Ar, *J* = 6.9 Hz), 6.9 (d, 2H, Ar, *J* = 6.6 Hz), 7.3 (d, 2H, Ar, *J* = 8.1 Hz), 7.4 (d, 2H, Ar, *J* = 8.7 Hz), 7.5 (d, 2H, Ar, *J* = 8.1 Hz), 7.6 (d, 2H, Ar, *J* = 8.7 Hz). ^{13}C APT NMR ($CDCl_3$, 75 MHz): δ 14.1 (2C), 22.8, 22.9, 26.2, 26.3, 29.3-29.6 (8C), 32.0, 32.1, 43.7, 68.3, 68.4, 82.2, 87.8, 90.2, 114.7, 114.9, 115.2, 121.8, 123.7, 126.1, 128.5, 132.0, 133.3, 141.0, 156.0, 159.5, 161.0. EI-MS: *m/z* 607 [M^+], 331, 258, 218 (100). Anal. Calcd for $C_{41}H_{53}NO_3$: C, 81.01; H, 8.79; N, 2.30. Found: C, 81.21; H, 8.83; N, 2.45. IR ν_{max}/cm^{-1}: 2922, 2852, 1603, 1591, 1516, 1468, 1251, 1180, 1108, 898, 829, 719, 666 (neat).

Acknowledgments

Acknowledgementes. The authors acknowledge MCT/CNPq Universal n° 471194/2008-5, MCT/CNPq nº 555785/2006-8, PROCAD-2007-CAPES and INCT-CMN for financial support and Prof. Renato Catalunã for ESI-MS facilities. B.C.A. and A.S. are undergraduate students and thank PIBIC-UFRGS for their fellowship. The authors thank also the referees for valuable suggestions and additions to this work.

References

[1] Carmella, P.; Grunanger, P. *1,3-Dipolar Cycloaddition Chemistry;* Padwa, A., Ed.; Wiley: New York, 1984; Vol. 1, pp. 291–392.

[2] Kozikowski, A.P. *Acc. Chem. Res*. **1984**, 17, 410–416.

[3] Torsell, K.B.G. *Nitrile Oxides, Nitrones and Nitronates* VCH: Weinheim, 1988.

[4] Padwa, A.; Schoffstall, A.M. *Advanced Cycloaddition Chemistry;* Curran,D.P., Ed.; JAI: Greenwich,CT, 1990.

[5] Gothelf, K.V.; Jorgensen, K.A. *Chem. Rev.* **1998**, 98, 863–909.

[6] Curran, D.P. *Advances in Cycloadditions*; Curran, D.P., Ed.; JAI: Greenwich, CT, Vol. 1, 1988; Curran, D.P.; Zhang, J. J. Chem. Soc. Perkin Trans. 1 1991, 2613–2625.

[7] Jager, V.; Muller, I. *Tetrahedron* **1985**, 41, 3519–3528.

[8] Habeeb, A.G.; Praveen Rao, P.N.; Knaus, E.E. *J. Med. Chem.* **2001**, 44, 2921–2927.

[9] Andre´s J.I.; Alca´ zar, J.; Alonso, J.M.; De Lucas, A.I.; Iturrino, L.; Biesmans, I.; Megens, A.A. *Bioorg. Med. Chem.* **2006**, 14, 4361–4372.

[10] Hanka, L.J.; Gerpheide, S.A.; Spieles, P.R.; Martin, D.G.; Belter, P.A.; Coleman, T.A.; Meyer, H.F. *Antimicrob. Agents Chemother*. **1975**, 7, 807–810.

[11] Becker, N.; Carreira, E.M. *Org. Lett.* **2007**, 9, 3857–3858.

[12] Fader, L.D.; Carreira, E.M. *Org. Lett*. **2004**, 6, 2485–2488.

[13] Bruce, D.C.; Heyns, K.; Vill, V.; *Liq. Cryst.* **1997,** 23, 813–819.

[14] Bezborodov, V.; Kauhanka, N.; Lapanik, V. Mol. Cryst. *Liq. Cryst.* **2004**, 411, 1145–1152; Bezborodov, V.S.; Kauhanka, N.N.; Lapanik, V.I.; Lee, C.J. *Liq. Cryst*. **2003**, 30, 579–583.

[15] Kovganko, V.N.; Kovganko, N.N. Russ. J. Org. Chem. 2006, 42, 696–700; Kovganko, V.N.; Kovganko, N.N. Russ. *J. Org. Chem*. **2006**, 42, 243–248.

[16] Kauhanka, U.M.; Kauhanka, M.M. *Liq. Cryst*. **2006**, 33, 121–127.

[17] Tavares, A.; Schneider, P.H.; Merlo, A.A. Eur. *J. Org. Chem*. **2009,** 889–897.

[18] Passo, J.P.; Schneider, P.H.; Vilela, G.D.; Ritter, O.M.S.; Merlo, A.A. *Liq. Cryst*. **2008**, 34, 834–840.

[19] Ritter, O.M.S.; Passo, J.P.; Giacomelli, F.C.; Silveira, N.P.; Merlo, A.A. *Polym. Bull*. **2006**, 56, 549–561.

[20] Merlo, A.A.; Gallardo, H.; Taylor, T.R. *Química Nova* **2001**, 24, 354–362.

[21] Hsiue, G.-H.; Chen, J.-H. *Macromolecules* **1995**, 28, 4366–4376.

[22] Grundmann, C. *Synthesis* **1970**, 344–359.

[23] Liu, K-C.; Shelton, B.R.; Howe, R.K. *J. Org. Chem*. **1980**, 45, 3916–3918.

[24] Lee, G.A. *Synthesis* **1982**, 508–509.

[25] Das, B.; Holla, H.; Mahender, G.; Banerjee, J.; Reddy, M.R. *Tetrahedron Lett*. **2004**, 45, 7347–7350.

[26] Moriya, O.; Nakamura, H.; Kageyama, T.; Urata Y. *Tetrahedron Lett*. **1989**, 30, 3987–3990.

[27] Vasconcelos, U.B.; Vilela, G.D.; Schrader, A.; Gorges A.C.A.; Merlo, A.A. *Tetrahedron* **2008**, 64, 4619–4626; Vasconcelos, U.B.; Merlo A.A. Synthesis 2006, 7, 1141–1147; Vasconcelos, U.B.; Dalmolin, E.; Merlo, A.A. *Org. Lett*. **2005**, 7, 1027–1030.

[28] Hsu, H.-F.; Lin, W.-C.; Lai, Y.-H.; Lin, S.-Y. *Liq. Cryst*. **2003,** 30, 939–944.

[29] Chinchilla, R.; Najera, C. *Chem. Rev*. **2007**, 107, 874–922.

[30] Sonogashira, K.; Tohda, Y.; Hagihara, N. *Tetrahedron Lett*. **1975**, 16, 4467–4470.

[31] Cristiano, R.; Santos, D.M.P.O.; Conte, G.; Gallardo, H. *Liq. Cryst.* **2006**, 33, 997–1003.

[32] Gallardo, H.; Conte, G.; Bryk, F.; Lourenc¸o, M.C.S.; Costa, M.S.; Ferreira, V.F. *J. Braz. Chem. Soc.* **2007**, 18, 1285–1291.
[33] Wong, J.; Masson, P.; Nicoud, J.F. *Polym. Bull*. **1994**, 32, 265–272.
[34] Melissaris, A.P.; Litt, M.H. *Macromolecules* **1994**, 27, 883–887.
[35] Hilla, L.L.; Smith, J.M.; Brown, W.S.; Moore, L.R.; Guevera, P.; Pair, E.S.; Porter, J.; Chou, J.; Wolterman, C.J.; Craciun, R.; Dixon, D.A.; Shaughnessy, K.H. *Tetrahedron* **2008**, 64, 6920–6934.
[36] Nagy, A.; Kotschy, A. *Tetrahedron Lett.* **2008**, 49, 3782–3784.
[37] Wu, M.; Mao, J.; Guo, J.; Ji, S. *Eur. J. Org. Chem.* **2008**, 4050–4054.
[38] Tavares, A.; Livotto, P.R.; Gonc¸alves, P.F.B.; Merlo, A.A. J. Braz. Chem. Soc. **2009**, *20*, 1742.
[39] Price, D.W.; Dirk, S.M. Jr.; Maya, F.; Tour, J.M. Tetrahedron **2003**, *59*, 2497–2518.
[40] James, D.K.; Tour, J.M. *Aldrichim. Acta* **2006**, 39, 47–56.
[41] Gray, G.W.; Goodby, J.W.G. *Smectic Liquid Crystals. Textures and Structures*; Leonard Hill: London, 1984.
[42] Patil, H.P.; Liao, J.; Hedden, R.C. *Macromolecules* **2007**, 40, 6206–6216.
[43] Collings, P.J.; Hird, M. *Introduction to Liquid Crystals. Chemistry and Physics*; Taylor and Francis: London, 1997.
[44] Han, J.; Chang, X.-Y.; Zhu L.-R.; Wang, Y.-M.; Meng, J.-B.; Lai, S.-W.; Chui, S. S.-Y. *Liq. Cryst.* **2008**, 35, 1379–1394.
[45] Tanaka, M.; Haino, T.; Ideta, K.; Kubo, K.; Mori, A.; Fukazawa, Y. *Tetrahedron* **2007**, 63, 652–665.
[46] Weygand, C.; Gabler, R. *J. Prakt. Chem.* **1940**, 155, 332–341.
[47] Zhang, L.-H.; Chug, J.C.; Costello, T.D.; Valvis, I.; Ma, P.; Kauffman, S.; Ward, R. *J. Org. Chem*. **1997**, 62, 2466–2470.
[48] Field, L.; Hughmark, P.B.; Shumaker, S.H.; Marshall, W.S. *J. Am. Chem. Soc.* **1961**, 83, 1983–1987.
[49] Narsaiah, A.V. *Adv. Synth. Catal*. **2004**, 11, 1271–1274.

CAPÍTULO 6

CAPÍTULO 6.1 – Artigo submetido ao jornal *MATER. CHEM. PHYS.*

Thermal Elimination of *O*-Benzoyloximes. Consequences on the Chemical Stability and Mesomorphic Behaviour

Aline Tavares,[a] Bárbara C. Arruda,[a] Elvis S. Boes,[b] Valter Stefani,[a] Hubert K. Stassen,[b] Leandra F. Campo,[a] Ivan H. Bechtold,[c] and Aloir A. Merlo*[a]

Instituto de Química, UFRGS. Av. Bento Gonçalves, 9500. Agronomia. 91501-970, Porto Alegre, RS – Brasil.

We report the synthesis of a series of unstable fluorescent liquid-crystalline materials based on *O*-benzoyloximes (**6a-d**, **8**) by esterification of the corresponding 4-alkyloxybenzoic acid (**5a-d**) and 3-arylisoxazolyl-5-carboxylic acid (**7d**) with 4-{[6-octyloxy)naphthalen-2-yl]ethynyl}benzaldehyde oxime (**4**) and the characterization of these materials by ^{1}H, ^{13}C NMR, ATR/FT-IR spectroscopy and elemental analysis. The chemical stability and liquid-crystalline as well as the photophysical properties of the compounds are described and show to be dependent on the heating/cooling cycles. The *O*-benzoyloximes "aging" is strongly induced by heat. The changing in chemical stability and the liquid crystals properties of **6a-d** and **8** were evaluated during these thermal cycles together IR analysis. The data collected from the first heating/cooling cycle were different from that 2nd and 3rd. Also, IR analysis showed that all sample underwent a thermal degradation yielding the corresponding nitrile such **10** as evidenced by IR and NMR ^{1}H spectra. To the first heating the nematic and smectic C were observed. However, the mesomorphic behaviour changed to nematic and smectic A phase in the 2nd and 3rd heating/cooling cycles for compounds **6a-d**. To **8** smectic X and SmB mesophase was assigned to the first and to the 2nd/3rd cycles, respectively. The nature of these mesophase was characterized by X-ray experiments. The intermediate oxime **4** as well as aldehyde **3** are stable nematogenic liquid crystals. The UV/vis absorption spectra in organic solvents display tree absorption bands between 230-340 nm and the fluorescence spectra present only a broad and structureless emission band located around 430 nm. The electron donor–acceptor interactions have a pronounced effect on the photophysical properties; Stokes' shift and the quantum yield depends on the solvent polarity and emitted violet-blue light in solution and in the solid state is observed. In solution, these compounds are stable at least for 6 months when stored in the refrigerator. *Ab initio* calculations were performed in order to obtain information on the molecular structure and properties of the title compounds.

Introduction

Carbonyl compound derivatives possessing a carbon-nitrogen double bond have been recognized as attractive synthetic targets due to their potential application in medical and material chemistry.

Schiff bases, which are the most popular class of theses carbonyl derivatives, have been reported as important materials in the coordination chemistry,[1] analytical chemistry[2] and liquid crystal science.[3] Oximes are less popular than Schiff bases, but they are found in many practical applications.[4] For example, (*E*)- and (*Z*)-oximes were used to elucidate action mechanism of their dehydration catalyzed by liver cytochromes P450.[5] Bisaryloxime ethers were found to be active inhibitors in vitro of plasma protein transthyretin (TTR) which is responsible of amyloid fibril formation.[6] Perillartine is the oxime derived from perillaldehyde, found in *Perilla frutescens* (Lamiaceae). It is known as perilla sugar being 2000 times sweeter than sucrose.[7] Pralidoxime is another example of an oxime, which is able to bind to organophosphatate-inactivated acetylcholinesterase.[8] Benz-isoxazoles are present in a large number of important products with pharmacological properties and are synthesized by [3+2] cycloaddition reaction of a benzyne with a nitrile oxide.[9a] Isatin is a natural product found in plants of the *genus Isatis*. Many of its derivatives, which are used in drug synthesis are obtained from precursors derived from oximes.[9b] Oxime-derived, chloro-bridged palladacycles represent very efficient catalyst precursors for the Heck olefination of haloarenes.[9c] And, more recently oxime carbonates were introduced as a novel reagents for the instalation of Fmoc and Alloc protecting groups, free of side reactions.[9d]

As part of our continuing interest in synthesis of new liquid crystals (LC) derived from 3,5-disubstituted isoxazolines, from [3+2] 1,3-dipolar cycloaddition reaction between aryl nitrile oxide and alkene,[10] we explored the synthetic potential of the arylaldoximes, as a precursor of aryl nitrile oxide, in the preparation of new LC materials. The initial strategy utilizes naphtyl ethynylbenzaldehyde oxime (**4**), an advanced intermediate in our research program involving the preparation of novel isoxazoline liquid crystals, as key component for the synthesis of mesogenic *O*-benzoyloximes.

In the present article, we report the synthesis and the physical chemical behaviour of a series of *O*-benzoyloximes **6a-d** and **8** derivatives as well as the intermediate **3** and **4**. The liquid-crystalline properties, ATR/FT-IR spectra, DSC thermograms, X-ray experiments, absorption and fluorescence spectra are reported.

Results and discussion

Synthesis

Chart 1 describes the intermediates and the final liquid crystals synthesized in this work. A two-step process was applied to synthesize the *O*-benzoyloxime **4**. The route begins with a Sonogashira cross-coupling reaction[11] of the terminal acetylene **1**[12] and the commercial *p*-bromobenzaldehyde (**2**) in dry triethylamine. The following step produces the oxime **4** from a reaction of aldehyde **3** under mild conditions in an aqueous ethanol solution of hydroxylamine hydrochloride and sodium acetate.

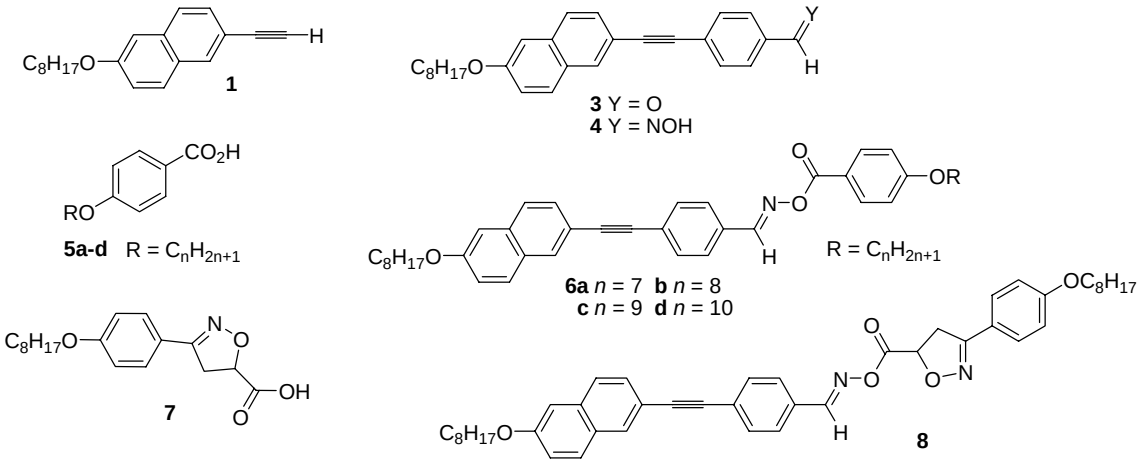

Chart 1. The chemical intermediates and the final liquid crystals **6a-d** and **8**.

The homologous series **6a-d** was prepared in order to investigate the effect of the benzoyl group on liquid crystals and photophysical properties. In addition, the benzoyl group linked to the oxime allows evaluating the conformational aspects related with rotamers around the N-O bond that are possible in these compounds (see theoretical discussion). Thus, four compounds **6a-d** were synthesized by esterification of oxime **4** with 4-alkoxybenzoic acids **5a-d**[13] using DCC/DMAP protocol.[14]

Considering our recent results using isoxazoline as molecular kits for liquid-crystalline materials[10e] we are reporting the synthesis and the LC behaviour of one member of LC containing isoxazoline ring. To compare, we selected the acid **7** as a chemical partner of the oxime **4**. The final compound **8** was then synthesized by application of the same reaction protocol as used for compounds **6a-d**.

Liquid-crystalline behaviour

The LC properties were investigated using differential scanning calorimetry (DSC) and polarizing optical microscopy (POM). The transition temperatures and thermodynamic data of compounds **3**, **4**, **6a-d** and **8** are summarized in Table 1. As expected, compounds **3** and **4** exhibited the enantiotropic nematic mesophase. When they were sandwiched between untreated glasses slides, birefringent droplets firstly appeared which vanished subsequently to give rise to large areas of planar orientation, schlieren texture on cooling from the isotropic state. These are the characteristic features of the nematic phase. The transformation of **3** into the oxime **4** showed that the presence of C=NOH group in substitution of C=O furnishes to a more stable mesophase probably due to the stronger dipole of the oxime and the association by intermolecular hydrogen bonds. This is also corroborated by the larger enthalpy value found for **4** for the transition of the nematic to the isotropic phase.

Compounds **6a-d**, and **8**, however, are thermally unstable. Thus, when the samples were subjected to the heating/cooling cycles, the DSC profiles exhibited different behaviours. As an example, the modification of the DSC traces in the heating/cooling cycles of the samples **6c** and **8** are represented in Figure 1 (a complete set of the DSC thermograms of all samples are included in SI section). The data in Table 1 were collected in the first and third cycles. It can be seen that LC properties of these compounds changed after the first heating/cooling cycle. The thermally induced degradations were more intense after the samples enter into isotropic phase during the first heating run. The DSC traces show that all samples when heated at first time presented irreversible endothermic transitions. For example, the selected peak at 155.3 °C as shown in Figure 1 at the top is associated to the transition Cr_2 to SmC phase, which disappeared after the first heating. The new and broad peak that arises around 139.7 °C – 143.3 °C is assigned now to the SmA → N → I transition by POM. After cooling and reheating the samples present a shift to lower temperature of the clear point around 30 °C for **6a-d** and *ca* 21 °C for **8**. In addition to the changes in all transition temperatures as seen in DSC traces, also the nature of the mesophase changed.

The nature of the mesophase of these esters was studied and characterized by POM and X-ray diffraction (see discussion below, Table 1 and 2 and Figure 3, 6 and 7). The mesophase textures, by POM, were assigned as smectic C and nematic for the first heating run. However, after the first heating the new textures that emerge from the samples were assigned as smectic A and nematic for **6a-d**. For the LC **8**, the mesophase texture during the first heating/cooling stage is inconclusive and named SmX. The texture of **8** was assigned as smectic B phase only after the first cycle.

It is worthwhile to mention the alteration in melting and clearing temperature and the asymmetry in the peak during the crystal → smectic A mesophase transition. The crystal → SmA phase transition is always accompanied by shoulders at both sides of the main peak. These anomalies are always present in the esters **6a-d**. As can be observed for **6c** (Fig. 1) two or more unsymmetrical and small endothermic peaks are detected at the flanks of the peak the crystal → SmA phase transition. The anomalies are not seen in the ester **8**. The origin of these anomalies is unknown, but the thermal history of these samples is probably associated by degradation process that affects the original mesomorphic behaviour of these materials.

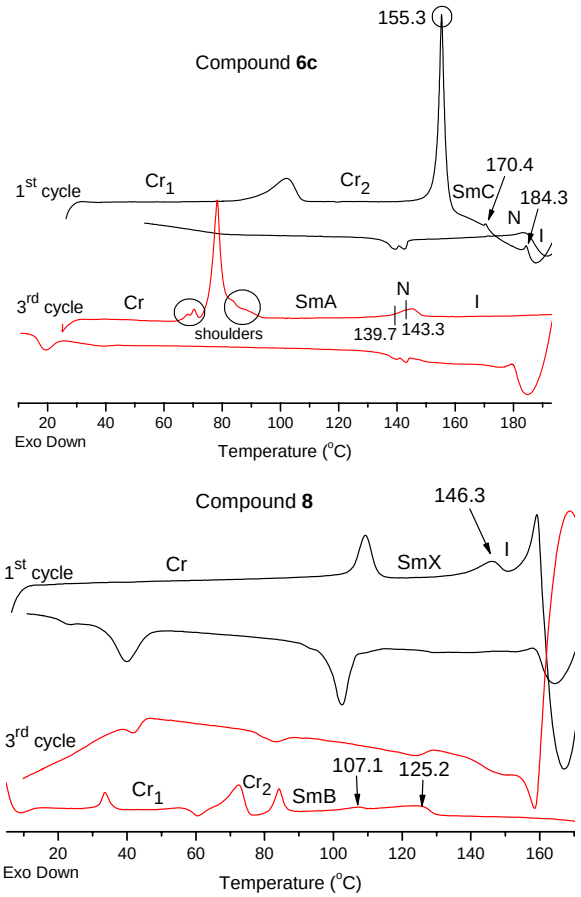

Fig. 1. DSC thermograms of **6c** and **8** on heating/cooling stages (1st and 3rd cycles) at rate 10 °C min^{-1}.

The modification of the DSC traces was observed even when the sample was submitted to heating/cooling cycles below the clearing temperature of the N – I transition. From these data, we can conclude that the thermal decomposition continuously grows. For example, on heating at 20 °C min^{-1} until 160.0 °C **6b** displayed, during the transition Cr_2 → SmC, T_{onset} at 128.5 °C, 111.9 °C and 86.3 °C to the 1st, 2nd and 3th heating/cooling cycles, respectively (Figure 2).

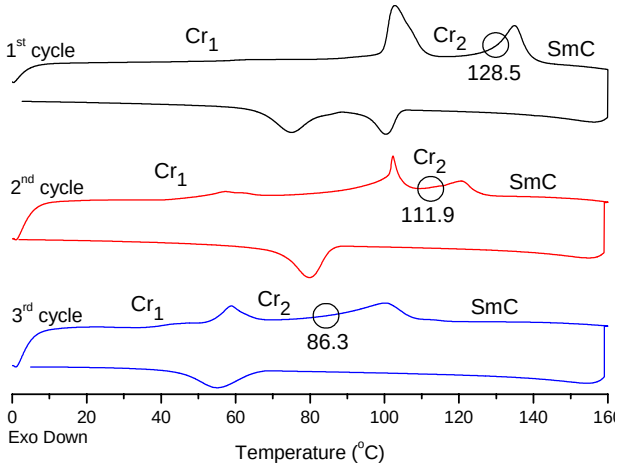

Fig. 2. DSC thermograms of **6b** on heating/cooling stages at rate 20 °C min^{-1}. The final temperature of the three heating/cooling cycle were acquired at twelve degrees (°C) below the clearing temperature of the N – I transition. The circle indicates the T_{onset} at 128.5 °C, 111.9 °C and 86.3 °C to the $Cr_2 \rightarrow$ SmC transition.

The X-ray diffraction experiments were carried out on compounds **6a** and **8**. For compound **6a** all the patterns recorded in the mesophase (at 100 °C) contain a sharp peak in the low-angle region, arising from the reflection of the X-ray beam on the smectic layers, and their corresponding higher order peaks. The inter-layer spacing was obtained by applying Bragg's law to the first maximum. The smectic order was confirmed by the ratio of the value obtained for the first peak with respect to the values obtained for the second order peaks. It is well known that this ratio must obey the relation 1:2:3:4… in smectic phases. Table 2 shows the inter-layer spacing for different heating/cooling cycles, where one can see that at the first heating cycle (heating the powder) the distance between the layers is 5.0 Å larger than for the second and third heating cycles. The strong reduction of the inter-layer spacing does not combine with the model described for SmA phase and based on its one-dimensional waves, i.e SmA_1 (monolayer), SmA_2 (bilayer) or SmA_d (where the periodicity d is intermediate between the monolayer and bilayer). This observation confirms that samples are changing their molecular structure by decomposition processes when heated. In spite of their thermal decomposition the products originated from heating are themselves LC. The layer spacing of the smectic phase is lower during the cooling cycles and no appreciable differences were observed between the three steps. In Table 2, the layer distances d of the smectic phases of **6a** were shorter than its calculated molecular length considering the distances between the far atoms with the addition of the Van der Waals radii from hydrogen atoms bonded to the first and last carbon atoms in the chain (Table 2). The value for the fully extended all *trans*-conformation is l = 43.1 Å. From the collected X-ray spectrum of the compound **6a** powder, before the first heating cycle, we obtained also a smectic structure with a spacing layer d_p = 39.3 Å. By considering d_p as the length adopted by the molecules in the smectic layers it is possible to conclude that the molecules are tilted to the normal plane with an angle $\theta = \cos^{-1}(d/d_p)$, which gives a tilt angle θ = 18 degrees. This observation is consistent with the POM texture observed for **6a** on the 1st heating which was assigned as SmC phase. For the 2nd and 3rd cycle the tilt angle assumes a higher value of θ = 35 degrees, which means a more tilted smectic phase! This result is conflicting to the fan focal conic and homeotropic texture observed by POM studies.

Table 1. Transition temperatures (°C) and enthalpy (kcal mol^{-1}, in brackets) for compounds **3**, **4**, **6a-d** and **8**.

LC	1st Heating/Cooling	ΔT_{N-I} [d]	3rd Heating/Cooling
3			Cr 107.5 (5.5) N 151.0 (0.04) I I 148.0 N 93.2 Cr
4			Cr 150.8 (4.1) N 176.0 (0.7) I I 173.2 N 132.3 Cr
6a	Cr_1 95.6 (1.14) Cr_2 139.3 (4.74) SmC 153.0 (0.14) N 175.4 (0.11) I I 145.8 N 132.3 SmA ..[a].. Cr	27.1	Cr 67.2 (6.16) SmA[b] 137.2 (0.31) N 148.3 (0.49) I I 146.1 N 133.6 SmA ..[a].. Cr
6b	Cr_1 99.7 (6.34) Cr_2 132.9 (5.73) SmC 169.9 (0.06) N 173.0 (0.04) I I 140.8 N 138.4 SmA ..[a].. Cr	29.7	Cr 66.5 (2.53) SmA[b] 130.7[c] N 143.3 (1.51) I I 139.9 N 128.9 SmA ..[a].. Cr
6c	Cr_1 101.8 (4.18) Cr_2 155.3 (10.05) SmC 170.4 (0.07) N 184.3 (0.17) I I 142.6 N 139.2 SmA ..[a].. Cr	39.0	Cr 78.3 (6.88) SmA[b] 139.7[c] N 145.3 (1.15) I I 143.2 N 139.7 SmA 19.4 Cr
6d	Cr_1 77.6 (0.38) Cr_2 107.9 (1.21) Cr_3 134.6 (6.24) SmC 170.1 (0.04) N 173.9 (0.10) I I 144.2 N 140.6 SmA 32.1 Cr	32.8	Cr 65.7 (9.78) SmA[b] 133.5[c] N 141.1 (1.58) I I 136.0 N 126.7[c] SmA 33.7 Cr
8	Cr 109.3 (2.39) SmX 146.3 (0.69) I I 127.4[c] SmB 102.5 Cr_2 39.7 Cr_1	21.1	Cr_1 72.6 (2.06) Cr_2 84.2 (0.94) SmB 125.2 (0.76) I I 123.7 SmB 82.8 Cr_2 42.0 Cr_1

Scan rate: 10 °C min^{-1} for all samples; Cr = Crystal phase; SmA = smectic A phase; SmB = smectic B phase, SmC = smectic C phase and N = nematic phase. a. Slow crystallization at room temperature (homeotropic and *fan*-focal conic texture). b. fan-shaped texture plus crystallines solid c. Transition temperatures were obtained from POM analyze. d. Range temperature taking into account the 1st and 3rd heating.

Considering that corresponding *O*-benzoyloximes when subjected to basic conditions yield the nitriles and benzoates,[15] we can speculate that the new texture is derived from the mixture 1:1 nitrile:benzoate formed during the first heating (see heat-promoted elimination from *cis* conformation in Figure 5b). The *l* value for the fully extended all *trans*-conformation of nitrile **10** is 26.4 Å. Considering this possibility, then the ratio d_p/l = 1.4 suggests a partially interdigitated smectic A phase – SmA_d.[16] However, the information about the interdigitation of the alkyl chains in the SmA mesophase suffers a serious drawback if we consider that this lamellar mesophase was thermally driven as a result of the decomposition processes. The possible degradation products nitrile[17] and 4-*n*-heptylbenzoic acid[18] display the following mesophase sequence: to nitrile **10**: Cr 95.2 N 157.5 I (DSC); to acid: Cr 101 SmC 107.5 N 145.3 I, respectively (see the ATR/FT-IR and mesophase texture analysis below).

Table 2. Inter-layer spacing (*d*) of **6a** for different heating/cooling cycles, obtained X-ray diffraction experiments in the SmA mesophase at 100 °C.

Entry	*d* heat (Å)	*d* cool (Å)
1st Cycle	37.3±0.1	31.2±0.1
2nd Cycle	32.3±0.1	31.4±0.1
3rd Cycle	32.3±0.1	31.7±0.1

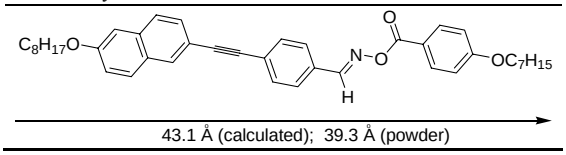

For **8** we investigated the phases by varying the temperature, the collected X-ray diffraction patterns for the third cooling cycle are shown in Figure 3. At 140 °C the compound is in the isotropic phase and as expected, no peaks are observed. For the temperature of 115 °C, an intense peak at the low angle region (2θ = 2.22°) is observed, which according to Bragg's Law results an inter-layer spacing of 39.8 Å. For angles of 2θ between 3.0° and 18° other five peaks can be seen, corresponding to distances of 20.0 Å, 13.6 Å, 8.0 Å, 6.7 Å and 5.0 Å. These distances prove the smectic character of the mesophase, because the ratio with the first maximum result in integers. In addition, a well-defined peak is observed at 2θ = 20.32°, corresponding to a distance of 4.4 Å, which is related to the (110) Miller reflection. The existence of this peak is consistent with a SmB phase.[19] At 75 °C other peaks above the (110) reflection can be seen. These peaks could not be assigned to specific ordered smectic phases. We suggest a crystalline phase that preserve a smectic order. Actually, the smectic order is still present at 30 °C, but the appearance of additional peaks at low and high angle regions indicate a second crystalline structure. It is important to emphasize that the SmB phase was observed during the heating and cooling only after the first heating/cooling process.

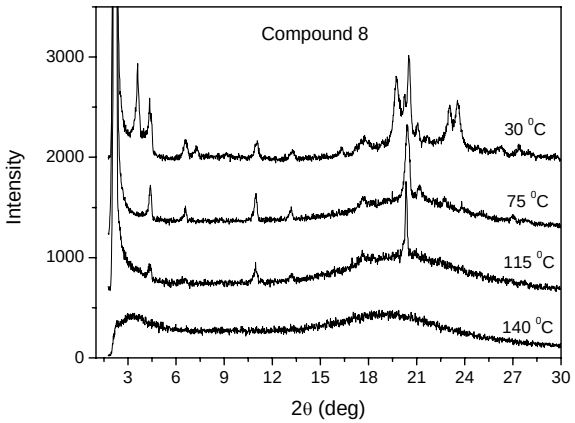

Fig. 3. X-ray diffraction patterns of **8** as a function of the temperature at the third cooling cycle.

Considering the DSC profile obtained during our thermal studies and the X-ray data, we believe that the decomposition is originated at a preferential conformation adopted by theses compounds when hetead yielding the corresponding nitrile and carboxylic acid. To test this hypothesis we performed a theoretical calculation in order to get additional information related with conformational preference (see discussion below and Figure 5a) and FT-IR studies. Next, we also synthesized the nitrile **10**[17] and when submited to heating, this compound displays the nematic mesophase that was observed to the esters **6a-d** after heating. The clear temperature of **10** are similar than those for **6a-d** after heated.

The degradation of these compounds was also observed in the ATR/FT-IR analysis. Figure 4 describes four ATR/FT-IR spectra of the same sample of **6c** under four different conditions: (a) before heating (no thermal history); (b) spectrum collected from the sample that underwent a many heating/cooling cycles, (c) spectrum recorded the same sample that remained overnight at room temperature; (d) ATR/FT-IR spectrum obtained from the batches of crystals (20 mg) of **6c** that were heated at 185 °C for 15 minutes and cooled to room temperature. After thermal treatment, **6c** was dissolved again in $CHCl_3$ and then the solvent was evaporated. The pale yellow solid obtained was washed with ethanol and dried. In (e) the spectrum of the synthesized nitrile-LC **10** is presented.[17]

The set of the ATR/FT-IR spectrum shows clearly a change in the region of 1600-1750 cm^{-1}. In (a), the **6c** displays a strong absorption at 1733 cm^{-1} which corresponds to the carbonyl group stretching. However, this absorption peak is shifted to lower frequency after heating/cooling cycles as show by (b) and (c) in Figure 4. The main modification is the appearance of a large peak at 1671 cm^{-1}. In (d) we can see that the **6c** does not return to the original condition. The absorption peak at 1671 cm^{-1} is accompanied by another peak at 2223 cm^{-1} which is an indication of the C≡N group resulting from the thermal decomposition due to an interaction that occurs an favourable *cis* conformation (see Figure 5a).

The absorption band at 2207 cm^{-1} is related to the C≡C group. The peak at 1090 cm^{-1} is assigned to the N-O-C group. The N-O-C stretching vibration appears in the recorded spectrum of the first heating (a) and its absent in the other spectra (b-d). The changes observed in the peaks at 1733 cm^{-1} and 1090 cm^{-1} clearly indicate that the decomposition is being induced continuously during the cycles of heating and cooling. The decomposition is indeed an elimination reaction induced by heat. The possible transition state to this elimination reaction can be described by the conformation *cis* in Figure 5 where the cleavage of C-H bond is promoted by the carbonyl group in the cyclic transition state.[15]

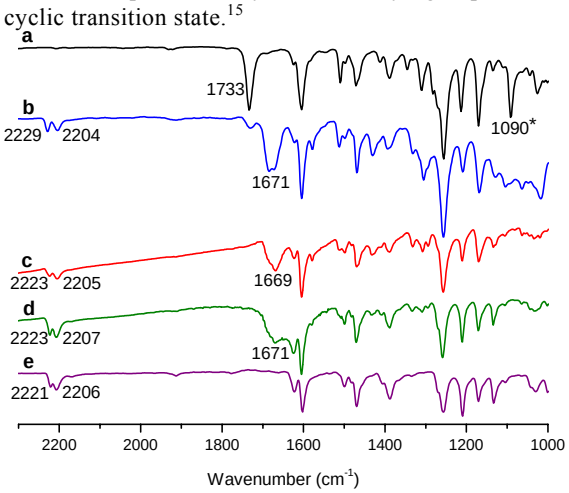

Fig. 4. Portion of the ATR/FT-IR spectra: (a) original sample of compound **6c** without heating/cooling cycles; (b) spectrum obtained of **6c** after many heating/cooling cycles using hot plate; (c) spectrum of the same sample **6c** in (b) after overnight at room temperature; (d) spectrum of **6c** after thermal and solvent treatment (see text for discussion); (e) compound **10**. "Asterisks" indicate the absorption band assigned to the N-O-C group present in **6c**.

The molecular size, calculated for this optimized structure as the distance between the hydrogen atoms located at opposite ends of the alkyl chains, is 43.1 Å. This is the length of the largest molecular axis. In addition we have studied the barrier height for the conformers *cis* and *trans* of this molecule corresponding to the rotation of the dihedral angle C-N-O-C generated by the rotation around the N-O bond. Therefore, we have optimized the molecule with dihedral angles C-N-O-C of 0.0 and 180.0 degrees corresponding to the *cis* and *trans* conformers respectively. We have found that the *cis* conformer is not a stationary point for this structure and we have performed the geometry optimization of this conformer keeping the dihedral angle C-N-O-C fixed at an angle of 0 degrees while allowing the optimization of all the other angles and bond lengths in the structure of the molecule in this conformation. In this case, we optimized the molecular structure with the molecule constrained to the *cis* conformer for the dihedral angle C-N-O-C.

Then we compared the energies calculated for the *trans* and *cis* conformers and we have found the difference of 7.39 kcal/mol (30.90 kJ/mol). This is the barrier height for the rotation of the dihedral angle C-N-O-C, corresponding to the difference in the energies calculated for the *cis* and *trans* conformer of this molecule.

We have also studied the possibility of a favourable interaction between the carbonyl oxygen and the hydrogen through the formation of hydrogen bond but the results show that this interaction is not favourable enough to compensate for the large repulsive interaction between the carbon atoms in the dihedral C-N-O-C. The distance between the carbon atoms is 3.373 Å in the *trans* conformer and 2.852 Å in the *cis* conformer.

The electrostatic analysis by Mulliken electronic population analysis also provides a clue to understand the high rotational barrier for the dihedral angle C-N-O-C in this molecule. In the *trans* conformer, the Mulliken charges for the carbon atoms in C-N-O-C are 0.2717 and 0.7311 respectively. In the *cis* conformer these charges are respectively 0.1785 and 0.7453. Just looking at these positive charges, we can already understand the source of the electrostatic repulsion between these atoms that partially accounts for the high rotational barrier about the N-O bond in this molecule. The distance between the hydrogen of the N=C-H group and the oxygen in the carbonyl group is 2.070 angstrons in the *cis* conformer. We have also observed a change in the Mulliken charges of this hydrogen from 0.0995 in the *trans* conformer to 0.1706 in the *cis* conformer while the charge on the carbonyl oxygen changed from -0.4333 in the *trans* to -0.4909 in the *cis* conformer indicating an electrostatic interaction between the oxygen and the hydrogen which loses part of its electronic density to the oxygen. This favourable electrostatic interaction acts in the direction of lowering the rotation barrier for the C-N-O-C dihedral angle.

The electrostatic analysis also provides us the dipole momentum for this molecule which is 4.23 D (debyes) for the *trans* conformer and 2.69 D for the *cis* conformer. The dipole vector points along the shortest molecular axis or in the direction orthogonal to the longest molecular axis. The high energy calculated for this rotational barrier prevents the rotation of the groups around the N-O bond at ordinary or room temperatures and contributes to enhance even more the structural rigidity of this molecule.

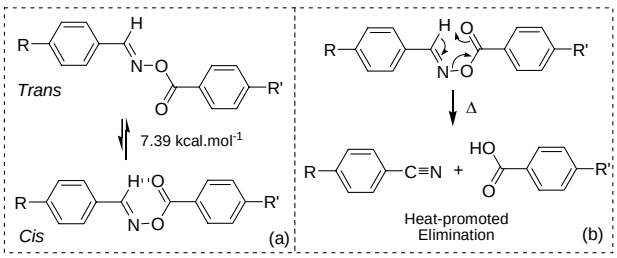

Fig. 5. *Trans* and *Cis* conformation for **6a** in (a) - the alkyloxy chains and naphtylacetilenic group have been omitted for clarity and in (b) the proposed elimination process induced by heat.

The most stable conformation obtained theoretically in this work is in agreement with previous work published by Dondas et al, describing the crystal structure of the *E*-benzaldehyde *O*-benzoyloxime.[21] They found that the crystalline structure of this aromatic oxime is better described by *trans* conformation where the C-N-O-C dihedral angle is approximately equal to 180.0 degrees.

Liquid Crystal Texture

For the discussion about the texture behaviour the compounds **6c** and **8** were selected. The Figures 6 and 7 show the relevant textures. For the ester **6c**, the sequence smectic C and nematic was seen only during the first heating (Fig 6a and 6b). When the samples were slowly heated, the schlieren texture appeared showing singularity lines with four dark brushes in some domains (Fig 6a). At SmC → N transition the sample become more fluid and schlieren texture showed singularity lines with two and four dark brushes and homeotropic texture (dark region) in the middle of Figure 6b.[22] On cooling from the isotropic liquid, the nematic phase appeared exhibiting planar thread-like texture (Fig 6c), which is characteristic of a liquid-crystalline nematic phase and, this texture changed to fan-shaped texture along with homeotropic texture of SmA phase when the sample entered to SmA phase (Fig 6d). The black area is caused by homeotropic orientation of molecules. The sample crystallizes slowly into a nice peacock "pavão" texture in (e) and (f).

The liquid-crystalline texture for **8** is shown in Figure 7. The mesophase identification was undertaken combining the X-ray data and POM analysis. Figures 7a and 7b present the crystal phases (Cr_1 and Cr_2, respectively) of **8**. The texture of the mesophase of **8** during the first heating is poorly defined and it is dificult to get some precise information about the nature of this mesophase. However, after the first heating/cooling cycle the sample displayed a mosaic texture which (Figure 7c-f) with the X-ray data was assigned as SmB phase.[23]

The thermal behaviour of the series **6a-d** displayed distinct behavior to **8**. These data suggested that the non-colinearity of the two planes of the isoxazoline ring (about 135.9°)[24] causes an influence on the stability of the mesophase. Due to the introduction of isoxazoline ring, the molecular symmetry is lowered changing the mesophase nature found in this work. The isoxazolinic system disfavours the interactions between the planar cores reducing the intermolecular forces responsabile for packing arrangements in the mesophase. It should be noted that the presence of the naphthalene ring induces the formation of more stable mesophase due to increased of molecular interactions.[25]

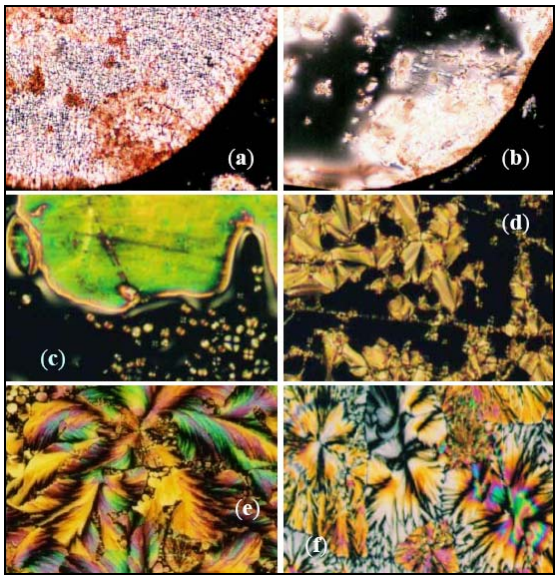

Fig. 6. Photomicrographs of the optical textures observed under POM of **6c** (magnification x10). In (a) a grainy schlieren texture of SmC phase at 169.0 °C; (b) schlieren and homeotropic texture (dark region at center) of N phase at 171.4 °C obtained during the first heating; (c) planar texture for N phase at 141.9 °C on cooling; (d) fan-shaped focal conic SmA with homeotropic domains textures at 125.5 °C; (e) and (f) peacock "pavão" texture of the crystal phase at rt.

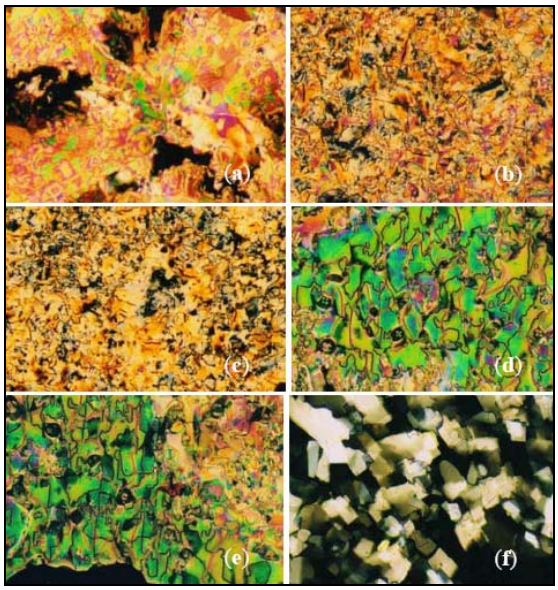

Fig. 7. Photomicrographs of the optical textures observed (magnification x10) for **8**. In (a) crystal phase Cr_1 at rt; (b) crystal phase Cr_2 at 75 °C; (c-f) mosaic SmB phase at 85 °C, 90 °C, 100 °C and 119 °C, respectively.

Photophysical Properties

The photophysical properties of compounds **3**, **4**, **6c** and **8** in dioxane, chloroform, ethanol and acetonitrile are listed in Table 3, and their UV spectra are shown in Figure 8. The spectra of all compounds clearly exhibit the two bands of the naphthalene ring[26] a major band at short wavelengths (220–260 nm), resulting from excitation along the major axis of the molecule (the β-band); and a two-peak band (*p*-band) between 250–300 nm. As has been observed by Marsh

et al,[26] upon addition of ethynyl group the major features of the absorption bands of naphthalene are preserved. On the other hand, the long-wavelength band around 340 nm can be attributed to the charge-transfer transition. In fact, a third band in these systems is evidently different from the spectra of naphthalene or ethynylnaphthalene[26,27] indicating that conjugation effects of the aryl group and the ethynyl-naphthalene are pronounced.

Although the free rotation of the ethynyl group may result in a steric effect that minimizes the conjugation effect of these groups,[28] the electronic interaction between the electrons of the aryl substituents and the 2-ethynyl-6-(octyloxy)-naphthalene ring plays an important role in activating the π-conjugation.[29] Thus, we assumed that the ground-state absorption can be attributed to the local excitation of the 2-ethynyl-6-(octyloxy)naphthalene chromophore. The absorption peaks of compounds **3**, **4**, **6c** and **8** show little dependence on the solvent polarity which implies that the solvent stabilization of the ground state species is not significant.

The fluorescence emission spectra of the compounds **3**, **4**, **6c** and **8** (Fig. 9) were recorded in the same solvents (dioxane, chloroform, ethanol and acetonitrile) and in the solid-state using excitation wavelength at 343 nm. Table 3 summarizes the emission maxima, Stokes' shift and quantum yield (ϕ) in the studied solvents and in the solid-state. The results show that all compounds emitted violet-blue light in solution and in the solid state. We observed constant emission band profiles from 290-350 nm range of excitation wavelength. The Stokes shift observed is very small (40-98 nm) suggesting similar geometry for the S_0 and S_1 states. All the fluorescence spectra are quite similar and the peaks appears at 350–550 nm with a hypsochromic shift produced in dioxane. The λ_{em} was shifted to longer wavelength (ca. 40 nm) when the aldehyde is the bearing group of the aryl ring. The spectra of the compounds in solution lose the characteristic of naphthalene fluorescence emission and show a broad and structureless emission which is solvent dependent. In the solid state the spectra are red-shifted and show some vibrational fine structure for isoxazoline **8**. The bands at 410 and 455 nm (Fig. 9 (D)) are assigned as solid-state bands and belong to crystal packings absent in solution.

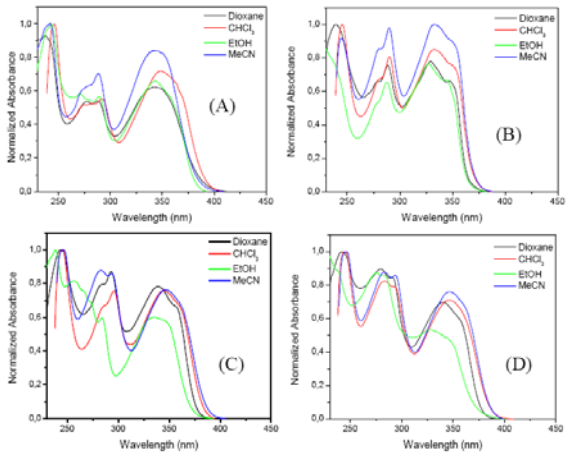

Fig. 8. Absorption spectra recorded in diferent solvents. Compounds: (A) aldehyde **3**, (B) oxime **4**, (C) esters **6c** and (D) **8**.

Table 3. Absorption and emission data of compounds **3**, **4**, **6c** and **8** in different solvents and in the solid-state (S-s).

Entry	Solvent	Absorption peaks (nm)	λ_{em} [(a)] (nm)	Stokes' shift/nm	ϕ[(b)]
3	Dioxane	243.5, 289.0, 343.5	384.4	40.9	0.20
	$CHCl_3$	246.5, 292.0, 349.5	440.6	91.1	0.11
	MeCN	242.0, 288.0, 343.4	441.6	93.7	0.17
	EtOH	237.0, 288.5, 342.0	423.6	98.2	
	S-s[c]	403.8	466.8	63.0	-
4	Dioxane	239.0, 288.5, 329.5	380.2	50.7	0.30
	$CHCl_3$	245.5, 290.5, 333.0	398.0	65.0	0.29
	MeCN	244.5, 290.0, 332.2	397.6	65.4	0.21
	EtOH	221.0, 287.5, 327.5	417.0	89.5	0.25
	S-s[c]	396.8	446.0	49.2	-
6c	Dioxane	243.5, 293.5, 339.5	398.8	59.3	0.70
	$CHCl_3$	245.5, 296.0, 344.0	418.4	74.4	0.10
	MeCN	238.5, 284.0, 341.5	412.8	71.3	0.27
	EtOH	246.6, 294.0, 346.5	434.6	88.1	0.25
	S-s[c]	353.4	436.6	83.2	-
8	Dioxane	242.0, 291.0, 340.0	405.6	65.6	0.47
	$CHCl_3$	245.0, 289.0, 346.5	412.2	65.7	0.17
	MeCN	246.5, 294.0, 346.5	409.0	62.5	0.18
	EtOH	285.0, 345.0	418.8	73.8	0.40
	S-s[c]	373.8	432.2	58.4	

a. λ_{ex} = 343 nm. b. Relative to quinine sulfate in 0.1 M H_2SO_4 as a standard (λ_{ex} = 343 nm, ϕ = 0.55). c. Solid-state.

Quantum yields have been measured in all solvents relative to quinine sulfate showing that efficiency is comparable to this standard but were found to be quite inferior to the 1-(phenylethynyl)naphthalene in cyclohexene (0.80).[30] As expected, the quantum yields of the esters **6c** and **8** were significantly larger than the analogous aldehyde **3** and oxime **4**. The ϕ of ester **6c** (70 %) is very high in dioxane. The ϕ of ester **8** (47 %) was also high and we envisage that the ϕ might be even larger in the solid-state for future organic light-emitting diodes (OLEDs) applications.

The photostability of these compounds was determined using the protocol established by Cho.[31] The control experiments were performed using a $CHCl_3$ solution of ester **6c**. The mixture was monitorated at 296 nm and 343 nm during six months maintaning the sample at 0°C. After this period, solution of **6c** became unstable as seen clearly by the changes in the UV spectrum described in Figure 10 which indicates that side reactions such as hydrolysis can occur. This photochemical behaviour was found for all the esters **6a-d** and **8**.

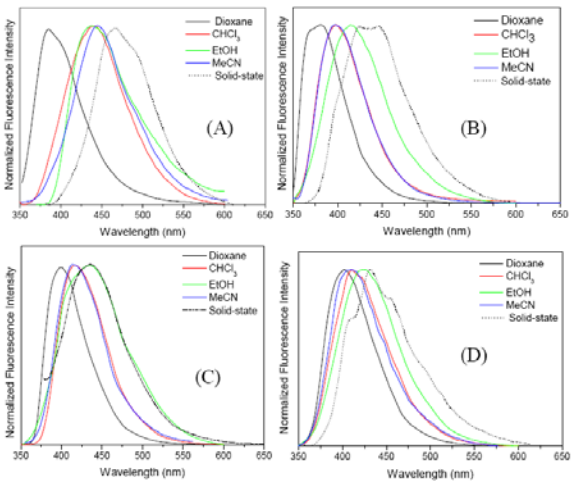

Fig. 9. Fluorescence emission spectra recorded in diferent solvents. Compound: (A) aldehyde **3**, (B) oxime **4**, (C) esteres **6c** and (D) **8**.

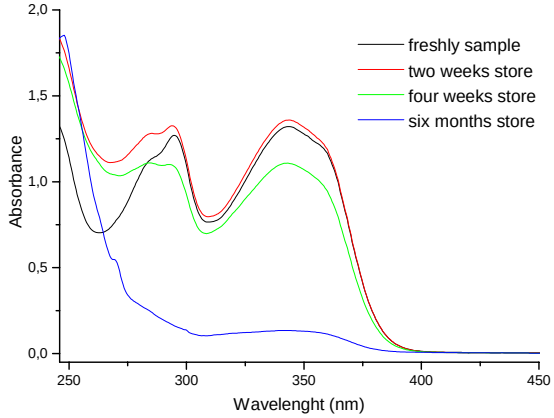

Fig. 10. UV-vis absorption spectra of 6c in different period of the time.

Experimental

Instruments and Techniques

Hydroxylamine hydrochloride, *N*-chlorosuccinimide (NCS), sodium acetate, ethanol, 4-bromobenzaldehyde, copper(I) iodide, triphenylphosphine, 1,3-dicyclohexylcarbodiimide (DCC) and 4-(*N*,*N*-dimethylamino)pyridine (DMAP) were used without further purification from Aldrich. Triethylamine (NEt_3) was distilled over potassium hydroxide. Tetra-hydrofuran (THF) was dried over sodium metal-benzophenone and distilled immediately before use. Anhydrous sodium sulphate (Na_2SO_4) was used to dry organic extracts. The *p*-*n*-alkoxybenzoic acids were prepared according to references 13 and 18. Bis-(triphenylphosphine) palladium (II) chloride [$PdCl_2(PPh_3)_2$] was prepared following the procedure reported by King and Negishi.[32] The melting points and mesophase transition temperatures and textures of the samples were measured on a Mettler Toledo FP82HT Hot Stage FP90 Central Processor and DSC 2910 TA Instruments. Nuclear magnetic resonance spectra were obtained on a Varian 300 MHz instrument. Chemical shift are given in parts per million (δ) and are referenced from tetramethylsilane (TMS). ATR/FTIR were recorded on a Varian 640-IR spectrometer (cm^{-1}). The DSC analyses were obtained on a DSC 2910 TA Instruments. Elemental analyses (CHN) were performed by Perkin-Elmer model 2400 CHN. UV vis absorption spectra were performed on a Perkin-Elmer model Lambda 16. Fluorescence emission and excitation spectra were measured in a Hitachi spectrofluorometer model F-4500. Spectrum correction was performed to enable measuring of a true spectrum by eliminating instrumental response such as wavelength characteristics of the monochromator or detector using rhodamine B as an internal standard (quantum counter). All experiments were performed at room temperature. The X-Ray diffraction experiments were realized with the X`Pert-PRO (PANalytical) diffractometer system using the linear monochromatic Cu $K\alpha_1$ beam (λ = 1.5405 Å), with an applied power of 1.2kVA. The scans were performed in continuous mode from 2° to 30° (2θ angle) and the diffracted radiation collected with the X'Celerator detector. The samples consist of a little amount of powder of the compounds on a glass plate and then placed in the diffractometer chamber on the TCU2000 - Temperature Control Unit (Anton Paar), which allows a precise control of the sample temperature during de measurement. The samples were submitted to heating and cooling cycles and the patterns collected at specific temperatures according to the transitions observed by POM and DSC. We used a rate of 10 °C/min. and waited 1 min. after each heating/cooling step.

Synthesis

2-Ethynyl-6-octyloxynaphthalene (1). This compound was prepared according to previous report.[12] Yield: 3.00 g (69%) as a white solid; mp 36

^{o}C; ν_{max}/cm^{-1} 3301 (≡C-H), 2939 (C-H_{ar}), 2921, 2852 (C-H_{alk}), 2102 (C≡C), 1625, 1600 (C=C_{ar}), 1469 (C=C_{ar}), 1390, 1226, 1041, 846, 812, 722 and 646; δ_H (300 MHz; $CDCl_3$; Me_4Si) 0.89 (m, 3H, CH_3), 1.40 (m, 10H, $(CH_2)_5$), 1.83 (m, 2H, CH_2CH$_2$O), 3.10 (s, 1H, HC≡C), 4.04 (t, *J* = 6.6 Hz, 2H, CH_2O), 7.07 (d, *J* = 2.4 Hz, 1H, Ar), 7.15 (dd, *J* = 9.0, 2.4 Hz, 1H, Ar), 7.47 (dd, *J* = 8.4, 1.5 Hz, 1H, Ar), 7.65 (m, 2H, Ar), 7.93 (s, 1H, Ar); δ_C (75 MHz; $CDCl_3$; Me_4Si) 14.1, 22.6, 26.1, 29.1, 29.2, 29.3, 31.8, 68.1, 76.6, 84.2, 106.4, 116.7, 119.7, 126.7, 128.1, 129.0, 129.2, 132.1, 134.4, 157.9.

4-[(6-Octyloxynaphthalen-2-yl)ethynyl]benzaldehyde (3). *Sonogashira's coupling.* A one-neck round-bottom flask equipped with septum stoppers was charged with NEt_3 (20 mL), 4-bromobenzaldehyde (0.8 mmol) and the alkyne (1.2 mmol) under argon atmosphere. The suspension was stirred for 30 min and then copper(I) iodide (CuI) (1.2 x 10^{-5} mol), triphenylphosphine (PPh_3) (4.0 x 10^{-5} mol) and *bis*-(triphenylphosphine)palladium (II) chloride [$PdCl_2(PPh_3)_2$] (0.8 x 10^{-5} mol) were then added. The mixture was heated under reflux for 48 h. After the solution to reach room temperature the solid was filtered through a Celite® pad and washed with diethyl ether. The filtrate was extracted with distilled H_2O (4 x 20 mL) and the organic extracts were dried (Na_2SO_4) and evaporated off. The solid was recrystallized twice from ethanol affording the product. Yield: 1.55 g (53%) as a yellow solid; mp 107.5 ^{o}C; ν_{max}/cm^{-1} 2955 (C-H_{ar}), 2919, 2871, 2850, 1690 (C=O), 1605 (C=C_{ar}), 1465 (C=C_{ar}), 1255, 1025, 860, 825, 720 and 666; δ_H (300 MHz; $CDCl_3$; Me_4Si) 0.89 (m, 3H, CH_3), 1.40 (m, 10H, $(CH_2)_5$), 1.86 (m, 2H, CH_2CH$_2$O), 4.08 (t, *J* = 6.6 Hz, 2H, CH_2O), 7.15 (m, 2H, Ar), 7.55 (m, 1H, Ar), 7.72 (m, 4H, Ar), 7.87 (d, *J* = 8.1 Hz, 2H, Ar), 8.00 (s, 1H, Ar), 10.02 (s, 1H, CHO); δ_C (75 MHz; $CDCl_3$; Me_4Si) 14.1, 22.6, 26.0, 29.1, 29.2, 29.3, 31.8, 68.0, 88.2, 94.3, 106.5, 117.0, 119.8, 126.9, 128.2, 128.7, 129.3, 129.5, 129.8, 131.7, 131.9, 134.5, 135.1, 158.1, 191.3.

4-[(6-octyloxynaphthalen-2-yl)ethynyl]benzaldehyde oxime (4). To alkylated product (23 mmol) and hydroxylamine hydrochloride (68 mmol) was added 40 mL of ethanol. The reaction mixture was stirred for 10 minutes and then sodium acetate (90 mmol) in distilled water (20 mL) was added. The mixture was heated at reflux during 1 hour. The reaction mixture was cooled and the white crystals were filtered off, washed with 50 mL of EtOH/H_2O mixture (15:35 mL) and dried under a reduced pressure. Yield: 1.45 g (94%) as a yellow solid; mp 150.8 ^{o}C; ν_{max}/cm^{-1} 2955 (C-H_{ar}), 2920, 2871, 2850, 1602 (C=C_{ar}), 1596 (C=N, shoulder), 1465 (C=C_{ar}), 1255, 1025, 860, 833 (N-O), 825, 720 and 666; δ_H (300 MHz; $CDCl_3$; Me_4Si) 0.89 (m, 3H, CH_3), 1.40 (m, 10H, $(CH_2)_5$), 1.85 (m, 2H, CH_2CH$_2$O), 4.01 (t, *J* = 6.6 Hz, 2H, CH_2O), 7.13 (m, 2H, Ar), 7.54 (m, 5H, Ar), 7.69 (t, *J* = 9.0 Hz, 2H, Ar), 7.98 (s, 1H, Ar), 8.15 (s, 1H, C*H*NOH); δ_C (75 MHz; $CDCl_3$/DMSO-d_6; Me_4Si) 13.0, 21.4, 24.8, 27.9, 28.0, 28.1, 30.5, 66.8, 87.7, 90.3, 105.4, 116.3, 118.7, 125.4, 125.8, 127.0, 127.6, 128.1, 129.4, 130.0, 130.5, 131.8, 133.1, 146.7, 156.8.

***p-n*-Alkoxybenzoic acid 5a-d.** These compounds were prepared according to reference 13 and 18.

Benzaldehyde *O*-benzoyloximes 6a-d. *The general protocol*. Oxime **3** (4.4 mmol) and *p-n*-alkoxybenzoic acid (4.4 mmol) were suspended in dry THF (30 mL) and stirring for 15 min under argon atmosphere. Then were added 1,3-dicyclohexylcarbodiimide (DCC) (6.6 mmol) and 4-(*N,N*-dimethylamino)pyridine (DMAP) (0.58 mmol). The reaction mixture was stirred for 24 h at room temperature. The white precipitate was filtered off and washed with THF. The solvent from the filtrate was evaporated and the solid was washed with diethyl ether and ethanol affording the pure product.

(*E*)-4-[(6-Octyloxynaphthalen-2-yl)ethynyl]benzaldehyde *O*-4-heptyloxybenzoyl oxime (6a). Yield: 155 mg (23%) as a white solid; mp 139.3 ^{o}C; found: C, 79.83; H, 8.03; N, 2.32%. $C_{41}H_{47}NO_4$ (617.83) requires C, 79.71; H, 7.67; N 2.27%; ν_{max}/cm^{-1} 2955 (C-H_{ar}), 2920, 2871, 2850, 1730 (C=O), 1605 (C=C_{ar}), 1600 (C=N, shoulder), 1510, 1465 (C=C_{ar}), 1350, 1310, 1255, 1090 (N-O-C), 1025, 860, 836 (N-OCO), 825, 760, 720, 690 and 666; δ_H (300 MHz; $CDCl_3$; Me_4Si) 0.88 (m, 6H, $(CH_3)_2$), 1.40 (m, 18H, $(CH_2)_9$), 1.79 (m, 4H, (CH_2CH$_2$O)$_2$), 4.02 (t, *J* = 6.3 Hz, 2H, CH_2O), 4.07 (t, *J* = 6.3 Hz, 2H, CH_2O), 6.95 (d, *J* = 9.0 Hz, 2H, Ar), 7.08-7.22 (m, 2H, Ar), 7.50-7.86 (m, 7H, Ar), 7.99 (s, 1H, Ar), 8.07 (d, *J* = 9.0 Hz, 2H, Ar), 8.53 (s, 1H, CHNO); δ_C (75 MHz; $CDCl_3$; Me_4Si) 14.1, 14.2, 22.6, 25.9, 26.1, 29.0, 29.2, 29.3, 29.4, 29.5, 29.6, 31.8, 31.9, 68.1, 68.2, 88.5, 92.9, 106.5, 107.4, 114.3, 117.4, 119.8, 120.3, 126.8, 126.9, 128.3, 128.8, 129.3, 129.7, 131.6, 131.8, 131.9, 134.4, 155.6, 158.0, 163.4, 163.7.

(*E*)-4-[(6-Octyloxynaphthalen-2-yl)ethynyl]benzaldehyde *O*-4-octyloxybenzoyl oxime (6b). Yield: 145 mg (20%) as a white solid; mp 132.9 ^{o}C; found: C, 79.55; H, 8.62; N 2.11%. $C_{42}H_{49}NO_4$ (631.86) requires C, 79.84; H, 7.82; N, 2.22%; ν_{max}/cm^{-1} 2955 (C-H_{ar}), 2920, 2871, 2850 (C-H_{alk}), 1730 (C=O), 1605 (C=C_{ar}), 1600 (C=N, shoulder), 1510, 1465 (C=C_{ar}), 1350, 1310, 1255, 1090 (N-O-C), 1025, 860, 836 (N-OCO), 825, 760, 720, 690 and 666; δ_H (300 MHz; $CDCl_3$; Me_4Si) 0.88 (m, 6H, $(CH_3)_2$), 1.40 (m, 20H, $(CH_2)_{10}$), 1.79 (m, 4H, (CH_2CH$_2$O)$_2$), 4.02 (t, *J* = 6.3 Hz, 2H, CH_2O), 4.07 (t, *J* = 6.3 Hz, 2H, CH_2O), 6.95 (d, *J* = 9.0 Hz, 2H, Ar), 7.08-7.22 (m, 2H, Ar), 7.50-7.86 (m, 7H, Ar), 7.99 (s, 1H, Ar), 8.07 (d, *J* = 9.0 Hz, 2H, Ar), 8.53 (s, 1H, CHNO); δ_C (75 MHz; $CDCl_3$; Me_4Si) 14.1, 14.2, 22.6, 25.9, 26.1, 29.0, 29.1, 29.2, 29.3, 29.4, 29.5, 29.6, 31.8, 31.9, 68.1, 68.2, 88.5, 92.9, 106.5, 107.4, 114.3,

117.4, 119.8, 120.3, 126.8, 126.9, 128.3, 128.8, 129.3, 129.7, 131.6, 131.8, 131.9, 134.4, 155.6, 158.0, 163.4, 163.7.

(*E*)-4-[(6-Octyloxynaphthalen-2-yl)ethynyl]benzaldehyde *O*-4-nonyloxybenzoyl oxime (6c). Yield: 163 mg (24%) as a white solid; mp 149.5 °C; found: C, 80.06; H, 7.93; N, 2.17%. $C_{43}H_{51}NO_4$ (645.88) requires C, 79.96; H, 7.96; N, 2.17%; ν_{max}/cm^{-1} 2955 (C-H_{ar}), 2920, 2871, 2850, 1730 (C=O), 1605 (C=C_{ar}), 1600 (C=N, shoulder), 1510, 1465 (C=C_{ar}), 1350, 1310, 1255, 1090 (N-O-C), 1025, 860, 836 (N-OCO), 825, 760, 720, 690 and 666; δ_H (300 MHz; $CDCl_3$; Me_4Si) 0.88 (m, 6H, $(CH_3)_2$), 1.40 (m, 22H, $(CH_2)_{11}$), 1.79 (m, 4H, $(CH_2CH_2O)_2$), 4.02 (t, *J* = 6.3 Hz, 2H, CH_2O), 4.07 (t, *J* = 6.3 Hz, 2H, CH_2O), 6.95 (d, *J* = 9.0 Hz, 2H, Ar), 7.08-7.22 (m, 2H, Ar), 7.50-7.86 (m, 7H, Ar), 7.99 (s, 1H, Ar), 8.07 (d, *J* = 9.0 Hz, 2H, Ar), 8.53 (s, 1H, CHNO); δ_C (75 MHz; $CDCl_3$; Me_4Si) 14.1, 14.2, 22.6, 22.7, 25.9, 26.1, 29.0, 29.1, 29.2, 29.3, 29.4, 29.5, 29.6, 31.8, 31.9, 68.1, 68.2, 88.5, 92.9, 106.5, 107.4, 114.3, 117.4, 119.8, 120.3, 126.8, 126.9, 128.3, 128.8, 129.3, 129.7, 131.6, 131.8, 131.9, 134.4, 155.6, 158.0, 163.4, 163.7.

(*E*)-4-[(6-Octyloxynaphthalen-2-yl)ethynyl]benzaldehyde *O*-4-decyloxybenzoyl oxime (6d). Yield: 165 mg (25%) as a white solid; mp 107.9 °C; found: C, 80.02; H, 7.85; N, 2.07%. $C_{44}H_{53}NO_4$ (659.91) requires C, 80.08; H, 8.10; N 2.12%; ν_{max}/cm^{-1} 2955 (C-H_{ar}), 2920, 2871, 2850, 1730 (C=O), 1605 (C=C_{ar}), 1600 (C=N, shoulder), 1510, 1465 (C=C_{ar}), 1350, 1310, 1255, 1090 (N-O-C), 1025, 860, 836 (N-OCO), 825, 760, 720, 690 and 666; δ_H (300 MHz; $CDCl_3$; Me_4Si) 0.88 (m, 6H, $(CH_3)_2$), 1.40 (m, 24H, $(CH_2)_{12}$), 1.79 (m, 4H, $(CH_2CH_2O)_2$), 4.02 (t, *J* = 6.3 Hz, 2H, CH_2O), 4.07 (t, *J* = 6.3 Hz, 2H, CH_2O), 6.95 (d, *J* = 9.0 Hz, 2H, Ar), 7.08-7.22 (m, 2H, Ar), 7.50-7.86 (m, 7H, Ar), 7.99 (s, 1H, Ar), 8.07 (d, *J* = 9.0 Hz, 2H, Ar), 8.53 (s, 1H, CHNO); δ_C (75 MHz; $CDCl_3$; Me_4Si) 14.1, 14.2, 22.6, 22.7, 25.9, 26.1, 29.0, 29.1, 29.2, 29.3, 29.4, 29.5, 29.6, 29.7, 31.8, 31.9, 68.1, 68.2, 88.5, 92.9, 106.5, 107.4, 114.3, 117.4, 119.8, 120.3, 126.8, 126.9, 128.3, 128.8, 129.3, 129.7, 131.6, 131.8, 131.9, 132.0, 134.4, 155.6, 158.0, 163.4, 163.7.

3-[4-(Octyloxy)phenyl]-4,5-dihydroisoxazole-5-carboxylic acid (7). This compound was prepared according to our previous report.[10e] Yield: 505 mg (66%) as a white solid; mp 143 °C; ν_{max}/cm^{-1} 2955, 2925, 2854, 1720 (C=O), 1610 (C=Car), 1600 (C=N), 1463 (C=Car), 1255, 1010, 860, 825, 720 and 666; δ_H (300 MHz; $CDCl_3$; Me_4Si) 0.89 (m, 3H, CH_3), 1.39 (m, 10H, $(CH_2)_5$), 1.79 (m, 2H, CH_2CH_2O), 3.63 (d, *J* = 9.0 Hz, 2H, CH_2CH), 3.98 (t, *J* = 6.6 Hz, 2H, CH_2O), 5.13 (t, *J* = 9.0 Hz, 1H, CH_2CH), 5.80 (b, 1H, OH), 6.90 (d, *J* = 8.7 Hz, 2H, Ar), 7.60 (d, *J* = 8.7 Hz, 2H, Ar); δ_C (75 MHz; $CDCl_3$/DMSO-d_6; Me_4Si) 13.7, 22.2, 25.6, 28.7, 28.8, 29.0, 31.4, 38.9, 67.7, 77.4, 114.3, 120.5, 128.1, 155.3, 160.5, 172.1.

(*E*)-4-[(6-Octyloxynaphthalen-2-yl)ethynyl]benzaldehyde *O*-3-(4-octyloxyphenyl)-4,5-dihydroisoxazole-5-carbonyl oxime (8). This compound was obtained by procedure similar to that used to prepare serie **6a-d**. Yield: 135 mg (30%) as a white solid; mp 110.4 °C; found: C, 77.19; H, 8.08; N, 3.82%. $C_{45}H_{52}N_2O_5$ (700.92) requires C, 77.11; H, 7.48; N, 4.00%; ν_{max}/cm^{-1} 2955 (C-H_{ar}), 2920, 2871, 2855, 1770 (C=O), 1605 (C=C_{ar}), 1596 (C=N, shoulder), 1515, 1465 (C=C_{ar}), 1350, 1310, 1255, 1187 (NO-CO), 1025, 1000 (C-ON isox.), 921 (CO-N isox.), 860, 836 (N-OCO), 825, 720, and 666; δ_H (300 MHz; $CDCl_3$; Me_4Si) 0.88 (m, 6H, $(CH_3)_2$), 1.40 (m, 20H, $(CH_2)_{10}$), 1.81 (m, 4H, $(CH_2CH_2O)_2$), 3.69 (dd, *J* = 16.8, 11.4 Hz, 1H, N=CC*H*HCH), 3.82 (dd, *J* = 16.8, 6.6 Hz, 1H, N=CCH*H*CH), 3.98 (t, *J* = 6.6 Hz, 2H, CH_2O), 4.08 (t, *J* = 6.3 Hz, 2H, CH_2O), 5.34 (m, 1H, CH_2CH), 6.92 (d, *J* = 9.0 Hz, 2H, Ar), 7.08-7.20 (m, 2H, Ar), 7.50-7.76 (m, 9H, Ar), 7.98 (s, 1H, Ar), 8.48 (s, 1H, CHNO); δ_C (75 MHz; $CDCl_3$/DMSO-d_6; Me_4Si) 14.1, 14.2, 22.7, 25.9, 26.0, 26.1, 29.0, 29.1, 29.2, 29.3, 29.4, 29.5, 31.8, 31.9, 39.4, 68.1, 68.2, 77.1, 88.3, 93.2, 106.5, 107.4, 114.7, 117.3, 119.9, 120.5, 126.9, 127.4, 128.3, 128.4, 128.5, 128.8, 129.3, 131.6, 131.9, 134.4, 155.8, 157.1, 158.1, 161.1, 167.9.

Conclusions

A novel series of thermal unstable aryl ethynylbenzalde-hyde *O*-benzoyloximes **6a-d** and **8** was synthesized and their LC and photophysical were evaluated. The heat-induced decomposition changed the mesomorphic behaviour. The thermal decomposition was analysed using DSC, X-ray, POM, ^{1}H NMR and IR data. The stability of these compounds was also checked by measuring the decrease in absorption of the *O*-benzoyloximes at 230-340 nm. For *O*-benzoyloximes **6a-d**, the smectic C and nematic phase were observed during the first heating. However, after heating, the samples displayed smectic A and nematic phases. The *O*-benzoyloximes **8** exhibits SmX followed by SmB in this heating/cooling cycles. The decomposition by heat of these compounds probably produced the nitrile correspondent as evidenced by IR and ^{1}H NMR spectra. In this sense, compound **10** was prepared and compared with the mixture produced during the "aging-heat" induced.

Acknowledgements

This work was supported by the Conselho Nacional de Desenvolvimento Científico, (MCT/CNPq Universal nº 471194/2008-5), PROCAD-CAPES, INCT-CMN. B. C. A. is an undergraduate student and thanks to CNPq-PIBIC-UFRGS for her fellowship. Thanks to FAPESC and Laboratório de Difração de Raios-X (LDRX-DF/UFSC) by the X-ray diffraction

experiments.

Notes and References

[a]Department of Organic Chemistry;
[b]Department of Physical Chemistry, Institute of Chemistry, UFRGS, Bento Gonçalves avenue, 9500, CEP 91501-970, Porto Alegre- RS, Brazil. Fax: 55 51 3308 7304; Tel: 55 51 3308 7316; E-mail: aloir@iq.ufrgs.br
[c]Department of Physics, UFSC, 88040-900 Florianópolis-SC, Brazil

†Electronic Supplementary Information (ESI) available: NMR ^{1}H and ^{13}C, ATR/FT-IR, DSC traces and LC texture figure. See DOI: 10.1039/b000000x/

1. (a) P. Mayer, K. C. Potgieter and T. I. A. Gerber, *Polyhedron*, 2010, **29**, 1423-1430. (b) S. Handa, V. Gnanadesikan, S. Matsunaga and M. Shibasaki, *J. Am. Chem. Soc.,* 2010, **132**, 4925-4934.
2. (a) S. Y. Doronin, N. M. Zadymova, V. Poteshnova, R. K. Chernova, A. A. Burgomistrova and N. A. Yurasov, *J. Anal. Chem*., 2010, **65**, 48-55. (b) K. Filipczak, J. Karolczak and M. Ziółek, *Photochem. Photobiol. Sci.*, 2009, **8**, 1603-1610.
3. (a) A. A. Merlo, H. Gallardo and T. R. Taylor, *Química Nova,* 2001, **24**, 354-362. (b) H. Pizzala, M. Carles, W. E. E. Stone and A. Thevand, *J. Chem. Soc. Perkin Trans. 2,* 2000, **5**, 935-939. (c) A. A. Merlo, P. R. Livotto, H. A. Gallardo and T. R. Taylor, *Mol. Cryst. and Liq. Cryst. Sci. and Techn. Sec. A-Mol. Cryst. and Liq. Cryst.,* 1998, **309**, 111-116.
4. (a) M. H. Abraham, J. G.-Lostes, J. E. C.-Muniz, W. S. Cain, C. F. Poole, S. N. Atapattu, R. J. Abraham and P. Leonardd, *New J. Chem*., 2009, **33**, 76-81. (b) P. A. Wood, R. S. Forgan, A. R. Lennie, S. Parsons, E. Pidcock, P. A. Tasker and J. E. Warren, *CrystEngComm*., 2008, **10**, 239-251. (c) D. L. de Murillas, R. Pinol, M. B. Ros, J. L. Serrano, T. Sierra and M. R. de la Fuente, *J. Mater. Chem.,* 2004, **14**, 1117-1127. (d) K. Kitahara, T. Toma, J. Shimokawa and T. Fukuyama, *Org. Lett.,* 2008, **10**, 2259-2261.
5. J.-L. Boucher, M. Delaforge and D. Mansuy, *Biochemistry,* 1994, **33**, 7811-7818.
6. (a) S. M. Johnson, H. M. Petrassi, H. E. Purkey, S. K. Palaninathan, N. N. Mohamedmohaideen, C. Nichols, K. P. Chiang, T. Walkup, J. C. Sacchettini, K. B. Sharpless and J. W. Kelly*, Med. Chem.*, 2005, **48**, 1576-1587. (b**)** P. De, Nonappa, K. Pandurangan, U. Maitra and S. Wailes, *Org. Lett.,* 2007, **9**, 2767-2770.
7. (a) A. Bassoli, G. Borgonovo, S. Caimi, L. Scaglioni, G. Morini, A. S. Moriello, V. Di Marzo and L. De Petrocellis, *Bioorganic & Medicinal Chemistry,* 2009, **17***,* 1636-1639. (b) D. Gamba, D. S. Pisoni, J. S. da Costa, C. L. Petzhold, A. C. A. Borges and M. A. Ceschi, *J. Braz. Chem. Soc.*, 2008, **19**, 1270-1276. (c) Q. A. R. de Almeida, M. L. O. Pereira, R. B. Coelho, E. M. de Carvalho, C. R. Kaiser, J. Jones Jr. and F. M. da Silva, *J. Braz. Chem. Soc.,* 2008, **19**, 894-902.
8. (a) S. Shrot, G. Markel, T. Dushnitsky, A. Krivoy, *NeuroToxicology*, **2009**, *30*, 167-173. (b) D. R. dos Santos, A. G. S. de Oliveira, R. L. Coelho, I. M. Begnini, R. F. Magnago and L. da Silva, *Arkivoc*, 2008, **xvii**, 157-166.
9. (a) A. V. Dubrovskiy and R. C. Larock*, Org. Lett.,* 2010, **12**, 1180-1183. (b) M. R. Almeida, G. G. Leitão, B. V. Silva, J. P. Barbosa and A. C. Pinto, *J. Braz. Chem. Soc.,* 2010, **21**, 764-769. (c) D. A. Alonso, C. Nájera, Mª C. Pacheco, *Adv. Synth. Catal*. 2002, **344**, 172-183. (d) S. N. Khattab, R. Subirós-Funosas, A. El-Faham and F. Albericio, *Eur. J. Org. Chem*. 2010, **2010**, 3275-3280.
10. (a) V. Bezborodov, N. Kauhanka and V. Lapanik, *Mol. Cryst. Liq. Cryst*., 2004, **411**, 1145-1152. (b) V. S. Bezborodov, N. N. Kauhanka, V. I. Lapanik and C. J. Lee, *Liq. Cryst*., 2003, **30**, 579-583. (c) D. C. Bruce, K. Heyns and V. Vill, *Liq. Cryst*., 1997, **23**, 813-819. (d) V. N. Kovganko and N. N. Kovganko, *Russian J. Org. Chem*., 2006, **42**, 430-434. (e) A. Tavares, P. H. Schneider and A. A. Merlo, *Eur. J. Org. Chem.,* 2009, **2009**, 889-897.
11. (a) K. Sonogashira, Y. Tohda and N. Hagihara, *Tetrahedron Lett.,* 1975, **16**, 4467-4470. (b) S. Takahashi, Y. Kuroyama, K. Sonogashira and N. Hagihara, *Synthesis*, 1980, 627-630. (c) R. Chinchilla and C. Nájera, *Chem. Rev*. 2007, **107**, 874-922.
12. (a) U. B. Vasconcelos and A. A. Merlo, *Synthesis,* 2006, **7**, 1141-1147. (b) U. B. Vasconcelos, G. D. Vilela, A. Schrader, A. C. A. Borges and A. A. Merlo, *Tetrahedron,* 2008, **64**, 4619-4626.
13. (a) S. I. Torgova, M. V. Petrov and A. Strigazzi, *Liq. Cryst*., 2001, **28**, 1439-1449. (b) A. L. Braga, D. S. Lüdtke, L. A. Wessjohann, M. W. Paixão and P. H. Schneider, *J. Mol. Catal. A* 2005, **229**, 47. (c) U. B. Vasconcelos, J. E. Braun, F. Ely, H. Gallardo and A. A. Merlo, *Liq. Cryst.*, 2000, **27**, 657-663.
14. B. Neises and W. Steglich, *Angew. Chem. Int. Ed. Engl*., 1978, **17**, 522-524.
15. (a) B. R. Cho, H. S. Chung and N. S. Cho, *J. Org. Chem.,* 1998, **63***,* 4685-4690. (b) B. R. Cho, W. J. Jang, J. T. Je and R. A. Bartsch, *J. Org. Chem.,* 1993, **58**, 3901-3904.
16. (a) S. Diele, S. Manke, W. Weibflog and D. Demus, *Liq. Cryst.,* 1989, **4**, 301-307. (b) M. Ragnolia, E. Puccia, M. Bertoluccia, B. Gallot and G. Galli, *J. Fluorine Chem.,* 2004, **125**, 283-292.
17. We have synthesized **10** using the Sonogashira protocol reacting **1** and **9** in 89% yield. The mesomorphic behaviour of **10** was analysed by DSC: *on heating* **Cr** 95.2 **N** 157.5 **I**; *on cooling* **I** 154.9 **N** 61.2 **Cr**. For related compounds see: (a) H.-F. Hsu, W.-C. Lin, Y.-H. Lai and S.-Y. Lin, *Liq. Cryst.*, 2003, **30**, 939-944. (b) M. Hird and K. J. Toyne, *Liq. Cryst.,* 1993, **14**, 741-761. (c) M. S. Wong and J.-F. Nicoud, *J. Chem. Soc., Chem. Commun*., 1994, 249-250.

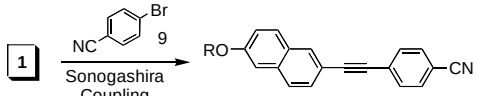

10 R = *n*-octyl

18. (a) W. Wan, C. Yang, H. Z. Jiang, H. M. Deng, J. Wang and J. Hao, *Liq. Cryst*., 2008, **35**, 665-673. (b) N. Gimeno, M. B. Ros, M. R. De la Fuente and J. L. Serrano, *Chem. Mater.,* 2008, **20***,* 1262-1271. (c) M. M. Naoum, G. R. Saad, R. I. Nessim, T. A. Abdel Aziz and H. Seliger, *Liq. Cryst*., 1997, **23**, 789-795. (d) D. Apreutesei and G. H. Mehl, *J. Mater. Chem*., 2007, **17**, 4711-4715.
19. (a) R. J. Birgeneau and J. D. Litster, *J. Physique Letters,* 1978, **39**, L-399-L-402. (b) Gou-Ping and Chang-Chien, *J. Polym. Sci. A,* 1998, **36**, 2849-2863.
20. M. J. Frisch, G. W. Trucks, H. B. Schlegel, G. E. Scuseria, M. A. Robb, J. R. Cheeseman, V. G. Zakrzewski, J. A. Montgomery, Jr., R. E. Stratmann, J. C. Burant, S. Dapprich, J. M. Millam, A. D. Daniels, K. N. Kudin, M. C. Strain, O. Farkas, J. Tomasi, V. Barone, M. Cossi, R. Cammi, B. Mennucci, C. Pomelli, C. Adamo, S. Clifford, J. Ochterski, G. A. Petersson, P. Y. Ayala, Q. Cui, K. Morokuma, D. K. Malick, A. D. Rabuck, K. Raghavachari, J. B. Foresman, J. Cioslowski, J. V. Ortiz, A. G. Baboul, B. B. Stefanov, G. Liu, A. Liashenko, P. Piskorz, I. Komaromi, R. Gomperts, R. L. Martin, D. J. Fox, T. Keith, M. A. Al-Laham, C. Y. Peng, A. Nanayakkara, M. Challacombe, P. M. W. Gill, B. Johnson, W. Chen, M. W. Wong, J. L. Andres, C. Gonzalez, M. Head-Gordon, E. S. Replogle, and J. A. Pople, *Gaussian, Inc*., Pittsburgh PA, 1998.
21. O. Altinbas, H. A. Dondas, H. Arslan, N. Külcü and C. Killner, *Z. Kristallogr.,* 2004, **219**, 379-380.
22. The LC textures are typical according to the reference (a) G. W. Gray and J. W. Goodby, *Smectic Liquid Crystals: Textures and Structures*, Leonard Hill, Glasgow and London, **1984**. (b) I. Dierking, *Texture of Liquid Crystals*, Wiley-VHC, **2003**. (c) D. Demus and L. Richter, *Texture of Liquid Crystals*, VEB, Leipzig, **1978**. (d) L. Li, C. D. Jones,

J. Magolan and R. P. Lemieux, *J. Mater. Chem.* 2007, **17**, 2313-2318. (e) K. Ayub, M. Moran, C. Lazar and R. P. Lemieux, *J. Mater. Chem.,* 2010, **20**, 6655-6661.
23. (a) W. Pyżuk, A. Krówczynsk and E. Górecka, *Mol Cryst. and Liq. Cryst.,* 1993, **237**, 75-84. (b) Y. Shimizu, K. Oikawa, K. Nakayama and D. Guillon, *J. Mater. Chem*., 2007, **17**, 4223-4229.
24. A. Tavares, P. R. Livotto, P. F. B. Gonçalves and A. A. Merlo, *J. Braz. Chem. Soc.,* 2009, **20**, 1742-1752.
25. J. Belmar, M. Parra, C. Zuñiga, G. Fuentes, M. Marcos and J. L. Serrano, *Liq. Cryst*., 1999, **26**, 9-15.
26. N. D. Marsh, C. J. Mikolajczak and M. J. Wornat, *Spectrochim. Acta*, *Part A*, 2000, **56**, 1499-1511.
27. F. Cataldo, *Polym. Degrad. Stab.*, 2004, **83**, 59-66.
28. R. Thomas, S. Lakshmi, S. K. Pati and G. U. Kulkarni, *J. Phys. Chem. B*, 2006, **110**, 24674-24677.
29. A recent report of a series of photophysical measurements of the parent species 6-methoxy-naphthalene-2-ethynylbenzaldehyde. H.-M. Guo and F. J. Tanaka, *J. Org. Chem.*, 2009, **72**, 2417-2424.
30. D. J. Keddie, K. E. Fairfull-S and S. E. Bottle, *Org. Biomol. Chem*., 2008, **6**, 3135-3143.
31. B. R. Cho, K. D. Kim, J. C. Lee and N. S. Cho, *J. Am. Chem. Soc.,* 1988, **10**, 6145-6148.
32. A. O. King and E. Negishi, *J. Org. Chem*., 1978, **43**, 358-360.

SUPPORTING INFORMATION – CAPÍTULO 6.1

Thermal Elimination of *O*-Benzoyloximes. Consequences on the Chemical Stability and Mesomorphic Behaviour

Aline Tavares,[a] Bárbara C. Arruda,[a] Elvis S. Boes,[b] Valter Stefani,[a] Hubert K. Stassen,[b] Leandra F. Campo,[a] Ivan H. Bechtold,[c] and Aloir A. Merlo*[a]

Instituto de Química, UFRGS. Av. Bento Gonçalves, 9500. Agronomia. 91501-970, Porto Alegre, RS – Brasil.

^{1}H, ^{13}C RMN and ATR/FT-IR data

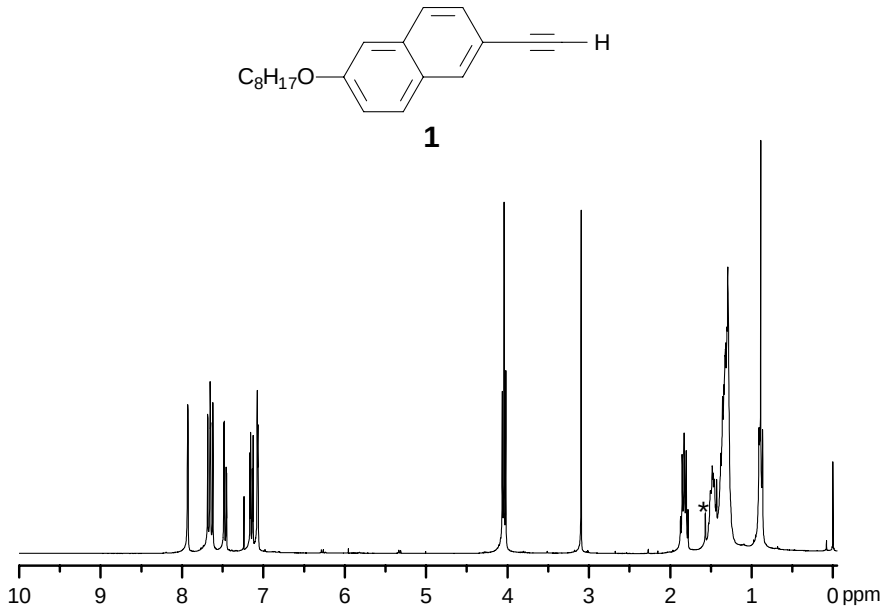

Figure 1. ^{1}H NMR spectrum of compound **1** ($CDCl_3$, 300 MHz). *Solvent impurity.

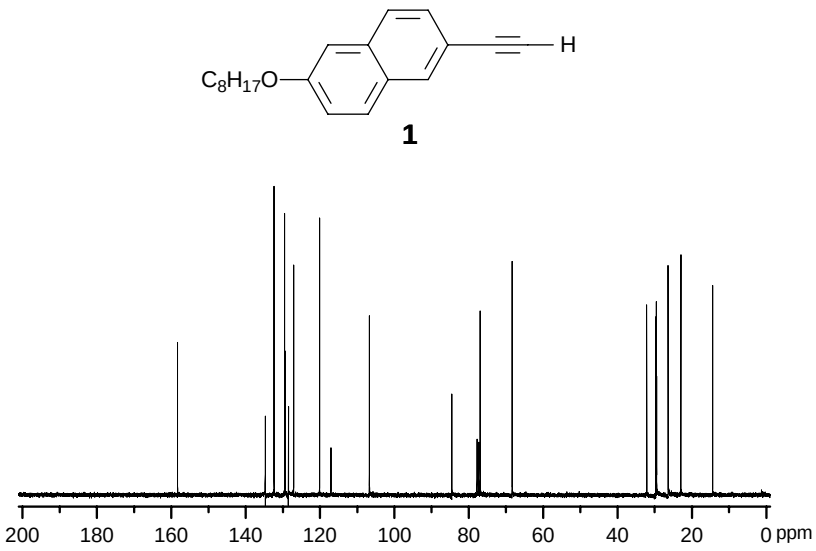

Figure 2. ^{13}C NMR spectrum of compound **1** ($CDCl_3$, 75 MHz).

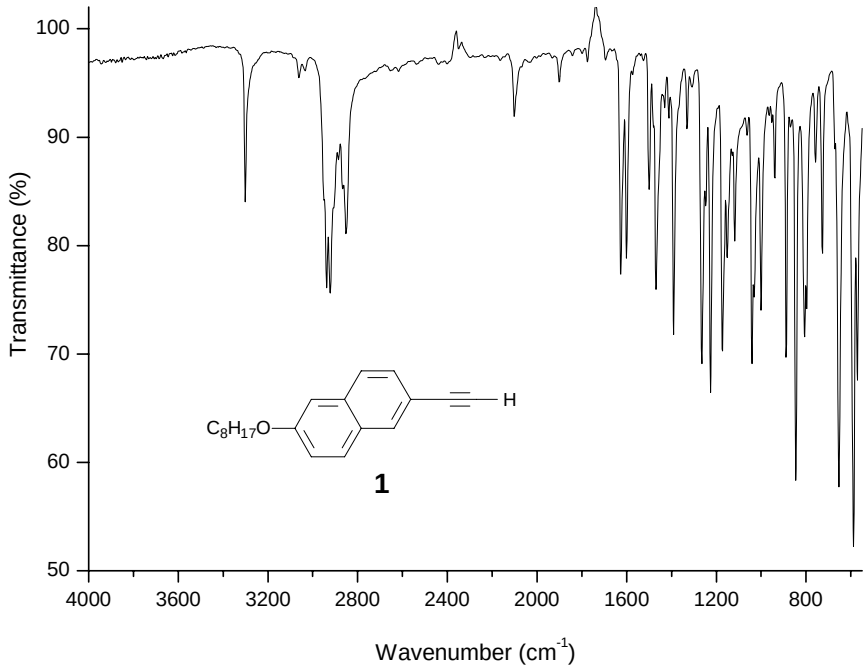

Figure 3. ATR/FT-IR absorption spectrum of compound **1**.

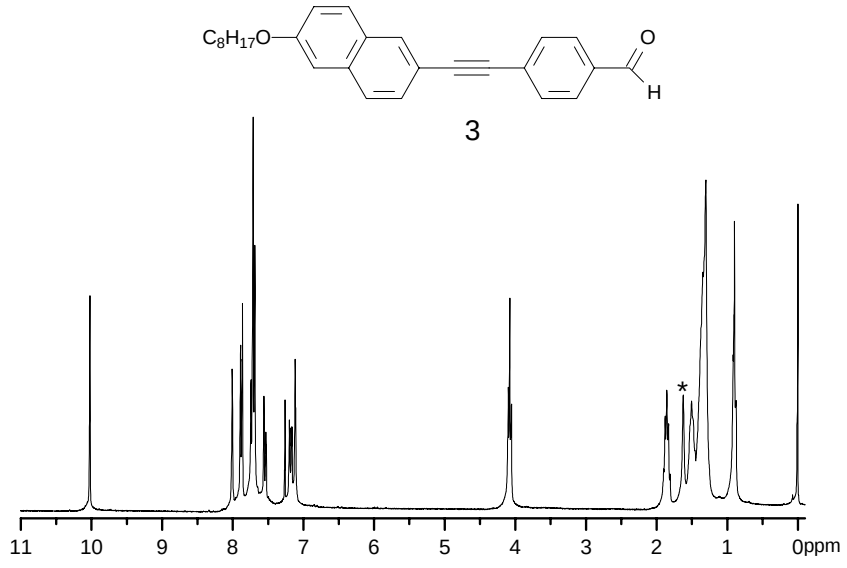

Figure 4. ^{1}H NMR spectrum of compound **3** ($CDCl_3$, 300 MHz). *Solvent impurity.

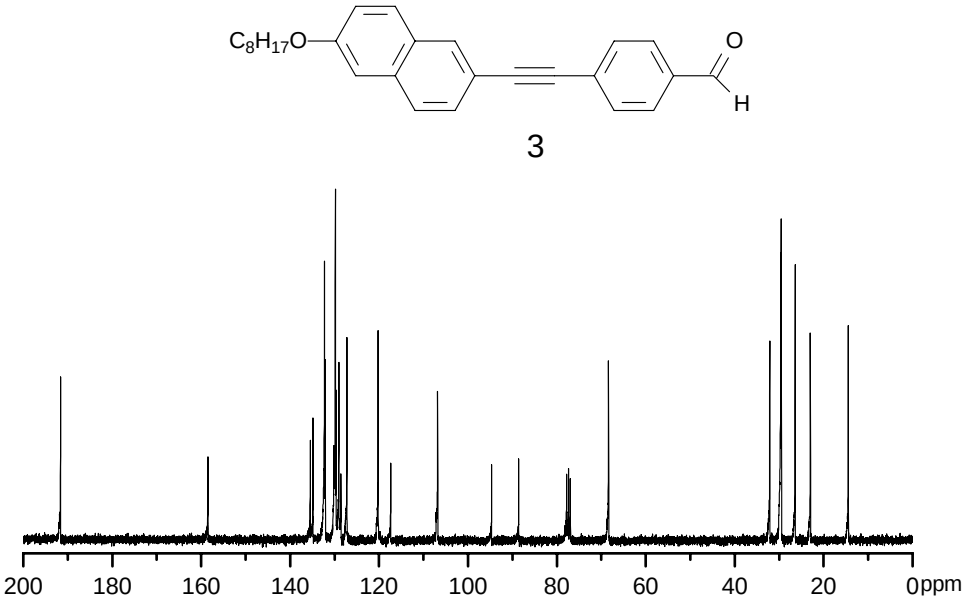

Figure 5. ^{13}C NMR spectrum of compound **3** ($CDCl_3$, 75 MHz).

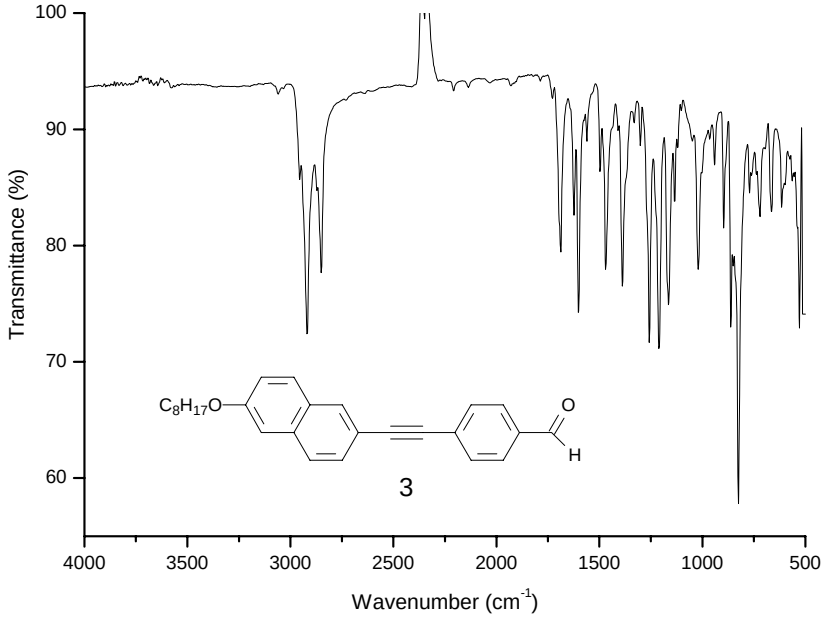

Figure 6. ATR/FT-IR absorption spectrum of compound **3**.

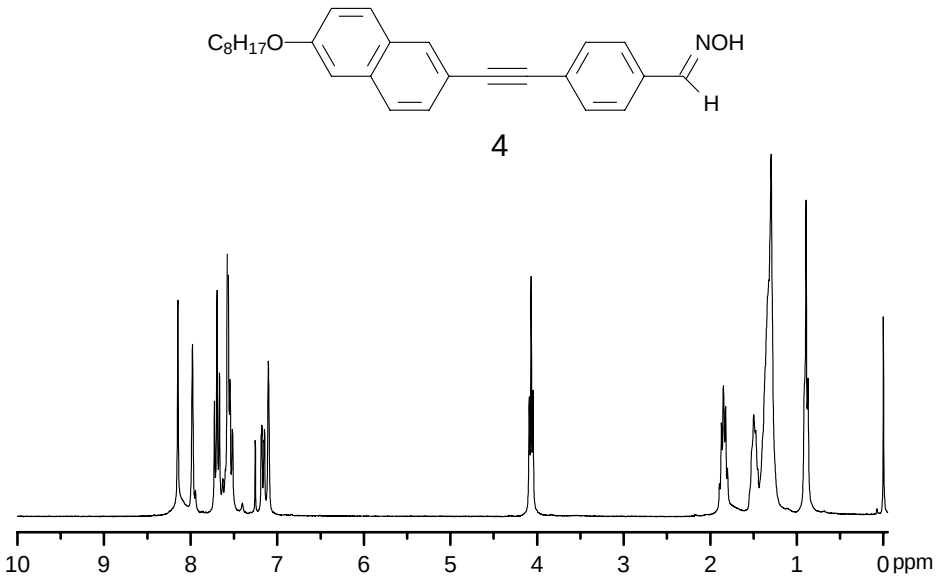

Figure 7. ^{1}H NMR spectrum of compound **4** ($CDCl_3$, 300 MHz).

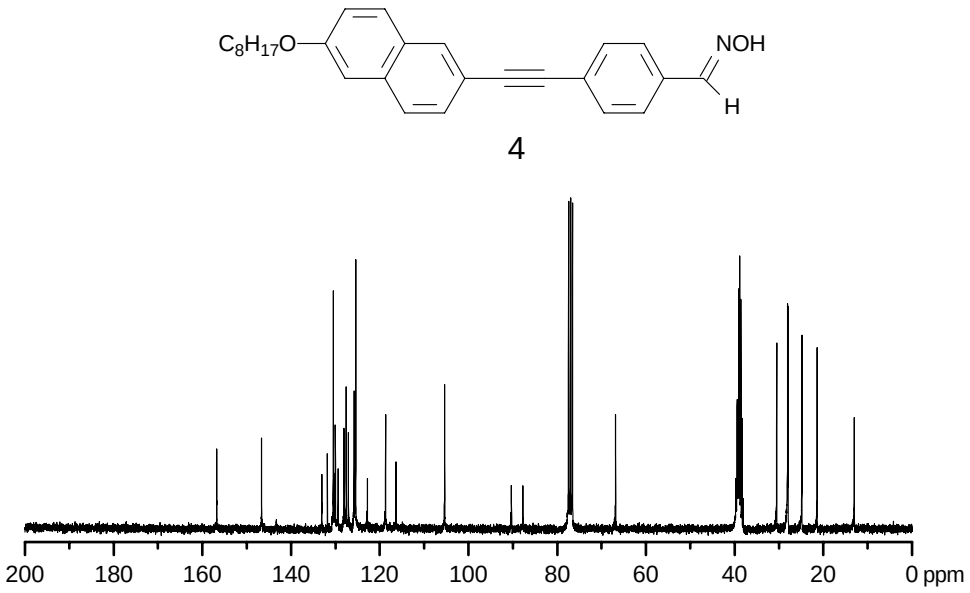

Figure 8. ^{13}C NMR spectrum of compound **4** ($CDCl_3$/DMSO-d_6, 75 MHz).

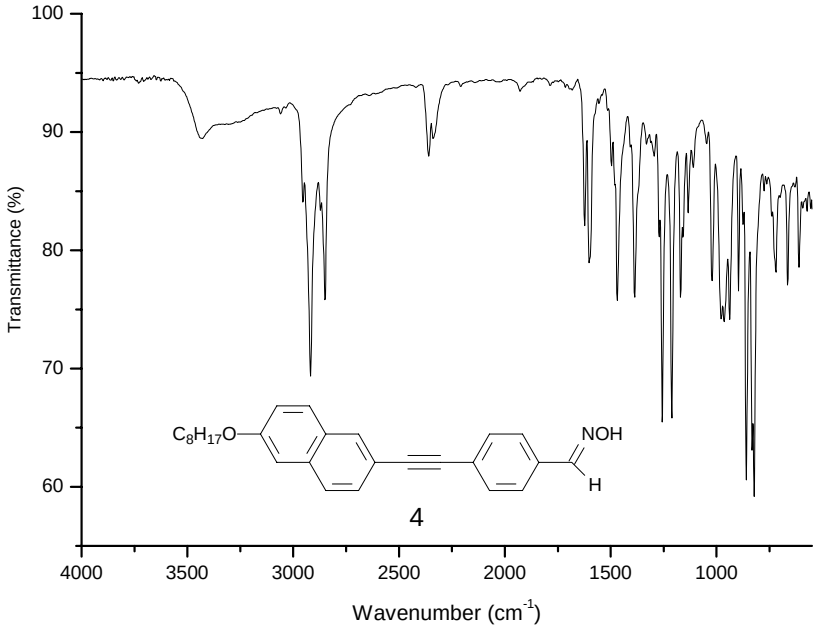

Figure 9. ATR/FT-IR absorption spectrum of compound **4**.

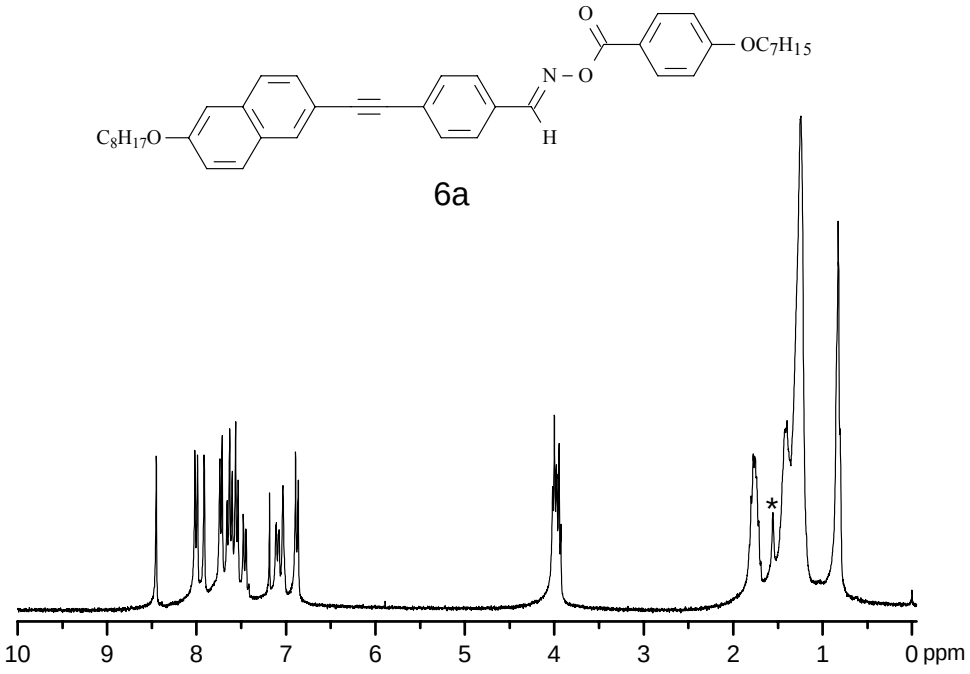

Figure 10. ^{1}H NMR spectrum of compound **6a** ($CDCl_3$, 300 MHz). *Solvent impurity.

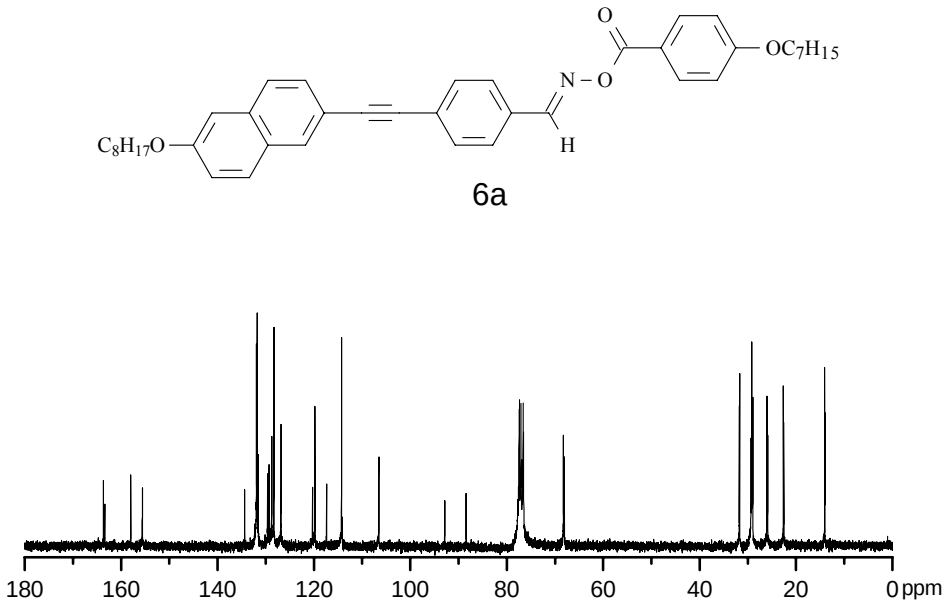

Figure 11. ^{13}C NMR spectrum of compound **6a** ($CDCl_3$, 75 MHz).

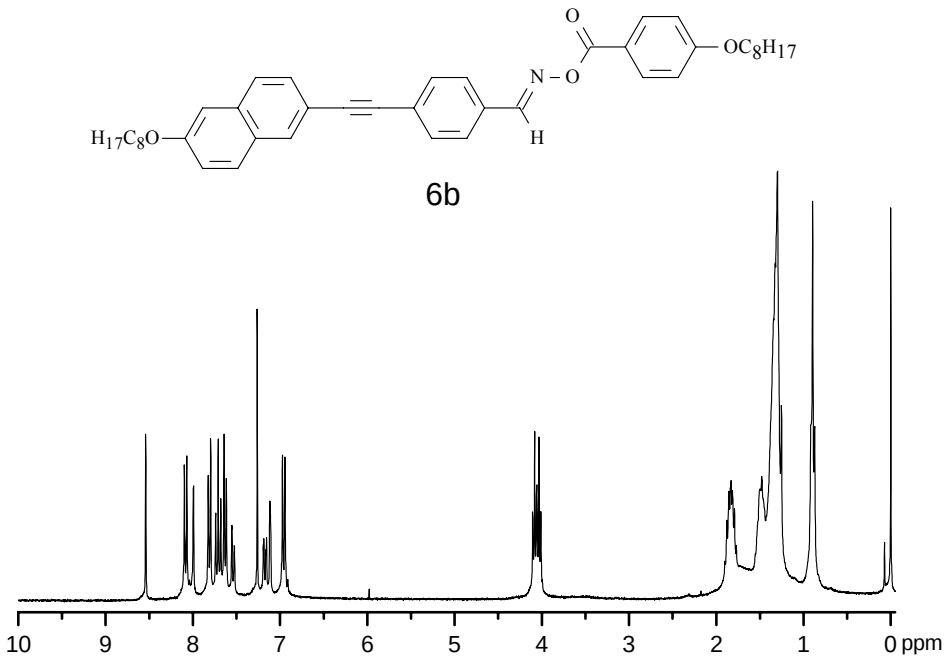

Figure 12. ^{1}H NMR spectrum of compound **6b** ($CDCl_3$, 300 MHz).

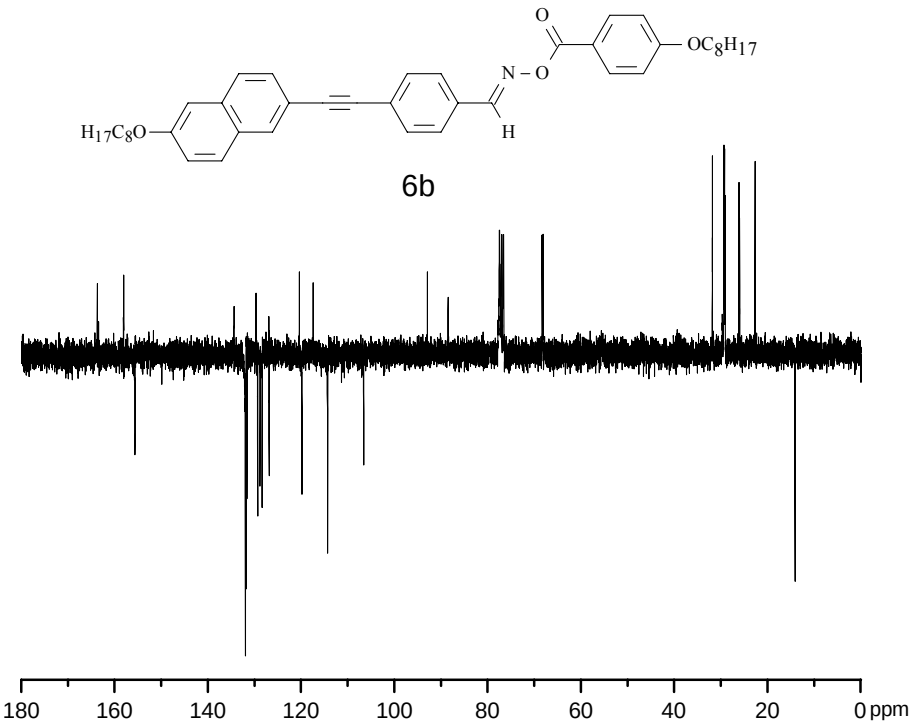

Figure 13. ^{13}C NMR spectrum of compound **6b** ($CDCl_3$, 75 MHz).

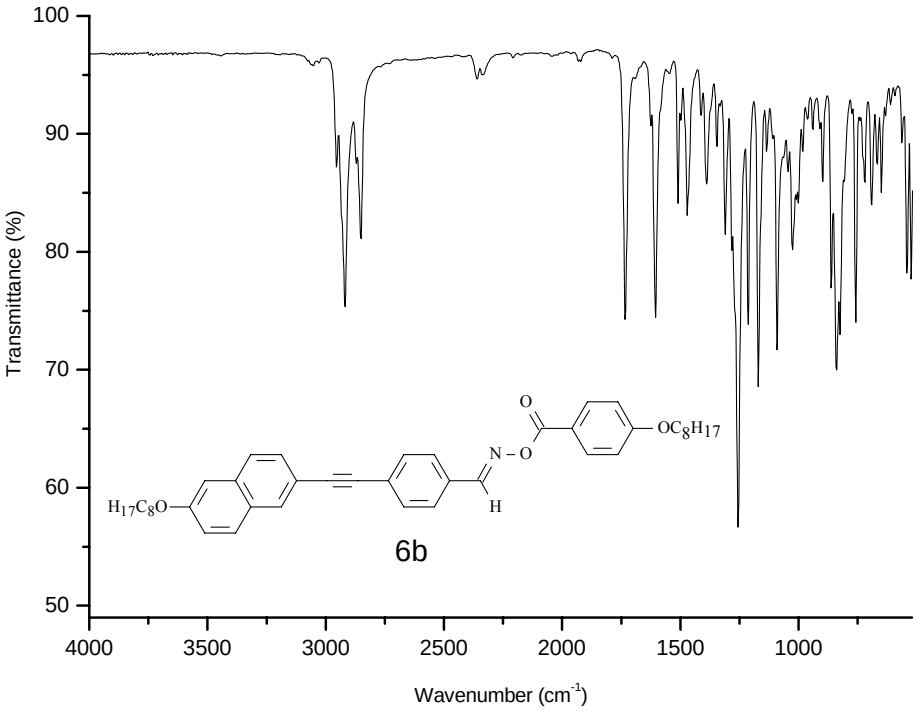

Figure 14. ATR/FT-IR absorption spectrum of compound **6b**.

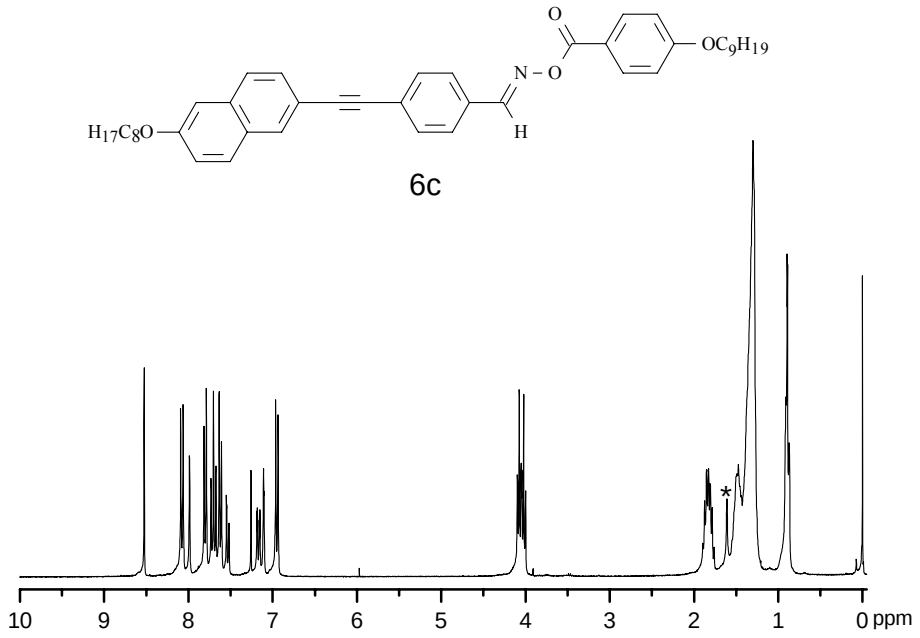

Figure 15. ^{1}H NMR spectrum of compound **6c** ($CDCl_3$, 300 MHz). *Solvent impurity.

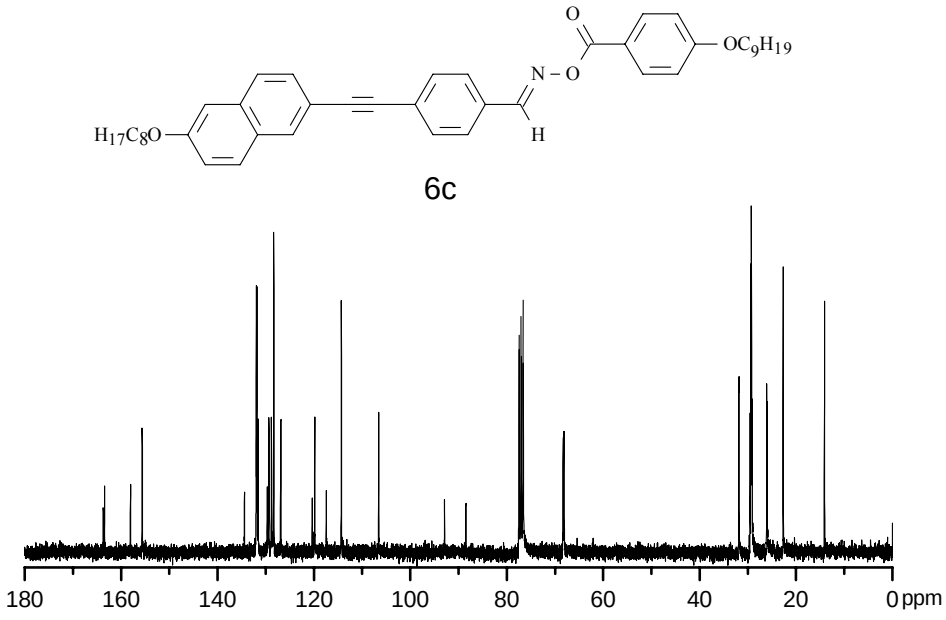

Figure 16. ^{13}C NMR spectrum of compound **6c** ($CDCl_3$, 75 MHz).

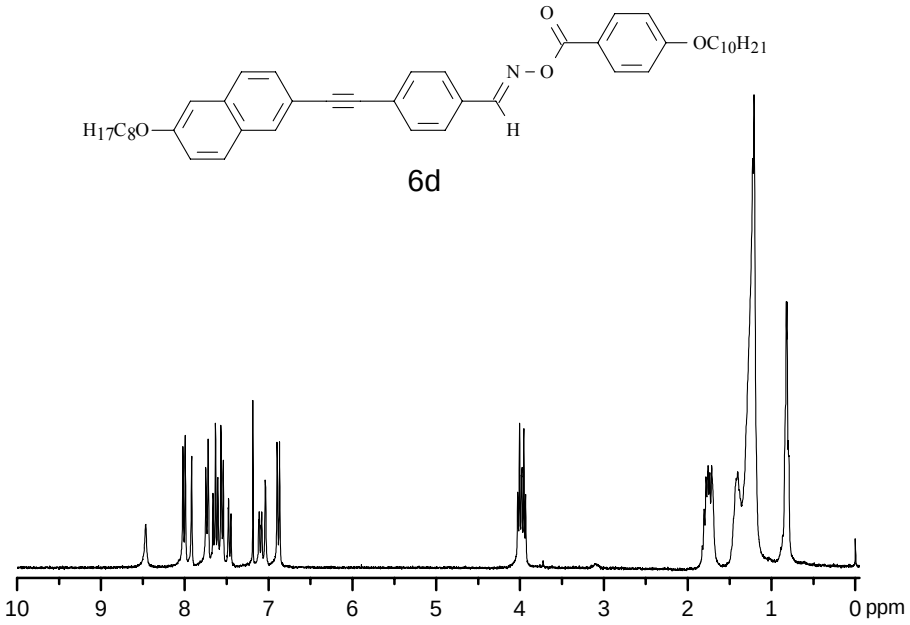

Figure 17. ^{1}H NMR spectrum of compound **6d** ($CDCl_3$, 300 MHz).

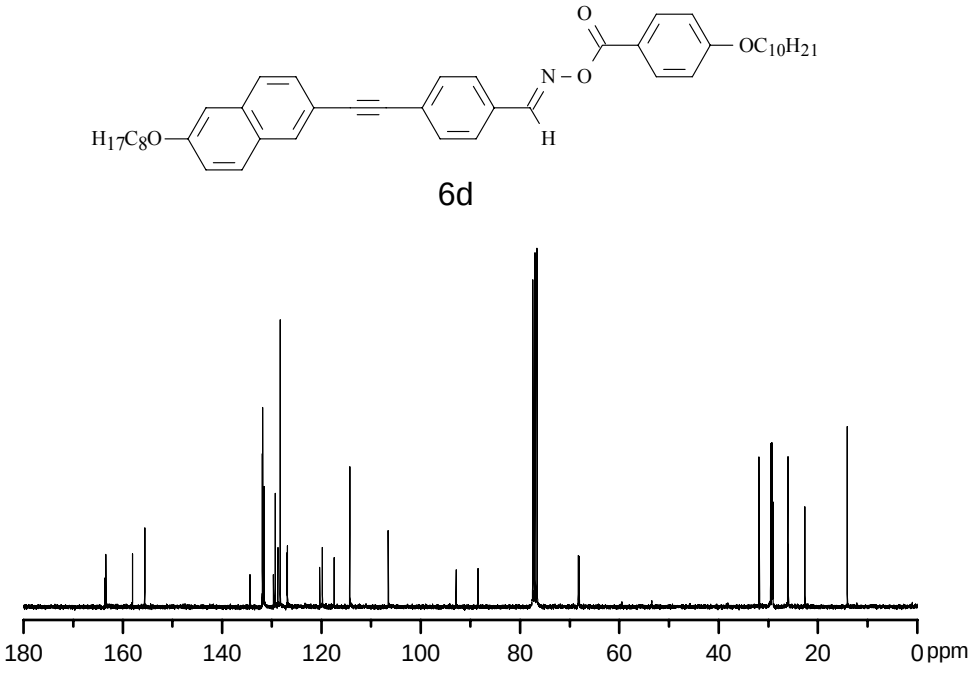

Figure 18. ^{13}C NMR spectrum of compound **6d** ($CDCl_3$, 75 MHz).

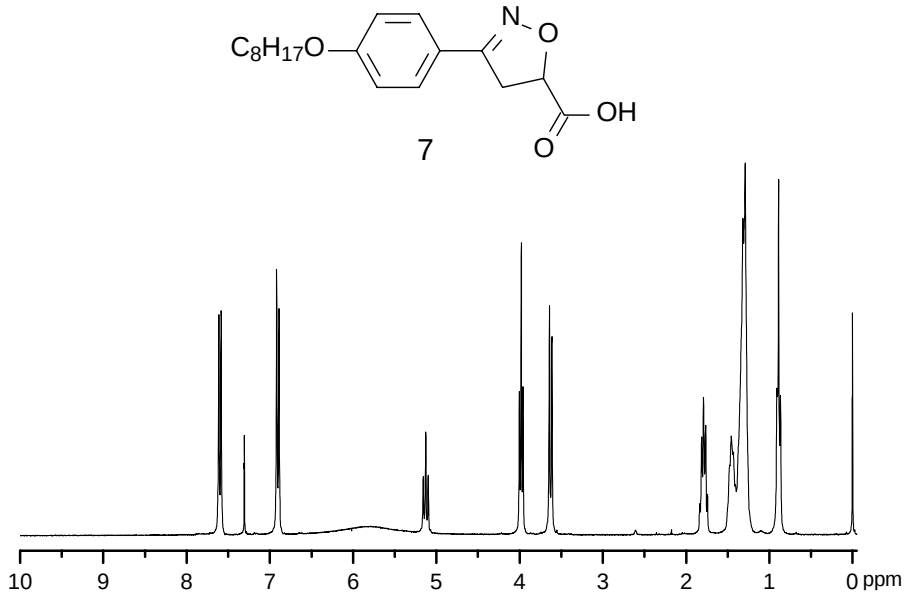

Figure 19. ^{1}H NMR spectrum of compound **7** ($CDCl_3$, 300 MHz).

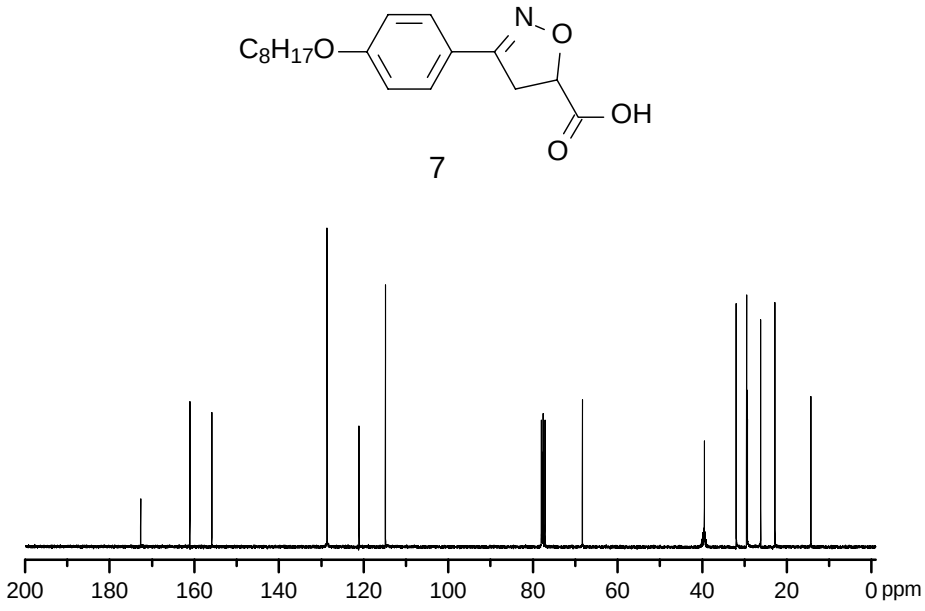

Figure 20. ^{13}C NMR spectrum of compound **7** ($CDCl_3$/DMSO-d_6, 75 MHz).

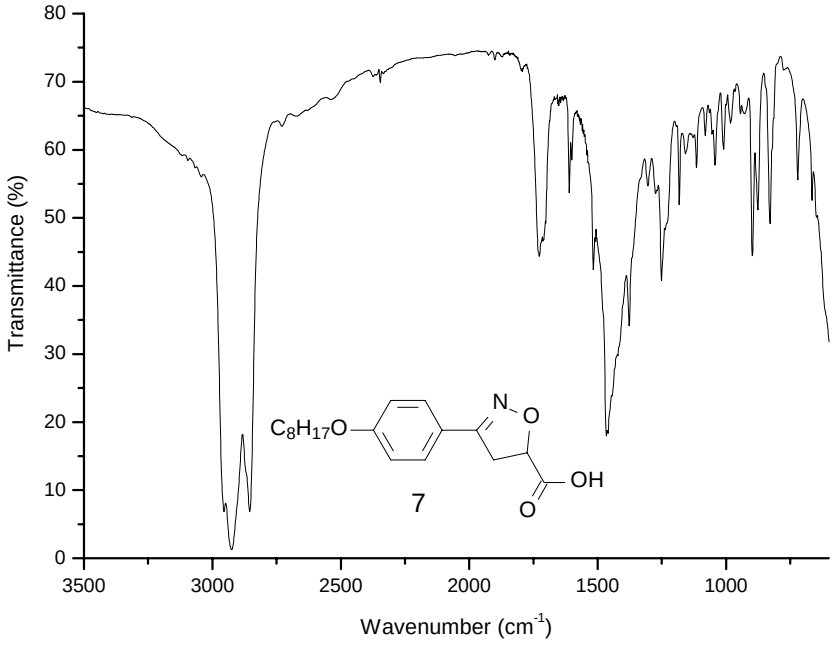

Figure 21. FT-IR absorption spectrum of compound **7** (nujol).

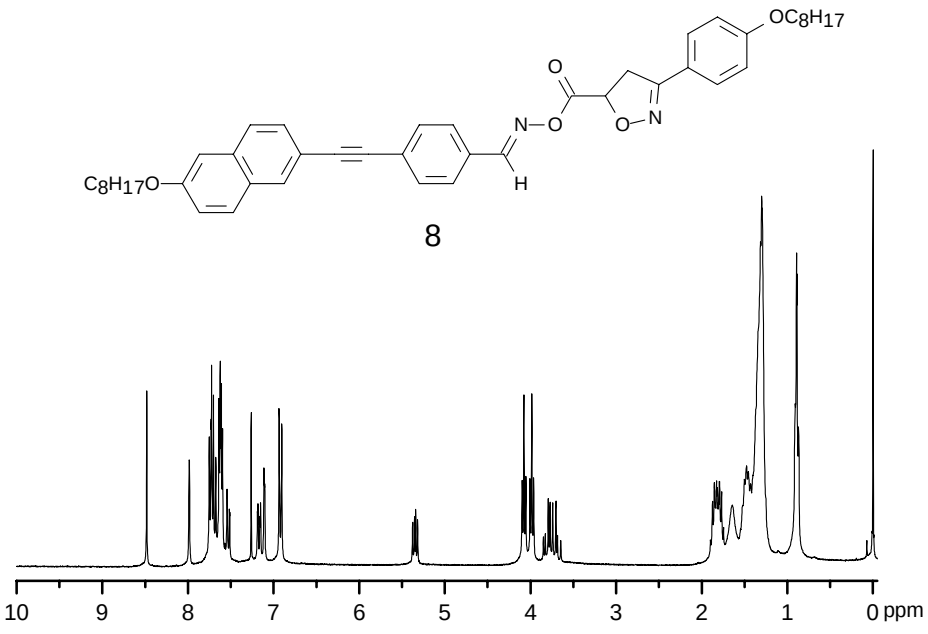

Figure 22. ^{1}H NMR spectrum of compound **8** ($CDCl_3$, 300 MHz).

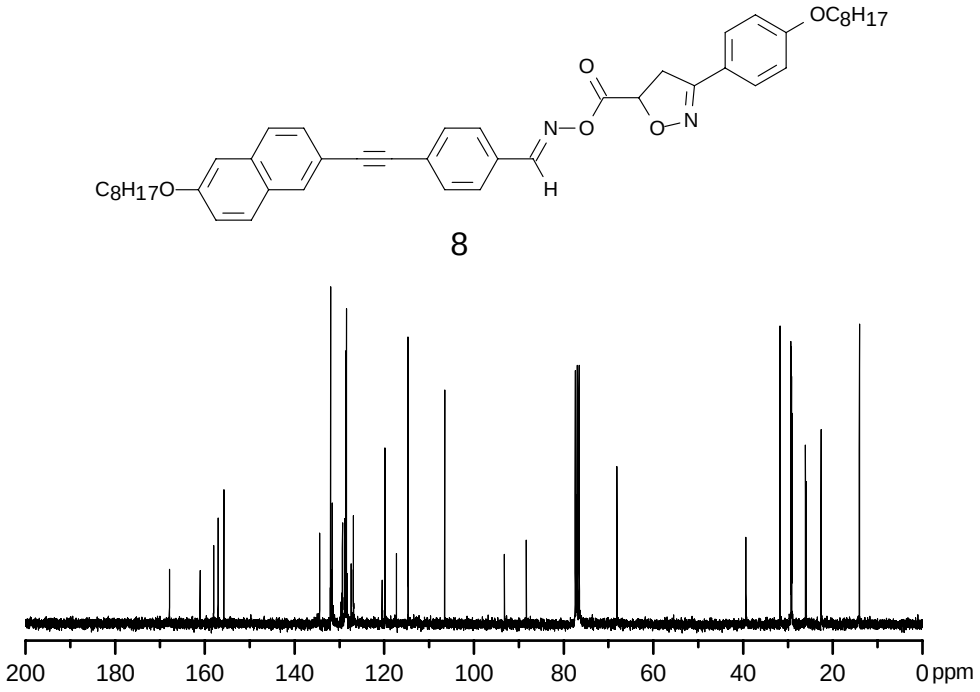

Figure 23. ^{13}C NMR spectrum of compound **8** ($CDCl_3$, 75 MHz).

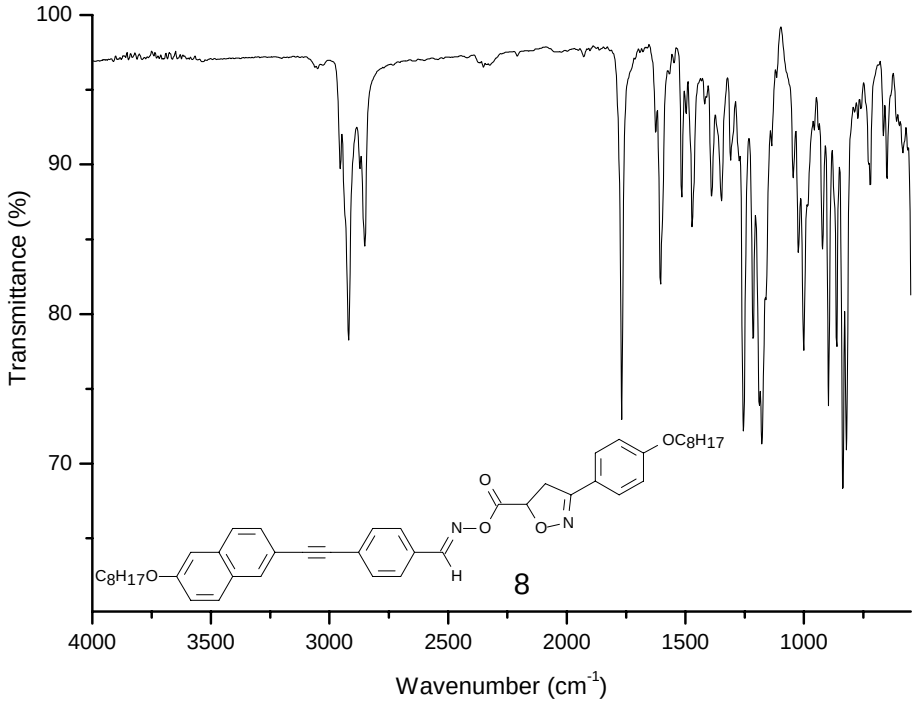

Figure 24. ATR/FT-IR absorption spectrum of compound **8**.

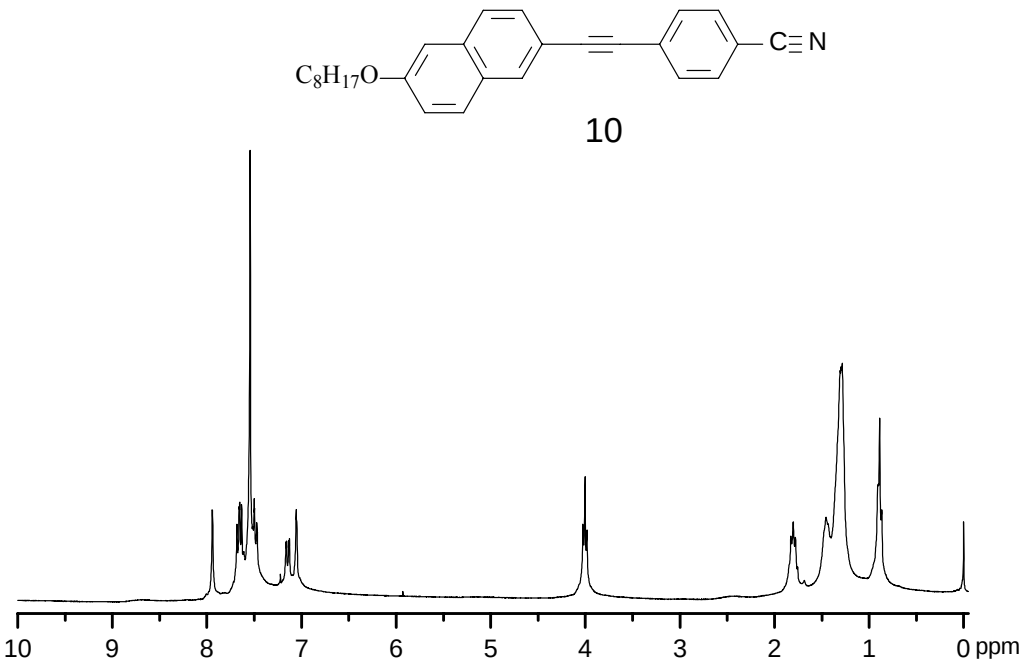

Figure 25. ^{1}H NMR spectrum of compound **10** ($CDCl_3$, 300 MHz).

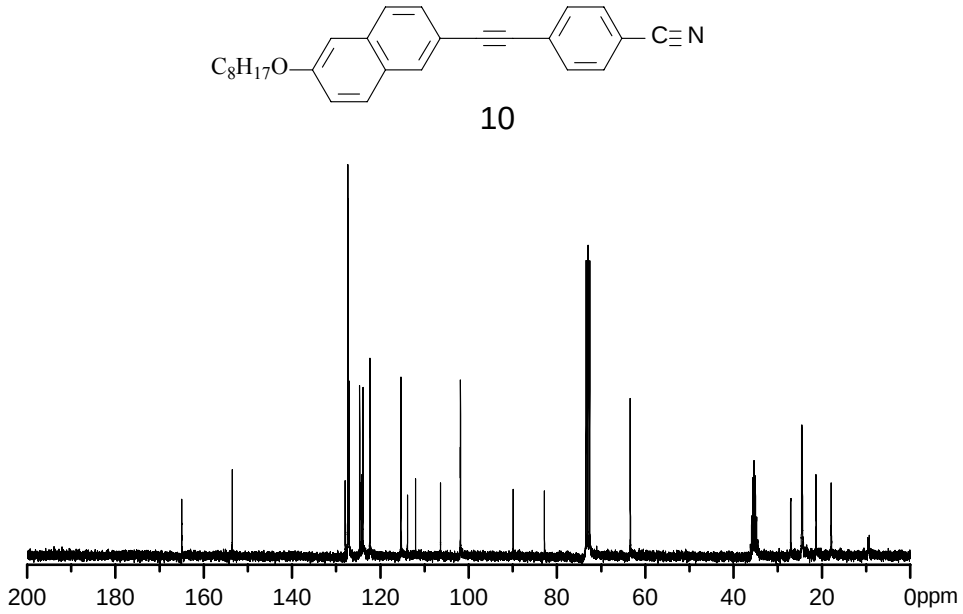

Figure 26. ^{13}C NMR spectrum of compound **10** ($CDCl_3$/DMSO-d_6, 75 MHz).

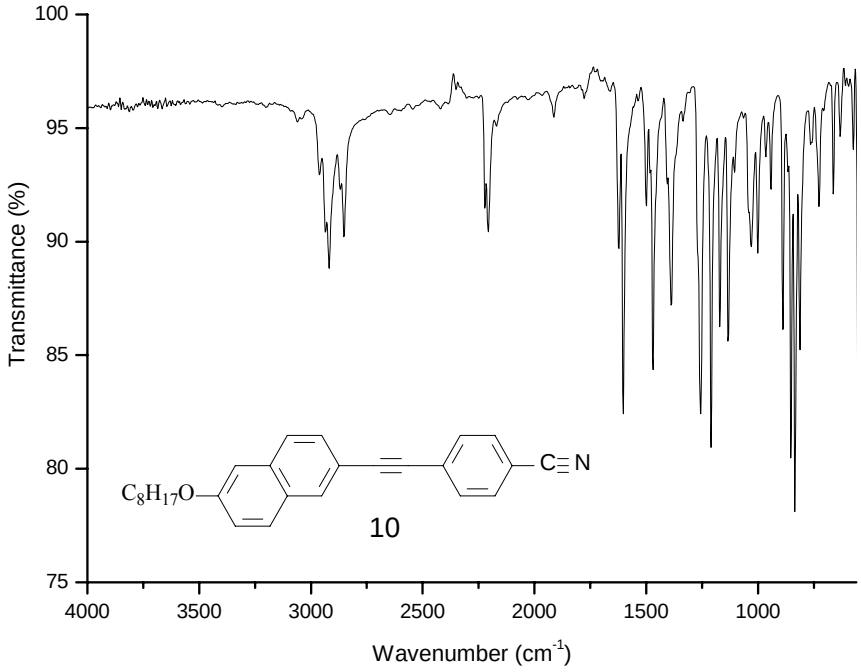

Figure 27. ATR/FT-IR absorption spectrum of compound **10**.

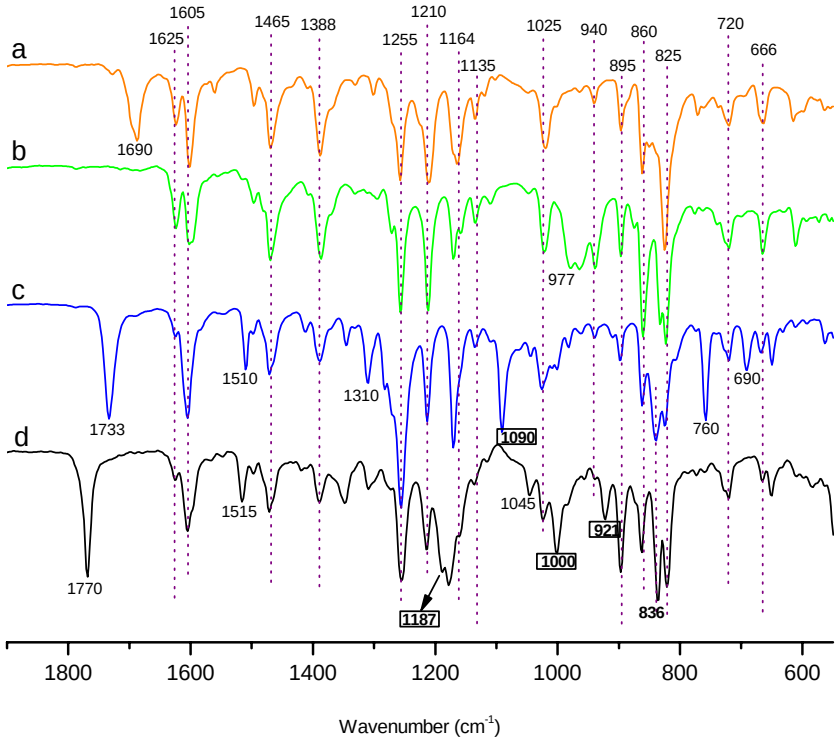

Figure 28. ATR/FT-IR absorption spectra of compounds (a) aldehyde **3**, (b) oxime **4**, (c) ester **6b** and (d) ester **8**.

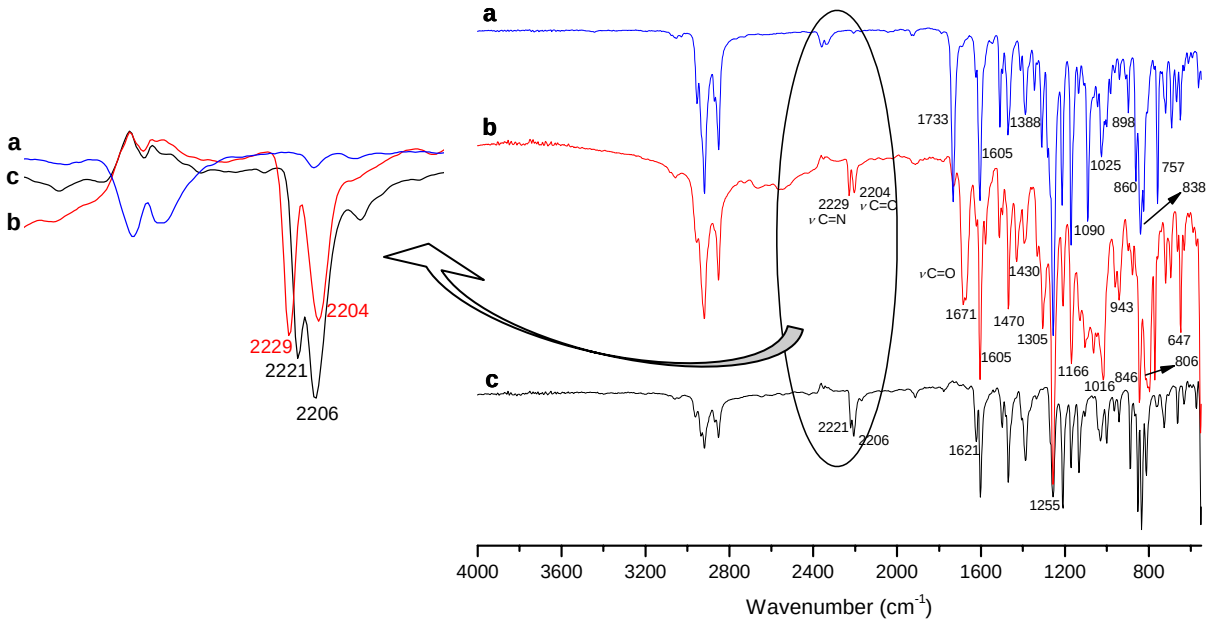

Figure 29. ATR/FT-IR absorption spectra of compounds (a) ester **6c**, (b) ester **6c** that underwent a many heating/cooling cycles and (c) nitrile **10**.

DSC traces

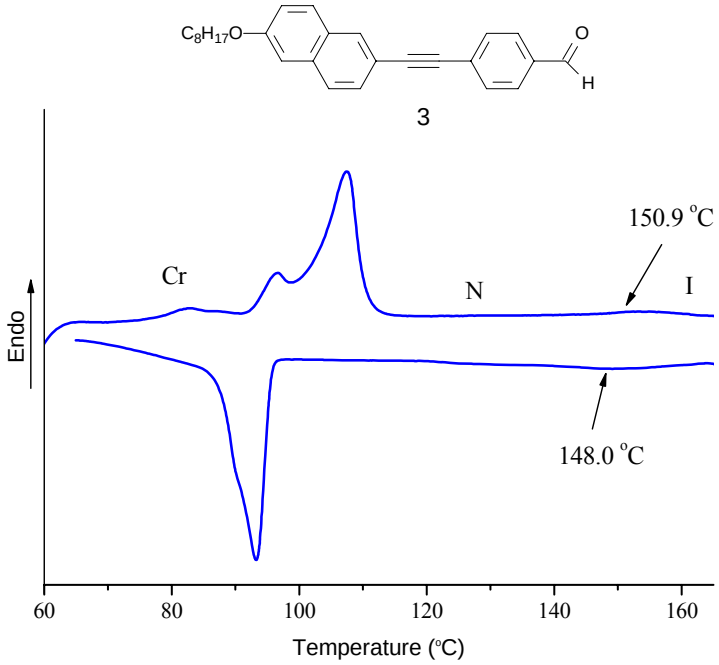

Figure 30. DSC traces of compound **3** with phase transition temperatures on third heating/cooling stage at 10 °C min^{-1}.

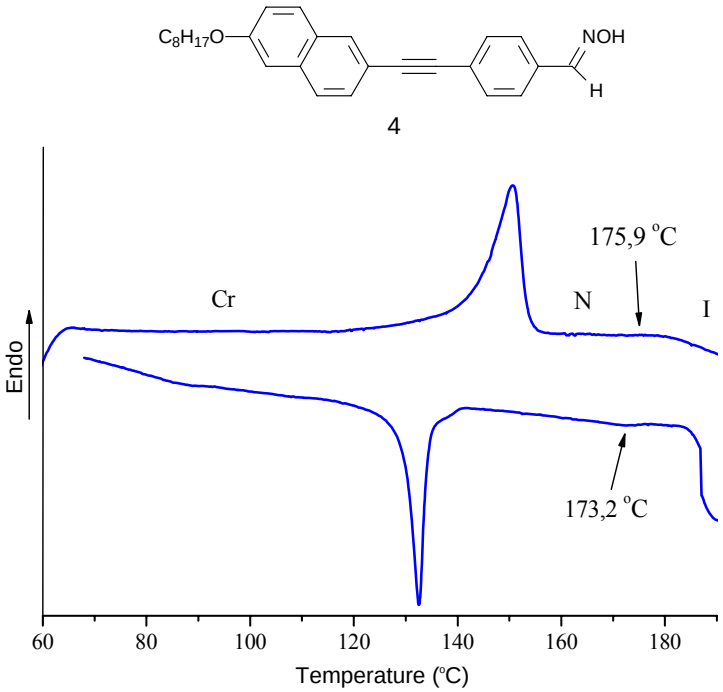

Figure 31. DSC traces of compound **4** with phase transition temperatures on third heating/cooling stage at 10 °C min^{-1}.

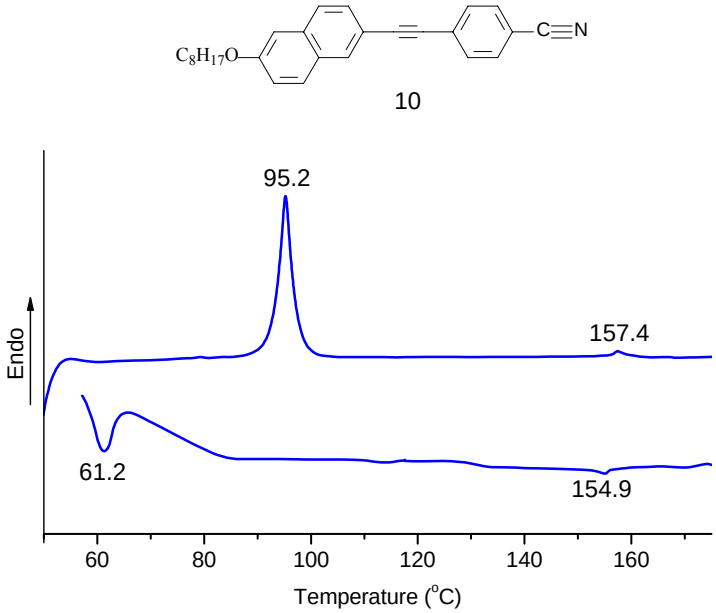

Figure 32. DSC traces with phase transition temperatures of compound **10** on third heating/cooling stages at 10 $^{o}C\ min^{-1}$.

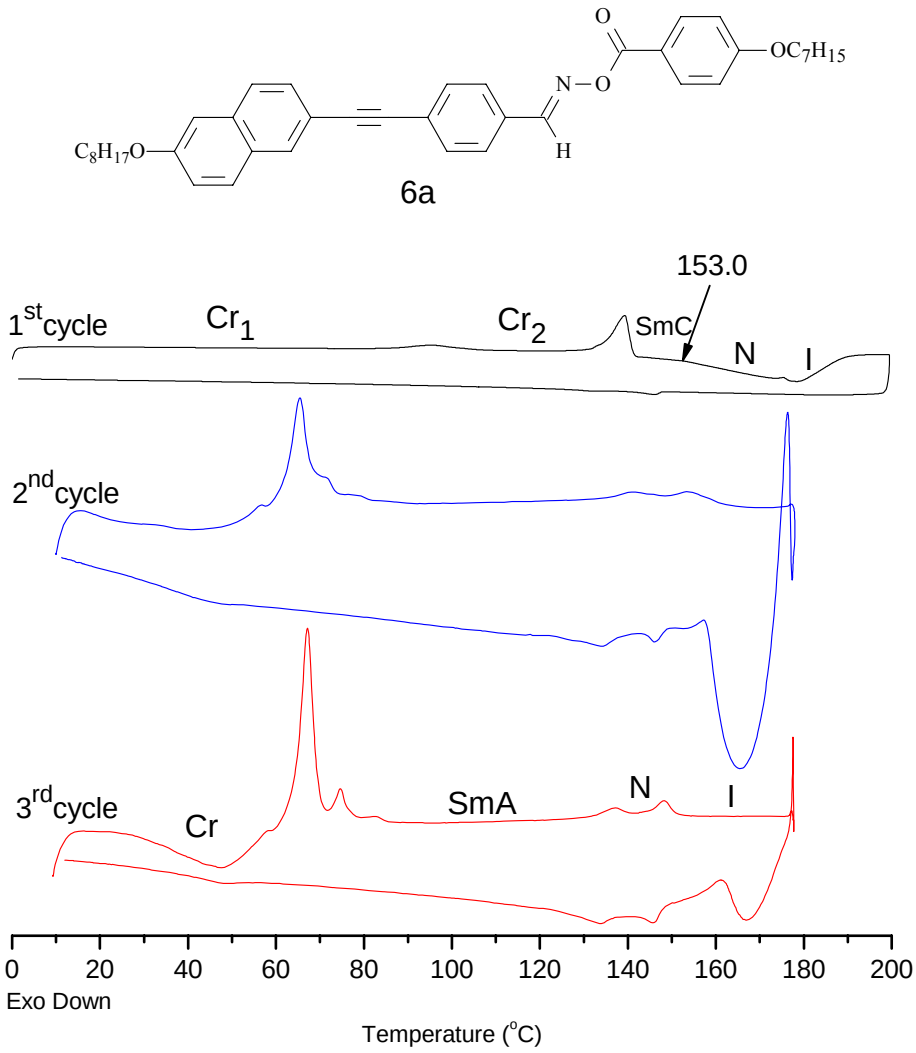

Figure 33. DSC traces of compound **6a** on first, second and third heating/cooling stages at rate 10 °C min^{-1}.

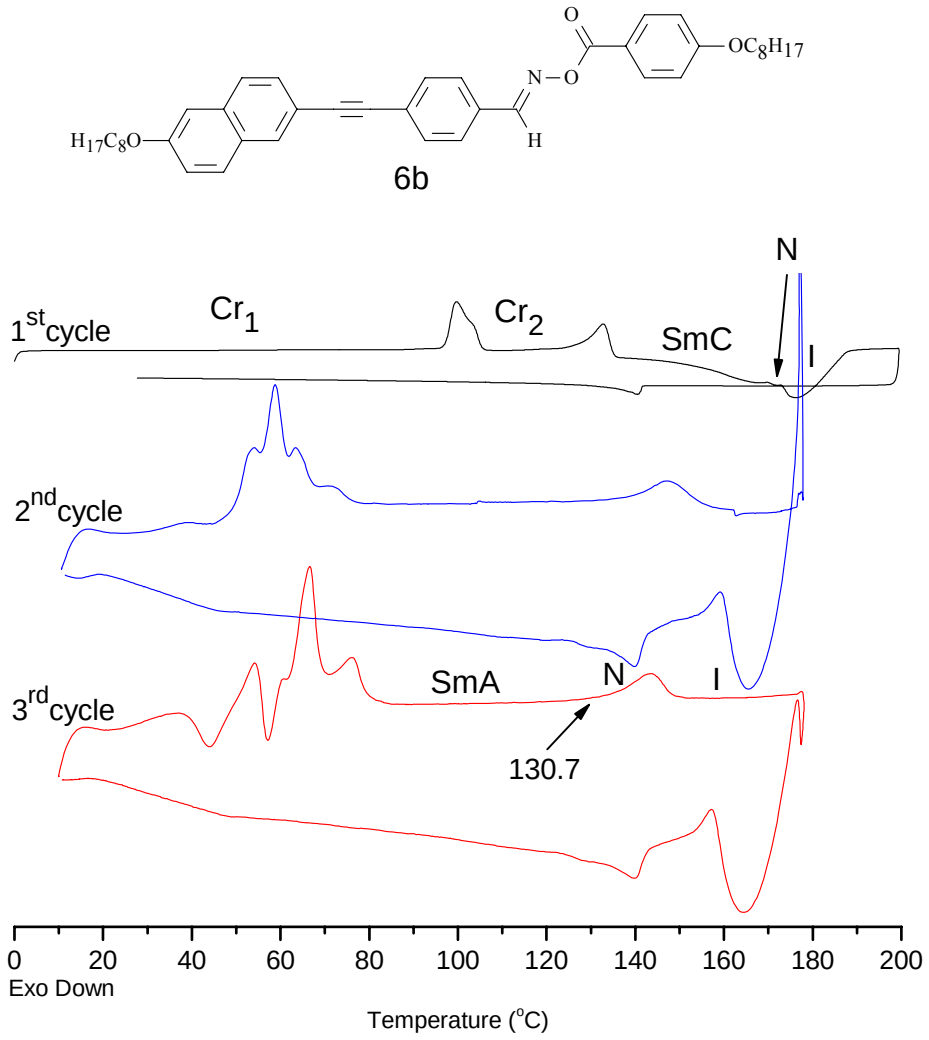

Figure 34. DSC traces of compound **6b** on first, second and third heating/cooling stages at rate 10 ^{o}C min^{-1}.

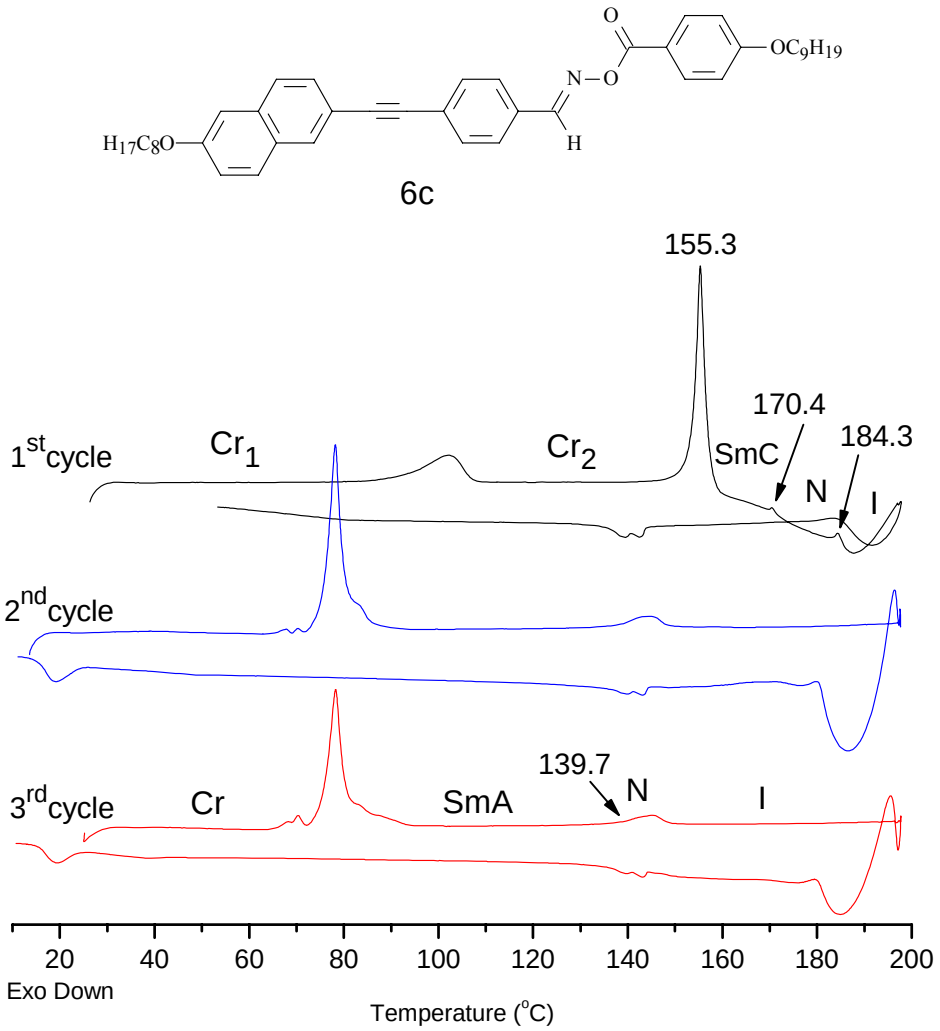

Figure 35. DSC traces of compound **6c** on first, second and third heating/cooling stages at rate 10 °C min^{-1}.

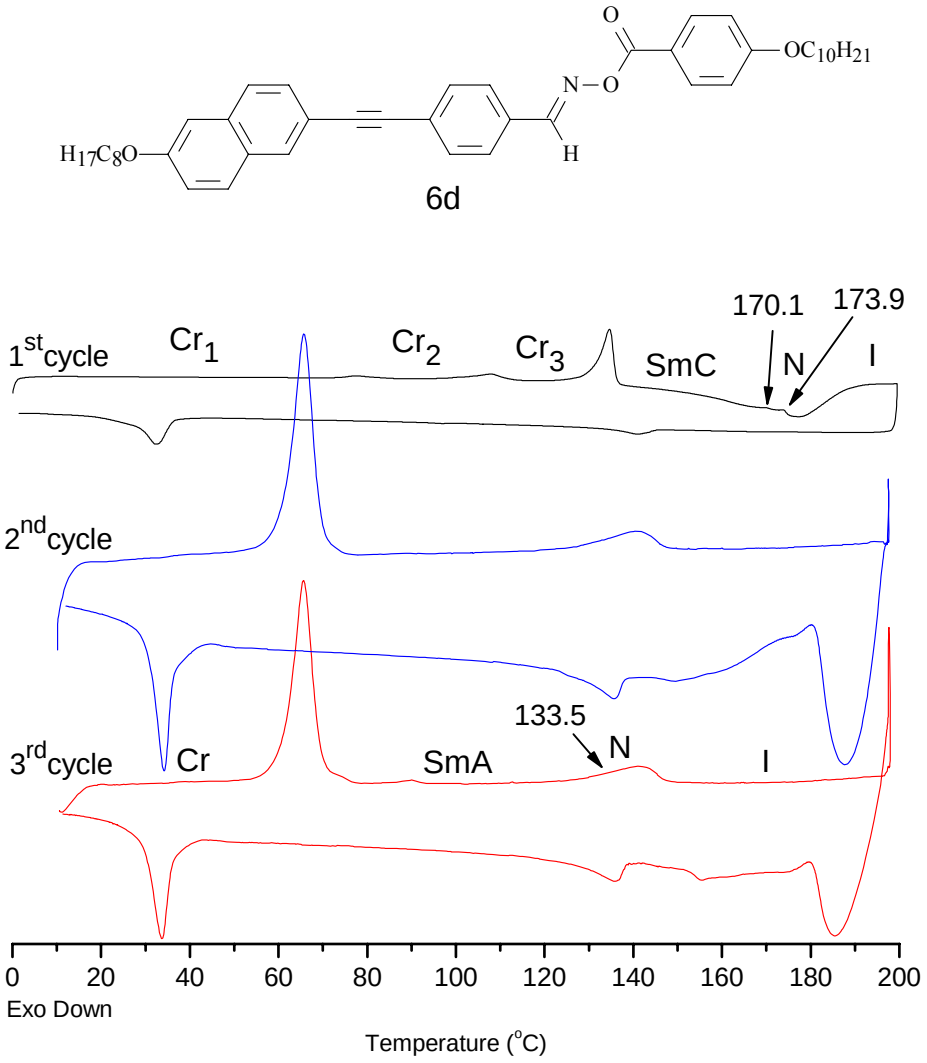

Figure 36. DSC traces of compound **6d** on first, second and third heating/cooling stages at rate 10 °C min^{-1}.

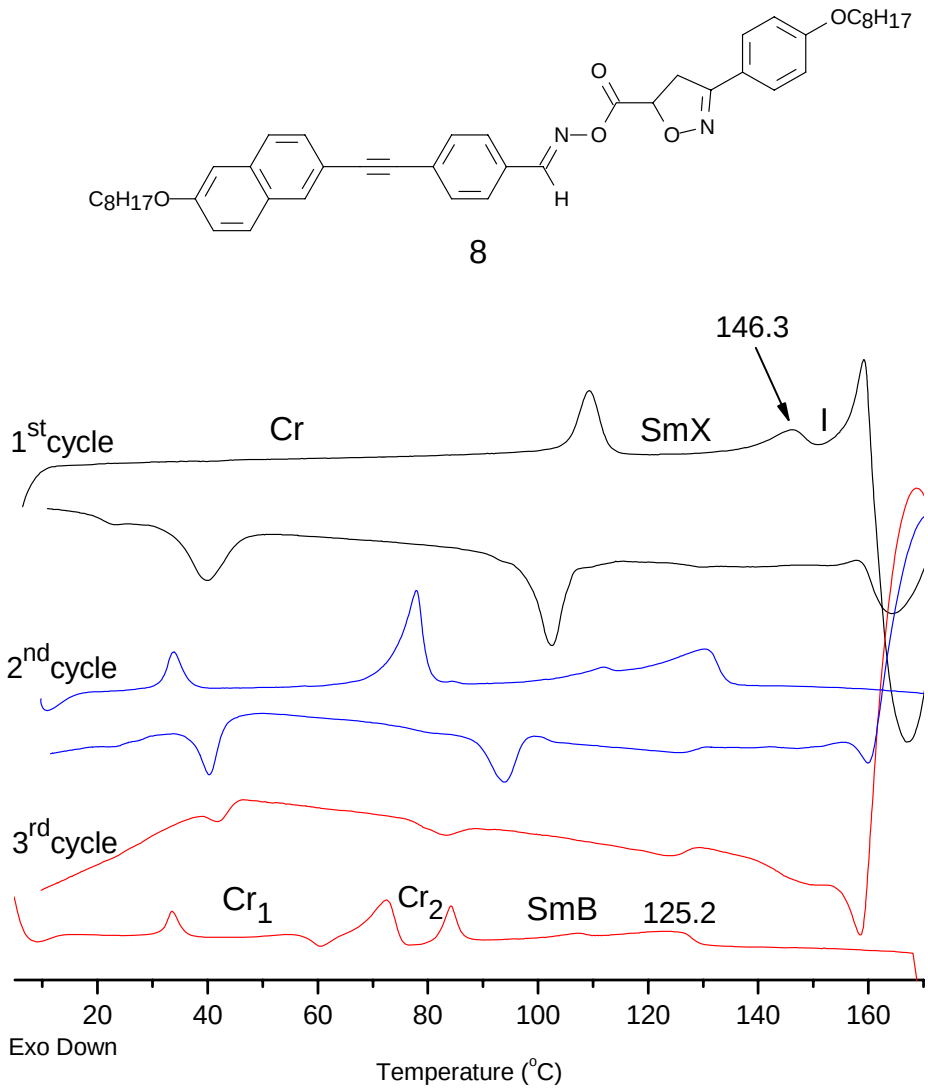

Figure 37. DSC traces of compound **8** on first, second and third heating/cooling stages at 10 ^{o}C min^{-1}.

Polarizing optical photomicrographs that appear in the text (x10)

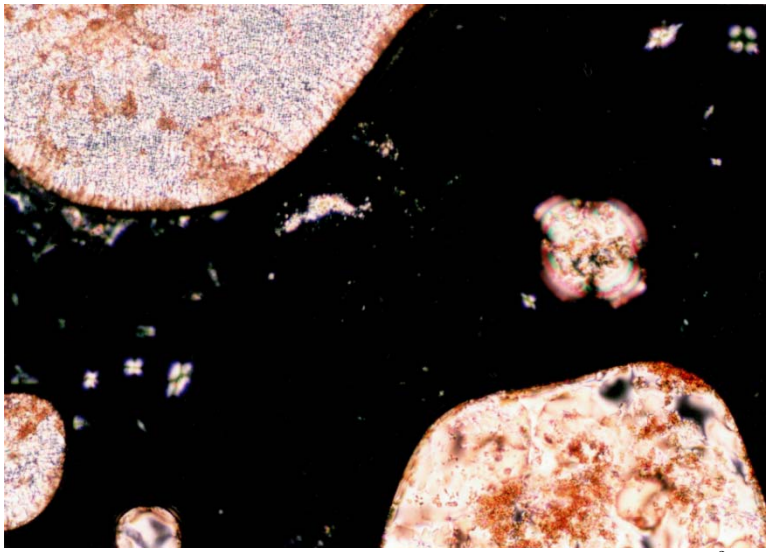

Figure 38. Grainy schlieren texture of SmC phase of **6c** on cooling at 169 ^{o}C (Fig. 6a).

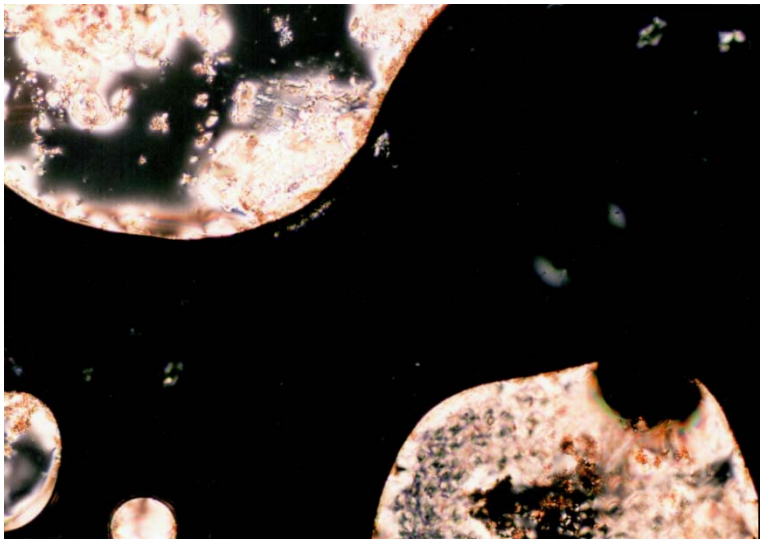

Figure 39. Schlieren and homeotropic texture of N phase of **6c** on first heating at 171.4 ^{o}C (Fig. 6b).

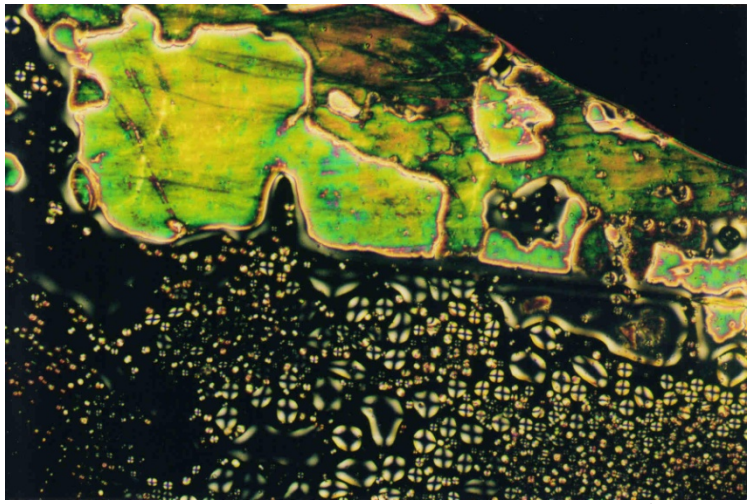

Figure 40. Planar texture of N phase of **6c** on cooling at 141.9 ^{o}C (Fig. 6c).

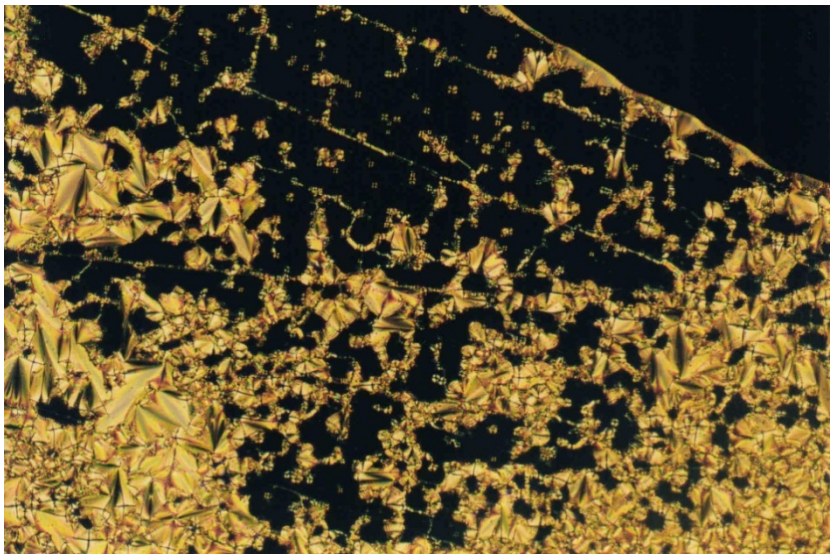

Figure 41. Fan-shaped focal conic texture of SmA phase with homeotropic domains of **6c** on cooling at 125.5 ^{o}C (Fig. 6d).

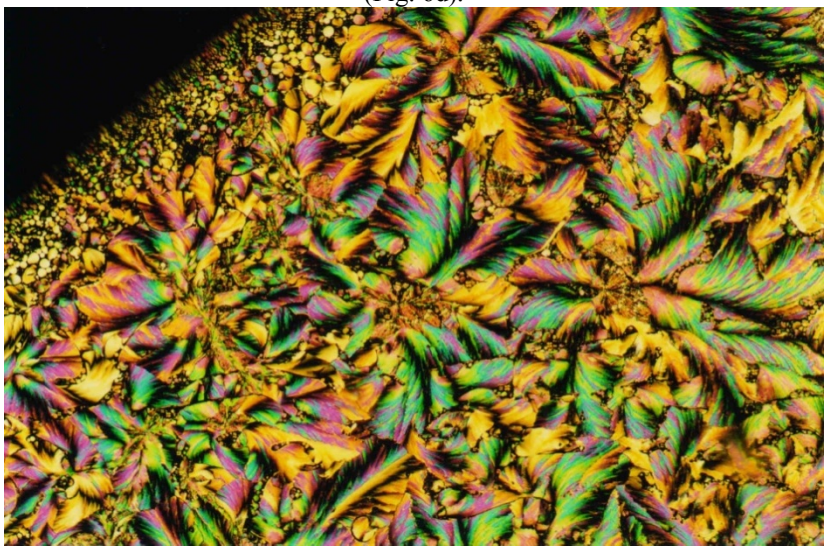

Figure 42. Peacock texture of crystal phase of **6c** at room temperature (Fig. 6e).

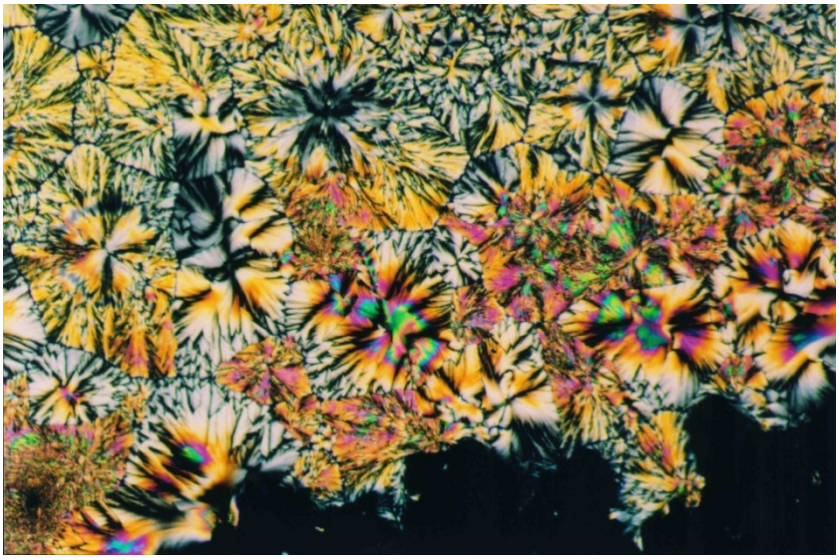

Figure 43. Peacock texture of crystal phase of **6c** at room temperature (Fig. 6f).

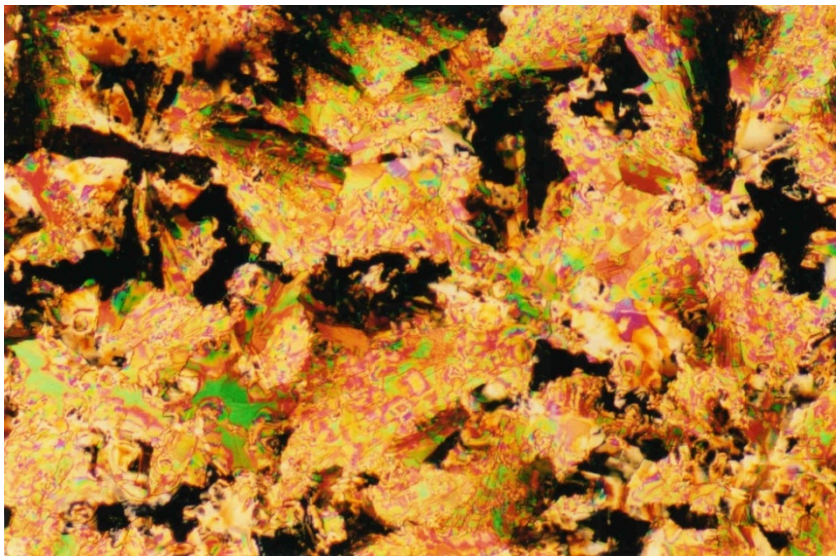

Figure 44. Crystal phase Cr_1 of **8** at room temperature (Fig. 7a).

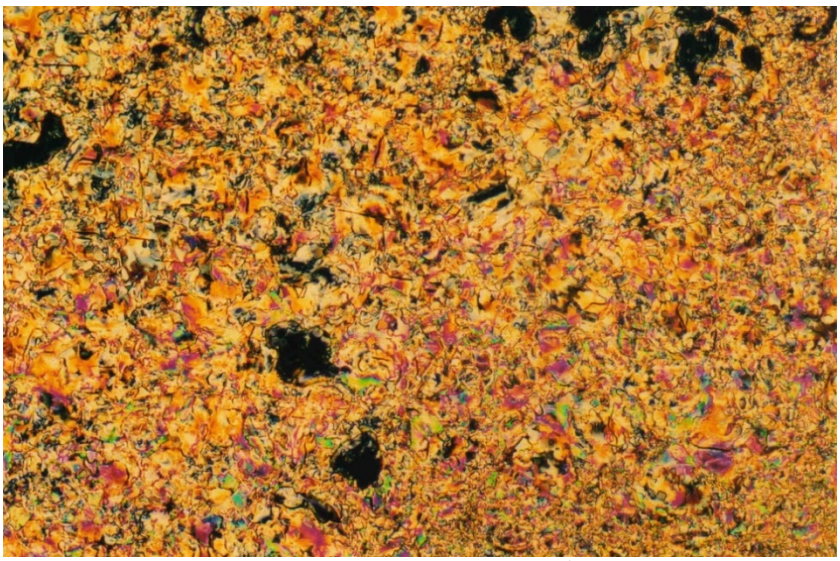

Figure 45. Crystal phase Cr_2 of **8** at 75 ^{o}C (Fig. 7b).

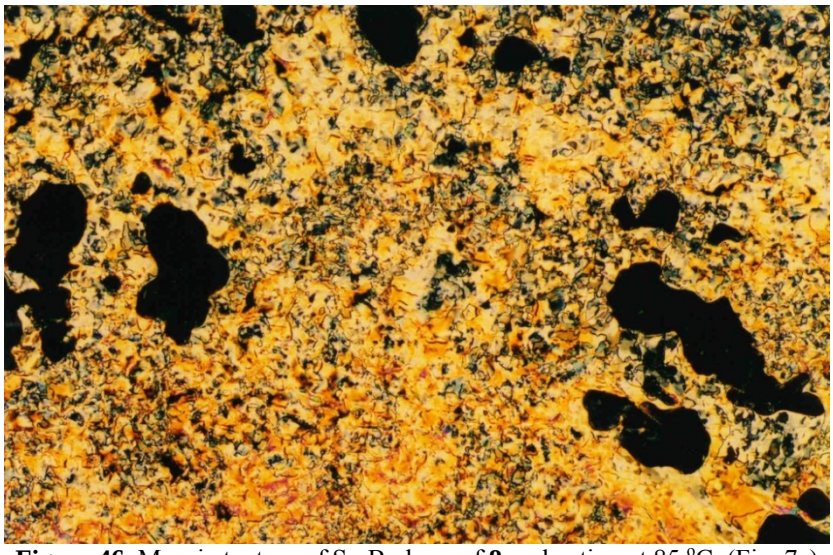

Figure 46. Mosaic texture of SmB phase of **8** on heating at 85 ^{o}C (Fig. 7c)

.

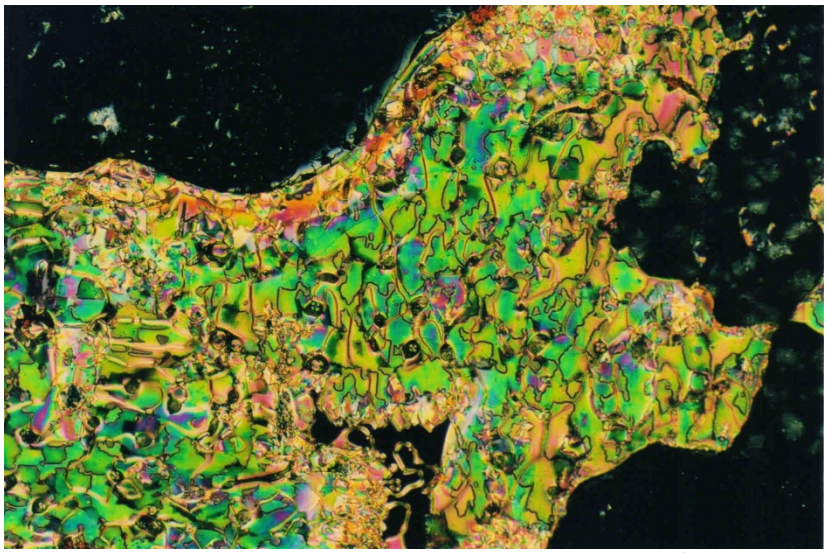

Figure 47. Mosaic texture of SmB phase of **8** on heating at 90 ^{o}C (Fig. 7d).

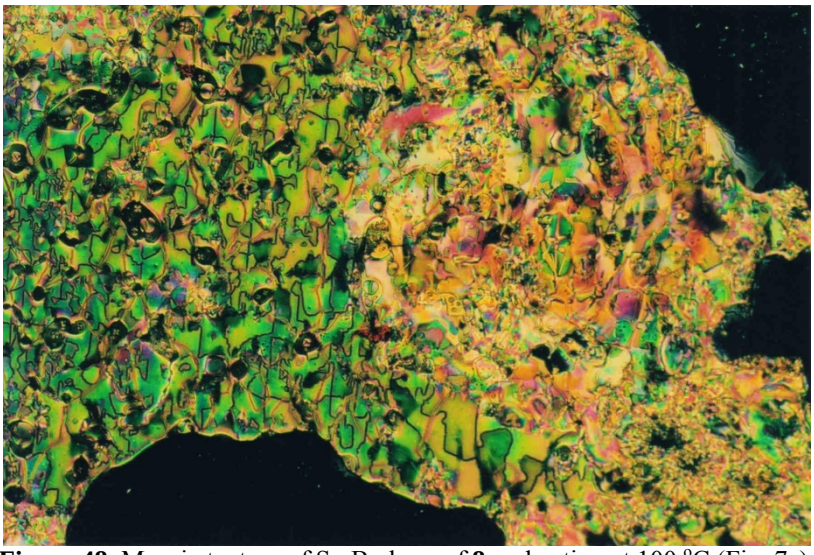

Figure 48. Mosaic texture of SmB phase of **8** on heating at 100 ^{o}C (Fig. 7e).

Figure 49. Mosaic texture of SmB phase of **8** on heating at 119 ^{o}C (Fig. 7f).

Polarizing optical photomicrographs from the same region (x10)

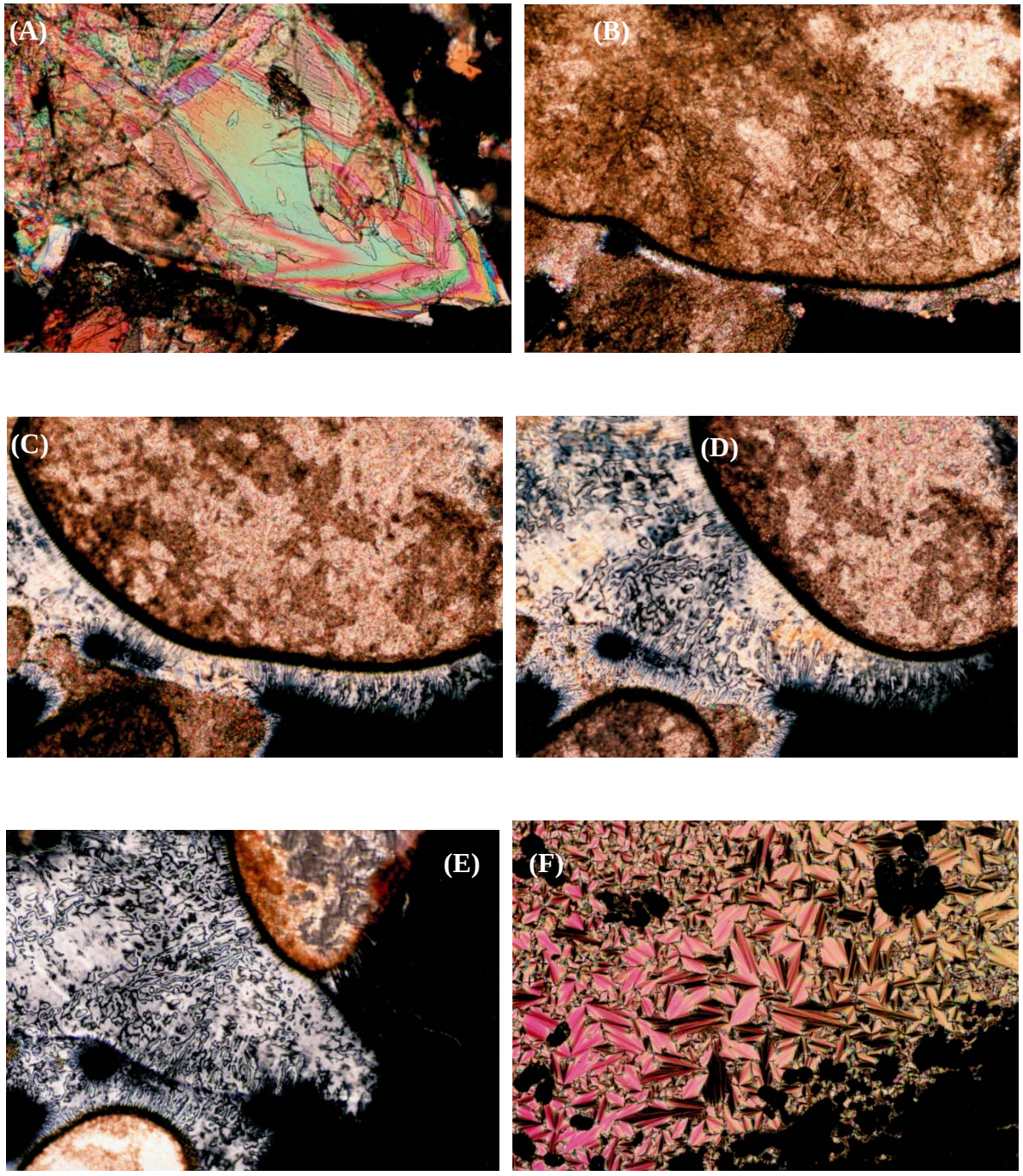

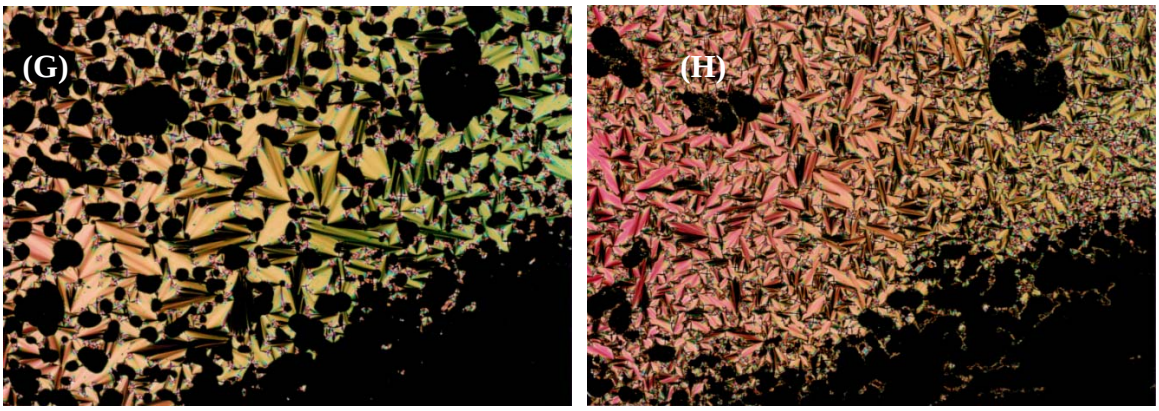

Figure 50. Photomicrographs of the optical textures under POM of **6c** obtained for the same region of the sample (magnification x10). In (A) crystal phase at 75.9 °C obtained before any heating/cooling cycles; (B) SmC phase at 143.9 °C obtained on first heating; (C-E) schlierem texture of SmC phase at 145.8 °C, 147.0 °C and 149.3 °C, respectively, obtained on first heating; (F) fan-shaped focal conic texture of SmA phase at 70.8 °C on first cooling; (G) fan-shaped focal conic texture of SmA phase with isotropic dark texture at 133.8 °C on second heating; (H) fan-shaped focal conic texture of SmA phase at 70.8 °C on second cooling.

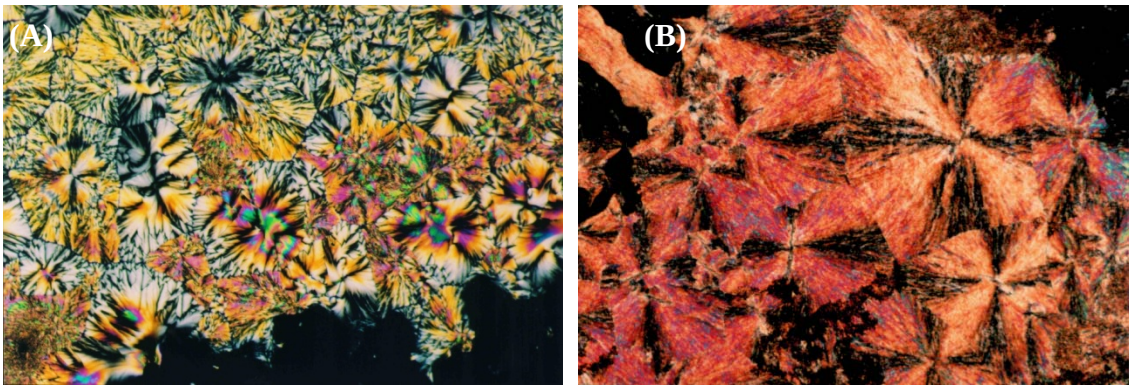

Figure 51. (A) Peacock texture of crystal phase at room temperature of compound **6c**; (B) Spherulite texture of crystal phase of the physical mixture consisting of acid **5a** and nitrile **10**, at room temperature.

CAPÍTULO 6.2 – Trabalho em fase final de redação.

The 2:1 Cycloadduct from [3+2] 1,3-Dipolar Cycloaddition Reaction. Synthesis and Liquid Crystal Behavior.

Tavares, A.; Gonçalves, P. F. B.; Bechtold, I. H. and Merlo, A. A.

Instituto de Química, UFRGS. Av. Bento Gonçalves, 9500. Agronomia. 91501-970, Porto Alegre, RS – Brasil.

Abstract: A novel series of liquid crystals (LC) **11a-d** was synthesized and the LC behavior reported. The new liquid crystals were characterized as a 2:1 cycloadduct which were obtained from the double [3+2] 1,3-dipolar cycloaddition reaction between the nitrile oxide **8** and the vinylacetic acid (**9**). Firstly, the cycloaddition of **8** and **9** gave the initial 1:1 cycloadduct **10**. Subsequently, the cycloadduct **10** acts as more reactive dipolarophile reacting with a second equivalent of nitrile oxide **8** yielded the 2:1 cycloadduct **11a-d** LC. All the **11a-d** compounds exhibiting the enantiotropic smectic I mesophase showed lower chemical stability during mesophase to isotropic liquid transition. Thermal decomposition was observed in all heating and cooling cycles. A theoretical calculation were performed using DFT methods at level B3LYP/aug-cc-pVDZ in order to get some information about the energetic profile of this 2:1 1,3-dipolar cycloaddition. The DFT studies revealed that double [3+2] 1,3-dipolar cycloaddition reaction is quite possible.

Introduction

The 5-membered heterocyclic compounds containing a heteroatom are found widely in nature with diverse biological function. The diversity of this class of organic compounds is one of the most important aspects to be considered. A lot of examples of the pentagonal ring can be mentioned such as imidazoles,[1a] tetrazoles,[1b] oxadiazoles,[1c] isoxazoles,[1d] furans[1e] and others.[1f-j] In this context the 3,5-, 3,4-, and 4,5-disubstituted isoxazoline ring plays a pivotal

[1] (a) Voss, M. E.; Beer, C. M.; Mitchell, S. A.; Blomgren, P. A.; Zhichkin, P. E. *Tetrahedron*, **2008**, *64*, 645; (b) McKie, A. H.; Friedland, S.; Hof, F. *Org. Lett*. **2008**, *10*, 4653; (c) Karthikeyan, M. S.; Prasad, D. J.; Mahalinga, M.; Holla, B. S.; Kumari, N. S. *Eur. J. Med. Chem.* **2008**, *43*, 25; (d) Willy, B.; Rominger, F.; Muller, T. J. J. *Synthesis,* **2008**, 293; (e) Sperry, J. B.; Wright, D. L. *Curr. Opin. In Drug Disc. & Dev.* **2005**, *8*, 723; (f) Yamamoto, H.; Hayashi, S.; Kubo, M.; Harada, M.;

position at 5-membered heterocyclic chemistry. For instance, the 4,5-disubstituted-4-isoxazolines such **1** are a novel inhibitors of cyclooxygenase-2 with analgesic and antiinflammatory activity and constitute as alternative to the nonsteroidal anti-inflammatory drugs for the treatment of arthritic inflammation and pain.[2]

Wityak and co-workers reported that isoxazolinylacetamides bearing a phosphoramidate group α- to the carboxylate moiety are able to bind GPIIb/IIIa with high affinity and display potent antagonists of ADP mediated platelet aggregation.[3] In depression diseases the isoxazoline derivatives such as **2** has proven to be the most potent α_2-adrenoceptor blockers within this chemical, while keeping potent 5-HT reuptake inhibiting activity.[4] Acivicin[5] **3** a new chloroisoxazoline amino acid antitumor antimetabolites and an inhibitor of γ-glutamil transpeptidase-GGT is a natural product which was obtained from *Streptomyces sviceus*. From synthetic point of view the isoxazolines are important molecular precursor for the preparation of, for instance β-hydroxyketone[6], **4**, a polyketide fragments[7] and others. This class of organic compounds is very important due to their diversity in nature and they exhibit diverse biological activities and pharmacological properties.

Hasegawa, M.; Noguchi, M.; Sumimoto, M.; Hori, K. *Eur. J. Org. Chem*. **2007**, 2859; (g) Zimmermann, P. J.; Lee, J. Y.; Hlobilova, I.; Endermann, R.; Habich, D.; Jager, V. *Eur. J. Org. Chem*. **2005**, 3450; (h) Evans, D. A. *Aldrichimica Acta* **1982**, *15*, 23; (i) Fernandes, M. S.; Merlo, A. A. *Synthetic Commun.* **2003**, *33,* 1167; (j) Zanatta, N.; Schneider, J. M. F. M.; Schneider, P. H.; Wouters, A. D.; Bonacorso, H. G.; Martins, M. A. P.; Wessjohann, L. A. *J. Org. Chem*. **2006**, *71,* 6996.

[2] Habeeb, A. G.; Rao, P. N. P; Knaus, E. E. *J. Med. Chem.* **2001**, *44,* 2921.

[3] (a) Wityak, J.; Tobin, A. E.; Mousa, S. A.; Wexler, R. R.; Olson, R. E.; *Bioorg. Med. Chem. Let.* **1999**, *9*, 123; (b) Wityak, J.; Sielecki, T. M.; Pinto, D. J.; Sze, J. Y.; Liu, J.; Tobin, A. E.; Wang, S.; Jiang, B.; Emmett, G.; Ma, P.; Mousa, S. A.; Olson, R. E.; Wexler, R. R. J. *Med. Chem.* **1997**, *40,* 50; (c) Xue, C.-B.; Wityak, J.; Sielecki, T. M.; Pinto, D. J.; Batt, D. G.; Cain, G. A.; Sworin, M.; Rockwell, A. L.; Roderick, J. J.; Wang, S.; Orwat, M. J.; Frietze, W. E.; Bostrom, L. L.; Liu, J.; Higley, C. A.; Rankin, F. W.; Tobin, A. E.; Emmett, G.; Lalka, G. K.; Sze, J. Y.; Di Meo, S. V.; Mousa, S. A.; Thoolen, M. J.; Racanelli, A. L.; Hausner, E. A.; Reilly, T. M.; DeGrado, W. F.; Wexler, R. R.; Olson, R. E. J. *Med. Chem.* **1997**, *40,* 2064.

[4] Andrés J. I.; Alcázar, J.; Alonso, J. M.; De Lucas, A. I.; Iturrino, L.; Biesmans, I.; Megens, A. A.; *Bioorg. Med. Chem.* **2006**, *14,* 4361.

[5] Hanka, L. J.; Gerpheide, S. A.; Spieles, P. R.; Martin, D. G.; Belter, P. A.; Coleman, T. A.; Meyer, H. F. *Antimicrob. Agents Ch.* **1975**, *7,* 807.

[6] Becker, N.; Carreira, E. M. *Org. Lett*. **2007**, *9*, 3857.

[7] Fader, L. D.; Carreira, E. M. *Org. Lett*. **2004**, *6*, 2485.

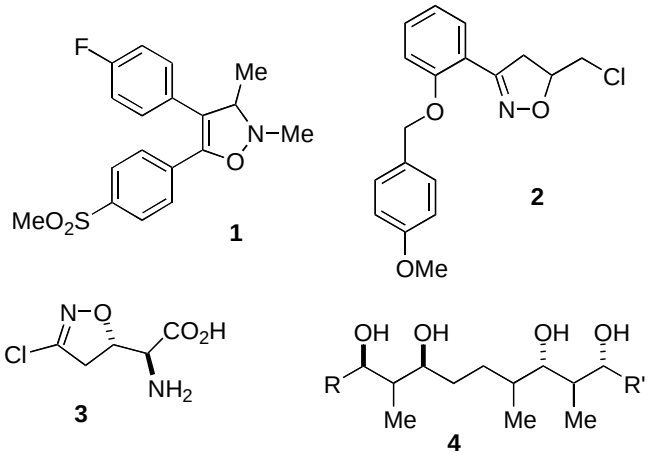

Because of the diverse chemical transformations available to the isoxazoline ring, organic compounds possessing this heterocyclic represent an attractive way to obtain new types of organic materials with potential technological applications.[8]

In our search for new LC molecules we have used the [3+2] 1,3-dipolar cycloaddition as a suitable methodology to prepare the hard core of the heterocyclic liquid crystals compounds. It is well-established that the reaction of nitriles oxides with alkenes as dipolarophile gives raises the expected 1:1 cycloadducts. However if alkene is less reactive than the normal cycloadduct, a second cycloaddition event takes place. In this sense the reaction can follow another way in which the isoxazoline product acts as dipolarophile due to its high reactivity when compared with the alkene. Under such circumstance the 2:1 cycloadducts can be obtained.[9] The Scheme 1 outlines the preparation of 2:1 cycloadducts considering the low reactivity of the alkene as dipolarophile.

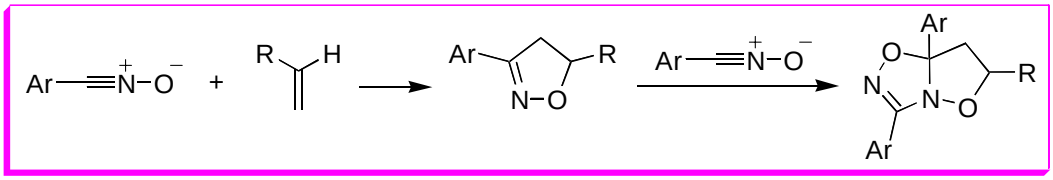

Scheme 1. The 2:1 cycloadduct obtained by double [3+2] 1,3-dipolar cycloaddition reaction.

Herein we wish to report on the synthesis and the mesomorphic behavior of liquid crystals from [3+2] 1,3-dipolar cycloaddition of nitrile oxides with electron-deficient alkenes as depicted in Scheme 1.

Synthesis

[8] Kauhanka, U. M.; Kauhanka, M. M. *Liq. Cryst.* **2006**, *33*, 121.
[9] Wang, J.-F.; Wei, D.-Q.; Wang, C.-F.; Ye, Y.; Li, Y.-X.; Luo, Y.; Wang, W.-W.; Liu, L.-Z.; Zhao, Y.-F. *J. Theoretical & Computational Chem.* **2007**, *6*, 861.

The Scheme 2 describes the synthesis of the homologous series **11a-d** obtained as a 2:1 cycloadducts. The initial step was the alkylation reaction of benzaldehyde **5** with 1-bromoalkanes given the alkylated products **6** in 90-95% yields.[10] Next, the addition of hydroxylamine chloridrate to **6** yielded the corresponding oximes **7** in good yields.[11] The nitrile oxide **8**, which was generated *in situ* by exposing to the NCS oxidant agent, reacted regioselectively with vinylacetic acid **9** to given the desired products **11a-d**.

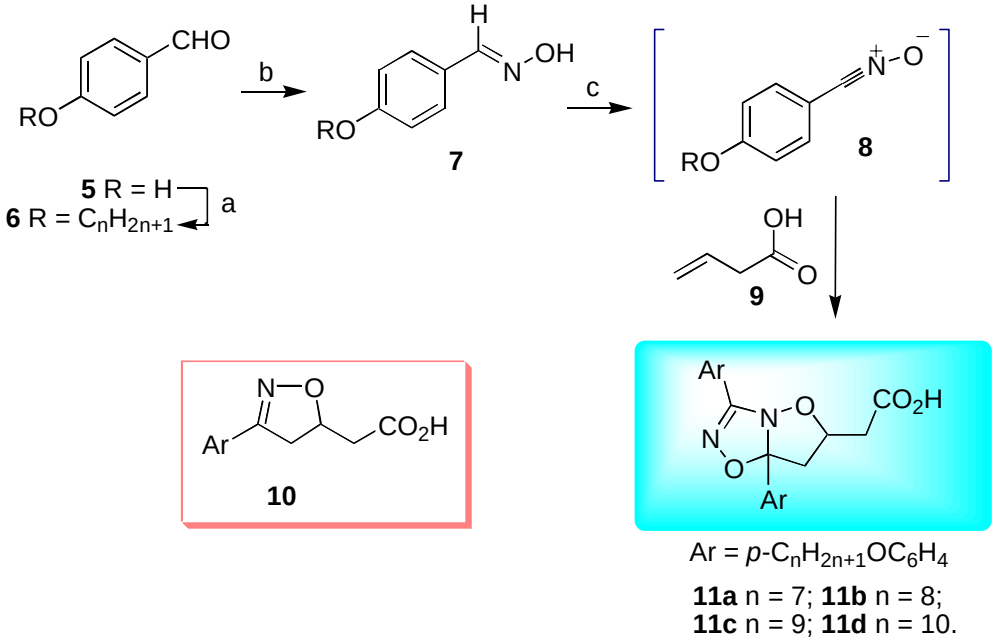

Conditions: a) RBr, KOH, DMF, C_6H_6 (90-95%); b) $HONH_2$.HCl; AcONa, EtOH, H_2O (73-93%); c) Vinylacetic acid (**9**), NCS, pyridine, $CHCl_3$ (40-55%).

Scheme 2. Preparation of LC compounds **11a-d**.

The formation of these novel 2:1 cycloadducts **11a-d** can be envisage by an initial dipolar cycloaddition of the nitrile oxide **8** across the ethylenic bond of **9** to give the expected 3,5-isoxazoline as a transient intermediate 1:1 cycloadduct **10**. The next step proceeds by a second dipolar cycloaddition of the nitrile oxide **8** across the bond C=N of the transient intermediate **10**. The obtainment of the 2:1 cycloadduct in this step is due to the more reactivity of the C=N double bond in **10** than the double bond in the dipolarophile **9**. The enhance reactivity of the **10** can be attributed to the presence of the oxygen atom in isoxazoline ring. The electron

[10] (a) Passo, J. A.; Vilela, G. D.; Schneider, P. H.; Ritter, O. M. S.; Merlo, A. A.; *Liq. Cryst*. **2008**, *35*, 833; (b) Ritter, O. M. S.; Giacomelli, F. C.; Passo, J. A.; Silveira, N. P.; Merlo, A. A. *Polymer Bull.* **2006**, *56,* 549.
[11] (a) Tavares, A.; Schneider, P. H.; Merlo, A. A. *Eur. J. Org. Chem.* **2009**, 889; (b) Tanaka, M.; Haino, T.; Ideta, K.; Kubo, K.; Mori, A.; Fukuzawa, Y. *Tetrahedron* **2007**, *63*, 652; (c) Weygand, C.; Gabler, R. *J. Prakt. Chem.* **1940**, *155*, 332.

attracting power of the oxygen atom favors the polarization of the C=N double bond in the orientation suitable with the cycloaddition of nitrile oxide **8**.

Theorectical calculations. To further our DFT studies we choose benzonitrile oxide (**12**) as a 1,3-dipole partner of the vinylacetic acid (**9**) in the 1,3-dipolar cycloadditions reactions. The DFT calculation reveal that the following mechanism is quite possible: it starts as a normal 1,3-dipolar cycloaddition reaction to produce 1:1 product **13**; then the benzonitrile oxide continues to react with **13** and gives the corresponding cycloadduct 2:1 **14**. In order to direct our analysis, we decided to calculate the FMO energies of the initial and intermediate dipolarophile **8** and **13** and the 1,3-dipolar reagent **12**. The calculated HOMO and LUMO energies of the reactants are depicted in Figure 1. As stated above, we calculated the FMO for dipole **12** without alkyl chain bonded to benzene ring as well as the dipolarophiles **8** and the isoxazoline **13** (as a 1:1 cycloadduct of the first cycloaddition). The calculated data predict that at the beginning of the reaction the interactions I and II are possible. The energy gap of I is smaller than II and, this suggest that the cycloaddition process is controlled by $HOMO_{(dipolarophile)}$-$LUMO_{(1,3\text{-}dipole)}$. As the reaction move forward the concentration of the **8** decreases and due to higher reactivity of dipolarophile **13** than **8** it competes by the nitrile oxide **12**. So, the second cycloaddition is favoring to occur now between the new dipolarophile **13** and **12**. The calculations showed that the interaction described by IV is highly favored over I by $\Delta E \sim 0.04$ eV. The dominant interactions that control the approach of both reactants depend on the relative levels of the FMOs. Furthermore, it is important to consider that the levels of HOMO and LUMO can be affected by (de)stabilizing effects such as complexation of Lewis acid and hydrogen-bond interactions.[12]

The regioselectivity observed can also be rationalized using the orbital coefficients of the HOMO and LUMO and it's in accordance with literature.[13,14,15]

[12] (a) Laszlo, P.; Lucche, J. *Actual. Chim.* **1984**, 42; (b) Curran, D. P.; Kim, B. H.; Piyasena, H. P.; Loncharich, R. J.; Houk, K. N. *J. Org. Chem.* **1987**, *52*, 2137; (c) Desimoni, G.; Faita, G.; Pasini, D.; Righetti, P. P. *Tetrahedron* **1992**, *48*, 1667.
[13] Jeddeloh, M. R.; Holden, J. B.; Nouri, D. H.; Kurth, M. J. *J. Comb. Chem.* **2007**, *9,* 1041.
[14] Houk, K. N. *Acc. Chem. Res.* **1975**, *8*, 361.
[15] Sustmann, R. *Tetrahedron Lett.* **1971**, *12*, 2717.

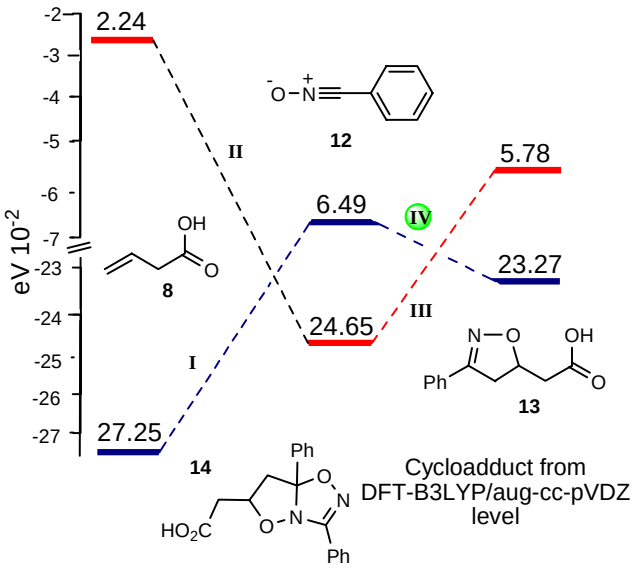

Figure 1. FMO energies (eV x10^{-2}; HOMO and LUMO) calculated at B3LYP/aug-cc-pVDZ level of the vinylacetic acid (**9**), benzonitrile oxide (**12**) and isoxazoline (**13**).

The structural characterization of the new liquid-crystalline cycloadducts **11a-d** were made by means of combustion analysis, ^{1}H, ^{13}C NMR spectroscopic techniques (H,H-COSY, HMQC and HMBC), EI-MS and HRMS (ESI). For example, the electrospray ionization mass spectrometry showed two characteristic peaks for the **11a** cycloadduct (ESI-MS) at *m/z* 553.3298 related to protonated molecular ion $[M+1]^+$. At *m/z* 575.3068, a second peak is visible and it is associated with sodium + molecular ion $[M+Na]^+$. The possible pattern of fragmentation of the **11a** is followed. The elimination of vinylacetic (86 amu) from the peak $[M+1]^+$ gave the ion at *m/z* 466 not visible. However **11b**, **11c** and **11d** showed [M - 86]+ at *m/z* 495, *m/z* 522 *m/z* 551 which is related with the protonated ion obtained from elimination of vinylacetic from the peak $[M+1]^+$. Further fragmentation of the ion fragment at *m/z* 466 produced ion at *m/z* 235 [233 +2H] which correspond to the M+ of nitrile oxide **10**. To the **11b**, **11c** and **11d** cycloadducts ions at *m/z* 249, 262 e 276 are visible at spectra which correspond to the protonated form of the ion of the nitrile oxide **10** derived from **11b**, **11c** and **11d** cycloadducts, respectively.

The base peak of this MS study was found at *m/z* 135 which is formed by the loss of alkene C_7H_{14} (from the alkyl chain). The ion at *m/z* 134 corresponds to the non protonated form. The ion at *m/z* 233 was probably formed by a retrocycloaddition [3+2] reaction of the fragment ion at *m/z* 466. Calculated mass ($M+H^+$, 552.3298) and the observed mass of the ion $[M+H]^+$ are in accordance with an elemental composition of $C_{32}H_{44}N_2O_6$ of the **11a** cycloadduct. The Figure 2 illustrates the fragmentation of **11a-d** obtained by low-resolution mass spectra.

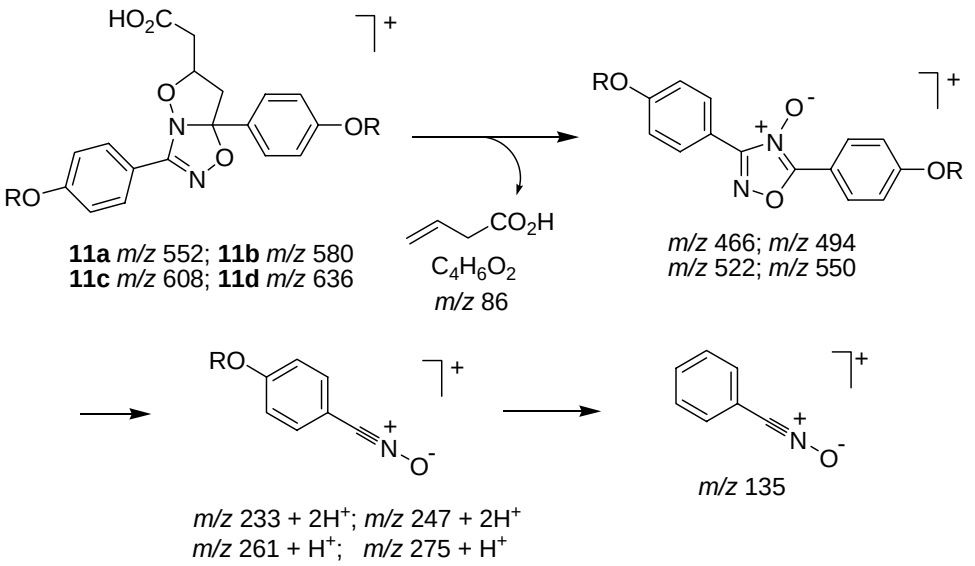

Figure 2. Fragmentation pattern of the 2:1 cycloadducts **11a-d** (*m/z* for the main fragment are given).

The correct structure of adducts **11a-d** was establish by ^{1}H and ^{13}C chemical shifts and coupling constants. The ^{1}H NMR spectrum of cycloadduct **11a** (Figures 3 and 4), for instance, exhibited four sets of doublet of doublets centred at δ 2.87, δ 3.05, δ 3.28 and δ 3.59 ppm, which belong to ABX and AMX patterns arising from chemically and magnetically non-equivalent protons H_9', H_9, H_3' and H_3, respectively. The $H_2 - H_3$ and $H_2 - H_9$ coupling constants are $^{2}J_{gem}$ = 16.8 Hz, $^{3}J_{cis}$ = 10.5 Hz, $^{3}J_{trans}$ = 6.9 Hz and $^{2}J_{gem}$ = 15.6 Hz, $^{3}J_{cis}$ = 6.0 Hz, $^{3}J_{trans}$ = 7.5 Hz, respectively. These attributions are consistent to the coupling constants describe by the Karplus correlation[16]. The proton H_2 is observed as a multiplet at δ 5.17 ppm. In the ^{13}C NMR spectrum of **11a** we can observed six signals centred at δ 37.5, δ 40.4, δ 76.3, δ 156.4, δ 166.3 and δ 168.8 ppm to the carbon atoms C_9, C_3, C_2, C_4, C_7 and C_{10}, respectively (Figure 4).

[16] Fieser, L. M.; Fieser, M. *Natural Products Related to Phenanthrene,* Reinhold, New York, 1949, p. 184.

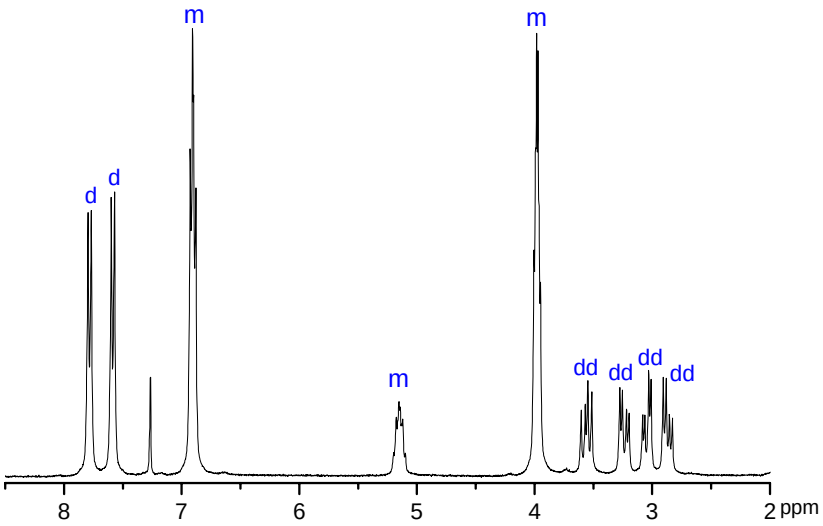

Figure 3. Partial ^{1}H NMR spectrum for compound **11a**.

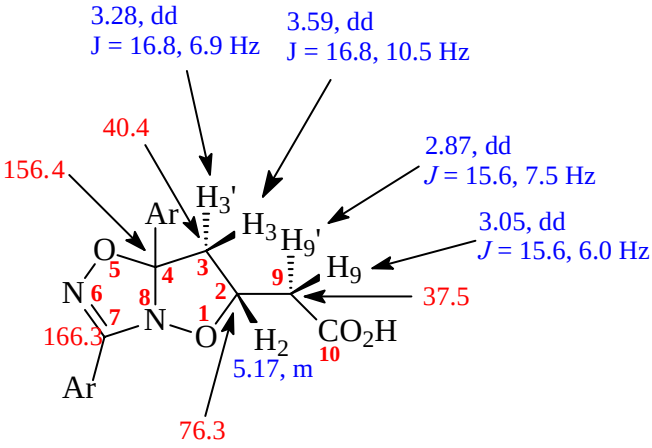

Figure 4. Representative ^{1}H and ^{13}C chemical shifts for compound **11a**.

We also used in addition to confirm the structure assignments of isoxazolinas **11a-d**, COSY, HMQC and HMBC experiments. In the COSY spectra (Figure 5), the more deshielded protons H_{12} and H_{17} (due to the withdrawing effect of the pentagonal rings) has correlation with the dublets centred at δ 6.89 and δ 6.93 ppm concerning to the other aromatic protons H_{13} and H_{18}. The multiplet at δ 5.17 has correlation with the protons H_3 and H_9 and then it is the H_2. The multiplet at δ 3.98 has correlation with the protons at δ 1.79 and then it is assigned as the protons H_{15} and H_{20}.

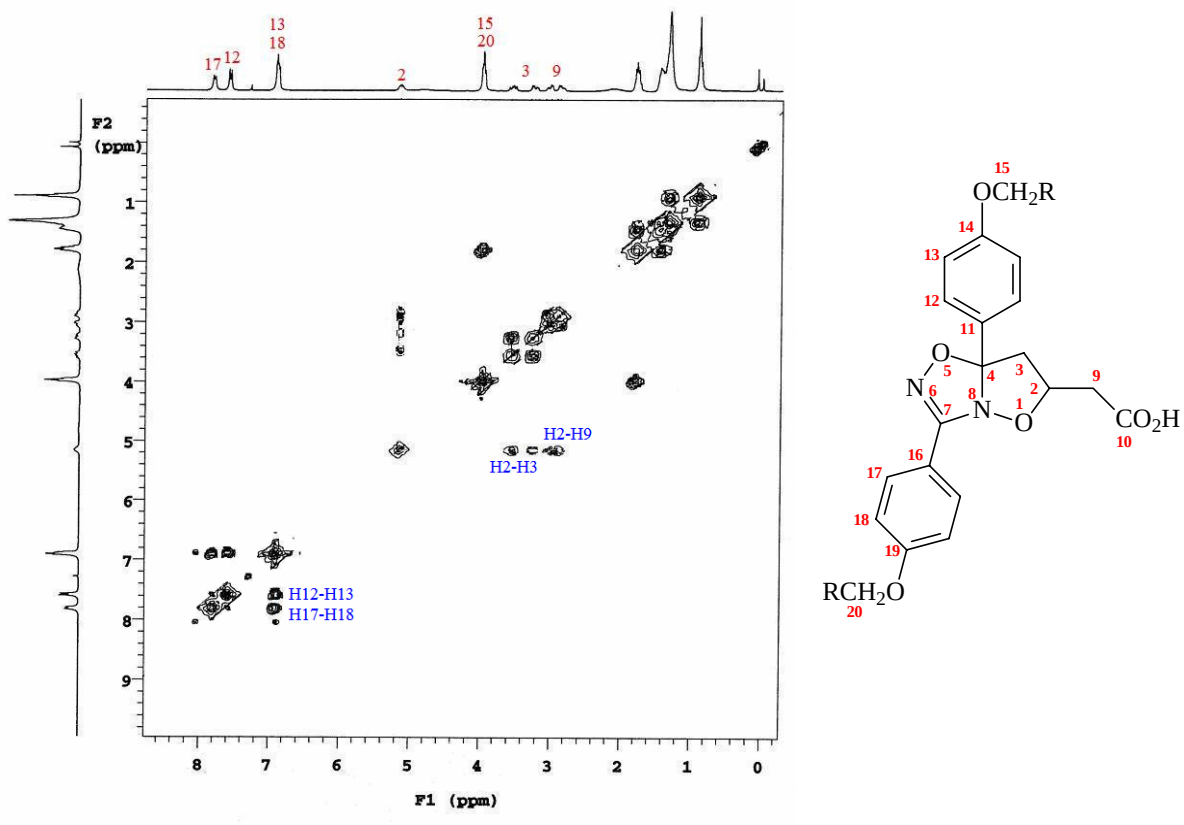

Figure 5. COSY spectrum of compound **11a**.

The HMQC experiments confirmed the position of aliphatic and aromatic carbon atoms. From Figure 6 we see that H_9 and H_9' correlated with C_9 (at δ 37.5 ppm) and H_3 and H_3' correlated with C_3 (at δ 40.4 ppm). Similarly, the same experiment correlated H_{13} and H_{18} with C_{13} (at δ 111.8 ppm) and C_{18} (at δ 114.4 ppm), respectively. And, the H_{12} and H_{17} are connected to C_{12} (at δ 128.3 ppm) and C_{17} (at δ 129.5 ppm), respectively. The HMQC bidimensional examination clearly indicated that H_2 is attached to carbon atom C_2 (at δ 76.3 ppm), whereas H_{15} and H_{20} are connected to C_{15} (at δ 68.1 ppm) and C_{20} (at δ 68.2 ppm), respectively. Thus, we have been able to establish the identities of all hydrogen and carbon atoms of belong to the framework of the bicyclic **11a**, as well as the hydrogen and carbon atoms of belong to the aromatic ring.

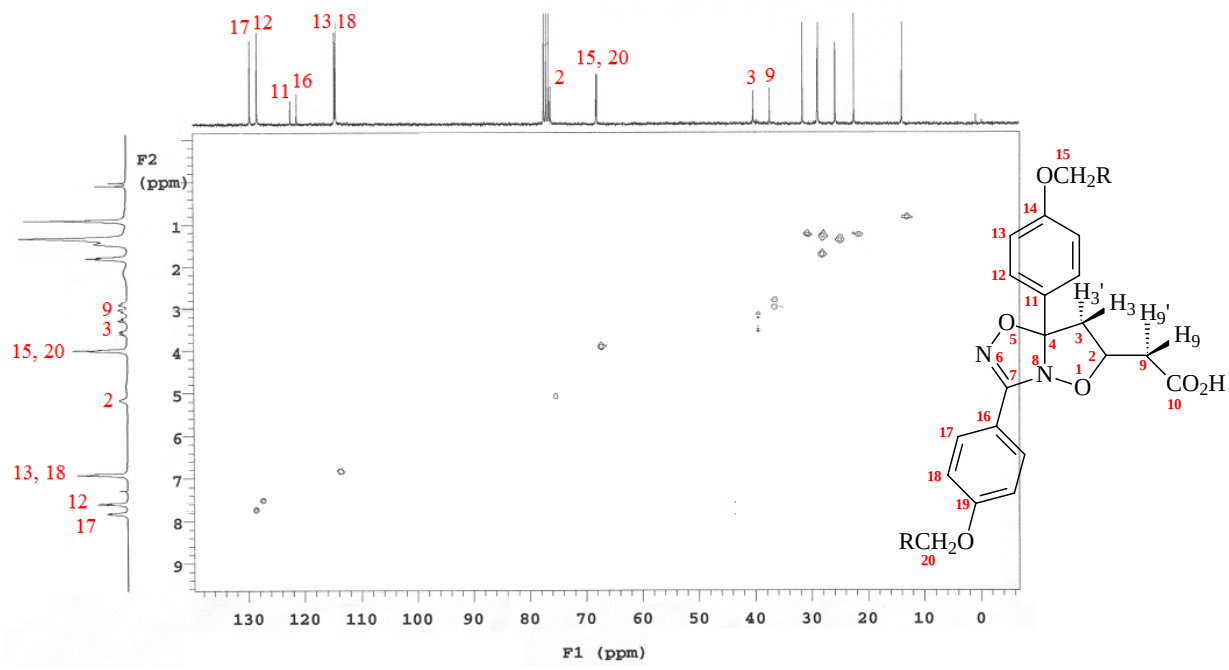

Figure 6. HMQC spectrum of compound **11a**.

Next, we turned our attention to the quaternary carbon atoms in **11a**. The Figure 7 depicts a portion of HMBC spectrum of the aromatic region of compound **11a**. First, carbon atom C_{10} (at δ 168.8 ppm) is correlated with two doublet of dublets H_9 and H_9'. The carbon atom C_7 (at δ 166.3 ppm) correlates with the dublets centred at δ 7.85 ppm, attributed to the hydrogen atom H_{17}. Both, carbon atoms C_{19} (at δ 162.7 ppm) and C_{14} (at δ 160.8 ppm) are correlated with the multiplet of H_{15} and H_{20} at δ 3.98 ppm, as expected. From the HMBC spectrum is seen others correlations of these carbon atoms with aromatic hydrogen atoms, such as H_{12}, H_{13}, H_{17} and H_{18}. Finally, the coupling of the carbon atom signal at δ 156.4 ppm with two doublet of dublets H_3 and $H_{3'}$ and with the proton H_{12} at δ 7.60 ppm are indicating that this carbon atom must be the C_4[17].

[17] (a) Gibert, J-P.; Jacquier, R.; Pétrus, C. *Bull. Soc. Chim. France*, **1979**, n 5-6, II-282-288; (b) Albini, F. M.; Vitali, D.; Oberti, R.; Caramella, P. *J. Chem. Research (S)* **1980**, 348; (c) Albini, F. M.; Vitali, D.; Oberti, R.; Caramella, P. *J. Chem. Research (M)* **1980**, 4355; (d) Gandolfi, R.; Tonoletti, G.; Rastelli, A.; Bagatti, M. *J. Org. Chem.* **1993**, *58*, 6038.

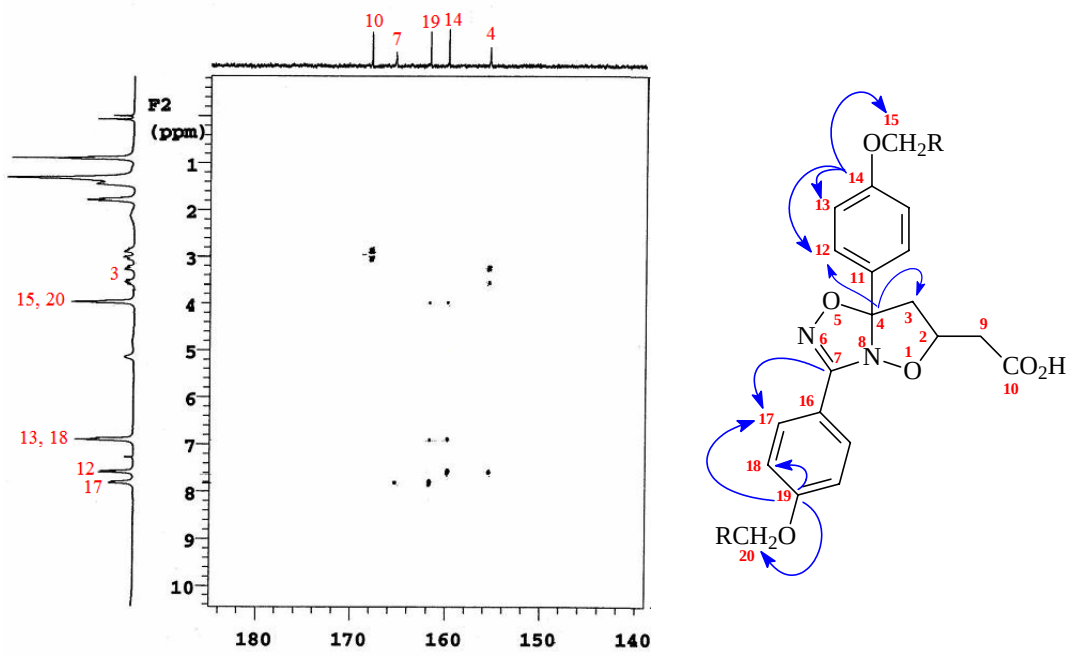

Figure 7. HMBC spectrum of compound **11a** depicting the aromatic region.

Mesomorphic Behavior and Thermal Analysis. The solid sample of **11a** was subjected for thermogravimetric analysis (TGA) (Figure 8). The curve of the solid sample showed no apparent weight loss at 50-140 ^{o}C. Above this temperature, the TGA curve displayed two decomposition modes. The first weight loss (*ca* 30 %) started at around 140-200 ^{o}C is probably related to elimination of vinylacetic and occluded solvent of crystallization. The second and third weight loss (*ca* 51 %) started at around 220-290 ^{o}C and the whole decomposition is completed near 500-600 ^{o}C.

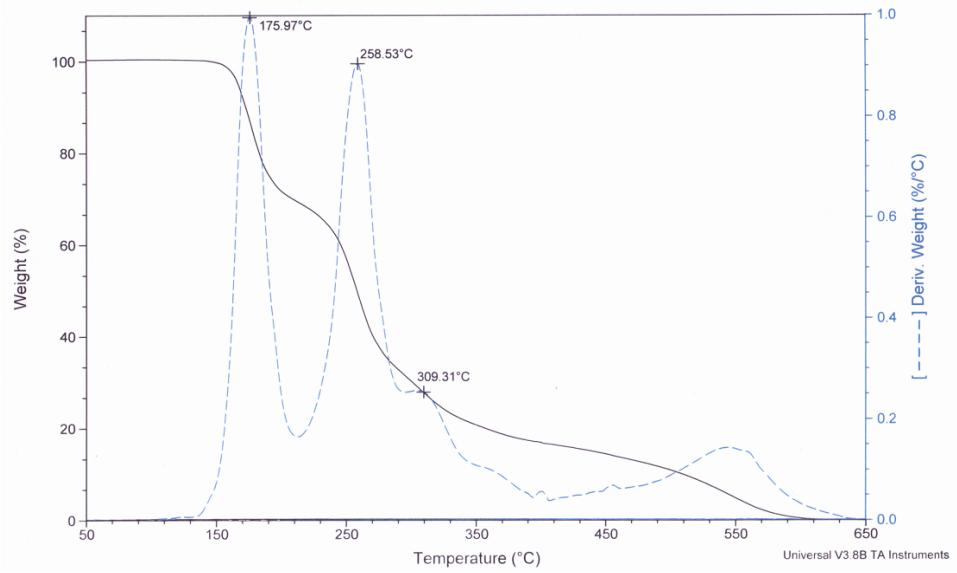

Figure 8. TGA/DTG curve for **11a**.

The LC properties of the cycloadduct 2:1 were investigated using differential scanning calorimetry (DSC) and polarizing optical microscopy (POM).[18] Thermal data were collected by POM (Figure 9) in the 1st heating cycle and by DSC (Figure 10) in the 2nd heating cycle. The data are compiled in Table 1. The nature of the mesophase and the transition temperatures were determined based on the first heating scan due to the decomposition which was observed when the samples were heated. The chemical instability of **11a-d** was seen during POM studies and from their DSC traces. The data in Table 1 was collected by POM. The onset temperature (T_{onset}) also was collected from the 1st and 2nd heating scan. Considering the instability of these compounds and the troubles associated with the exactly determination of the transition SmC to SmA, we decided to grouped them. The onset temperature, T_{onset}, shows a good correlation with the temperature observed by POM. Also, the size and the peak sharpness give us an indication that something is happening when the samples melt to liquid-crystalline state. For instance, T_{onset} for **11a** is 125.8 ^{o}C, and this is *ca* the temperature (126.1 ^{o}C) in which compound **11a** enters into the SmC mesophase, as observed by POM. In this sense, thermal response of the sample using onset temperature or the data by POM can deduced. The peak temperature at 133.4 ^{o}C is inappropriate to correlated with transitions SmC to SmA due to the size of the peak as a consequence of the thermal degradations. The thermal behavior after the first heating remains the same as can be seen in Figure 10. The onset temperature listed in Table 1 and the microscopic observation reveal that the decomposition induced by heat yielded a new mixture which was LC itself. However, we could not observe the focal conic-fan texture in this series of cycloadducts **11a-d** after heated. The mesophase SmC was characterized as solely (Figure 9D).

[18] (a) Gray, G. W.; Goodby, J. W.; *Smectic Liquid Crystals: Textures and Structures*, Leonard Hill, Glasgow and London, 1984; (b) Li, L.; Jones, C. D.; Magolan, J.; Lemieux, R. P. *J. Mat. Chem.* **2007**, *17*, 2313; (c) Godzwon, J.; Sienkowska, M. J.; Galewski, Z. *Thermochimica Acta* **2009**, *491*, 71; (d) Weissflog, W.; Dunemann, U.; Findeisen-Tandel, S.; Tamba, M. G.; Kresse, H.; Pelzl, G.; Diele, S.; Baumeister, U.; Eremin, A.; Sternb, S.; Stannarius, R. *Soft Matter*. **2009**, *5*, 1840.

Table 1. Transitions temperatures (°C) of cycloadducts **11a-d**.

Compound	Heating cycle[a,b]								T_{onset}[c]	T_{onset}[d]	ΔT[e]
	Cr[f]			SmC		SmA		I			
11a	•	126.1	•	[b]	•	136.7	I	•	125.8	110.6	13.3
11b	•	140.5	•	[b]	•	141.7	I	•	138.4	112.0	14.7
11c	•	132.5	•	[b]	•	141.0	I	•	133.7	110.9	19.0
11d	•	130.2	•	[b]	•	135.8	I	•	130.9	109.6	20.3

[a]Data obtained by POM; [b]The transition temperature was not determined. Due to the instability of the samples during the 1st heating scan the range of mesophase was taken into account as being (SmC + SmA) transition; [c,d]Determined by DSC (10 °C min^{-1}) during the 1st heating and 2nd heating scan, respectively; [e]Peak size; [f]Transitions between crystal – crystal phase was often observed for solution-crystallized virgin samples of a majority of 2:1 cycloadducts in the first heating cycle. Such polymorphism may be due to the differences in molecular structures. Polymorphic forms were vanished after the first heating/cooling cycles because of thermal degradation of the compounds.

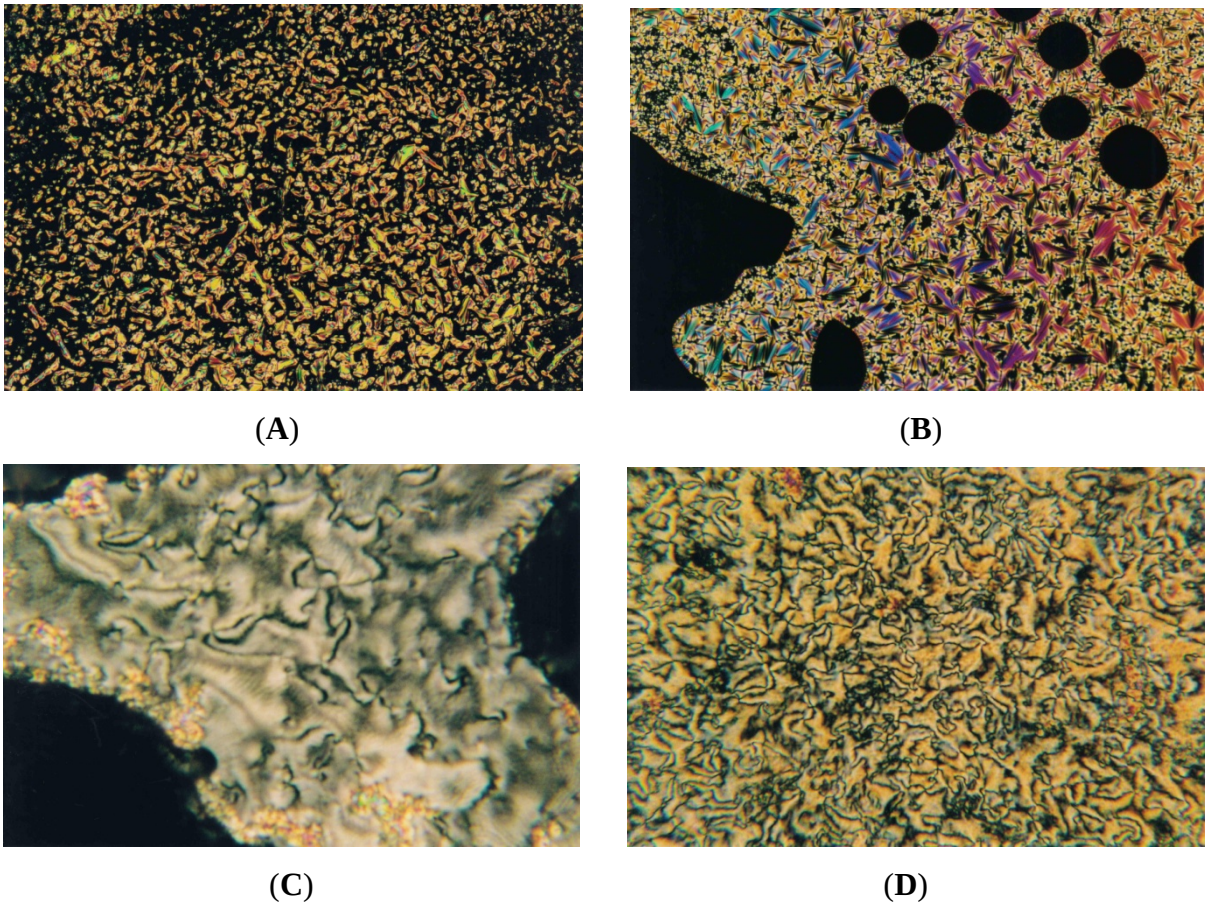

(**A**) (**B**)

(**C**) (**D**)

Figure 9. Textures of smectics phase exhibited by the compounds **11a,c,d** on first heating scan. (**A**) Batonnet forms of the SmA phase at 128.4 °C to the **11a**; (**B**) focal conic-fan texture of SmA phase at 135.0 °C exhibited by **11c**. In the same sample, extinct region (black circle at middle of the picture) was also observed, indicating thermal decomposition of the samples; (**C**) and (**D**) Schlieren texture of SmC phase exhibited by **11a** and **11d** at room temperature, respectively.

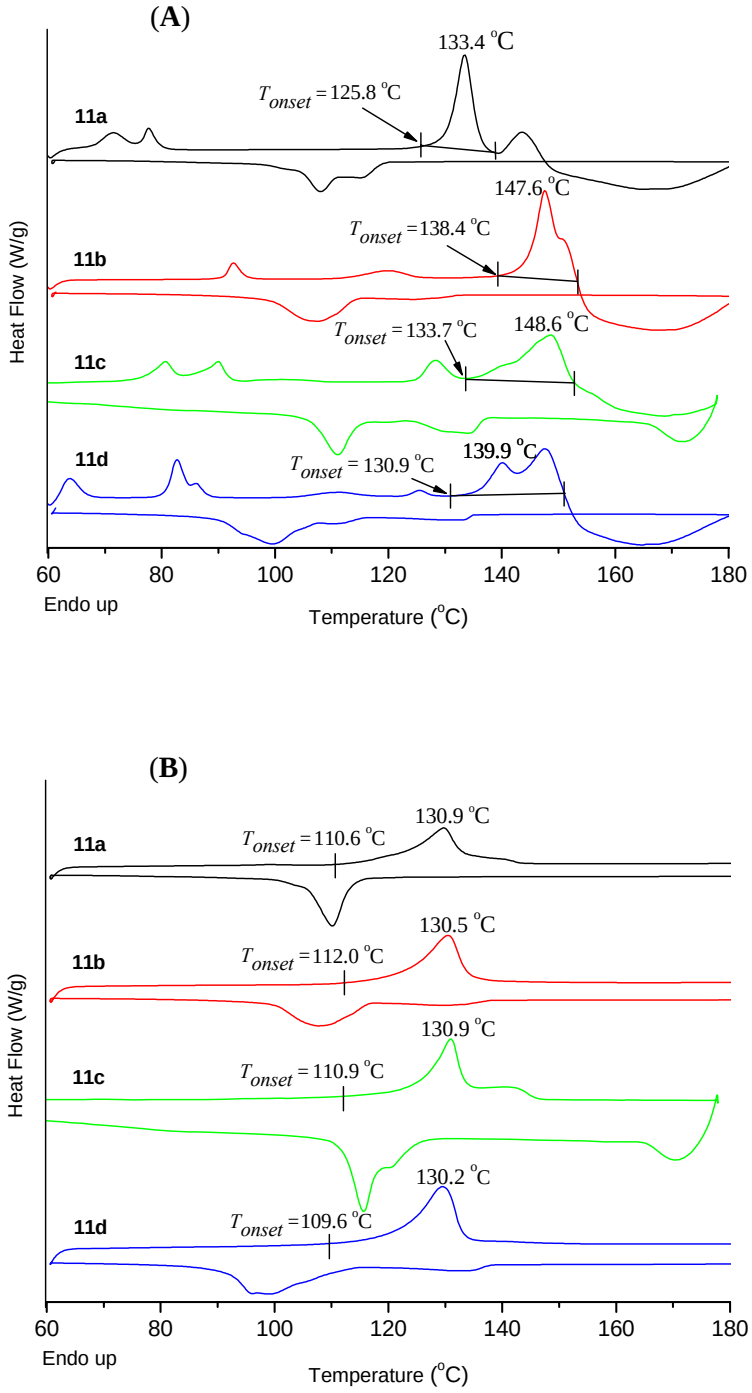

Figure 10. DSC thermograms of **11a-d** on heating/cooling stages: in (**A**) 1st run; (**B**) 2nd run, at rate 10 °C min^{-1}.

Conclusion

In this work we prepared new homologous series of bicyclic compounds **11a-d** *via* 1,3-dipolar cycloaddition reaction between dipolarophile vinylacetic acid and nitrile oxides with 47-53% in yield. The mesomorphic behavior was investigating using POM, DSC and TGA

techniques. On heating, the compounds showed morphological changes, which are thermal decomposition. The compounds **11a-d** exhibits SmA and SmC in the 1st heating/cooling cycle.

Acknowledgments. This work was supported by Conselho Nacional de Desenvolvimento Científico e Tecnológico (project MCT/CNPq nº 555785/2006-8 and Edital Universal/CNPq n° 471194-2008-5), PROCAD-2007/CAPES, INCT-CMN and Coordenação de Aperfeiçoamento de Pessoal de Nível Superior (CAPES) for fellowship. We also thank Prof. Jairton Dupont (IQ-UFRGS) and Antonio de Amorim Borges (IQ-UFRGS) for ESI-MS facilities.

Experimental Section

Instruments and Techniques. 4-Hydroxybenzaldehyde, 1-bromoalkanes, hydroxylamine hydrochloride, acrylic acid, *N*-chlorosuccinimide (NCS), sodium acetate and vinylacetic acid were purchased from Aldrich and used as received unless otherwise specified. Pyridine and toluene were distilled under reduced pressure under argon immediately before use. All other commercial solvents and reagents were used without further purification. The melting points and mesophase transition temperatures and textures of the samples were determined using an Olympus BX43 polarizing microscope in conjunction with a Mettler FP-90 controller and FPHT82 heating stage and DSC 2910 TA Instruments. The rate of heating or cooling was 10 ^{o}C min^{-1}. Nuclear magnetic resonance spectra were obtained on a Varian 300 MHz instrument. Chemical shift are given in parts per million (δ) and are referenced from tetramethylsilane (TMS). Infrared spectra were recorded on a Perkin-Elmer Spectrum One FTIR Spectrometer Instruments using NaCl plates in case of solids and as thin film supported between NaCl plates in case of liquids and are reporter as wavenumber (cm^{-1}). Low-resolution mass spectra were obtained on a Shimadzu CG-MS-QP5050 Mass Spectrometer interfaced with a Shimadzu GC-17A. Gas Chromatograph equipped with a DB-17 MS capillary column. ESI-MS data were collected on a Waters® Micromass® Q-Tof micro™ mass spectrometer with Z-spray electrospray source. Samples were infused from a 100 µL gas-tight syringe at 5 µL min^{-1}, via a syringe pump. Instrument settings were unexceptional: capillary voltage 4500 V, cone voltage 50 V, source temperature 100 ^{o}C, desolvation gas temperature 100 ^{o}C. Nitrogen was used as the desolvation gas. CHN analyses were performed on a Perkin-Elmer 2400 CHN Elemental Analyzer.

Synthesis and characterization

The synthesis of the 4-alkyloxybenzaldehyde (**6a-d**) and the benzaldehydes oximes **7a-d** were prepared according to the procedure describe in reference 11a.

General procedure for the cycloaddition reactions. To an ice-cooled solution of $CHCl_3$ (13 mL), vinylacetic acid (**9**) (4.8 mmol), pyridine (6.3 mmol) and *N*-chlorosuccinimide (NCS) (4.8 mmol) under argon atmosphere was added dropwise a solution of the corresponding oxime **7a-d** (4.2 mmol) in $CHCl_3$ (3 mL) for 40 min. The reaction was then stirred at room temperature for 4 h. The solution was washed with water and dried with Na_2SO_4 anhydrous. The filtrate was evaporated under a reduced pressure and the residue was purified by recrystallisation in toluene (3 times) and one in ethanol to give the products **11a-d** as a white solid.

3,7a-*bis*(4-Heptyloxyphenyl)-7,7a-dihydro-6*H*-isoxazolo[2,3-*d*][1,2,4]oxadiazol-6-yl)acetic acid (11a). Yield: 0.710g, 53%; white solid; m. p. 125.8 ^oC. HRMS (ESI): *m/z* calcd for $[M]^+$ 552.3199, found $[M+1]^+$ 553.3298; $[M+Na]^+$ calcd 575.3097, found 575.3068. EI-MS: *m/z* 533 ($[M + H]^+$), 235, 135 (100 %), 134, 107. ^1H NMR (300 MHz, $CDCl_3$) δ 0.89 (m, 6H, $(CH_3)_2$), 1.38 (m, 16H, $(CH_2)_8$), 1.79 (m, 4H, $(C\underline{H}_2CH_2O)_2$), 2.87 (dd, 1H, NCC$\underline{H}$HCH, *J* = 15.6, 7.5 Hz), 3.05 (dd, 1H, NCCH$\underline{H}$CH, *J* = 15.6, 6.0 Hz), 3.28 (dd, 1H, CHC$\underline{H}$HCO$_2$H, *J* = 16.8, 6.9 Hz), 3.59 (dd, 1H, CHCH$\underline{H}$CO$_2$H, *J* = 16.8, 10.5 Hz), 3.98 (m, 4H, $(CH_2O)_2$), 5.17 (m, 1H), 6.89 (d, 2H, Ar, *J* = 8.4 Hz), 6.93 (d, 2H, Ar, *J* = 8.4 Hz), 7.60 (d, 2H, Ar, *J* = 8,7 Hz), 7.85 (d, 2H, Ar, *J* = 8.7 Hz); ^{13}C NMR (75 MHz, $CDCl_3$/DMSO-d_6) δ 14.0, 22.5, 25.8, 25.9, 28.9, 29.0, 29.1, 31.7, 37.5, 40.4, 68.1, 68.2, 76.3, 114.4, 114.6, 121.3, 122.4, 128.3, 129.5, 156.4, 160.8, 162.7, 166.3, 168.8; IR 3228, 2924, 2854, 1787, 1684, 1608, 1517, 1464, 1377, 1254, 1176, 1098, 1015, 876, 834, 812, 722, 666; Elemental analysis (%) for $C_{32}H_{44}N_2O_6$ (XXX): calcd. C 69.53, H 8.02, N 5.06; found C 68.93, H 8.03, N 4.79.

3,7a-*bis*(4-Octyloxyphenyl)-7,7a-dihydro-6*H*-isoxazolo[2,3-*d*][1,2,4]oxadiazol-6-yl)acetic acid (11b). Yield: 0.680g, 48%; white solid; m. p. 138.4 ^oC. EI-MS: *m/z* 581 ($[M + H]^+$), 495, 249 (100%), 135, 120, 107.^1H NMR (300 MHz, $CDCl_3$) δ 0.89 (m, 6H, $(CH_3)_2$), 1.40 (m, 20H, $(CH_2)_{10}$), 1.79 (m, 4H, $(C\underline{H}_2CH_2O)_2$), 2.87 (dd, 1H, NCC$\underline{H}$HCH, *J* = 15.6, 7.5 Hz), 3.05 (dd, 1H, NCCH$\underline{H}$CH, *J* = 15.6, 6.0 Hz), 3.24 (dd, 1H, CHC$\underline{H}$HCO$_2$H, *J* = 16.8, 6.9 Hz), 3.56 (dd, 1H, CHCH$\underline{H}$CO$_2$H, *J* = 16.8, 10.5 Hz), 3.98 (m, 4H, $(CH_2O)_2$), 5.16 (m, 1H), 6.88 (d, 2H, Ar, *J* = 8.7 Hz), 6.91 (d, 2H, Ar, *J* = 8.4 Hz), 7.60 (d, 2H, Ar, *J* = 8,7 Hz), 7.85 (d, 2H,

Ar, *J* = 8.7 Hz); ^{13}C NMR (75 MHz, $CDCl_3$/DMSO-d_6) δ 14.0, 22.6, 25.8, 25.9, 29.0, 29.1, 29.2, 29.3, 31.7, 37.5, 40.4, 68.1, 68.2, 76.2, 114.4, 114.6, 121.2, 122.2, 128.3, 129.5, 156.4, 160.8, 162.8, 166.4, 168.8; IR 3228, 2924, 2854, 1785, 1684, 1609, 1518, 1464, 1377, 1255, 1176, 1099, 1017, 877, 834, 812, 722, 666. Elemental analysis (%) for $C_{34}H_{48}N_2O_6$ (580.76): calcd. C 70.32, H 8.33, N 4.82; found C 70.28, H 8.46, N 4.84.

3,7a-*bis*(4-Nonyloxyphenyl)-7,7a-dihydro-6*H*-isoxazolo[2,3-*d*][1,2,4]oxadiazol-6-yl)acetic acid (11c). Yield: 0.725g, 50%; white solid; m. p. 133.7 °C. EI-MS: *m/z* 609 ($[M + H]^+$), 523, 262 (100%), 135, 120, 107. ^{1}H NMR (300 MHz, $CDCl_3$) δ 0.89 (m, 6H, $(CH_3)_2$), 1.39 (m, 24H, $(CH_2)_{12}$), 1.79 (m, 4H, $(C\underline{H}_2CH_2O)_2$), 2.88 (dd, 1H, NCC$\underline{H}$HCH, *J* = 15.6, 7.5 Hz), 3.05 (dd, 1H, NCCH$\underline{H}$CH, *J* = 15.6, 6.0 Hz), 3.25 (dd, 1H, CHC$\underline{H}$HCO$_2$H, *J* = 16.8, 6.9 Hz), 3.58 (dd, 1H, CHCH$\underline{H}$CO$_2$H, *J* = 16.8, 10.5 Hz), 3.98 (m, 4H, $(CH_2O)_2$), 5.17 (m, 1H), 6.91 (m, 4H, Ar), 7.60 (d, 2H, Ar, *J* = 8,7 Hz), 7.78 (d, 2H, Ar, *J* = 8.7 Hz); ^{13}C NMR (75 MHz, $CDCl_3$/DMSO-d_6) δ 14.2, 22.7, 25.8, 29.1, 29.2, 29.3, 29.4, 29.5, 31.8, 37.5, 40.4, 68.2, 68.3, 76.3, 114.3, 114.7, 121.3, 122.4, 128.3, 129.8, 156.4, 160.8, 162.5, 166.3, 168.9; IR 3229, 2924, 2854, 1785, 1684, 1609, 1518, 1464, 1377, 1256, 1176, 1098, 1016, 878, 834, 813, 722, 666. Elemental analysis (%) for $C_{36}H_{52}N_2O_6$ (608.82): calcd. C 71.02, H 8.61, N 4.60; found C 71.06, H 8.72, N 4.59.

3,7a-*bis*(4-Decyloxyphenyl)-7,7a-dihydro-6*H*-isoxazolo[2,3-*d*][1,2,4]oxadiazol-6-yl)acetic acid (11d). Yield: 0.720g, 47%; white solid; m. p. 130.9 °C. EI-MS: *m/z* 637 ($[M + H]^+$), 551, 276, 135 (100%), 120, 107. ^{1}H NMR (300 MHz, $CDCl_3$) δ 0.88 (m, 6H, $(CH_3)_2$), 1.39 (m, 28H, $(CH_2)_{14}$), 1.79 (m, 4H, $(C\underline{H}_2CH_2O)_2$), 2.87 (dd, 1H, NCC$\underline{H}$HCH, *J* = 15.6, 7.5 Hz), 3.06 (dd, 1H, NCCH$\underline{H}$CH, *J* = 15.6, 6.0 Hz), 3.25 (dd, 1H, CHC$\underline{H}$HCO$_2$H, *J* = 16.8, 6.9 Hz), 3.57 (dd, 1H, CHCH$\underline{H}$CO$_2$H, *J* = 16.8, 10.5 Hz), 3.98 (m, 4H, $(CH_2O)_2$), 5.17 (m, 1H), 6.91 (m, 4H, Ar), 7.58 (d, 2H, Ar, *J* = 8,7 Hz), 7.80 (d, 2H, Ar, *J* = 8.7 Hz); ^{13}C NMR (75 MHz, $CDCl_3$/DMSO-d_6) δ 14.0, 22.2, 25.5, 25.9, 28.6, 28.7, 28.8, 28.9, 29.0, 31.4, 37.2, 40.0, 67.6, 67.7, 76.0, 113.7, 114.2, 121.0, 122.4, 127.8, 129.3, 155.9, 160.3, 161.9, 166.3, 168.2; IR 3228, 2924, 2854, 1787, 1684, 1609, 1517, 1464, 1377, 1256, 1176, 1097, 1017, 876, 834, 812, 722, 666. Elemental analysis (%) for $C_{38}H_{56}N_2O_6$ (636.87): calcd. C 71.67, H 8.86, N 4.40; found C 71.63, H 8.90, N 4.32.

SUPPORTING INFORMATION – CAPÍTULO 6.2

The 2:1 Cycloadduct from [3+2] 1,3-Dipolar Cycloaddition Reaction. Synthesis and Liquid Crystal Behavior.

Tavares, A.; Gonçalves, P. F. B. and Merlo, A. A.

Instituto de Química, UFRGS. Av. Bento Gonçalves, 9500. Agronomia. 91501-970, Porto Alegre, RS – Brasil.

***e-mail: aloir@iq.ufrgs.br**

Tel.: +55 51 33087316; fax: +55 51 33087304

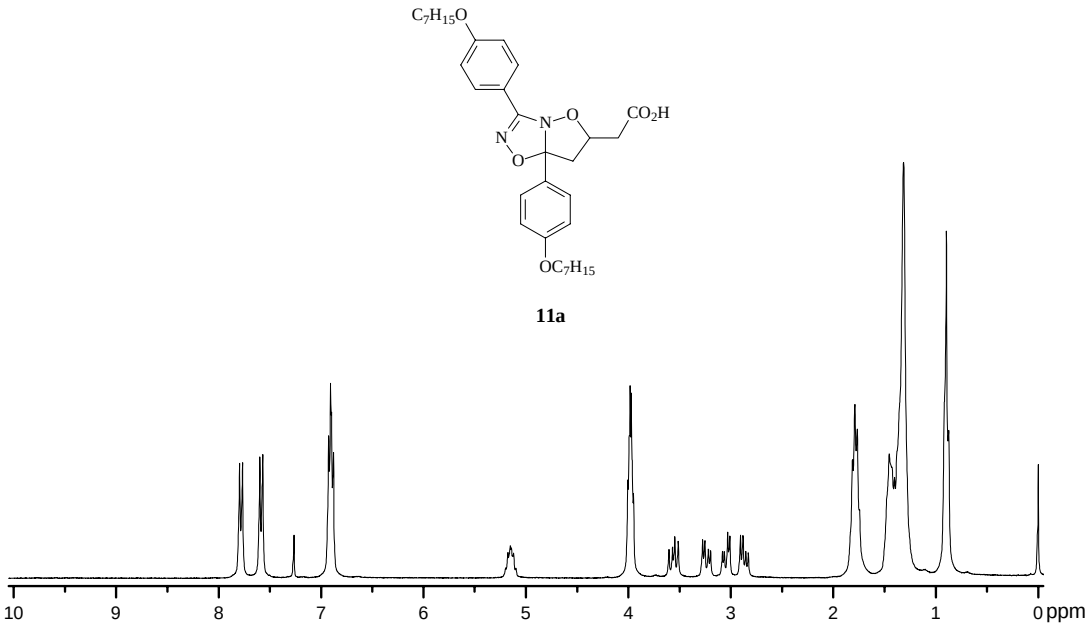

Figure 1. ^{1}H NMR spectrum of compound **11a** (300 MHz, $CDCl_3$).

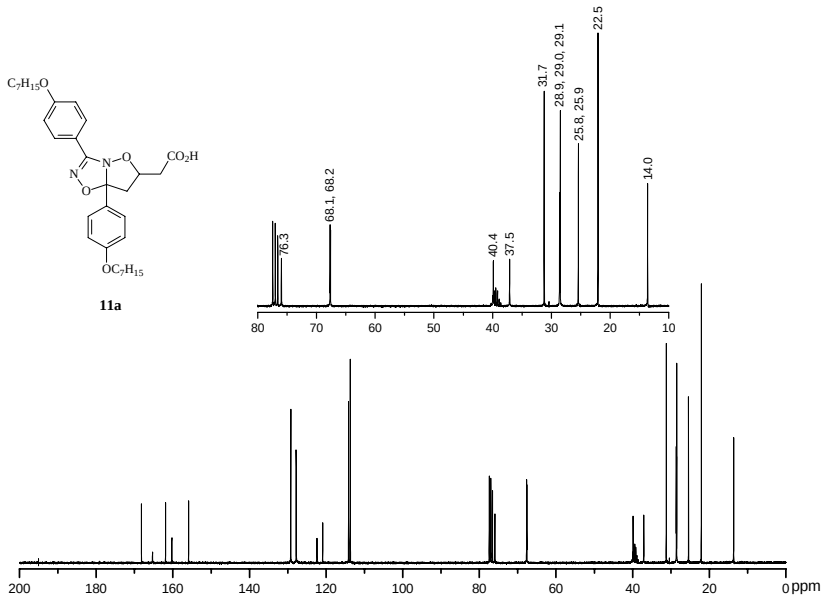

Figure 2. ^{13}C NMR spectrum of compound **11a** (75 MHz, $CDCl_3$/DMSO-d_6).

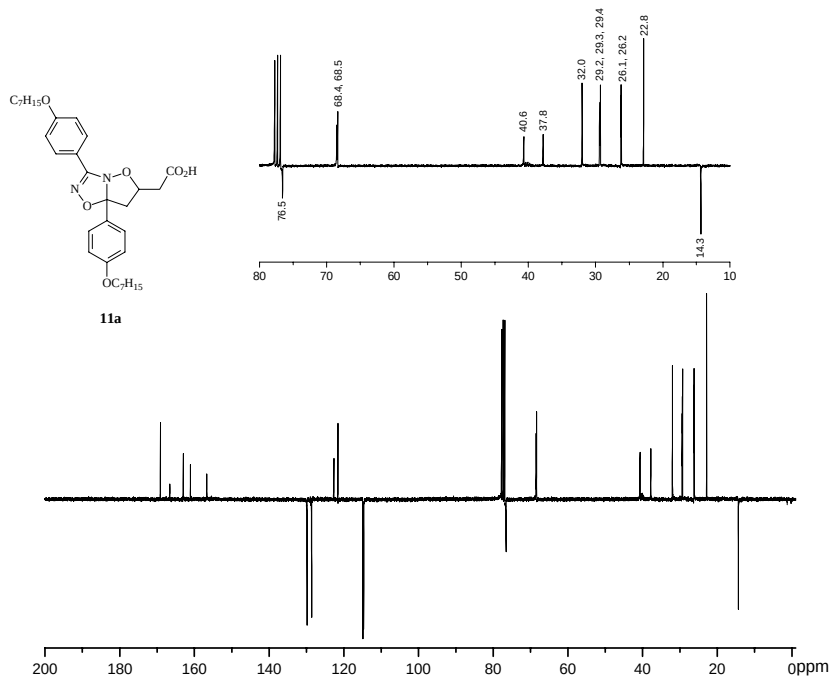

Figure 3. APT NMR spectrum of compound **11a** (75 MHz, $CDCl_3$/DMSO-d_6).

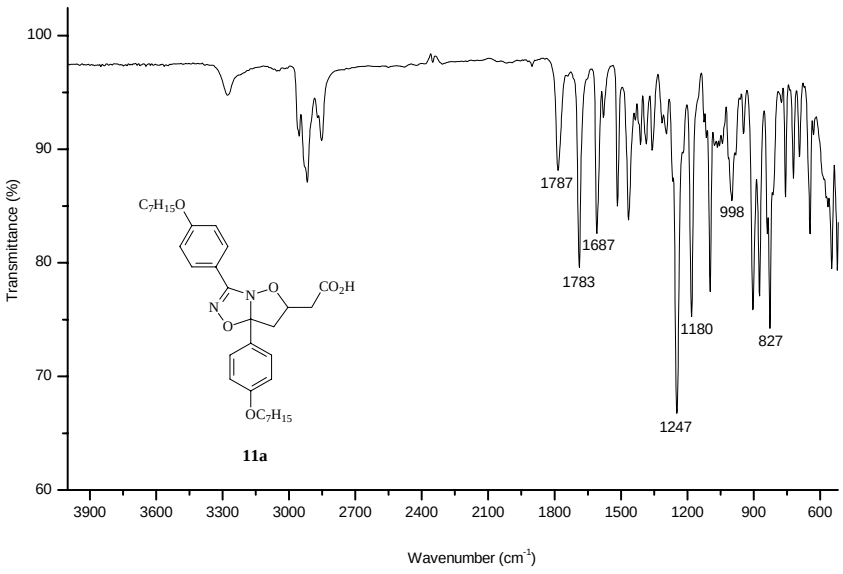

Figure 4. ATR spectrum of compound **11a**.

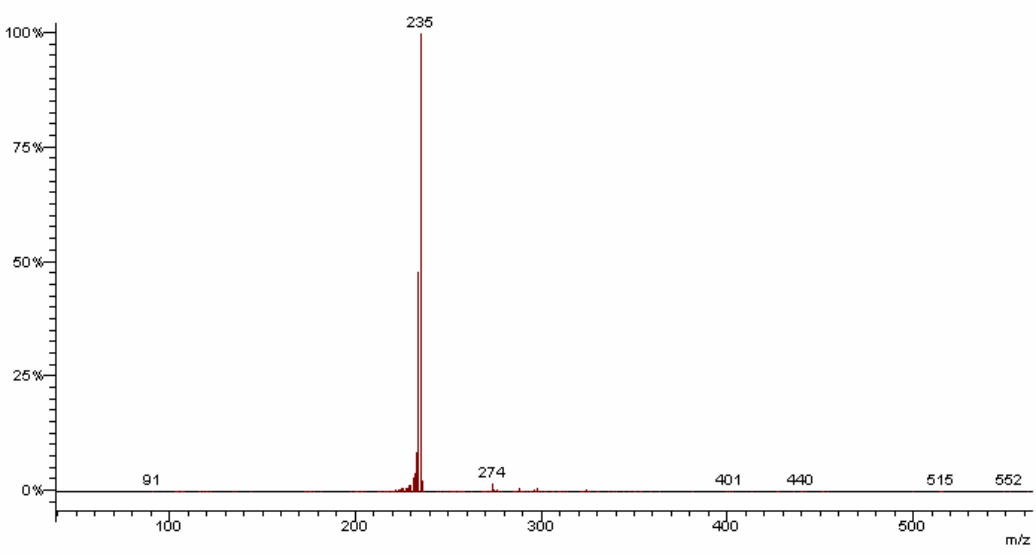

Figure 5. Mass spectra (EI-MS) of compound **11a**.

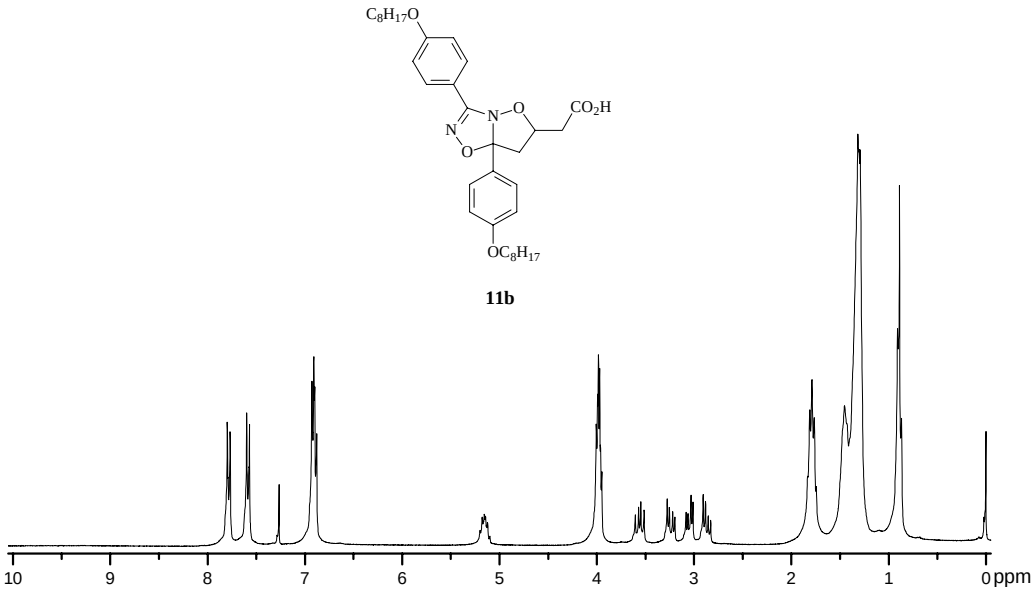

Figure 6. ^{1}H NMR spectrum of compound **11b** (300 MHz, $CDCl_3$).

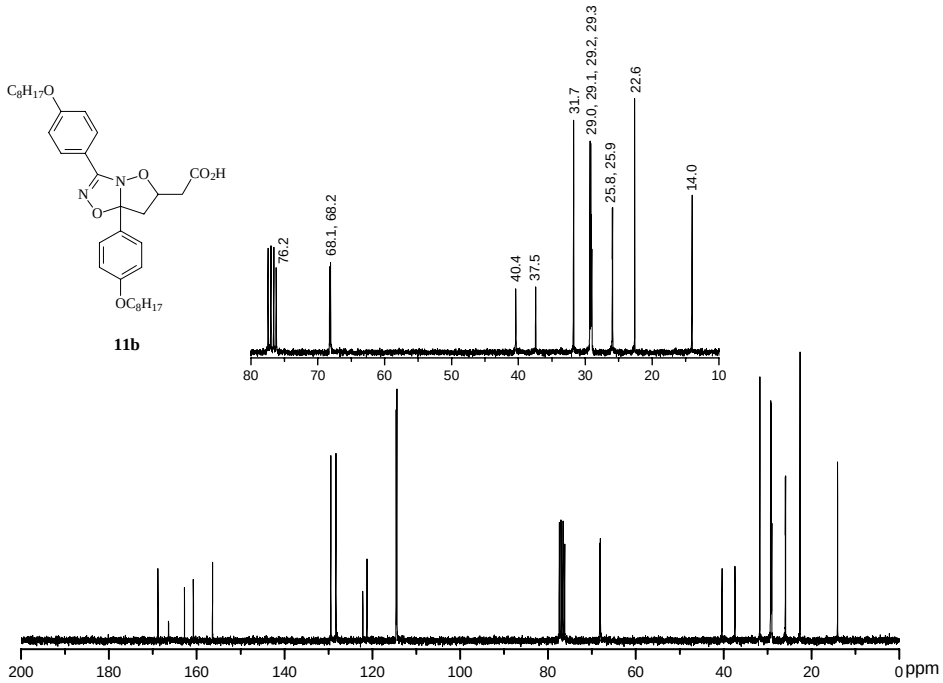

Figure 7. ^{13}C NMR spectrum of compound **11b** (75 MHz, $CDCl_3$).

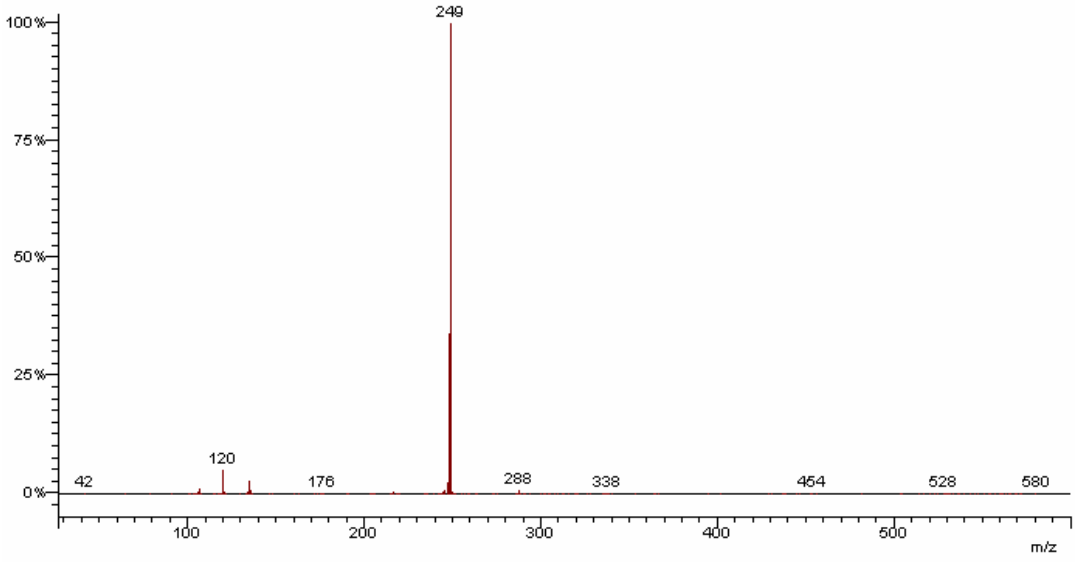

Figure 8. Mass spectra (EI-MS) of compound **11b**.

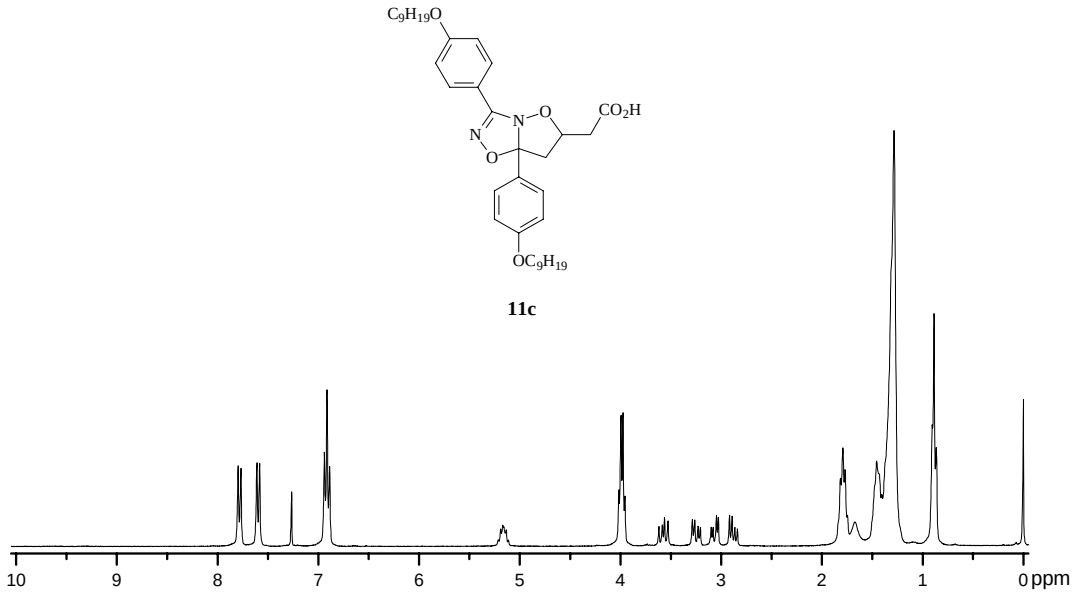

Figure 9. ^{1}H NMR spectrum of compound **11c** (300 MHz, $CDCl_3$).

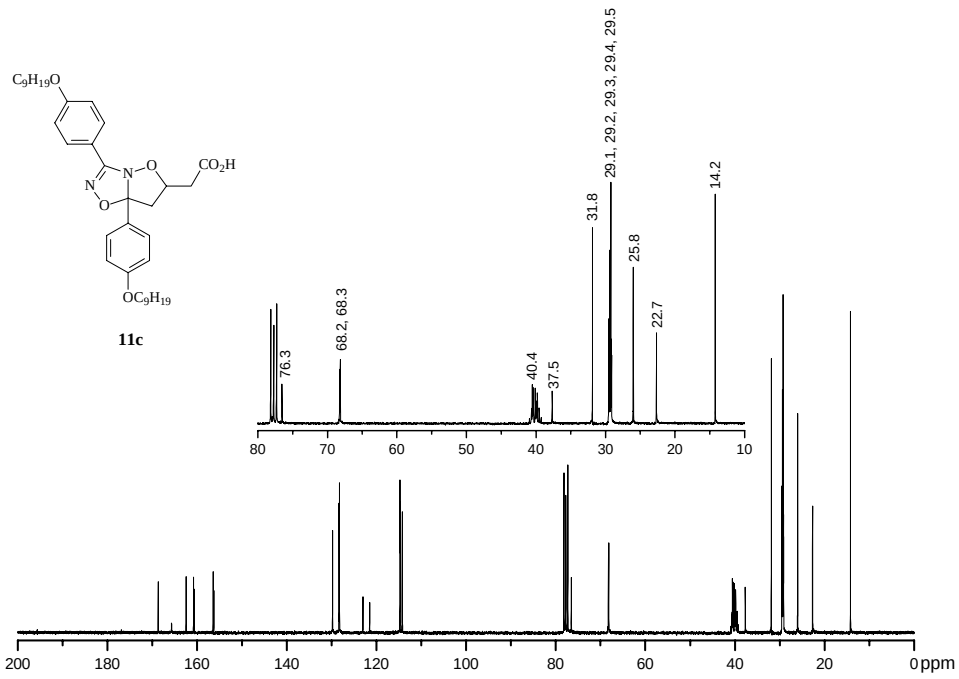

Figure 10. ^{13}C NMR spectrum of compound **11c** (75 MHz, $CDCl_3$/DMSO-d_6).

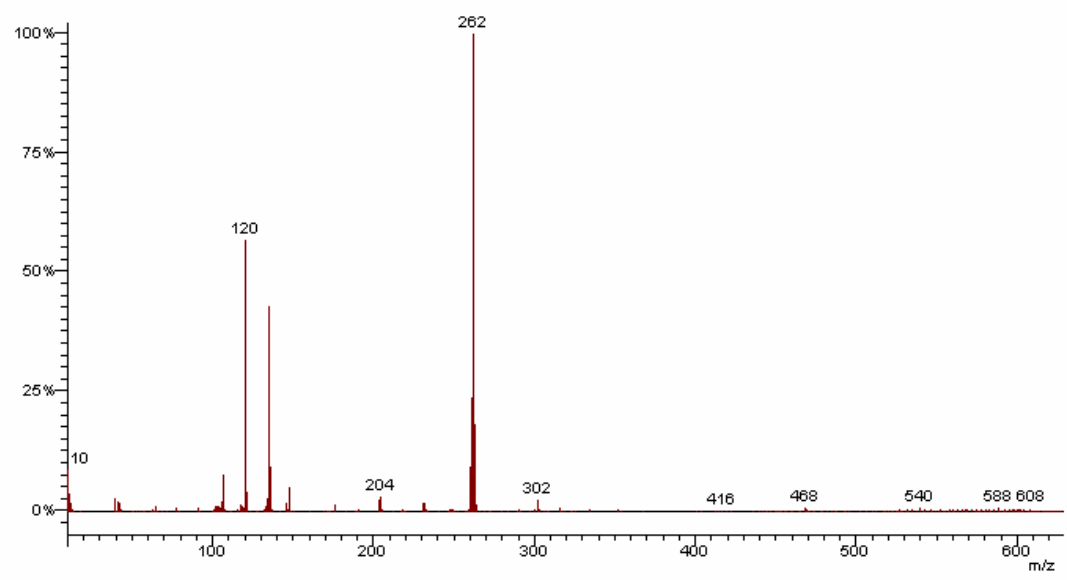

Figure 11. Mass spectra (EI-MS) of compound **11c.**

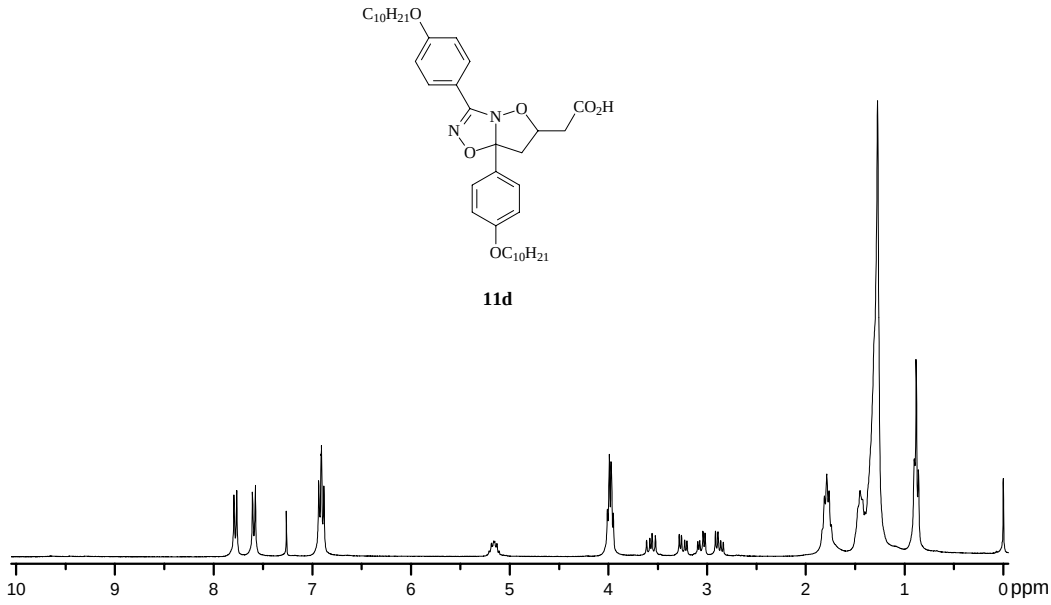

11d

Figure 12. ^{1}H NMR spectrum of compound **11d** (300 MHz, $CDCl_3$).

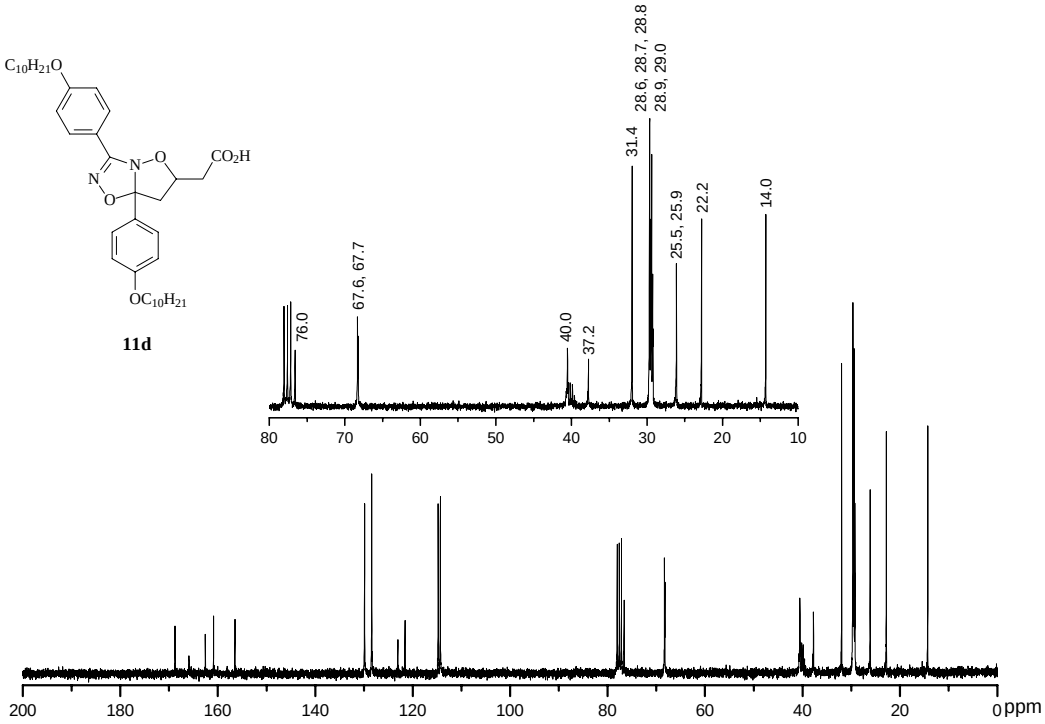

Figure 13. ^{13}C NMR spectrum of compound **11d** (75 MHz, $CDCl_3$/DMSO-d_6).

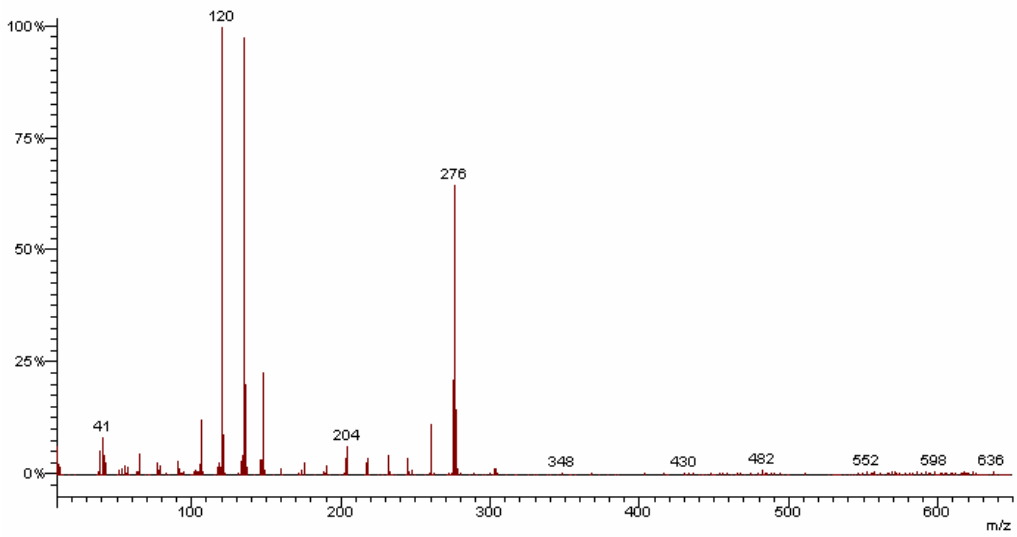

Figure 14. Mass spectra (EI-MS) of compound **11d.**

CAPÍTULO 6.3 – Trabalho em fase final de redação.

Síntese e Propriedades Mesomórficas dos Ésteres Aromáticos 3,5-dissubstituídos Benzoatos de 4,5-dihidroisoxazoíla

Tavares, A.; Gonçalves, P. F. B.; Merlo, A. A.

Instituto de Química, UFRGS. Av. Bento Gonçalves, 9500. Agronomia. 91501-970, Porto Alegre, RS – Brasil.

Resumo: Neste trabalho é discutida a síntese e as propriedades mesomórficas de novos ésteres liquido-cristalinos **5a-d** e **9a-d** contendo o anel isoxazolínico 3,5-dissubstituído. Alguns compostos finais apresentaram propriedades líquido-cristalinas nemática ou esmética C. As propriedades estruturais das séries de cristais líquidos foram estudadas usando o método DFT no nível B3LYP/ccpVDZ. As isoxazolinas intermediárias **3a-d** foram sintetizados via reação de cicloadição [3+2] 1,3-dipolar entre óxidos de nitrila, os quais foram gerados pela oxidação *in situ* a partir das respectivas oximas aromáticas, e os dipolarófilos derivados do álcool alílico (CH_2=CH(CH_2)$_n$OH, n = 1, 2, 3 e 4). Os ésteres finais **5a-d** foram sintetizados via reação de esterificação direta de **3a-d** com o ácido *p*-*n*-deciloxibenzóico **4**. A série dos ésteres **9a-d** foram sintetizadas via derivatização das respectivas isoxazolinas **3a-d** em ésteres bromados intermediários **7a-d**, seguido da reação de Sonogashira com o alcino **8**.

Abstract: The synthesis and liquid-crystalline properties of novel esters **5a-d** and **9a-d** containing the 3,5-dissubstituted isoxazoline ring are reported. Some final compounds showed smectic C (SmC) and nematic (N) phase. Theoretical calculations were performed using the DFT B3LYP/ccpVDZ level. The intermediate isoxazolines **3a-d** were synthesized by cycloaddition reaction [3 + 2] 1,3-dipolar between nitrile oxides, which were generated by oxidation *in situ* from the respective aromatic oximes and dipolarophiles derived from allyl alcohol (CH_2=CH (CH_2)nOH, n = 1, 2, 3 and 4). Esters **5a-d** were synthesized through esterification of **3a-d** and *p*-*n*-deciloxibenzoic **4**. The series of esters **9a-d** were synthesized by derivatization of isoxazolinas **3a-d** into bromoesters **7a-d** followed by reaction of Sonogashira with alkyne **8**.

Introdução

As moléculas que contêm anéis heterocíclicos constituem uma classe de importantes produtos e que despertam interesse na pesquisa já há bastante tempo devido às diversas aplicações destes compostos nas áreas biológica, química e tecnológica. Por exemplo, os isoxazóis e isoxazolinas, além de apresentarem atividade biológica bem conhecida[1], são heterociclos que podem fornecer importantes intermediários em síntese orgânica na preparação de estruturas bifuncionais como β-hidroxicetonas, cetonas α-β insaturadas, 1,3-aminoácidos, 1,3-dióis, os quais são obtidos diretamente a partir da clivagem redutiva do anel ou de reações consecutivas.[2] Além disso, constituem importantes blocos de construção para a preparação de produtos farmacêuticos e naturais.[3]

Também, é conhecido que compostos que contêm anéis heterocíclicos de 5 membros e grupos mesógenos como tolano, naftila e bifenila podem apresentar propriedades líquido-cristalinas.[4] As principais características estruturais que uma molécula na forma de bastão deve apresentar para o aparecimento de mesofase são: *i.* forma alongada; *ii.* rigidez; *iii.* dipolos permanentes e grupos polarizáveis e *iv.* grupos finais com dipolo fraco. A presença de heteroátomos atua no aumento do dipolo da molécula e da anisotropia dielétrica levando a uma organização a nível molecular através da geração de interações eletrostáticas entre as moléculas. Hoje em dia derivados desses compostos também vêm mostrando grande relevância na síntese de materiais semicondutores[5].

---

[1] (a) Shah, T.; Desai, V. *J. Serb. Chem. Soc.* **2007**, *72*, 443; (b) Gaonkar, S. L.; Rai, K. M. L.; Prabhuswamy, B. *Med. Chem. Res.* **2007**, *15*, 407; (c) Xiang, Y.; Chen, J.; Schinazi, R. F.; Zhao, K. *Bioorg. Med. Chem. Lett.* **1996**, *6*, 1051; (d) Zhang, L.; Anzalone, L.; Ma, P.; Kauffman, G. S.; Storace, L.; Ward, R. *Tetrahedron Lett*. **1996**, *37*, 4455; (e) Dallanoce, C.; Meroni, G.; De Amici, M.; Hoffmann, C.; Klotz, K-N.; De Micheli, C. *Bioorg. Med. Chem.* **2006**, *14*, 4393; (f) Wade, P. A.; Pillay, M. K.; Singh, S. M. *Tetrahedron Lett.* **1982**, *23*, 4563.

[2] (a) Kozikowski, A. P. *Acc. Chem. Res.* **1984**, *17*, 410; (b) Fuller, A. A.; Chen, B.; Minter,A. R.; Mapp, A. K. *J. Am. Chem. Soc.* **2005**, *127*, 5376; (c) Aschwanden, P.; Kvaerno, L.; Geisser, R. W.; Kleinbeck, F.; Carreira, E. M. *Org. Lett.* **2005**, *7*, 5741.

[3] (a) Traxler, P.; Trinks, U.; Buchdunger, E.; Mett, H.; Meyer, T.; Muller, M.; Regenass, U.; Rosel, J.; Lydon, N.; *J. Med. Chem.* **1995**, *38*, 2441; (b) Dimmock, J. R.; Sidhu, K. K.; Chen, M.; Reid, R. S.; Allen, T. M.; Kao, G. Y.; Truitt, G. A. *Eur. J. Med. Chem.* **1993**, *28*, 313.

[4] (a) Byron, D. J.; Harwood, D. J.; Wilson, R. C. *J. Chem. Soc. Perkin Trans. II* **1983**, *197*; (b) Tavares, A.; Schneider, P. H.; Merlo, A. A. *Eur. J. Org. Chem.* **2009**, 889; (c) Tavares, A.; Livotto, P. R.; Gonçalves, P. F. B.; Merlo, A. A. *J. Braz. Chem. Soc*. **2009**, *9*, 1742; (d) Tavares, A.; Ritter, O. M. S.; Vasconcelos, U. B.; Arruda, B. C.; Schrader, A.; Schneider, P. H.; Merlo, A. A. *Liq. Cryst.* **2010**, *37*, 159; (e) Vasconcelos, U. B.; Merlo, A. A. Synthesis **2006**, *7*, 1141; (f) Cristiano, R.; Santos, D. M. O.; Gallardo, H. *Liq. Cryst.* **2005**, *32*, 7; (g) Giménez, R.; Piñol, M.; Serrano, J. L. *Chem. Mater.* **2004**, *16*, 1377; (h) Merlo, A. A.; Braun, J. E.; Vasconcelos, U. B. *Liq. Cryst.* **2000**, *27*, 657.

[5] (a) Inokuchi, H. *Org. Elet.* **2006**, *7*, 62; (b) Oyston, S.; Wang, C.; Hughes, G.; Batsanov, A. F.; Perepichka, I. F.; Bryce, M. R.; Ahn, J. H.; Pearson, C.; Petty, M. C. *J. Mater. Chem.* **2005***, 15*, 194; (c) Vieira, A. A.; Cristiano, R.; Bortoluzzi, A. J.; Gallardo, H. *J. Mol. Struct*, **2008**, *875*, 364.

Os heterociclos de 5 membros como as isoxazolinas, isoxazóis, pirazóis e triazóis são convenientemente preparados a partir da reação de cicloadição 1,3-dipolar.[6] Por exemplo, a cicloadição entre oximas substituídas e alcenos ou alcinos terminais em meio básico é a metodologia amplamente utilizada para a preparação de 2-isoxazolinas e isoxazóis, respectivamente.

Previamente publicamos trabalhos sobre a síntese e estudo das propriedades líquido-cristalinas de isoxazolinas 3,5-dissubstituídas onde foi observada uma influência do número de carbonos das cadeias carbônicas laterais nas características estruturais e estabilidade dos compostos.

Em continuação ao nosso trabalho na preparação de compostos contendo isoxazolinas, neste trabalho informamos a síntese e investigação das propriedades líquido-cristalinas de duas novas séries homólogas **5a-d** e **9a-d** com destaque para a variação do número de átomos de carbonos metilênicos na estrutura molecular destes compostos.

Resultados e Discussão

A rota sintética utilizada para a síntese das isoxazolinas **3a-d** está descrita no Esquema 1. O aldeído **2** foi sintetizado a partir da alquilação do 4-hidroxibenzaldeído **1** com bromooctano com rendimento de 72%.[4b] As isoxazolinas foram obtidas a partir da reação de cicloadição [3+2] 1,3-dipolar entre o óxido de nitrila gerado *in situ* a partir da 4-*n*-octiloxibenzaldeído oxima a 4 diferentes dipolarófilos derivados de álcoois alílicos produzindo as isoxazolinas **3a-d** com 33-36% de rendimento. Os compostos foram caracterizados por RMN de ^{1}H e ^{13}C como o cicloaduto 3,5-dissubstituído, obtido a partir da adição do oxigênio do óxido de nitrila ao carbono mais substituído da ligação C=C.

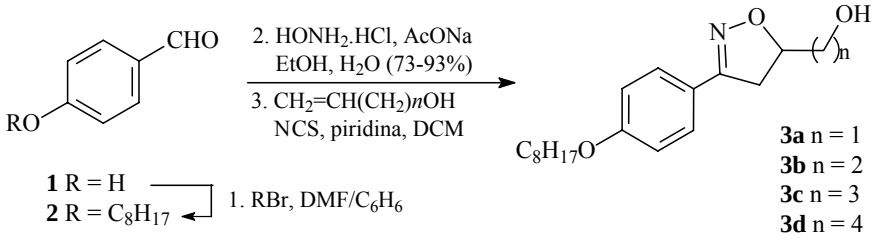

Esquema 1. Rota sintética utilizada para a preparação dos compostos isoxazolínicos **3a-d**.

[6] (a) Jäger, V.; Colinas, P. A. "*Nitrile Oxides*" em *The Chemistry of Heterocyclic Compounds*. Vol. 59; Padwa, A. e Pearson, W. H., Eds.; Wiley: New York, 2002; (b) Carey, F. A.; Sundberg, R. J. *Advanced Organic Chemistry, Part B: Reactions and Synthesis*. Plenum Press, 2008; (c) Huisgen R. 1*,3-Dipolar Cycloadditon Chemistry*. Padwa, A., Ed.; Vol. 1. Wiley: New York, 1984.

O desenho e a síntese dos cristais líquidos **5a-d** e **9a-d** foram baseados considerando as características estruturais necessárias para o aparecimento de mesofase assim como a viabilidade de síntese. Nesse sentido, os compostos isoxazolínicos **3a-d** não apresentaram propriedades líquido-cristalinas, pois podem ser consideradas moléculas de baixa anisometria de forma. Já os compostos **5a-d** (Esquema 2), que possuem uma estrutura molecular mais alongada, apresentaram fase líquido-cristalina esmética. Estes compostos foram preparados a partir da reação de esterificação entre os compostos isoxazolínicos **3a-d** e o ácido *p*-*n*-deciloxibenzóico **4** na presença de DCC e DMAP catalítico em solução de THF.

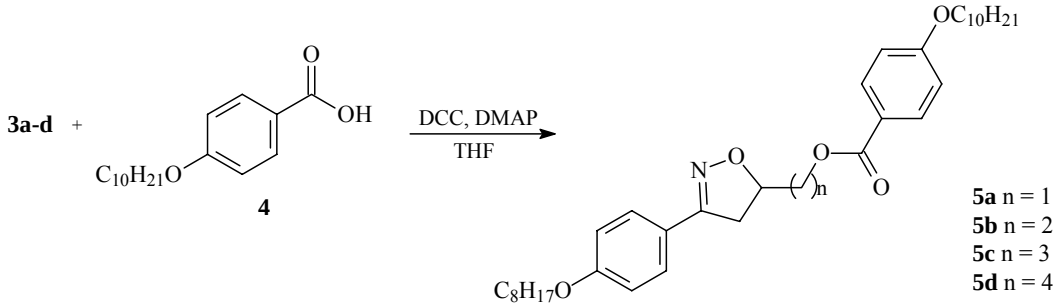

Esquema 2. Caminho sintético para a preparação de ésteres isoxazolínicos.

Os compostos **7a-d** (Esquema 3) são os precursores para a síntese dos materiais líquido-cristalinos finais **9a-d**. Estes compostos foram preparados a partir da reação de esterificação entre os compostos isoxazolínicos **3a-d** e o ácido *p*-bromobenzóico **6** na presença de DCC e DMAP catalítico em THF.

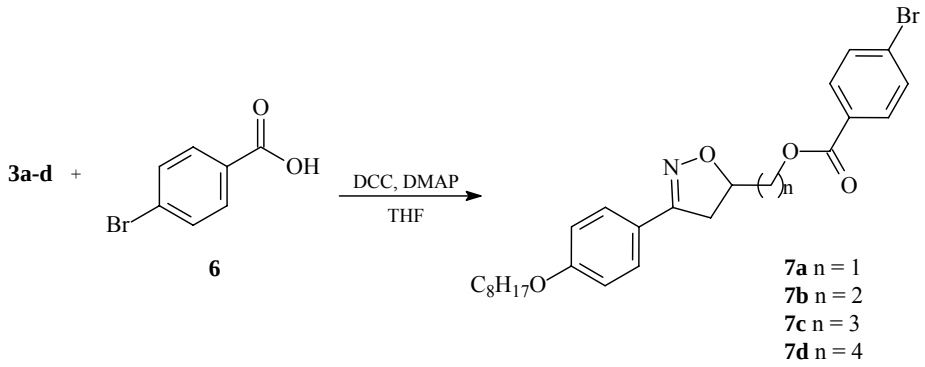

Esquema 3. Caminho sintético para a preparação de compostos precursores de cristais líquidos.

Apesar de apresentarem um grupo polarizável - condição que pode gerar mesofase – os compostos não apresentaram comportamento líquido-cristalino. Devido a isso não foram realizadas análises de DSC destes compostos, onde os dados de temperatura apresentados na

Tabela 1 foram obtidos somente por microscopia óptica. As moléculas desta série apresentam uma razão comprimento/largura (*l*/*d)* menores que as da série **5a-d** devido à ausência de uma das cadeias alquílicas terminais. Além da menor razão *l*/*d*, a presença do átomo de bromo gera um dipolo terminal intenso o suficiente para formar interações muito fortes entre as moléculas segundo o eixo molecular maior, favorecendo apenas a transição direta da fase cristal para a fase isotrópica.

Os compostos **9a-d** de acordo com o Esquema 4 foram preparados a partir da reação de acoplamento de Sonogashira entre os compostos isoxazolínicos **7a-d** e o alcino terminal **8** na presença de catalisador de paládio, CuI e PPh_3 em Et_3N.

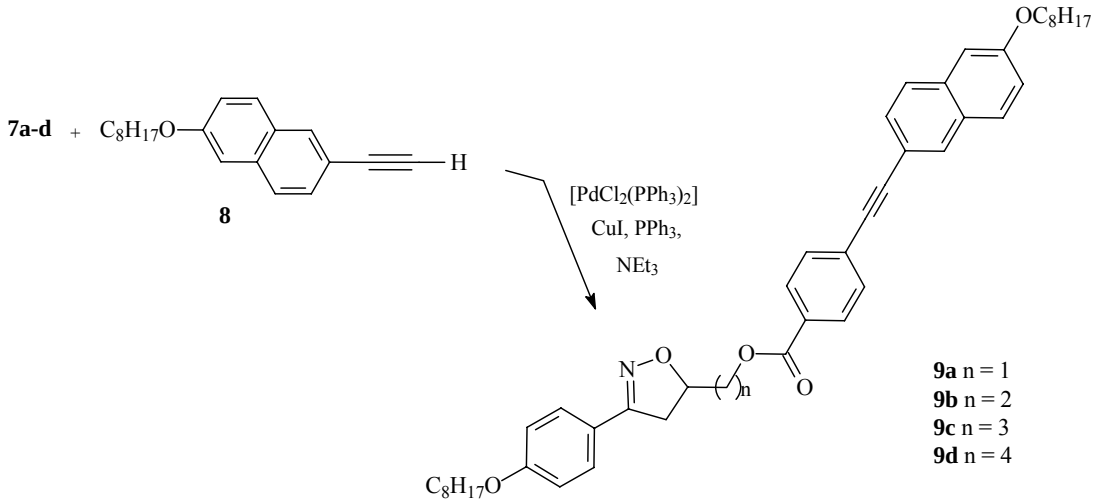

Esquema 4. Caminho sintético para a preparação dos ésteres isoxazolínicos **9a-d** contendo o grupo naftila.

A mesofase para os compostos da série **5** foi identificada como SmC a partir da observação da textura de leque quebrado por microscopia óptica (Figuras 1A e 1B). A identificação da mesofase N dos compostos da série **9** foi realizada a partir da observação visual das texturas *Schlieren* e planar (Figuras 1C e 1D) em microscópio óptico e pelos baixos valores de entalpia da transição I→mesofase. Os compostos desta série têm estrutura molecular em forma de bastão mais pronunciada que a dos compostos das séries **5** e **7** e, conseqüentemente, apresentaram mesofase mais estável (enantiotrópica) que os compostos da série **5**. As temperaturas de transição de fase e os dados calorimétricos estão apresentados na Tabela 1.

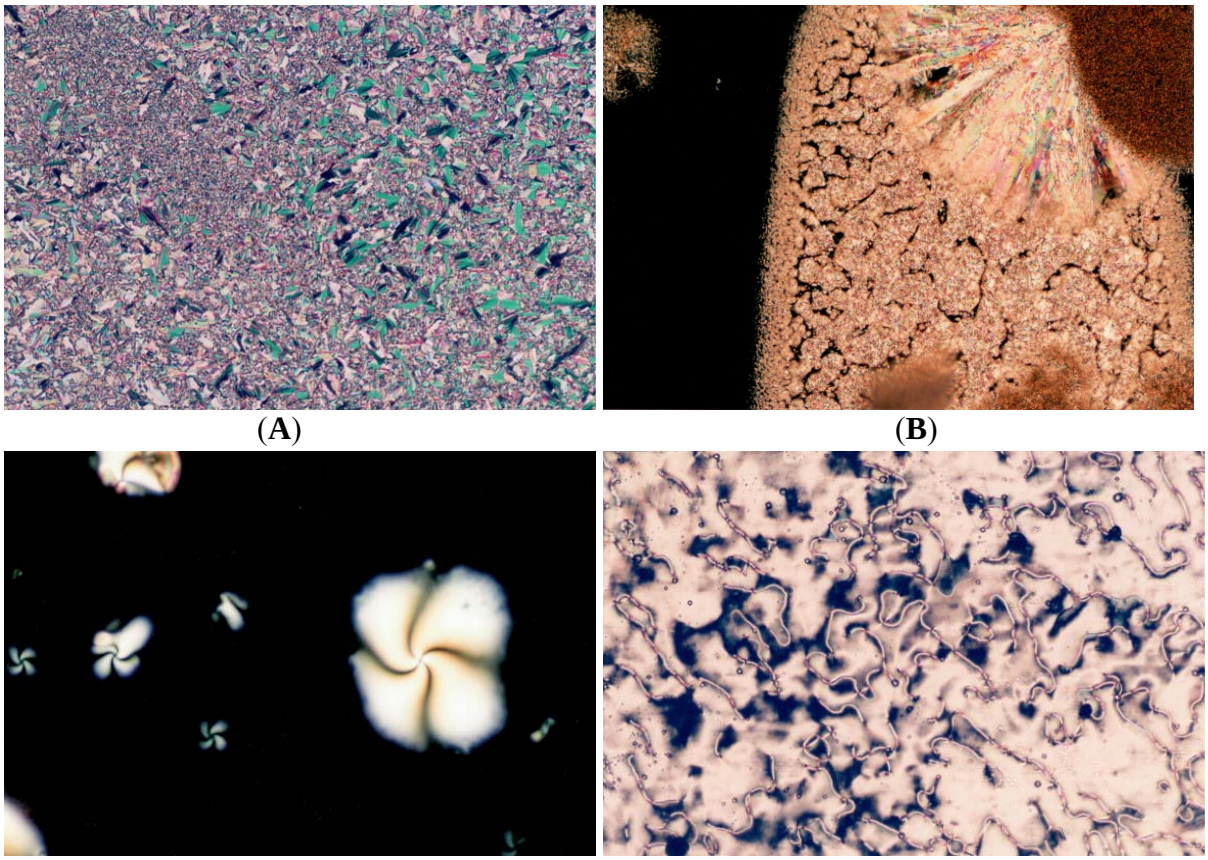

(**A**) (**B**)

(**C**) (**D**)

Figura 1. Fotomicrografias das texturas obtidas por microscopia óptica no resfriamento (x10) da: (A) textura de leque quebrado da mesofase SmC exibida pelo composto **5a** a 78,9 ^{o}C; (B) coexistência da textura de leque quebrado da mesofase SmC e da fase cristal exibida pelo composto **5d** a 55,8 ^{o}C no resfriamento rápido; (C) textura Schlieren da mesofase N exibida pelo composto **9b** a 129,6 ^{o}C; (D) textura planar da mesofase N exibida pelo composto **9d** a 120,6 ^{o}C.

Os compostos da série **5a-d** diferem entre si no número de carbonos da cadeia alquílica interna. De acordo com os dados de DSC mostrados na Tabela 1, os compostos **5a** e **5b** apresentaram comportamento monotrópico com 2 picos exotérmicos durante o segundo resfriamento. Os picos correspondentes à transição isotrópico-SmC para estes compostos foram em 82,8 ^{o}C e 61,0 ^{o}C, respectivamente. Já os homólogos superiores **5c** e **5d** não apresentaram comportamento mesomórfico possível de ser observado pela análise de DSC. Porém, no resfriamento rápido da temperatura (amostra exposta ao ambiente externo) foi possível observar a fase SmC (homeotrópica) durante o processo de cristalização (Figura 4B, para o composto **5d**).

A Figura 2 (A) mostra a variação nas temperaturas de transição com o aumento do número de átomos de carbonos na cadeia carbônica interna. Ambas as transições cristal-isotrópico e isotrópico-SmC (para os compostos **5a** e **5b**) diminuem à medida que a cadeia aumenta. Também, é observado um efeito par-ímpar nestas transições, o que pode ser entendido como

uma conseqüência do parâmetro de ordem com respeito ao eixo molecular.[7] Os valores de entalpia também mostraram este efeito. O comportamento da entropia indica a natureza da transição envolvida. Na Figura 2 (B) pode-se observar uma tendência crescente no valor das entropias de fusão com o aumento do número de átomos de carbonos metilênicos, além do efeito par-ímpar. Os maiores valores de entropia são observados para os compostos com número ímpar de átomos de carbonos (**5a** e **5c**), o que está indicando um melhor empacotamento molecular destas moléculas na transição do que aquelas com número par de átomos de carbono, o que pode ser conseqüência de uma maior linearidade daquelas moléculas.

Tabela 1. Temperaturas de transição* (°C) e valores de variação de entalpia (kcal mol^{-1}) e entropia das séries homólogas **5a-d**, **7a-d** e **9a-d**.

Composto	Temperaturas de transição de fase		ΔT^c	Valores de entalpia		$\Delta S/R^e$ ($x10^{-5}$)
	Aquecimento	Resfriamento		Fusão[d]	I - fase – Cr	
5a	Cr 103,0 I	I 82,8 SmC 73,7 Cr	9,1	17,95	I 3,12 SmC 10,29 Cr	2,4
5b	Cr 72,3 I	I 61,0 SmC 53,6 Cr	7,4	8,67	I 2,06 SmC 4,15 Cr	1,2
5c	Cr 85,3 I	I 65,8 Cr[b]	-	23,13	-	3,2
5d	Cr 68,3 I	I 57,1 Cr[b]	-	13,37	-	1,9
7a	Cr 115,2 I[a]	I 103,8 Cr [a]	-	-	-	-
7b	Cr 89,9 I[a]	I 77,5 Cr [a,b]	-	-	-	-
7c	Cr 98,8 I[a]	I 80,5 Cr [a,b]	-	-	-	-
7d	Cr 73,1 I[a]	I 60,8 Cr [a,b]	-	-	-	-
9a	Cr 145,8 N 161,7 I	I 160,7 N 134,8 Cr	15,9	10,65	I 0,51 N 10,75 Cr	1,2
9b	Cr 124,7 N 136,1[a] I	I 135,8 N 120,2 Cr	11,4	5,34	I 1,38 N 9,2 Cr	0,7
9c	Cr 129,3 N 148,7 I	I 149,0 N 113,6 Cr	19,4	11,46	I 0,23 N 11,71 Cr	1,4
9d	Cr 109,7 N 135,3 I	I 142,0 N 100,9 Cr	25,6	6,85	I 0,78 N 10,90 Cr	0,9

*Temperaturas de início (T_{onset}). Dados obtidos do DSC com velocidade de aquecimento e resfriamento de 10 °C min^{-1}; Cr = fase cristal; SmC = esmética C; N = nemática; I = líquido isotrópico. [a]As temperaturas foram obtidas por análise de microscopia óptica. [b]Após resfriamento rápido a amostra apresentou mesofase SmC. [c]Faixa de existência de mesofase no resfriamento para os compostos **5a** e **5b** e aquecimento para **9a-d**. [d]Valores de entalpia (segundo ciclo de aquecimento/resfriamento) obtidos na transição Cr-I para os compostos da série **5a-d** e na transição Cr-N para a série **9a-d**. [e]Valores de entropia de fusão obtidos na transição Cr-I para os compostos da série **5a-d** e na transição Cr-N para a série **9a-d**. R = 8,31 J K^{-1} mol^{-1}.

[7] (a) Pink, D. P. *J. Chem. Phys.* **1975**, *63*, 2533; (b) Imrie, C. T.; Henderson, P. A. *Chem. Soc. Rev*. **2007**, *36*, 2096; (c) Carnelley, T. *Philos. Mag*. **1882**, *13*, 112.

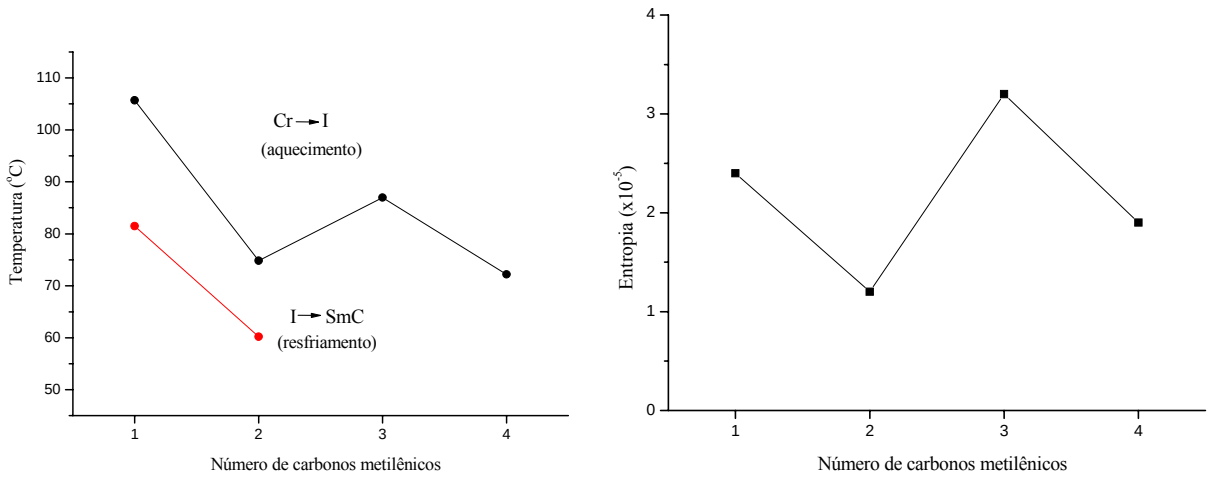

Figura 2. Gráficos do número de átomos de carbono metilênicos (*n*) na cadeia alquílica interna para os compostos da série **5a-d** em função (A) das temperaturas de transição de fase e (B) da entropia da transição Cr→I.

Os compostos da série **9a-d** diferem entre si no número de carbonos da cadeia alquílica interna, assim como a série **5a-d**. De acordo com os dados de DSC (Tabela 1 e Figura 3), todos os compostos desta série apresentaram mesofase nemática enantiotrópica. No aquecimento, a faixa de existência de mesofase aumenta à medida que aumenta o número de carbonos na série: para **9a** $\Delta T = 15,9\ ^{o}C$ e para **9d** $\Delta T = 25,6\ ^{o}C$.

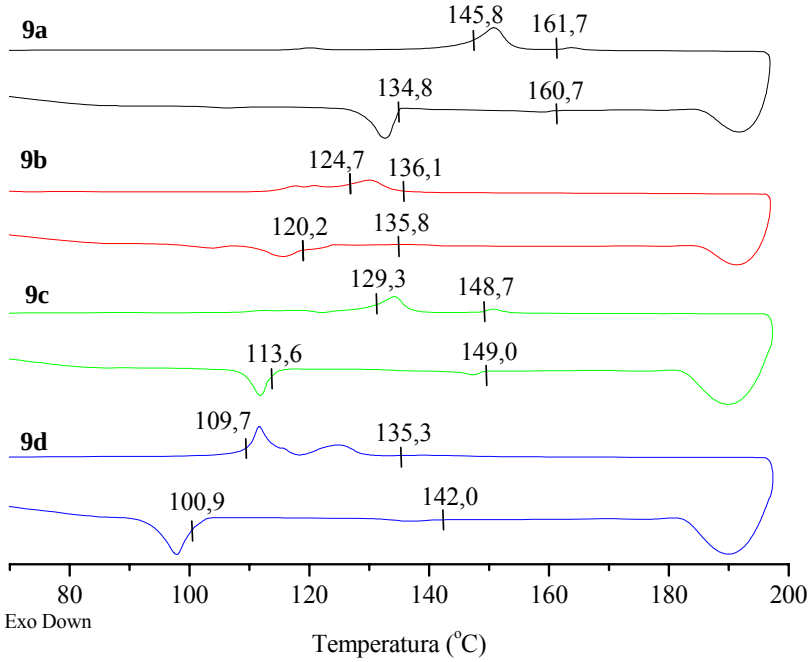

Figura 3. Termogramas de DSC dos compostos da série **9a-d** na segunda corrida de aquecimento/resfriamento. Todas as corridas foram realizadas com velocidade de 10 $^{o}C\ min^{-1}$.

A Figura 4A mostra a variação das temperaturas de transição com o aumento do número de átomos de carbonos na cadeia carbônica interna. Ambas as transições isotrópico→N e cristal→N diminuem à medida que a cadeia aumenta, assim como pode ser observado um efeito par-ímpar nestas transições. Os valores de entalpia também mostraram este efeito e são consistentes com a mesofase N menos ordenada. Os valores de entropia apresentaram o mesmo comportamento que os compostos da série **5**, porém neste caso os valores são menores uma vez que se trata de transições Cr→mesofase, as quais são fases mais ordenadas que a fase isotrópica (Figura 4B).

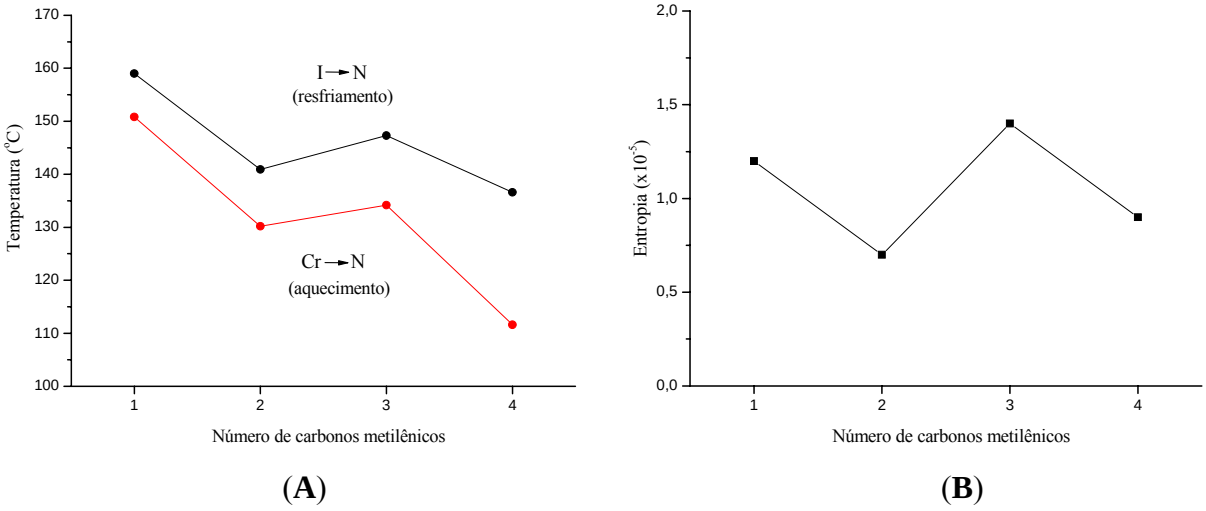

(**A**) (**B**)

Figura 4. Gráficos do número de átomos de carbono metilênicos (*n*) na cadeia alquílica interna para os compostos da série **9a-d** em função (A) das temperaturas de transição de fase e (B) da entropia da transição Cr→N (aquecimento).

Cálculos Teóricos

Foram realizados estudos teóricos para avaliar a influência do número de carbonos na cadeia alquílica interna nos valores de momento de dipolo, energia de Hartree e orbitais moleculares de fronteira HOMO e LUMO. Na Tabela 2 podem-se observar os valores de energia calculados para os compostos da série **5**.

Tabela 2. Valores de momento de dipolo, energia de Hartree e diferença de energia entre os orbitais HOMO e LUMO para os compostos **5a-d**.

Composto	Momento de dipolo, μ (D)	Energia de Hartree (kcal mol^{-1})	$\Delta E_{HOMO-LUMO}$
5a	1,2172	0	0,16762
5b	4,8048	39,289	0,16991
5c	1,0963	78,575	0,16916
5d	4,7261	117,863	0,16896

Os compostos **5a** e **5c** (com n = 1 e n = 3, respectivamente) apresentaram valores de momento de dipolo menores do que os compostos com número par de carbonos metilênicos na cadeia interna. Para **5a** μ= 1,2172, **5b** μ= 4,8048, **5c** μ= 1,0963 e **5d** μ= 4,7261.

A análise da conformação mais estável para cada composto desta série (Figura 5) mostrou que para os compostos **5a** e **5c** os eixos moleculares são relativamente colineares e coplanares, o que vai permitir um melhor empacotamento molecular na transição líquido-cristalina. Este efeito também pode ser observado nos maiores valores de entalpia encontrados para os compostos **5a** e **5c** (Tabela 1).

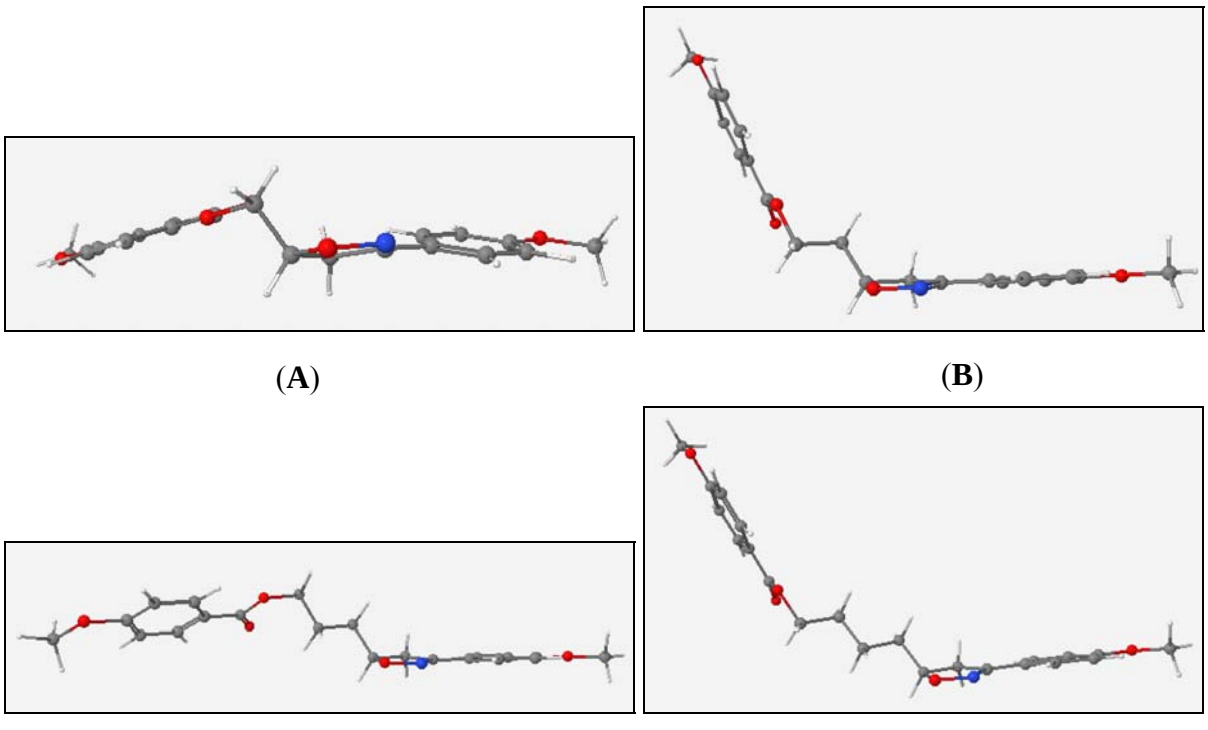

(**A**) (**B**)

(**C**) (**D**)

Figura 5. Conformação mais estável dos compostos da série **5a-d** com diferentes comprimentos de espaçadores obtidos por cálculos computacionais: (A) uma unidade metilênica, (B) duas unidades metilênicas, (C) três unidades metilênicas e (D) quatro unidades metilênicas.

Conclusão

Foram sintetizadas duas novas séries de compostos líquido-cristalinos contendo o anel isoxazolínico. Foram analisadas as propriedades mesomórficas destes materiais em relação às temperaturas de transição e estrutura química. A estrutura dos compostos foi confirmada por RMN de ^{1}H, ^{13}C, IV e CHN. As medidas de DSC confirmaram a natureza líquido-cristalina dos novos compostos sintetizados. Os compostos **9a-d**, que têm geometria mais próxima a um bastão, apresentaram mesofase mais estável.

Parte experimental

Material

Etanol, éter etílico, ácido *p*-bromobenzóico, iodeto de cobre(I) (CuI), trifenilfosfina (PPh_3), 4-(*N,N*-dimetilamino)piridina (DMAP) e 1,3-diciclohexilcarbodiimida (DCC) foram utilizados sem purificação. O ácido *p*-*n*-deciloxibenzóico[8] e o 2-etinil-6-(octiloxi)naftaleno[9] foram preparados de acordo com a literatura. O cloreto de *bis*-(trifenilfosfina)paládio (II) [$PdCl_2(PPh_3)_2$] foi preparado seguindo o procedimento reportado na referência 10. A trietilamina (Et_3N) foi destilada com hidróxido de potássio. O tetrahidrofurano (THF) foi seco sob sódio metálico e benzofenona e destilado imediatamente antes do uso. Foi utilizado sulfato de sódio anidro (Na_2SO_4) como secante das fases orgânicas.

Caracterização

Os espectros de ressonância magnética nuclear foram obtidos em um equipamento Varian de 300MHz. Os deslocamentos químicos foram dados em partes por milhão (δ) utilizando o tetrametilsilano (TMS) como padrão. Os espectros de ATR foram obtidos em um equipamento Varian 640-IR entre 4000 e 500 cm^{-1} e resolução de 4 cm^{-1}. Todos os espectros foram realizados com 16 *scans* e são dados em número de onda (cm^{-1}). As análises elementares foram realizadas em um equipamento Perkin-Elmer modelo 2400. As análises de DSC foram realizadas em um equipamento DSC 2910 TA Instruments.

Caracterização térmica

[8] N. Gimeno, M. B. Ros, M. R. De la Fuente, J. L. Serrano, *Chem. Mater.* **2008**, *20*, 1262.
[9] Vasconcelos, U. B.; Vilela, G. D.; Schrader, A.; Borges, A. C. A.; Merlo, A. A.; *Tetrahedron* **2008**, *64*, 4619.
[10] King, A. O.; Negishi, E. *J. Org. Chem*. **1978**, *43*, 358.

As temperaturas de transição de fase e caracterização das texturas foram determinadas em um microscópio Mettler Toledo equipado com processador central FP90 e célula de medição térmica FP82HT, conectado a uma câmera Olympus BX41. A velocidade de aquecimento e resfriamento foi de 10 ºC min^{-1}.

Cálculos teóricos

As energias e geometria correspondentes foram obtidas por otimização completa sem restrições. Os cálculos foram realizados com o programa GAUSSIAN 98[11] usando o híbrido funcional B3LYP[12] empregando as funções de base 6-31G*(*d,p).

Sínteses

A síntese da série (3-[4-(alquiloxi)fenil]-4,5-dihidroisoxazol-5-il)hidroxialquil (**3a-d**) foi realizada de acordo com a referência 4b.

(3-(4-(Octiloxi)fenil)-4,5-dihidroisoxazol-5-il)metanol (3a): Rendimento: 219 mg, 36%; sólido branco; p. f. 94.0 °C. ^{1}H NMR ($CDCl_3$): δ = 0.89 (m, 3 H, CH_3), 1.41 [m, 10 H, $(CH_2)_5$], 1.78 (m, 2 H, C*H*$_2$CH$_2$O), 2.09 (br., 1 H, OH), 3.24 (dd, $^2J_{gem}$ = 16.8 Hz, $^3J_{trans}$ = 8.1 Hz, 1 H, N=CC*H*HCH), 3.34 (dd, $^2J_{gem}$ = 16.8 Hz, $^3J_{cis}$ = 10.5 Hz, 1 H, N=CCH*H*CH), 3.67 (dd, $^2J_{gem}$ = 12.0 Hz, $^3J_{trans}$ = 4.8 Hz, 1 H, CHC*H*HOH), 3.83 (dd, $^2J_{gem}$ =12.0 Hz, $^3J_{cis}$ = 3.3 Hz, 1 H, CHCH*H*OH), 3.96 (t, *J* = 6.6 Hz, 2 H, CH_2O), 4.81 (m, 1 H), 6.87 (d, *J* = 9.0 Hz, 2 H, Ar), 7.56 (d, *J* = 8.7 Hz, 2 H, Ar) ppm. ^{13}C NMR ($CDCl_3$): δ = 13.9, 22.5, 25.8, 29.0, 29.1, 29.2, 31.7, 36.5, 63.4, 68.0, 80.9, 114.5, 121.4, 128.1, 156.5, 160.5 ppm. ATR: ν = 2954, 2919, 2871, 2854, 1606, 1594, 1515, 1255, 1181, 1045, 896, 819, 642 cm^{-1}. $C_{18}H_{27}NO_3$ (305.42): calcd. C 70.79, H 8.91, N 4.59; found C 70.65, H 8.86, N 4.80.

2-(3-(4-(Octiloxi)fenil)-4,5-dihidroisoxazol-5-il)etanol (3b): Rendimento: 44 mg, 35%; sólido branco; p. f. 106.9 °C. ^{1}H NMR ($CDCl_3$): δ = 0.91 (m, 3 H, CH_3), 1.41 [m, 10 H, $(CH_2)_5$], 1.81 (m, 2 H, C*H*$_2$CH$_2$O), 1.97 (m, 2 H, CHC*H*$_2$CH$_2$OH), 3.06 (dd, $^2J_{gem}$ = 16.5 Hz,

[11] Frisch, M. J.; Trucks, G. W.; Schlegel, H. B.; Scuseria, G. E.; Robb, M. A.; Cheeseman, J. R.; Zakrzewski, V. G.; Montgomery J. A.; Stratmann, Jr., R. E.; Burant, J. C.; Dapprich, S.; Millam, J. M.; Daniels, A. D.; Kudin, K. N.; Strain, M. C.; Farkas, O.; Tomasi, J.; Barone, V.; Cossi, M.; Cammi, R.; Mennucci, B.; Pomelli, C.; Adamo, C.; Clifford, S.; Ochterski, J.; Petersson, G. A.; Ayala, P. Y.; Cui, Q.; Morokuma, K.; Malick, D. K.; Rabuck, A. D.; Raghavachari, K.; Foresman, J. B.; Cioslowski, J.; Ortiz, J. V.; Stefanov, B. B.; Liu, G.; Liashenko, A.; Piskorz, P.; Komaromi, I.; Gomperts, R.; Martin, R. L.; Fox, D. J.; Keith, T.; Al-Laham, M. A.; Peng, C. Y.; Nanayakkara, A.; Gonzalez, C.; Challacombe, M.; Gill, P. M. W.; Johnson, B.; Chen, W.; Wong, M. W.; Andres, J. L.; Gonzalez, C.; Head-Gordon, M.; Replogle, E. S.; Pople, J. A.; *Gaussian 98, Revision A.5.* Gaussian, Inc., Pittsburgh, PA. **1998**.

[12] a. Becke, A. D.; *J. Chem. Phys.* **1993**, *98*, 5648; b. Lee, C.; Yang, W.; Parr, R. G.; *Phys. Rev. B* **1988**, *37*, 785.

$^{3}J_{trans}$ = 7.8 Hz, 1 H, N=CC*H*HCH), 3.47 (dd, $^{2}J_{gem}$ = 16.5 Hz, $^{3}J_{cis}$ = 10.5 Hz, 1 H, N=CCH*H*CH), 3.88 (t, *J* = 6.3 Hz, 2 H, C*H*$_2$OH), 3.99 (t, *J* = 6.3 Hz, 2 H, CH$_2$O), 4.91 (m, 1 H), 6.92 (d, *J* = 9.0 Hz, 2 H, Ar), 7.60 (d, *J* = 9.0 Hz, 2 H, Ar) ppm. ATR: ν = 2954, 2919, 2871, 2854, 1606, 1594, 1515, 1255, 1181, 1045, 896, 819, 642 cm^{-1}.

3-(3-(4-(Octiloxi)fenil)-4,5-dihidroisoxazol-5-il)propan-1-ol (3c): Rendimento: 48 mg, 36%; sólido branco; p. f. 97.1 °C. ^{1}H NMR (CDCl$_3$): δ = 0.91 (m, 3 H, CH$_3$), 1.41 [m, 10 H, (CH$_2$)$_5$], 1.70 (m, 6 H, CH(C*H*$_2$)$_2$CH$_2$OH, C*H*$_2$CH$_2$O), 2.89 (dd, $^{2}J_{gem}$ = 16.5 Hz, $^{3}J_{trans}$ = 7.8 Hz, 1 H, N=CC*H*HCH), 3.33 (dd, $^{2}J_{gem}$ = 16.0 Hz, $^{3}J_{cis}$ = 10.2 Hz, 1 H, N=CCH*H*CH), 3.64 (m, 2 H, C*H*$_2$OH), 3.90 (t, *J* = 6.6 Hz, 2 H, CH$_2$O), 4.67 (m, 1 H), 6.82 (d, *J* = 8.7 Hz, 2 H, Ar), 7.50 (d, *J* = 8.7 Hz, 2 H, Ar) ppm. ATR: ν = 2954, 2919, 2871, 2854, 1606, 1594, 1515, 1255, 1181, 1045, 896, 819, 642 cm^{-1}.

4-(3-(4-(Octiloxi)fenil)-4,5-dihidroisoxazol-5-il)butan-1-ol (3d): Rendimento: 45 mg, 33%; sólido branco; p. f. 102.8 °C. ^{1}H NMR (CDCl$_3$): δ = 0.91 (m, 3 H, CH$_3$), 1.60 [m, 18 H, (CH$_2$)$_5$, CH(C*H*$_2$)$_3$CH$_2$OH, C*H*$_2$CH$_2$O], 2.98 (dd, $^{2}J_{gem}$ = 16.5 Hz, $^{3}J_{trans}$ = 8.1 Hz, 1 H, N=CC*H*HCH), 3.40 (dd, $^{2}J_{gem}$ = 16.5 Hz, $^{3}J_{cis}$ = 10.5 Hz, 1 H, N=CCH*H*CH), 3.70 (t, *J* = 6.3 Hz, 2 H, C*H*$_2$OH), 4.00 (t, *J* = 6.3 Hz, 2 H, CH$_2$O), 4.73 (m, 1 H), 6.93 (d, *J* = 9.7 Hz, 2 H, Ar), 7.61 (d, *J* = 9.7 Hz, 2 H, Ar) ppm. ^{13}C NMR (CDCl$_3$): 13.9, 21.7, 22.4, 25.8, 29.0, 29.1, 29.2, 31.6, 32.2, 34.8, 40.0, 62.1, 67.9, 80.8, 114.4, 121.9, 127.9, 156.0, 160.4 ppm. ATR: ν = 2954, 2919, 2871, 2854, 1606, 1594, 1515, 1255, 1181, 1045, 896, 819, 642 cm^{-1}.

Síntese da série 5a-d. O álcool correspondente (**3a-d)** (4,2 x 10^{-4} mol) e o ácido *p-n*-deciloxibenzóico (4,2 x 10^{-4} mol) foram suspensos em THF seco (5 mL) e a solução agitada durante 15 minutos sob atmosfera inerte. Após, DCC (5,8 x 10^{-4} mol) e DMAP (5,2 x 10^{-5} mol) foram adicionados ao balão. A reação permaneceu sob agitação durante 24 horas em temperatura ambiente. O sólido branco que se formou foi filtrado e o solvente evaporado. O produto puro foi obtido após 2 recristalizações em etanol.

(3-(4-(Octiloxifenil)-4,5-dihidroisoxazol-5-il)metil 4-(deciloxi)benzoato (5a): Rendimento: 192 mg, 81%; sólido branco; p. f. 103.0 ^{o}C. ^{1}H NMR (CDCl$_3$): δ = 0.89 [m, 6 H, (CH$_3$)$_2$], 1.38 [m, 24 H, (CH$_2$)$_{12}$], 1.79 [m, 4 H, (C*H*$_2$CH$_2$O)$_2$], 3.22 (dd, $^{2}J_{gem}$ = 16.5 Hz, $^{3}J_{trans}$ = 6.9 Hz, 1 H, N=CC*H*HCH), 3.49 (dd, $^{2}J_{gem}$ = 16.8 Hz, $^{3}J_{cis}$ = 10.8 Hz, 1 H, N=CCH*H*CH), 3.98 [t, *J* = 6.6 Hz, 4 H, (CH$_2$O)$_2$], 4.44 (m, 2 H, CHC*H*$_2$OCO), 5.05 (m, 1 H), 6.85 (d, *J* = 9.0 Hz, 2 H, Ar), 6.91 (d, *J* = 8.7 Hz, 2 H, Ar), 7.61 (d, *J* = 8.7 Hz, 2 H, Ar), 7.95 (d, *J* = 9.0 Hz, 2 H,

Ar) ppm. ATR: ν = 2954, 2919, 2871, 2854, 1714, 1606, 1515, 1469, 1255, 1172, 1110, 1045, 896, 819, 767, 696, 642 cm^{-1}.

2-(3-(4-Octiloxi)fenil)-4,5-dihidroisoxazol-5-il)etil 4-(deciloxi)benzoato (5b): Rendimento: 69 mg, 30%; sólido branco; p. f. 72.3 °C. ^{1}H NMR ($CDCl_3$): δ = 0.89 [m, 6 H, $(CH_3)_2$], 1.38 [m, 24 H, $(CH_2)_{12}$], 1.82 [m, 4 H, $(CH_2CH_2O)_2$], 2.10 (m, 1 H, CHC*H*HCH$_2$OCO), 2.23 (m, 1 H, CHCH*H*CH$_2$OCO), 3.08 (dd, $^2J_{gem}$ = 16.2 Hz, $^3J_{trans}$ = 7.5 Hz, 1 H, N=CC*H*HCH), 3.49 (dd, $^2J_{gem}$ = 16.2 Hz, $^3J_{cis}$ = 9.9 Hz, 1 H, N=CCH*H*CH), 4.00 (t, *J* = 6.6 Hz, 2 H, CH$_2$O), 4.03 (t, *J* = 6.9 Hz, 2 H, CH$_2$O), 4.50 (m, 2 H, CHCH$_2$C*H*$_2$OCO), 4.93 (m, 1 H), 6.92 (d, *J* = 8.7 Hz, 4 H, Ar), 7.61 (d, *J* = 8.7 Hz, 2 H, Ar), 7.98 (d, *J* = 8.4 Hz, 2 H, Ar) ppm. ATR: ν = 2954, 2919, 2871, 2854, 1714, 1606, 1515, 1469, 1255, 1172, 1110, 1045, 896, 819, 767, 696, 642 cm^{-1}.

3-(3-(4-(Octiloxi)fenil)-4,5-dihidroisoxazol-5-il)propil 4-(deciloxi)benzoato (5c): Rendimento: 118 mg, 52%; sólido branco; p. f. 85.3 °C. ^{1}H NMR ($CDCl_3$): δ = 0.89 [m, 6 H, $(CH_3)_2$], 1.38 [m, 24 H, $(CH_2)_{12}$], 1.79 [m, 4 H, $(CH_2CH_2O)_2$], 1.93 (m, 4 H, CHC*H*$_2$C*H*$_2$CH$_2$OCO), 2.97 (dd, $^2J_{gem}$ = 16.5 Hz, $^3J_{trans}$ = 7.8 Hz, 1 H, N=CC*H*HCH), 3.41 (dd, $^2J_{gem}$ = 16.2 Hz, $^3J_{cis}$ = 10.5 Hz, 1 H, N=CCH*H*CH), 3.97 (t, *J* = 6.6 Hz, 2 H, CH$_2$O), 4.00 (t, *J* = 6.6 Hz, 2 H, CH$_2$O), 4.34 (m, 2 H, CHCH$_2$CH$_2$C*H*$_2$OCO), 4.80 (m, 1 H), 6.89 (d, *J* = 9.0 Hz, 4 H, Ar), 7.58 (d, *J* = 8.7 Hz, 2 H, Ar), 7.97 (d, *J* = 9.0 Hz, 2 H, Ar) ppm. ATR: ν = 2954, 2919, 2871, 2854, 1714, 1606, 1515, 1469, 1255, 1172, 1110, 1045, 896, 819, 767, 696, 642 cm^{-1}.

4-(3-(4-(Octiloxi)fenil)-4,5-dihidroisoxazol-5-il)butil 4-(deciloxi)benzoato (5d): Rendimento: 81 mg, 36%; sólido branco; p. f. 68.3 °C. ^{1}H NMR ($CDCl_3$): δ = 0.89 [m, 6 H, $(CH_3)_2$], 1.38 [m, 24 H, $(CH_2)_{12}$], 1.70 [m, 10 H, CH(C*H*$_2$)$_3$CH$_2$OCO, (C*H*$_2$CH$_2$O)$_2$], 2.87 (dd, $^2J_{gem}$ = 16.2 Hz, $^3J_{trans}$ = 8.1 Hz, 1 H, N=CC*H*HCH), 3.30 (dd, $^2J_{gem}$ = 16.2 Hz, $^3J_{cis}$ = 10.2 Hz, 1 H, N=CCH*H*CH), 3.90 (t, *J* = 6.9 Hz, 2 H, CH$_2$O), 3.92 (t, *J* = 6.6 Hz, 2 H, CH$_2$O), 4.23 (t, *J* = 6.3 Hz, 2H, CH(CH$_2$)$_3$C*H*$_2$OCO), 4.64 (m, 1 H), 6.82 (d, *J* = 9.0 Hz, 4 H, Ar), 7.51 (d, *J* = 8.7 Hz, 2 H, Ar), 7.90 (d, *J* = 9.0 Hz, 2 H, Ar) ppm. ATR: ν = 2954, 2919, 2871, 2854, 1714, 1606, 1515, 1469, 1255, 1172, 1110, 1045, 896, 819, 767, 696, 642 cm^{-1}.

Síntese da série 7a-d. O álcool correspondente (**3a-d)** (1,1 x 10^{-3} mol) e o ácido *p*-bromobenzóico (1,1 x 10^{-3} mol) foram suspensos em THF seco (13 mL) e a solução agitada durante 15 minutos sob atmosfera inerte. Após, DCC (1,5 x 10^{-3} mol) and DMAP (1,3 x 10^{-4}

mol) foram adicionados ao balão. A reação permaneceu sob agitação durante 24 horas sob atmosfera inerte e temperatura ambiente. O sólido branco que se formou foi filtrado e o solvente evaporado. O produto puro foi obtido após 2 recristalizações em etanol.

(3-(4-(Octiloxi)fenil)-4,5-dihidroisoxazol-5-il]metil 4-bromobenzoato (7a): Rendimento: 262 mg, 49%; sólido branco; p. f. 115.2 (MOLP) °C. ^{1}H NMR ($CDCl_3$): δ = 0.89 (m, 3 H, CH_3), 1.38 [m, 10 H, $(CH_2)_5$], 1.80 (m, 2 H, C*H*$_2$CH$_2$O), 3.21 (dd, $^{2}J_{gem}$ = 16.8 Hz, $^{3}J_{trans}$ = 6.6 Hz, 1 H, N=CC*H*HCH), 3.51 (dd, $^{2}J_{gem}$ = 16.5 Hz, $^{3}J_{cis}$ = 10.8 Hz, 1 H, N=CCH*H*CH), 3.99 (t, *J* = 6.6 Hz, 2 H, CH$_2$O), 4.41 (dd, $^{2}J_{gem}$ = 11.7 Hz, $^{3}J_{trans}$ = 5.4 Hz, 1 H, CHC*H*HOCO), 4.50 (dd, $^{2}J_{gem}$ =11.7 Hz, $^{3}J_{cis}$ = 4.2 Hz, 1 H, CHCH*H*OCO), 5.10 (m, 1 H), 6.91 (d, *J* = 9.0 Hz, 2 H, Ar), 7.52 (d, *J* = 8.4 Hz, 2 H, Ar), 7.60 (d, *J* = 9.0 Hz, 2 H, Ar), 7.86 (d, *J* = 8.7 Hz, 2 H, Ar) ppm. ^{13}C NMR ($CDCl_3$): 14.0, 22.5, 25.9, 29.0, 29.1, 29.2, 31.7, 37.5, 65.8, 68.0, 77.5, 114.5, 114.6, 121.2, 128.0, 128.1, 128.2, 128.3, 131.1, 131.2, 131.7, 131.8, 155.7, 160.7, 165.5 ppm. ATR: ν = 2954, 2919, 2871, 2854, 1720, 1606, 1591, 1515, 1438, 1388, 1255, 1172, 1110, 1068, 1045, 1012, 921, 896, 819, 755, 684, 642 cm^{-1}.

2-(3-(4-(Octiloxi)fenil)-4,5-dihidroisoxazol-5-il)etil 4-bromobenzoato (7b): Rendimento: 308 mg, 56%; sólido branco; p. f. 89.9 (MOLP) °C. ^{1}H NMR ($CDCl_3$): δ = 0.90 (m, 3 H, CH_3), 1.38 [m, 10 H, $(CH_2)_5$], 1.81 (m, 2 H, C*H*$_2$CH$_2$O), 2.17 (m, 2 H, CHC*H*$_2$CH$_2$OCO), 3.07 (dd, $^{2}J_{gem}$ = 16.5 Hz, $^{3}J_{trans}$ = 7.5 Hz, 1 H, N=CC*H*HCH), 3.50 (dd, $^{2}J_{gem}$ = 16.5 Hz, $^{3}J_{cis}$ = 10.2 Hz, 1 H, N=CCH*H*CH), 4.00 (t, *J* = 6.6 Hz, 2 H, CH$_2$O), 4.54 (m, 2 H, CHCH$_2$C*H*$_2$OCO), 4.92 (m, 1 H), 6.92 (d, *J* = 9.0 Hz, 2 H, Ar), 7.58 (d, *J* = 8.7 Hz, 2 H, Ar), 7.61 (d, *J* = 9.0 Hz, 2 H, Ar), 7.91 (d, *J* = 8.4 Hz, 2 H, Ar) ppm. ^{13}C NMR ($CDCl_3$): 14.0, 22.5, 25.9, 29.0, 29.1, 29.2, 31.7, 34.3, 40.4, 61.7, 68.0, 77.5, 114.5, 114.6, 121.2, 128.0, 128.1, 128.2, 128.3, 131.1, 131.2, 131.7, 131.8, 155.9, 160.5, 165.5 ppm. ATR: ν = 2954, 2919, 2871, 2854, 1720, 1606, 1591, 1515, 1438, 1388, 1255, 1172, 1110, 1068, 1045, 1012, 921, 896, 819, 755, 684, 642 cm^{-1}.

3-(3-(4-(Octiloxi)fenil)-4,5-dihidroisoxazol-5-il)propil 4-bromobenzoato (7c): Rendimento: 323 mg, 57%; sólido branco; p. f. 98.8 (MOLP) °C. ^{1}H NMR ($CDCl_3$): δ = 0.89 (m, 3 H, CH_3), 1.38 [m, 10 H, $(CH_2)_5$], 1.80 (m, 2 H, C*H*$_2$CH$_2$O), 1.96 (m, 4 H, CHC*H*$_2$C*H*$_2$CH$_2$OCO), 2.97 (dd, $^{2}J_{gem}$ = 16.5 Hz, $^{3}J_{trans}$ = 7.8 Hz, 1 H, N=CC*H*HCH), 3.43 (dd, $^{2}J_{gem}$ = 16.2 Hz, $^{3}J_{cis}$ = 10.2 Hz, 1 H, N=CCH*H*CH), 3.98 (t, *J* = 6.6 Hz, 2 H, CH$_2$O), 4.39 (m, 2 H, CHCH$_2$CH$_2$C*H*$_2$OCO), 4.77 (m, 1 H), 6.90 (d, *J* = 9.0 Hz, 2 H, Ar), 7.56 (d, *J* = 8.4

Hz, 2 H, Ar), 7.59 (d, J = 9.0 Hz, 2 H, Ar), 7.90 (d, J = 8.7 Hz, 2 H, Ar) ppm. ^{13}C NMR ($CDCl_3$): 13.9, 22.0, 25.8, 28.3, 28.9, 29.0, 29.1, 31.6, 34.7, 40.1, 64.8, 67.9, 80.5, 114.5, 114.6, 121.2, 128.0, 128.1, 128.2, 128.3, 131.1, 131.2, 131.7, 131.8, 155.8, 160.3, 165.5 ppm. ATR: ν = 2954, 2919, 2871, 2854, 1720, 1606, 1591, 1515, 1438, 1388, 1255, 1172, 1110, 1068, 1045, 1012, 921, 896, 819, 755, 684, 642 cm^{-1}.

4-(3-(4-(Octiloxi)fenil)-4,5-dihidroisoxazol-5-il)butil 4-bromobenzoato (7d): Rendimento: 286 mg, 44%; sólido branco; p. f. 73.1 (MOLP) ^{o}C. ^{1}H NMR ($CDCl_3$): δ = 0.89 (m, 3 H, CH_3), 1.38 [m, 10 H, $(CH_2)_5$], 1.80 (m, 2 H, CH_2CH_2O), 1.96 (m, 6 H, CHCH_2CH_2CH_2CH_2OCO), 2.97 (dd, $^2J_{gem}$ = 16.5 Hz, $^3J_{trans}$ = 7.8 Hz, 1 H, N=CCHHCH), 3.43 (dd, $^2J_{gem}$ = 16.2 Hz, $^3J_{cis}$ = 10.2 Hz, 1 H, N=CCHHCH), 3.98 (t, J = 6.6 Hz, 2 H, CH_2O), 4.39 (m, 2 H, CHCH_2CH_2CH_2OCO), 4.77 (m, 1 H), 6.90 (d, J = 9.0 Hz, 2 H, Ar), 7.56 (d, J = 8.4 Hz, 2 H, Ar), 7.59 (d, J = 9.0 Hz, 2 H, Ar), 7.90 (d, J = 8.7 Hz, 2 H, Ar) ppm. ^{13}C NMR ($CDCl_3$): 13.9, 22.0, 22.4, 25.8, 28.3, 28.9, 29.0, 29.1, 31.6, 34.7, 40.1, 64.8, 67.9, 80.5, 114.5, 114.6, 121.2, 128.0, 128.1, 128.2, 128.3, 131.1, 131.2, 131.7, 131.8, 155.8, 160.3, 165.5 ppm. ATR: ν = 2954, 2919, 2871, 2854, 1720, 1606, 1591, 1515, 1438, 1388, 1255, 1172, 1110, 1068, 1045, 1012, 921, 896, 819, 755, 684, 642 cm^{-1}.

Síntese da série 9a-d. *Acoplamento de Sonogashira:* em um Schlenk, sob atmosfera de argônio, foram adicionados o éster **7a-d** correspondente (0,4 x 10^{-3} mol), 2-etinil-6-octiloxinaftaleno (0,5 x 10^{-3} mol), THF (2,4 mL) e Et_3N (0,6 mL). A mistura foi agitada por 20 minutos e então CuI (0,8 x 10^{-5} mol), PPh_3 (2,5 x 10^{-5} mol) e $[PdCl_2(PPh_3)_2]$ (0,5 x 10^{-5} mol) foram adicionados. A mistura foi agitada sob refluxo por 24 horas. A solução resfriou até a temperatura ambiente e foi filtrada sobre Celite®, lavando-se com éter. O filtrado foi lavado com água (4 x 20 mL) e a fase etérea foi seca sob Na_2SO_4 e concentrada em rota-evaporador. O produto foi obtido puro após 2 recristalizações em etanol.

(3-(4-(Octiloxi)fenil)-4,5-dihidroisoxazol-5-il)metil 4-((6-(octiloxi)naftalen-2-il)etinil)benzoato (9a): Rendimento: 230 mg, 66%; sólido amarelo; p. f. 145.8 ^{o}C. ^{1}H NMR ($CDCl_3$): δ = 0.82 [m, 6 H, $(CH_3)_2$], 1.22 [m, 20 H, $(CH_2)_{10}$], 1.74 [m, 4 H, $(CH_2CH_2O)_2$], 3.14 (dd, $^2J_{gem}$ = 16.5 Hz, $^3J_{trans}$ = 7.2 Hz, 1 H, N=CCHHCH), 3.43 (dd, $^2J_{gem}$ = 16.5 Hz, $^3J_{cis}$ = 10.8 Hz, 1 H, N=CCHHCH), 3.90 (t, J = 6.6 Hz, 2 H, CH_2O), 3.99 (t, J = 6.6 Hz, 2 H, CH_2O), 4.40 (m, 2 H, CHCH_2OCO), 5.01 (m, 1 H), 6.84 (d, J = 8.4 Hz, 2 H, Ar), 6.98-7.15 (m, 2 H, Ar), 7.38-7.74 (m, 8 H, Ar), 7.92 (d, J = 6.6 Hz, 2 H, Ar) ppm. ATR: ν = 2954, 2919,

2871, 2854, 1714, 1606, 1594, 1515, 1469, 1388, 1255, 1213, 1172, 1110, 1045, 943, 896, 858, 819, 767, 696, 642 cm^{-1}.

2-(3-(4-(Octiloxi)fenil)-4,5-dihidroisoxazol-5-il)etil 4-((6-(octiloxi)naftalen-2-il)etinil)benzoato (9b): Rendimento: 222 mg, 65%; sólido rosa; p. f. 124.7 °C. ^{1}H NMR ($CDCl_3$): δ = 0.90 [m, 6 H, $(CH_3)_2$], 1.24 [m, 20 H, $(CH_2)_{10}$], 1.80 [m, 4 H, $(CH_2CH_2O)_2$], 2.20 (m, 2 H, $CHCH_2CH_2OCO$), 3.06 (dd, $^2J_{gem}$ = 16.5 Hz, $^3J_{trans}$ = 7.2 Hz, 1 H, N=CCHHCH), 3.47 (dd, $^2J_{gem}$ = 16.2 Hz, $^3J_{cis}$ = 10.5 Hz, 1 H, N=CCHHCH), 3.97 (t, J = 6.3 Hz, 2 H, CH_2O), 4.07 (t, J = 6.3 Hz, 2 H, CH_2O), 4.53 (m, 2 H, $CHCH_2CH_2OCO$), 4.91 (m, 1 H), 6.90 (d, J = 9.0 Hz, 2 H, Ar), 7.07-7.21 (m, 2 H, Ar), 7.47-7.76 (m, 8 H, Ar), 8.01 (d, J = 8.4 Hz, 2 H, Ar) ppm. ATR: ν = 2954, 2919, 2871, 2854, 1714, 1606, 1594, 1515, 1469, 1388, 1255, 1213, 1172, 1110, 1045, 943, 896, 858, 819, 767, 696, 642 cm^{-1}.

3-(3-(4-(Octiloxi)fenil)-4,5-dihidroisoxazol-5-il)propil 4-((6-(octiloxi)naftalen-2-il)etinil)benzoato (9c): Rendimento: 164 mg, 48%; sólido amarelo; p. f. 129.3 °C. ^{1}H NMR ($CDCl_3$): δ = 0.88 [m, 6 H, $(CH_3)_2$], 1.30 [m, 20 H, $(CH_2)_{10}$], 1.70-2.08 [m, 8 H, $(CH_2CH_2O)_2$, $CHCH_2CH_2CH_2OCO$), 3.00 (dd, $^2J_{gem}$ = 16.5 Hz, $^3J_{trans}$ = 7.8 Hz, 1 H, N=CCHHCH), 3.42 (dd, $^2J_{gem}$ = 16.5 Hz, $^3J_{cis}$ = 10.2 Hz, 1 H, N=CCHHCH), 3.97 (t, J = 6.3 Hz, 2 H, CH_2O), 4.07 (t, J = 6.3 Hz, 2 H, CH_2O), 4.40 (m, 2 H, $CHCH_2CH_2OCO$), 4.78 (m, 1 H), 6.90 (d, J = 9.0 Hz, 2 H, Ar), 7.07-7.21 (m, 2 H, Ar), 7.47-7.76 (m, 8 H, Ar), 8.01 (d, J = 8.4 Hz, 2 H, Ar). ATR: ν = 2954, 2919, 2871, 2854, 1714, 1606, 1594, 1515, 1469, 1388, 1255, 1213, 1172, 1110, 1045, 943, 896, 858, 819, 767, 696, 642 cm^{-1}.

4-(3-(4-(Octiloxi)fenil)-4,5-dihidroisoxazol-5-il]butil 4-((6-(octiloxi)naftalen-2-il)etinil)benzoato (9d): Rendimento: 237 mg, 92%; sólido amarelo; p. f. 109.7 °C. ^{1}H NMR ($CDCl_3$): δ = 0.90 [m, 6 H, $(CH_3)_2$], 1.28 [m, 20 H, $(CH_2)_{10}$], 1.62-1.92 [m, 10 H, $(CH_2CH_2O)_2$, $CHCH_2CH_2CH_2CH_2OCO$), 2.94 (dd, $^2J_{gem}$ = 16.2 Hz, $^3J_{trans}$ = 8.1 Hz, 1 H, N=CCHHCH), 3.38 (dd, $^2J_{gem}$ = 16.2 Hz, $^3J_{cis}$ = 10.5 Hz, 1 H, N=CCHHCH), 3.98 (t, J = 6.3 Hz, 2 H, CH_2O), 4.07 (t, J = 6.3 Hz, 2 H, CH_2O), 4.35 (m, 2 H, $CHCH_2CH_2OCO$), 4.72 (m, 1 H), 6.90 (d, J = 9.0 Hz, 2 H, Ar), 7.07-7.21 (m, 2 H, Ar), 7.47-7.76 (m, 8 H, Ar), 8.01 (d, J = 8.4 Hz, 2 H, Ar). ATR: ν = 2954, 2919, 2871, 2854, 1714, 1606, 1594, 1515, 1469, 1388, 1255, 1213, 1172, 1110, 1045, 943, 896, 858, 819, 767, 696, 642 cm^{-1}.

SUPPORTING INFORMATION – CAPÍTULO 6.3

Síntese e Propriedades Mesomórficas dos Ésteres Aromáticos 3,5-dissubstituídos Benzoatos de 4,5-dihidroisoxazoíla

Tavares, A.; Gonçalves, P. F. B.; Merlo, A. A.

Instituto de Química, UFRGS. Av. Bento Gonçalves, 9500. Agronomia. 91501-970, Porto Alegre, RS – Brasil.

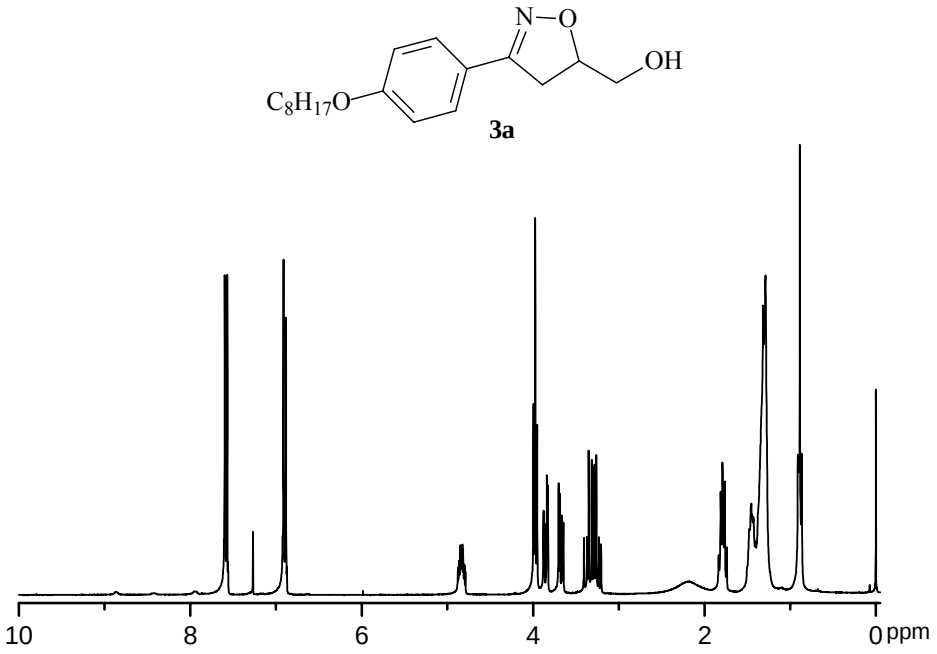

Figura 1. Espectro de ^{1}H NMR do composto **3a** ($CDCl_3$, 300 MHz).

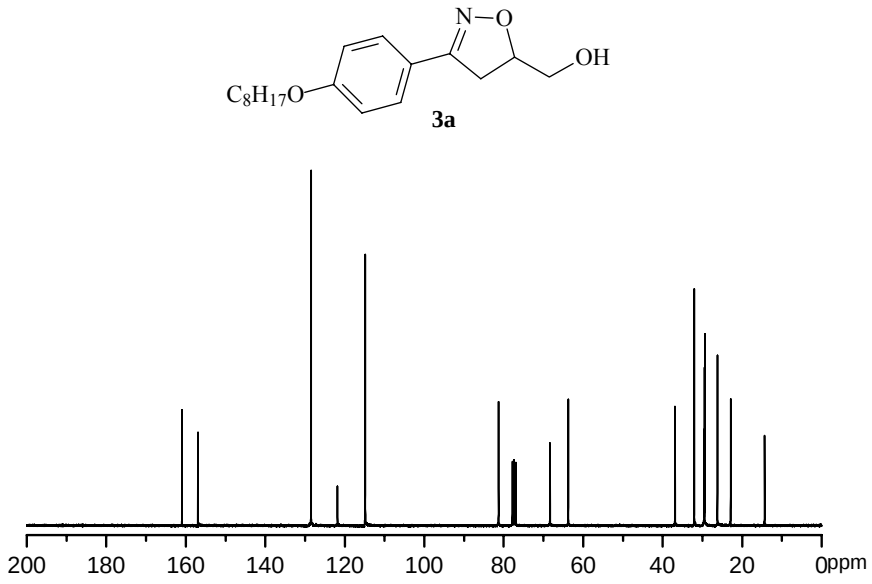

Figura 2. Espectro de ^{13}C NMR do composto **3a** ($CDCl_3$, 300 MHz).

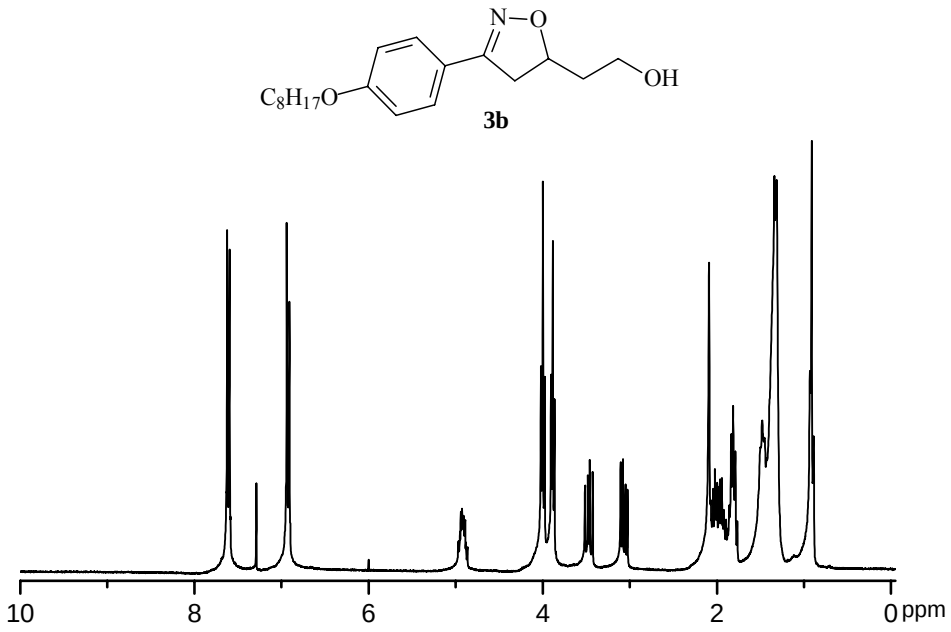

Figura 3. Espectro de ^{1}H NMR do composto **3b** ($CDCl_3$, 300 MHz).

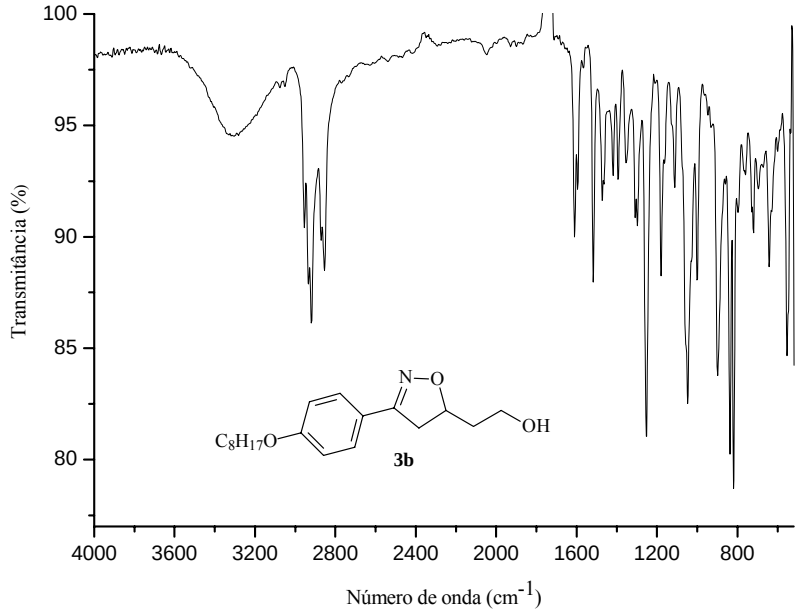

Figura 4. Espectro de ATR/FT-IR do composto **3b**.

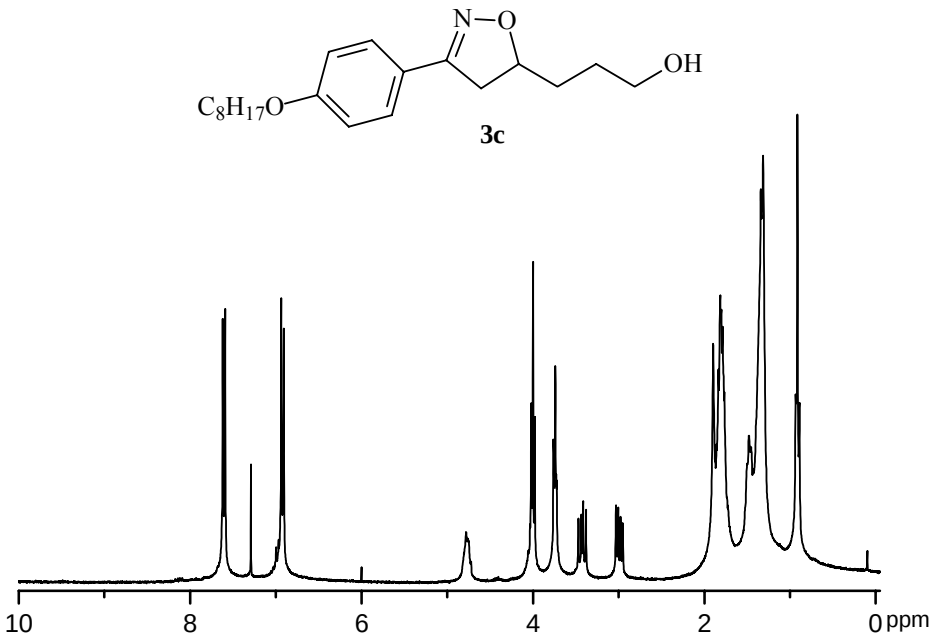

Figura 5. Espectro de ^{1}H NMR do composto **3c** ($CDCl_3$, 300 MHz).

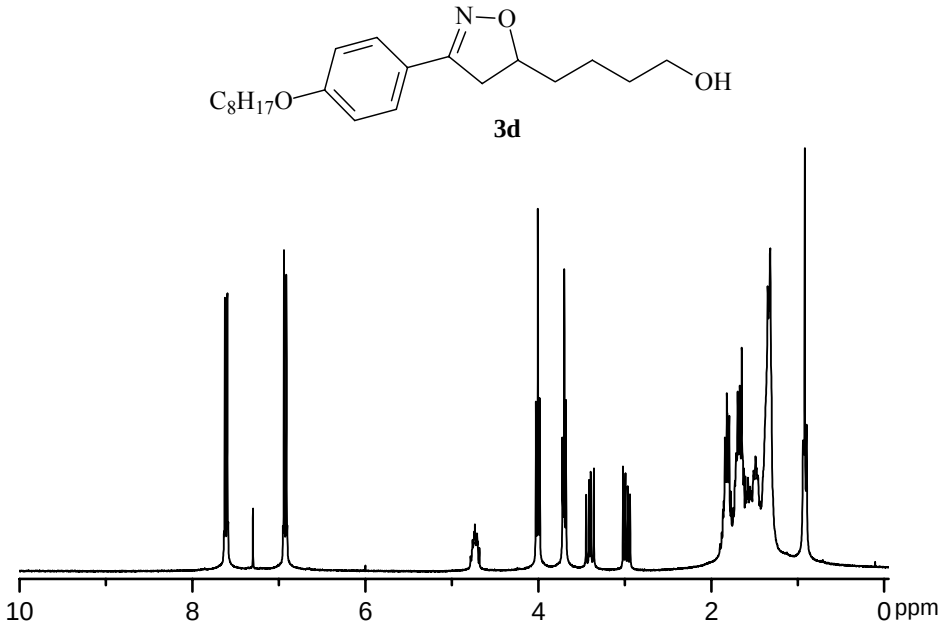

Figura 6. Espectro de ^{1}H NMR do composto **3d** ($CDCl_3$, 300 MHz).

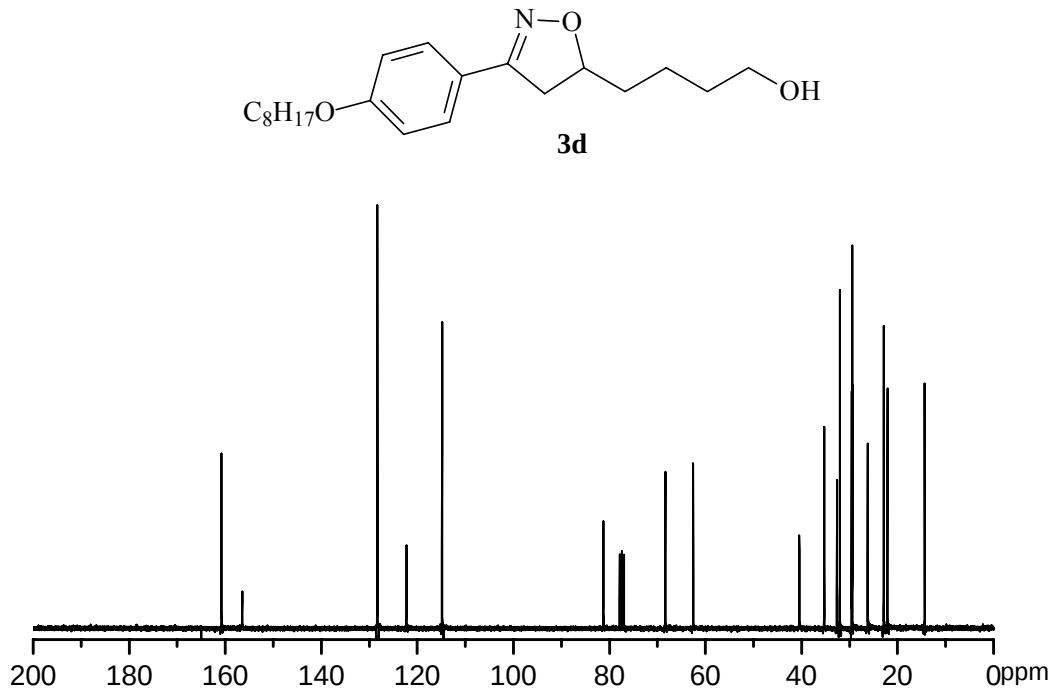

Figura 7. Espectro de ^{13}C NMR do composto **3d** ($CDCl_3$, 300 MHz).

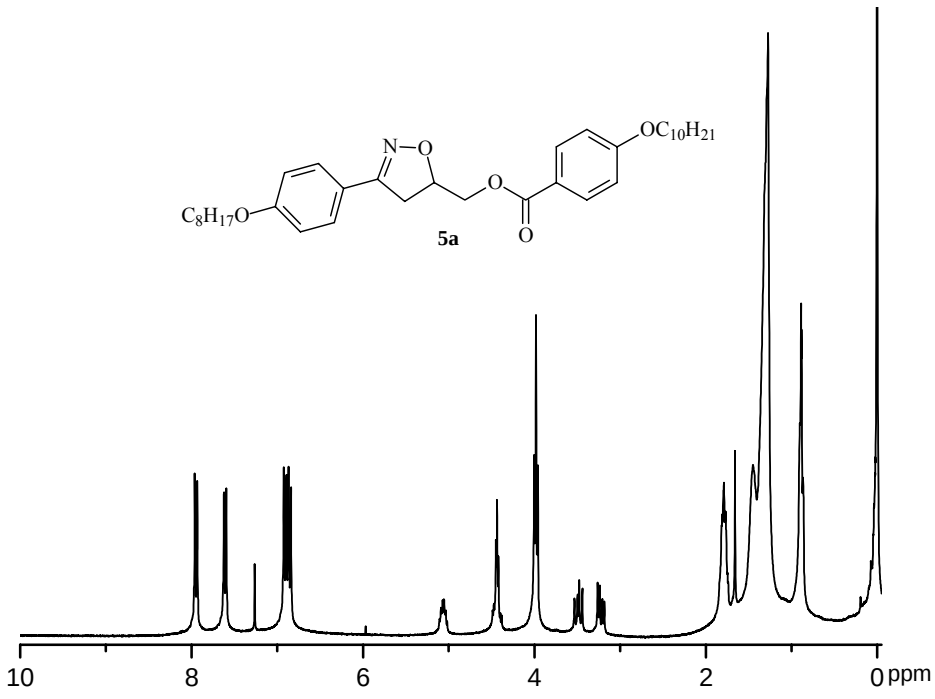

Figura 8. Espectro de ^{1}H NMR do composto **5a** ($CDCl_3$, 300 MHz).

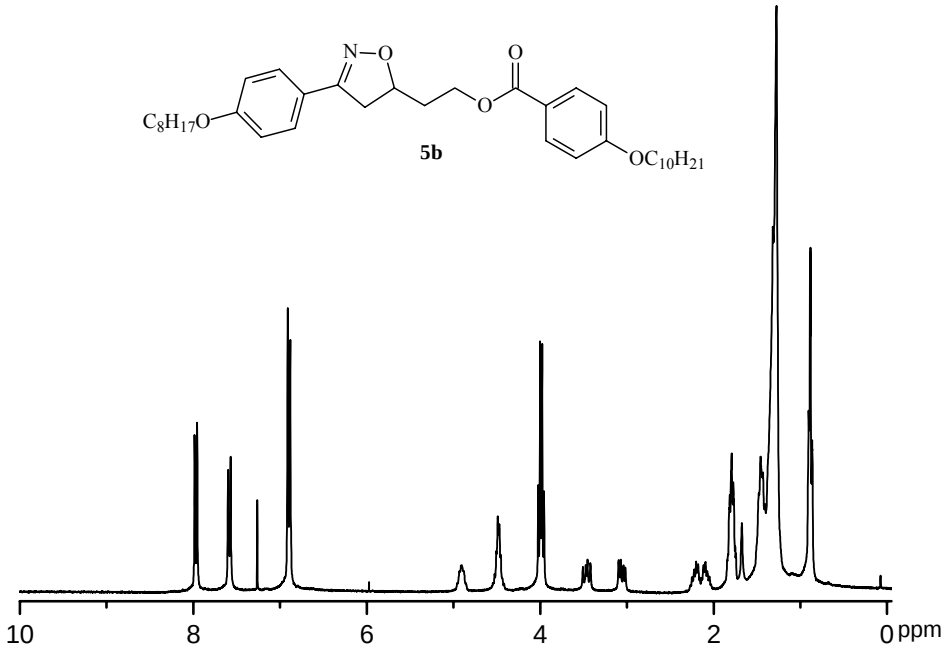

Figura 9. Espectro de ^{1}H NMR do composto **5b** ($CDCl_3$, 300 MHz).

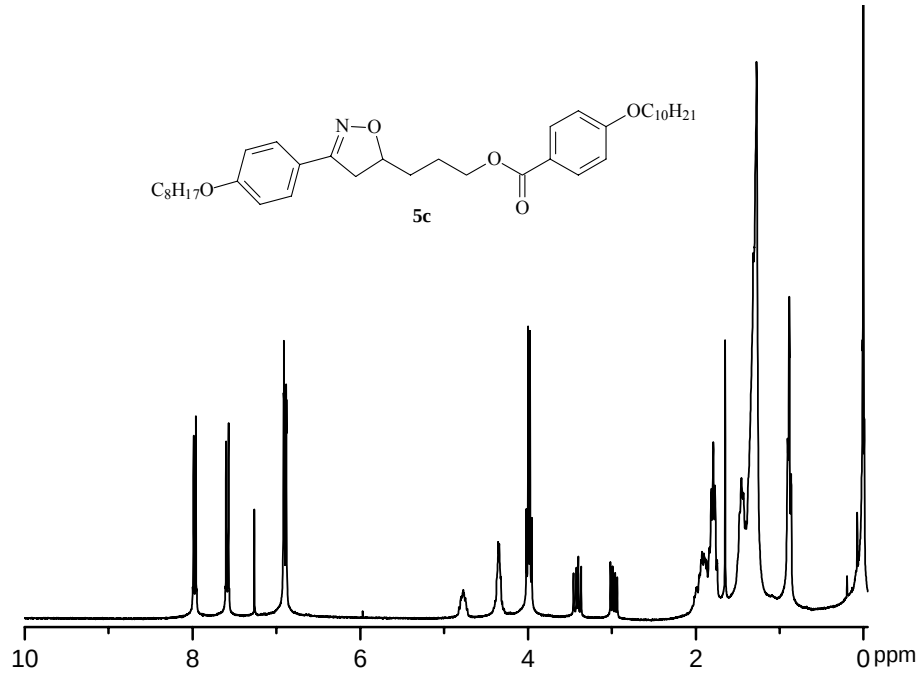

Figura 10. Espectro de ^{1}H NMR do composto **5c** ($CDCl_3$, 300 MHz).

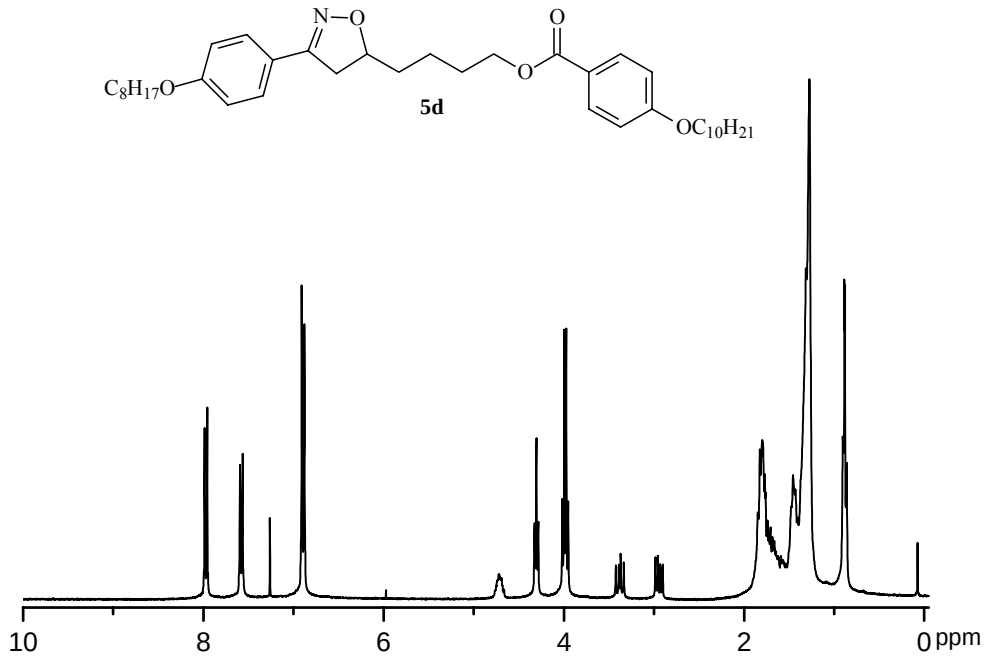

Figura 11. Espectro de ^{1}H NMR do composto **5d** ($CDCl_3$, 300 MHz).

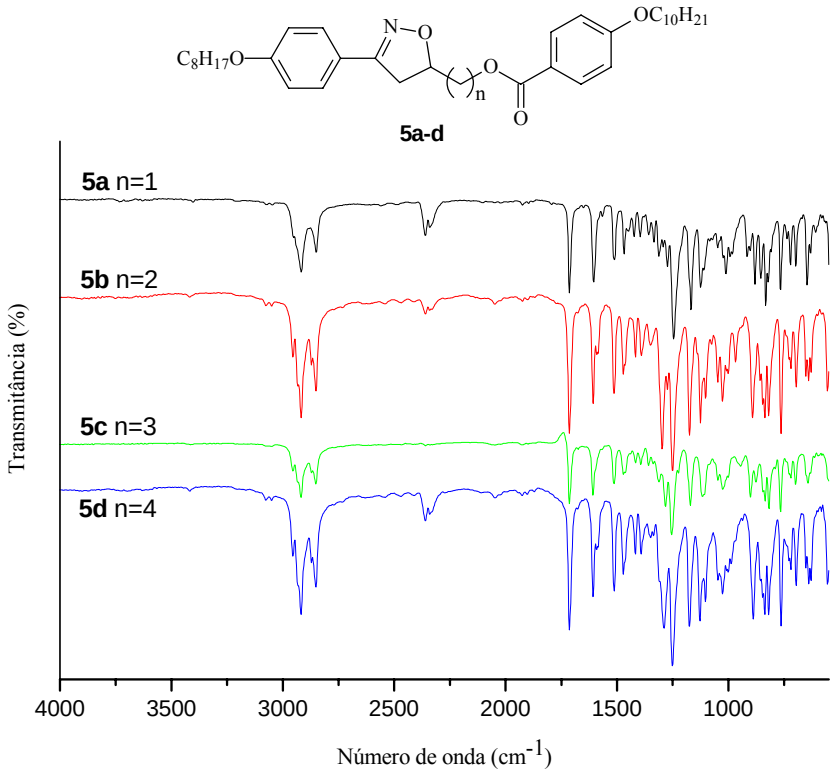

Figura 12. Espectros de ATR/FT-IR dos compostos da série **5a-d**. n = número de carbonos metilênicos.

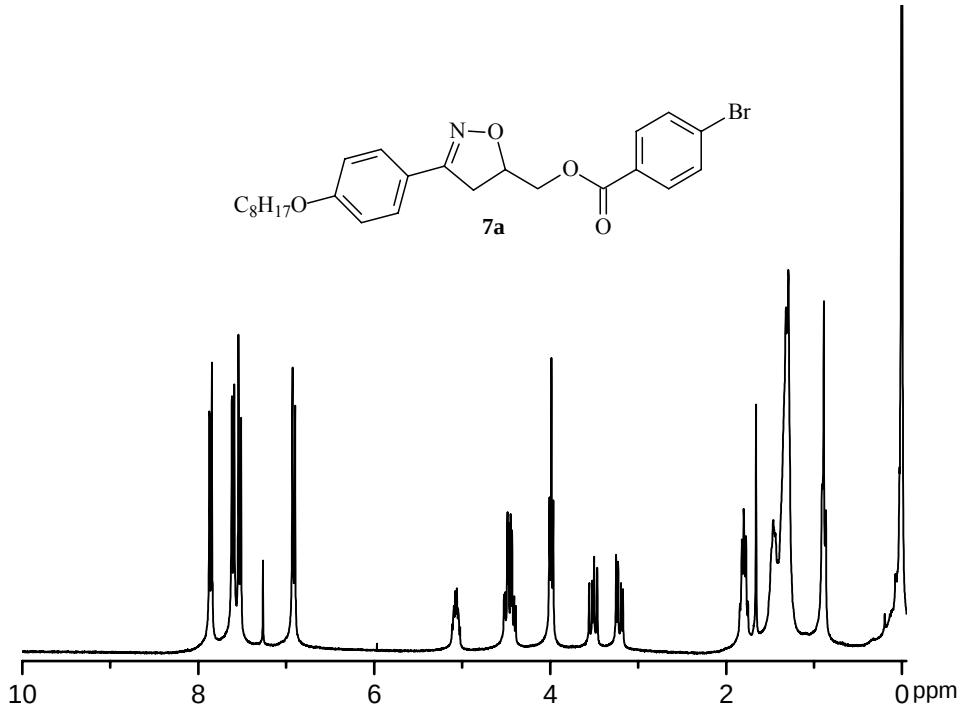

Figura 13. Espectro de ^{1}H NMR do composto **7a** ($CDCl_3$, 300 MHz).

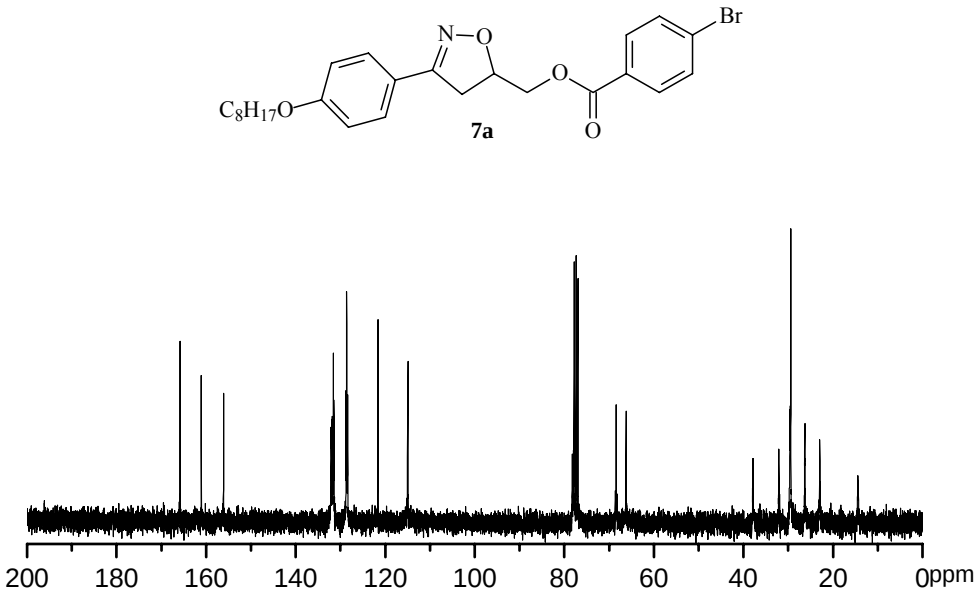

Figura 14. Espectro de ^{13}C NMR do composto **7a** ($CDCl_3$, 300 MHz).

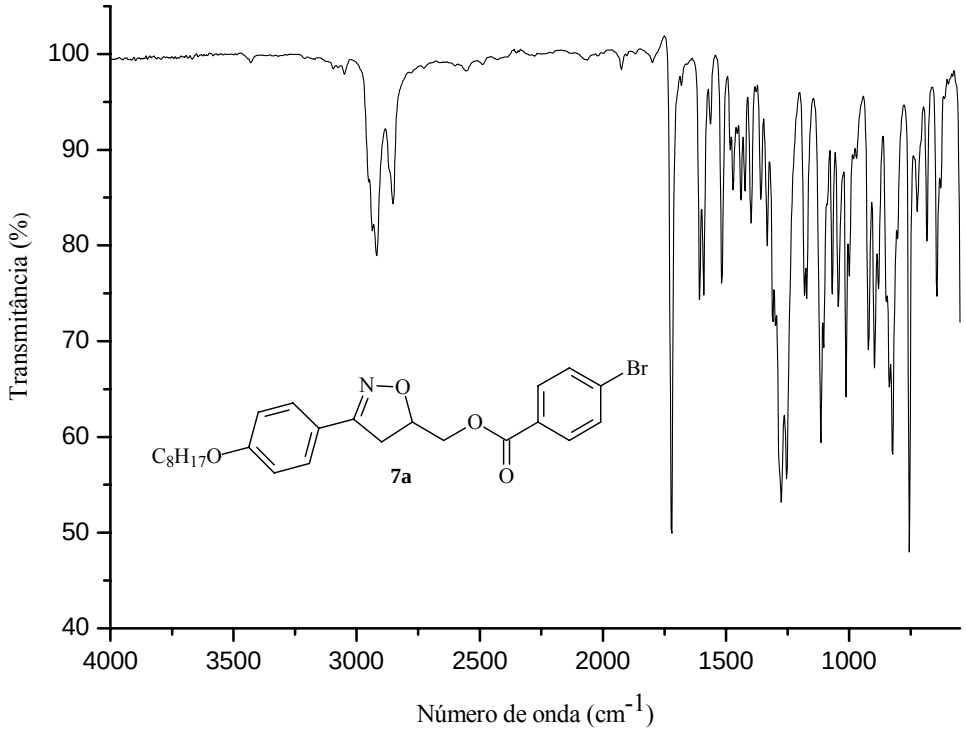

Figura 15. Espectro de ATR/FT-IR do composto **7a**.

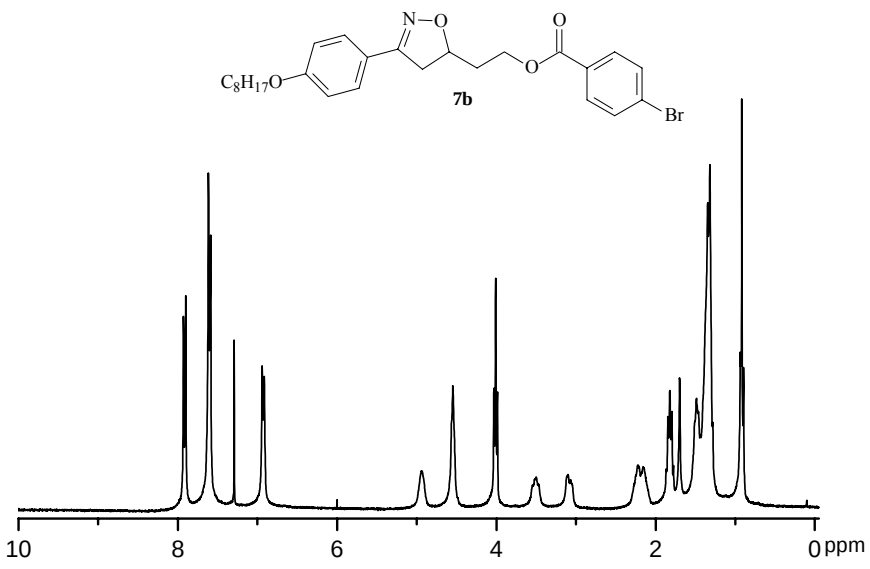

Figura 16. Espectro de ^{1}H NMR do composto **7b** ($CDCl_3$, 300 MHz).

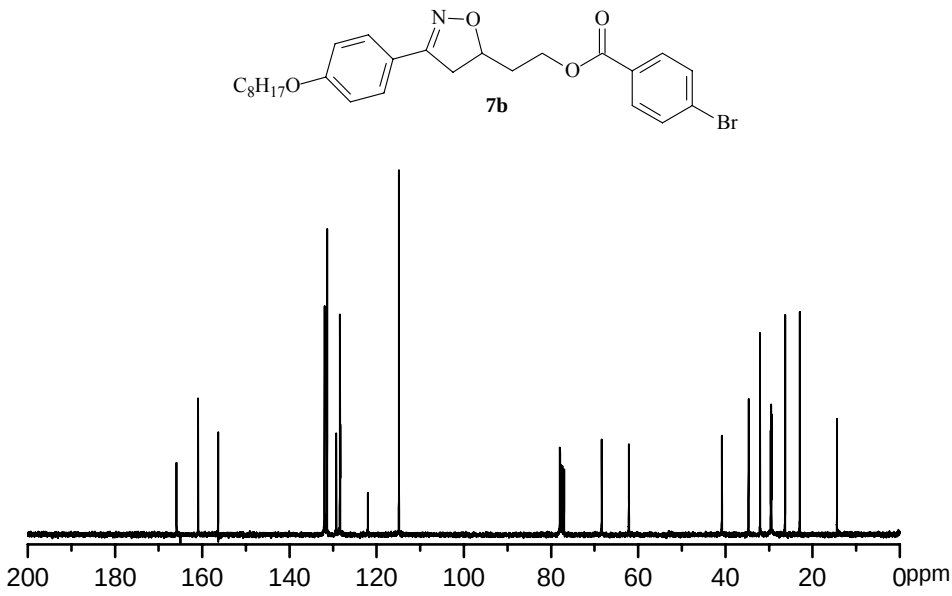

Figura 17. Espectro de ^{13}C NMR do composto **7b** ($CDCl_3$, 300 MHz).

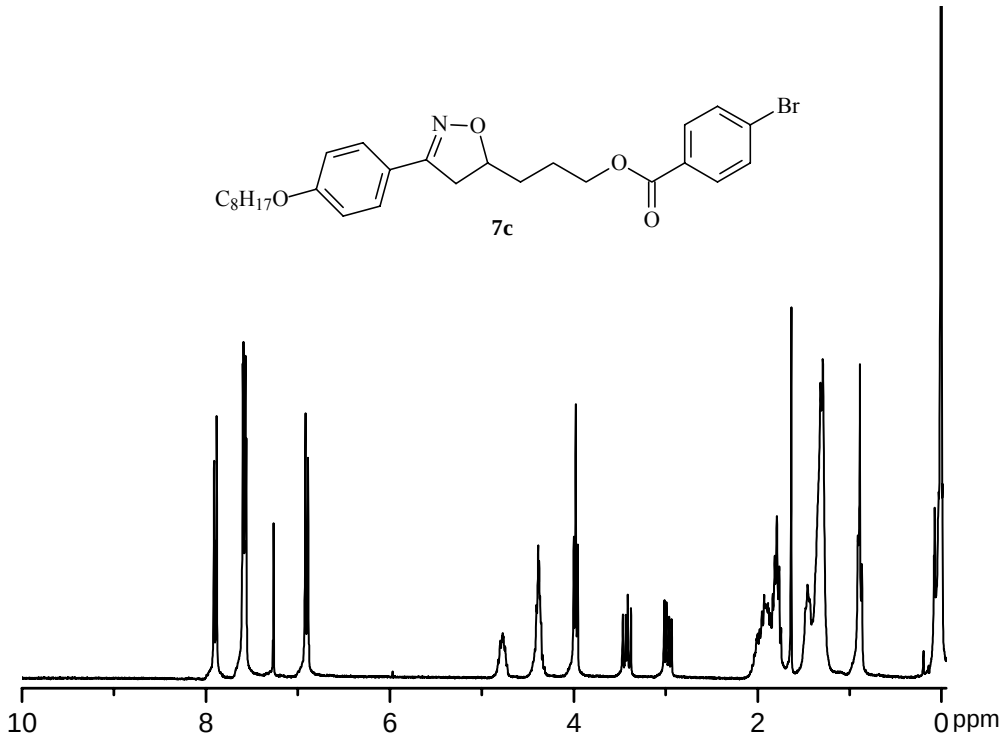

Figura 18. Espectro de ^{1}H NMR do composto **7c** ($CDCl_3$, 300 MHz).

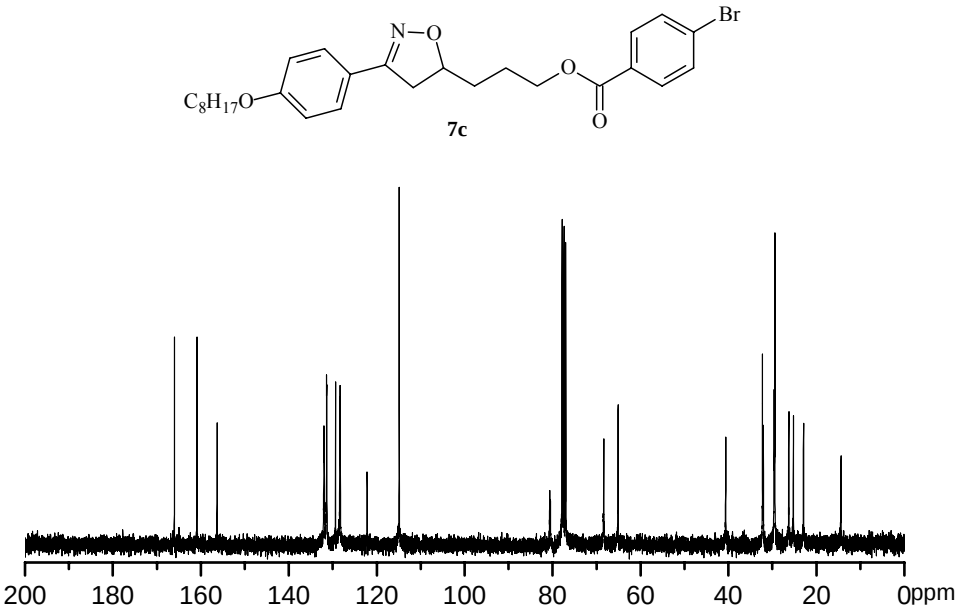

Figura 19. Espectro de ^{13}C NMR do composto **7c** ($CDCl_3$, 300 MHz).

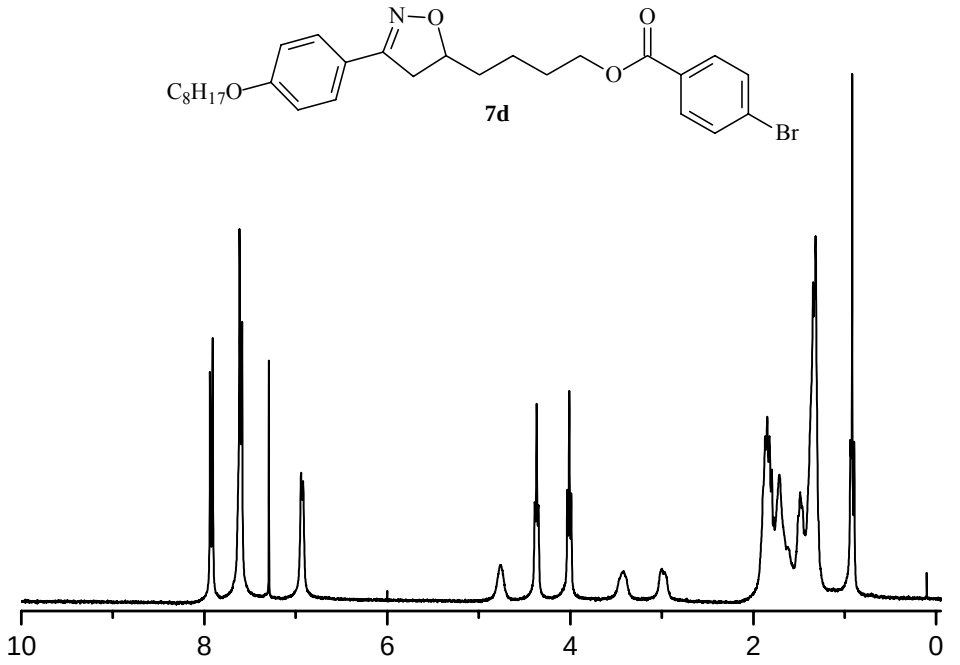

Figura 20. Espectro de ^{1}H NMR do composto **7d** ($CDCl_3$, 300 MHz).

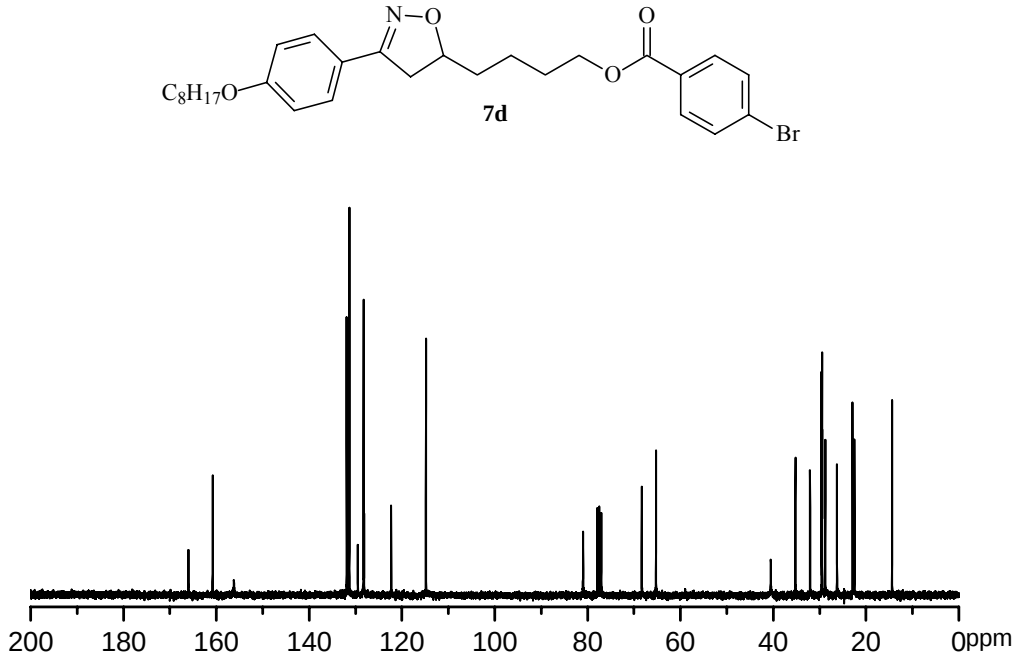

Figura 21. Espectro de ^{13}C NMR do composto **7d** ($CDCl_3$, 300 MHz)..

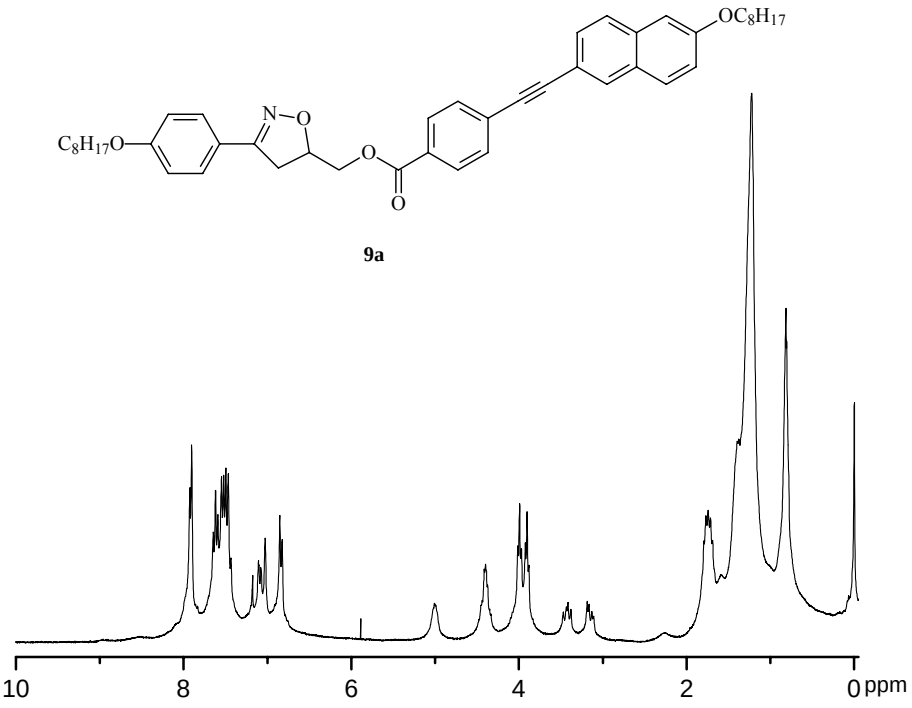

Figura 22. Espectro de ^{1}H NMR do composto **9a** ($CDCl_3$, 300 MHz).

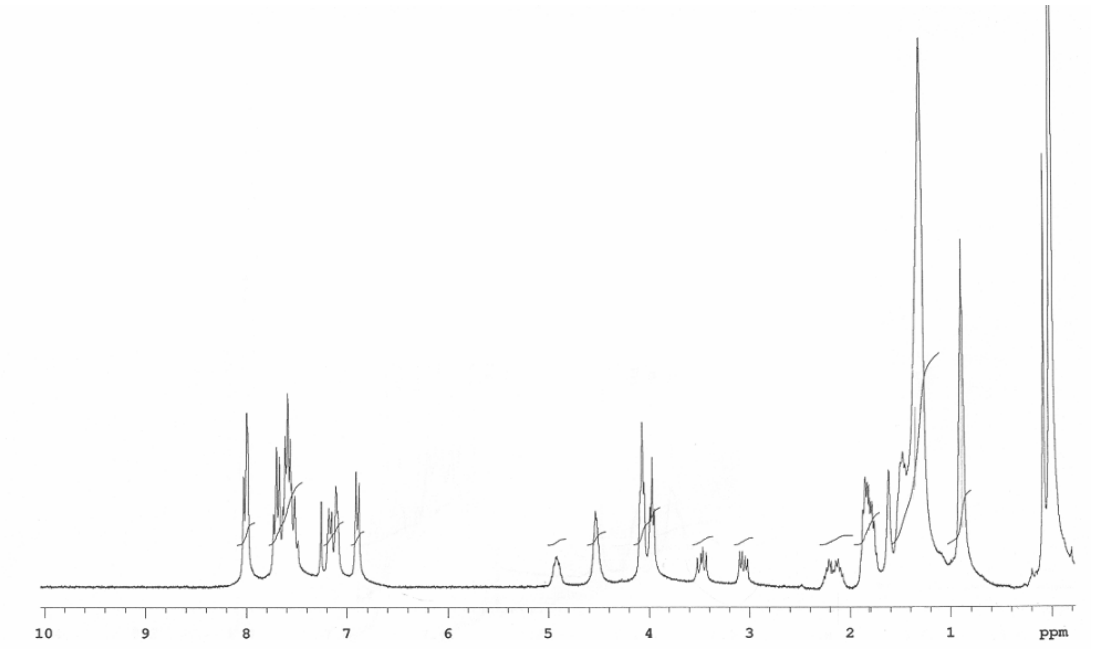

Figura 23. Espectro de ^{1}H NMR do composto **9b** ($CDCl_3$, 300 MHz).

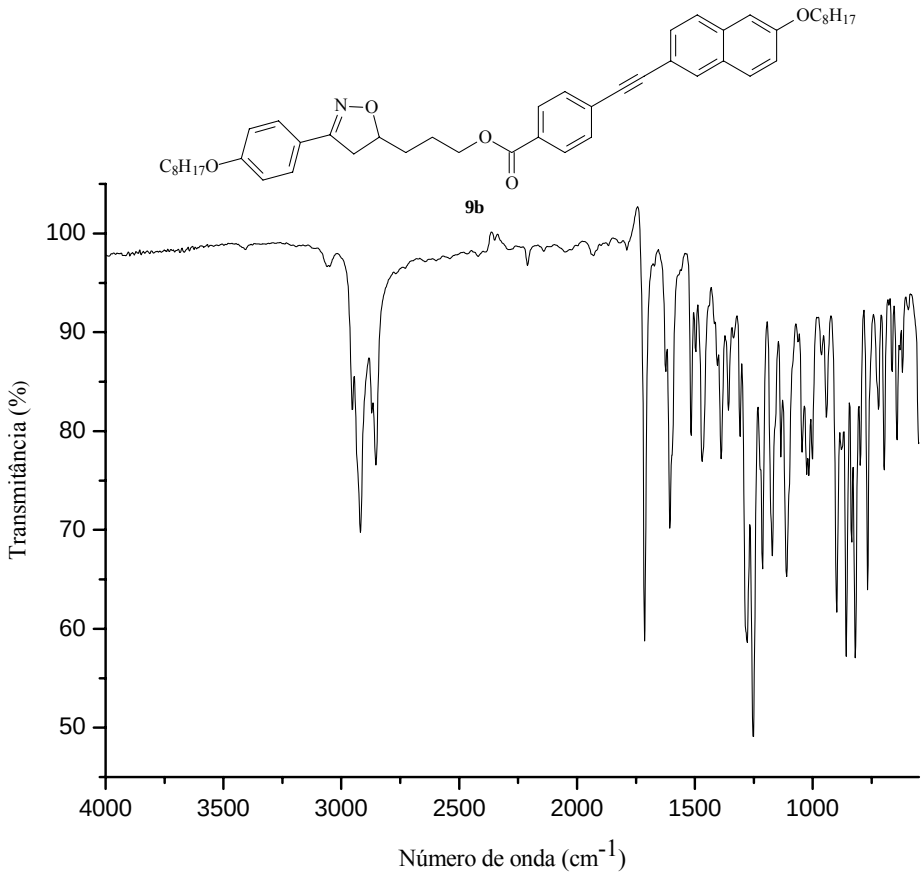

Figura 24. Espectro de ATR/FT-IR do composto **9b**.

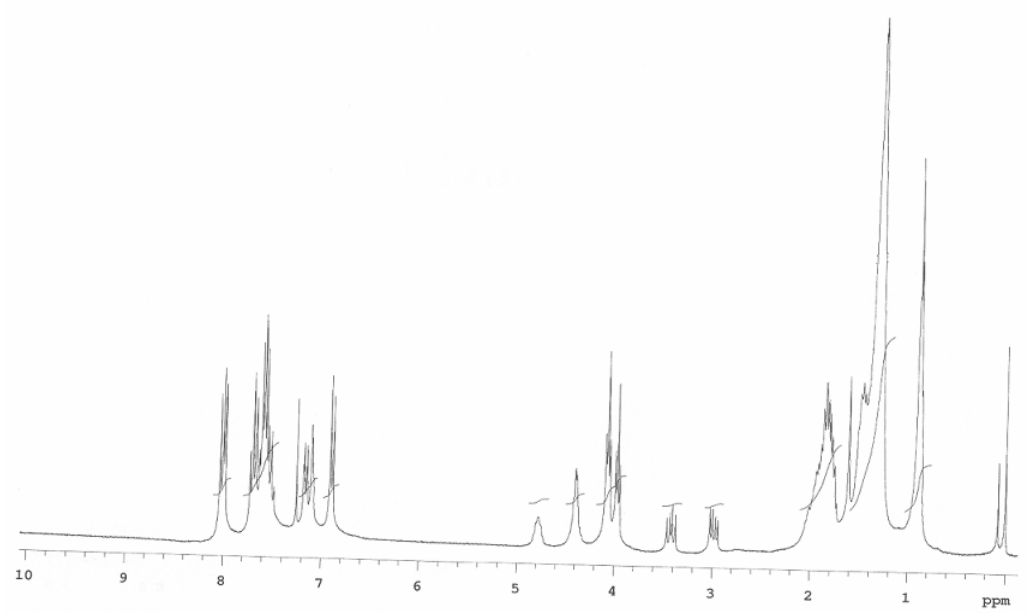

Figura 25. Espectro de ^{1}H NMR do composto **9c** ($CDCl_3$, 300 MHz).

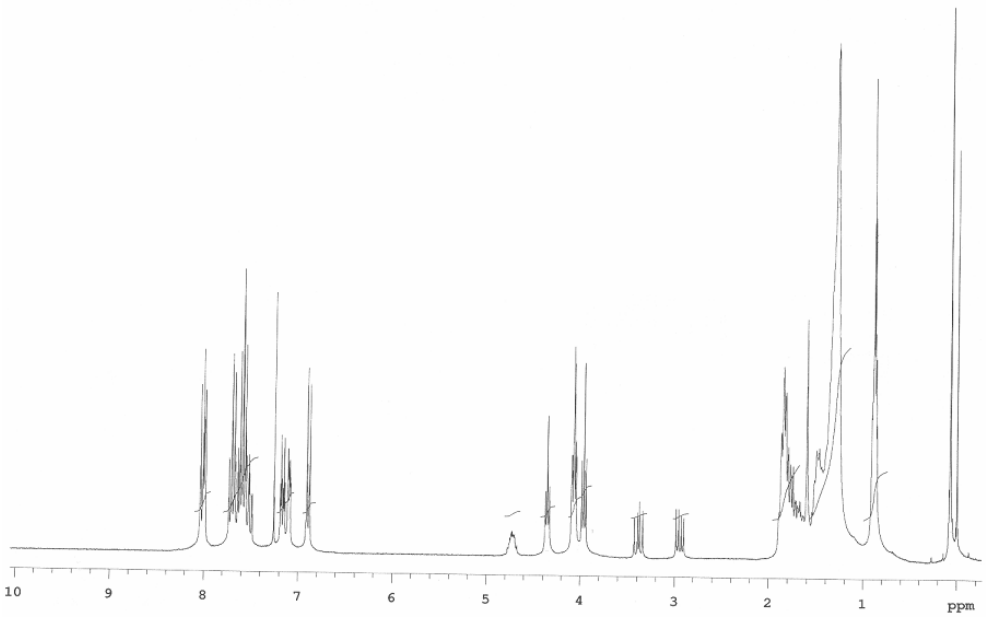

Figura 26. Espectro de ^{1}H NMR do composto **9d** ($CDCl_3$, 300 MHz).

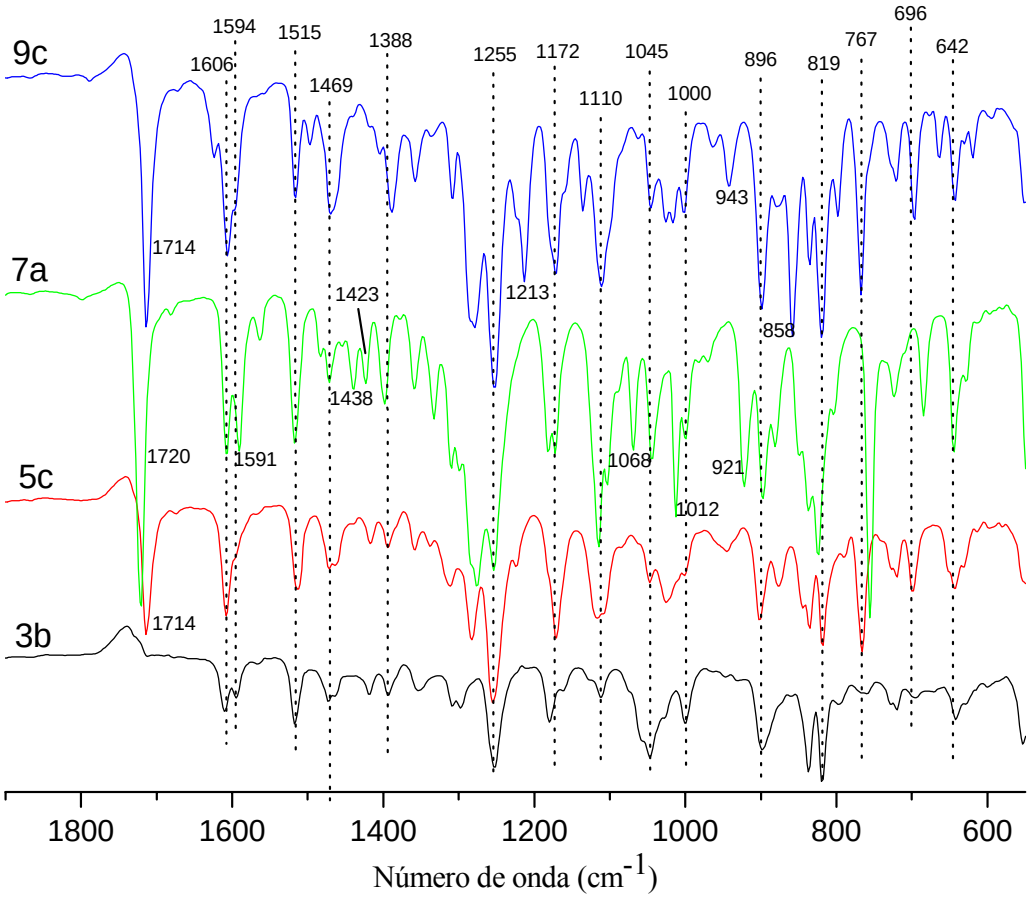

Figura 27. Sobreposição dos espectros parciais de ATR/FT-IR dos compostos **9c**, **7a**, **5c** e **3b**.

7. CONCLUSÕES

A utilização da reação de cicloadição [3+2] 1,3-dipolar para a obtenção do anel heterocíclico isoxazolina 3,5-dissubstituído mostrou-se altamente eficiente e regiosseletiva, permitindo a obtenção de uma coleção de compostos isoxazolínicos. Através do redimensionamento da anisometria geométrica destes precursores foram sintetizadas séries de compostos líquido-cristalinos. A caracterização dos produtos foi feita através da análise dos dados obtidos pelas técnicas espectroscópicas de RMN de ^{1}H e ^{13}C, IV e análise elementar. As propriedades mesomórficas foram avaliadas por DSC e MOLP.

Alguns precursores isoxazolínicos foram selecionados para serem transformados em cristais líquidos. A principal reação empregada foi o acoplamento de Sonogashira entre haletos de arila e arilacetilenos terminais. A tripla ligação entre os dois anéis aromáticos mostrou-se eficaz por contribuir na polarizabilidade, linearidade e rigidez das moléculas finais, uma vez que tais compostos apresentaram propriedades líquido-cristalinas. O aumento do comprimento molecular através das cadeias carbônicas laterais estabilizou as mesofases devido ao aumento da anisotropia geométrica. Estes fatores são importantes e determinam muitas das propriedades físicas dos compostos finais.

Nas reações de cicloadição 1,3-dipolar utilizando o ácido vinilacético como dipolarófilo obteve-se exclusivamente o cicloaduto 2:1 e não o esperado cicloaduto 1:1. Estudos *ab initio* sugerem que o cicloaduto 2:1 é formado porque a interação do orbital LUMO do composto 1,3-dipolar é mais favorável com o HOMO do cicloaduto 1:1 intermediário do que com o HOMO do dipolarófilo inicial. O estudo mesomórfico mostrou que os compostos apresentam mesofase esmética, com decomposição térmica da amostra.

Uma série de *O*-benzoiloximas foi sintetizada através da reação de esterificação entre oximas aromáticas e diferentes derivados de ácidos benzóicos. Os compostos apresentaram as mesofases SmA e N enantiotrópicas. Também, exibiram fluorescência azul em solução e no estado sólido. A incorporação do anel isoxazolina na estrutura molecular destes compostos mostrou uma quebra na planaridade da molécula, confirmada pela textura SmB observada por MOLP.

8. PERSPECTIVAS

8.1 Preparação do anel isoxazol.

Comparado ao anel isoxazolina, o anel isoxazol pode ser mais promissor para gerar propriedades líquido-cristalinas[1]. Isto porque este anel possui polarizabilidade anisotrópica de forma suficiente para induzir mesofase, além de ser aromático, conferindo uma maior conjugação e planaridade à molécula.

Estudos preliminares apresentados nesta Tese já mostraram bons resultados em relação à geração de mesomorfismo em um composto que continha o anel isoxazol[2]. Uma vez que este anel pode ser obtido a partir de uma etapa de oxidação do anel isoxazolina e que inúmeros compostos isoxazolínicos já foram sintetizados, é interessante preparar e estudar o comportamento térmico dos compostos isoxazólicos.

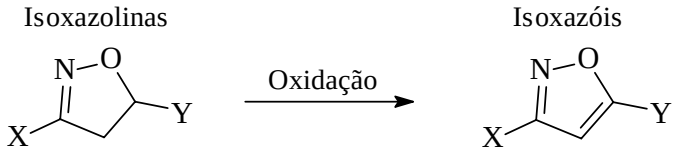

Esquema 8. Síntese de isoxazóis.

8.2 Preparação de carboniluréias.

Uma propriedade interessante que pode ser observada em moléculas que contêm grupos funcionais do tipo uréia, amida, ácidos, entre outros, é a gelatinização[3]. Um gel será formado sempre que tais moléculas, através de um processo de auto-organização, formarem uma rede de fibras tridimensional com grande área superficial sólida na qual um solvente é imobilizado. O fenômeno da automontagem das fibras é originado nas interações intermoleculares como ligações de hidrogênio, interações π-π e forças de van der Waals.

Os compostos que contêm o grupo carboniluréia também são bastante difundidos na área da agroquímica[4] (atuando como inseticidas reguladores do crescimento) e na área de saúde[5], agindo como drogas anticâncer.

[1] Vilela, G. D. Dissertação de Mestrado, **2010**. Programa de Pós-Graduação em Química, UFRGS.
[2] Tavares, A.; Schneider, P. H.; Merlo, A. A. *Eur. J. Org. Chem.* **2009**, 889.
[3] Miravet, J. F.; Escuder, B. *Org. Lett.* **2005**, *7*, 4791.
[4] Imran, M. Khan, S. A. *Indian J. of Heterocyclic Chem.* **2004**, *13*, 213.
[5] Zhang, Y.; Lukacova, V.; Bartus, V.; Nie, X.; Sun, G.; Manivannan, E.; Ghorpade, S. R.; Jin, X.; Manyem, S.; Sibi, M. P.; Cook, G. R.; Balaz, S. *Chem. Biol. Drug. Des.* **2008**, *72*, 237.

Nesse sentido, é interessante desenvolver rotas de síntese de carboniluréias que possuam anéis isoxazolínicos ou isoxazólicos (Figura 40) pois, assim, este material poderá apresentar a propriedade da gelatinização e comportamento mesomórfico.

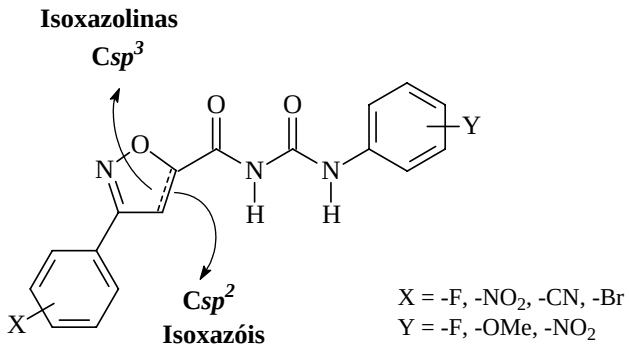

Figura 40. Estrutura química de carboniluréias dissubstituídas.

Também, estabelecidas as melhores condições de síntese dessas moléculas, pode-se estender a metodologia para sua versão assimétrica, produzindo uma coleção de carboniluréias dissubstituídas quirais.

8.3 Preparação de compostos perfluorados.

Compostos fluorados possuem, em geral, alta atividade sob o ponto de vista biológico[6], principalmente devido a sua capacidade de modular propriedades físico-químicas como acidez, basicidade e lipofilicidade da molécula[7].

Deste modo, pode ser interessante introduzir átomos de flúor na estrutura química de compostos isoxazolínicos a fim de produzir novos derivados fluorados ou perfluorados, como o composto da Figura 41, buscando-se atividade biológica.

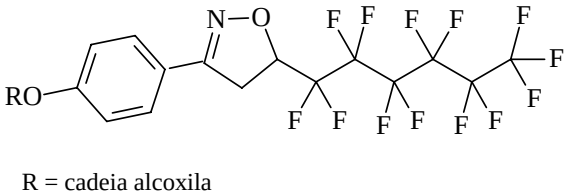

Figura 41. Exemplo de isoxazolina perfluorada.

[6] Kirk, K.L. *J. Fluorine Chem*. **2006**, *127*, 1013–1029.
[7] Dolbier, W. R. Jr. *J. Fluorine Chem.* **2005**, *126*, 157–163.